INFORMATION TO USERS

GAS-PHASE LUMINESCENCE OF AROMATIC CARBONYL COMPOUNDS AND THE DESIGN AND USE OF A GAS CHROMATOGRAPHIC DETECTOR

by

Zhong-Ping Lin

*Submitted in partial fulfillment of the requirements
for the degree of Doctor of Philosophy*

at

Dalhousie University
Halifax, Nova Scotia, Canada
October, 1997

Your file Votre référence

Our file Notre référence

Canada

DALHOUSIE UNIVERSITY

DEPARTMENT OF CHEMISTRY

The undersigned hereby certify that they have read and recommend to the Faculty of Graduate Studies for acceptance a thesis entitled "GAS-PHASE LUMINESCENCE OF AROMATIC CARBONYL COMPOUNDS AND THE DESIGN AND USE OF A GAS CHROMATOGRAPHIC DETECTOR"

by Zhong-Ping Lin

in partial fulfillment of the requirements for the degree of Doctor of Philosophy.

Dated October 3, 1997

External Examiner ___

Research Supervisor ___

Examining Committee ___

___

___
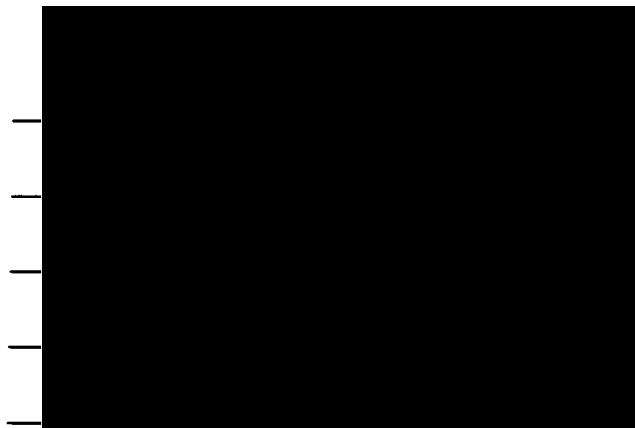
DALHOUSIE UNIVERSITY

DATE: <u>October 3, 1997</u>

AUTHOR: <u>Zhong-Ping Lin</u>

TITLE: <u>GAS-PHASE LUMINESCENCE OF AROMATIC CARBONYL</u>

<u>COMPOUNDS AND THE DESIGN AND USE OF A GAS</u>

<u>CHROMATOGRAPHIC DETECTOR"</u>

DEPARTMENT OR SCHOOL: <u>Chemistry</u>

DEGREE: <u>Ph.D.</u>   CONVOCATION: <u>May</u>   Year: <u>1998</u>

iii

I would like to dedicate this thesis to
my teachers and my family for all of their support

TABLE OF CONTENTS

Chapter 3   CHROMATOGRAPHIC DETECTION BY GAS-PHASE LUMINESCENCE SPECTROMETRY

Chapter 4   GAS-PHASE LUMINESCENCE OF AROYL COMPOUNDS

LIST OF FIGURES

x

xi

xviii

LIST OF TABLES

ABSTRACT

Certain types of aroyl compounds produce gas-phase luminescence in excited nitrogen. A novel, radioactively stimulated, high-voltage, low-current discharge in high-purity nitrogen was used to excite aroyl compounds. Based on gas-phase luminescence, a new single-channel aroyl luminescence detector (ALD) was designed and constructed. Aroyl compounds can be detected with unique selectivity and extreme sensitivity in the ALD. The detection limit was about 0.1 femtomol/second for a strongly luminescing compound like benzaldehyde. The linear range of calibration curves was about 4 orders of magnitude.

The gas-phase luminescence spectra of about sixty aroyl compounds were mapped. Gas-phase phosphorescence spectra are rare in the literature but, where available, they agreed with the ALD spectra. Most ALD spectra had never been obtained before in the gas phase. The triplet state energies were calculated. The substituent effects on the triplet energy (0-0 band) of substituted benzaldehydes, acetophenones and benzophenones; the luminescence quenching by oxygen and hydrocarbons; and the luminescence enhancement by argon and helium were also investigated. Our speculative luminescence mechanism for aroyl compounds in excited nitrogen suggests that ground-state N_2 is excited by collision with a fast electron in the mild discharge, and that this is followed by efficient triplet-triplet energy transfer from N_2 (A $^3\Sigma_u^+$) to the aroyl compound.

The single-channel ALD was converted to dual-channel operation to demonstrate the possibility of computer-mediated, compound-specific detection by dual-channel photometry. Response ratios of sixteen components of test mixture were examined, and turned out to remain constant in the ALD from close to their limit of detection to well beyond their range of linear calibration. Each individual compound could be successfully retrieved from the chromatographic file of the separated mixture as a single-peak Condac chromatogram in the presence, and even in the absence, of an optical filter or dispersive device. It is reasonable to conclude that several other detectors should likewise be able to provide virtually compound-specific response for analytical ends. In real samples, overlap between adjacent peaks often takes place. In extreme cases, overlapping peaks may co-elute completely, appearing as a single peak. In this case, quantitation is considered impossible. Yet, dual-channel chromatograms were successfully used for quantitating two perfectly co-eluting model analytes. This simple technique of resolving two peaks of identical retention into two quantifiable subtraction chromatograms is not restricted to the ALD, but can be carried out on various types of dual-channel detectors.

Finally, a triple-channel aroyl luminescence detector was designed and constructed. It can be used to acquire gas-phase luminescence spectra from a single chromatographic peak and generate response ratios of aroyl compounds. Based on the spectrum, retention time and spectral response ratio, particular aroyl compounds can be identified in complex mixtures. They can also be quantitatively determined with high sensitivity (picogram range) in a non-dispersive channel. This methodology was employed to analyze some aroyl compounds in essential oils and complex environmental samples such as a standard marine sediment. Further demonstrated analytical applicabilities include the highly sensitive and selective determination of alcohols coupled with luminescing aroyl moiety, and the direct-injection sampling of room air for luminscing products of incomplete combustion.

LIST OF ABBREVIATIONS

A: ampere

ALD: aroyl luminescence detector

amol: atto mole

AP: acetophenone

AW: acid washed

BA: benzaldehyde

BP: benzophenone

ca: circa

CH: channel

CHROM: chromatograms(a computer program name)

cm: centimeter

cm^{-1}: wavelength number

CNMA: cinnamaldehyde

Condac: conditional access

DC: direct current

DL: detection limit

ECD: electron capture detector

e.g.:   [L *exempli gratia*] for example

eV: electron volt

fg: femto gram

FID:	flame ionization detector
FPD:	flame photometric detector
FT/IR:	fourier transform infrared
fmol:	femto mole
g:	gram
GC:	gas chromatography
i.d.:	inside diameter
i.e.:	[L *id est*] that is
IP:	ionization potential
ISPBA:	4-isopropylbenzaldehyde
kV:	kilo volt
LC:	liquid chromatography
LP:	long pass
mA:	milli ampere
m/e:	mass to charge ratio
mL/min:	milliliters per minute
mm:	millimeter
mM:	milli molarity
mmol:	milli mole
ms:	milli second
MS:	mass spectrometry
N:	noise

nA:	nano ampere
ng:	nanogram
nm:	nanometer
nmol:	nanomole
NPPD:	nitrogen plasma photometric detector
ns:	nano second
pA:	pico ampere
PAH:	polynuclear aromatic compound
PAK:	polynuclear aromatic ketone
pg:	picogram
PMT:	photomultiplier tube
p-p:	peak to peak
ppb:	part per billion
ppm:	part per million
R:	response
RR:	response ratio
RSD:	relative standard deviation
sec:	second
S:	singlet
S/N:	signal to noise ratio
SP:	short pass
T:	triplet

t_R: retention time

μg: microgram

μL: microliter

μmol: micro mole

μs: micro second

v/v: volume to volume ratio

w/w: weight to weight ratio

ACKNOWLEDGMENTS

Without my supervisor Dr. Walter A. Aue's encouragement, understanding and intelligent supervision, this thesis would have been impossible to complete. I am also deeply indebted to him for offering me the opportunity to study at Dalhousie and to be one of his students. This will be the most unforgettable memory in my lifetime.

Special thanks go to the members of my supervisory committee Dr. Amares Chatt, Dr. James A. Pincock and Dr. Philip D. Pacey for reading and correcting this thesis.

Much appreciation is extended to one of our group members, Dr. Nancy Lowery, for correcting and smoothing English for the draft of this thesis, to Mr. Brain Millier for his valuable assistance in electronic work and to Mr. Cecil. G. Eisener for his fine work in building various parts of these detectors.

I also wish to thank other group members Drs. Xun-Yun Sun, Hameraj Singh, Kevin B. Thurbide, Taghi Khayamian and all of the departmental staff for their various forms of assistance during my years at Dalhousie.

Finally I would like to acknowledge Dalhousie University for my graduate fellowship, the Chemistry Department for offering me a teaching assistantship and to thank my wife and her family, in China, for taking care of our little son Frank and for their understanding.

My thesis supervisor, Dr. Walter A. Aue, has the unrestricted right to use any or all of this thesis, and its technical and descriptive content, in whatever way he deems appropriate.

_____
Author's Signature

October 3, 1997
Date

Chapter 1

INTRODUCTION

1.1 Gas Chromatography(GC) and Detectors

Gas chromatography still stands as one of the leading techniques in analytical chemistry. It is widely used in environmental analysis, medicine, industry, space research, and geology, among other fields, for the separation and determination of volatile chemical substances. Meanwhile, the rapid progress in high technology constantly poses new challenges for this powerful technique. As we know, a detection device for qualitative and quantitative determination of the components after their separation is central to chromatographic instrumentation, and progress in gas chromatography very strongly depends on the development of its detectors.

The GC detectors developed in the last few decades can be divided into two types: universal and selective detectors (1, 2). According to their mode of operation, most GC detectors are based on one of several mechanisms: gas-phase ionization, photometry, electrochemistry, or bulk property measurements. The flame ionization detector (FID), the helium ionization detector (HID), the photoionization detector (PID), the nitrogen/phosphorus detector (NPD), the surface ionization detector (SID), the electron capture detector (ECD), and the ion mobility detector (IMD) are well-known chromatographic detectors under the general category of gas-phase ionization. Among these detectors, the FID is the most common detector for GC because of its universality, high sensitivity, wide linear response range and simplicity of design. The

1

second most often used detector is the ECD, which features excellent sensitivity and selectivity for certain compounds containing halogens or nitro groups (3). The photometic detection for GC includes atomic emission, molecular emission, atomic absorption, and molecular absorption. In general, absorption methods are less sensitive than emission detection methods because it is far easier to detect a weak signal on a low background than to observe a small decrease in a large signal. This is why emission detectors are more attractive than absorbance detectors such as the atomic absorption detector, the UV/visible absorption detector and the infrared absorption detector. One of the best known emission detectors is the flame photometric detector (FPD). Although it can sense many metal elements (4), it is used primarily for the selective detection of phosphorus and sulfur containing compounds. The greatest interest in photometric detection for GC over the past few years has been in the area of atomic emission spectrometry (AES) (5). This technique uses microwave-induced plasmas (MIPs) as the primary energy sources, and has proved to be a versatile, sensitive and element-selective detector for gas chromatography. Among electrochemical detectors, the Hall electrolytic conductivity detector is the most widely used and accepted GC detector. GC detectors which are based on monitoring changes in bulk properties include the thermal conductivity detector (TCD) and the surface acoustic wave crystal detector.

Mass spectrometric detection for GC (GC/MS), which does not neatly fit into the categories listed above, has become the most common of GC detector for determination of the structure and elemental composition of the components of complex mixtures (6). In this combined technique, GC is able to separate multi-component mixtures into single

components with high separation efficiency, and MS operates as a chromatographic detector with a high identification ability. With the advancement of computer technology, libraries of compounds may be installed with most instruments, thus promoting unambiguous identification of the compounds in complex mixtures. Some hyphenated techniques including GC/FT-IR/MS and GC/MS/MS are more powerful analytical tools in chromatographic identification. The invention of new GC detectors and the improvement of existing ones are still challenging tasks for analytical chemists (7).

1.2 Molecular Emission Photometric Detector in Chromatography

The most common GC detectors which involve the emission of light from molecules are the flame photometric detector, the chemiluminescence detector, the flame infrared emission detector, the gas-phase fluorescence detector, and the plasma emission detector, depending on the methods by which the analyte, or its products, is excited. In the FPD, the excitation energy of excited products comes from chemical reactions in the flame (8). The excited molecules emit photons while decaying to the ground state. This excitation is of a chemical nature and the emission is therefore called flame chemiluminescence. For example, sulfur- and phosphorous-containing organic compounds can be detected by measuring the intensity of the S_2^* (at 394 nm) and HPO* (at 526 nm) chemiluminescent bands emitted in a low temperature hydrogen-air (oxygen) flame. When chemiluminescence in hydrogen-air (oxygen) flames is not possible, analytes can be detected by thermal emission or the emission from products formed by

their interaction with a sensitizer in a hydrogen-air flame (8). The chemiluminescence

detectors usually utilize excitation energy supplied by the reaction with ozone. For

example, sulfur-containing compounds can be determined by means of excited SO_2^* at

300 to 400 nm, where the SO_2^* is formed as a result of the oxidation of those compounds

by ozone. Generally, chemiluminescence is possible when: (a) the free energy of the

reaction is sufficient to form excited products; and (b) preferable excited products form.

The chemiluminescent process can involve the following reactions:

$$A + B \rightarrow M^* \qquad \text{(formation of excited molecules} \qquad (1.1)$$
$$\text{caused by chemical reaction)}$$

$$M^* \rightarrow M + h\nu \qquad \text{(emission)} \qquad (1.2)$$

$$M^* \rightarrow M \qquad \text{(deactivation of excited molecules} \qquad (1.3)$$
$$\text{by quenching, internal deactivation,}$$
$$\text{or energy transfer)}$$
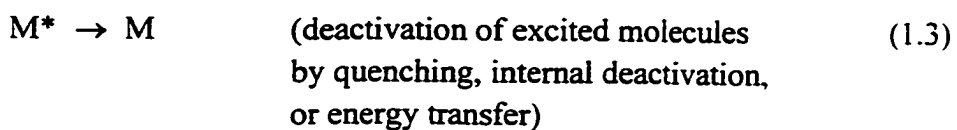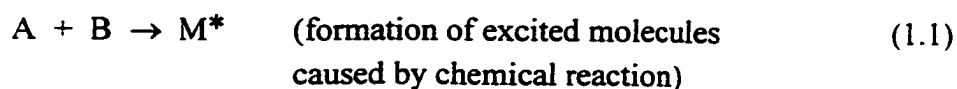
The flame infrared detector for GC is based on monitoring molecular emission

from terminal combustion products, i.e. CO_2, HCl and HF, to achieve carbon-, chlorine-,

and fluorine-specific detection in a hydrogen/air flame (9). The detection limits and

selectivities are not competitive with those of other selective detectors, but one advantage

of the flame infrared detector is that it can be used with nonselective FID detection.

Molecular fluorescence spectrometry offers a number of potential advantages for

detection in GC, including very high sensitivity, high selectivity, fast response, the

generation of spectral information useful for compound identification and freedom from

influence of column temperature and flow rate (10). Although the earliest fluorometric

GC detector operated by trapping column eluent in a liquid solvent followed by

measuring room-temperature solution fluorescence (11), later designs for fluorescence GC detectors have used measurement of gas-phase fluorescence, with a heated transfer line carrying the GC eluent to a heated detector cell (12). In gas-phase fluorescence detection, both electron impact (EI) and optical (conventional lamps and lasers) excitation are used to induce fluorescence. Gierczok and co-workers (13) discussed the characteristics of electron impact-induced fragmentation as a means of producing emissive fragments from various non-fluorescent organic molecules and pointed out its potential advantages as a technique for GC detection. The interfacing technique of EI-fluorescence apparatus to a GC were reported by Wehry and co-workers (14). This detector can be operated in either a universal or selective mode, depending on whether single or multiple-wavelength detection of fluorescence is utilized. With optical excitation, Thomas and co-workers (15) found that polynuclear aromatic compounds (PAH) could be detected by simultaneous UV-absorbance and fluorescence measurement. while Creaser and co-workers (16) reported that the addition of the vapor of a fluorescent compound (naphthalene) provided a means for direct gas-phase fluorescence detection of fluorescent species as positive peaks and indirect detection of nonfluorescent species as negative peaks. These detectors were capable of achieving subnanogram limits of detection for fluorescing compounds. A major shortcoming of these detectors was the fact that molecular fluorescence spectra of hot gases at relatively high temperatures tended to be broader than their counterparts measured in liquid solution due to vibrational and rotational sequence congestion. In order to achieve high spectral resolution and improve selectivity in gas-phase fluorometric GC detection, both matrix isolation (17)

and supersonic jet (18) fluorescence spectrometry were used as low-temperature measurement techniques. Supersonic jet expansions are extremely useful for high-spectral-resolution fluorescence measurements. In a free jet expansion, the analyte molecules are present as isolated ultracold gas-phase species. Gauterman and co-workers (19) described capillary gas chromatography/pulsed supersonic jet/fluorescence excitation spectroscopy as a promising analytical tool which was capable of separating and identifying structural isomers of PAH's in complex environmental samples. Although the various plasmas are mainly used for atomic emission detection in GC (5), plasmas may also give rise to molecular emission. This will be discussed in the following section.

1.3 Active Nitrogen Plasma Photometric GC Detector

The most important plasma emission detectors (PED's) use the microwave-induced and -sustained helium plasma (MIP), the direct-current argon plasma (DCP), the alternating current plasma (ACP), the capacitively coupled plasma (CCP), the radio-frequency-induced plasma (RFP), and the inductively coupled argon plasma (ICP) as primary energy sources. The ICP has been little used for GC detection, but is finding favor as a mass spectral ion source in the GC-ICPMS mode. The plasma gases are usually rare gases (He and Ar), but air and nitrogen have been used as well. The plasma consists of a mass of predominantly ionized or excited gases. The analyte excitation results from electron impact and from collision with metastable atoms of the plasma gas. Specific emissions from the excited species are monitored to reveal the presence of particular compounds or elements in the GC effluent stream.

Using nitrogen as the plasma support gas creates a new kind of GC detector based on "active nitrogen" (20). The term "active nitrogen" refers to any excited forms of nitrogen: molecular, atomic, even ionic or, more often, a mixture of these. The high chemical activity of active nitrogen is attributed to ground state nitrogen atoms, nitrogen molecular ions and various electronically and vibrationally excited nitrogen molecules. Ground state $N(^4S)$ atoms and excited molecules, probably $N_2(A\ ^3\Sigma_u^+)$, are considered to be the main contributors to the chemical reactivity (21). There are various methods for producing active nitrogen. Active nitrogen is usually produced by an electric discharge through nitrogen. Other discharges such as high-frequency electrodeless discharge, high voltage ac and dc discharge, hollow cathode dc discharge, ozonizer-type discharge, arc discharge, and microwave discharge, etc., can also be used to activate nitrogen. The energy of the excited metastables of nitrogen molecules can be used to excite analyte molecules by energy transfer. Then, the excited analyte molecules will return to the ground state by specific luminescence emission. The active-nitrogen plasma photometric detector is based on monitoring the intensity of the emission spectra of the excited analytes.

The active-nitrogen detector offers both atomic and molecular luminescence detection. In 1972, D'Silva and co-workers reported the first analytical use of active nitrogen (22). The active nitrogen was generated in an Ar/N_2 mixture by X-ray excitation and was used to excite mercury vapour. Mercury could be determined down to the ppb level by monitoring the Hg 253.7 nm emission. Later, Cappelle and co-workers (23, 24), with a microwave discharge, produced active nitrogen which in turn excited thermally

vaporized Bi and Ge. Detection limits of about 10^4 and 10^8 atoms/cm^3 for Bi and Ge, respectively, were reported. This technique was named Metastable Transfer Emission Spectroscopy (MTES), and it was estimated that half of the stable elements in the periodic table are accessible by this method. MTES has been used for Pb (25-27), Ag, Bi, Cd, Cu, Mg and Tl (26,27) detection. Dodge and co-workers (28) developed another approach for the excitation of metals by using a high voltage dielectric discharge to generate a high concentration of metastable species $N_2(A\ ^3\Sigma_u^+)$. The technique was called Metastable Energy Transfer for Atomic Luminescence (METAL). Detection limits for Hg and Zn were $\sim 10^8$ atoms/cm^3 and 10^7 atoms/cm^3, respectively. In 1981, D'Silva, and co-workers reported an Atmospheric Pressure Active Nitrogen Afterglow (APAN) detector (29), which was based on generating active nitrogen by means of an electrodeless ozonizer-type discharge, mixing of the hydrides of several metals with active nitrogen in the afterglow plasma, and monitoring the characteristic atomic emission lines of the metals of interest. The detection limits were similar to those obtained in atomic absorption spectrometry. So far, considerably fewer analytical studies have investigated the molecular emission induced by active nitrogen. Several reseachers have examined the application of an active-nitrogen-induced chemiluminescence detector for gas chromatography (30-33). They used the MTES system which consisted of a microwave stimulated nitrogen plasma at low pressure (8-30 torr) and the APAN system in which the nitrogen was activated by a high-voltage dielectric discharge. In both systems, virtually all carbon compounds reacted with active nitrogen to produce electronically excited cyanogen radicals (CN). The GC detection was

based on observing the strong emission at 388.3 nm from the CN (B $^2\Sigma^+ \to$ X $^2\Sigma^+$) system when hydrocarbons were present in the GC detection cell. For organometallics (32), detection can be performed by monitoring not only CN band emission, but also the characteristic atomic emission lines for the metal of interest. For oxygen-containing compounds, either NO (A $^2\Sigma^+ \to$ X $^2\Pi$) or OH (A $^2\Sigma^+ \to$ X $^2\Pi$) emission can be monitored (34). One percent HCl added into nitrogen was found to enhance hydrocarbon response because of increased degradation of the hydrocarbons in the MTES system. It is claimed that active nitrogen, with its nearly universal response to hydrocarbons and wavelength selective detection of many different elements, has a significant advantage over the flame ionization detector, which can only be used in a "universal" mode.

Active nitrogen has also been used as a low energy source for the excitation of line and band spectra of many atoms and molecules (35). The first analytically useful molecular spectra of inorganic S-, P-, B-, Cl- Br- and I-containing compounds were obtained from the APAN system by Rice and co-workers in 1984 (36), with a detection limit down to several nanograms per second. By monitoring the SN and PN emission of sulphur and phosphorus compounds in the MTES system (37), and the emission from molecular species of oxygen-containing compounds (38,39), sulphur and phosphorus compounds in the gaseous and aqueous phase, and oxygen-containing impurities in nitrogen and argon can be determined. These molecular emissions originate from small fragments of the analyte molecule, rather from the intact molecule itself. In 1984, Winefordner and co-workers (40) reported the chemiluminescence spectra of intact benzene, naphthalene and anthracene molecules. The

authors used a gentle molecular excitation source based on energy transfer from metastable nitrogen molecules in a nitrogen afterglow, which was generated by a dielectric discharge through flowing nitrogen. The limits of detection for several polycyclic aromatic hydrocarbons (PAHs) by active nitrogen-induced chemiluminescence were in the tenths-of-a-nanogram range with single channel detection. A hydrocarbon and a PAH mixture could be separated on a gas chromatographic column with multichannel detection. This was the first report of GC detection based on the luminescence from an intact analyte molecule excited by active nitrogen.

In 1987, Tang and Aue reported GC determination of benzaldehyde (41) and anthraquinone (42) by gas-phase luminescence in excited nitrogen, which was produced by a very mild, radioactively stimulated DC discharge. The detection limits for benzaldehyde and anthraquinone were extremely low, down to 0.1 pg/s and 0.05 pg/s, respectively. This gas-phase luminescence in excited nitrogen showed high selectivity to certain aroyl-type molecules. The authors found that a strong electrical field was necessary for producing a large number of metastable energy transfers and hence a strong detector response; however, in the absence of the strong electrical field, the energy derived solely from the beta decay of ^{63}Ni still produced considerable luminescence from some aroyl-containing molecules (43). Minimum detectable amounts were, however, about fifty times higher in the radioactive plasma than that in the strong electrical field. Since a radioactive plasma is conventionally used in the electron capture detector (ECD) operated with N_2 as a carrier gas, aroyl compounds luminesce in the ECD and can be specifically determined by a second, photometric channel (44).

1.4 Objectives

As mentioned above, this radioactively stimulated nitrogen plasma can be applied for highly selective and extraordinarily sensitive determination of certain aromatic aldehydes. ketones and quinones. It is very interesting to note the difference of analyte response behaviour between the so called "active nitrogen" systems (atmospheric pressure active nitrogen (APAN) spectrometry, metastable transfer emission spectroscopy (MTES), etc.) and the so called "excited nitrogen" system. The former systems showed the typical excited molecular fragments (CN, NO, PN, SN, etc.) emission (30-33, 37) or molecular luminescence from intact polycyclic aromatics (34). The latter system failed to show any response from either molecular fragments or from intact polycyclic aromatics, but it can generate luminescence from selected aroyl compounds with high sensitivity and selectivity. All other types of organic compounds tested produced no detectable luminescence in this radioactively stimulated excited nitrogen. The questions are whether typical active nitrogen systems are comparable in their manner of operation to the excited nitrogen system, why only some aroyl compounds luminesce strongly in excited nitrogen, and what is the origin and nature of the luminescence. The APAN and MTES systems not only formed and excited the CN radical, but also excited atomic emission of metal and non-metal elements. Can the excited nitrogen system also serve as an excitation energy source for atomic emission? The earlier reported nitrogen plasma photometric detector was based on a modified Shimadzu FPD (44). Although this detector showed unusually high sensitivity for aroyl compounds, some technical factors still limited the further improvement of its sensitivity. In this work a new "nitrogen plasma photometric detector" (NPPD) called

Aroyl Luminescence Detector (ALD) was designed and constructed. It was then necessary

to carry out analytical applications of this new energy transfer system, to study the ALD's

operating mechanisms, and to map and characterize the gas-phase luminescence spectra.

Chapter 2

EXPERIMENTAL

2.1 General

In this study, a Tracor model 550 gas chromatograph (Serial number: 740103; Austin, TX, USA) equipped with a flame ionization detector was used.

2.1.1 Experimental Set-up and General GC Conditions

Figure 2.1 is a block diagram of the experimental set-up used in this study. Nitrogen served as GC carrier gas, purge gas and reagent gas for the aroyl luminescence detector (ALD). The FID used prepurified hydrogen and extra dry air. All flowmeters were calibrated with a soap bubble flowmeter. Prior to entering the injection part, nitrogen gas was purified by passage through molecular sieve 5A (Guild Corporation, Bethel Park, PA, USA) and heated zirconium sponge ("gas purifier"; Supelco, Bellefonte, PA, USA). Carrier gas (nitrogen line 1) and make-up gas (nitrogen line 2) were mixed, if needed, with a doping gas at the entrance of the ALD. Nitrogen line 3 provided purge gas to flush air or impurities out of the detector. A sample splitter was employed to divide the column effluent for ALD and FID detection. The FID was used to confirm the response of an analyte in the ALD or signal the passage of compounds that did not respond in the ALD. In most cases, the ALD was equipped with more than one channel (up to three channels available) for the recording of two-channel response ratios or the mapping of luminescence spectra. A 12-kV Spellman (Model: HS5P30/CR/X769;

13
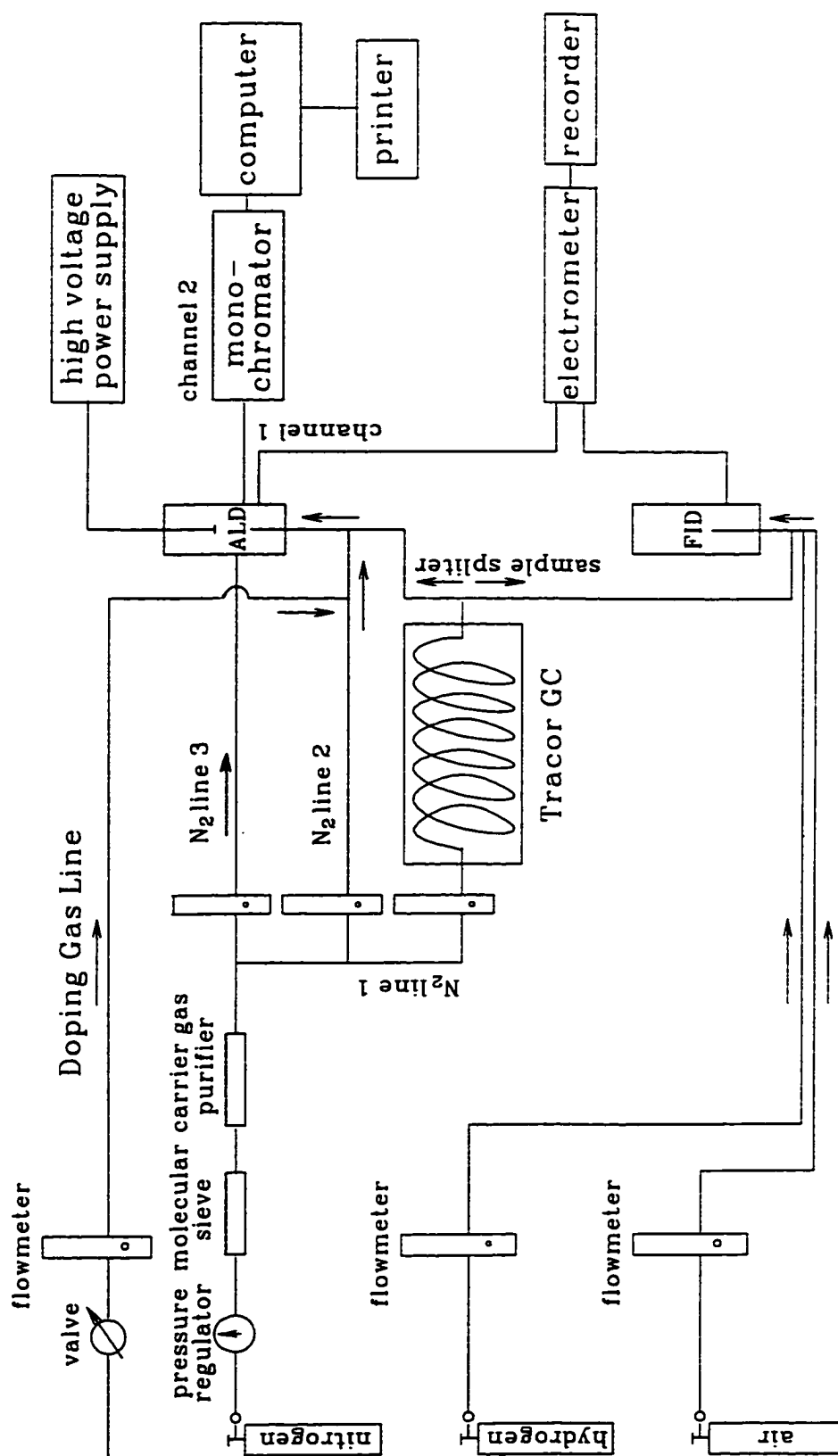
Figure 2.1 Block diagram of the experimental set-up.

High Voltage Electronics Corporation, Bronx, NY, USA) or 5-kV HIPOtronics (Model: #R10B; Brewster, NY, USA) DC high voltage power supply was employed to polarize the electrode in the ALD. For safety, a current-limiting resistor of 5×10^6 ohms was installed between the DC power supply and the electrode.

The photons emitted from the analyte in the detector cell were converted to an electric signal and amplified by a Hamamatsu photomultiplier tube (PMT) (Hamamatsu Corporation, Middlesex, NJ, USA) and a Tracor electrometer. Most of the work was performed with either an R-268 (for experimental optimization and calibration curves) or an R-374 (for measurement of luminescence spectra) PMT with occasional use of an R-2228. The signal was displayed on a Linear two-pen chart recorder or stored in a computer for different types of manipulation. Either Ditric (no longer in business) or Oriel (250 Long Beach Blvd., P. O. Box 872, Stratford, CT, USA) optical filters were used if needed.

The two different packed columns used for chromatographic separation were 100 X 0.2 cm i. d. borosilicate glass tubing packed with 5% OV 101 on 100/120 mesh acid-washed (AW) Chromosorb W (used in Chapter 3 and 4) and the same glass tubing packed with 5% Carbowax 20M on 100/120 mesh AW Chromosorb W (used in Chapter 4, 5 and 6). The gas chromatograph provided for both isothermal and temperature-programmed operation of the column. The temperatures of the injection port and the detector base were usually kept at 250 °C (about 50 °C higher than that of the maximum column temperature).

2.1.2 Gases, Chemicals and Materials

Nitrogen (prepurified, 99.998%), hydrogen (prepurified, 99.99%) and air (extra dry, maximum moisture of 10 ppm) were the products of Linde (Linde Union Carbide Canada Ltd., Toronto, ON, Canada). Argon, helium, methane and propane were ultra-high-purity gases from Matheson (Matheson Gas Products, Toronto, ON, Canada). Carbon monoxide gas (99+%) was purchased from Aldrich (Aldrich Chemical Company, Inc., Milwaukee, WI, USA).

All the chemicals (with 95+% purity) used in this study were from commercial sources: Aldrich Chemical Company; Fluka Chemical Corp. (Ronkonkoma, NY, USA; and SIGMA Chemical Company (St. Louis, MO, USA). All samples were dissolved in hexane or acetone and stored in 15-mL screw-cap glass sample vials with Teflon liner, or in crimp-top glass vials, at approximately 0 to 5 °C. The liquid and gas syringes were from Hamilton (Reno, Nevada, USA). Most of the other GC accessories were obtained from Chromatographic Specialties Ltd. (Brockville, ON, Canada).

The soil sample was taken from the parking lot on Dalhousie campus. The incense sample was purchased from local stores. The Canadian certified marine sediment sample (PACS-1) was provided by Dr. Michael Siu at the National Research Council (Ottawa, ON, Canada). A few of the essential oils used in this study were ordered from chemical supply houses (SIGMA, Roth, USA). However, most of them were Dr. Walter A. Aue's private collection which were purchased from a local health food shop; with one exception they came from Aura Cacia (P. O. Box 399, Weaverville, CA, USA).

2.2 The Novel Design of the Aroyl Luminescence Detector (ALD)

2.2.1 Single-Channel Aroyl Luminescence Detector

A detailed diagram of the single-channel aroyl luminescence detector is shown in Figure 2.2. The *de novo* design of this detector was based on the earlier reported nitrogen plasma photometric detector (NPPD) (44). The ALD consisted of a detector cell and one photometric detection channel. The two basic requirements in designing this detector were (a) to ensure that it is gas tight, and (b) to get maximal light output from the emission zone. Bearing this in mind, the detector cell was constructed with a 7.5 cm X 8 mm i. d. quartz tube of 1 mm thickness, which was fixed on the detector base with a Supelco nut and a lab-made Teflon ferrule. A high-voltage electrode was inserted from the top of the detector into the quartz tube. The electrode was held by a Supelco nut and insulated from the detector body. The distance between the electrode and the nozzle (counter electrode) was adjustable, but was normally kept at 4 mm. A 1-mm high ^{63}Ni cylindrical foil was placed inside the quartz tube, with the lower edge of the foil at the same level as the top of the nozzle. The detector volume was about 200 μL so that chromatographic resolution of peaks could be maintained. A 6-inch long and 6 mm o.d. high-quality glass image conduit (Edmund, Scientific, Barrington, NJ, USA), shielded from light by an aluminum housing, was inserted through the detector wall and moved against the quartz tube to pick up as much light as possible. The other end of this optical channel was the photocathode of the Hamamatsu photomutiplier tube, leaving a space
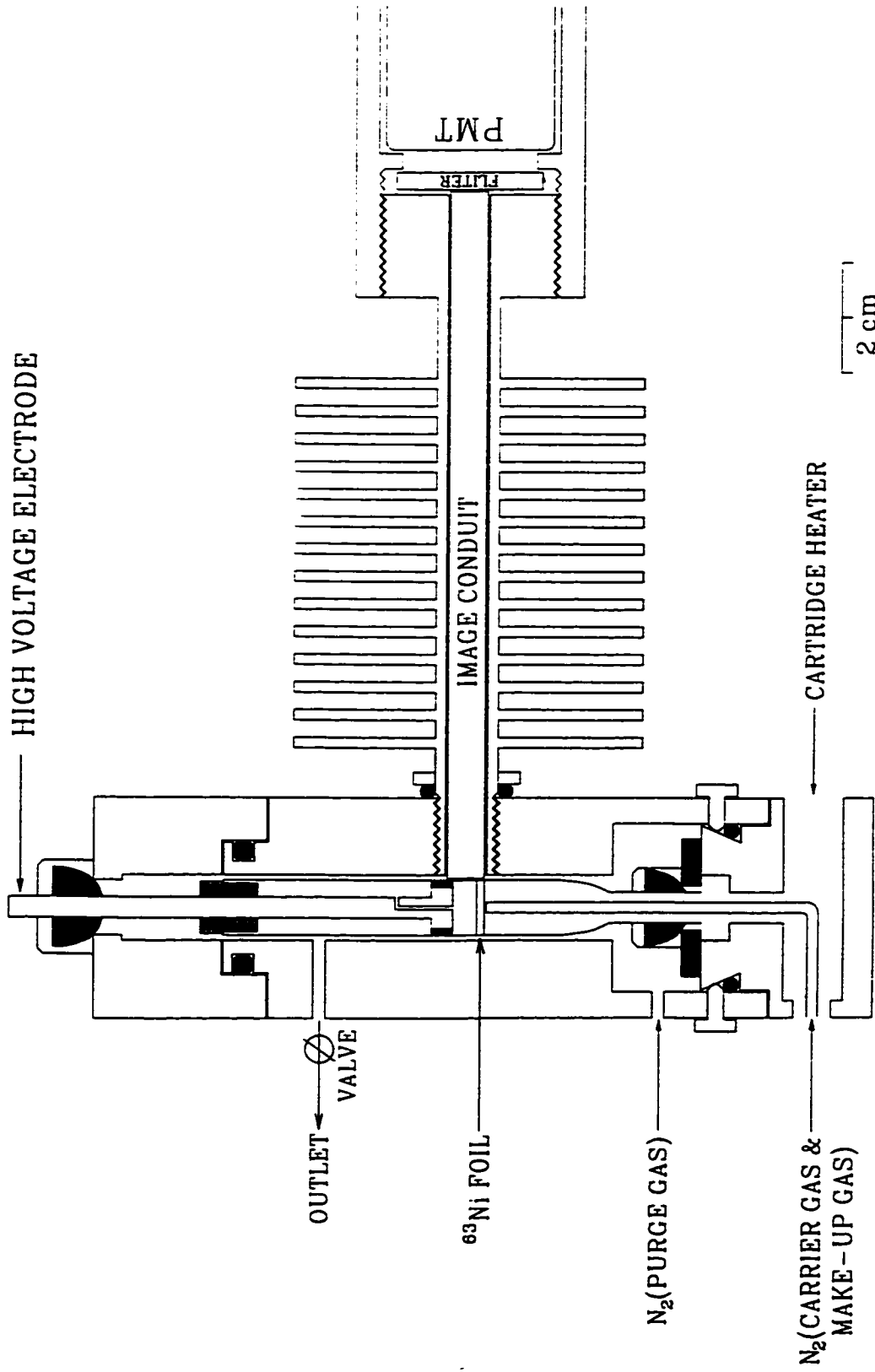
Figure 2.2 Blueprint of single-channel aroyl luminescence detector.

wide enough to insert an optical filter if desired. The detector was made light-tight and also gas-tight by using silicone O-rings, Teflon ferrules and stoppers. Even so. a purge gas line, connected to the detector, was necessary for flushing the diffusing air or impurities out of the detector. The detector was exhausted through a long copper tube. which prevented the entry of light, and a valve was put in the exhaust line to keep the detector at a slight overpressure, which helped to minimize the back diffusion of atmospheric oxygen. This valve can be connected to pressure gauges or MaCleod gauges for pressure measurements.

2.2.2 Dual-Channel Aroyl Luminescence Detector

The dual-channel aroyl luminescence detector was made from the single-channel ALD by inserting a vertical, mirror-finished aluminum wedge as a beam splitter. Figure 2.3 gives a schematic representation of the dual-channel ALD. The photometric detection channel of the ALD employed a lab-made Al mirror to deflect the diffuse light beam by $90°$ onto the photocathode of a photomultiplier tube. The Al mirror was cut at a $45°$ angle from a 1-inch aluminum rod, and was placed between two 40-mm ports. Each of the two ports held one PMT. In front of the PMTs, there were two filter boxes in which various optical filters could be put if needed. The Al mirror was designed to slide into a 1-inch port through a silica O-ring, and was easily moved and rotated to the optimized position of equal and maximal light reaching the two PMTs.

HIGH VOLTAGE ELECTRODE

PMT

FILTER

Al MIRROR

FILTER

PMT

IMAGE CONDUIT

CARTRIDGE HEATER

2 cm

OUTLET

VALVE

^{63}Ni FOIL

N$_2$(PURGE GAS)

N$_2$(CARRIER GAS & MAKE–UP GAS)
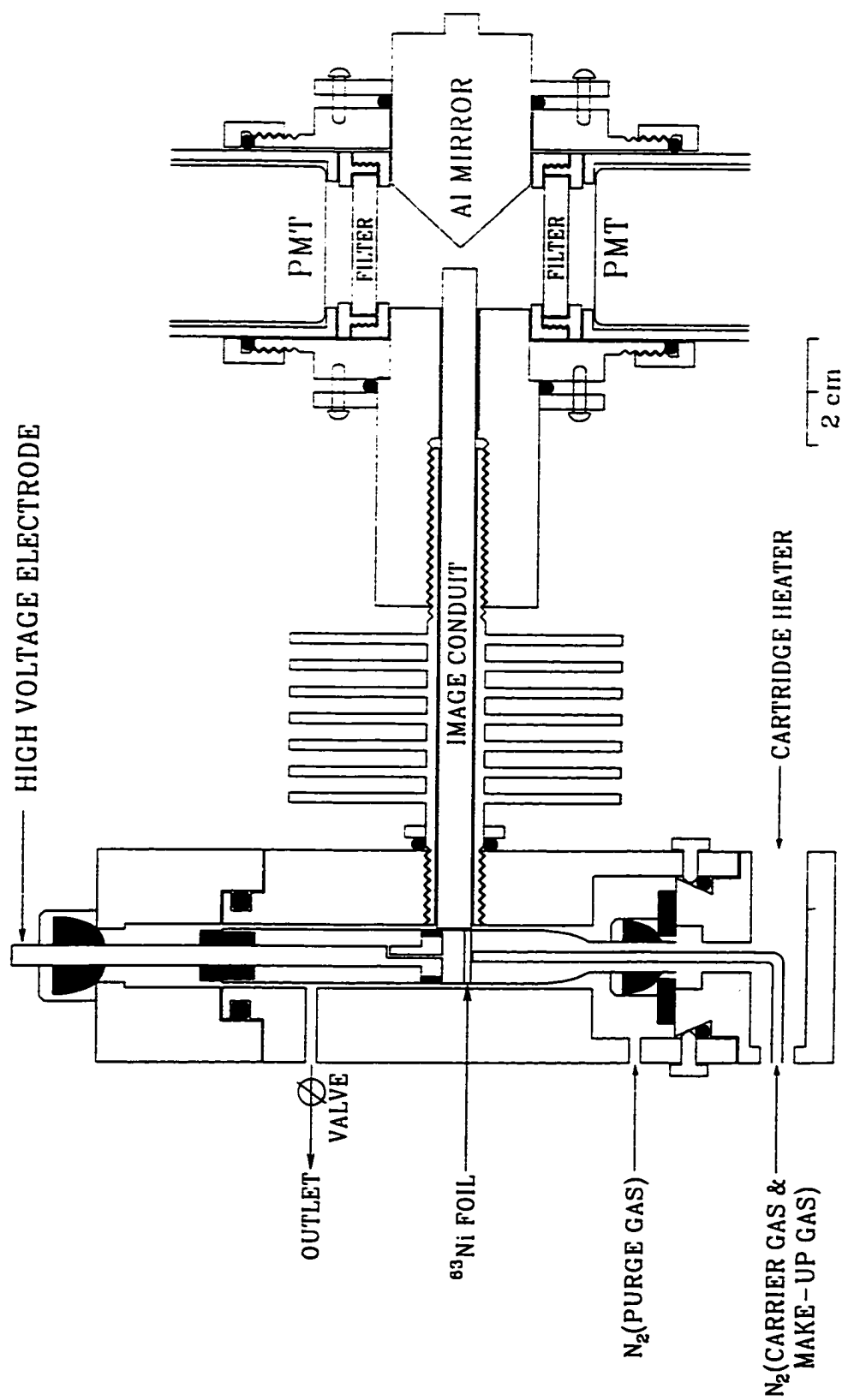
Figure 2.3   Blueprint of dual-channel aroyl luminescence detector.

2.2.3 Triple-Channel Aroyl Luminescence Detector

The triple-channel aroyl luminescence detector consisted of a detector cell, two photometric detection channels (response-ratio channels) and one spectral channel. Figure 2.4 shows a schematic diagram of the triple-channel ALD detection unit. The detector cell was built as similar to that in the single-channel ALD. The two photometric detection channels consisted of a bifurcated optical fiber bundle (Item 77533; Oriel, 250 Long Blvd., Stratford, CT, USA) with optical filters as needed and two Hamamatsu R-268 PMTs installed in lab-made housings. An aluminum tube was used to hold the optical fiber bundle, and was placed in a light guide housing with a spherical mirror of 31 mm diameter and 15 mm focal length at one end. This aluminum mirror, with a 6 mm diameter hole in the center so that the optical fiber could pick up the optical emission, was inserted through the detector wall to focus (roughly) the luminescence onto the slit of a monochromator. This spectral channel consisted of an aluminum tunnel used to connect the detector body and the monochromator, a quartz window installed at the end of the tunnel to make the detector gas-tight, a monochromator, and a Hamamatsu PMT to record the luminescence spectrum. The distances from both the mirror and the monochromator to the emission zone could be adjusted. The purpose of adjustment was to focus the beam onto, and almost filling the acceptance cone of, the monochromator aperture, and to maintain optimal light throughput. In order to keep the PMT's and the monochromator cool, both the photometric detection channels and the spectral channel were equipped with water-flushed cooling coils. In addition, the spectral channel could be replaced by a PMT held in a water-cooled housing for more sensitive detection. The
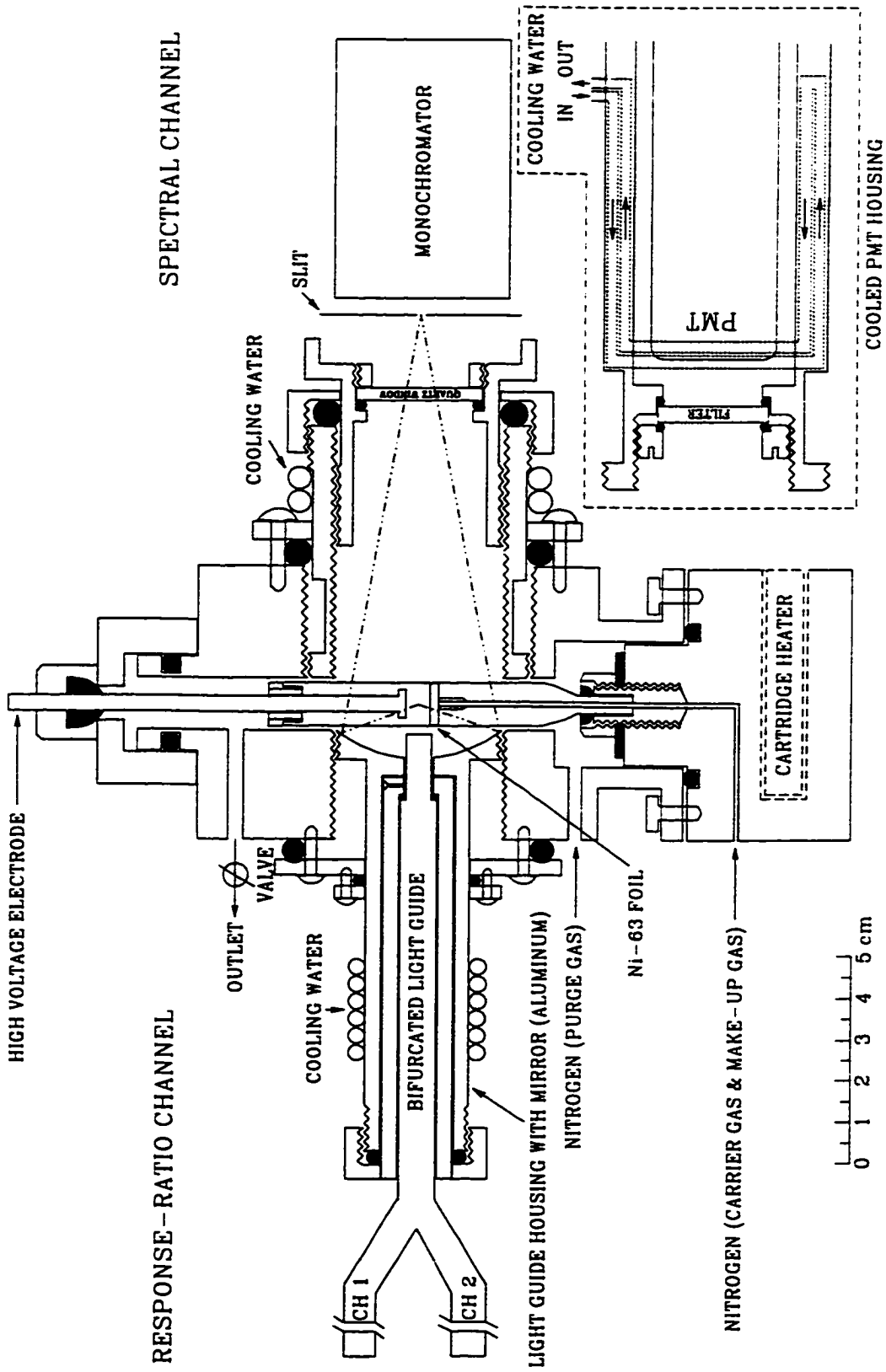
Figure 2.4 Blueprint of triple-channel aroyl luminescence detector.

whole detector was built gas-tight by using silicone O-rings and Teflon ferrules.

2.3   Spectral Measurements

A spectrum provides important information for analytical ends and for the study of the photochemical and photophysical behavior of the tested molecule in the gas phase. In this study, the spectra were obtained by using a Hamamatsu R-374 PMT (180-850 nm), different monochromators, and different measurement modes. The spectra were not corrected for the PMT's response profile and the monochromator's transmission efficiency.

2.3.1 Repeated Injection Mode

In the single-channel ALD, the image conduit was replaced by a quartz rod of equal dimensions. Either a Jarrell-Ash model 82-415 quarter-meter monochromator with 1180 grooves/mm grating blazed for 500 nm and a pair of slits (0.5, 1, 2 or 4 mm) or an Oriel model 7155 filter monochromator (range 400 nm to 700 nm; for weakly emitting compounds) with slit options of 1, 2, 4, and 6 mm, were employed to map the spectra. In this mode, analytes were repeatedly injected while the wavelength drive was manually advanced.

2.3.2 Continuous Doping Mode

In this mode, spectra were obtained from the quarter-meter monochromator mentioned above. Liquid analytes were vaporized in a doping vessel to present a

constant, nitrogen-diluted stream to the ALD. For solid compounds, the analytes were placed in a capillary tube which was inserted into the GC injection port, and heated to a sufficient temperature to produce a constant analyte stream. The luminescence from the analyte was scanned by an automatic wavelength drive.

2.3.3 Single-Peak Mode

The triple-channel ALD and an Oriel model 77250 eighth-meter monochromator, with a No. 77298 grating and 0.02 to 3.2 mm variable slits, were used in this mode. The single-peak mode used here had been developed for accurate and either highly sensitive or highly resolved spectral scans of single GC peaks from a dual-channel FPD in our laboratory (45). When the analyte was introduced as a chromatographic peak, a No. 77325 stepping motor driven by a lab-built circuit with scan speeds from 0.25 to 315 nm/min was used to scan the GC peak. In order to compensate adequately for the analyte's increasing and decreasing concentration, the true intensity distribution of the spectrum can only be obtained from the ratio of two observation channels. One would serve as the dispersive/spectral channel. The other was used as non-dispersive channel of constant wavelength (one of the response-ratio channels). The spectrum from the dispersive and the chromatogram from the non-dispersive channel were simultaneously recorded by a dual-channel program called CHROM 8 (46). The stored data were exported as an ASCII file into a commercial program SigmaPlot (Jandel Scientific, San Rafael, CA, USA) for futher data manipulation.

2.4 Experiments of Luminescence Quenching and Enhancing

Luminescence quenching and enhancing experiments were carried out by introducing the quenchers or enhancing reagents into the ALD through either a restricted 1/8" copper tube and a Nupro fine valve or an exponential dilution flask. The various doping concentrations were built up in the detector by changing the flow rate of dopants in the doping gas line (Figure 2.1). The output concentration (C) of the exponential dilution flask can be calculated by:

$$C = C_0 e^{-(Ft/V)} \qquad (2.1)$$

where C_0 is the original quencher concentration in the flask; F is the flow rate of the purge gas (nitrogen); V is the volume of the diluting flask (in this work, a lab-made 310 mL glass vessel was used); and t is the time. The required concentration at time t can be obtained by setting the original quencher concentration and the purge gas flow rate. In the diluting flask, the quenchers were mixed with purge gas by a magnetic stirrer.

2.5 Discharge Current Measurement

In the aroyl luminescence detector, nitrogen functioned as both carrier and reagent gas. A radioactively stimulated discharge in nitrogen operated in the detector cell. A simple floating circuit was used to measure the discharge current. The Spellman high-voltage power supply was electrically insulated from ground, its positive output was connected to the detector and its negative output to an electrometer.

2.6   Triplet-State Lifetime Measurement

A block diagram of the instrument for the triplet-state life time measurement is shown in Figure 2.5. It was different from all pulse techniques for measuring phosphorescence decay which employ short-duration (microsecond range) flash light sources (47) that this method applied a pulsed high voltage source with changeable pulse duration. This technique involved measuring the change in luminescence intensity at selected wavelength over the time after the high voltage pulse, by means of a photomultiplier tube, an amplifier and a digital oscilloscope. A lab-made microprocessor-based square-wave pulse generator, capable of repeating a given sequence of up to three individually definable pulses, was used to trigger the high-voltage pulser. The high-voltage pulser was a lab-built unit with five changeable amplitude settings and an output of 6.8 kV to 10.2 kV. The sequence repetition rate, as well as the delay time and width of each of the pulses within a given sequence, were entered on a terminal connected to the pulser through an RS-232 serial port. The emission from excited molecules in the ALD cell was monitored by two R-268 PMT's (one channel with a 340 nm band-pass glass filter for the nitrogen second positive system emission; another channel with a 460 nm long-pass glass filter for the aroyl phosphorescence), both amplified by a lab-made fast dual-channel amplifier (rise time: 60 μs). The emission traces were displayed on or stored in a digital oscilloscope (Tektronix Model 2232, Beaverton, OR, USA) in the average mode or the sampling mode. The acquired data in
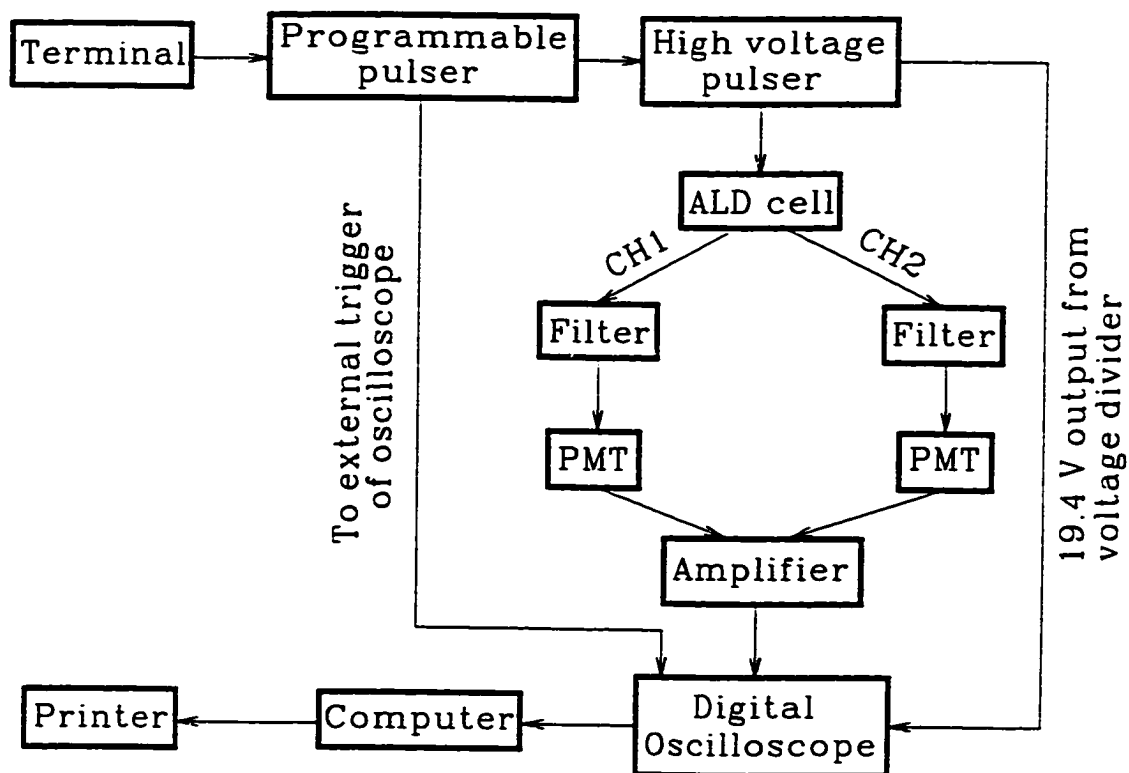
Figure 2.5   Block diagram of the instrument for the triplet-state lifetime measurement.

the oscilloscope memory were converted to an ASCII file by using the General Purpose Interface Bus (GPIB) and a dual-trace collection program written by Dr. Peter Wentzell (Department of Chemistry, Dalhousie University) for the TEK 2232.

Chapter 3

CHROMATOGRAPHIC DETECTION
BY GAS-PHASE LUMINESCENCE SPECTROMETRY

3.1 Introduction

The development of sensitive and selective detectors has played a major role in the establishment of gas chromatography as an indispensable analytical tool. As reviewed in Chapter 1, molecular emission spectrometry as a detection method for GC has received significant attention. Among the molecular photometric detectors, the nitrogen plasma photometric detector (NPPD) (44) was deemed "the most novel optical detector" (48). The NPPD was based on gas-phase luminescence derived from radioactively stimulated excited nitrogen, and could be employed for highly sensitive and selective determination of certain aroyl compounds (41-43). The new detector did not, however, receive much attention from the analytical community. This is not surprising: very few applications have been carried out on this kind of detector, and the detector is not commercially available.

The analytical characteristics of this nitrogen plasma photometric detector are not well understood and its intriguing energy-transfer mechanism remains largely undefined. As well, the exploratory prototype of this detector, a modified Shimadzu FPD, was not totally gas-tight (an oxygen-free environment is necessary to obtain maximum emission intensity), and the light transmission of this system was limited by the Shimadsu FPD's original construction. This study was, therefore, designed to further improve the NPPD's sensitivity by constructing from scratch a dedicated aroyl luminescence detector (ALD),

28

to explore its analytical characteristics and operating mechanisms, and to demonstrate its potential applicability to various analytical problems.

3.2 Experimental

3.2.1 Optimization of ALD Performance

The single-channel ALD (Figure 2.2) and benzaldehyde as a test analyte were used throughout the course of optimization. The main parameters involved were the geometry of the high-voltage electrode and its surface condition, the imposed DC voltage, the interelectrode distance, the detector temperature and the nitrogen flow rate.

Five electrodes with different geometric shapes (Figure 3.1) were tested in the ALD. The surface condition of the electorde was one of the most important factors for achieving the highest possible signal to noise ratio (S/N). The electrodes were highly polished by using a silicon carbide-grease mixture (LC-1200 EF 1200 silicon carbide, Small Parts Inc., Miami Lake, FL, USA). A rough electrode surface gave rise to sparking or larger noise. In order to maintain a stable plasma discharge in the detector cell, sparking should be avoided. For the five electrodes, the sparking voltage decreased in the following order: (1) brass "big foot" electrode with Teflon gasket (stopper); (2) stainless steel "big foot" electrode; (3) stainless steel flat electrode; (4) stainless steel round electrode; and (5) stainless steel sharp electrode. The brass "big foot" electrode with Teflon gasket can tolerate the highest DC voltage without sparking. The need for using a Ni-63 foil was confirmed. Without foil, both background emission and aroyl luminescence vanished. Although the nitrogen plasma was stimulated by the
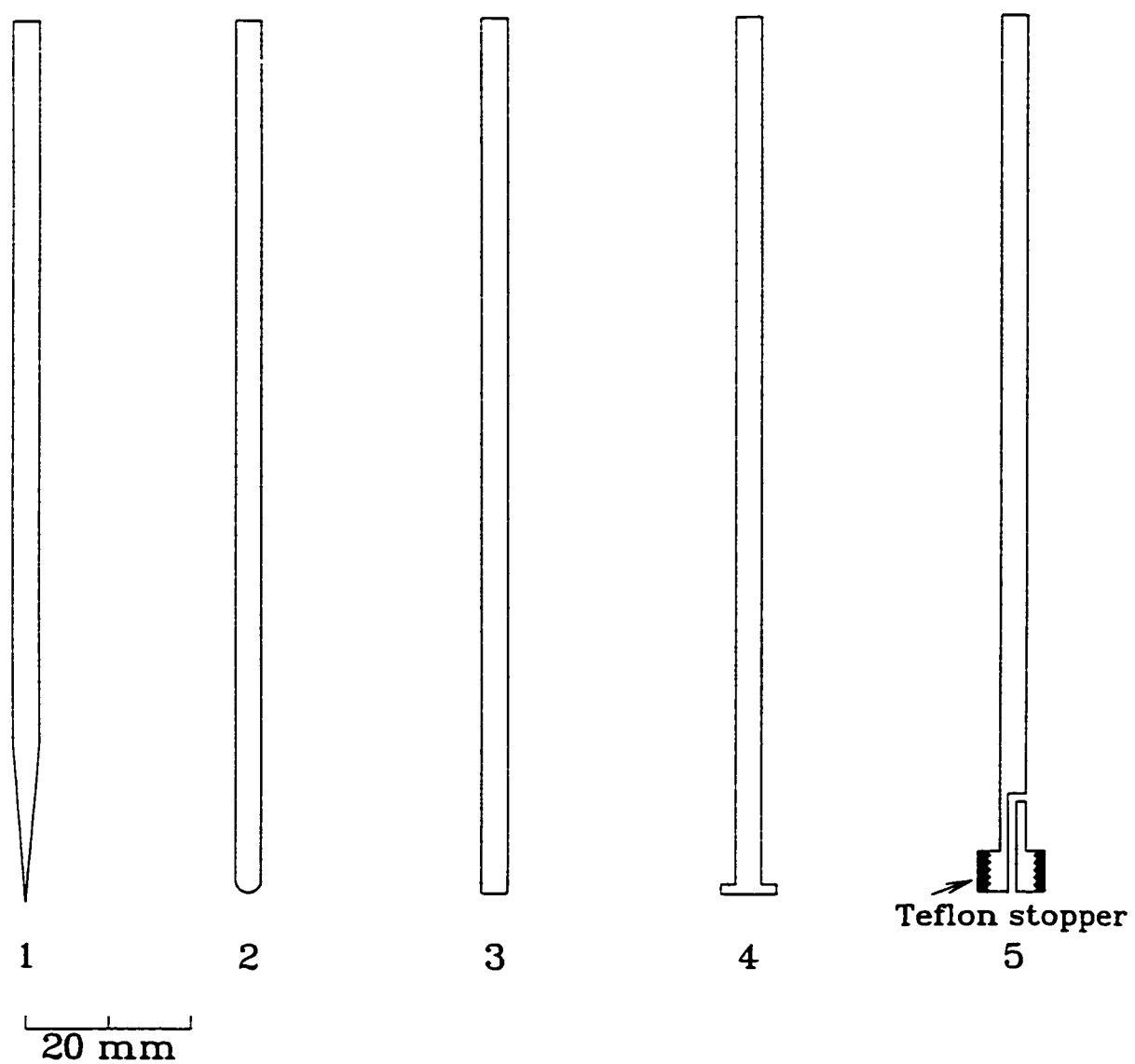
Figure 3.1 Various electrodes used in the aroyl luminescence detector.
1. stainless steel sharp electrode; 2. stainless steel round electrode; 3. stainless steel flat electrode; 4. stainless steel "big foot" electrode; 5. brass "big foot" electrode with Teflon stopper.

radioactivity, a high DC voltage was also an important factor contributing to an intense gas-phase emission. Figures 3.2 and 3.3 show the luminescence of N_2 and benzaldehyde versus the DC voltage. Up to a point, the higher the applied DC voltage, the stronger the luminescence and the better the S/N ratio (Figure 3.4). All the data used for plotting are the averages of several measurements. A positive DC voltage gave a much better S/N ratio than a negative one, mainly due to the larger noise of the latter. The emission zone, as viewed by dark-adapted eye, was situated just below the electrode, and the larger the electrode surface area, the bigger the emission zone. The end of the electrode carried a Teflon stopper (gasket), which was friction fit into the chimney. A 1-mm hole was drilled through the electrode to serve as an outlet. With this electrode configuration, the ALD gave the best response. Therefore, a highly polished brass "big foot" electrode with a Teflon gasket, polarized by a positive (and high) DC voltage, was used for all further studies.

The interelectrode distance was quite critical: the shorter the distance, the greater the S/N ratio. However, too short a distance would give rise to sparking and thus disturb the stability of the background. For the best monitoring of the luminescence zone with a 6 mm diameter image conduit, an interelectrode distance of 4 mm was chosen as optimum. Figure 3.5 shows the variation of benzaldehyde response in the ALD as a function of detector temperature. The response of benzaldehyde increased as the temperature rose. Although the background emission also increased, the baseline noise remained at about the same level. When the detector temperature exceeded 180 °C, the luminescence of benzaldehyde started decreasing. This behavior is possibly due to the
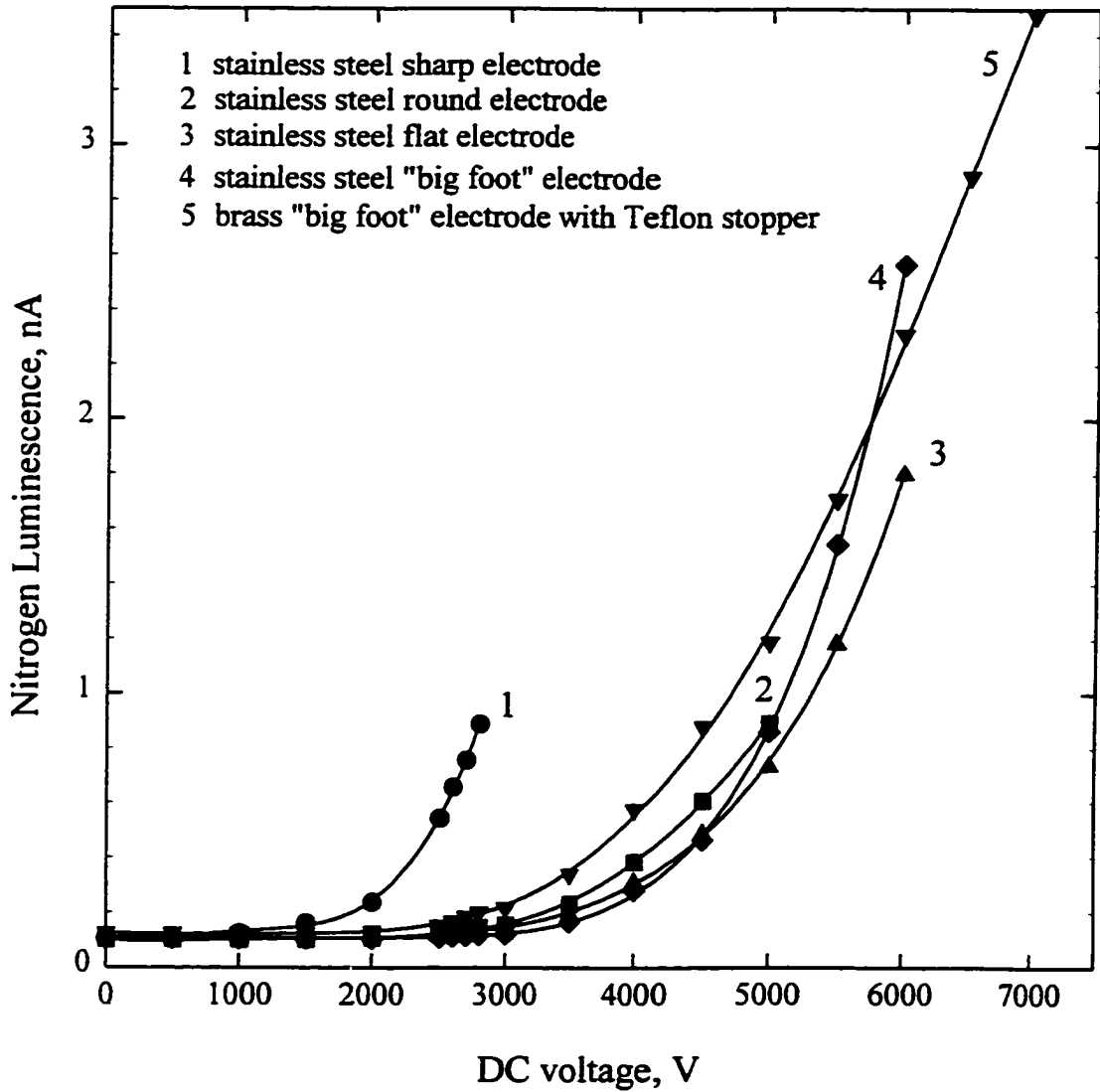
Figure 3.2 Nitrogen luminescence versus DC voltage of the aroyl luminescence detector. Detector temperature: 180 °C; PMT (R-374) voltage: -700 V; N_2 flow rate: 10 mL/min (carrier gas), 100 mL/min (make-up gas) and 50 mL/min (purge gas).
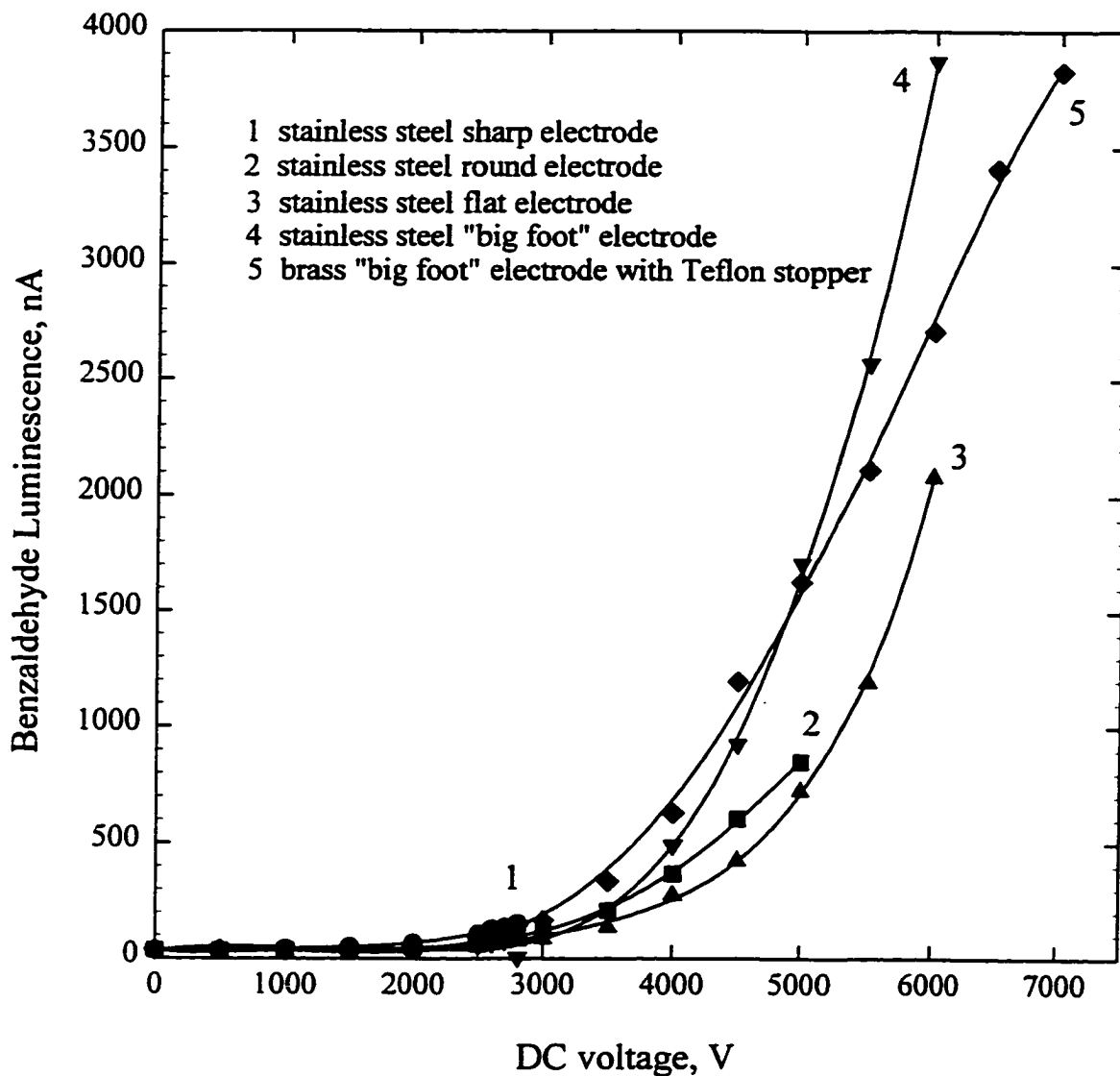
Figure 3.3 Benzaldehyde luminescence versus DC voltage of the aroyl luminescence detector. Column temperature: 55 °C; 1 ng benzaldehyde injected. Other conditions as in Figure 3.2.
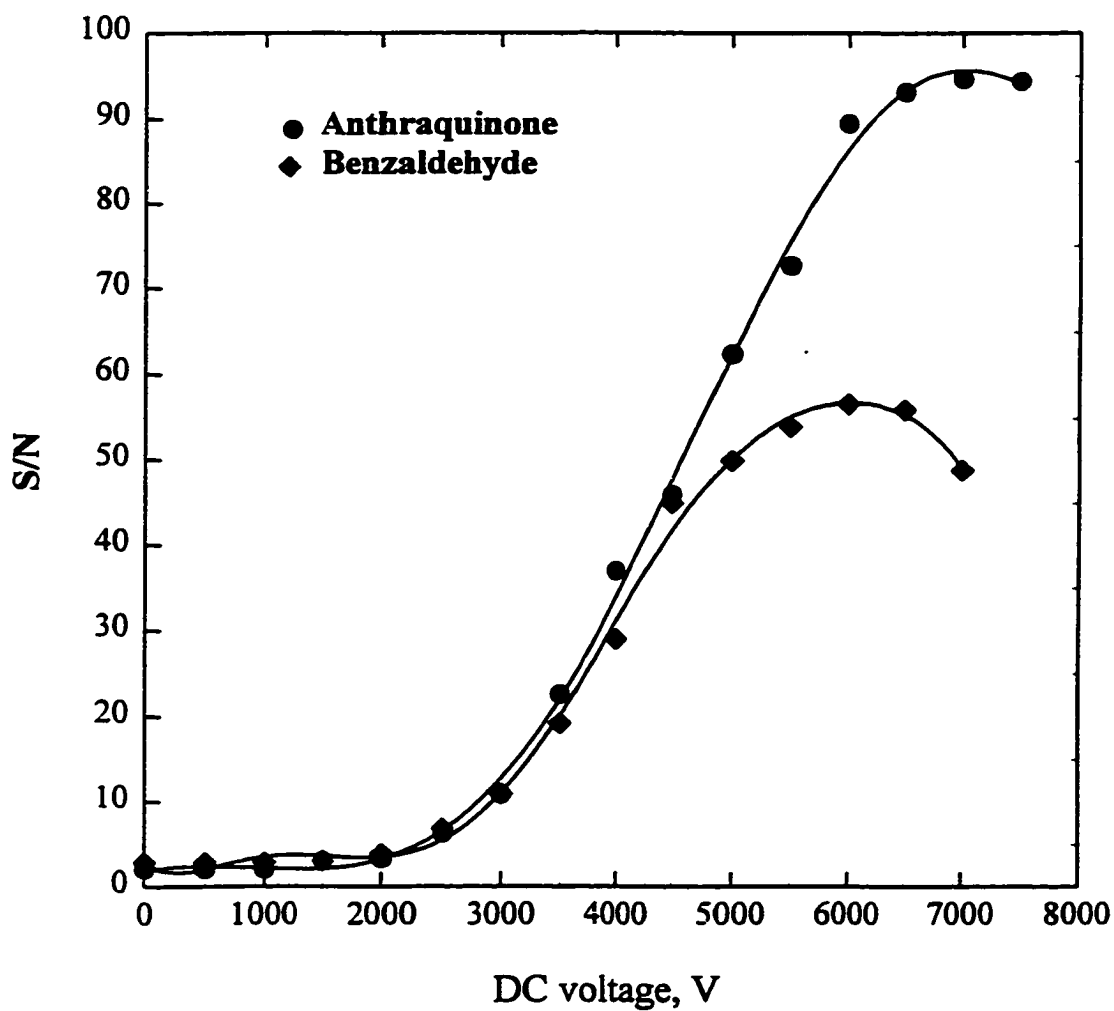
Figure 3.4   The signal/noise ratio of benzaldehyde and anthraquinone versus DC voltage in the aroyl luminescence detector. Column temperature: 55 °C (benzaldehyde); 165 °C (anthraquinone). Other conditions as in Figure 3.2.
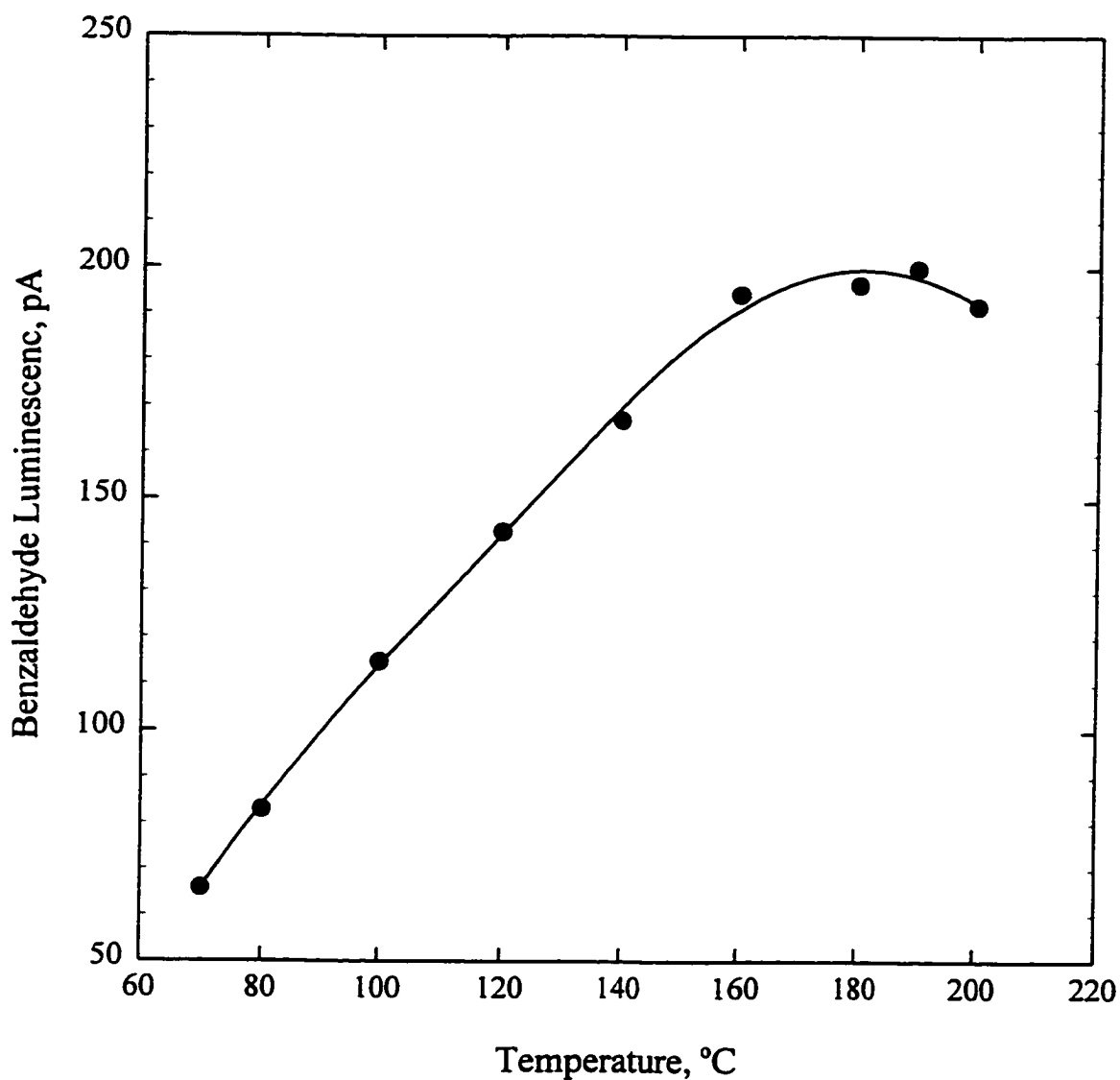
Figure 3.5 The effect of detector base temperature on benzaldehyde luminescence. DC voltage: +6000 V; PMT (R-374) voltage: -700 V; column temperature: 55 °C; 0.2 ng benzaldehyde injected. N_2 flow rate as in Figure 3.2.

collision quenching of excited benzaldehyde at higher temperatures. The optimum temperature varied with different analytes, but the reasons for this were not further investigated.

The nitrogen flow was very important in the process of optimization. The carrier gas flow rate was chosen to give proper separation conditions of various analytes. In addition, both make-up nitrogen and nitrogen purge gas were necessary for the optimal response of analytes. The luminescence profile of benzaldehyde, anthrone, and nitrogen background versus the make-up nitrogen flow rate is shown in Figure 3.6. The responses of the two analytes increased steadily with increasing nitrogen flow. A plateau was obtained at flow rates of about 180 mL/min, but the response dropped when the flow rate was over about 325 mL/min. The nitrogen background emission also increased with nitrogen flow, but reached a maximum at flow rates greater than about 50 mL/min. The increased make-up nitrogen flow did increase the baseline noise. Figure 3.7 demonstrates the necessity of supplying a considerable flow of purge gas in order to flush atmospheric oxygen and impurities out of the detector housing. The most important process of optimization was to keep the entire detector *gas-tight*, because oxygen is an extremely efficient quencher of analyte luminescence (see section 4.8.2). This process involved putting a Teflon stopper on top of the chimney and using a valve on the exhaust line to keep the detector at a slight overpressure, which minimized the back-diffusion of atmospheric oxygen.

In addition, the best performance of the ALD was attained by choosing an optical filter based on the luminescence spectrum of analyte to minimize interference, and by
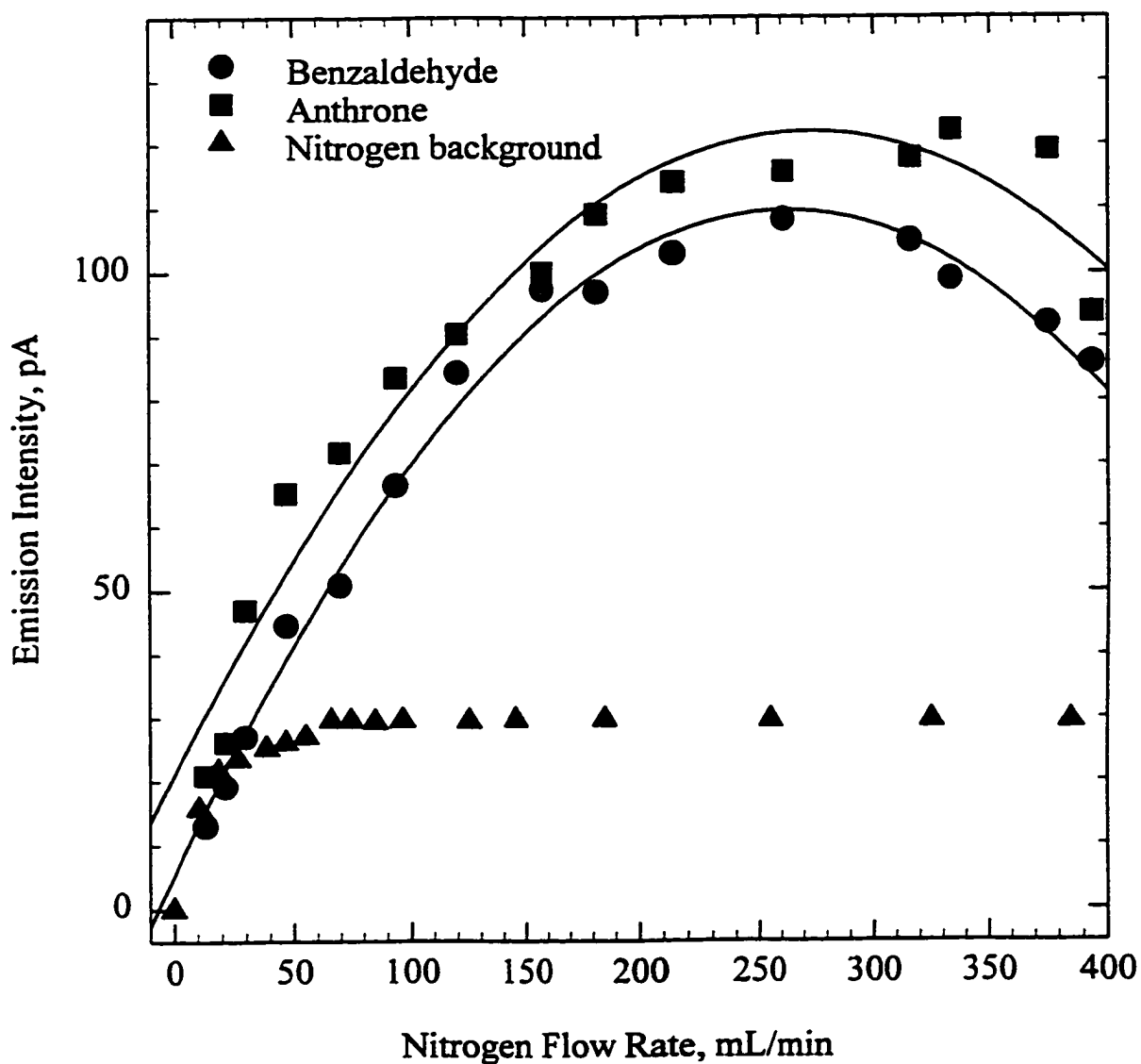
Figure 3.6 The effect of nitrogen flow rate (carrier and make-up gas) on the emission intensity of benzaldehyde, anthrone and nitrogen background emission. A 340 nm interference filter used for monitoring nitrogen background emission; DC voltage: +6000 V; PMT (R-374) voltage: -700 V; detector temperature: 180 °C; column temperature: 55 °C (benzaldehyde); 165 °C (anthrone); 0.2 ng benzaldehyde injected; 0.2 ng anthrone injected.
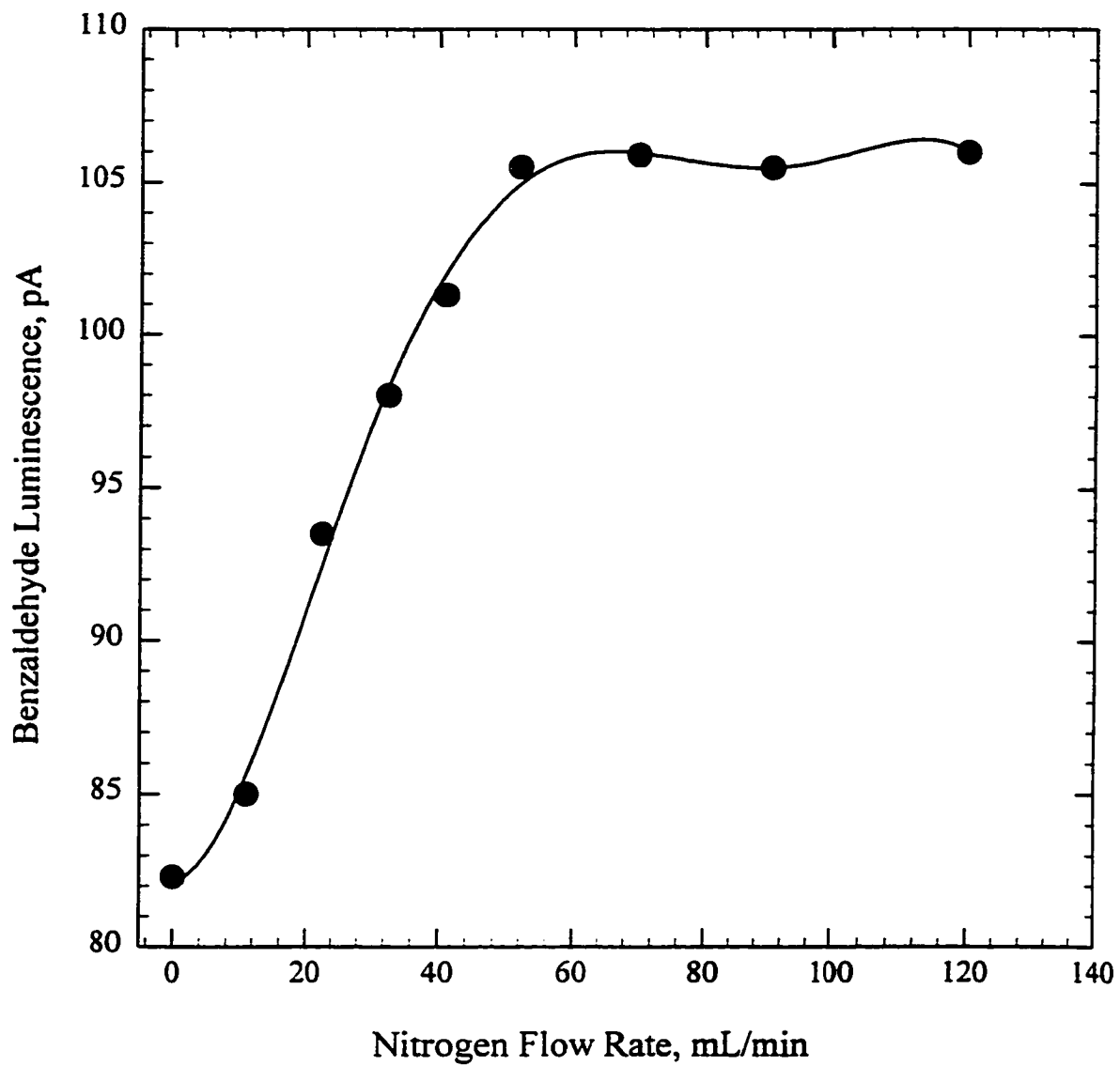
Figure 3.7 The effect of nitrogen purge gas flow rate on the benzaldehyde luminescence. 0.1 ng benzaldehyde injected. Other conditions as in Figure 3.6.

using a simple RC electronic filter to reduce noise. After optimization, the newly designed ALD achieved much better sensitivity than its NPPD predecessor (44).

3.2.2 Sample Preparation

3.2.2.1 Sampling of Room Air

Room air was sampled with a 10-mL gas-tight Hamilton syringe in a medium-sized (ca. 60 m^3) laboratory of the Chemistry Building at Dalhousie University after the burning of one stick of Tibetan healing incense. A 10 mL sample of room air was taken and directly injected into the GC-ALD system for analysis. A blank of laboratory air was run before an incense stick was lit, in order to ensure the absence of any compound responding in the ALD.

3.2.2.2 Soil Sample

A soil sample was taken from the parking lot on Dalhousie campus, and dried in a desiccator over silica gel at room temperature for 24 hours. A 1-2g sample was weighed and placed in a lab-made solid sampler (Figure 3.8). The GC column temperature was maintained at room temperature while the GC injection port and the solid sampler were heated to 250 °C for 2 hours (the solid sampler was heated at 300 °C for 2 hours and checked for freedom from contamination before it was used). Then a temperature program from room temperature to 190 °C with a program rate of 7.5 °C/min was used to heat the GC column.
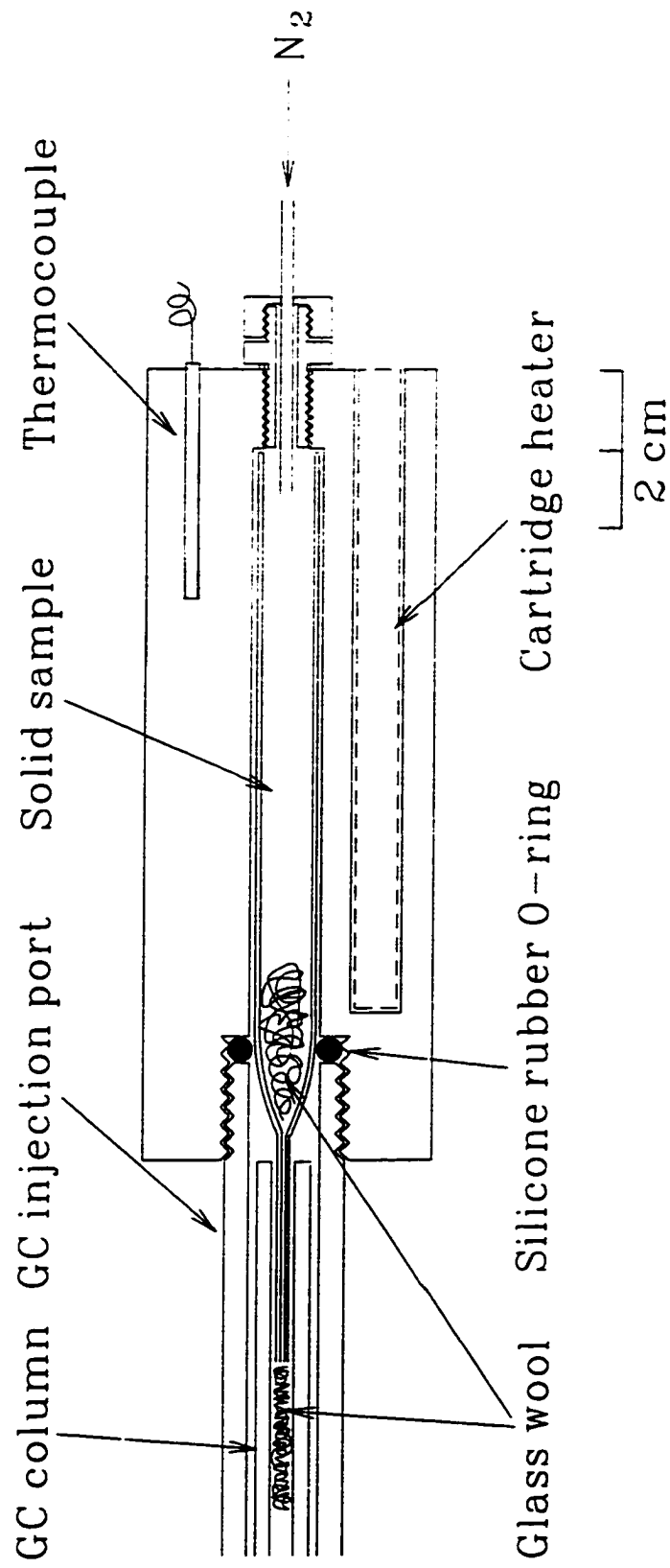
Figure 3.8 Blueprint of solid sampler.

3.2.2.3 Derivatization of Alcohols

Preparation of p-formylbenzoyl chloride: To a round-bottomed flask equipped with a stirrer, dropping funnel and condenser with drying tube, was added 10 g (0.067 mole) of 4-carboxybenzaldehyde. Then 31 g (0.268 mole) of thionyl chloride was added dropwise. When all materials had been added, the mixture was refluxed at 80 °C for 3 hours while hydrochloric acid and sulfur dioxide were given off. The excess thionyl chloride was distilled off at atmospheric pressure to give a solid residue which, upon recrystallization from dichloromethane, yielded 11.2 g of p-formylbenzoyl chloride (m.p. 48 °C) (48a) (~ 80 % yield). Mass spectrum: m/e (relative intensity) 167.8 (M^+, 4), 132.9 (100) (Figure 3.9).

Derivatization procedure: To a 0.4 mL standard solution containing 0.1-50 nano mol of a variety of alcohols was added 0.4 mL of 1.25 mM p-formylbenzoyl chloride (in diethyl ether) and 0.2 mL of 1% (v/v%) pyridine. The mixture was heated at 60 °C for 10 min after tightly capping the tube. In order to remove the excess of reagent (the acid chloride), the reaction mixture was well mixed and incubated again at 60 °C for 10 min after addition of 1 mL of 50 mM aqueous cysteic acid solution. One μL of the organic layer was injected into the GC-ALD system. The derivatization process is summarized in Figure 3. 10.

Preparation of esters: 0.25 mole each of four alcohols (methanol, ethanol, 1-chloroethanol and 1-heptanol) and 0.05 mole p-formylbenzoyl chloride in diethyl ether were mixed and, after addition of several drops of pyridine, the mixture was heated at 60 °C for 2 hours in flame-dried glassware. The precipitated pyridine•HCl was removed by
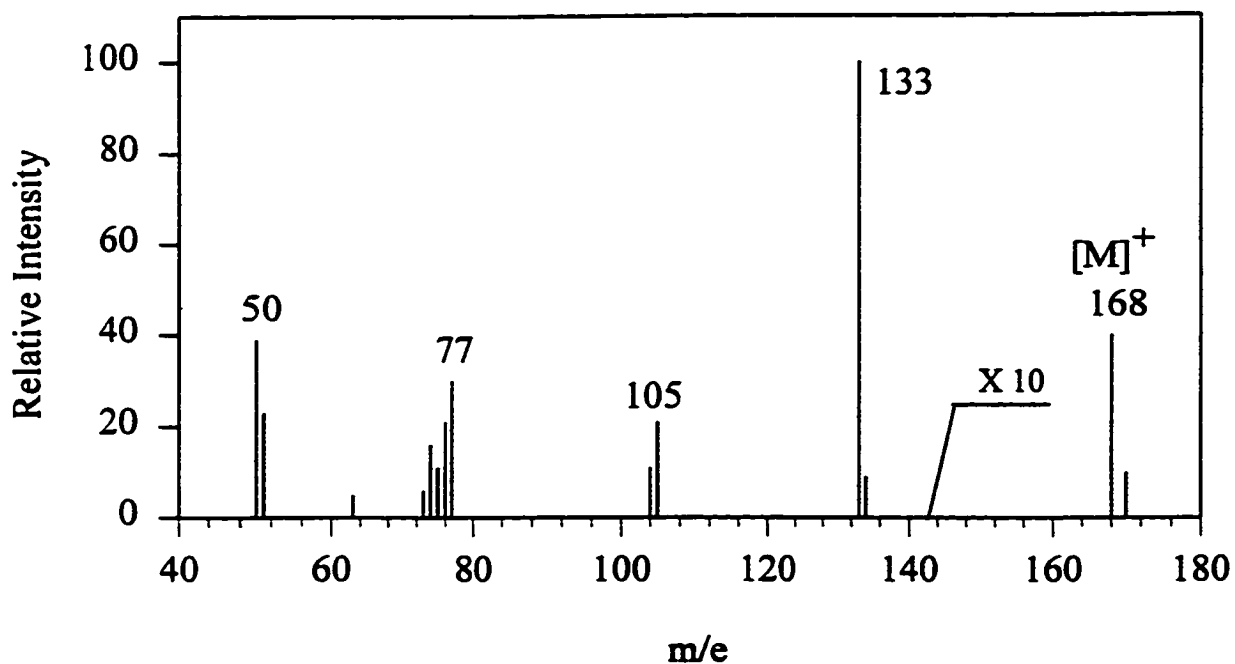
Figure 3.9   Mass spectrum of p-formylbenzoyl chloride.
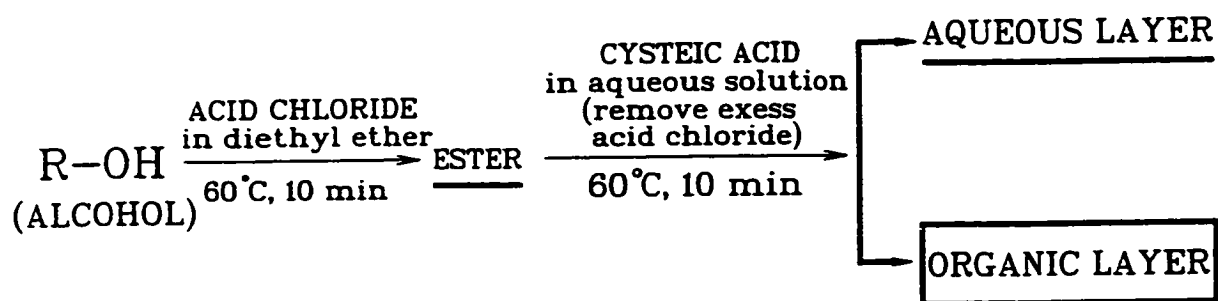
Figure 3.10   Outline of chemical derivatization of alcohols.

filtration. The solvent and excess alcohols were removed in vacuum, and the residue was recrystallized from 1:1(v/v) 2-propanol/hexane solution. The prepared esters were used for measurements of gas-phase luminescence and mass spectra (see section 3.4.3.2).

3.3 Analytical Characteristics

3.3.1 Selectivity

Very few kinds of organic compounds gave positive response in the new ALD. Only certain compounds containing an aroyl moiety in the form of an aromatic aldehyde. ketone or quinone responded strongly. Most aliphatic compounds and aromatic nitriles. esters, chlorides, alcohols, amines and sulfides did not respond even at the 1 μg level. An FID with temperature programmed separation was employed to check if these organics did go through the GC column or not. Non-responding and responding aroyl compounds. together with their relative luminescence intensities are listed in Table 1 and Table 2. respectively.

Some heavy molecules such as 2,2,2-triphenyl acetophenone, 5,12-naphthacene-quinone, 1,4-chrysenequinone, 1-pyrenecarboxaldehyde, 1-acetylpyrene, and 2-naphthoflavone did not pass through the GC column up to the ALD's normal operating temperature.

The results revealed that compounds that do not contain an aroyl moiety do not respond and, with several exceptions, that an aroyl moiety in the form of an aromatic aldehyde, ketone or quinone is a necessary structure for luminesceence in the ALD. Among aroyl compounds, particular subsituents such as nitro-, amino- and hydroxy-

Table 3.1   Non-responding Compounds Tested in the ALD

Alkyl hydrocarbons	Fluoranthene
Alkyl aldehydes	Pyrene
Alkyl ketones	Benzo-a-pyrene
Alkyl alcohols	2H-pyran-2-one
Alkyl amines	Biacetyl
Alkyl nitriles	Acetylacetone
Alkyl sulfides	p-Benzoquinone
Alkyl halides	Phenyl-1,4-benzoquinone
Alkyl esters	Pyridazine
Alkyl ethers	Pyrazine
Benzene	Pyrimidine
Nitrobenzene	Pyridine
1,3,5-Triethylbenzene	Bipyridyl
Benzonitrile	Quinoxaline
Benzyl ether	Quinoline
Benzyl chloride	Isoquinoline
Benzyl alcohol	1-Benzosuberone
Benzyl amine	Piperonal
Diphenyl ether	2-Phenyl-1,3-indandione
Diphenyl sulfide	Benzalphthalide
Benzoyl chloride	Furil
Phenyl acetate	Benzil
Phenylacetaldehyde	Cumarin
Benzyl acetate	Flavone
Phenylacetonitrile	3H-1,2-Benzodithiol-3-one
2-Phenylethyl acetate	1,1'-Carbonyldiimidazole
Phenyl-2-propanone	3-Formylchromone
2-Phenylethyl alcohol	3-Formyl-6-nitrochromone
3-Phenyl-1-propanol	2-Fluorenecarboxaldehyde
Naphthalene	Dibenzoylmethane
1-Methylnaphthalene	1-Benzoylacetone
Acenaphthene	n-Butyrophenone
Anthracene	Dibenzosuberenone
Phenanthrene	Benzanthrone

Table 3.2 Aroyl Compounds Tested in the ALD (Intensity Relative to 100 for Benzaldehyde)
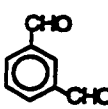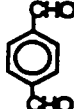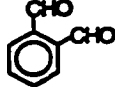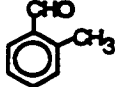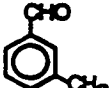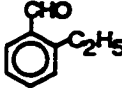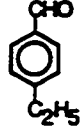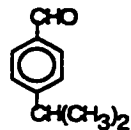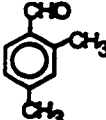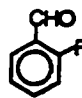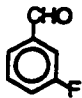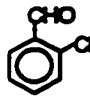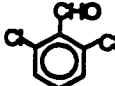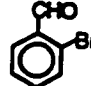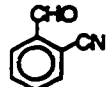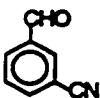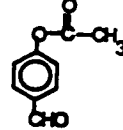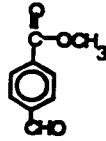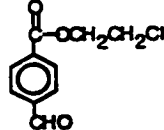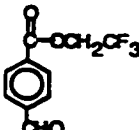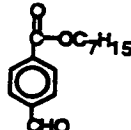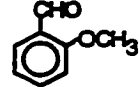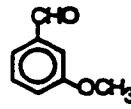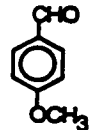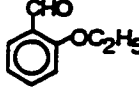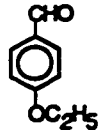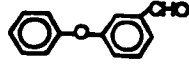
benzaldehyde (100)

isophthalaldehyde (92)

terephthal- aldehyde (105)

phthalaldehyde (0)

2-methylbenz- aldehyde (0)

3-methylbenz- aldehyde (125)

4-methylbenz- aldehyde (120)

2-ethylbenz- aldehyde (0)

4-ethylbenz- aldehyde (138)

4-isopropylbenz- aldehyde (165)

2,4-dimethylbenz- aldehyde (0)

biphenyl-4-carbox- aldehyde (0.2)

2-fluorobenz- aldehyde (71)

3-fluorobenz- aldehyde (75)

4-fluorobenz- aldehyde (81)

2-chlorobenz- aldehyde (10)

4-chlorobenz- aldehyde (45)

2,6-dichlorobenz- aldehyde (3)

2-bromobenz- aldehyde (0)

4-bromobenz- aldehyde (0)

2-cyanobenz- aldehyde (0)

3-cyanobenz- aldehyde (172)

4-cyanobenz- aldehyde (100)

4-acetoxybenz- aldehyde (45)

methyl 4-formyl- benzoate (75)

ethyl 4-formyl- benzoate (70)

2-chloroethyl 4- formylbenzoate (61)

2,2,2-trifluoro- ethyl 4-formyl- benzoate (73)

heptyl 4-formyl- benzoate (60)

2-methoxybenz- aldehyde (0)

3-methoxybenz- benzoate (38)

4-methoxybenz- aldehyde (7)

2-ethoxybenz- aldehyde (0)

4-ethoxybenz- aldehyde (2)

3-phenoxybenz- aldehyde (0.5)

Table 3.2 (continued)
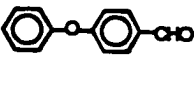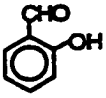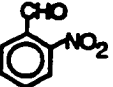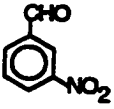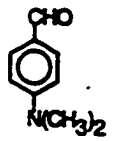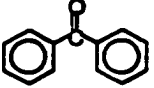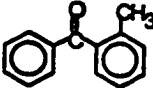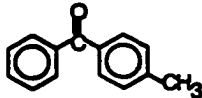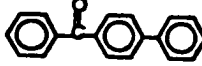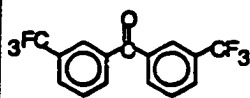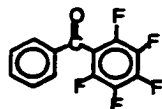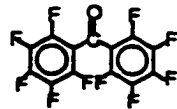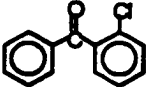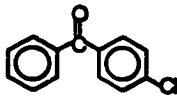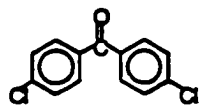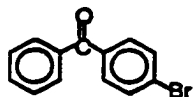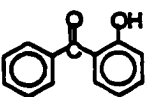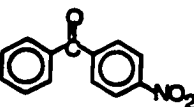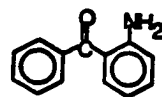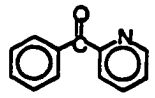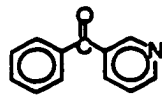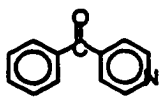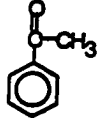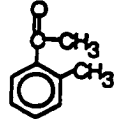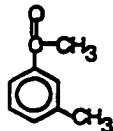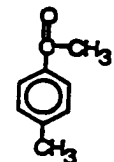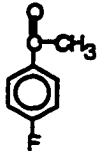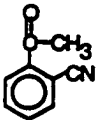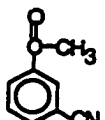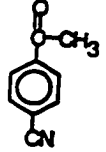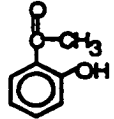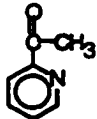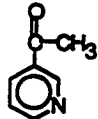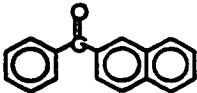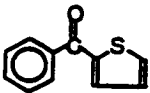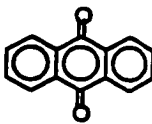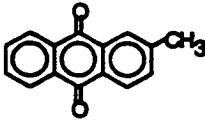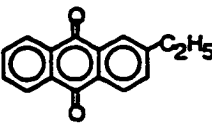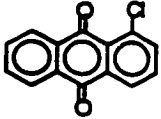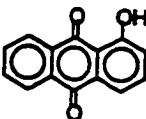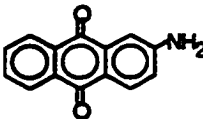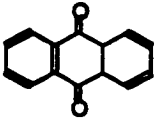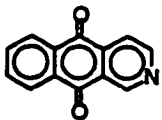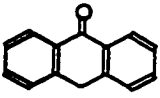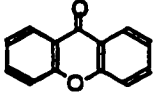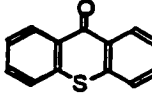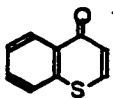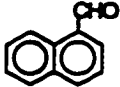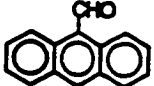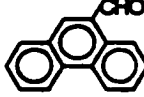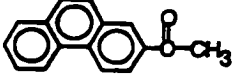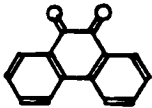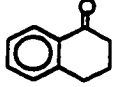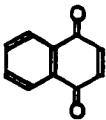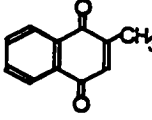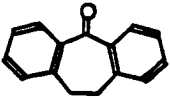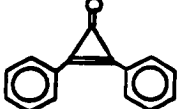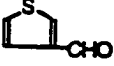
4-phenoxybenz-aldehyde (0)	2-hydroxybenz-aldehyde (0)	2-nitrobenz-aldehyde (0)	3-nitrobenz-aldehyde (0)	4-nitrobenz-aldehyde (0)
4-(dimethyl-amino)benz-aldehyde (0)	benzophenone (100)	2-methylbenzo-phenone (0)	4-methylbenzo-phenone (84)	4-benzoyl-biphenyl (3.6)
3,3'-bis(trifluoro-methyl)benzo-phenone (47)	2,3,4,5,6-penta-fluorobenzo-phenone (0.02)	decafluorobenzo-phenone (0)	2-chlorobenzo-phenone (4)	4-chlorobenzo-phenone (46)
4,4'-dichloro-benzophenone (42)	4-bromobenzo-phenone (0)	2-hydroxybenzo-phenone (0)	4-nitrobenzo-phenone (0)	2-aminobenzo-phenone (0)
2-benzoyl-pyridine (0.4)	3-benzoyl-pyridine (1)	4-benzoyl-pyridine (25)	acetophenone (28)	2-methylaceto-phenone (0)
3-methylaceto-phenone (50)	4-methylaceto-phenone (32)	4-fluoroaceto-phenone (50)	2-acetylbenzo-nitrile (0)	3-acetylbenzo-nitrile (56)
4-acetylbenzo-nitrile (134)	2-hydroxyaceto-phenone (0)	2-acetylpyridine (0.1)	3-acetylpyridine (0.3)	4-acetylpyridine (3)

Table 3.2 (continued)

propiophenone (0.1)	2-benzoyl-naphthalene (0.5)	2-benzoyl-thiophene (0.02)	anthraquinone (1400)	2-methylanthra-quinone (500)
2-ethylanthra-quinone (250)	1-chloroanthra-quinone (30)	1-hydroxyanthra-quinone (0)	2-aminoanthra-quinone (0)	1,4,4a,9a-tetra-hydroanthra-quinone (210)
benz(g)isoquinol-5,10-dione (100)	anthrone (300)	xanthone (3000)	thio-xanthene-9-one (1280)	thiochroman-4-one (0.01)
1-naphthaldehyde (0.1)	2-naphthaldehyde (0.1)	9-anthraldehyde (1.2)	phenanthrene-9-carboxaldehyde (0.1)	2-acetylphen-anthrene (0.1)
phenanthrene-quinone (0.6)	α-tetralone (12)	1,4-naphtho-quinone (2)	2-methyl-1,4-naphthoquinone (2)	dibenzosuberone (5)
trans-cinnam-aldehyde (0.5)	diphenylcyclo-propenone (0.1)	3-thiophene-carboxaldehyde (0.01)		

groups and substituents in particular positions on the aromatic ring (the "ortho effects" will be discussed in Chapter 4) may minimize or even eliminate luminescence. One exceptional finding was that dimanganese decacarbonyl showed a good response in the ALD (intenisity relative to benzaldehyde: 25%). The reason for this is unknown.

The ability of the ALD to perform highly selective determinations of certain aroyl compounds in complex mixtures is illustrated in Figure 3.11. Figure 3.11A shows the chromatogram of a condensate of pyrolyzed peat moss obtained by using the aroyl luminescence detector. Figure 3.11B is an FID chromatogram for the same sample. Non-luminescent compounds, such as hydrocarbons, alcohols and aromatic nitriles. etc.. in amounts about 10^5 times greater than that of the well-responding aroyl compounds. did not appear or showed only a weak negative signal (they depressed the background luminescence). Only several aroyl compounds did appear in the ALD chromatogram.

3.3.2 Sensitivity

The ALD response to aroyl compounds was characterized by examining the photometric behavior of benzaldehyde and anthraquinone. Benzaldehyde was chosen as representative because it is the simplest of the aromatic aldehyde family and possesses the greatest analytical importance due to its industrial uses. Anthraquinone was chosen because of its extremely strong luminescence in the ALD and also because of its industrial usefulness. Figure 3.12 shows the calibration curves of both benzaldehyde and anthraquinone. Based on the spectral measurements (Chapter 4), which indicate that the
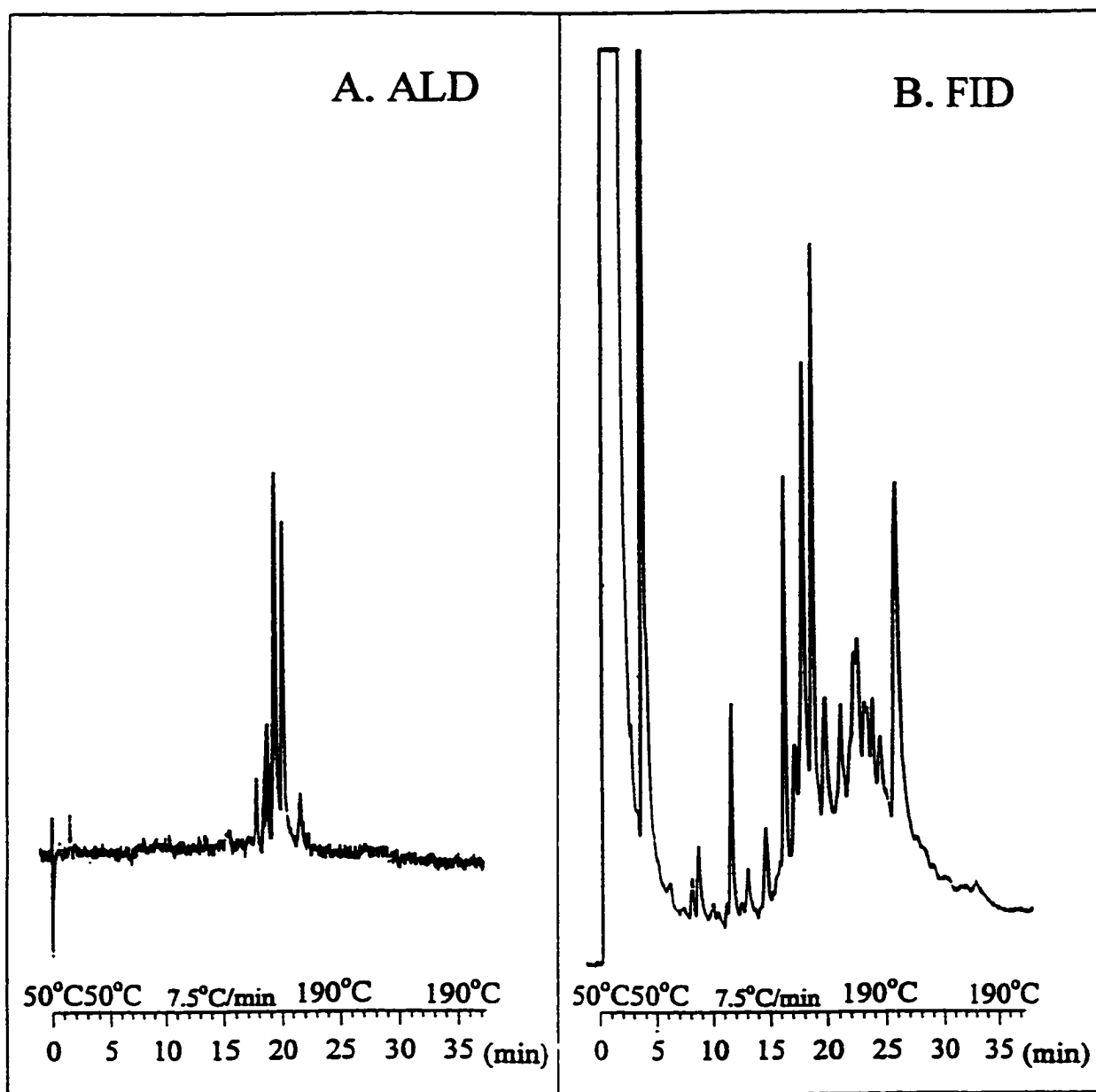
Figure 3.11 Chromatograms of a condensate from the pyrolysis of peat moss.
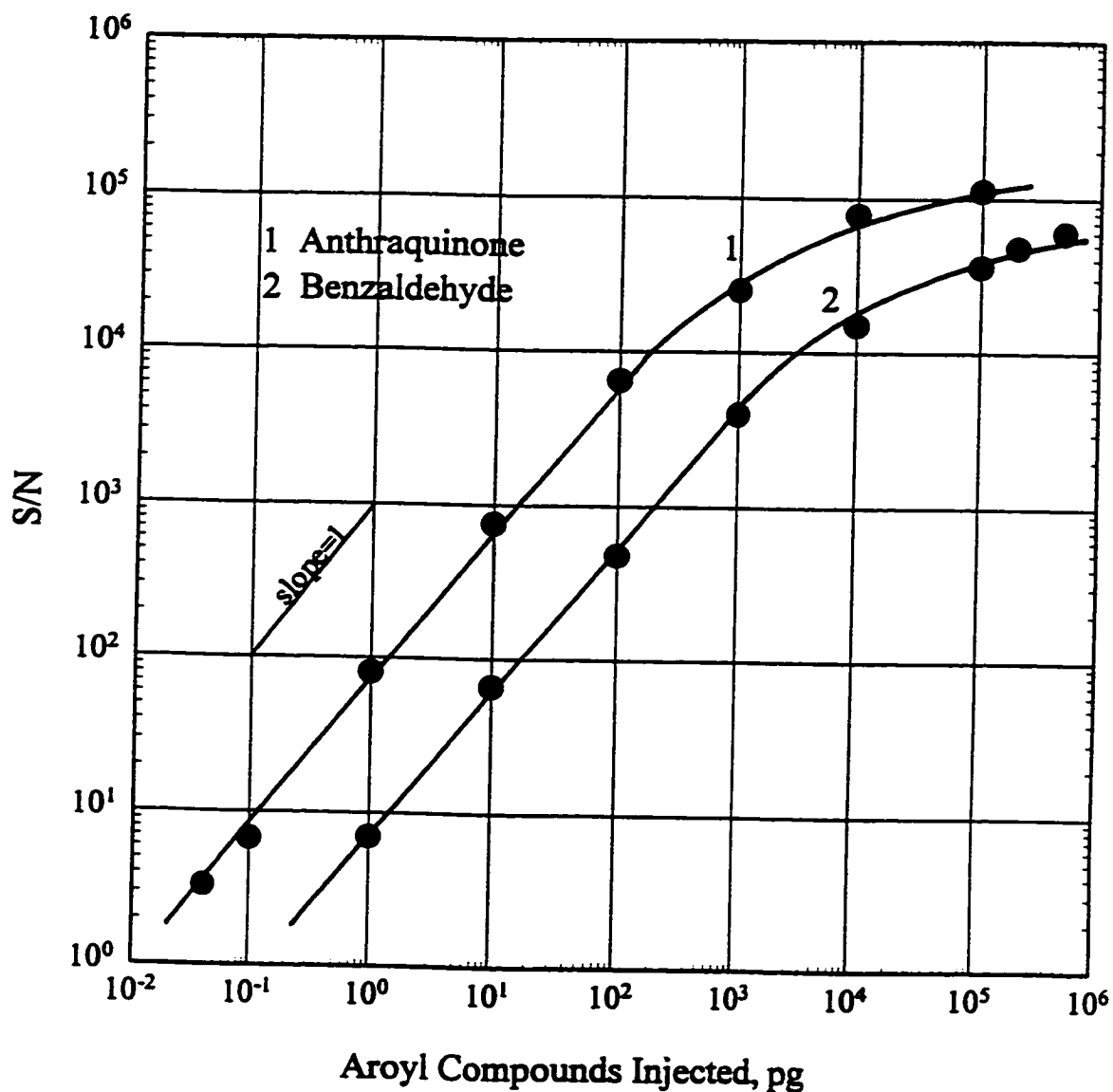
Figure 3.12 Calibration curves of benzaldehyde and anthraquinone at optimal conditions. DC voltage: +7000 V; PMT (R-374) voltage: -800 V; detector temperature: 180 °C; column temperature: 35 → 65 °C @ 10 °C/min for benzaldehyde; 35→ 170 °C @ 15 °C/min for anthraquinone; 460 nm longpass filter; RC time constant: 1 second; N_2 flow rate: 10 mL/min (carrier gas), 150 mL/min (make-up gas) and 100 mL/min (purge gas).

nitrogen background emission occurred in the 300-400 nm region, and that benzaldehyde and anthraquinone luminesce strongly around 460 nm and in 460-490 nm region, respectively, a 460 nm colored-glass long-pass filter was employed for the photometric measurement of both compounds. Other experimental conditions were as outlined in the experimental section. The minimum detectable amounts of benzaldehyde and anthraquinone were determined at a signal/noise ratio (where noise is the peak-to-peak fluctuation of the baseline over ca 1 min) of 2 as approximately 0.3 pg or 30 fg/s or 0.3 fmol/s for benzaldehyde and 24 fg or 2.4 fg/s or 12 amol/s for anthraquinone, respectively. The minimum detectable amounts of benzaldehyde and anthraquinone in the improved ALD are 3 times and 20 times lower, respectively, than those in the ALD's predecessor (the "NPPD") (44). The improved minimum detectable amounts can be attributed to gas-tightness of the ALD, greater light transmission and other factors such as a higher applied DC voltage, better polishing of the electrode, use of purge gas, etc..

3.3.3 Dynamic Range

The response was found to be linear on a log/log plot over about four orders of magnitude for both benzaldehyde and anthraquinone.

3.3.4 Quenching of Luminescence by Oxygen and Solvents

As for other photometric GC detectors, the obvious problem for the ALD is the quenching effect. The gas-phase luminescence of aroyl compounds was quenched strongly by trace amounts of oxygen in the carrier gas, or by back-diffusion of

atmospheric oxygen. The strong quenching effect of oxygen—which is expected for luminescence measurements of any sort and is commonly attributed to oxygen triplet diradical state—was confirmed by the improved response after installation of a valve on the exhaust line which kept the detector at a slight overpressure and thus minimized the back—diffusion of atmospheric oxygen. It was also necessary to use a heated oxygen scavenger cartridge to purify the nitrogen. Also, the luminescence of benzaldehyde was reduced when trace amounts of oxygen were introduced into the carrier gas stream (see section 4.8.2).

Various solvents efficiently quenched the luminescence of benzaldehyde. This quenching of benzaldehyde by solvents can be eliminated by temperature programming. In this mode the emission intensity of benzaldehyde was larger than in the isothermal mode (when the benzaldehyde eluted on the solvent tail). The solvent-quenching effect was also confirmed by dissolving benzaldehyde in a solvent with a high boiling point. Benzaldehyde then eluted prior to the solvent peak, and its response was close to that obtained in the temperature programmed mode. The solvent-quenching effect is illustrated in Figure 3.13.

3.4 Analytical Applications

The aroyl luminescence detector is one of the most sensitive and selective GC sensing devices. It can provide simple, characteristic gas chromatograms. Its unique selectivity—very few peaks show up—and its extraordinary sensitivity—in the subpicogram range—allow well separated peaks to be obtained from a complex mixture even under

	(1)	(2)	(3)
Solvent:	hexane	hexane	hexadecane
Mode:	isothermal 55 °C	temperature programming 30 → 80 °C	temperature programming 30 → 170 °C
Relative Response:	63.2%	95.8%	100%
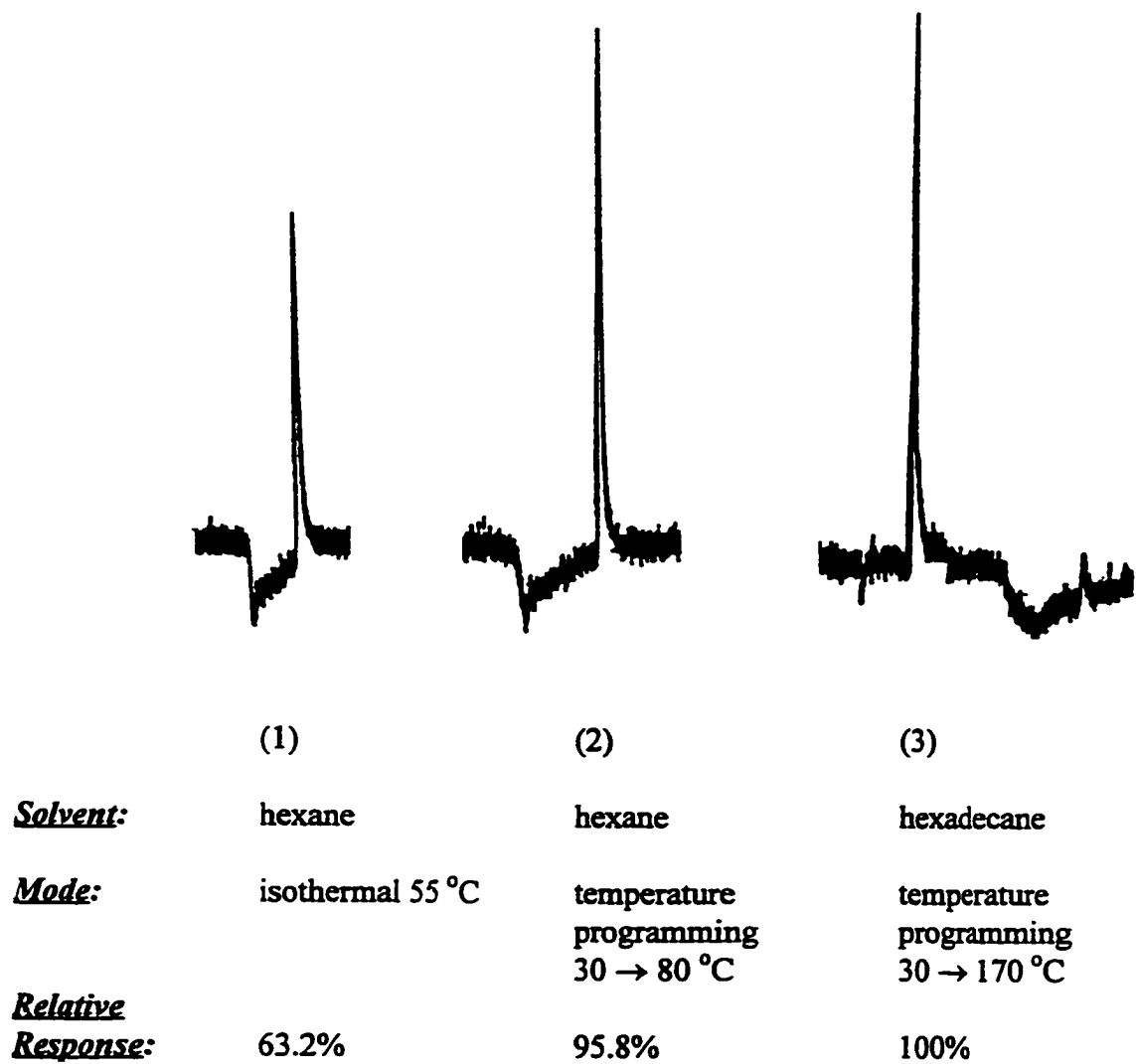
Figure 3.13   Quenching effect of benzaldehyde luminescence by hexane in the ALD.

conditions of low chromatographic resolution. Potential applications of the ALD in chemical analysis were explored by the analysis of several real-life samples.

3.4.1 Direct Injection of Room Air

3.4.1.1 Introduction

Indoor air has an important impact on a person's well-being. As a consequence. air pollution needs to be strictly and carefully controlled. However, air is probably one of the most difficult environmental matrices to handle. The sampling and analysis of organic compounds in air remain a challenge. Also, due to the low concentration of pollutants in the atmosphere, an enrichment step is often needed to reach acceptable detection limits.

Smoke—or, more specifically, the products of incomplete combustion—is the major contributor to air pollution and has been the object of much scientific inquiry (49. 50). The most often employed analytical methodology relies on preconcentration followed by gas-liquid chromtography/mass spectrometry. A variety of other techniques (after preconcentration) are also used (51). What is rare, however, is the direct injection into a gas chromatograph of a smoke-containing atmosphere. Direct injection of atmospheric samples might circumvent the problems typically associated with preconcentration. It does, however, require a detector of high sensitivity. Furthermore, the complexity of smoke composition suggests that the detector should also be selective to a particularly interesting type of chemical structure. The aroyl luminescence detector appears to meet these requirements.

3.4.1.2 Results and Discussion

Smoldering sticks of incense did introduce a variety of ALD-active compounds into the air of the laboratory. Different types of incense, of Tibetan, Indian and Japanese origin, yielded very similar chromatograms. Figure3.14 shows a typical chromatogram of 10 mL air drawn from the laboratory after one stick of incense had been burned. It demonstrates that direct injection of room air provided enough volatile smoke components for detection by the ALD. Some smoke components, such as the very common benzaldehyde, were easily identified. The identification of others will depend on the availability of authentic standards, or the use of far more expensive and labor-intensive techniques.

In fact, even the continued persistence of these smoke components can be followed for a considerable period of time. Figure 3.15 shows the decay of benzaldehyde and anthraquinone concentration in laboratory air over several hours after one stick of incense has been burned and suggests two distinct first-order processes of benzaldehyde and anthraquinone loss from the atmosphere. These may be the faster dispersal and sorption on various surfaces in the room (including unprotected syringe needles); and after slow desorption, the removal by ventilation—similar to the familiar household effect of curtains retaining the smell of cigarettes for a long time. However, the precise chemistry that produced Figure 3.15 was not further investigated.
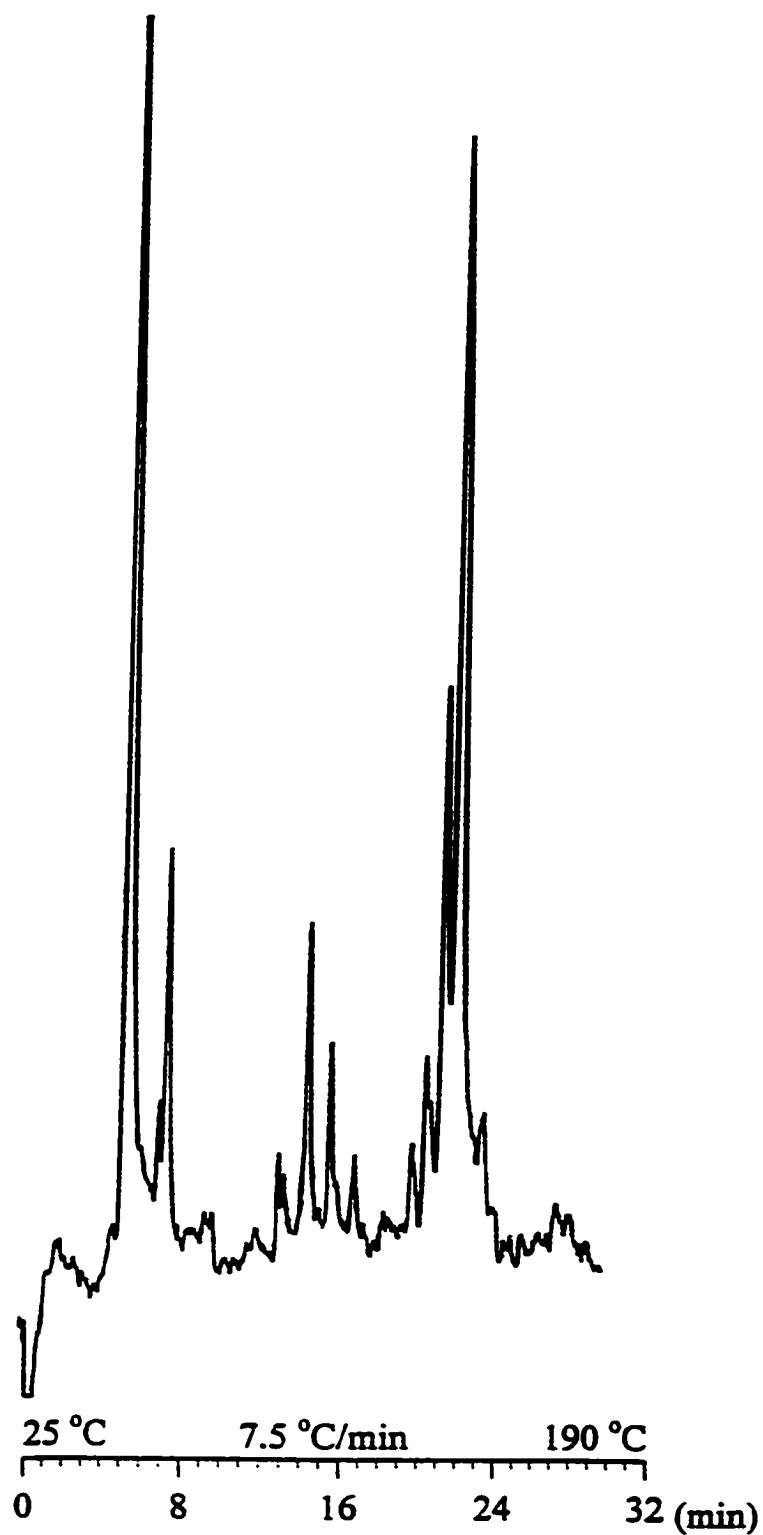
Figure 3.14 Chromatograms of room air (10 mL injected) after burning one stick (ca 1.5 g) of Tibetan healing incense in a laboratory of ca 60 m³ volume.
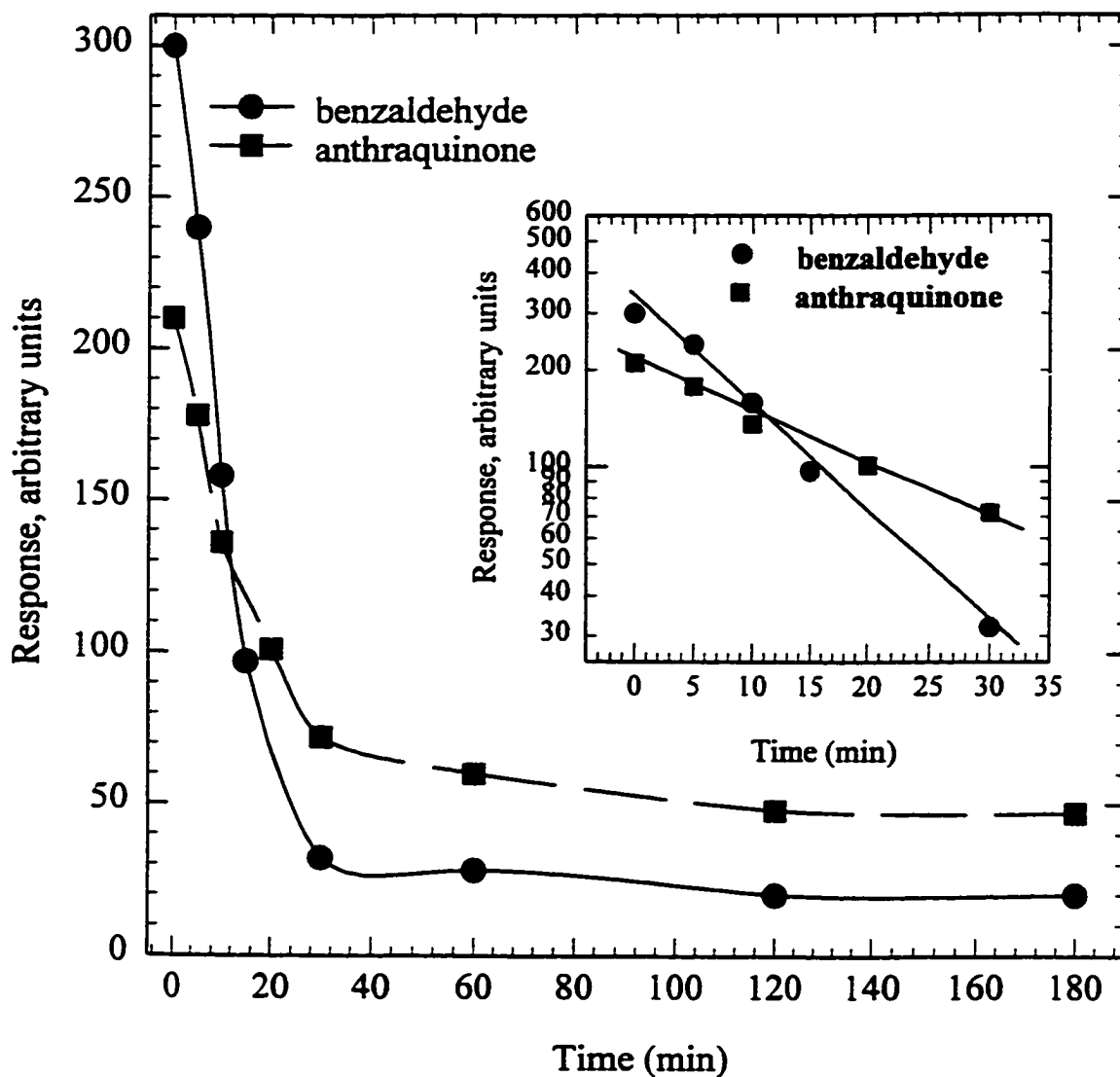
Figure 3.15 Persistence of aroyl compounds in room air after burning one stick of Tibetan healing incense.

3.4.2 Determination of Aroyl Compounds in a Soil Sample

3.4.2.1 Introduction

Organic compounds in soil can be translocated into plants. Therefore, knowledge of the presence of toxic or carcinogenic substances in soil is very important. Previous work has shown that polynuclear aromatic hydrocarbons (PAH's) have been found in the soil and soil-related samples like sediments (52, 53), and that PAH's released into the air with particular matter from combustion sources occur together with polynuclear aromatic ketones (PAK's) and other derivatives of PAH's (54, 55). These emitted compounds eventually transfer into surface soil by settlement of air particulate matter.

Recently, many "chemicals" have gained notoriety as a result of the refinement of advanced analytical instruments such as the gas chromatograph-mass spectrometer, and the extensive studies of biolological effects. Some aroyl compounds, particularly those of the polynuclear variety, are suspect because of their structural similarity to proven carcinogens. Indeed, oxygenated fractions of polynuclear aromatics such as PAK's show stronger mutagenicity in the Ames test than their purely hydrocarbonaceous analogues (56). However, PAK's are more polar than PAH's and may be more rapidly dissipated by leaching and degradation. Therefore, a sensitive detector is required for the determination of trace amounts of PAK's in surface soil. The ALD should be a good candidate. In this study, the ALD was used for the analysis of aroyl components in surface soil, albeit only in a qualitative manner, in order to illustrate the applicability of the new methodology to real-life samples.

3.4.2.2 Results and Discussion

The sampling procedure was described in section 3.2.2.2. The gas chromatogram of headspace from 0.25 g soil, which was heated in N_2 at different temperatures, is presented in Figure 3.16. It demonstrates that trace amounts of aroyl compounds do exist in surface soil. The experiment also showed that, as the baking temperature increased, the number and luminescent intensity of detectable compounds increased and reached a maximum at approximately 250 °C. The identification of most of these compounds will depend on the availability of authentic standards (see Chapter 6). Also, this chromatographic information could be very useful for other identification methodologies such GC/MS or LC/MS.

3.4.3 Determination of Alcohols by Chemical Derivatization

3.4.3.1 Introduction

As previously mentioned, aroyl compounds can be detected both sensitively and selectively in the ALD by monitoring their gas-phase luminescence. The high selectivity could be considered as either an advantage (for luminescent compounds) or a disadvantage (for non-luminescent compounds). However, proper chemical derivatization could convert a non-luminescent analyte to a luminescent derivative for its photometric detection in the ALD. A compound containing the aroyl moiety (e.g. a suitably substituted aromatic aldehyde or ketone) can be employed as the derivatizing agent. Gas chromatographic determination of aliphatic alcohols as their ester derivatives was used to demonstrate the possibility of highly sensitive determination of non-

25 °C   7.5 °C/min   190 °C

0   8   16   24   32 (min)
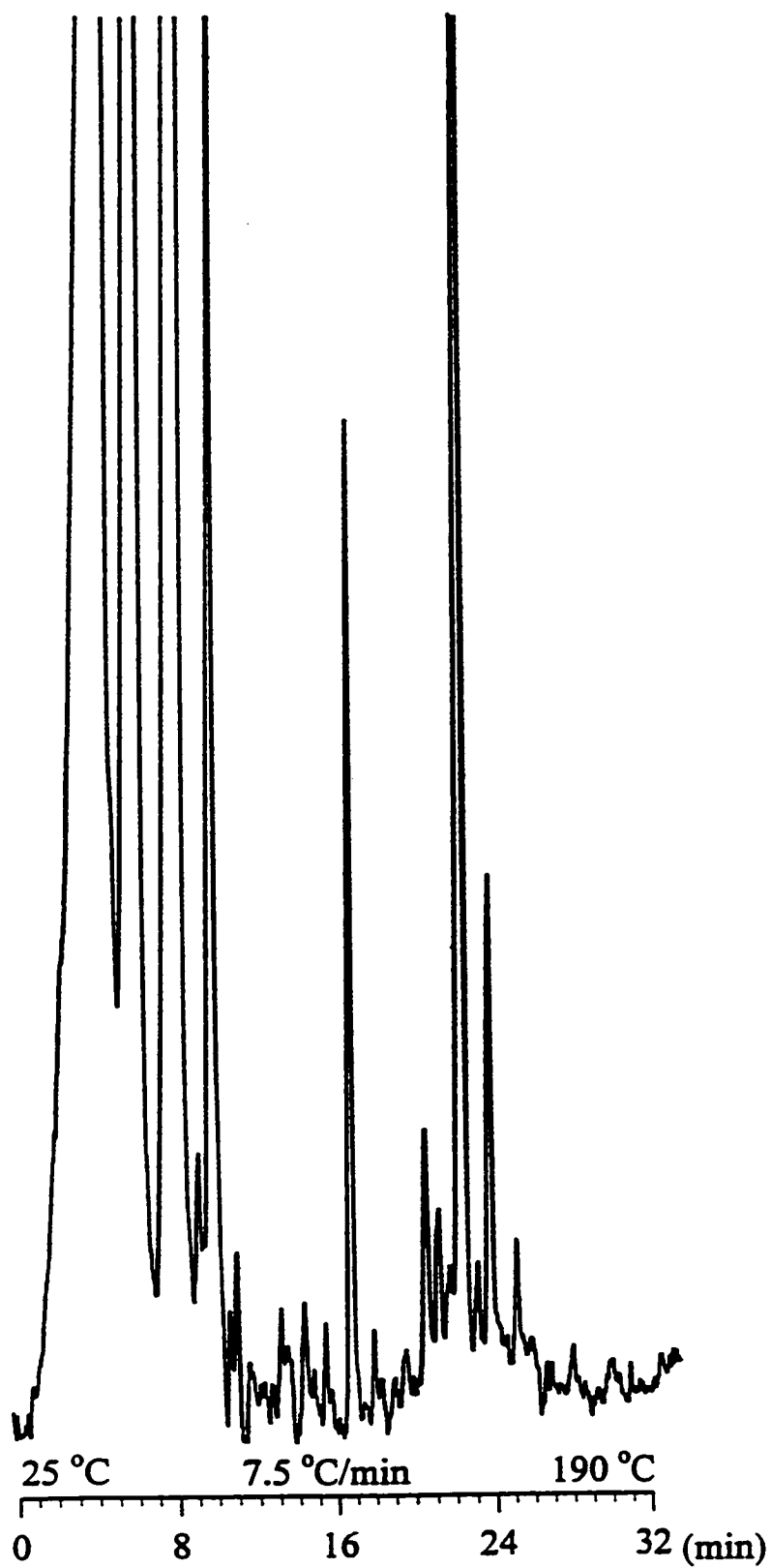
Figure 3.16 Chromatogram of atmosphere above soil which was heated in N_2 at 250 °C for 30 min.

luminescent analytes by chemical derivatization.

The identification and quantitative determination of alcohols (e.g. in food aromas, beverages, natural products and biological systems) is a commonly encountered problem in organic analysis. Most monofunctional alcohols have sufficient volatility for GC or GC/MS analysis, however, chemical derivatization may improve their GC behavior or impart higher detectability. Various alkyl, acyl, and silyl derivatives have been used for this purpose (57).

In this study, in order to increase the detectability of the aliphatic alcohols, the alcohols were converted into the corresponding ALD-active esters by reaction with p-formylbenzoyl chloride, and the esters produced were analyzed directly by GC-ALD. The reaction is illustrated in the following scheme:

$$OHC-C_6H_4-COCl + ROH \rightarrow OHC-C_6H_4-COOR + HCl \qquad (4.1)$$
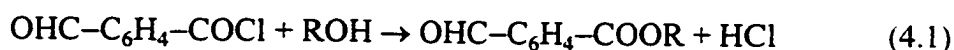
3.4.3.2 Results and Discussion

The derivatization process of alcohols is shown in Figure 3.10. The evaluation of reaction condition is shown in Figure 3.17 (the plot of mole ratio (acid chloride/alcohol) vs. reaction percentage) and Figure 3.18 (the effect of reaction time). The reaction was quantitative when the molar acid chloride/alcohol ratio exceeded 1000:1, and the reaction time was longer than 10 min at 60°C.

Figure 3.19 shows a typical chromatogram of the ester derivatives of 10 alcohols with the ALD. The derivatives were volatile, stable, eluted as well separated symmetrical peaks, and provided an excellent ALD response.

The retention times of the homologous ester derivatives were plotted against their carbon numbers. As shown in Figure 3.20, and as expected for a temperature-programmed separation, a linear dependence was found between the retention times and the carbon numbers of the alcohol molecules. The alcohols can thus be identified.

The derivatives of several alcohols were prepared for the measurements of mass spectra and gas-phase luminescence spectra. Mass spectra were obtained with a Consolidated-Electrodynamics-Corporation Model 21-110 mass spectrometer, operated at 70 eV ionizing energy. The electron inpact spectra of methyl 4-formylbenzoate, ethyl 4-formylbenzoate, 2-chloroethyl 4-formylbenzoate and hepyl 4-formylbenzoate are shown in Figure 3.21(A-D). All derivatives gave molecular ions with the expected m/e values. A large peak at m/e 133, corresponding to the elimination of the -OR group from the molecular ion, was present and this ion gave the base peak for all the ester derivatives. The ion fragment peak at m/e 105, $[OHC-C_6H_4-]+$, has also been found to be characteristic of these derivatives. Figure 3.22 shows the gas-phase luminescence spectra of the ester derivatives of five alcohols in excited nitrogen. The spectral distribution of these derivatives are similar and represent their phosphorescence spectra (see Chapter 4).

3.5 Conclusions

The newly designed and constructed aroyl luminescence detector possesses excellent sensitivity for the selective determination of certain aroyl compounds. Detection limits are down to 0.3 pg for benzaldehyde and 24 fg for anathraquinone, which are about 3 times and 20 times better, respectively, than those of the nitrogen
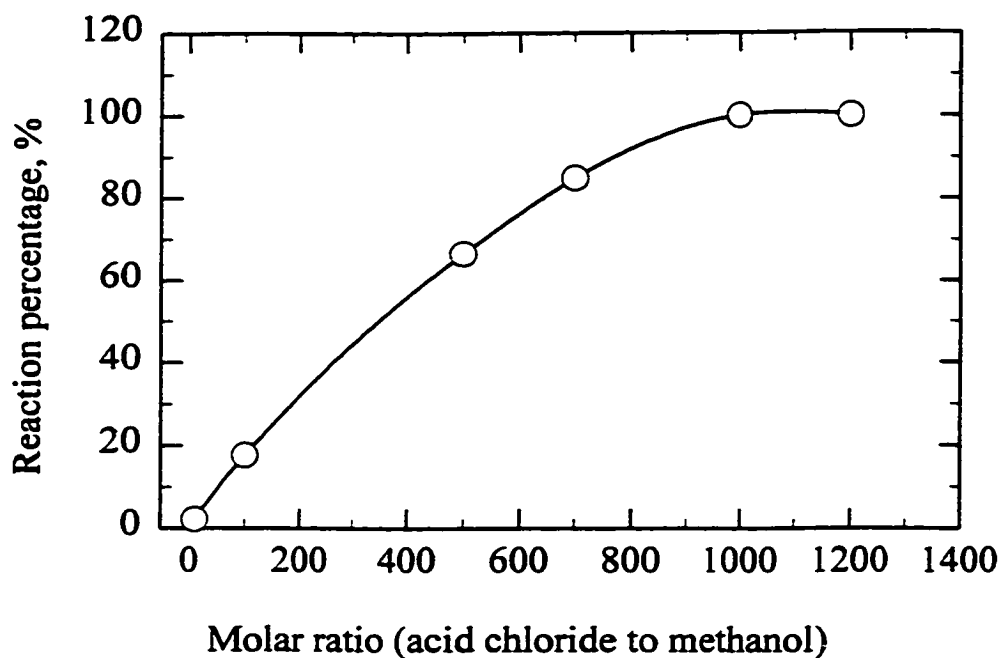
Figure 3.17 Effect of molar ratio of acid chloride to methanol (0.05 nmoles in diethyl ether) on percent yield. Reaction time: 10 min; Reaction temperature: 60 °C.
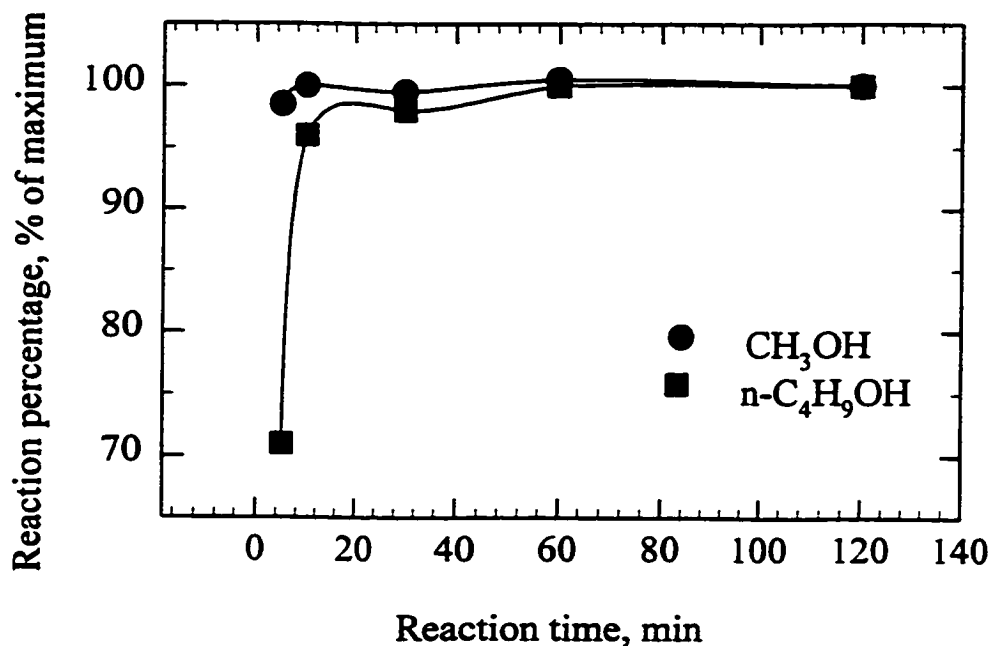
Figure 3.18 Effect of reaction time on reaction percentage. Alcohols: 0.05 nmoles; Acid chloride: 50 nmoles; Reaction temperature: 60 °C.
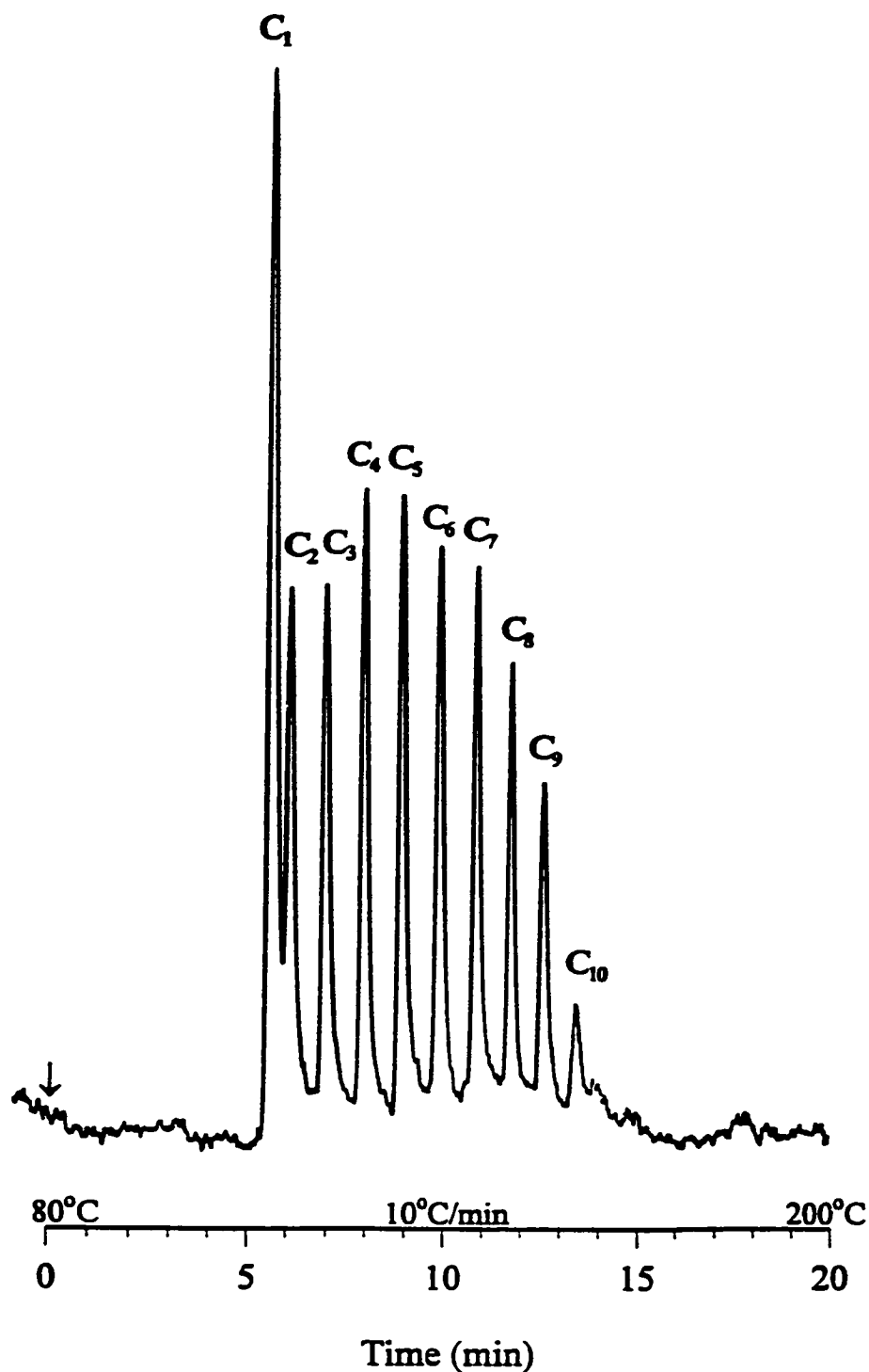
Figure 3.19 A typical gas chromatogram for 10 ester derivatives of alcohols with the ALD. $C_1=CH_3OH$; $C_2=C_2H_5OH$; $C_3=n-C_3H_7OH$; $C_4=n-C_4H_9OH$; $C_5=n-C_5H_{11}OH$; $C_6=n-C_6H_{13}OH$; $C_7=n-C_7H_{15}OH$; $C_8=n-C_8H_{17}OH$; $C_9=n-C_9H_{19}OH$; $C_{10}=n-C_{10}H_{21}OH$. The sample contained a mixture of acid chloride (25 mmoles) and alcohols (2.5 µmoles of each) in 1 mL diethyl ether; Reaction time: 10 min; Reaction temperature: 60 °C; Sample volume: 0.25 µL.
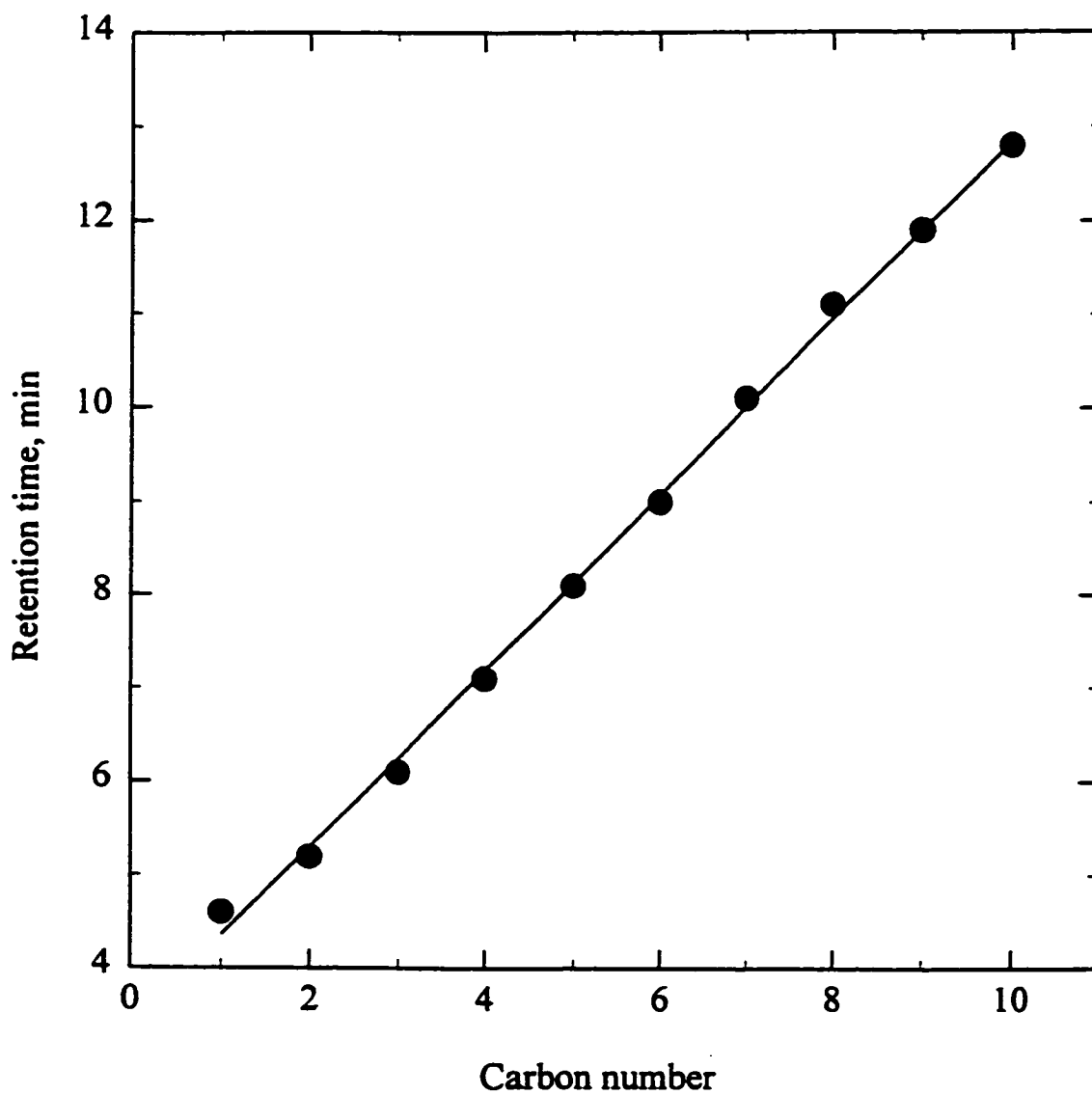
Figure 3.20   Plot of retention time of esters versus carbon number in alkyl group of ester derivatives. Column temperature: 80 → 200 °C @ 7.5 °C/min.
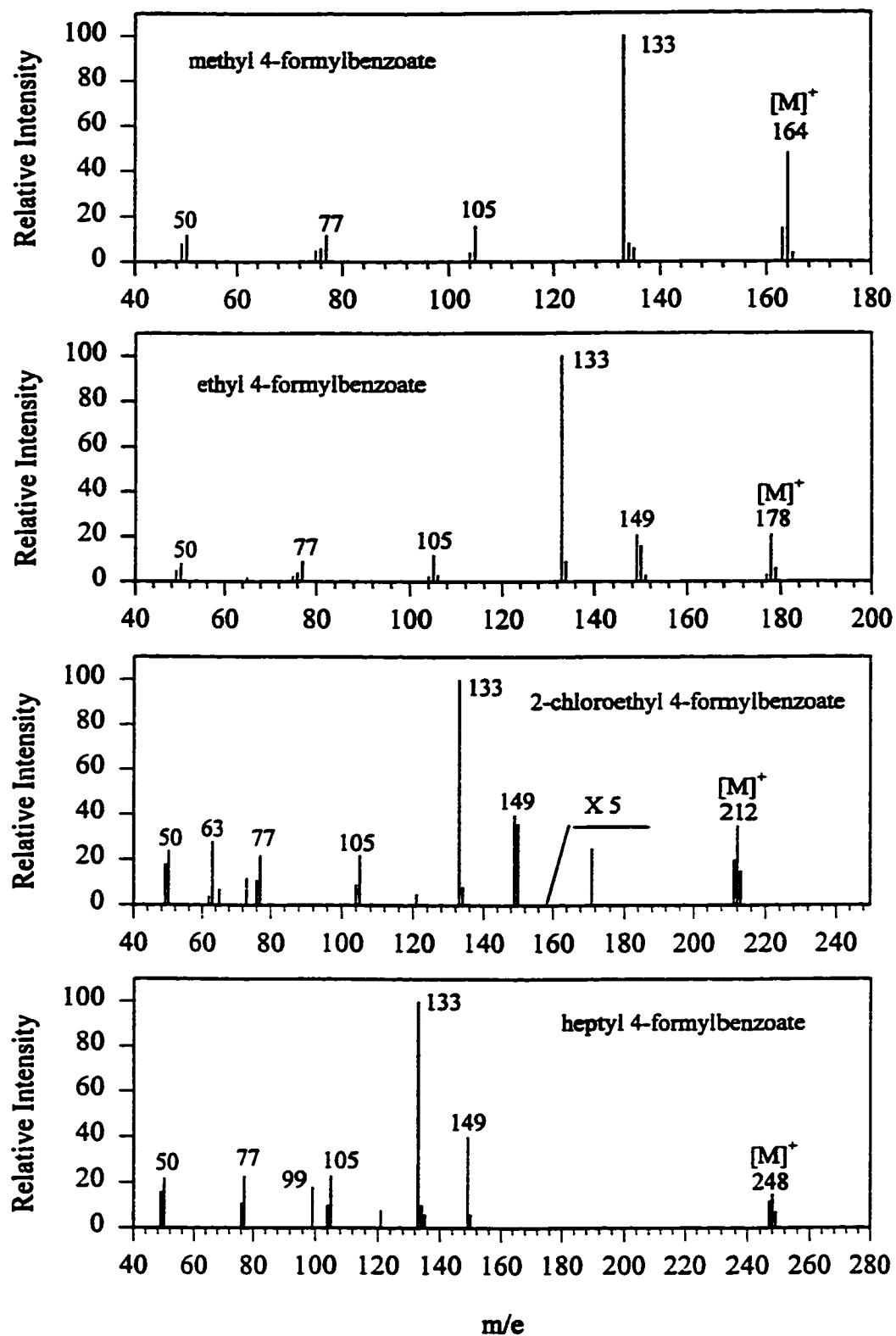
Figure 3.21   Mass spectra of four esters.
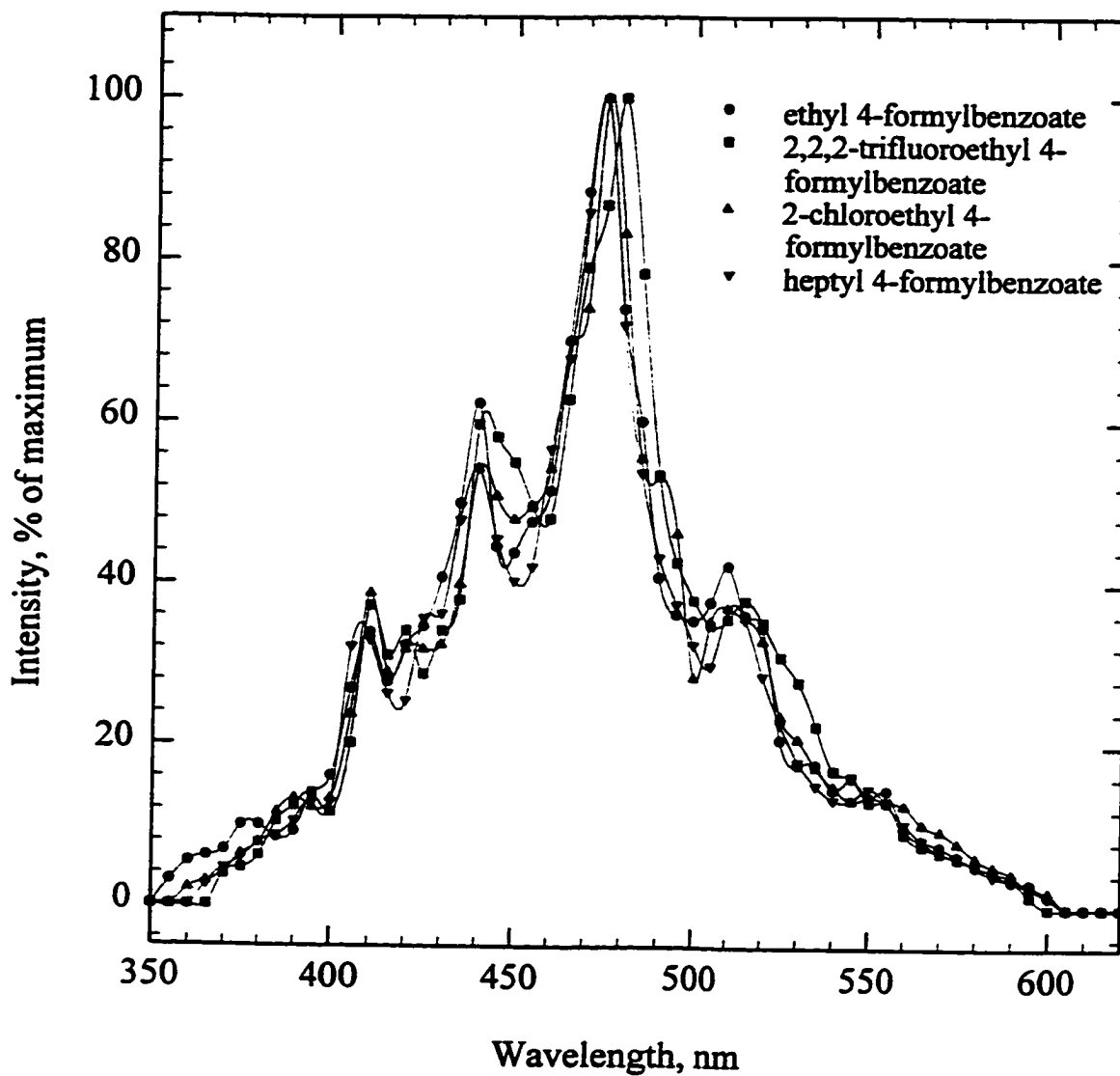
Figure 3.22   Gas-phase luminescence spectra of the ester derivatives of four alcohols in excited nitrogen. 1/4 meter grating monochromator, 2 mm slits (6.6 nm bandpass). R-268 PMT.

plasma photometric detector predecessor. This is mainly due to the improved gas-tightness and light transmission efficiency of the ALD. The ALD responds to certain types of aromatic carbonyl compounds, i.e., aromatic aldehydes, ketones and quinones. Not all of these basic structures respond, and certain substitutents ($-OH$, NH_2, etc., as well as alkyl in the ortho position) quench luminescence. The ALD is the detector of high sensitivity and selectivity for aroyl compounds in real-life samples. An entirely new chemical derivatization process was proposed and demonstrated for indirect determination of trace levels of alcohols as their 4-formylbenzoic esters.

The ALD is a novel GC photometric detector based on monitoring the gas-phase luminescence of certain analytes excited by metastable nitrogen molecules. The interpretation of the gas-phase luminescence spectra and the discussion of the intriguing excitation mechanism will be presented in Chapter 4.

Chapter 4

GAS-PHASE LUMINESCENCE OF AROYL COMPOUNDS

4.1 Introduction

Luminescence is defined generally as radiation emitted by atoms or molecules when they undergo a radiative transition from an excited energy level to a lower energy level. Atoms or molecules can be excited to higher energy states by an external light source (UV light, visible light, or laser), by a chemical reaction, and by electron impact (electrical energy). The emissions from these transitions are referred to as photoluminescence, chemiluminescence, and electroluminescence, respectively. In addition, the excited states can be produced by other excitation sources such as plasmas and discharges, which are mainly used for excitation of atomic luminescence (58).

The theory of molecular luminescence has been discussed extensively in the literature (10, 59-63). In order of increasing energy, molecules have translational, rotational, vibrational and electronic excited states. The initial stage of a molecule before excitation is usually the singlet ground electronic state S_0. As a result of excitation. an atom or molecule is promoted to a higher electronic state. There are several paths open to the excited species to lose its energy. (1) It may, before any emission of luminescent radiation or photochemical reaction occurs, undergo a series of extremely rapid events. These include vibrational relaxation (the process of dissipating excess vibrational energy by loss in thermal energy, proceeding to the lowest vibrational level ($v=0$) of the electronically excited state); and two other nonradiative processes: internal conversion (a

rapid, radiationless transfer of energy to the lowest excited singlet state) and intersystem crossing (a transfer from lowest excited singlet to excited triplet states). (2) The excited species may luminesce. Two radiative processes are called fluorescence [the two states involved in the transition have the same multiplicity ($\Delta S=0$)] and phosphorescence [the two states differ in multiplicity ($\Delta S \geq 1$)]. (3) The excited species may collide with another molecule and react with it. (4) The excited species may collide with other molecules and pass on to them some or all of its excitation energy, which can either cause reaction in the other molecule, or can gradually be degraded into heat. (5) The excited species itself may undergo a chemical reaction if the excitation energy goes into breaking or rearranging chemical bonds.

The various energy states and luminescence processes of a molecule are usually shown in Jablonski diagrams such as that in Figure 4.1. Rotational sub-levels are not shown because they are so closely spaced as to form a near continuum. The transition from an excited singlet state to a singlet ground state (prompt fluorescence) is spin-allowed and thus occurs with a high degree of probability and the relatively short life time of 10^{-10} to 10^{-7} second. On the other hand, the transition from a triplet excited state to a singlet ground state (phosphorescence) is a spin-forbidden process with a relatively long life time from 10^{-4} to 10 seconds. Because of this, phosphorescence is a relatively slow process compared to other processes associated with excited molecules, and the triplet state suffers from a high possibility of collisional quenching by impurity or solvent molecules. Another pathway shown in figure 4.1 is the reverse intersystem crossing ($T_1 \rightarrow S_1$). This happens if the energy difference between the singlet and triplet state is

Singlet States   Triplet States
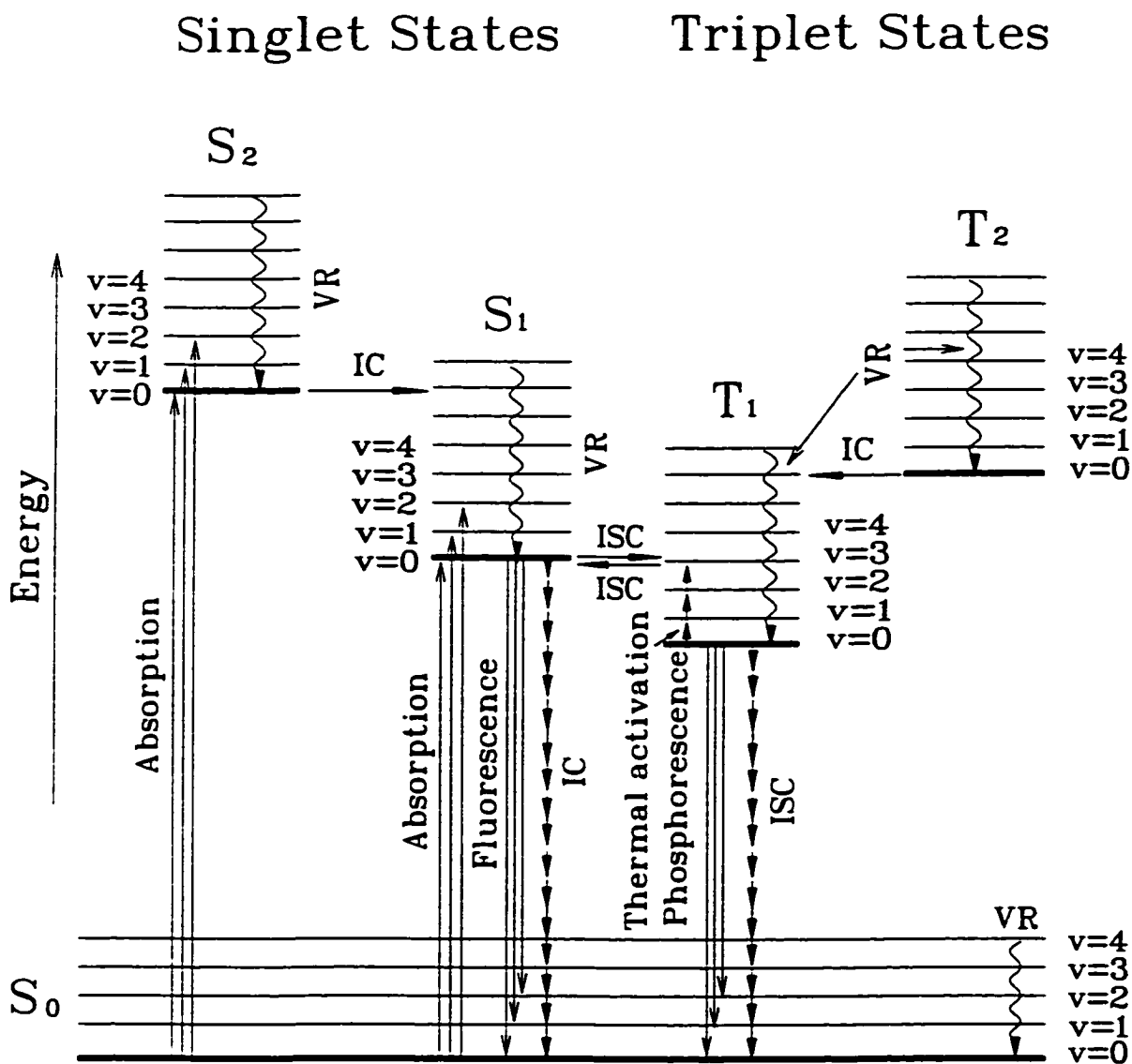
Figure 4.1   Jablonski diagram showing some of the radiative and non-radiative processes available to molecules (VR=vibrational relaxation; IC=internal conversion; ISC=intersystem crossing).

small, so it is probable that T_1 can be activated to S_1 by thermal excitation. This process gives rise to the so-called E-type delayed fluorescence, which is highly temperature-dependent and has a lifetime approximately equal to that of phosphorescence. Another type of delayed fluorescence is called P-type fluorescence, which is produced by a triplet-triplet annihilation process: $T_1 + T_1 \rightarrow S_1 + S_0$. The spectroscopic nature of the luminescence, including energy levels in a luminescent molecule, and shape and intensity of the spectrum, may differ due to environmental effects. In solution at room temperature, the interaction of solvent with the upper and lower electronic levels may lead to a wavelength shift of a given vibrational level observed in emission and absorption. Spectral features are very broad due to the vibrational sequence and strong solvent interactions. The luminescence intensity is generally very low because of the high collision number in condensed phases (as opposed to a low-pressure gas). In order to obtain a high resolution spectrum and high luminescence intensity, a low-temperature environment is required, which can be achieved by freezing the solution to form a rigid glass at the temperature of liquid nitrogen (77K). For analytical purposes, several low-temperature spectroscopies have been developed, including Shpol'skii spectrometry, matrix isolation spectrometry, and fluorescence line narrowing spectrometry (10. 64). However, at low pressure in the gas phase, molecular interactions are minimized and the rate of collision is relatively smaller. Thus unperturbed luminescence spectra of the isolated molecules can be approximated. However, as pressure increases, the excited molecules usually lose their energy by collisional quenching before they have a chance to emit. For spectroscopic studies, preparation of internally cold, isolated gas phase

molecules has been traditionally desired by spectroscopists. This can be achieved by the use of supersonic free jets or supersonic molecular beams which retain the advantages of solid state or matrix isolation spectroscopy without the disadvantage of intermolecular perturbations (65).

The photophysics and photochemistry of organic molecules have been extensively studied, usually by using optical excitation (66, 67) and electron impact (68, 69). However, most of investigations have been restricted to the condensed phases in which organic molecules do not show some of the photochemical or photophysical properties that can be observed in the gas phase. In the present study, a radioactively stimulated, high-voltage, low-current discharge in high-purity nitrogen was used as a novel source for the excitation of certain aromatic carbonyl compounds at atmospheric pressure and high temperature in the gas phase. The emission spectra of many aroyl compounds were measured and compared with the spectral data from other excitation systems (if available in the literature). The substituent effects on the triplet energy, the luminescence quenching effects (by oxygen and hydrocarbons), and the enhancing effects of argon or helium were also investigated. The objective here was to develop an understanding of the general photophysical characteristics of gas-phase molecules under these specific conditions (high temperature and atmospheric pressure) and to try to explore the intriguing energy-transfer-excitation mechanism.

4.2 Experimental

The luminescence measurements were made in three different modes (see Chapter

2). For the strongly luminescent compounds such as benzaldehyde, the gas-phase spectrum was obtained with a Jarrell-Ash model 82-415 quarter-meter monochromator and an Oriel model 77250 eighth-meter monochromator. The spectral distributions with the two monochromators were identical except for the different intensity distributions due to the distinct light transmission profiles of the grating (Figure 4.2 and 4.3). In most cases, the spectra obtained by single-peak mode (scanning a single chromatographic peak with dual-channel correction for the variable concentration) with the eighth-meter monochromator are reported. For some weakly emitting compounds, such as 1,4-naphthoquinone, a low-resolution device with a far higher light throughput. the Oriel model 7155 "filter monochromator", was employed to map the spectra.

In single-peak mode, in order to obtain accurate and either highly sensitive or highly resolved spectra, a sample amount greater than 10 ng was required for injection into the triple-channel ALD system. The spectra could still be measured from a peak produced from less than 10 ng, though with some loss in resolution. To secure a good spectrum from a single peak, samples in amounts corresponding to the upper end of their linear calibration ranges were introduced into the ALD. A background spectrum of pure nitrogen (the so-called second positive system) persisted in the ALD (Figure 4.4A). In order to obtain spectra that accurately correlate spectral information with concentration. the spectral background had to be deducted from the raw spectrum of the dispersive channel (Figure 4.4B). The net raw spectrum—the output of the dispersive-channel scan minus the spectral background—was divided by the chromatographic signal from the nondispersive channel (Figure 4.4C). These corrections are easy to implement, either by
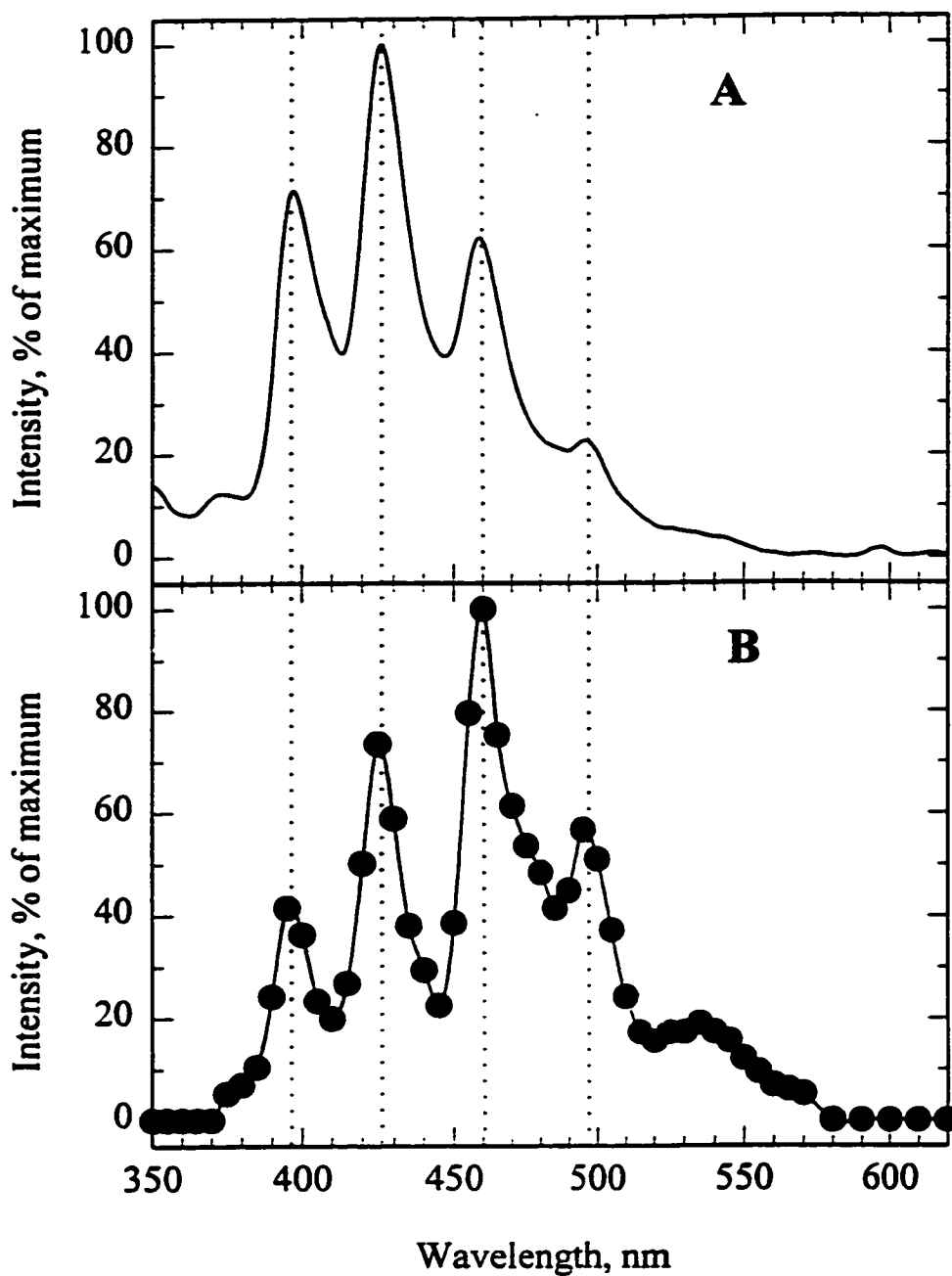
Figure 4.2 Gas-phase luminescence spectra of benzaldehyde in excited nitrogen obtained from a 100 ng peak with 1/8 meter grating monochromator (A) and by repeatedly injecting 100 ng benzaldehyde with 1/4 meter grating monochromator (B). R-374 PMT, Bandpass: 6.6 nm.
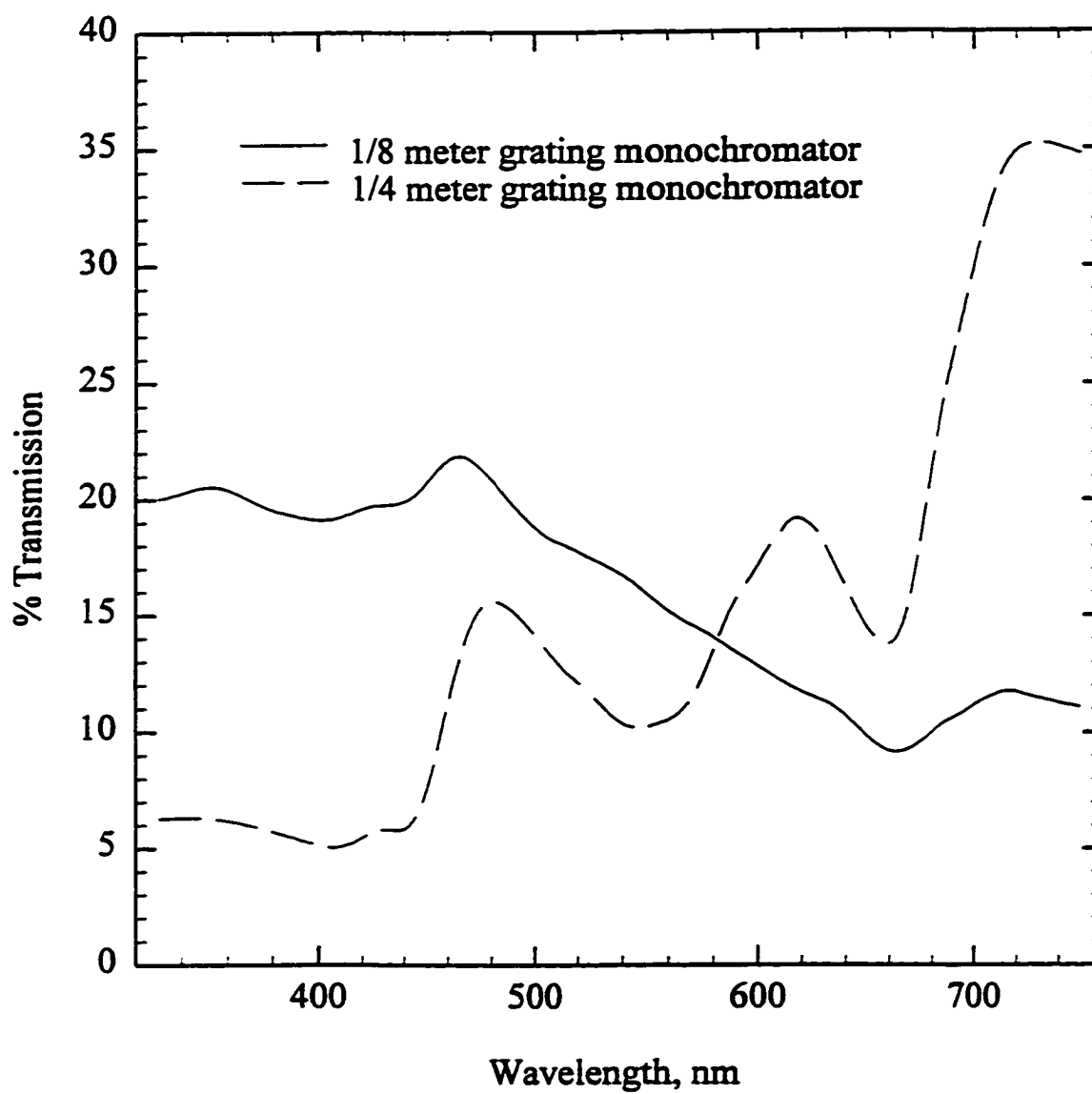
Figure 4.3   Light transmission efficiencies of two monochromators.
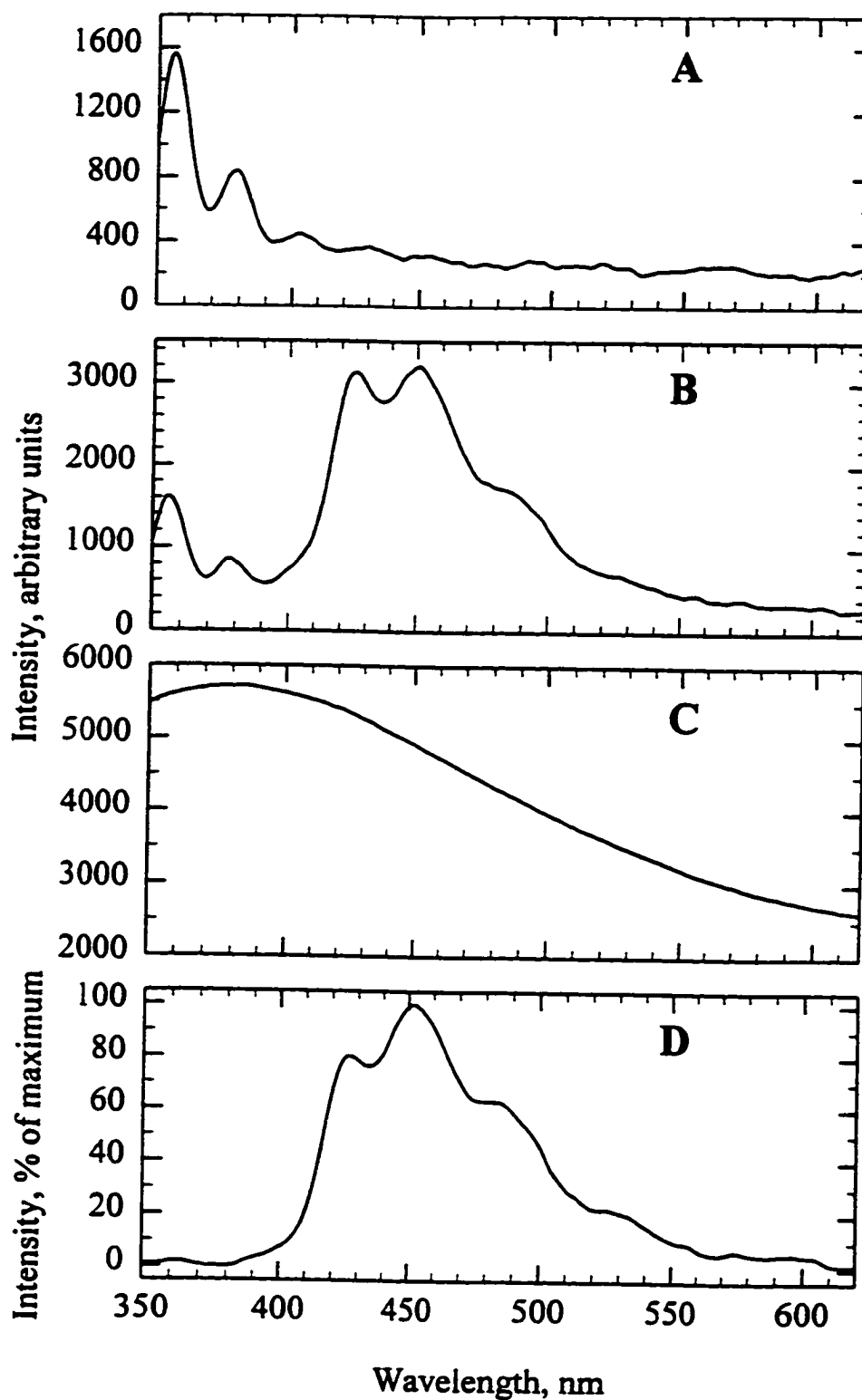
Figure 4.4 A. Background spectrum in the ALD; B. The raw spectrum from the dispersive channel; C. The chromatographic signal from the nondispersive channel; D. The referenced gas-phase luminescence spectrum of benz(g)isoquinolone-5,10-dione.
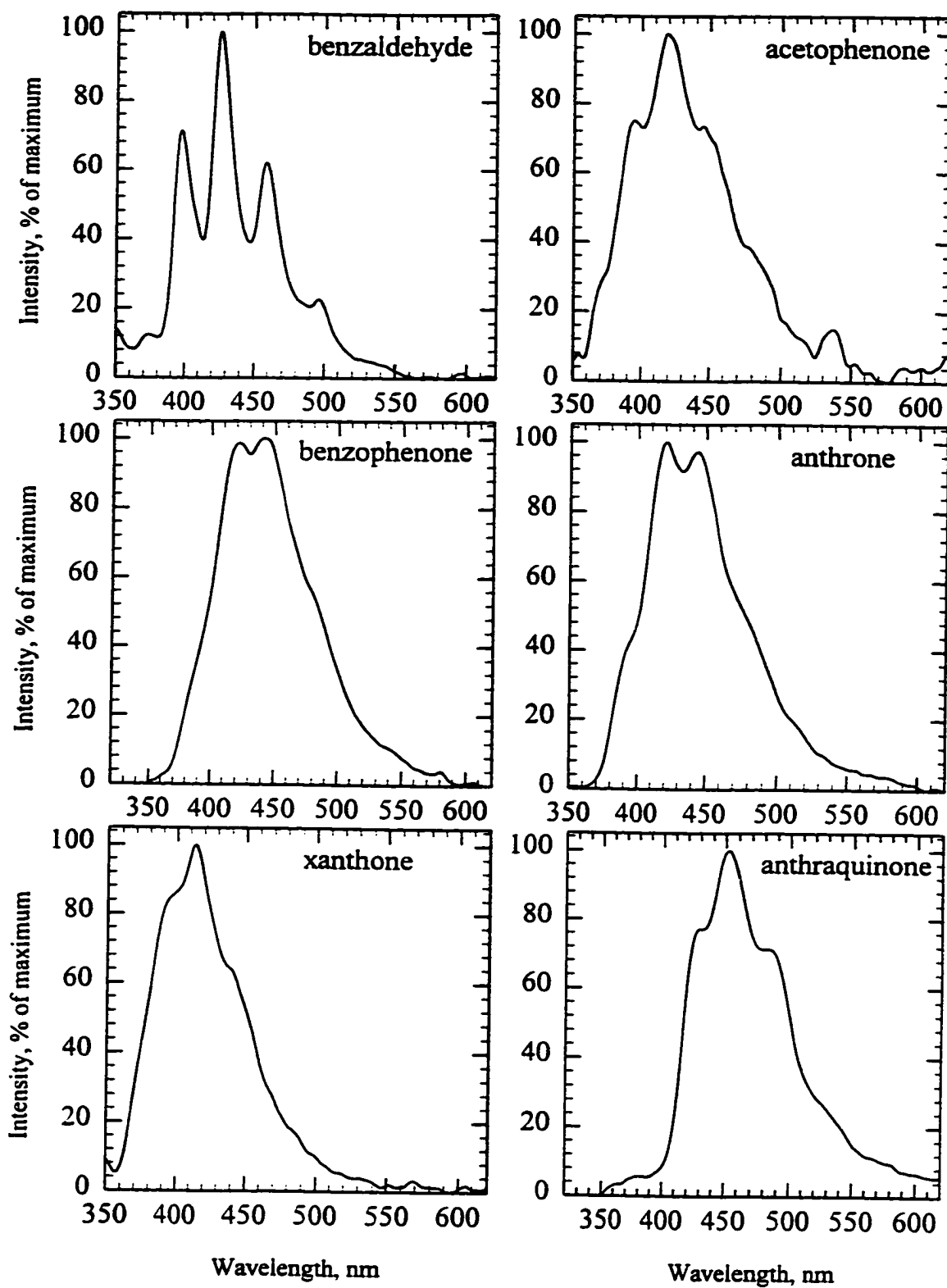
Figure 4.4. E. The gas-phase luminescence spectra of some typical aroyl compounds obtained by the single-peak mode.

a suitable algorithm as found in the CHROM 8 program (46), or by a spreadsheet. The referenced gas-phase luminescence spectrum of benz(g)isoquinolone-5,10-dione is shown in Figure 4.4D. The gas-phase luminescence spectra of some typical aroyl compounds obtained by the single-peak mode are shawn in Figure 4.4E. All referenced spectra reported in this study are not corrected for photomultiplier quantum yield. monochromator grating efficiency and other instrumental variables. The wavelength indicator on the monochromator was calibrated from time to time using the mercury lines as a standard.

Figure 4.5 shows the gas-phase luminescence spectra of benzaldehyde measured by the 1/8 meter monochromator with different slit widths. In general, the narrower the slit width the better the resolution, and conversely, the wider the slit width the greater the light throughput. However, under this specific luminescent condition (high temperature and atmospheric-pressure gas phase), as the slit width decreased, the spectral resolution did not improve too much. This broad-band spectrum is due to the fact that at high temperature the population of higher vibrational energy levels is larger, and the rotational sub-levels are so closely spaced as to form a near continuum. Based on this fact. the slit width for luminescence spectrum measurements was usually set to 2 mm or 1 mm. The scan rate was 300 nm/min.

4.3 Spectra and Interpretation

The photochemical behavior and photophysical properties of aromatic carbonyl compounds have been thoroughly studied both in condensed phase and in the gas phase. It is generally assumed that unsubstituted aromatic carbonyl compounds emit solely
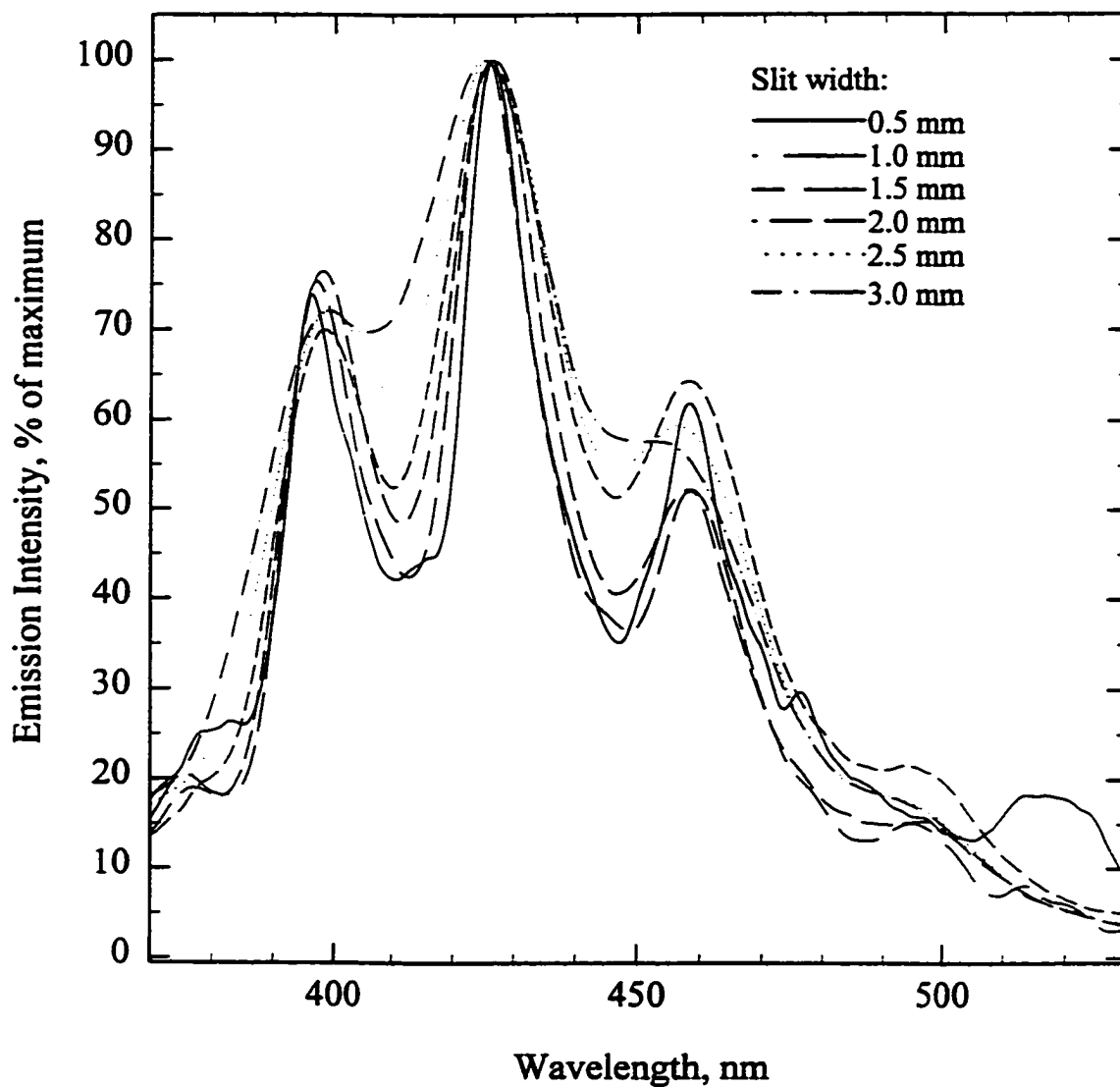
Figure 4.5   Gas-phase luminescence spectrum of benzaldehyde in excited nitrogen obtained from a 100 ng peak with the 1/8 meter grating monochromator, R-374 PMT and different slit widths.

phosphorescence because the overall intersystem crossing $S_1 \rightarrow T_1$ is very efficient (70.

71). Certain substituted aromatic carbonyl compounds show solely phosphorescence:

others show both fluorescence and phosphorescence (59). Many photochemical reactions

proceed from the triplet state (72). The nature of the lowest excited state is a subject of

great interest. It is well established that the lowest excited triplet state, T_1, of typical

aromatic carbonyl compounds such as benzaldehyde or benzophenone is $^3(n,\pi^*)$, both in

non-polar solvents or in the gas phase, while the T_1 state of some substituted compounds,

possessing an electron-donating group at the para position, is attributed to the $^3(\pi,\pi^*)$

state (67, 73). The nature of the triplet state can be assigned to π,π^* or n,π^* based on

several factors including (1) lifetime and polarization; (2) electron spin resonance; (3)

triplet-singlet splitting; (4) vibrational structure, and (5) the heavy atom solvent effect on

the $\pi^* \leftarrow n$ absorption. It is very common that the emission spectra from an n,π^* state of

aromatic carbonyls will contain the $C=O$ vibrational structure. All these investigations

were carried out by using optical light sources or electron impact. In this study, as well as

in studies involving the ALD's predecessor (41-44), it was found that certain aromatic

carbonyl compounds luminesce in the radioactively stimulated, high-voltage, low-current

nitrogen discharge; other do not. It is therefore of substantial interest to investigate the

photophysical properties of the luminescent aroyls in excited nitrogen.

4.3.1 Benzaldehydes

The spectral distribution of luminescence originating from benzaldehyde in excited

nitrogen is shown in Figure 4.6. Benzaldehyde, the simplest aromatic carbonyl molecule,
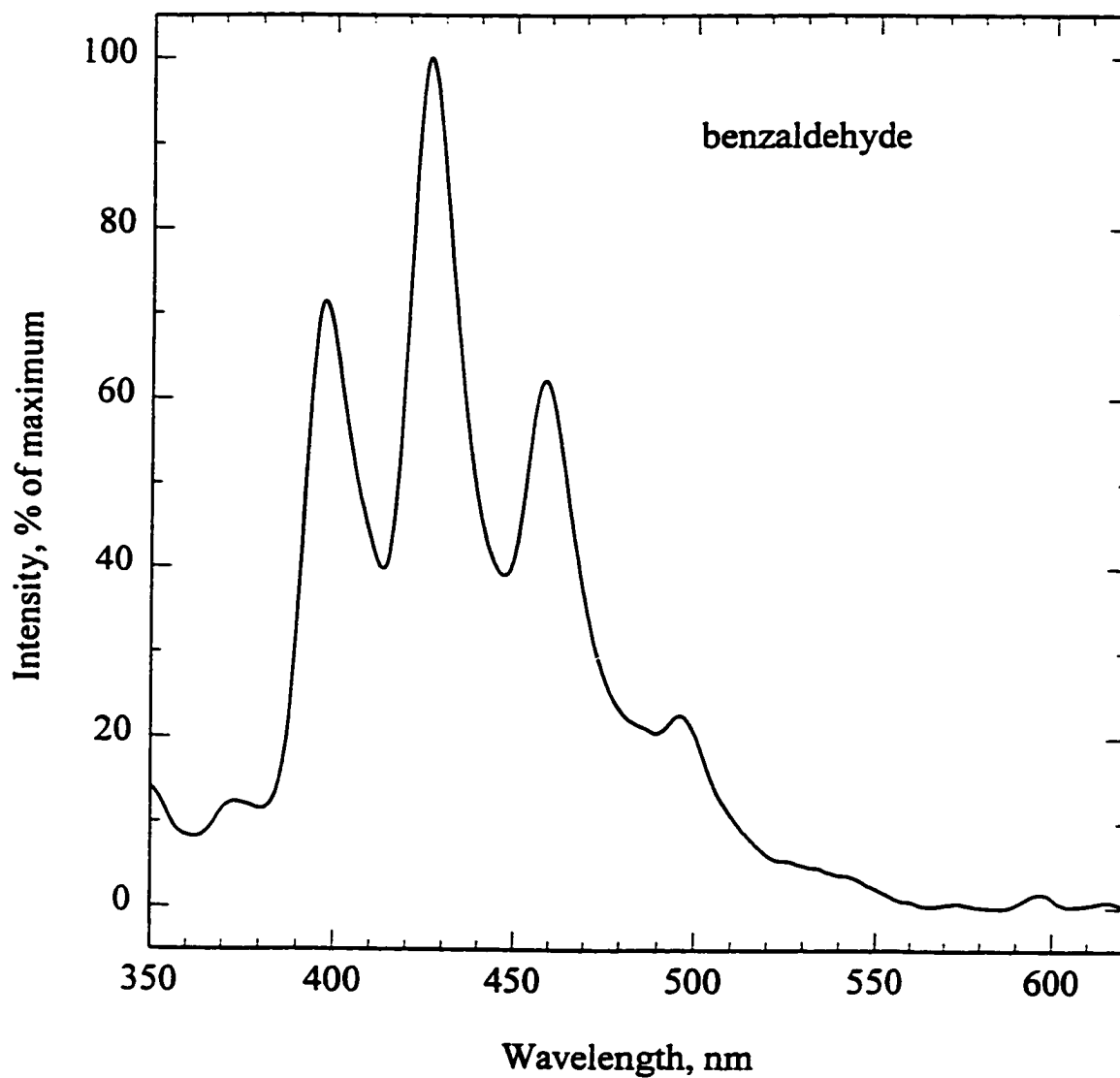
Figure 4.6   Gas-phase luminescence spectrum of benzaldehyde in excited nitrogen obtained by using 1/8 meter grating monochromator, R-374 PMT and single-peak mode. Bandpass: 6.6 nm.

has been spectroscopically and photochemically well investigated (66, 74-77), and these studies have served as the basis for understanding more complex aromatic carbonyl spectra. As mentioned before, the unsubstituted carbonyl-containing molecules usually emit solely phosphorescence (59). The phosphorescence of benzaldehyde can be induced by optical excitation (67, 75-78), electron impact (68) or active nitrogen (79) in the condensed phase (67, 75, 76) or in the gas phase (68, 79-82). The spectrum obtained in this study exhibits prominent peaks at 397, 427, 460 and 498 nm, respectively. This spectrum resembles the phosphorescence spectrum of benzaldehyde measured in a rigid medium (67) or in the gas phase (68, 79-82), apart from the fact that the spectrum obtained in this study is broader than that measured at room temperature and low pressure in the gas phase because of the effect of temperature broadening on the vibrational structure. A prominent C=O stretching vibrational progression with a frequency of about 1703 cm^{-1} is shown in the gas-phase luminescence spectrum (Table 4.1). Based on these observations, we can safely assign the present luminescence spectrum as that of benzaldehyde phosphorescence. Prominent peaks at 397, 427, 460 and 498 nm were assigned as the 0-0 band and progressions in the C=O stretching mode, respectively. The phosphorescence of benzaldehyde originates from the T_1 (n,π*) → S_0 transition. T_1 (n.π*) at 397 nm (25189 cm^{-1} or 3.12 eV or 301 kJ/mol) is the lowest triplet state in benzaldehyde (59, 67). This assignment is in agreement with the previously reported assignment (67, 68), and is useful in locating T (n,π*) triplet states in substituted benzaldehydes.

Table 4.1 Vibrational Analysis of Luminescence Spectrum of Benzaldehyde in the Gas Phase

v (cm^{-1})	Δv (cm^{-1})	Attribution
25189 (397 nm)	0	0-0
23419 (427 nm)	1770	1729
21739 (460 nm)	3449	2 X 1729 = 3458
20080 (498 nm)	5108	3 X 1729 = 5187

Figure 3.22 and Figures 4.7-4.25 show the gas-phase luminescence spectra of a number of substituted benzaldehydes. The spectral shapes of the emission observed from these substituted benzaldehydes are quite similar to that of benzaldehyde except for the spectral shift due to substituent effects. All of these spectra exhibit a vibrational progression characteristic of the C=O stretching frequency (1700 cm^{-1}). When the emission occurs from a T (π,π^*) state, the vibrational structure of the phosphorescence spectrum is variable. Therefore, similar assignment of the gas-phase luminescence spectra as their phosphorescence spectra can be made with respect to these substituted benzaldehydes. The spectroscopic data obtained are summarized in Table 4.2. and are in agreement with vapor phase data when these are available (81), or close to the data obtained in a non-polar solvent (78). It is seen from this table that electron-donating groups at the para-position cause a blue shift of the T_1 (n,π^*) → S_0 transitions except for the T_1 (n,π^*) → S_0 transitions of 4-chlorobenzaldehyde, but a red shift is seen for electron-withdrawing groups at the para-position. On the other hand, the T_1 (n,π^*) → S_0 transitions are red-shifted in meta-substituted benzaldehydes relative to those of benzaldehyde. It is interesting to note that, in 4-fluorobenzaldehyde, the T_1 (n,π^*) → S_0

Figure 4.7 Gas-phase luminescence spectrum of isophthalaldehyde in excited nitrogen obtained by using 1/8 meter grating monochromator, R-374 PMT and single-peak mode. Bandpass: 6.6 nm.
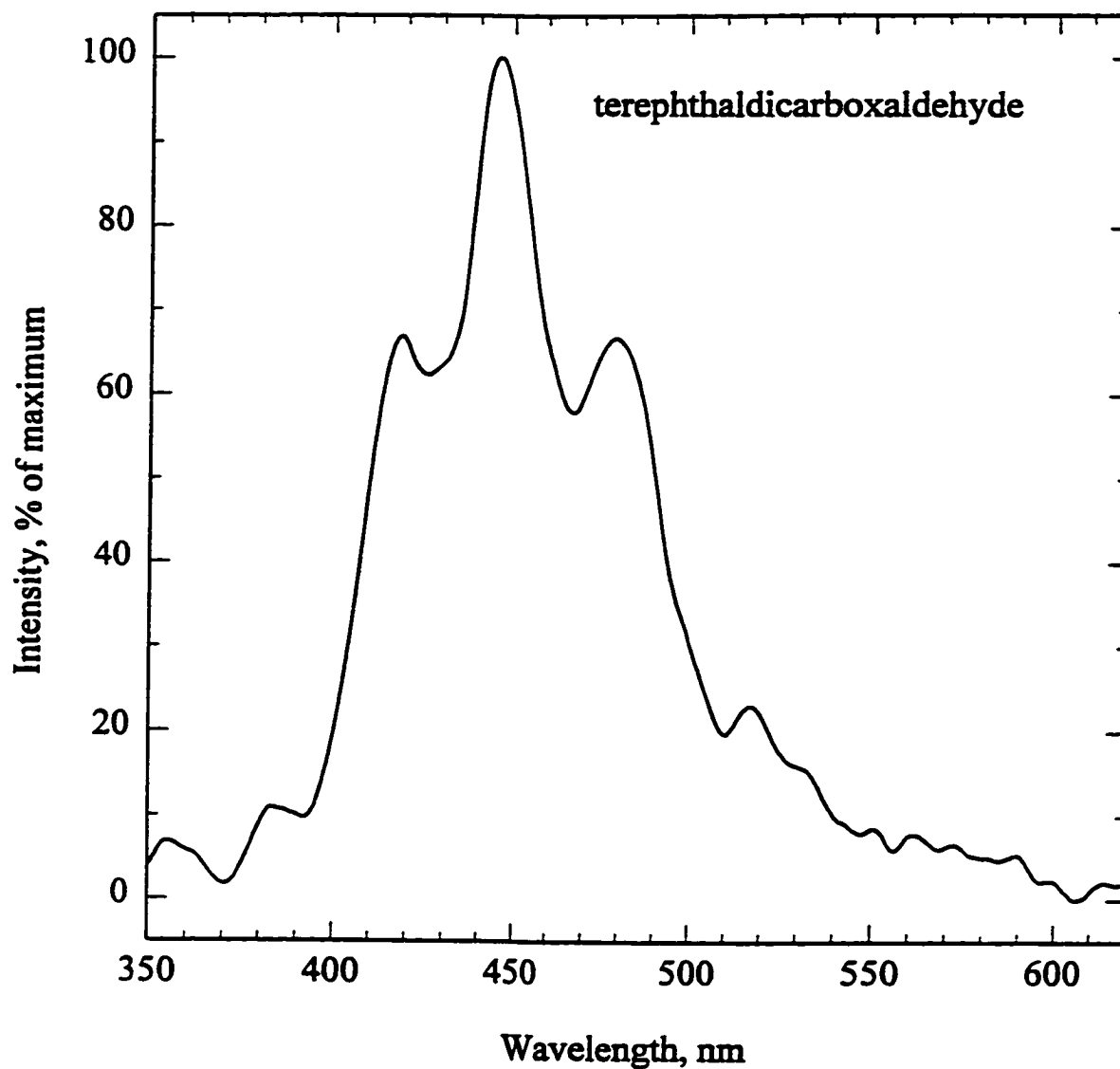
Figure 4.8   Gas-phase luminescence spectrum of terephthaldicarboxaldehyde in excited nitrogen obtained by using 1/8 meter grating monochromator, R-374 PMT and single-peak mode. Bandpass: 6.6 nm.

Figure 4.9   Gas-phase luminescence spectrum of 3-methylbenzaldehyde in excited nitrogen obtained by using 1/8 meter grating monochromator, R-374 PMT and single-peak mode. Bandpass: 6.6 nm.

Figure 4.10 Gas-phase luminescence spectrum of 4-methylbenzaldehyde in excited nitrogen obtained by using 1/8 meter grating monochromator, R-374 PMT and single-peak mode. Bandpass: 6.6 nm.

Figure 4.11 Gas-phase luminescence spectrum of 4-ethylbenzaldehyde in excited nitrogen obtained by using 1/8 meter grating monochromator, R-374 PMT and single-peak mode. Bandpass: 6.6 nm.

Figure 4.12   Gas-phase luminescence spectrum of 4-isopropylbenzaldehyde in excited nitrogen obtained by using 1/8 meter grating monochromator, R-374 PMT and single-peak mode. Bandpass: 6.6 nm.

Figure 4.13 Gas-phase luminescence spectrum of 2-fluorobenzaldehyde in excited nitrogen obtained by using 1/8 meter grating monochromator, R-374 PMT and single-peak mode. Bandpass: 6.6 nm.

Figure 4.14   Gas-phase luminescence spectrum of 3-fluorobenzaldehyde in excited nitrogen obtained by using 1/8 meter grating monochromator, R-374 PMT and single-peak mode. Bandpass: 6.6 nm.
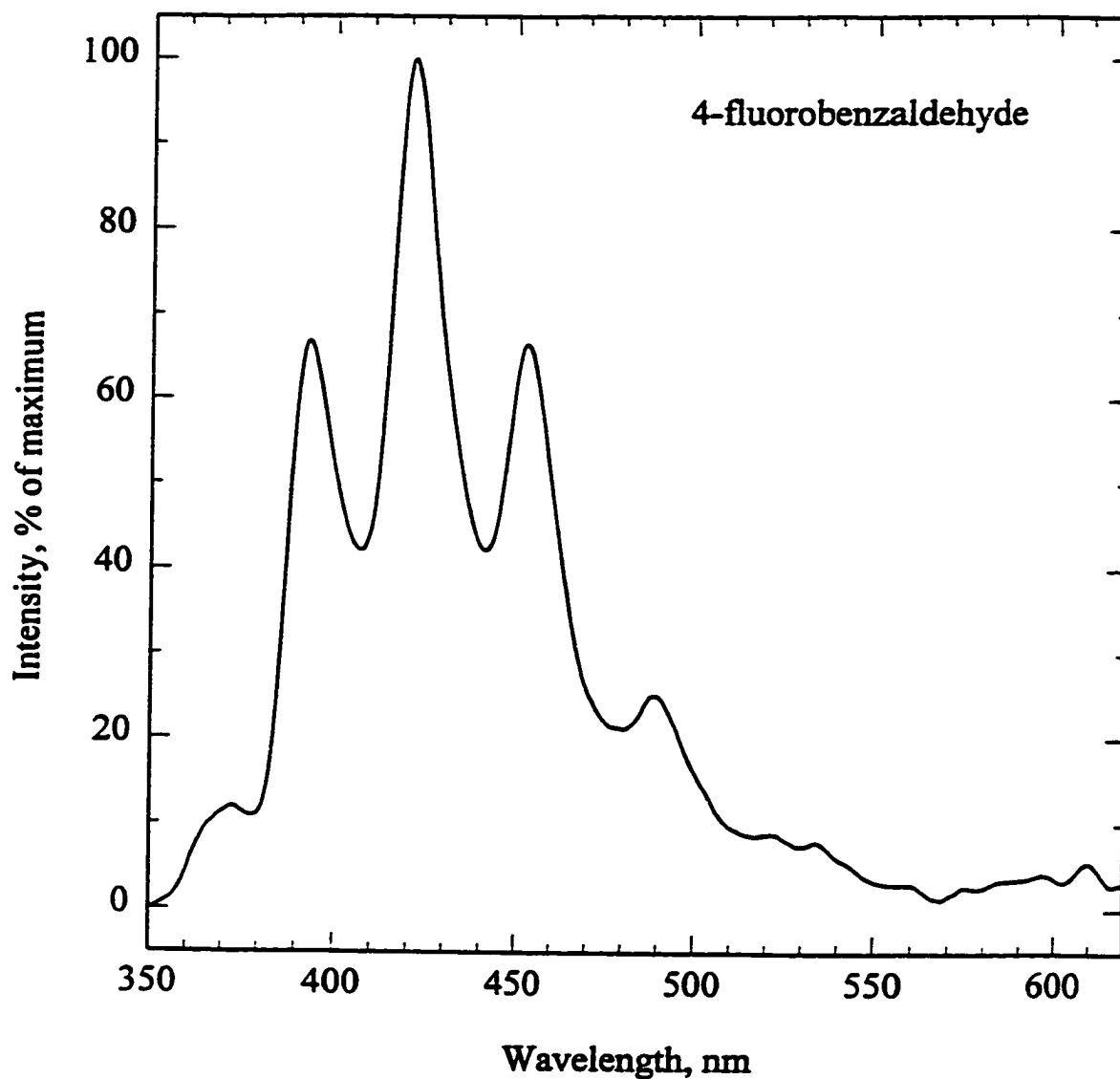
Figure 4.15 Gas-phase luminescence spectrum of 4-fluorobenzaldehyde in excited nitrogen obtained by using 1/8 meter grating monochromator, R-374 PMT and single-peak mode. Bandpass: 6.6 nm.
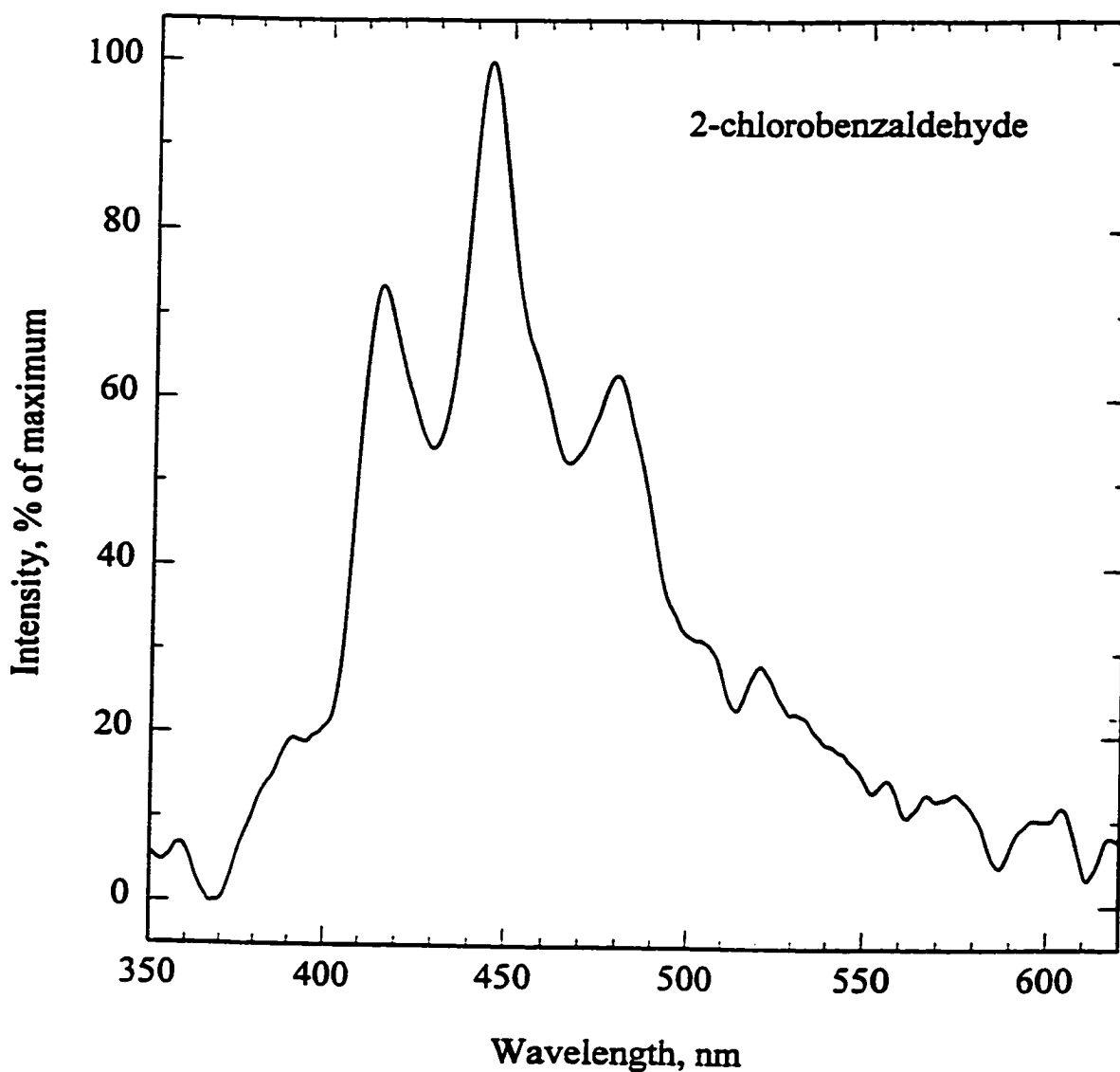
Figure 4.16 Gas-phase luminescence spectrum of 2-chlorobenzaldehyde in excited nitrogen obtained by using 1/8 meter grating monochromator, R-374 PMT and single-peak mode. Bandpass: 6.6 nm.
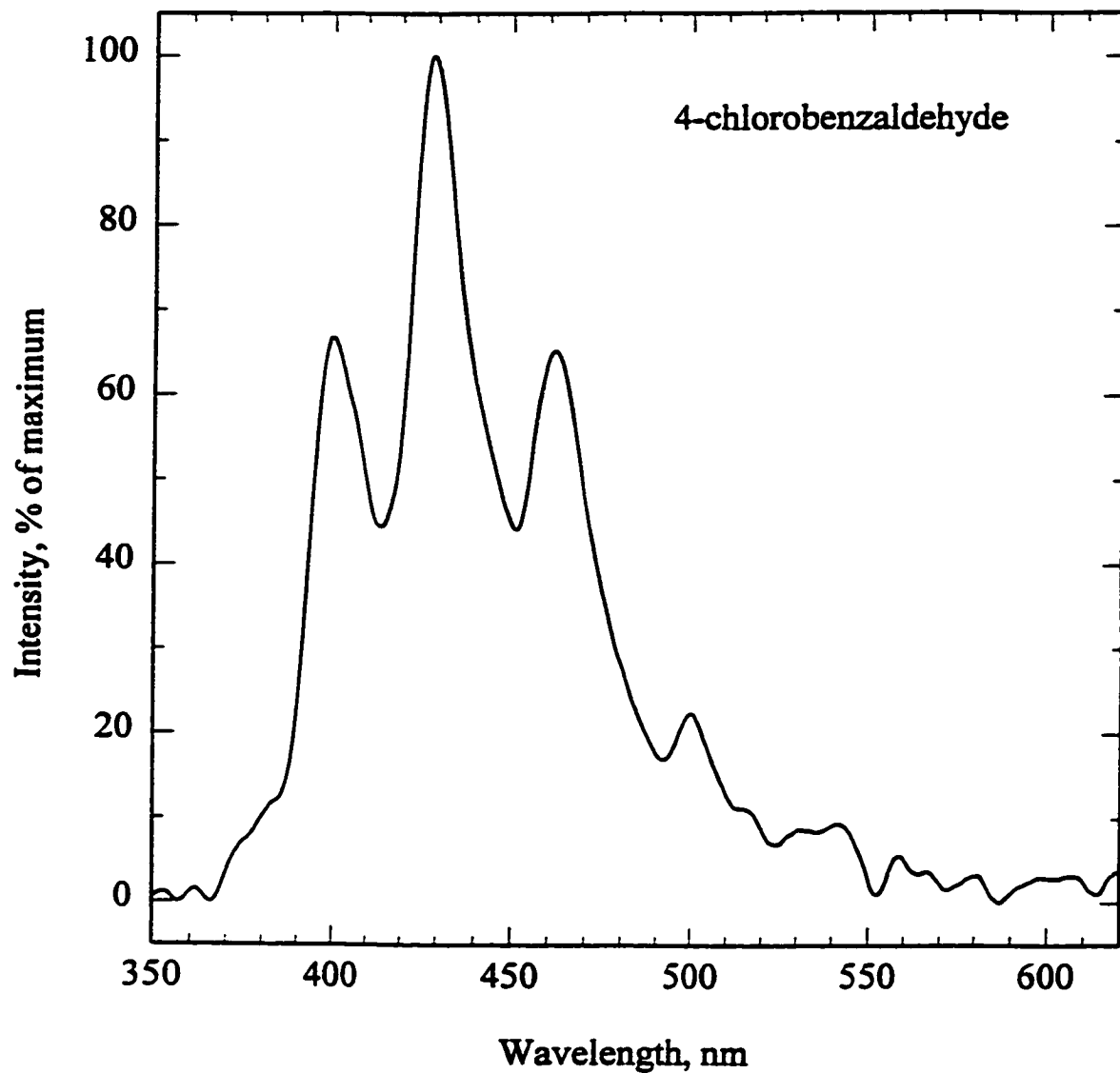
Figure 4.17 Gas-phase luminescence spectrum of 4-chlorobenzaldehyde in excited nitrogen obtained by using 1/8 meter grating monochromator, R-374 PMT and single-peak mode. Bandpass: 6.6 nm.
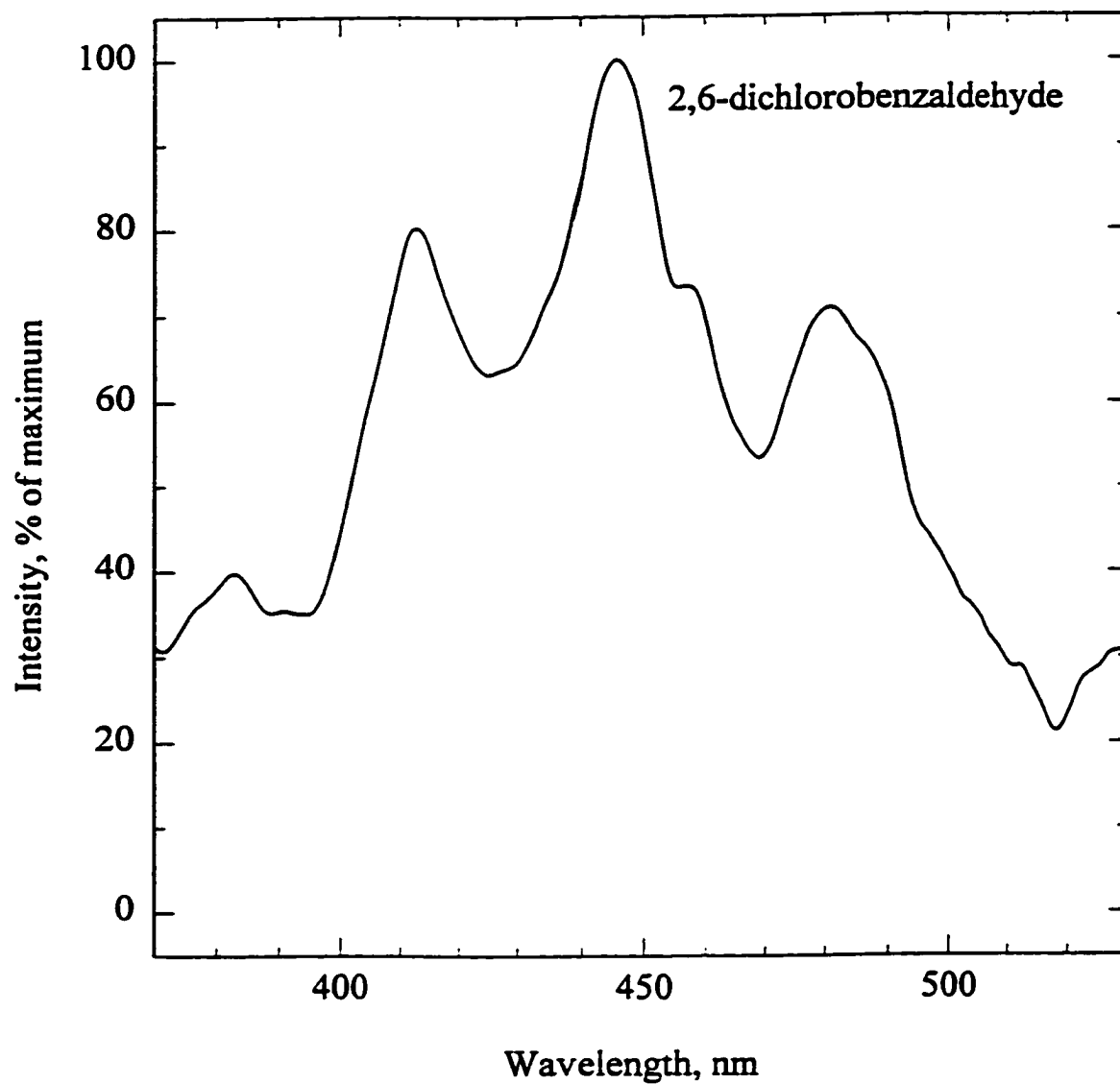
Figure 4.18   Gas-phase luminescence spectrum of 2,6-dichlorobenzaldehyde in excited nitrogen obtained by using 1/8 meter grating monochromator, R-374 PMT and single-peak mode. Bandpass: 12.6 nm. Ar flow doped into nitrogen: 100 mL/min.
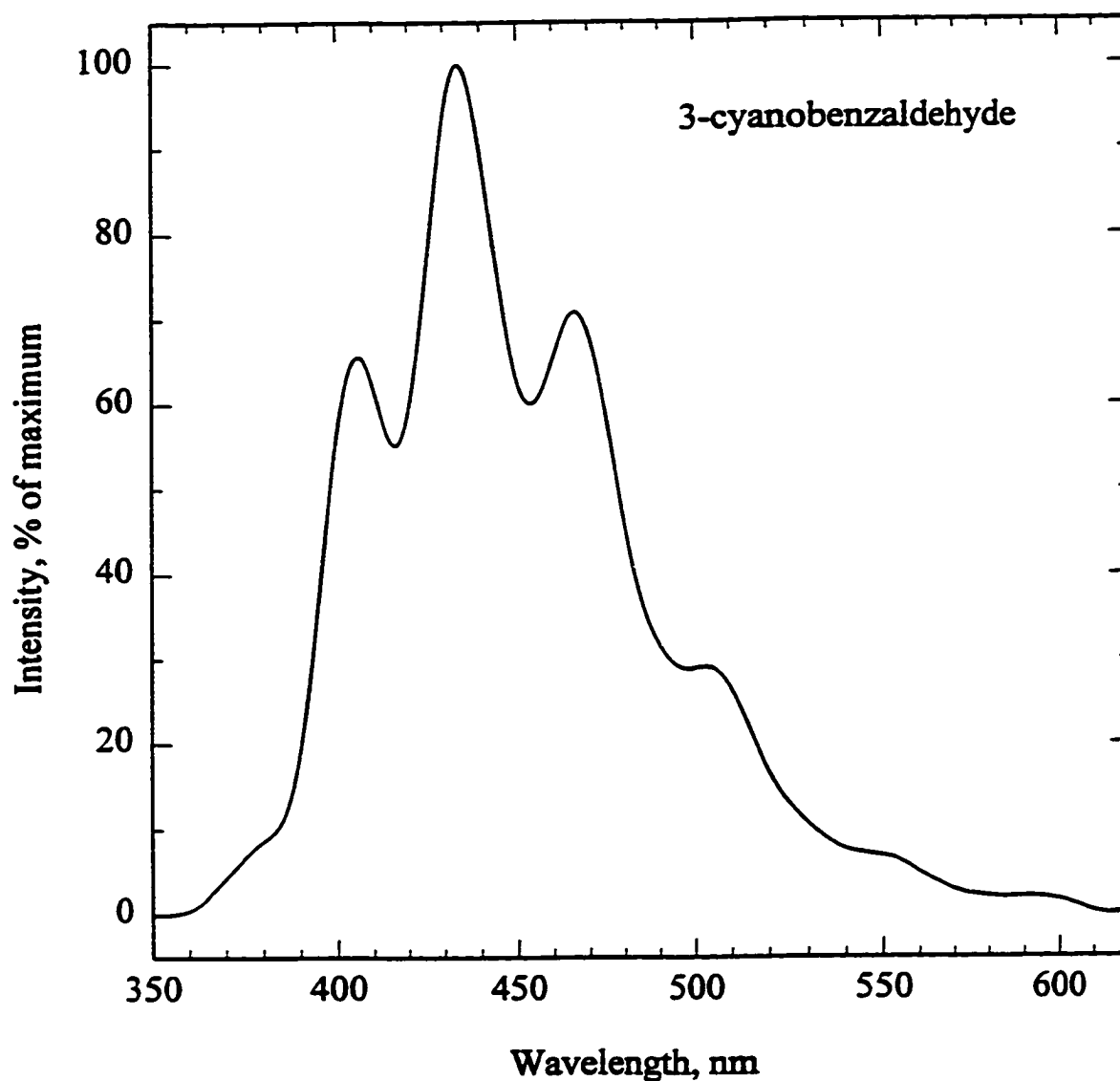
Figure 4.19 Gas-phase luminescence spectrum of 3-cyanobenzaldehyde in excited nitrogen obtained by using 1/8 meter grating monochromator, R-374 PMT and single-peak mode. Bandpass: 12.6 nm.
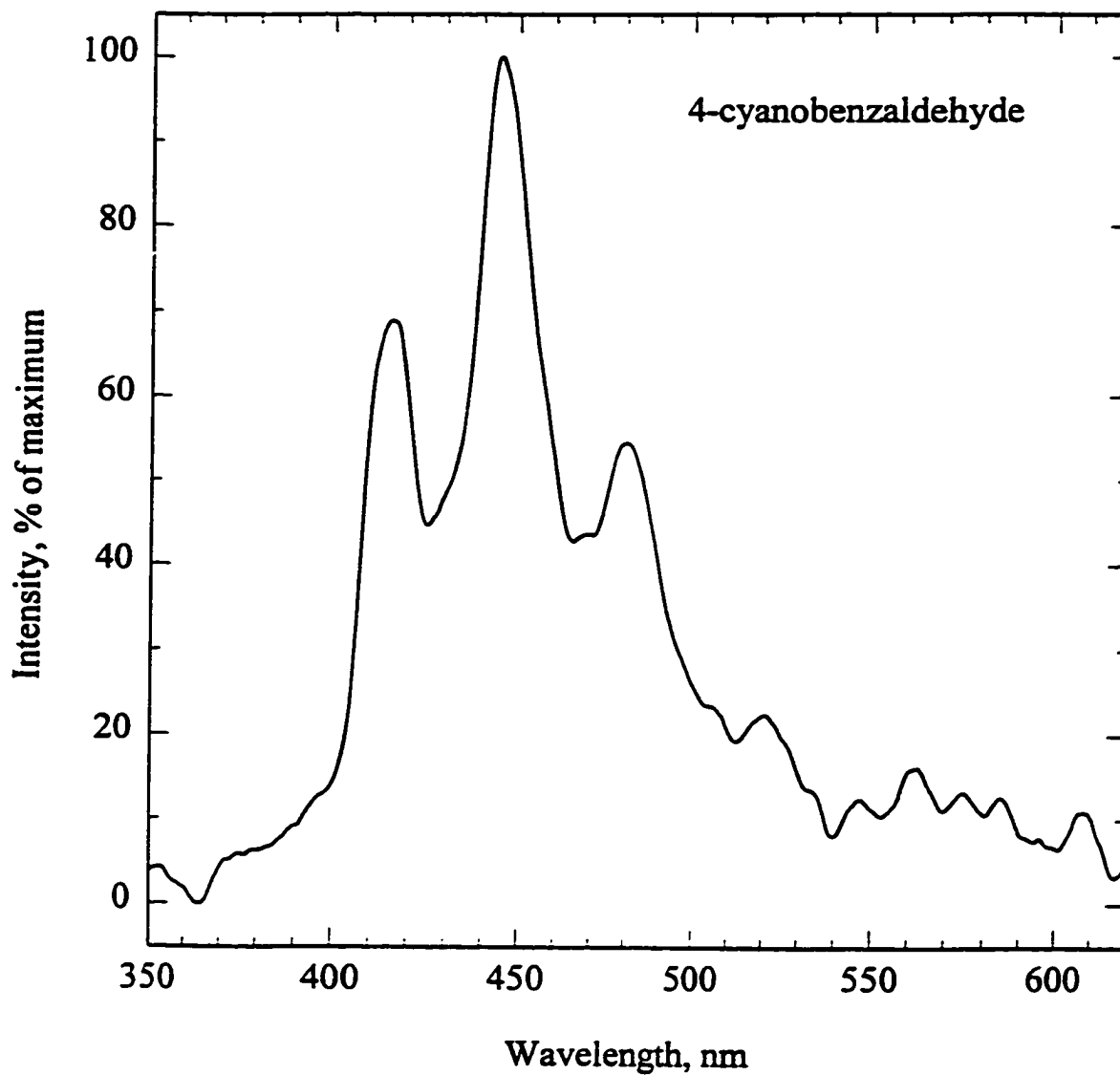
Figure 4.20 Gas-phase luminescence spectrum of 4-cyanobenzaldehyde in excited nitrogen obtained by using 1/8 meter grating monochromator, R-374 PMT and single-peak mode. Bandpass: 6.6 nm.
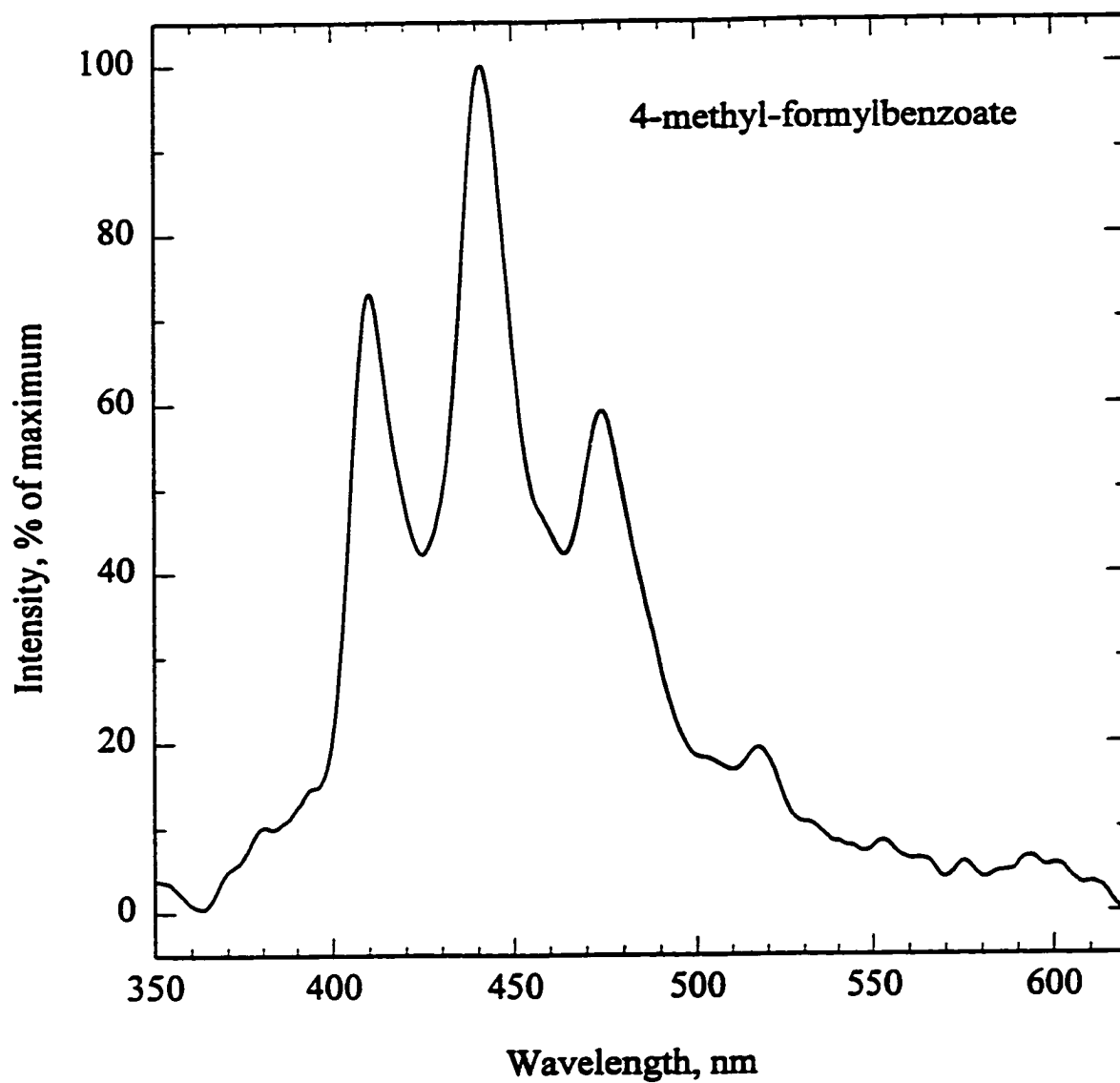
Figure 4.21   Gas-phase luminescence spectrum of 4-methyl-formylbenzoate in excited nitrogen obtained by using 1/8 meter grating monochromator, R-374 PMT and single-peak mode. Bandpass: 6.6 nm.
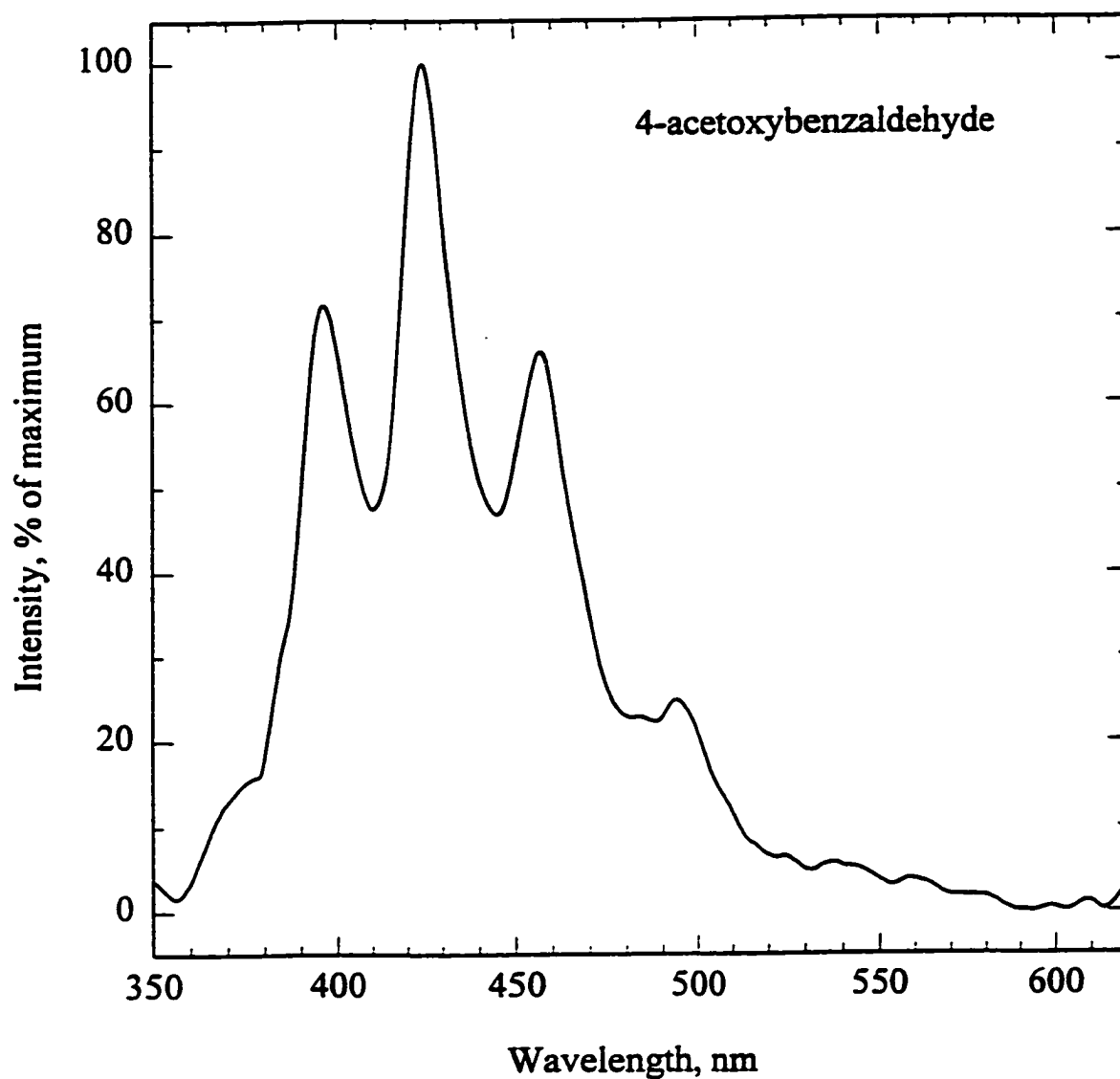
Figure 4.22   Gas-phase luminescence spectrum of 4-acetoxybenzaldehyde in excited nitrogen obtained by using 1/8 meter grating monochromator, R-374 PMT and single-peak mode. Bandpass: 6.6 nm.
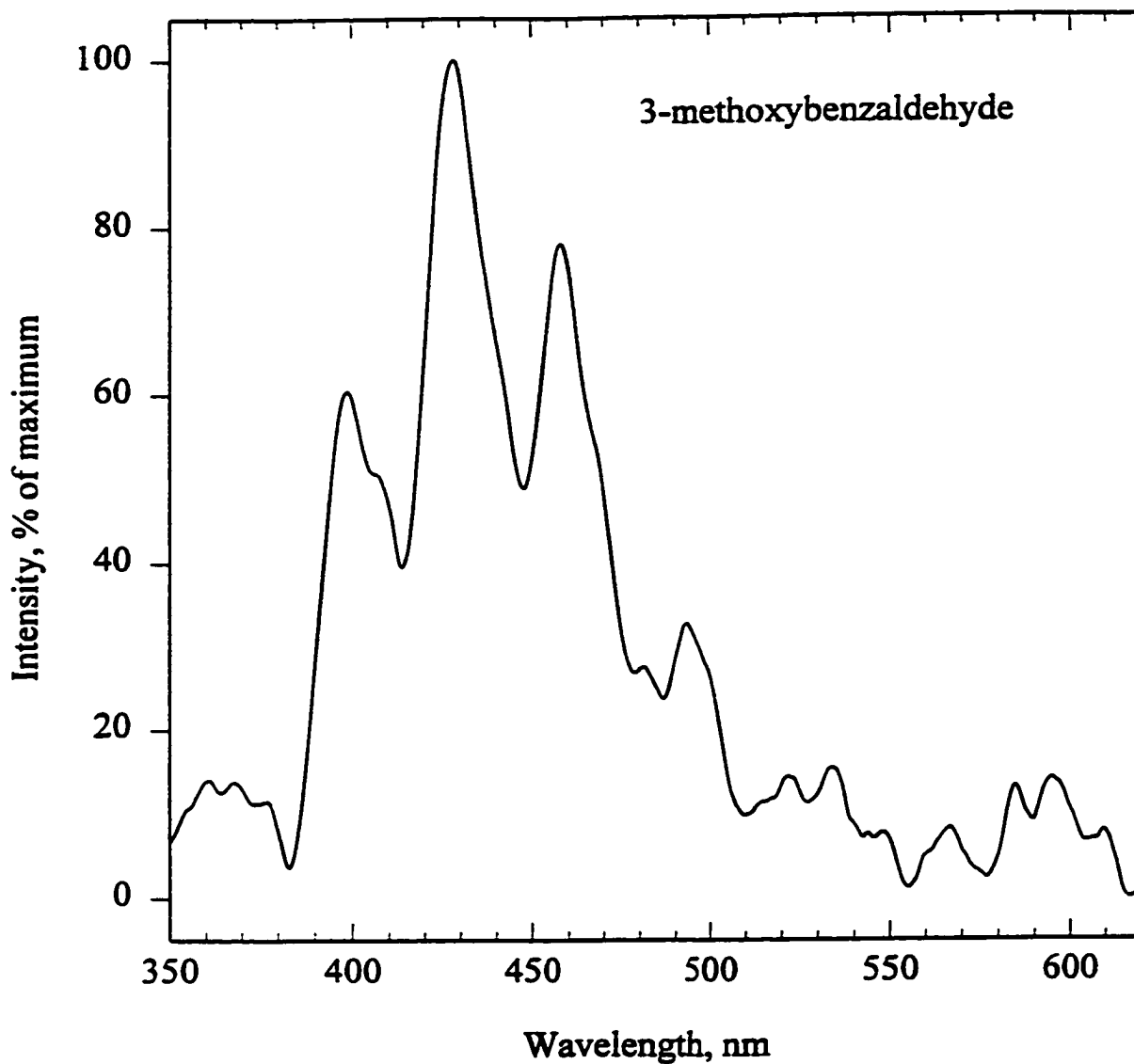
Figure 4.23 Gas-phase luminescence spectrum of 3-methoxybenzaldehyde in excited nitrogen obtained by using 1/8 meter grating monochromator, R-374 PMT and single-peak mode. Bandpass: 6.6 nm. Note: the features above ca 500 nm are due to noise.
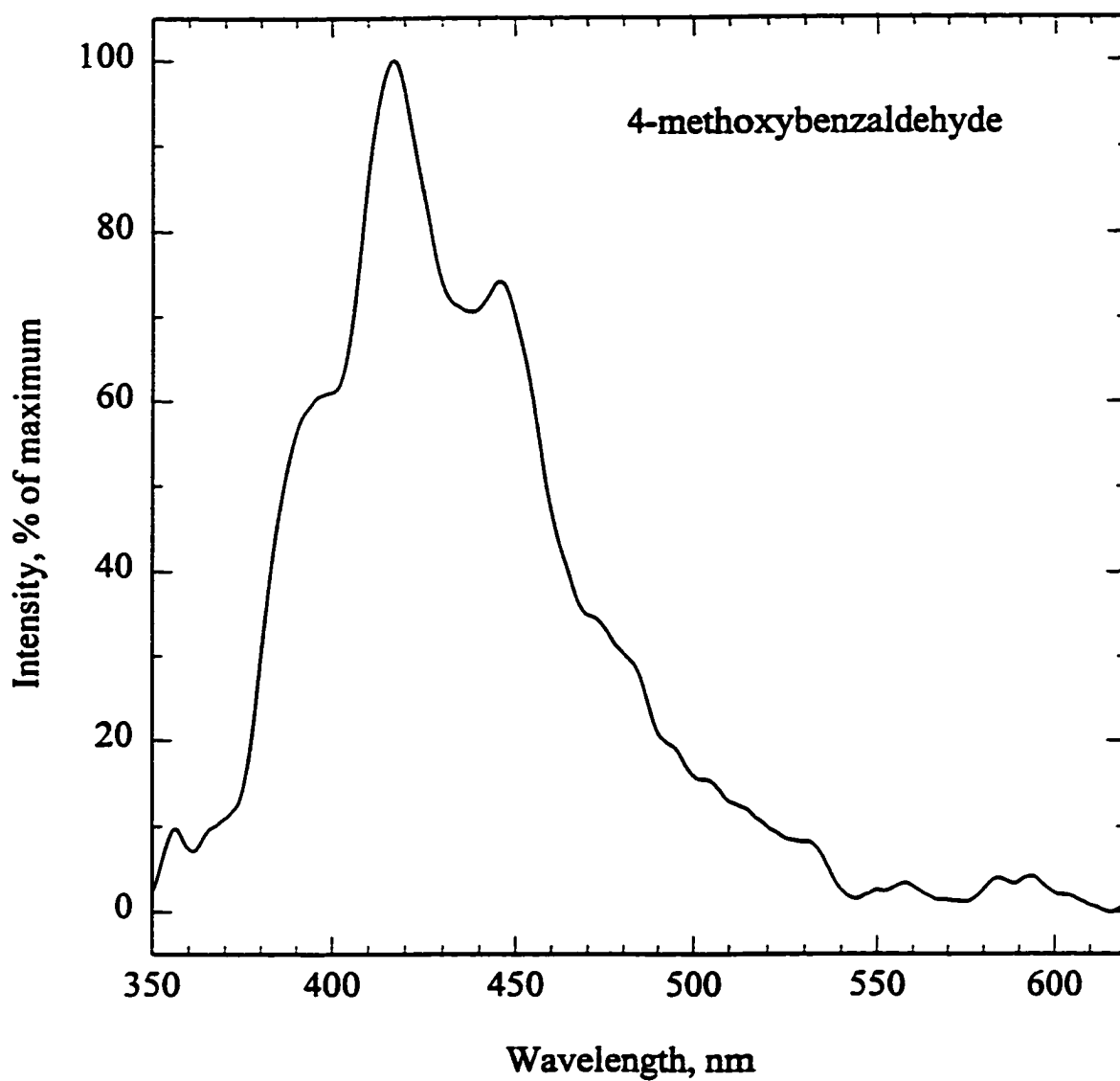
Figure 4.24 Gas-phase luminescence spectrum of 4-methoxybenzaldehyde in excited nitrogen obtained by using 1/8 meter grating monochromator, R-374 PMT and single-peak mode. Bandpass: 12.6 nm. Ar flow doped into nitrogen: 100 mL/min.
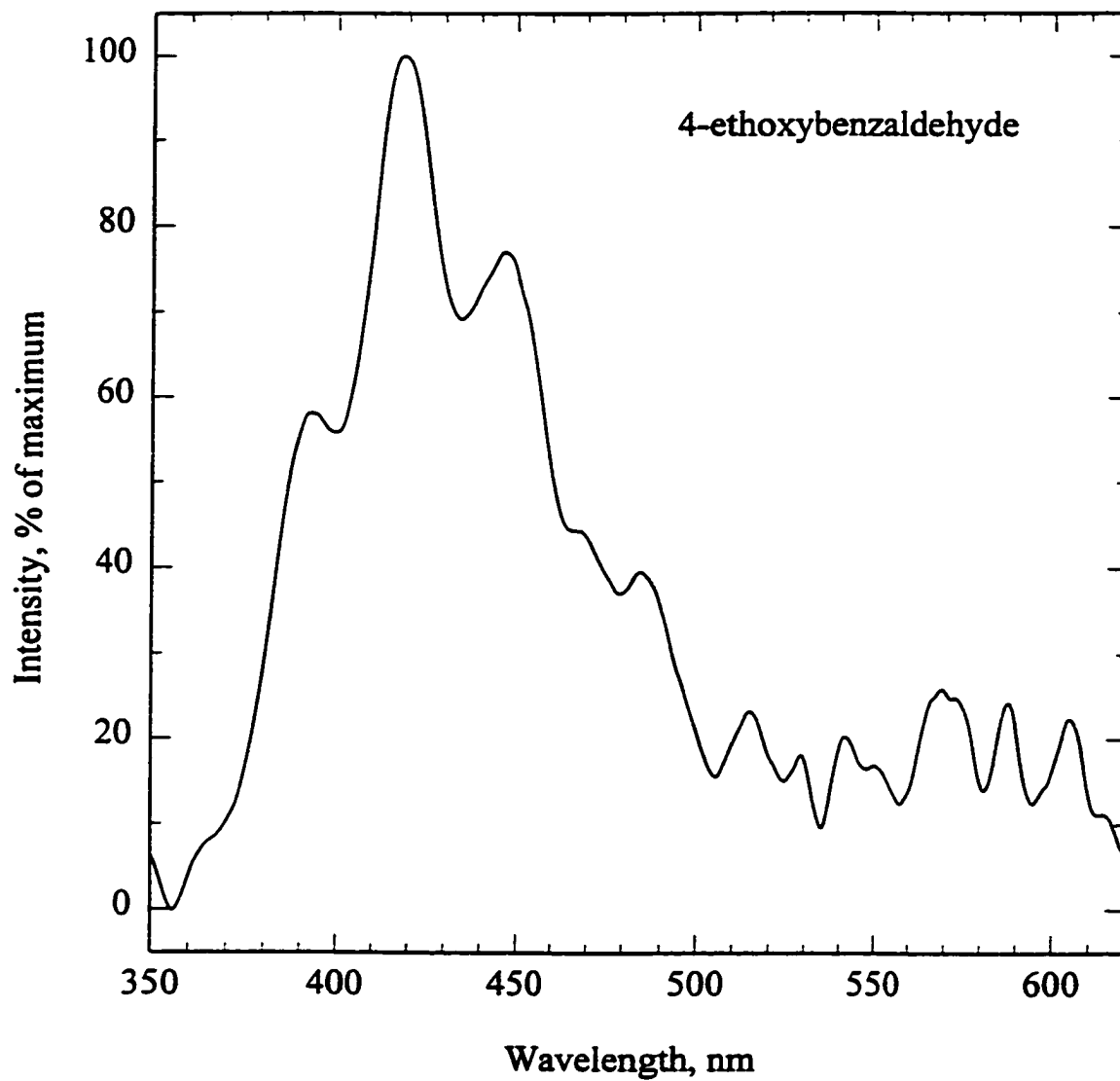
Figure 4.25 Gas-phase luminescence spectrum of 4-ethoxybenzaldehyde in excited nitrogen obtained by using 1/8 meter grating monochromator, R-374 PMT and single-peak mode. Bandpass: 12.6 nm. Ar flow doped into nitrogen: 100 mL/min. Note: the features above 500 nm are due to noise.

transition exhibits a large blue shift relative to benzaldehyde, and the 2- and 3-fluorobenzaldehydes show a red shift. This observation agrees with previously reported results (78, 83). From the substituent effect on the energy of the transitions, information

Table 4.2 Spectral Characteristics of Benzaldehyde and Some Substituted Benzaldehydes

Compound	Origin of T_1 $(n,\pi^*) \rightarrow$ S_0 transition, cm^{-1}	Substituent shifts of T_1 $(n,\pi^*) \rightarrow S_0$ [a], cm^{-1}	Type of lowest triplet
Benzaldehyde	25189 (397 nm)	0	n,π^*
Isophthalaldehyde	24876 (402 nm)	+313	n,π^*
Terephthal-dicarboxaldehyde	23866 (419 nm)	+1323	n,π^*
3-Methylbenzaldehyde	25126 (398 nm)	+63	n,π^*
4- Methylbenzaldehyde	25316 (395 nm)	-127	n,π^*
4-Ethylbenzaldehyde	25253 (396 nm)	-64	n,π^*
4-Isopropylbenzaldehyde	25253 (396 nm)	-64	n,π^*
2-Fluorobenzaldehyde	24510 (408 nm)	+679	n,π^*
3-Fluorobenzaldehyde	24876 (402 nm)	+313	n,π^*
4-Fluorobenzaldehyde	25381 (394 nm)	-192	n,π^*
2-Chlorobenzaldehyde	24038 (416 nm)	+1151	n,π^*
4-Chlorobenzaldehyde	25000 (400 nm)	+189	n,π^*
2,6-Dichlorobenzaldehyde	24213 (413 nm)	+976	n,π^*
3-Cyanobenzaldehyde	24631 (406 nm)	+558	n,π^*
4-Cyanobenzaldehyde	24096 (415 nm)	+1093	n,π^*
4-Acetoxybenzaldehyde	25253 (396 nm)	-64	n,π^*
3-Methoxybenzaldehyde	25000 (400 nm)	+189	n,π^*
4-Methoxybenzaldehyde	25381 (394 nm)	-192	n,π^*
4-Ethoxybenzaldehyde	25445 (393 nm)	-256	n,π^*
Methyl 4-formylbenzoate	24390 (410 nm)	+799	n,π^*
Ethyl 4-formylbenzoate	24390 (410 nm)	+799	n,π^*
2-Chloroethyl 4-formylbenzoate	24390 (410 nm)	+799	n,π^*
2,2,2-Trifluoroethyl 4-formylbenzoate	24390 (410 nm)	+799	n,π^*
Heptyl 4-formylbenzoate	24509 (408 nm)	+680	n,π^*

[a] the + and- signs indicate red and blue shifts, respectively.

concerning the variations of electron distributions accompanying electronic excitation and the nature of their low-lying triplet state can be gained (see section 4.4).

Figure 4.26 shows the gas-phase phosphorescence spectra at different temperatures. The spectra displayed the same shape and no spectral shift was observed with the variation of temperature. This means that the spectroscopic nature of benzaldehyde luminescence does not change as the temperature changes (i.e. that the thermal activation is not involved). The emission intensity of phosphorescence increased slightly as temperature increased, but the vibrational structure of the phosphorescence spectrum became more diffuse. This observation is in agreement with the results of photophysical studies of other aroyl compounds in the gas phase (84, 85), however, the results are inconsistent with those observed in rigid media (86, 87).

4.3.2 Acetophenones

Acetophenone is the simplest aromatic ketone and has long been the subject of spectroscopic and photophysical studies (67, 81, 87-91). However, ambiguity remains concerning the assignment of the lowest triplet state of acetophenone and substituted acetophenones in various environments (90, 92). The gas-phase luminescence spectra of acetophenone and some substituted acetophenones in excited nitrogen are shown in Figures 4.27-4.35. A severe loss of resolution is observed in these spectra compared to those of the benzaldehydes because the low frequency of torsional vibrations of the methyl group results in spectral congestion (91). The spectrum of acetophenone measured in this study exhibits prominent peaks at 394, 420, and 450 nm, respectively, and shows a
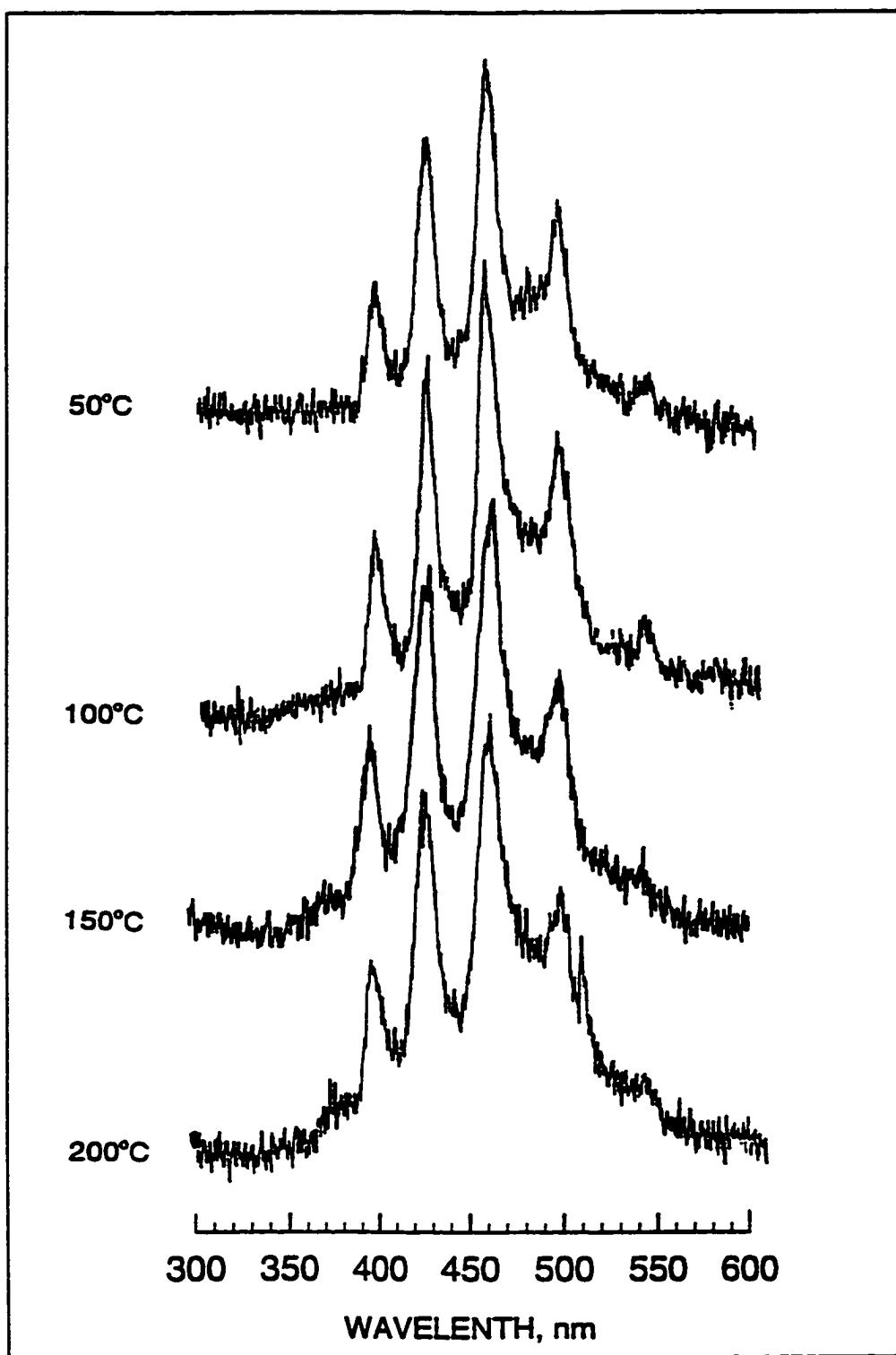
Figure 4.26 Gas-phase luminescence spectra of benzaldehyde in excited nitrogen at different temperatures obtained by using 1/4 meter grating monochromator, R-374 PMT and continuous doping mode. Bandpass: 6.6 nm.
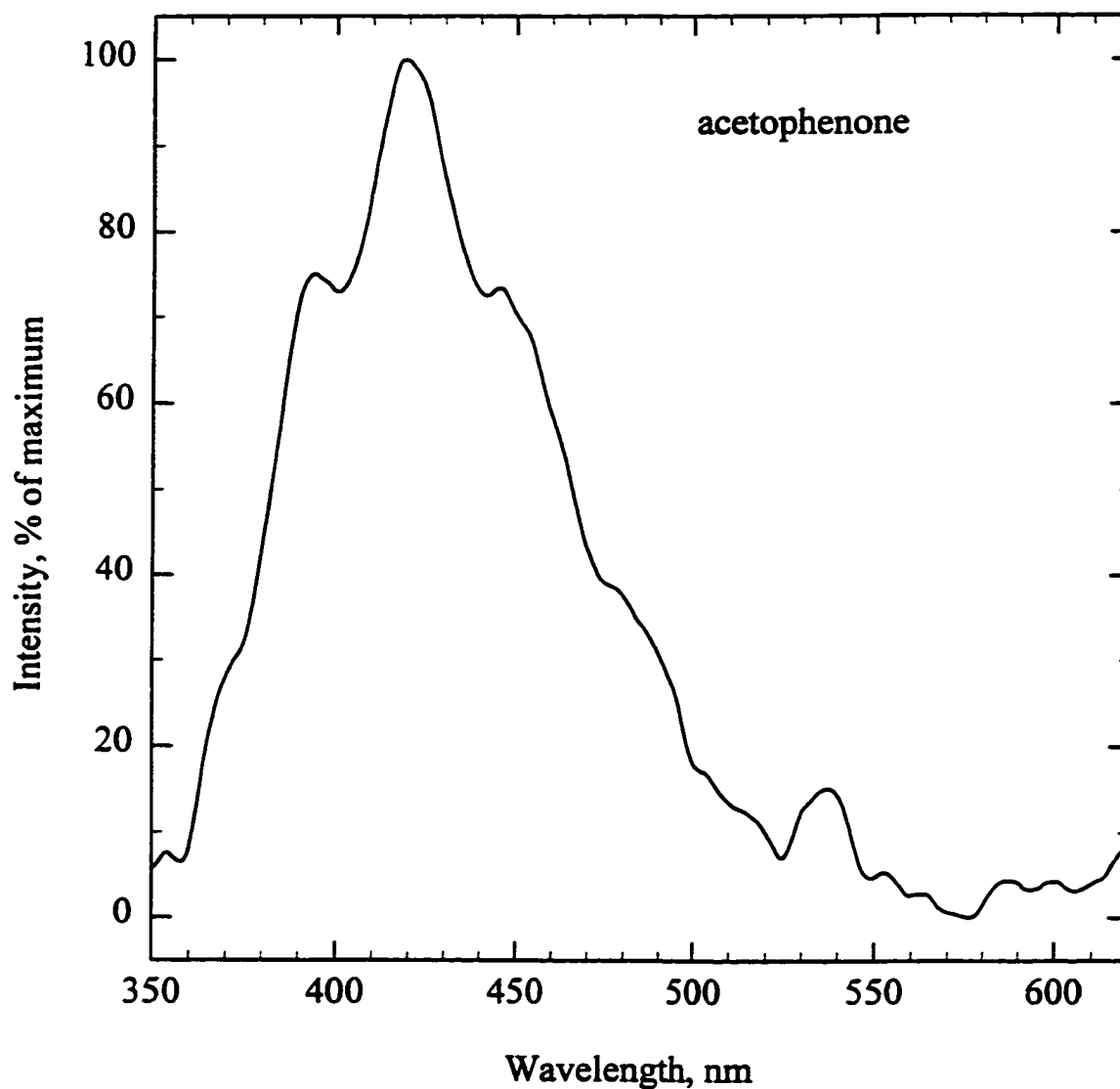
Figure 4.27   Gas-phase luminescence spectrum of acetophenone in excited nitrogen obtained by using 1/8 meter grating monochromator, R-374 PMT and single-peak mode. Bandpass: 6.6 nm. The hump at ca 540 nm is due to noise.
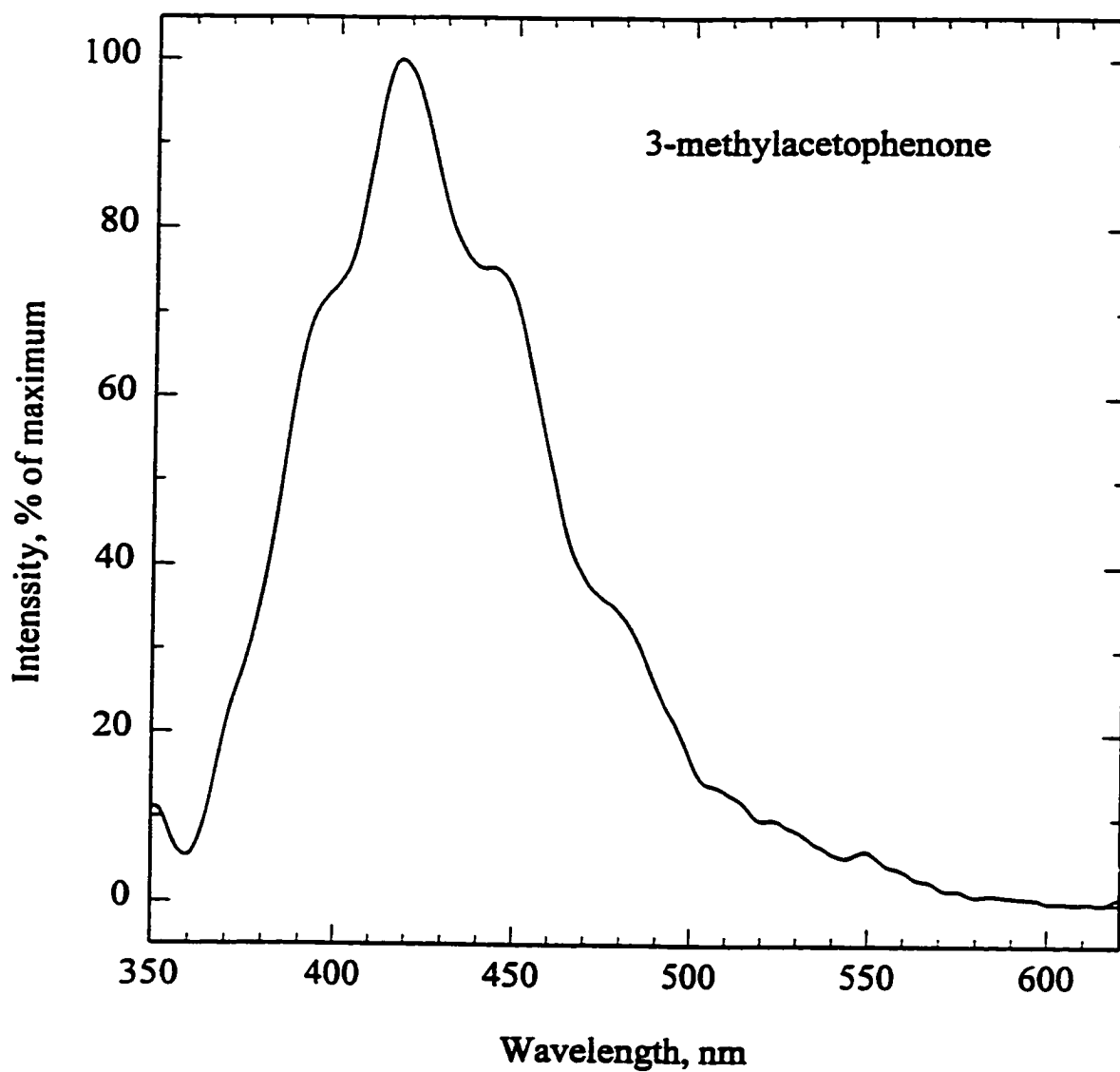
Figure 4.28   Gas-phase luminescence spectrum of 3-methylacetophenone in excited nitrogen obtained by using 1/8 meter grating monochromator, R-374 PMT and single-peak mode. Bandpass: 12.6 nm.
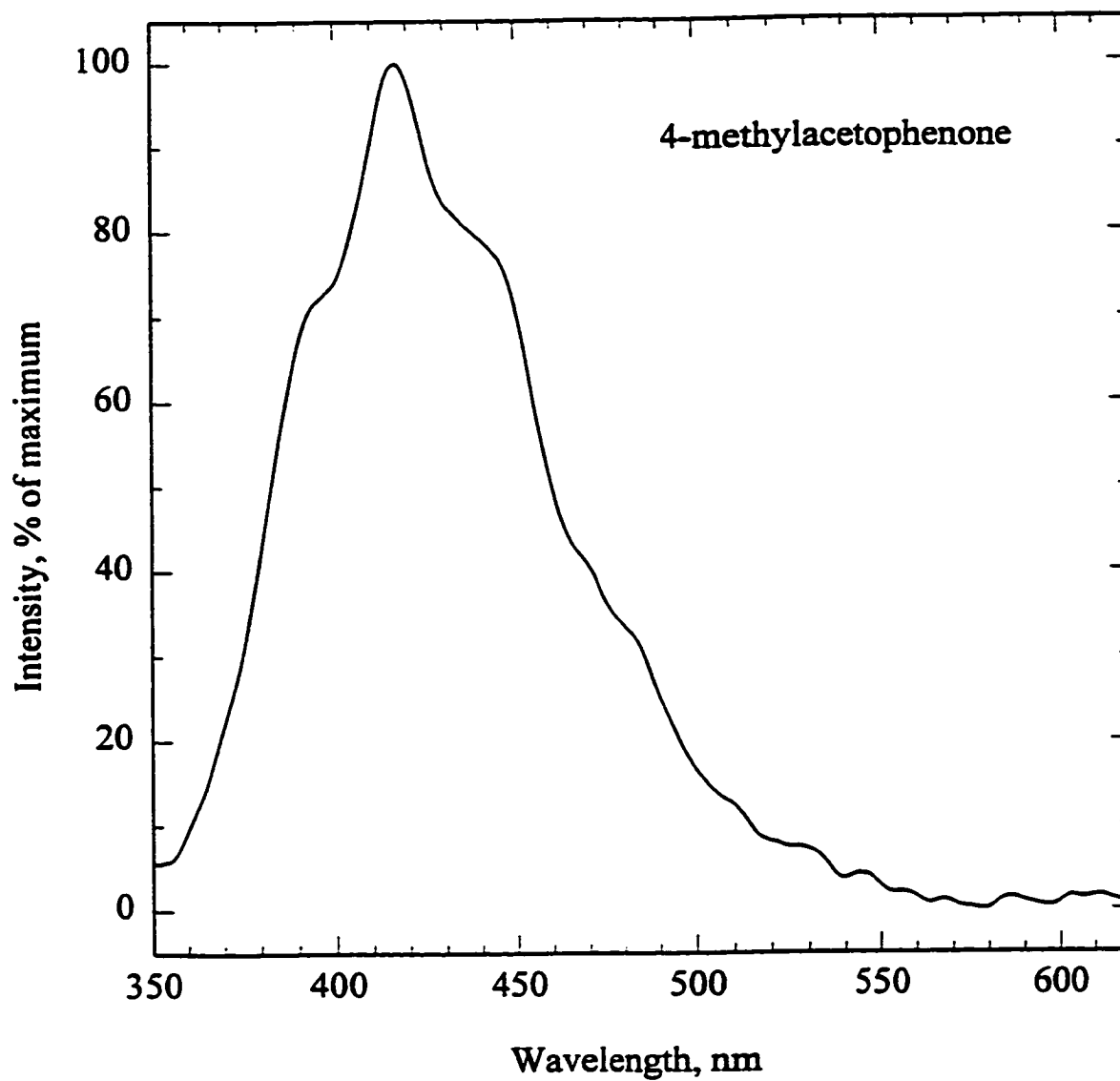
Figure 4.29 Gas-phase luminescence spectrum of 4-methylacetophenone in excited nitrogen obtained by using 1/8 meter grating monochromator, R-374 PMT and single-peak mode. Bandpass: 12.6 nm.

Figure 4.30   Gas-phase luminescence spectrum of 4-fluoroacetophenone in excited nitrogen obtained by using 1/8 meter grating monochromator, R-374 PMT and single-peak mode. Bandpass: 12.6 nm.

Figure 4.31   Gas-phase luminescence spectrum of 3-acetylbenzonitrile in excited nitrogen obtained by using 1/8 meter grating monochromator, R-374 PMT and single-peak mode. Bandpass: 12.6 nm.
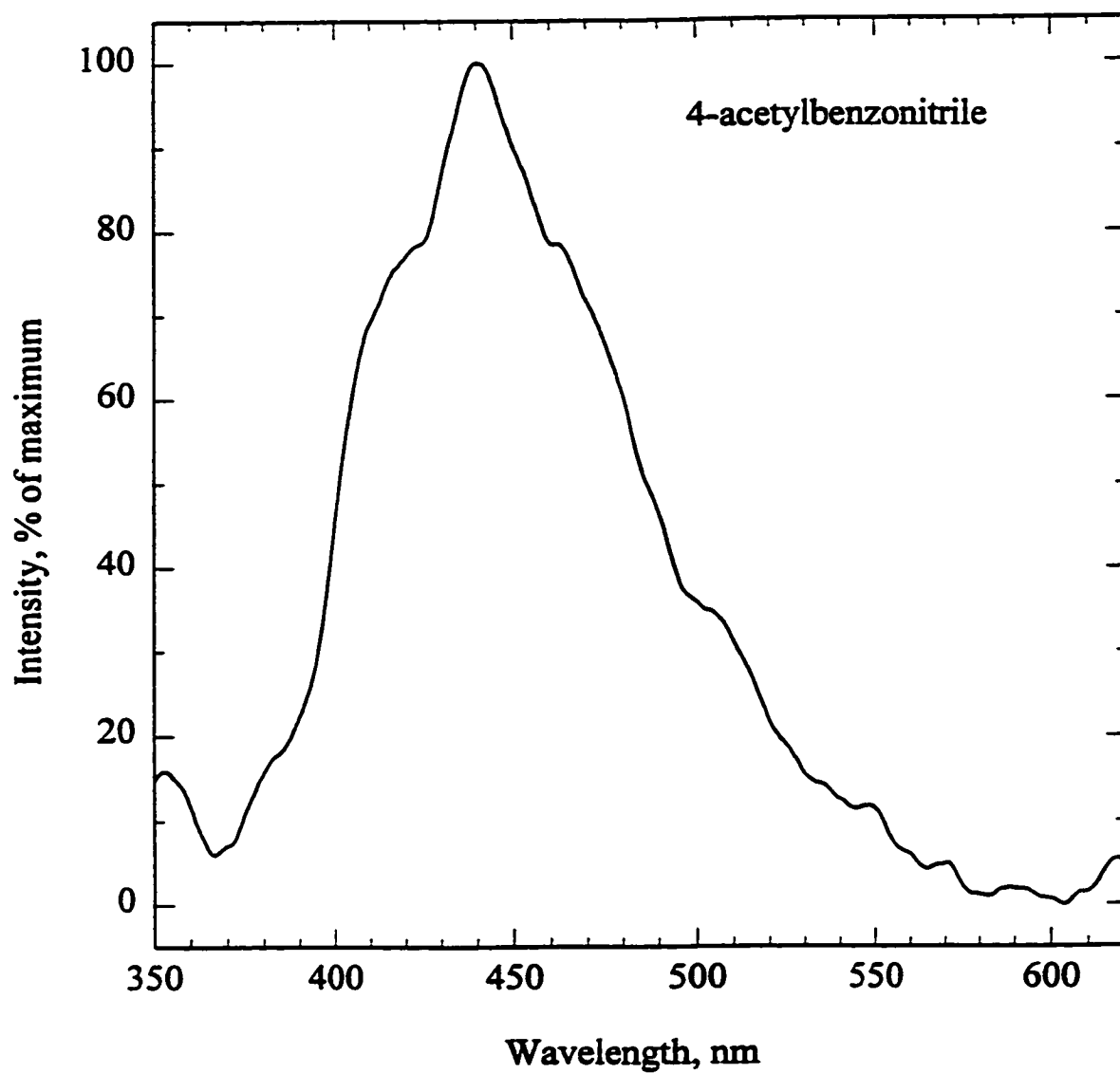
Figure 4.32   Gas-phase luminescence spectrum of 4-acetylbenzonitrile in excited nitrogen obtained by using 1/8 meter grating monochromator, R-374 PMT and single-peak mode. Bandpass: 12.6 nm.
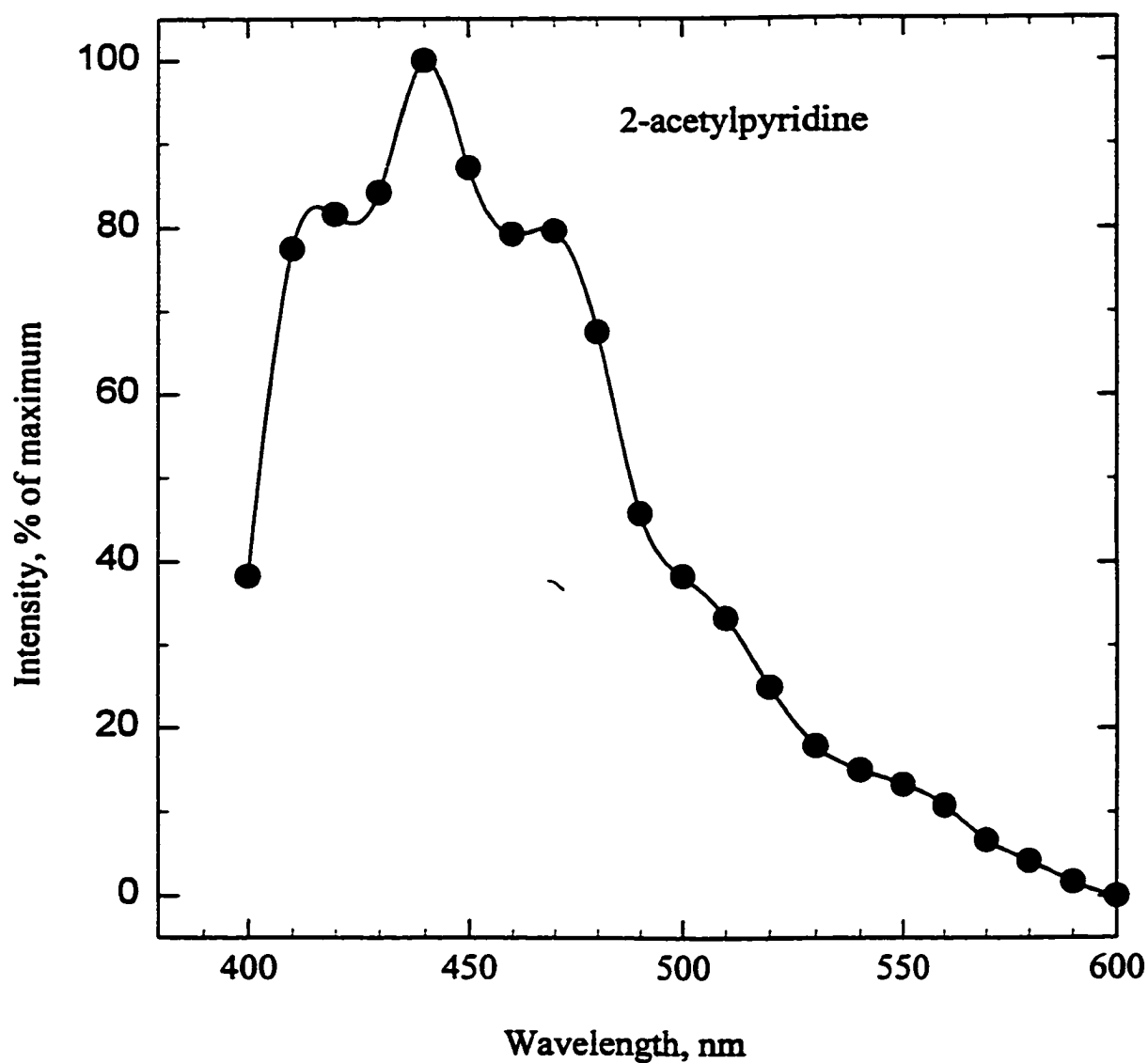
Figure 4.33   Gas-phase luminescence spectrum of 2-acetylpyridine in excited nitrogen obtained by using a filter monochromator, R-268 PMT and repeated injection mode. 2 mm slit (corresponding to a 13 nm bandpass at 400 nm).
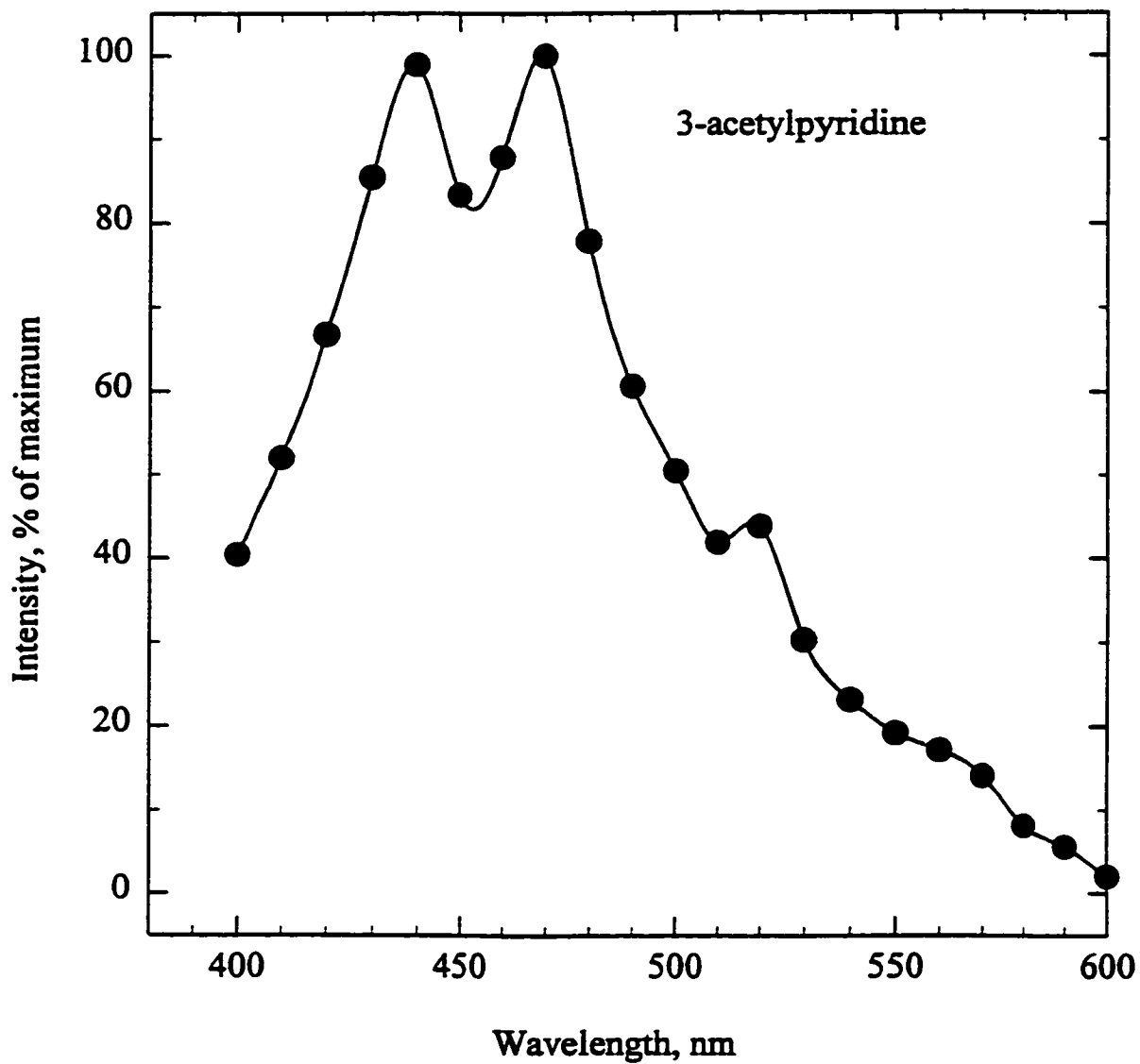
Figure 4.34   Gas-phase luminescence spectrum of 3-acetylpyridine in excited nitrogen obtained by using a filter monochromator, R-268 PMT and repeated injection mode. 2 mm slit (corresponding to a 13 nm bandpass at 400 nm).
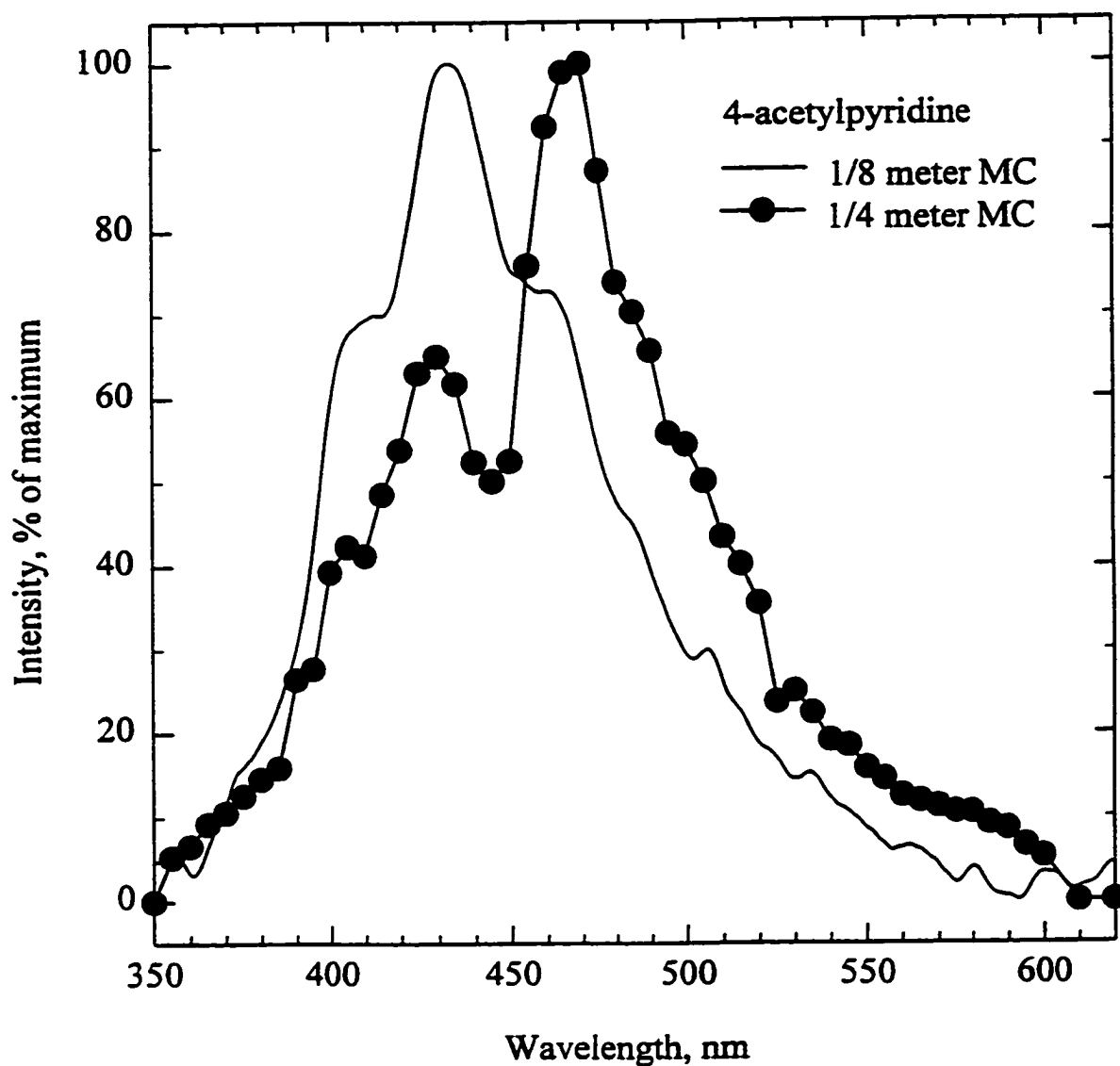
Figure 4.35 Gas-phase luminescence spectrum of 4-acetylpyridine in excited nitrogen obtained by using 1/8 meter grating monochromator with single-peak mode and 1/4 meter grating monochromator with repeated injection mode. R-374 PMT; Bandpass: 12.6 nm.

prominent C=O stretching vibrational progression with a frequency of about 1600 cm^{-1}.

This spectrum is very similar in shape to that of acetophenone phosphorescence obtained

in a rigid medium (67), the gas phase (81) and on Whatman No. 1 filter paper (87). Thus,

we conclude that the present gas-phase luminescence spectrum is mainly the

phosphorescence spectrum of acetophenone. The lowest triplet state of acetophenone in

the gas phase is of normal n, π^* character, because it is well known that n,π^*-type

phosphorescence spectra exhibit a clear progression of the carbonyl vibration (59). The

luminescence spectra of the substituted acetophenones were also considered to be

phosphorescence spectra because of their very similar spectral shapes to that of

acetophenone. Table 4.3 shows the spectroscopic data of acetophenone and some

substituted acetophenones.

Table 4.3 Spectral Characteristics of Acetophenone and Some Substituted Acetophenones

Compound	Origin of Phosphorescence, cm^{-1}	Substituent shifts of 0-0 transitions (cm^{-1}) [a]
Acetophenone	25381 (394 nm)	0
3'-Methylacetophenone	25445 (393 nm)	-64
4'-Methylacetophenone	25510 (392 nm)	-129
4'-Fluoroacetophenone	25510 (392 nm)	-129
3-Acetylbenzonitrile	24752 (404 nm)	+629
4-Acetylbenzonitrile	24272 (412 nm)	+1109
2-Acetylpyridine	24154 (414 nm)	+1227
4-Acetylpyridine	24449 (409 nm)	+932

[a] the + and - signs indicate red and blue shifts, respectively.

It is noted that the 0-0 transitions are blue-shifted with electron-donating groups,

and red-shifted with electron-withdrawing groups at the para-position in substituted acetophenones. The direction of shift is parallel between the substituted benzaldehydes and the substituted acetophenones. This similarity also reflects the similar nature of the triplet state which is T (n,π^*) for both substituted benzaldehydes and substituted acetophenones.

4.3.3 Benzophenones

Benzophenone has been investigated extensively as a triplet energy donor (63, 66) and its luminescence in various media was thoroughly studied (66, 67, 69, 70, 81, 87, 93, 94). In early papers, it was reported that benzophenone shows solely phosphorescence with a lowest T_1 (n,π^*) state in the rigid matrix at 77 K (66, 67, 93, 94). Sun and co-workers (84) demonstrated that luminescence of benzophenone in CCl_4 solutions consists mainly of delayed fluorescence and phosphorescence originating from thermally equilibrated S_1 and T_1 states. The observation of the delayed fluorescence of benzophenone in solution (95, 96) and in rigid media (97) was confirmed by other researchers. The valuable technique of gated nanosecond time resolved laser spectroscopy was developed, which can be used for the study of emission processes having low quantum efficiencies and/or several competing modes of emission (96). In the gaseous phase, the luminescence of benzophenone was first reported by Borisevich and co-workers and on the basis of an appreciable overlap of the absorption and emission spectra and long decay time of the emission, it was concluded that the luminescence is thermally activated delayed fluorescence (98). Dorokhin and co-workers (99) reported

the effect of temperature on the delayed luminescence of benzophenone, and it was shown that, as the temperature rises, the fraction of thermally activated delayed fluorescence in the total emission increases, as reported for benzophenone in the condensed phase (84, 97). Itoh and co-workers (81) interpreted the gas-phase emission spectrum of benzophenone as composed mainly of phosphorescence, accompanied by very weak E-type delayed fluorescence at shorter wavelengths. Inoue (69) measured the emission spectrum of benzophenone induced by electron impact, and assigned the spectrum as that of benzophenone phosphorescence with origin at 390 nm (25641 cm^{-1}).

Figure 4.36 shows the gas-phase luminescence spectrum of benzophenone in excited nitrogen. It was found that the spectrum measured from benzophenone vapor in excited nitrogen under that specific condition is very similar in shape to those spectra of benzophenone which are composed mainly of E-type fluorescence and phosphorescence (81, 84, 96, 97), and different from the pure phosphorescence spectra of benzophenone in rigid media (66, 67, 93, 94). Therefore, we concluded that the gas-phase luminescence of benzophenone consists mainly of E-type fluorescence and phosphorescence with origin at about 380 nm (26316 cm^{-1}) and 420 nm (23809 cm^{-1}), respectively. The gas-phase luminescence spectra of some substituted benzophenones are shown in Figures 4.37-4.46. Note that, aside from the strong emission features, noise is apparent in some of these figures, particularly at wavelengths above ca 500-550 nm (e.g. Figures 4.37 and 4.38). These spectra are very similar in shape to that of benzophenone. We also tentatively assign them as the spectra originated from E-type delayed fluorescence and phosphorescence.
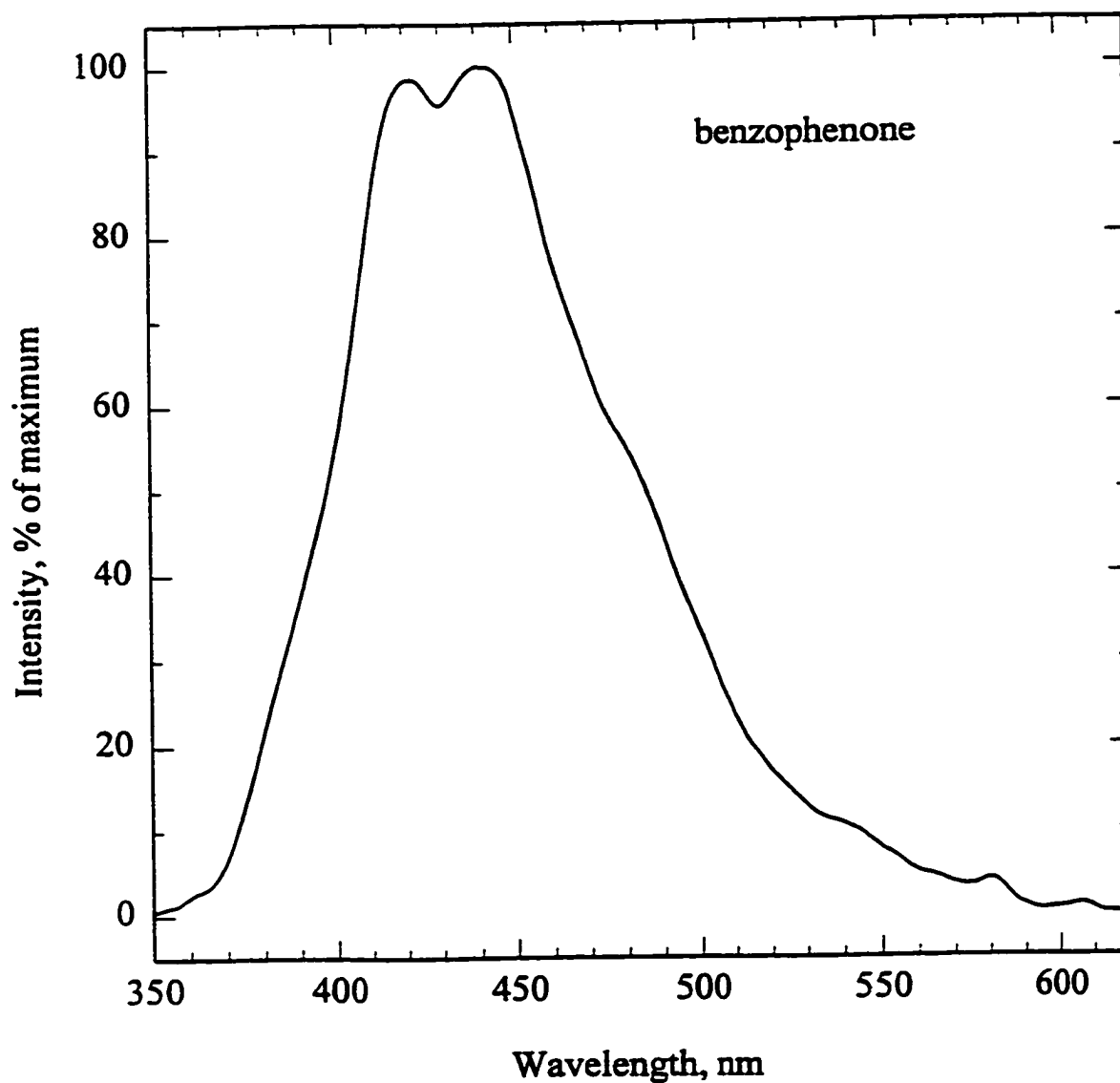
Figure 4.36 Gas-phase luminescence spectrum of benzophenone in excited nitrogen obtained by using 1/8 meter grating monochromator, R-374 PMT and single-peak mode. Bandpass: 12.6 nm.
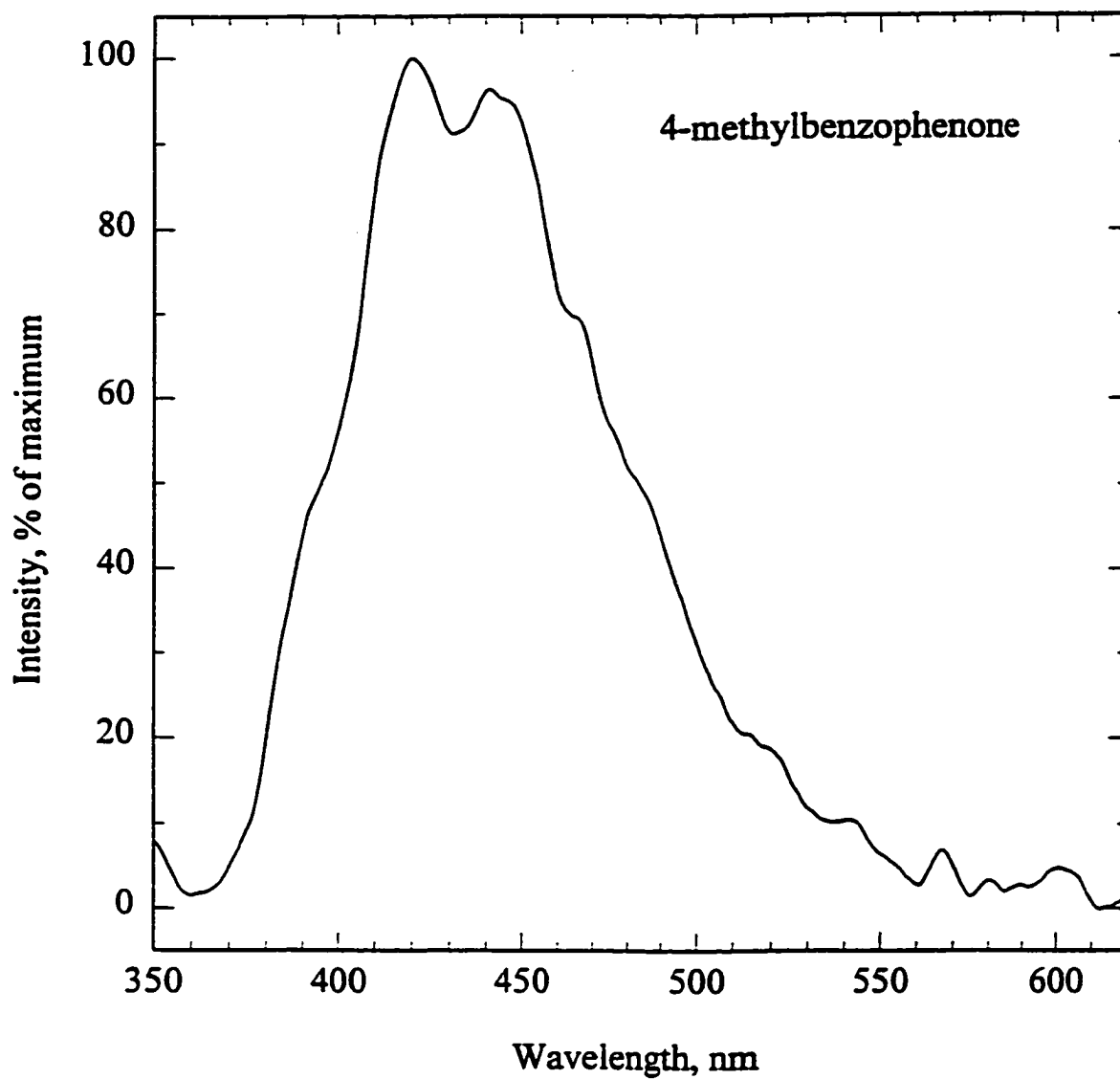
Figure 4.37 Gas-phase luminescence spectrum of 4-methylbenzophenone in excited nitrogen obtained by using 1/8 meter grating monochromator, R-374 PMT and single-peak mode. Bandpass: 12.6 nm.

Figure 4.38   Gas-phase luminescence spectrum of 2-chlorobenzophenone in excited nitrogen obtained by using 1/8 meter grating monochromator, R-374 PMT and single-peak mode. Bandpass: 12.6 nm. Ar doped into nitrogen: 100 mL/min.

Figure 4.39 Gas-phase luminescence spectrum of 4-chlorobenzophenone in excited nitrogen obtained by using 1/8 meter grating monochromator, R-374 PMT and single-peak mode. Bandpass: 12.6 nm.
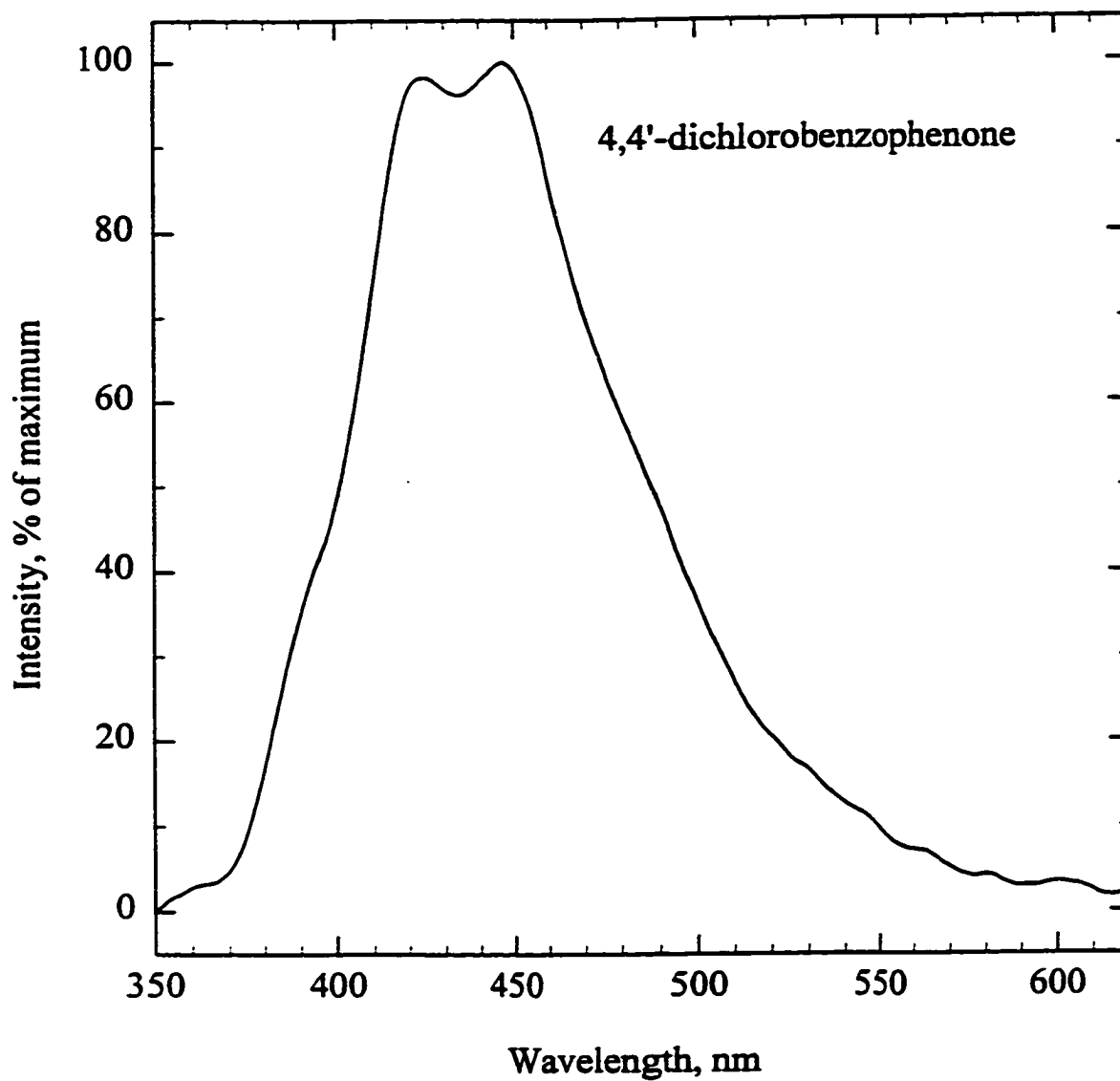
Figure 4.40 Gas-phase luminescence spectrum of 4,4'-dichlorobenzophenone in excited nitrogen obtained by using 1/8 meter grating monochromator, R-374 PMT and single-peak mode. Bandpass: 12.6 nm.

Figure 4.41 Gas-phase luminescence spectrum of 3,3'-bis(trifluoromethyl)-benzophenone in excited nitrogen obtained by using 1/8 meter grating monochromator, R-374 PMT and single-peak mode. Bandpass: 12.6 nm.

Figure 4.42   Gas-phase luminescence spectrum of 4-methoxybenzophenone in excited nitrogen obtained by using 1/8 meter grating monochromator, R-374 PMT and single-peak mode. Bandpass: 12.6 nm.

Figure 4.43   Gas-phase luminescence spectrum of 4-benzoylbiphenyl in excited nitrogen obtained by using a filter monochromator, R-268 PMT and repeated injection mode. 2 mm slit (corresponding to a 13 nm bandpass at 400 nm).

Figure 4.44   Gas-phase luminescence spectrum of 2-benzoylpyridine in excited nitrogen obtained by using a filter monochromator, R-268 PMT and repeated injection mode. 2 mm slit (corresponding to a 13 nm bandpass at 400 nm).
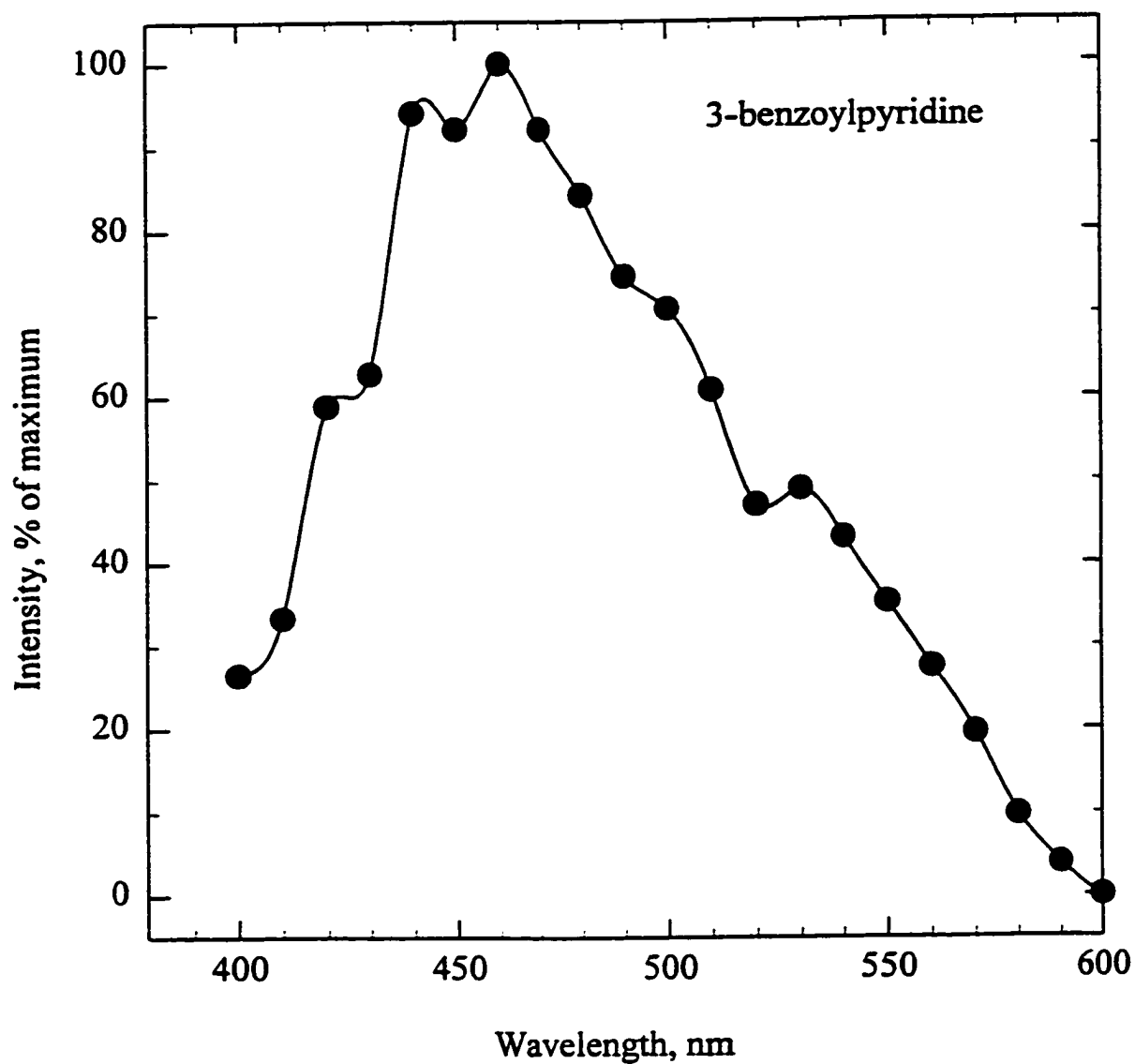
Figure 4.45   Gas-phase luminescence spectrum of 3-benzoylpyridine in excited nitrogen obtained by using a filter monochromator, R-268 PMT and repeated injection mode. 2 mm slit (corresponding to a 13 nm bandpass at 400 nm).
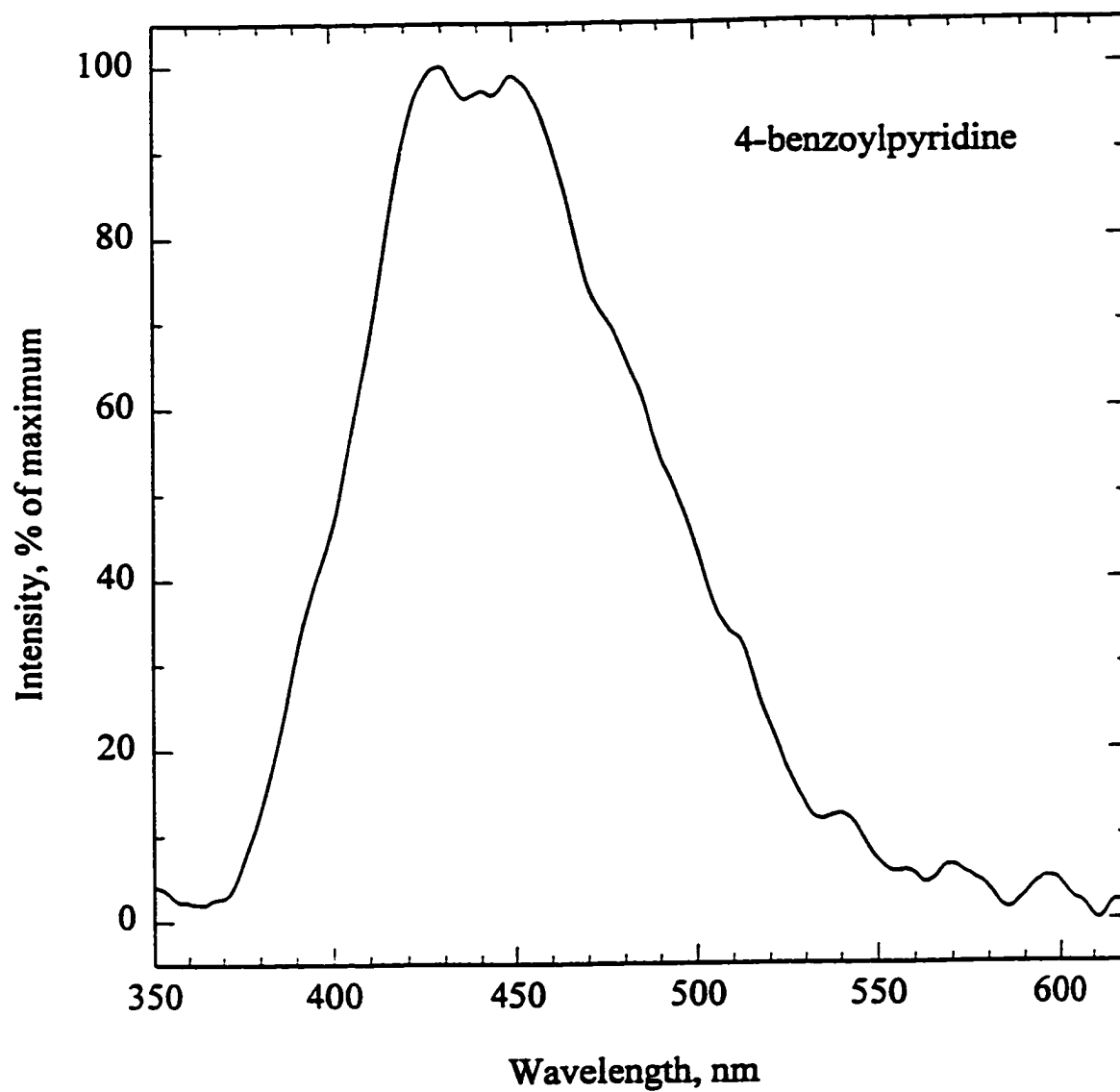
Figure 4.46   Gas-phase luminescence spectrum of 4-benzoylpyridine in excited nitrogen obtained by using 1/8 meter grating monochromator, R-374 PMT and single-peak mode. Bandpass: 12.6 nm.

The substituents only slightly shift the 0-0 transition of phosphorescence. but the direction of shift is parallel between the substituted benzophenones and the substituted benzaldehydes or acetophenones. Again, this similarity reflects the similar nature of the lowest triplet states of these aromatic carbonyl compounds.

4.3.4 Anthraquinones

Anthraquinone is another aromatic carbonyl compound whose photophysical and photochemical behavior has been extensively investigated (100-113). The compound. 9,10- anthraquinone, shows comparatively strong emission in the visible region in various rigid media (74, 100, 102) or in the gas phase (111-113). In the previous reports. the emission has been identified as phosphorescence from the lowest triplet state of the $n.\pi^*$ type, originating at about 455 nm (22,000 cm^{-1}) (102-104, 107, 109). It is also known that anthraquinone exhibits weak emission in the gas phase. The gas-phase emission was obtained by Singh and Singh (110) and later by Longin (111), with the aid of discharge excitation. The former authors regarded the luminescence in the 420-540 nm region as fluorescence and that in the 590-690 nm region as phosphorescence, while Longin assigned the emission to dual fluorescence with the origins at 421.4 and 422.7 nm. Later on, Rogozhin and co-workers (112) obtained highly resolved emission spectra of anthraquinone vapor at relatively high temperature. In order to interpret the emission nature of anthraquinone vapor, emission and excitation spectra of anthraquinone in the gas phase were measured and compared with those in the condensed phases by Itoh (113). Although the spectra obtained under different conditions were different with respect to

band resolution and shape, the interpretation of the auther was that the emission of anthraquinone vapor consists of $S_1(n,\pi^*) \rightarrow S_0$ fluorescence and $T_1(n,\pi^*) \rightarrow S_0$ phosphorescence, with origins at about 422 nm (23,700 cm^{-1}) and 455 nm (22.000 cm^{-1}). respectively.

In the present study, anthraquinone vapor exhibits very strong luminescence in excited nitrogen. Figure 4.47 shows the gas-phase luminescence spectrum of anthraquinone. The main peaks of this spectrum occur at around 425, 452, 487 and 530 nm. This spectrum is quite different from the phosphorescence spectra of anthraquinone obtained in rigid media and at low temperature (101,103, 107), but very similar with respect to band position and shape to those obtained by Longin (111) and Itoh (113) in the gas phase. Hence, we can assign the gas-phase luminescence to the $S_1(n,\pi^*) \rightarrow S_0$ E-type fluorescence and $T_1(n,\pi^*) \rightarrow S_0$ phosphorescence with origins at about 425 nm (23,529 cm^{-1}) and 452 nm (22,124 cm^{-1}), respectively. The prominent peaks at 452, 487. and 530 nm were assigned to the 0-0 band and C=O stretching modes, respectively. From the band position, the singlet-triplet energy gap, ΔE_{S-T}. is found to be 1405 cm^{-1}. Figure 4.48 shows that the ratio of the fluorescence intensity to the phosphorescence intensity increases with temperature. According to the relation (114) $I_F/I_P \propto \exp(-\Delta E_{S-T}/kT)$, where I_F, I_P, k and T represent the fluorescence and phosphorescence intensities. Boltzmann constant and absolute temperature, respectively, ΔE_{S-T} can be derived from the plot of $\ln(I_F/I_P)$ versus 1/T (Figure 4.49). The plot gives a straight line, and the value of ΔE_{S-T} calculated from the slope is 1367 cm^{-1}. This value agrees well with the singlet-triplet energy gap of 1405 cm^{-1} obtained from the band position, thus confirming
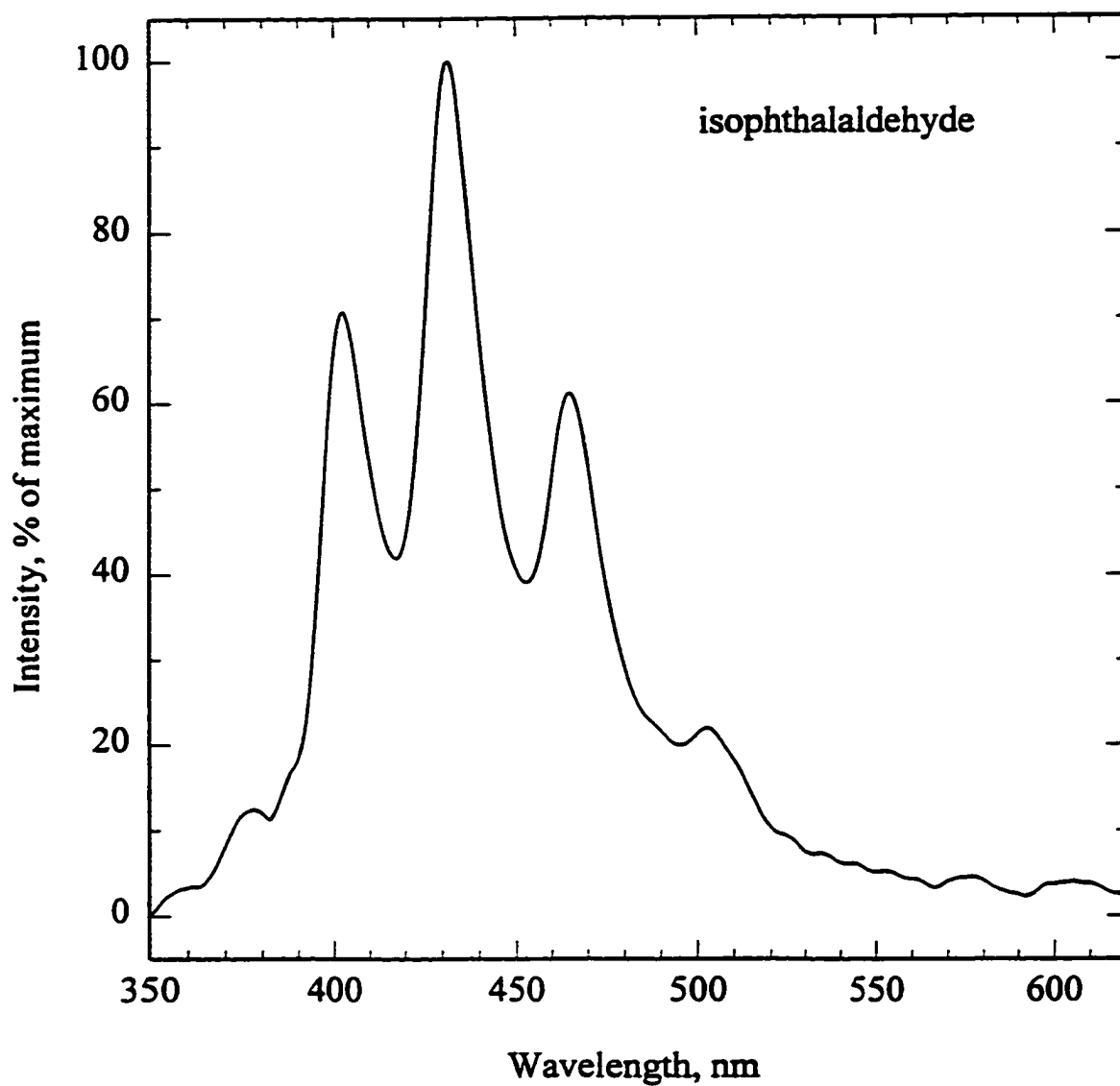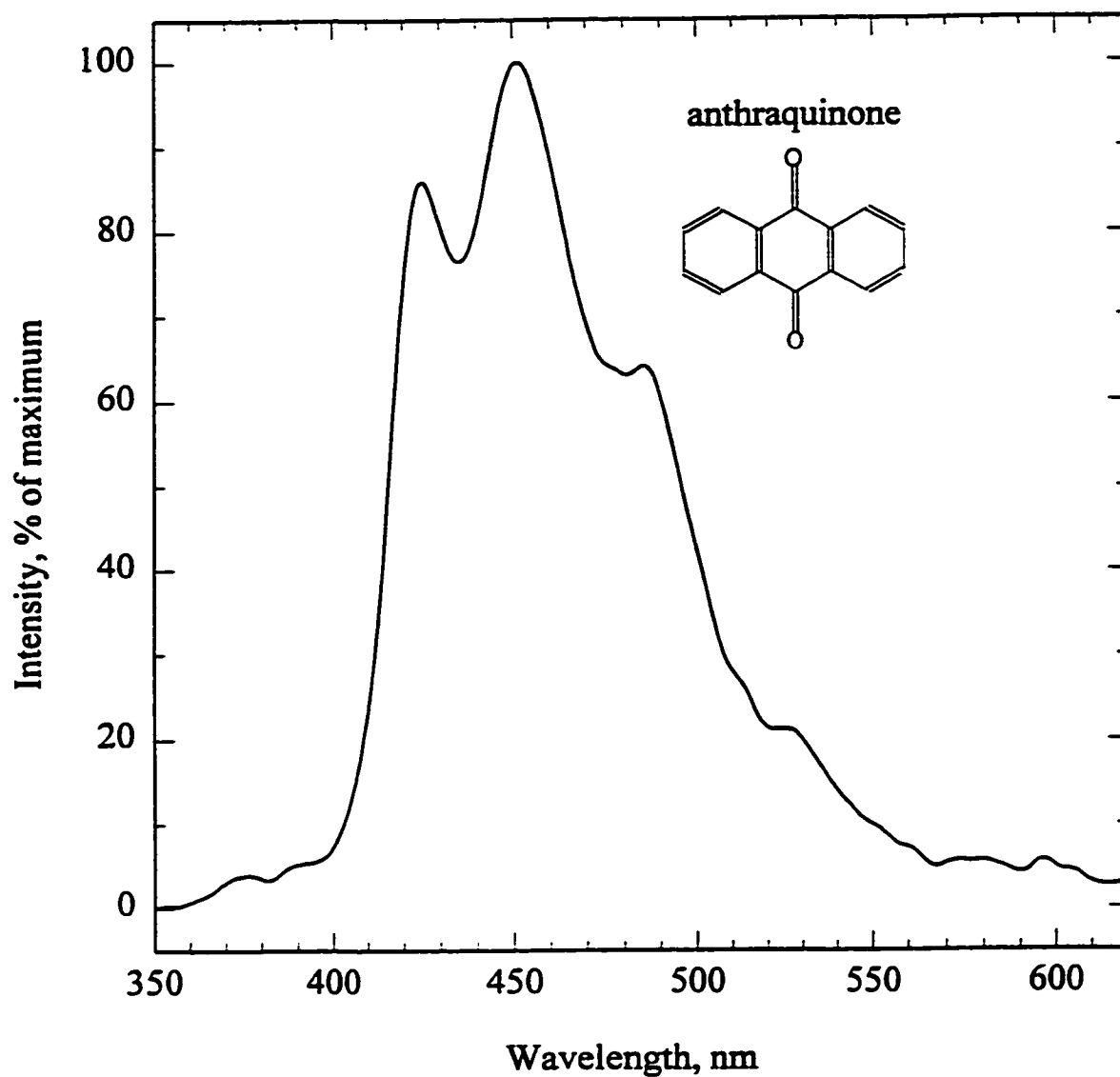
Figure 4.47　Gas-phase luminescence spectrum of anthraquinone in excited nitrogen obtained by using 1/8 meter grating monochromator, R-374 PMT and single-peak mode. Bandpass: 6.6 nm.
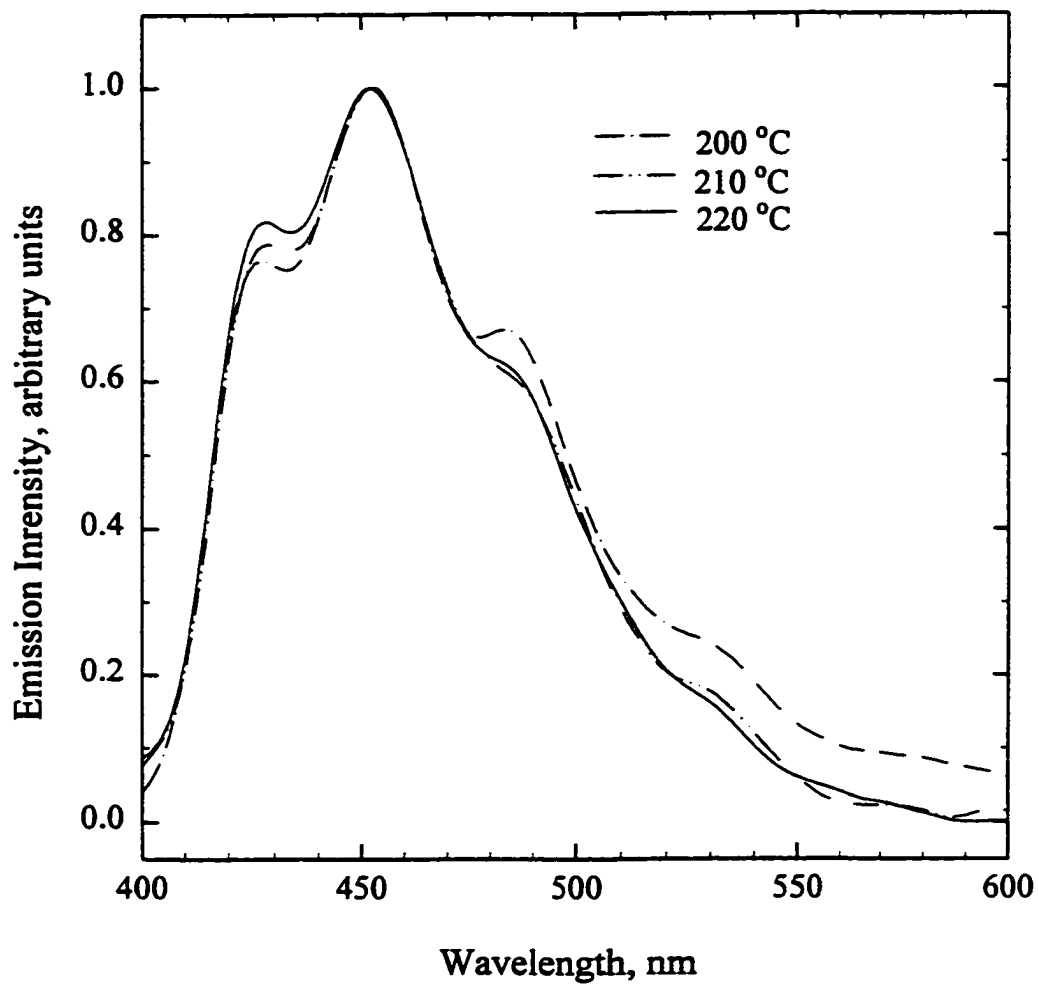
Figure 4.48 Gas-phase luminescence spectra of anthraquinone in excited nitrogen at different temperatures obtained by using 1/8 meter grating monochromator, R-374 PMT and single-peak mode. Bandpass: 6.6 nm.
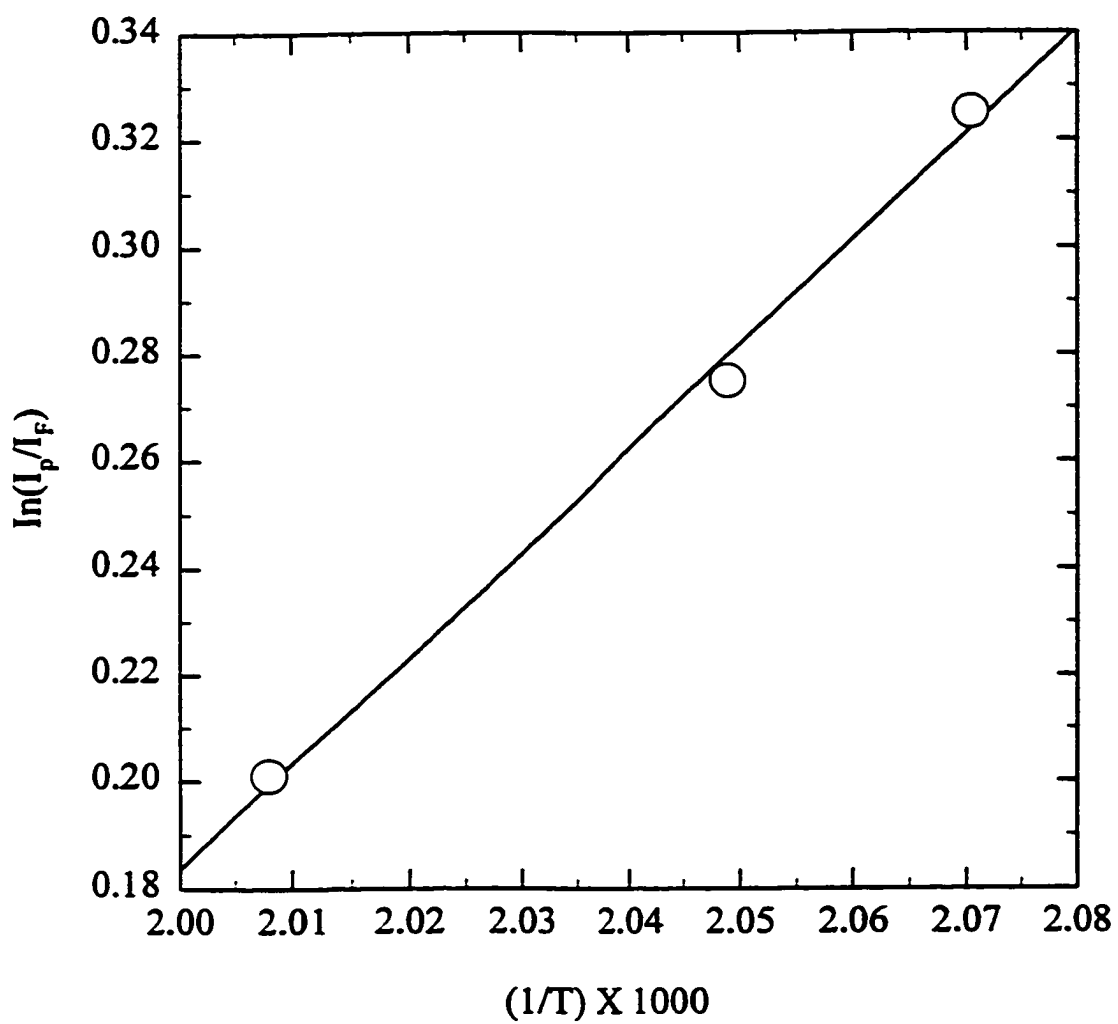
Figure 4.49   Temperature dependence of the intensity ratios of phosphorescence to fluorescence for anthraquinone in the gas phase.

the occurrence of E-type delayed fluorescence. Similar results were also obtained by Carlson and Hercules for the emission of anthraquinone in Freon (115) and by Itoh for the emission of anthraquinone vapor (113).

The gas-phase luminescence spectra of some substituted anthraquinones are shown in Figures 4.50-4.54. These spectra are essentially the same as the anthraquinone spectrum and have the principal vibrational structure of the carbonyl stretching frequency (1590-1660 cm^{-1}). Thus, all the spectra of these substituted anthraquinones can be regarded as consisting of the $S_1 \rightarrow S_0$ E-type fluorescence and $T_1 \rightarrow S_0$ phosphorescence from the T_1 state of an n,π^* character. It is noted that no spectrum shift was observed among these substituted anthraquinones (Table 4.4).

Table 4.4 Spectral Characteristics of Anthraquinone and Some Substituted Anthraquinones

Compound	Origin of Fluorescence, cm^{-1}	Origin of Phosphorescence, cm^{-1}
Anthraquinone	23,529 (425 nm)	22,124 (452 nm)
2-Methylanthraquinone	23,419 (427 nm)	22,124 (452 nm)
2-Ethylanthraquinone	23,419 (427 nm)	22,124 (452 nm)
1-Chloroanthraquinone	23,474 (426 nm)	22,124 (452 nm)
1,4,4a,9a-Tetrahydroanthraquinone	23,419 (427 nm)	22,124 (452 nm)
Benz(g)isoquinolon-5,10-dione	23,474 (426 nm)	22,124 (452 nm)

4.3.5 1,4 Naphthoquinone and Its 2-Methyl Derivative

1,4-Naphthoquinone is one of the prototype quinones and several studies were reported about its photophysical properties. Kuboyama recorded the strong emission of 1,4-naphthoquinone in the visible region in rigid glass solution at 77 K and the emission
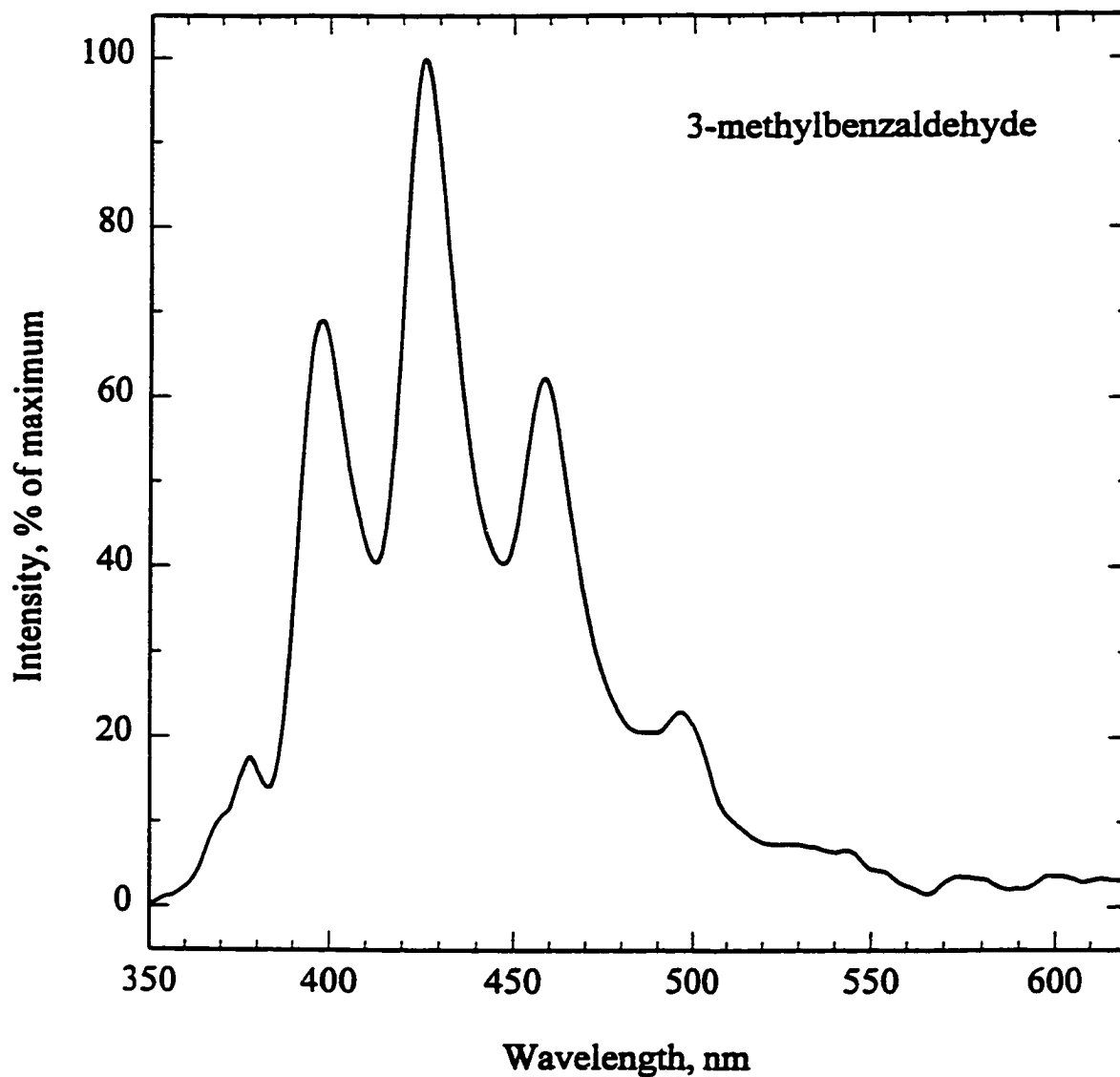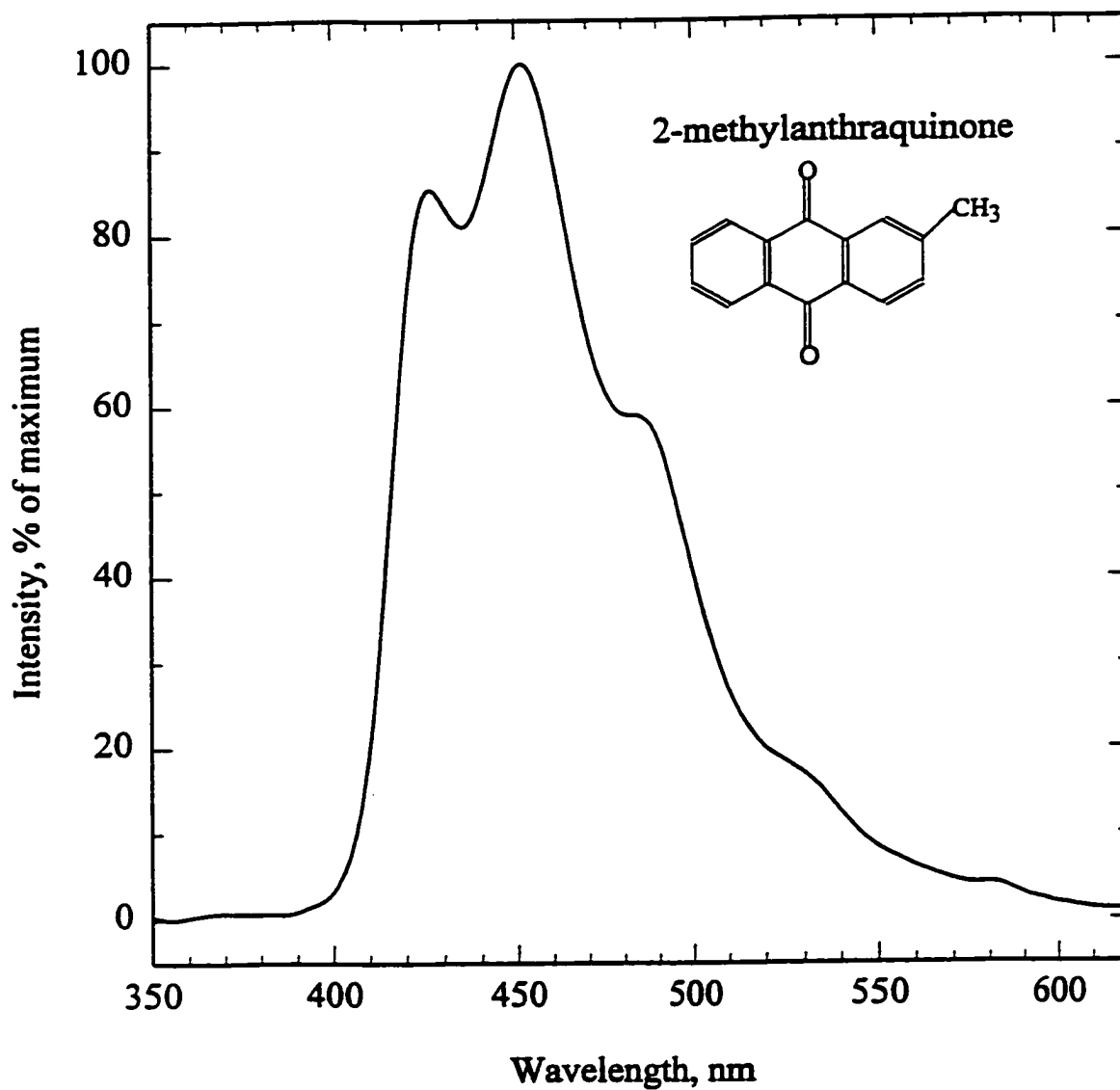
Figure 4.50   Gas-phase luminescence spectrum of 2-methylanthraquinone in excited nitrogen obtained by using 1/8 meter grating monochromator, R-374 PMT and single-peak mode. Bandpass: 6.6 nm.
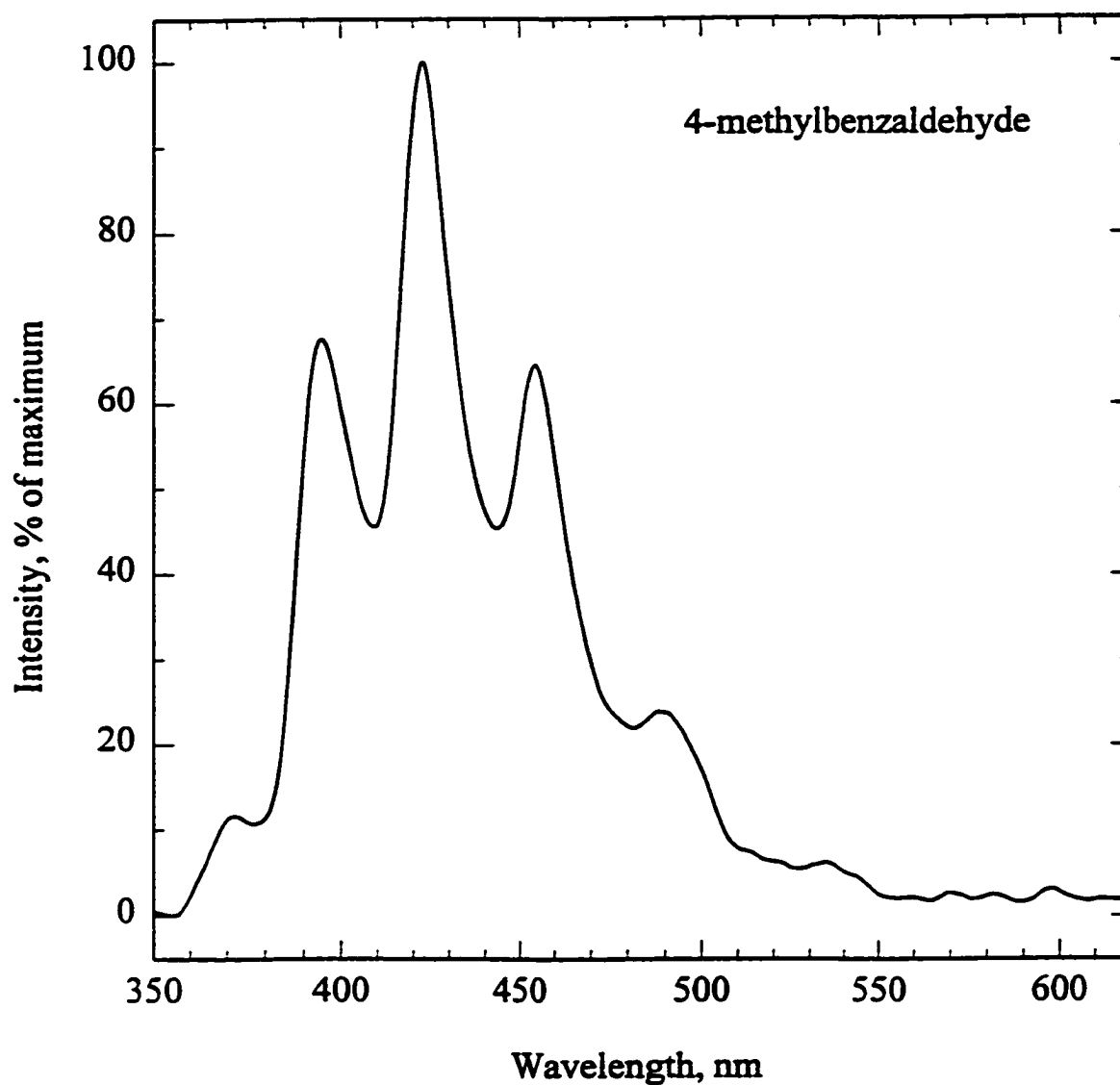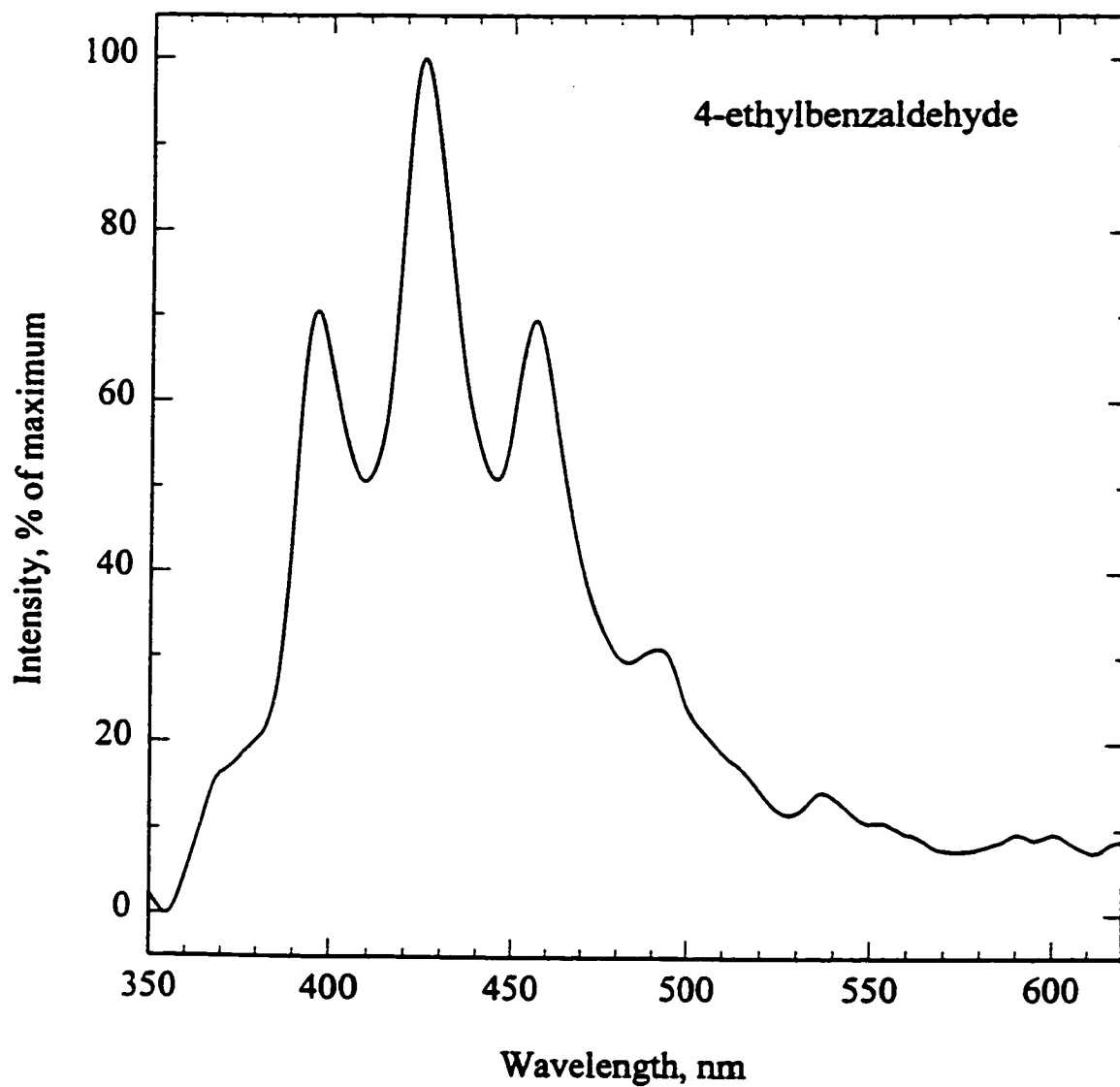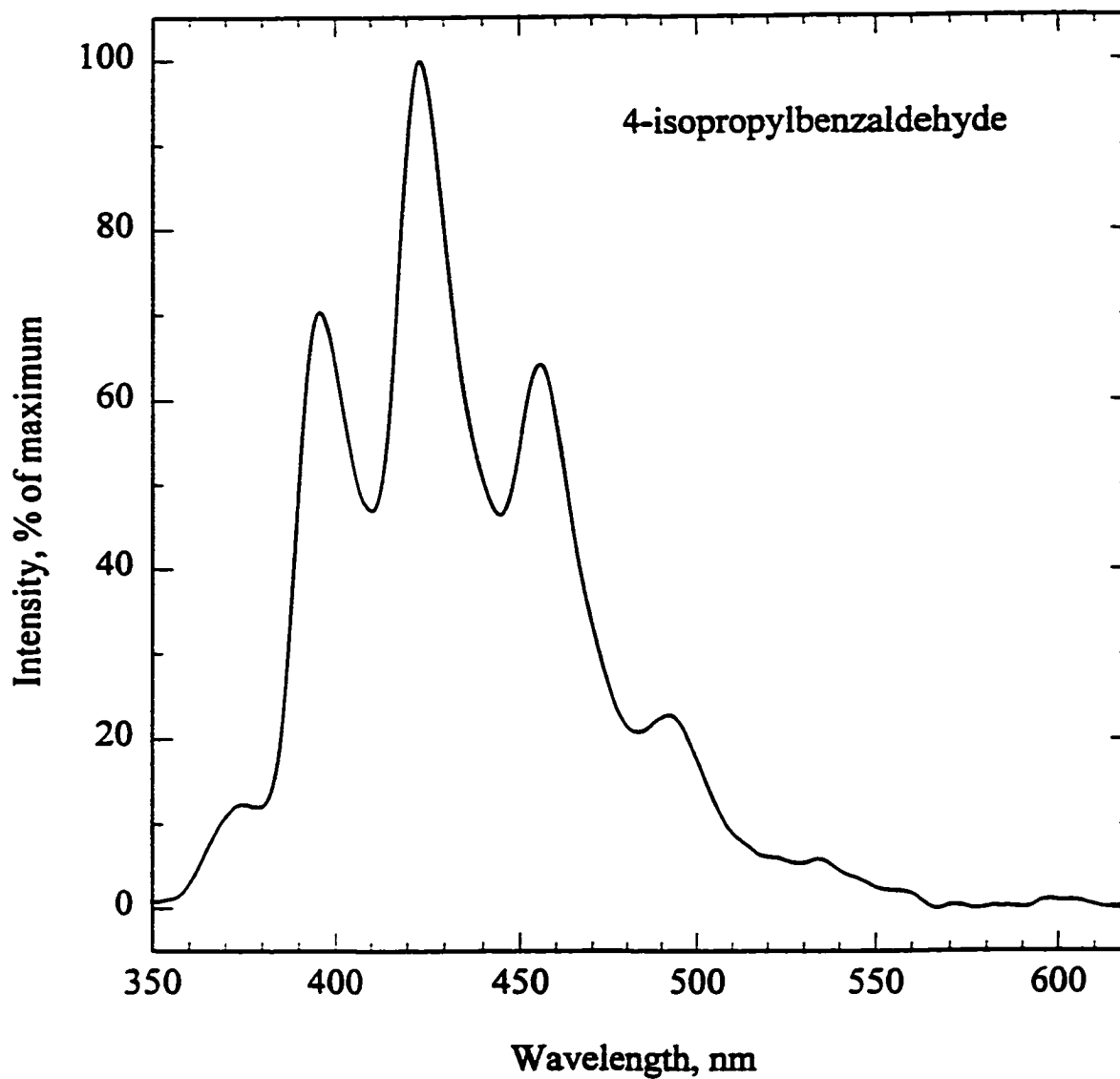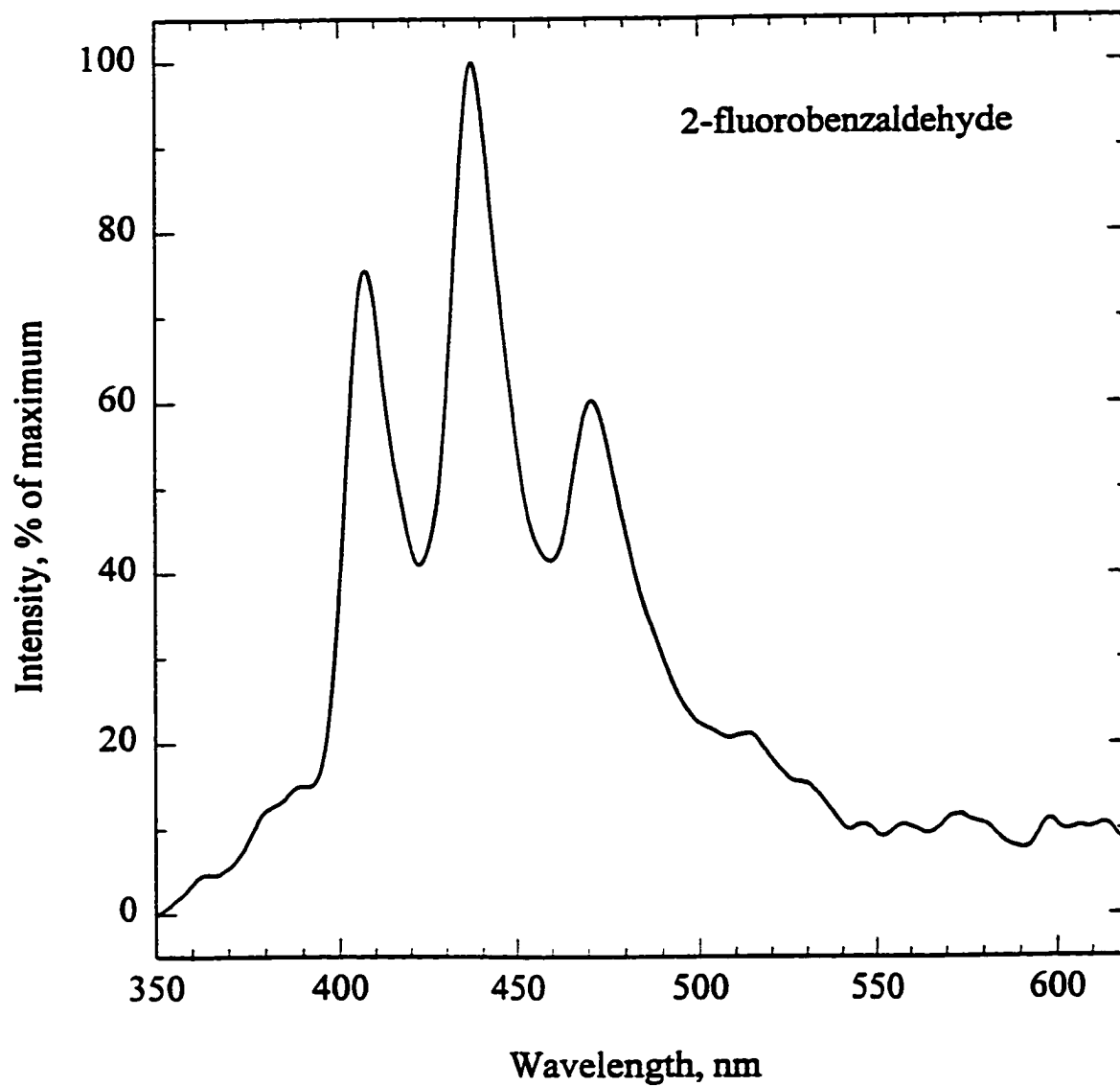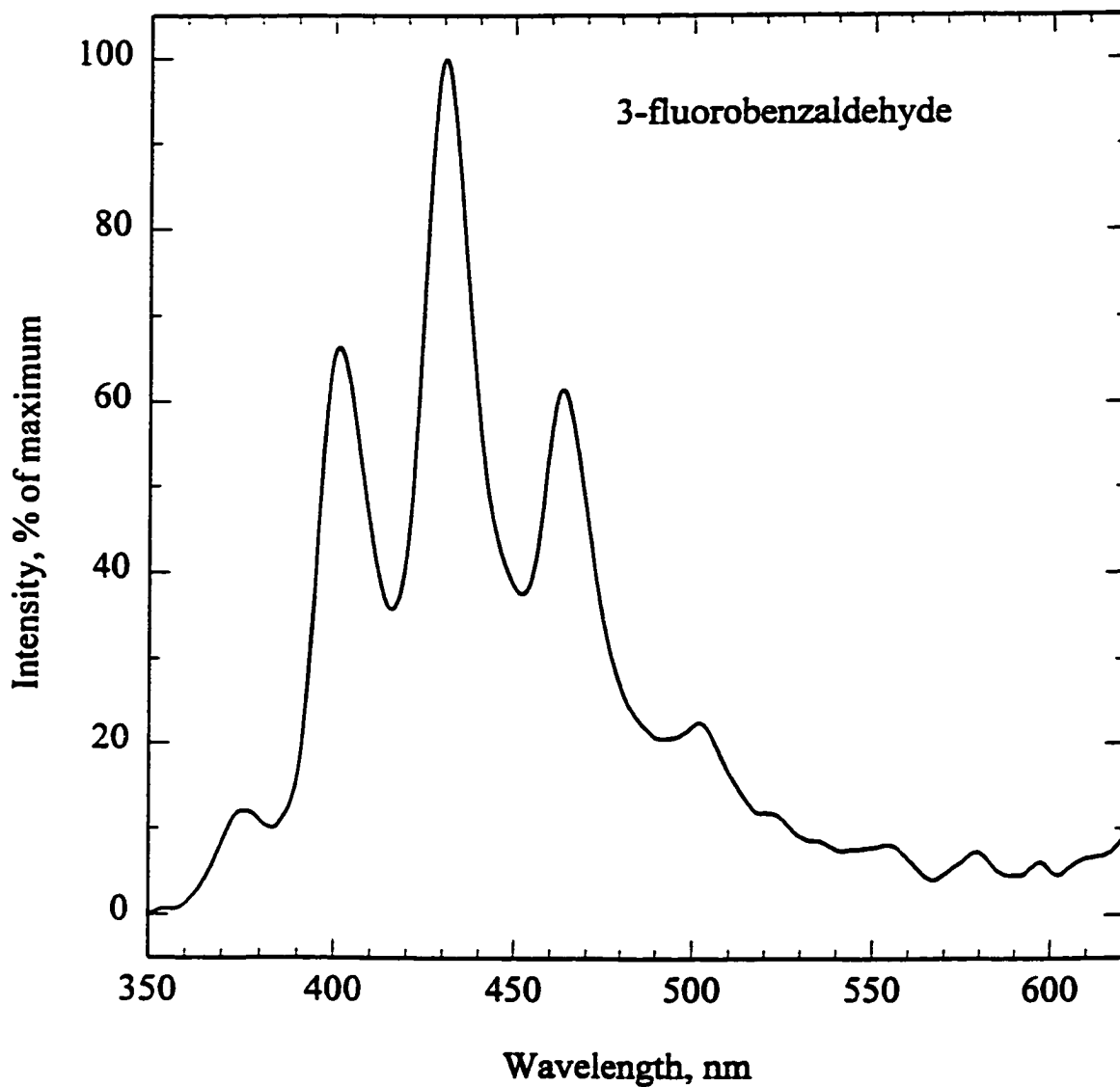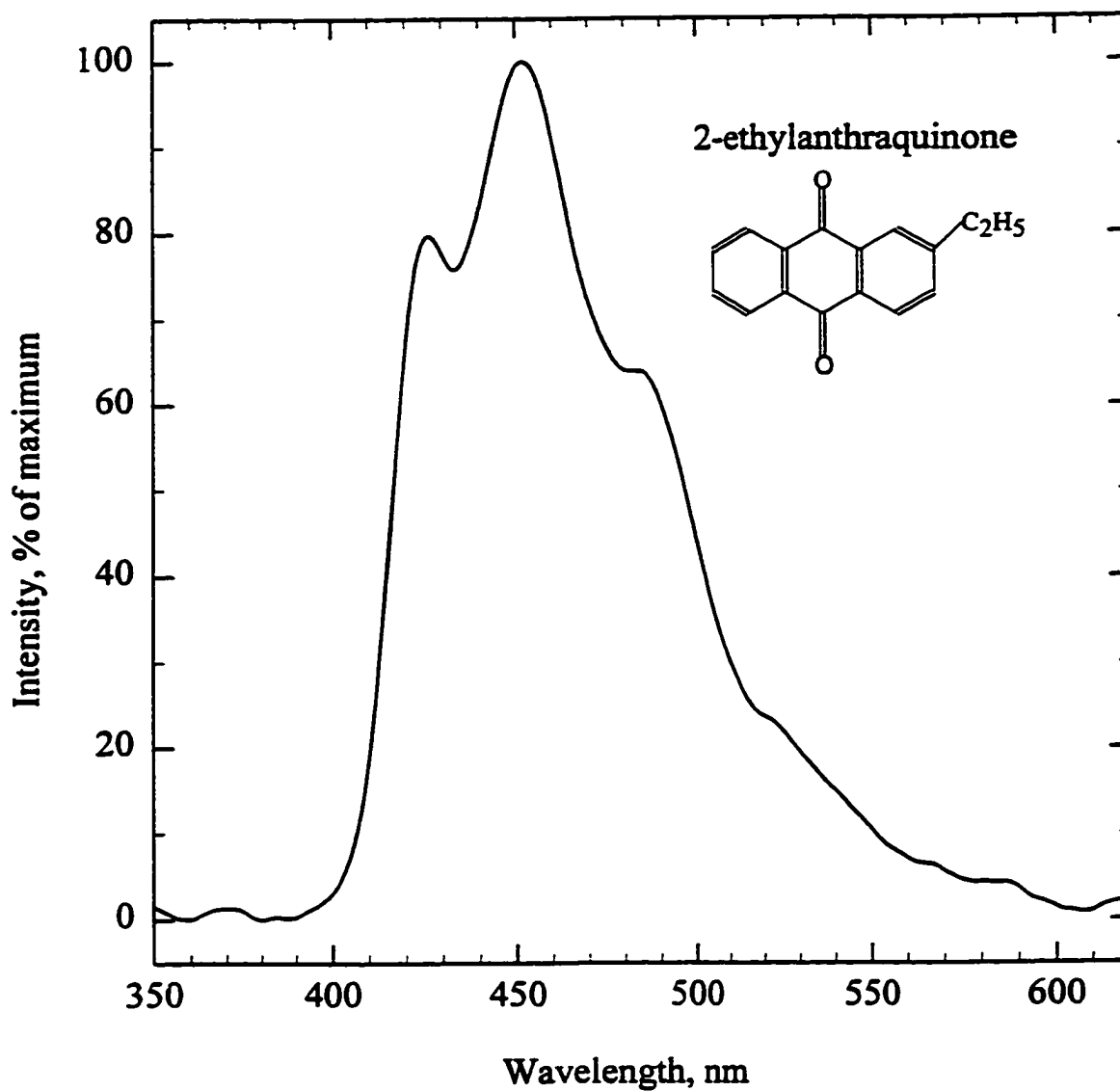
Figure 4.51   Gas-phase luminescence spectrum of 2-ethylanthraquinone in excited nitrogen obtained by using 1/8 meter grating monochromator, R-374 PMT and single-peak mode. Bandpass: 6.6 nm.
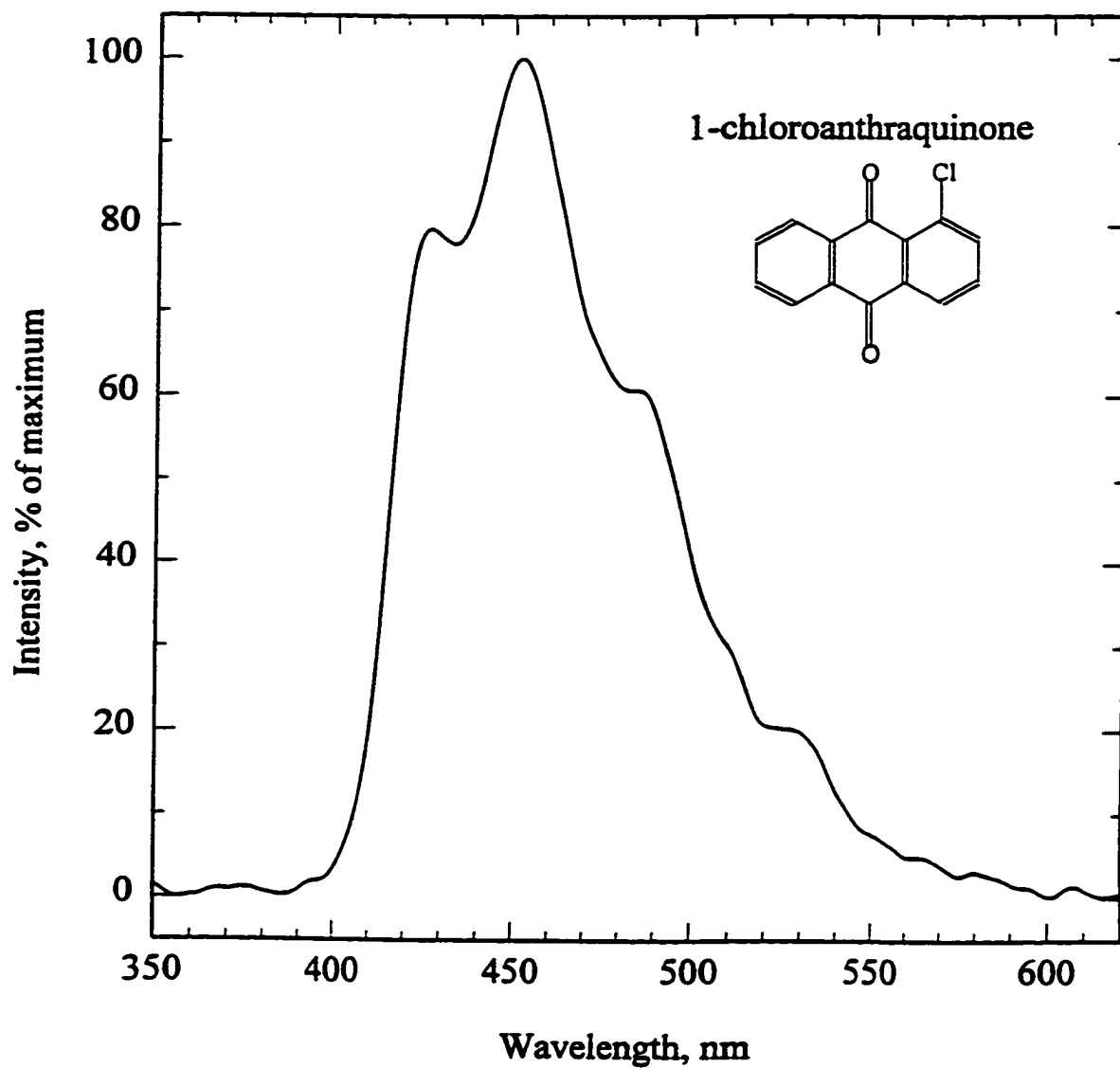
Figure 4.52   Gas-phase luminescence spectrum of 1-chloroanthraquinone in excited nitrogen obtained by using 1/8 meter grating monochromator, R-374 PMT and single-peak mode. Bandpass: 6.6 nm.
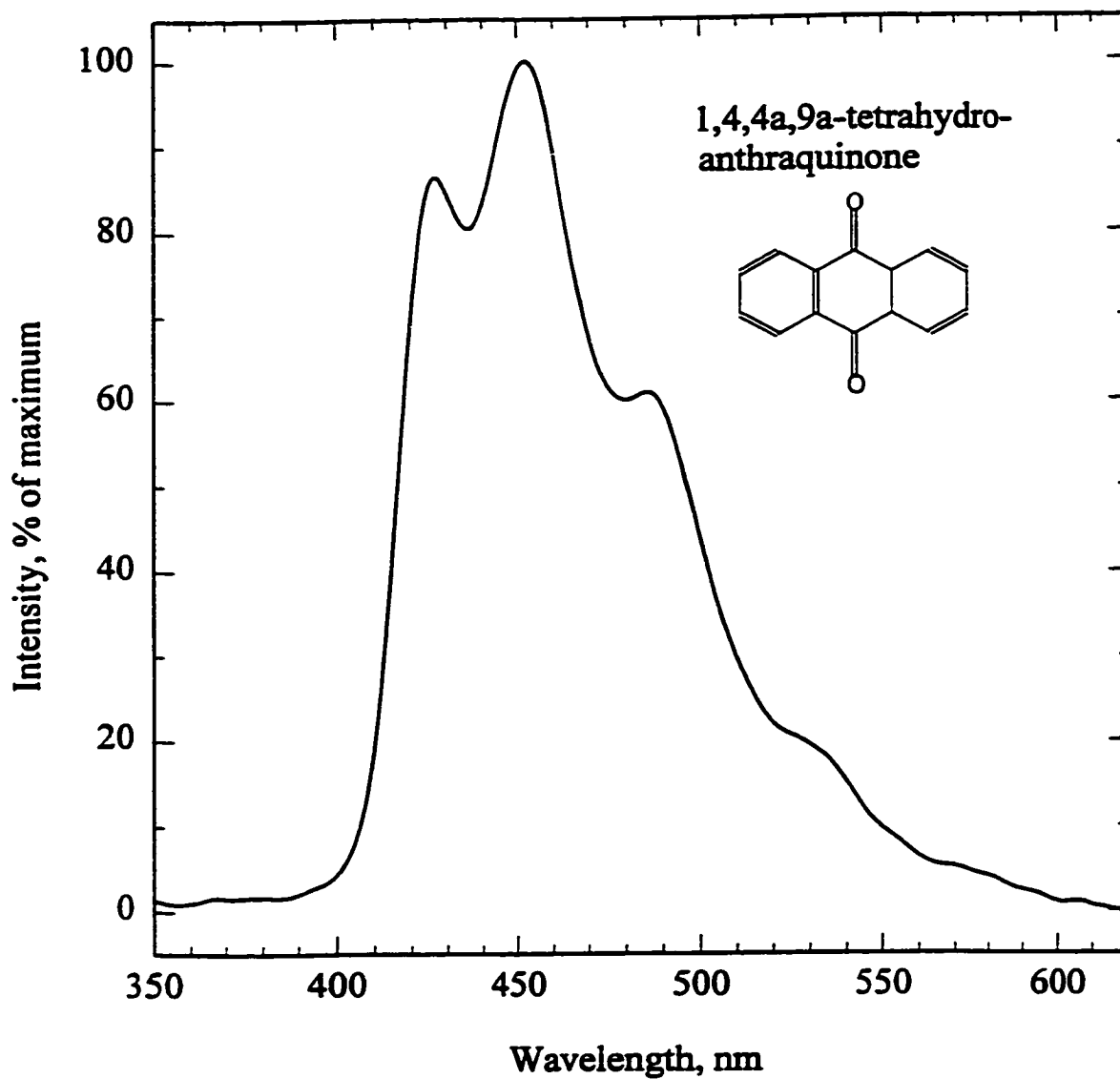
Figure 4.53   Gas-phase luminescence spectrum of 1,4,4a,9a-tetrahydroanthraquinone in excited nitrogen obtained by using 1/8 meter grating monochromator, R-374 PMT and single-peak mode. Bandpass: 6.6 nm.
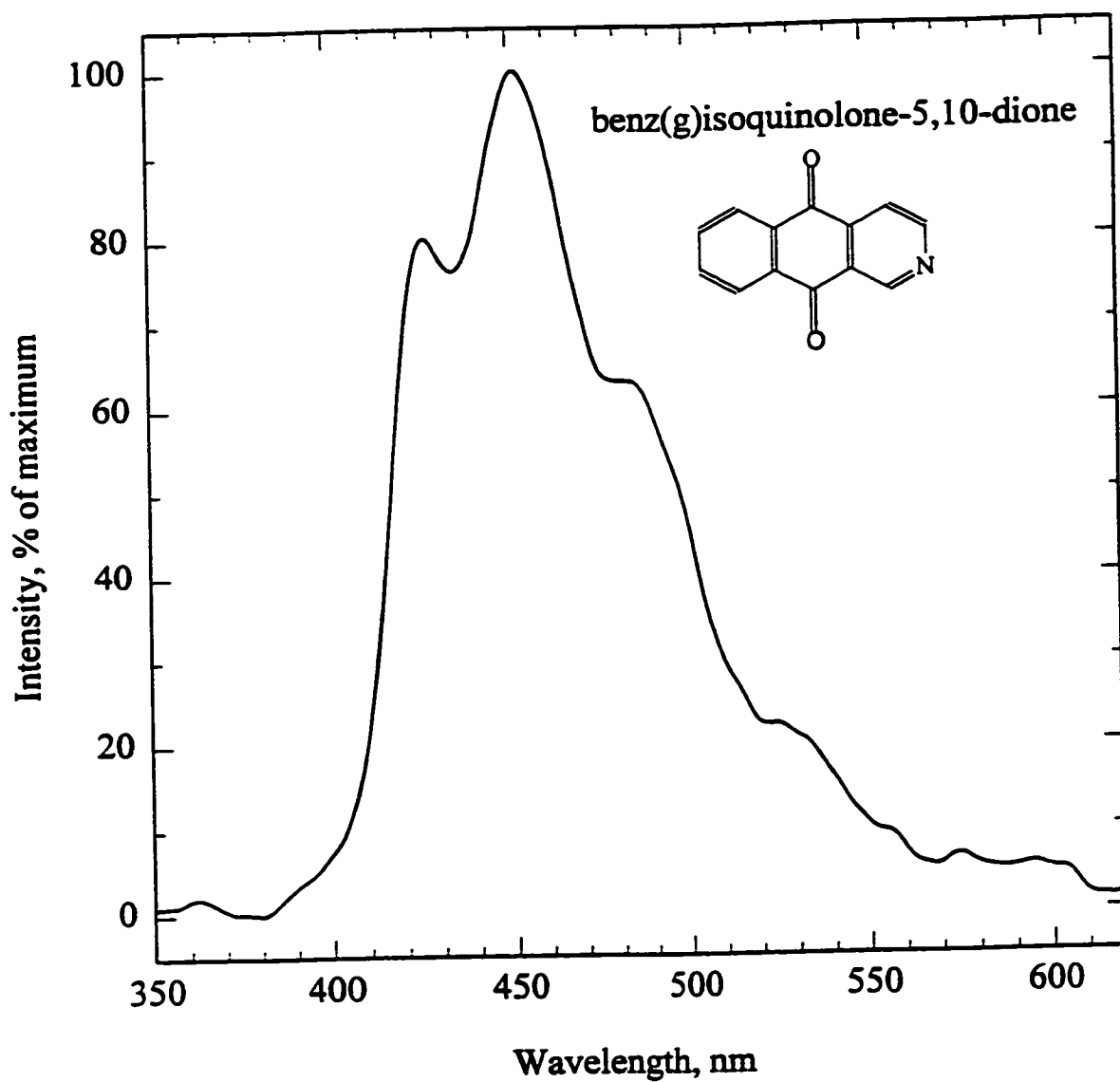
Figure 4.54 Gas-phase luminescence spectrum of benz(g)isoquinolone-5,10-dione in excited nitrogen obtained by using 1/8 meter grating monochromator, R-374 PMT and single-peak mode. Bandpass: 6.6 nm.

has been assigned as n,π^*-type phosphorescence from the lowest triplet state (102). In the gas phase, 1,4-naphthoquinone shows weak emission. The first gas-phase emission spectrum of 1,4-naphthoquinone was obtained in the presence of flowing vapor of benzene by Singh and Singh (116) and later by Longin (111) with the aid of discharge excitation. Singh and Singh assigned the emission as fluorescence and phosphorescence with the origins at 21,945 cm^{-1} (455 nm) and 18,782 cm^{-1} (532 nm), respectively, while Longin considered that the gas-phase emission consists of two kinds of fluorescence with the origins at 22,163 cm^{-1} (451.2 nm) and 21,974 cm^{-1} (455.1 nm). The carbonyl compounds, having a small singlet-triplet energy gap, often exhibit weak E-type delayed fluorescence (63). Itoh and Baba (117) took this into account in the assignment of the emitting states of 1,4-naphthoquinone and investigated the temperature dependence of the emission spectrum as well as the emission lifetime of 1,4-naphthoquinone vapor in the presence of added foreign gases. They showed that the emission consists of the phosphorescence from the lowest triplet state and the delayed fluorescence from the lowest singlet state with the origins at 20,460 cm^{-1} (488.8 nm) and 21,830 cm^{-1} (458.1 nm), respectively. They also reported the prompt fluorescence which originates from the $S_1(n,\pi^*)$ state in addition to the phosphorescence and E-type delayed fluorescence at low pressure (10^{-3}-10^{-1} Torr) (118). It is known that the non-fluorescent nature of the aromatic carbonyl compounds is due to fast intersystem crossing from the S_1 state to an excited triplet state. It was explained that the prompt fluorescence is due to isoenergetic intersystem crossing from the triplet to the S_1 state under collision-free conditions. More recently, Itoh (85) reported that the gas-phase emission spectrum of 1,4-naphthoquinone

consists of the dual phosphorescence from T_1 (n,π^*) and T_2 (n,π^*) with origins at 20,295

cm^{-1} (488.4 nm) and 20475 cm^{-1} (492.0 nm), respectively, in addition to the weak E-type

delayed fluorescence. This clarified the doublet structures in the main emission bands of

1,4-naphthoquinone vapor.

The emission spectra of 2-methyl-1,4-naphthoquinone vapor also were reported by

Baruah and co-workers (119) and later by Itoh and Baba (117). The former authors

interpreted the emission as consisting of fluorescence from a S_1 (n,π^*) state and

phosphorescence from a T_1 (n,π^*) state, with origins at 22,075 cm^{-1} (453.0 nm) and

20,262 cm^{-1} (493.5 nm), respectively, while the latter regarded the spectrum as consisting

of T_1(n,π^*)$\rightarrow$$S_0$ phosphorescence and weak E-type delayed fluorescence from S_1(n.π^*)

with origins at 20,340 cm^{-1} (491.6 nm) and 21,950 cm^{-1} (455.6 nm), respectively.

Figure 4.55 and Figure 4.56 show the gas-phase luminescence spectra of 1,4-

naphthoquinone and 2-methyl-1,4-naphthoquinone in excited nitrogen, respectively.

Their entire emission spectra lie in the visible region with broad and diffuse bands at

about 450, 485, 525, and 575 nm for 1,4-naphthoquinone and 455, 490, 530, and 480 nm

for 2-methyl-1,4-naphthoquinone, respectively, and show a prominent C=O stretching

vibrational progression. These spectra resemble the corresponding gas-phase emission

spectra obtained by Itoh and co-worker (85, 117, 118), and agree in band position with

these spectra recorded in ref. 111, 116 and 119. Therefore, we regard the gas-phase

luminescence spectra of 1,4-naphthoquinone and 2-methyl-1,4-naphthoquinone as

consisting of phosphorescence from T_1 (n,π^*) and E-type delayed fluorescence from S_1

(n,π^*) with origins at 22,222 cm^{-1} (450 nm) and 20,619 cm^{-1} (485 nm) for
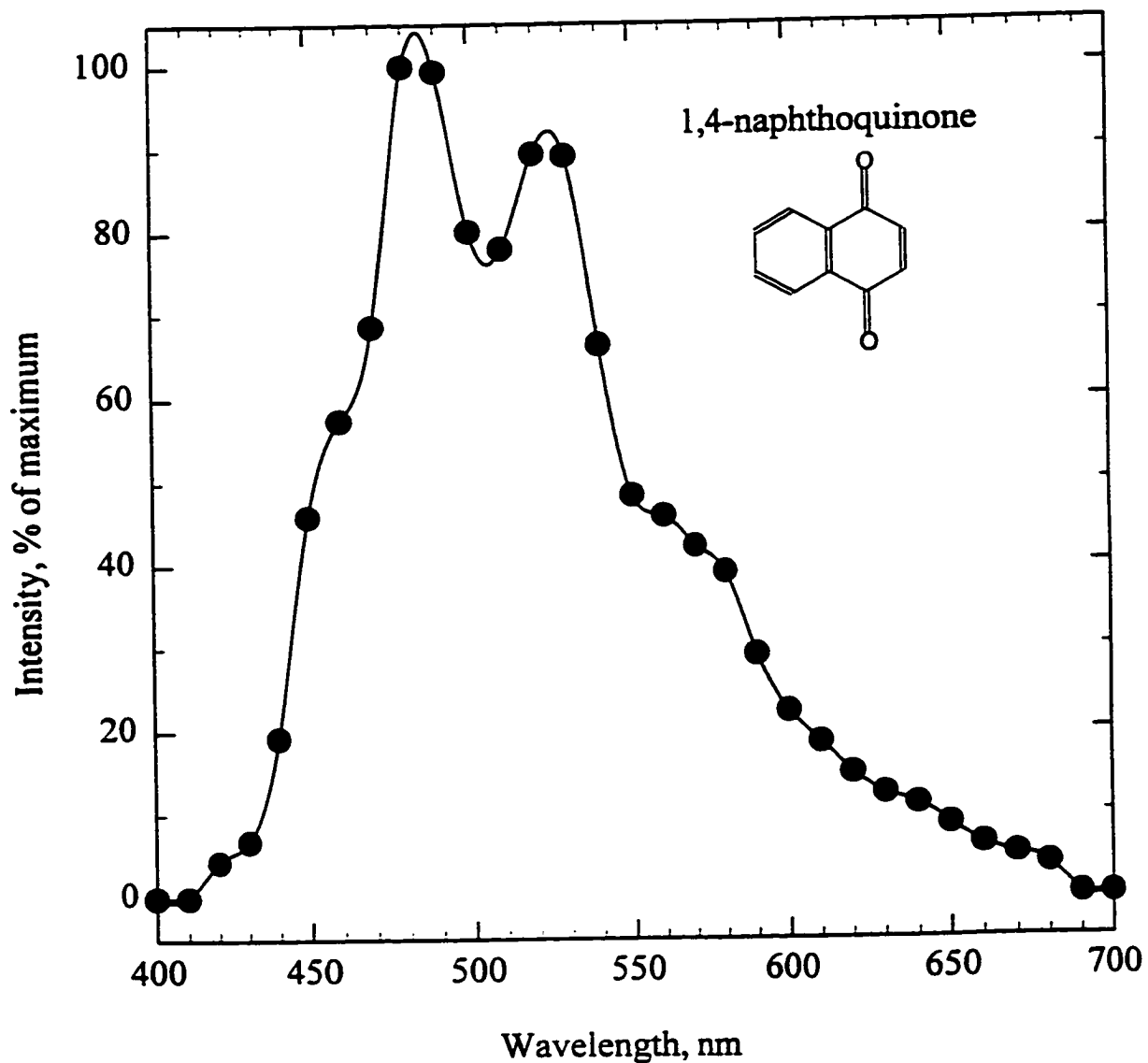
Figure 4.55 Gas-phase luminescence spectrum of 1,4-naphthoquinone in excited nitrogen obtained by using a filter monochromator, R-268 PMT and repeated injection mode. 2 mm slit (corresponding to a 13 nm bandpass at 400 nm).
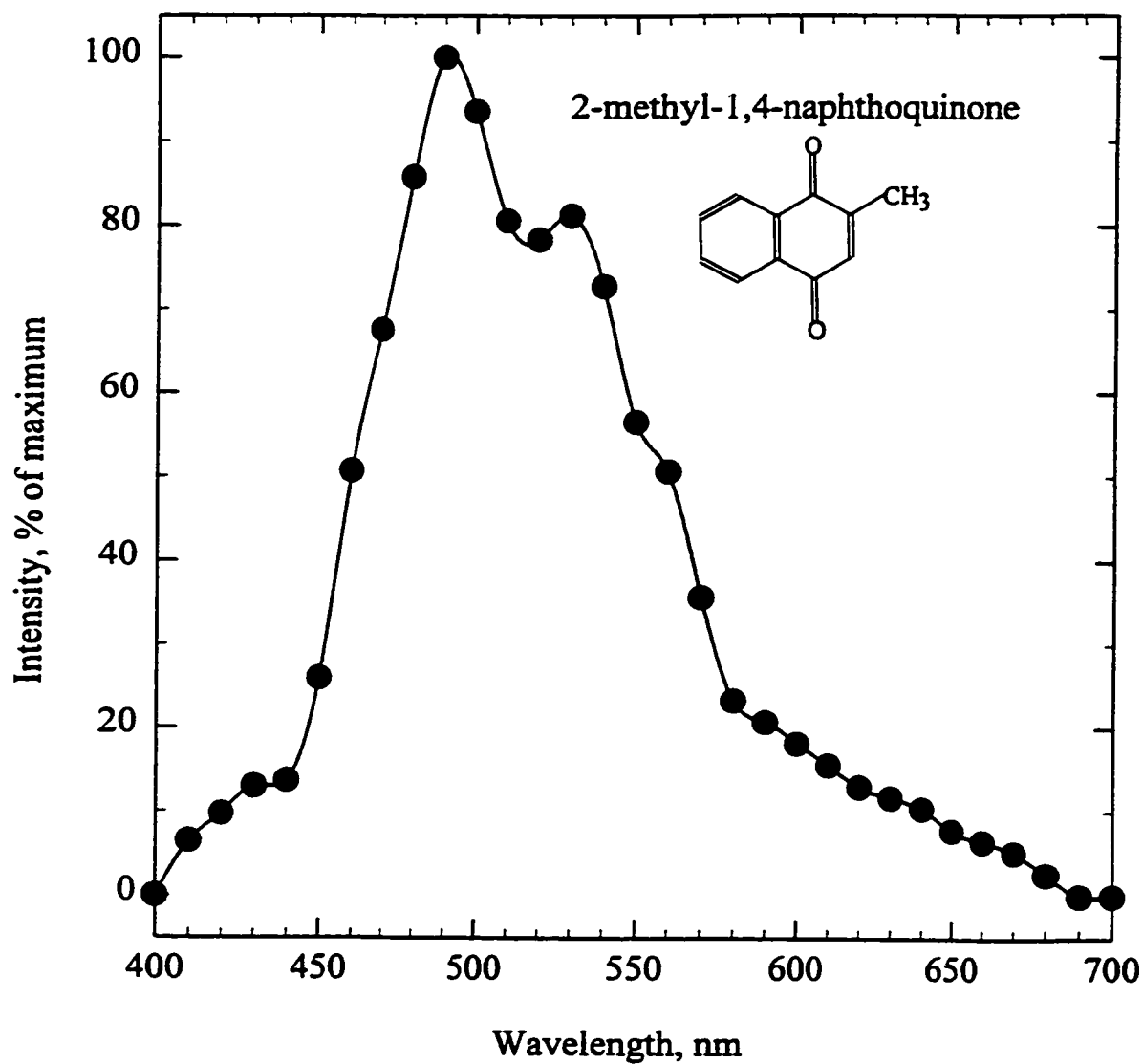
Figure 4.56 Gas-phase luminescence spectrum of 2-methyl-1,4 naphthoquinone in excited nitrogen obtained by using a filter monochromator, R-268 PMT and repeated injection mode. 2 mm slit (corresponding to a 13 nm bandpass at 400 nm).

1,4-naphthoquinone and 21,978 cm^{-1} (455 nm) and 20,408 cm^{-1} (490 nm) for 2-methyl-1,4-naphthoquinone, respectively.

4.3.6 Xanthone and Thioxanthone

Xanthone is one of certain carbonyl compounds which exhibit anomalous emission behavior. Pownall and Huber (120) reported that the emission spectrum of xanthone in 3-methylpentane at 77 K is the phosphorescence from a triplet n,π^* state with origin at 25,905 cm^{-1} (386 nm) and shows four fundamental vibrations with frequencies of 260, 530, 930 and 1665 cm^{-1}, while the phosphorescence in polar solvent originates from a triplet π,π^* state. Later, based on an emission study of xanthone at about 2 K and 77 K, Pownall and co-workers (121) concluded that xanthone exhibits "dual" phosphorescence at 77 K in a 3-methylpentane glass matrix which is due to emission from two triplet n,π^* states with origins at 25,905 cm^{-1} (386 nm) and 25,650 cm^{-1} (389 nm), respectively, and the phosphorescence spectrum is very sensitive to temperature. This phenomenon was confirmed by Terada and co-workers in polyethylene matrix (122), but the lowest triplet state was identified as π,π^* state which is in agreement with that in the crystal and in diphenylmethane matrix at 1.5 K (123). Kanda and co-workers (124) reported that xanthone shows phosphorescence consisting of mainly three emission systems whose origin bands are located at 25,751 cm^{-1} (389 nm), 25,766 cm^{-1} (388 nm) and 25,774 cm^{-1} (387 nm), respectively. They also gave a quantitative explanation for the origin of such multiple phosphorescence levels (125).

All these photophysical studies of xanthone were made in rigid media or in crystal systems. So far, the emission study of this molecule in the gas phase has not been done. In this study, xanthone luminesced strongly in the excited nitrogen in the gas phase and turns out to be the strongest emitter among the compounds investigated. Figure 4.57 shows the gas-phase luminescence spectrum of xanthone in excited nitrogen. The emission spectrum exhibits little structure and shows a maximum at about 24,154 cm^{-1} (414 nm) with two shoulders at about 25,773 cm^{-1} (388 nm) and 22,573 cm^{-1} (443 nm), respectively. These are the main peaks in phosphorescence spectrum of xanthone in 3-methylpentane at 77 K. In spite of the spectral congestion, the gas-phase spectrum is similar in band position to the phosphorescence spectrum of xanthone in 3-methylpentane at 77 K (120). It is reasonable to conclude that the gas-phase luminescence spectrum of xanthone in excited nitrogen is the phosphorescence from a T_1 (n,π*) state with a origin at about 25,773 cm^{-1} (388 nm). The bands at about 25,773 cm^{-1} (388 nm), 24,154 cm^{-1} (414 nm) and 22,573 cm^{-1} (443 nm) are assigned as the 0-0 band and progressions in the C=O stretching mode, respectively. However, the detailed analysis of vibrational structure cannot be made due to its structureless features.

Thio-xanthene-9-one also shows strong emission in excited nitrogen in the gas phase. The gas-phase emission spectrum of thio-xanthene-9-one (Figure 4.58) resembles that of xanthone upon a closer examination of the emission spectra, except for the change of the band intensity. Therefore, we tentatively assign the gas-phase emission spectrum of thio-xanthene-9-one to the phosphorescence from a triplet n,π* state with the origin at about 26,316 cm^{-1} (380 nm). The 0-0 band is the strongest in the phosphorescence
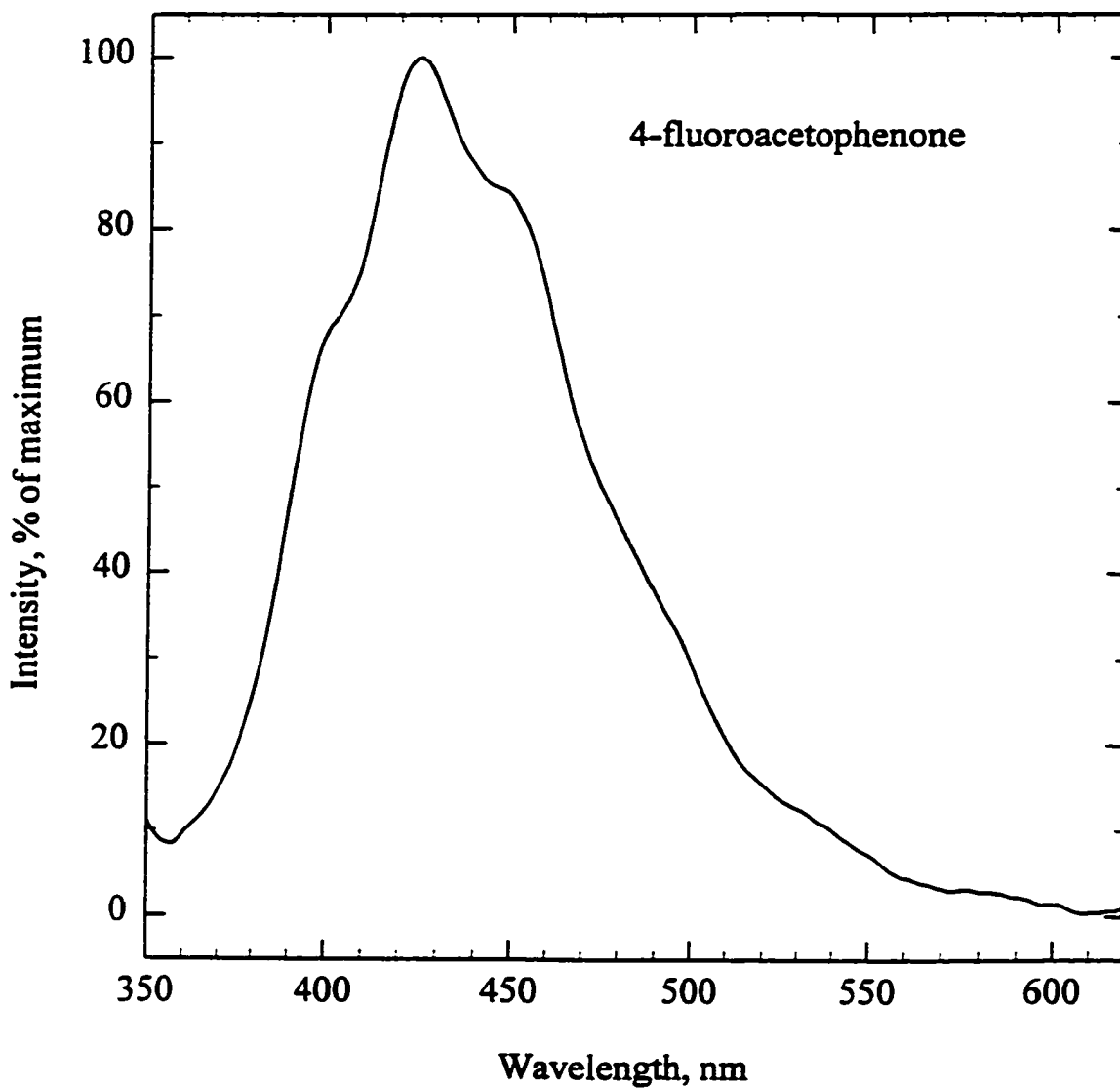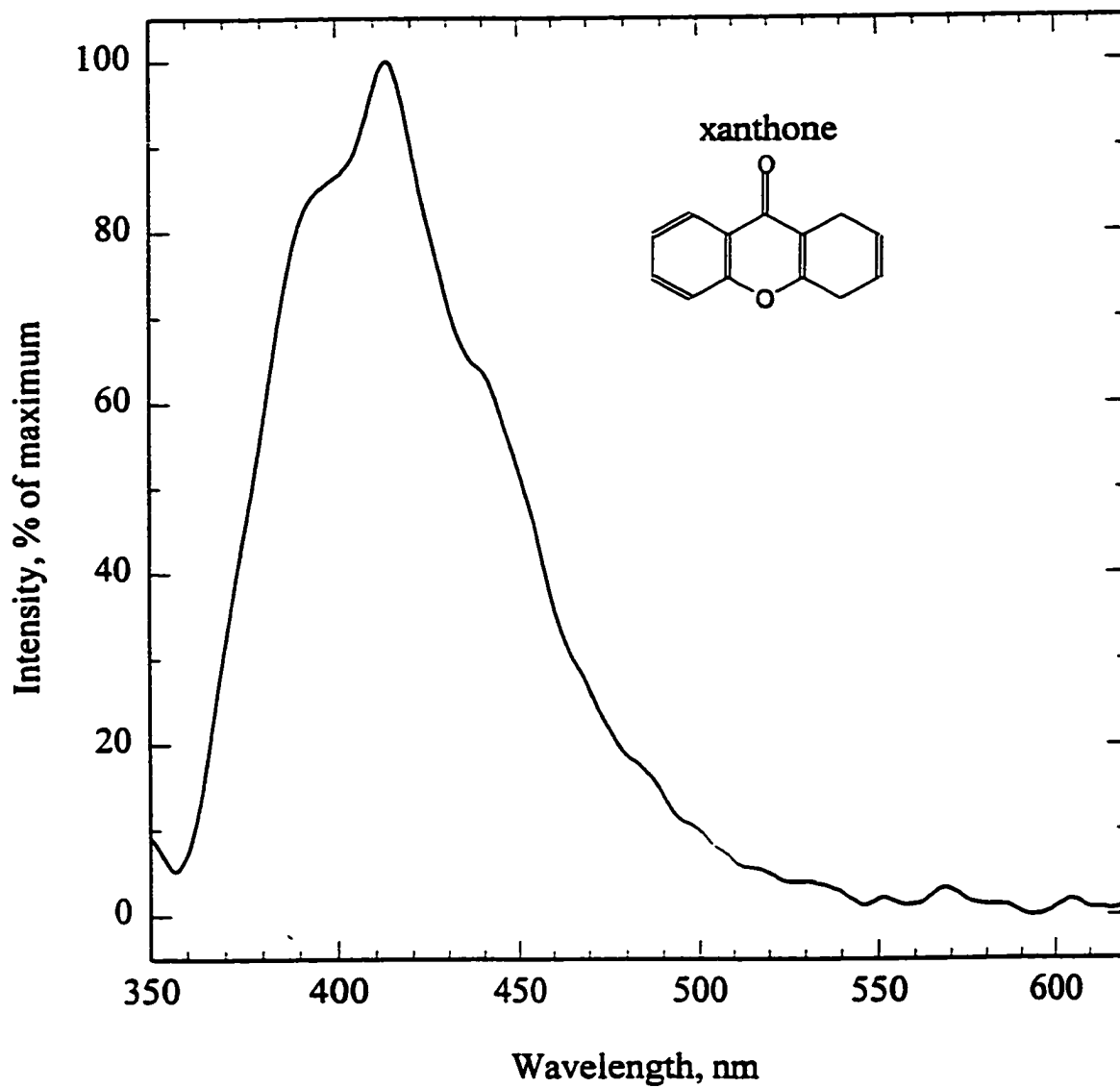
Figure 4.57 Gas-phase luminescence spectrum of xanthone in excited nitrogen obtained by using 1/8 meter grating monochromator, R-374 PMT and single-peak mode. Bandpass: 6.6 nm.
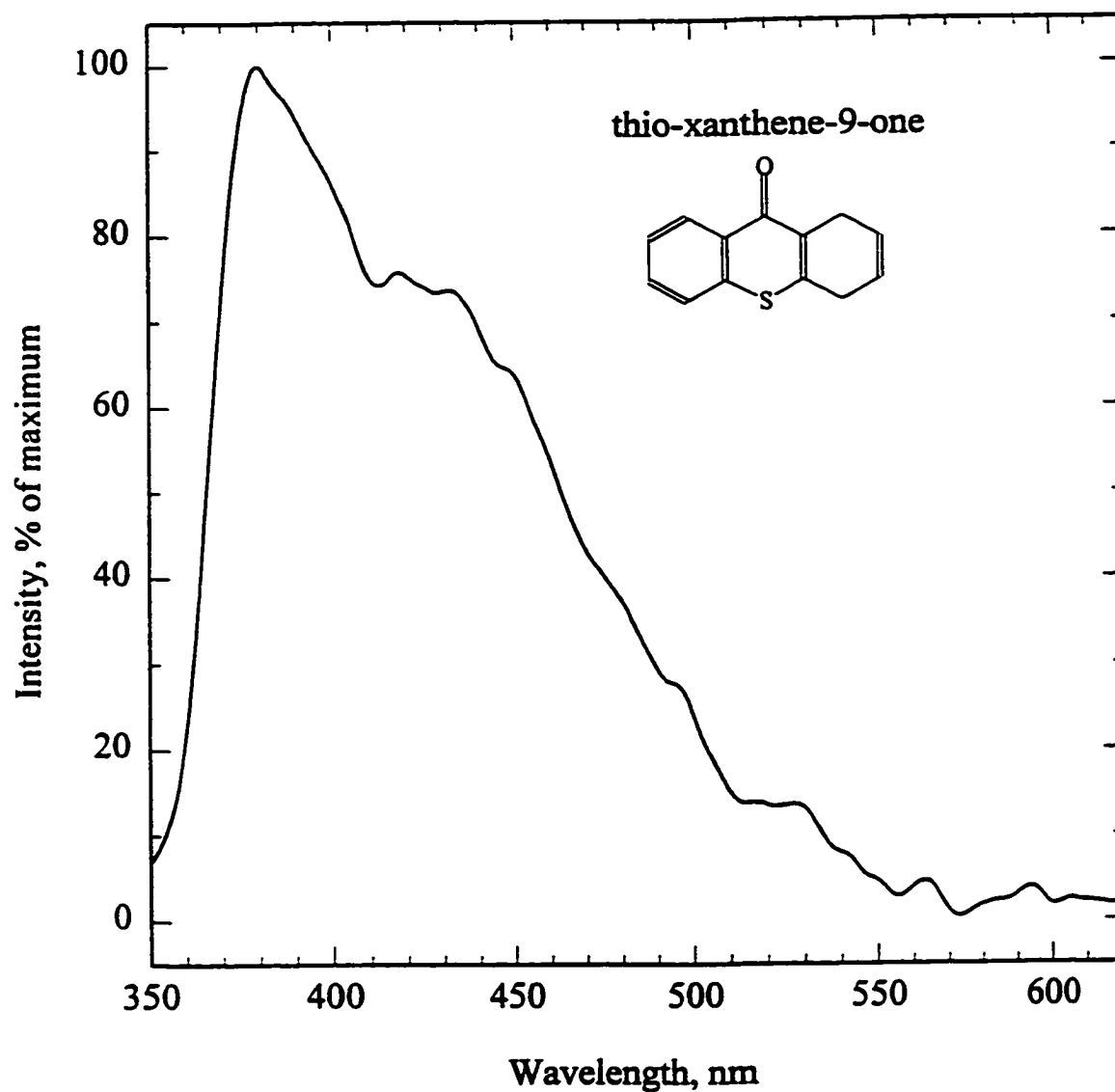
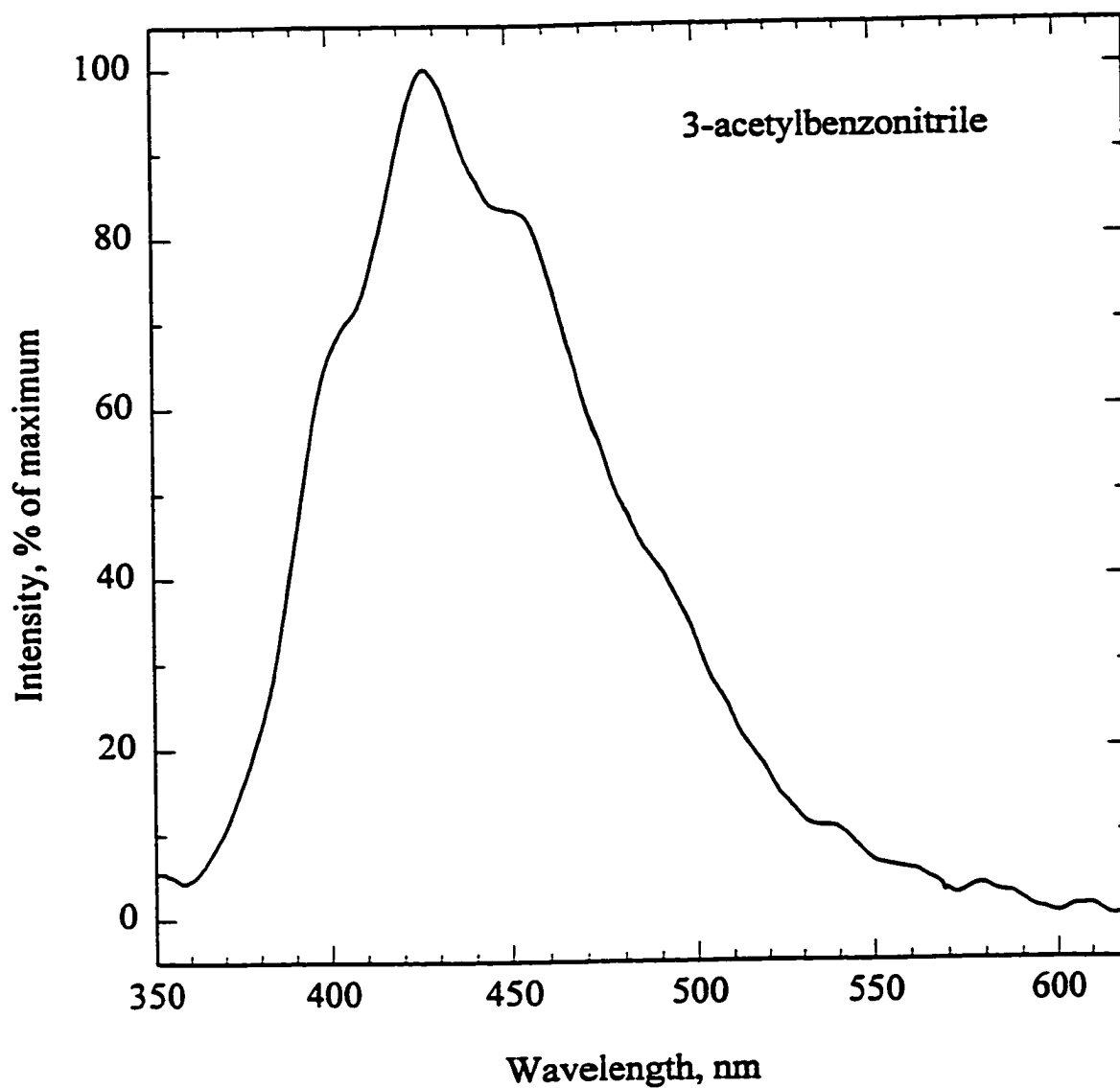**Figure 4.58** Gas-phase luminescence spectrum of thio-xanthene-9-one in excited nitrogen obtained by using 1/8 meter grating monochromator, R-374 PMT and single-peak mode. Bandpass: 6.6 nm.

spectrum of thio-xanthene-9-one. This is in striking contrast to the case of xanthone where the main radiative mechanism is possibly vibronic (see Figure 4.59). This result shows substantial difference from the few published emission data available on thio-xanthene-9-one (126).

4.3.7 α-Tetralone

The phosphorescence behavior of aromatic ketones is rather complex. A dual or even triple structured phosphorescence emission has been reported (124. 127-129). Several emission studies of α-tetralone have been done in rigid media (94.128-130) or in single crystal host of durene (131). It was reported that α-tetralone shows phosphorescence from a triplet n,π* state with origin at about 25,450 cm⁻¹ (393 nm) (94. 128-131). Kanda and co-workers (128) concluded that, unlike 1-indanone, which exhibits dual phosphorescence from a short-lived (1.5-2 msec) triplet n,π* state and a long-lived (0.15-0.22 sec) triplet state with mixed n,π* and π,π* character due to the reversible photochemical formation of the enolate anion, α-tetralone does not emit dual phosphorescence in accord with the lowered acidity. However, it was pointed out by Chu and Kearns (129) that this interpretation was incorrect and they observed the dual phosphorescence from α-tetralone and attributed the short-lived emission to emission from a T_1 (n,π*) state and the long-lived emission to emission of photoreduction products. Chu and Kearns (129) presented the authentic phosphorescence spectrum of α-tetralone from the triplet n,π* state with three main peaks at about 25,253 cm⁻¹
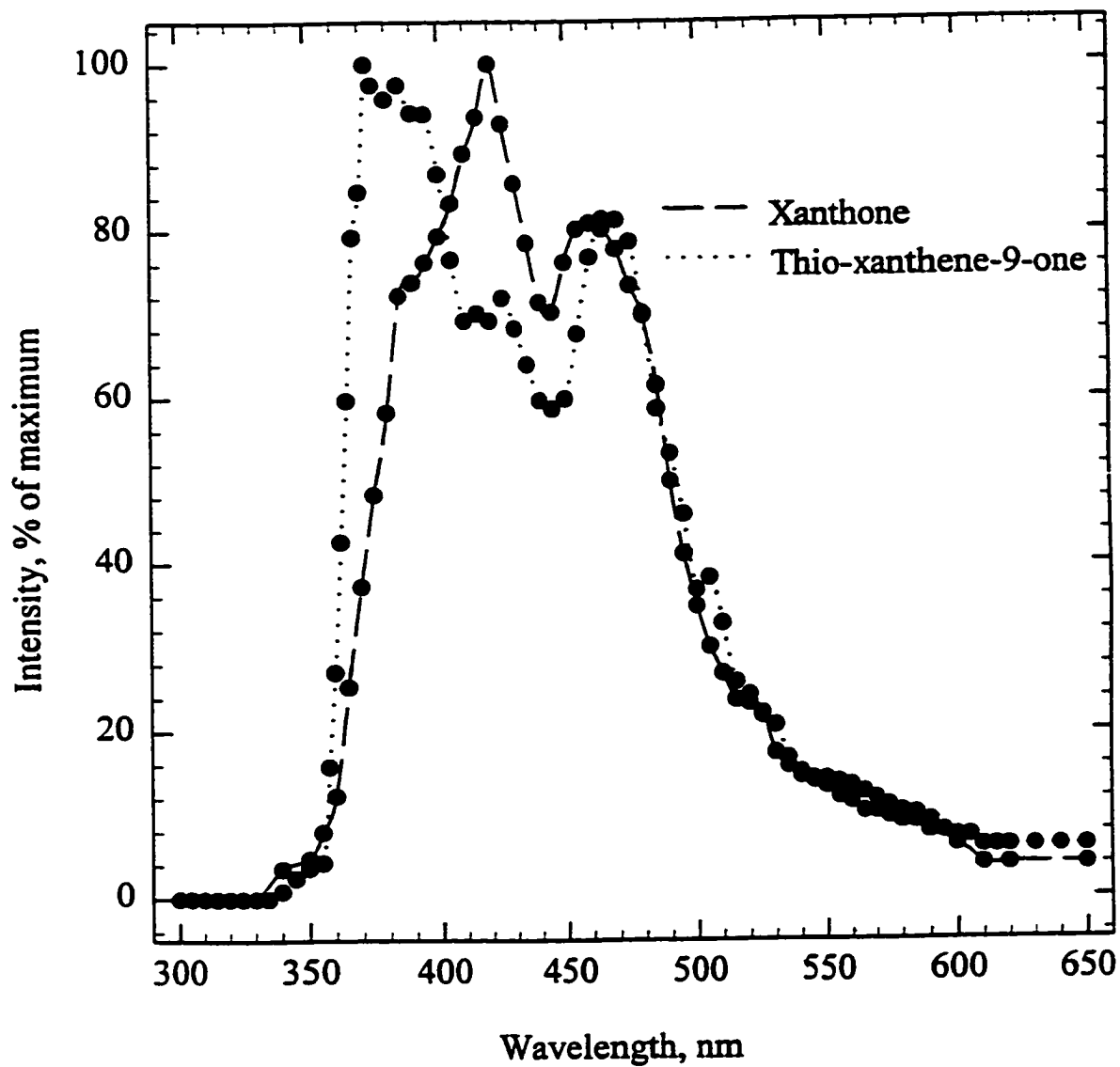
Figure 4.59 Comparison of gas-phase luminescence spectra of xanthone and thio-xanthene-9-one in excited nitrogen obtained by using 1/4 meter grating monochromator, R-374 PMT and repeated injection mode. Bandpass: 6.6 nm.

(396 nm) 23,641 cm^{-1} (423 nm) and 21,882 cm^{-1} (457 nm), respectively, and concluded that the emission spectra which had been published before had been mixtures of short- and long-lived components.

The emission spectrum of α-tetralone in the gas phase has not been reported before. It is for the first time that we present the gas-phase luminescence spectrum of α-tetralone (Figure 4.60) in excited nitrogen with added argon which enhances the emission intensity of some weakly luminescing aroyl compounds such as α-tetralone, 9-anthraldehyde and dibenzosuberenone (see section 4.9). The spectrum shows little structure with a maximum at 23,529 cm^{-1} (425 nm) and two shoulders at about 25,125 cm^{-1} (398 nm) and 21,925 cm^{-1} (456 nm). This spectrum is very similar in band position and emission band intensity to the phosphorescence spectrum of α-tetralone in rigid media (94, 128, 129). We tentatively assign the gas-phase luminescence spectrum of α-tetralone as the phosphorescence spectrum mainly from a T_1 (n,π*) state with origin at about 25,125 cm^{-1} (398 nm), but beyond this we have no detailed information about the nature of the excited triplet state.

4.3.8 Anthrone

The photophysical and photochemical behavior of carbonyl compounds has been the subject of numerous studies, while anthrone has received only very limited attention. In rigid media, it was reported that anthrone exhibits phosphorescence from the lowest n,π* state with origin at 25,150 cm^{-1} (397.6 nm) (66, 94, 132). The other prominent peaks occur at about 23,331 cm^{-1} (430 nm), 21,739 cm^{-1} (460 nm), 20,202 cm^{-1}
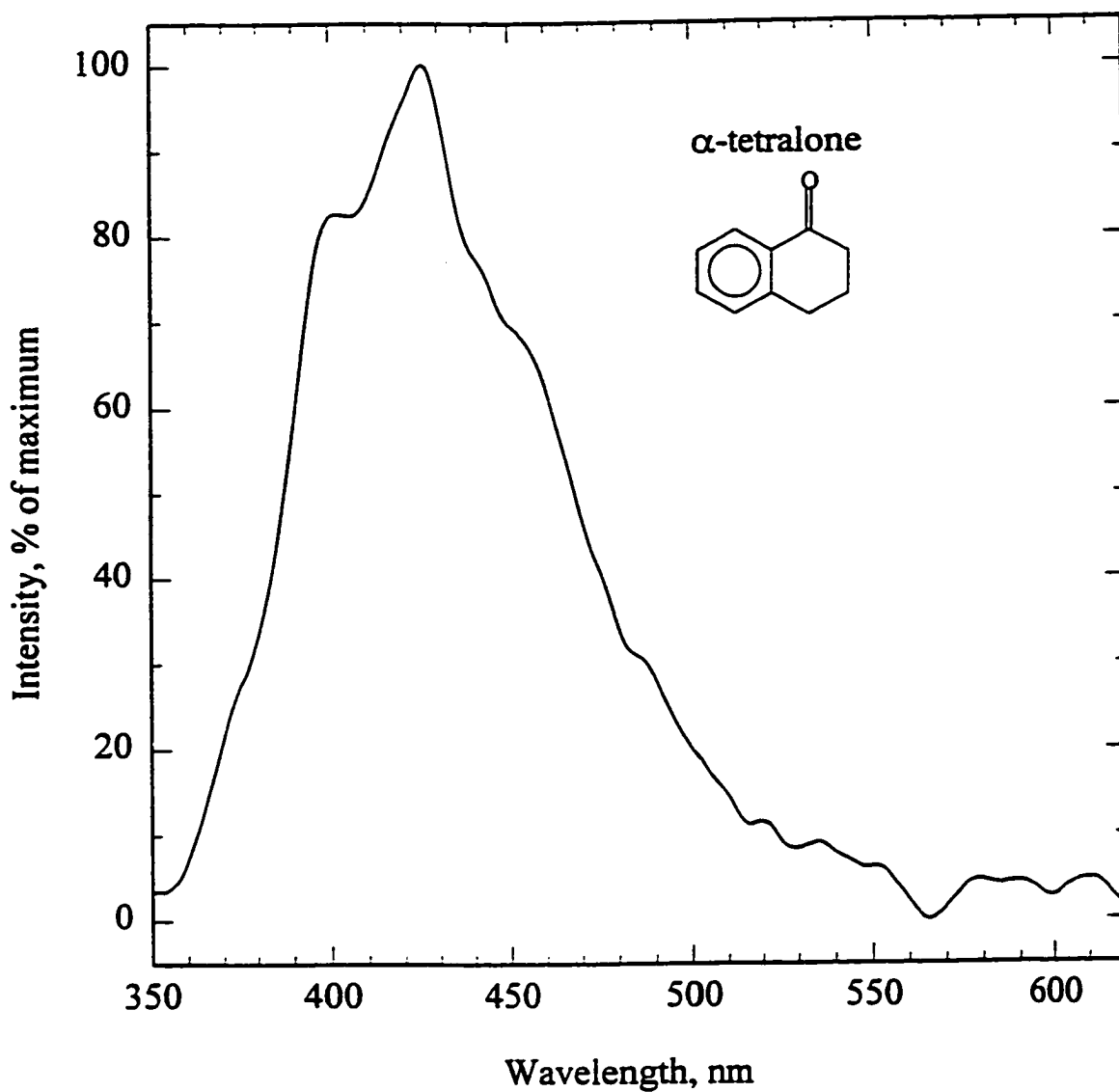
Figure 4.60 Gas-phase luminescence spectrum of α-tetralone in excited nitrogen obtained by using 1/8 meter grating monochromator, R-374 PMT and single-peak mode. Bandpass: 12.6 nm. Ar doped into nitrogen: 100 mL/min.

(495 nm) and 18,691 cm^{-1} (535 nm) and show the appearance of aromatic C=O vibrational frequency (94).

Figure 4.61 shows the gas-phase luminescence spectrum of anthrone in excited nitrogen. An examination of this spectrum indicates that although it is very different from the pure phosphorescence spectrum of anthrone in rigid media (94), it is very similar in spectral shape and band position to the gas-phase luminescence spectrum of benzophenone in excited nitrogen which is assigned as consisting of E-type delayed fluorescence and phosphorescence. Given the structural resemblance between anthrone and benzophenone and the similarity of their spectra, the same spectral assignment could be made for anthrone. A similar analogy in their photochemical behavior was reported by Scaiano and Lee (133).

4.3.9 9-Anthraldehyde

Yang (134) estimated, by analogy, that the low-lying triplet of 9-anthraldehyde is at about 14,800 cm^{-1} (676 nm) and π,π^* in nature. Warwick and Wells (135) confirmed the lowest π,π^* triplet state in 9-anthraldehyde by the oxygen perturbation technique. Hirayama (136) carried out the kinetic studies relevant to the excited singlet and triplet states on eighteen carbonyl compound of anthracene in EPA at 77 K and concluded that the 0-0 band of the fluorescence is at 21,598 cm^{-1} (463 nm) at 77 K and the phosphorescence from a triplet π,π^* state with origin at 13,790 cm^{-1} (725 nm) is very similar, in spectral shape and energy of the lowest triplet state, to that of anthracene.
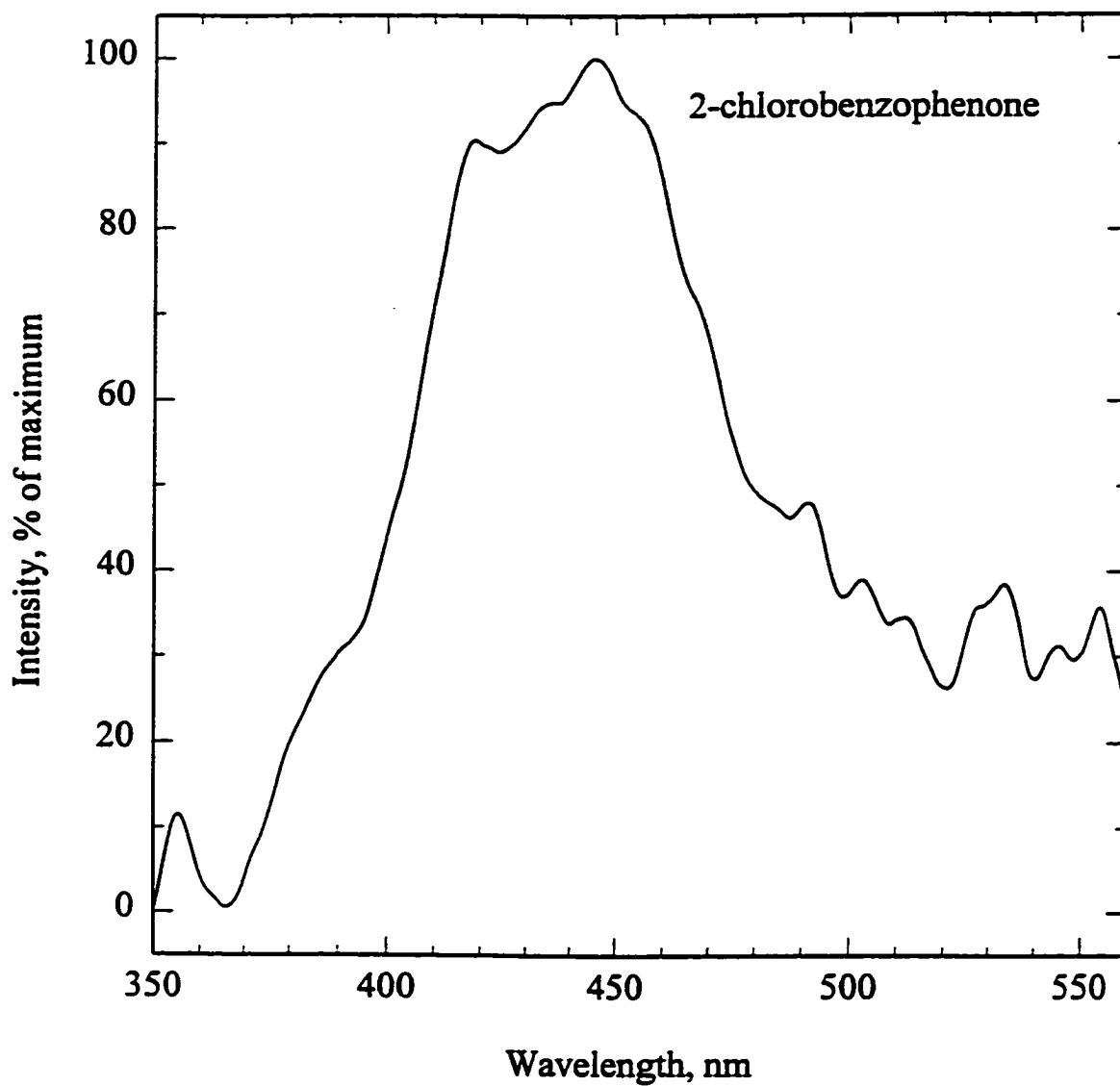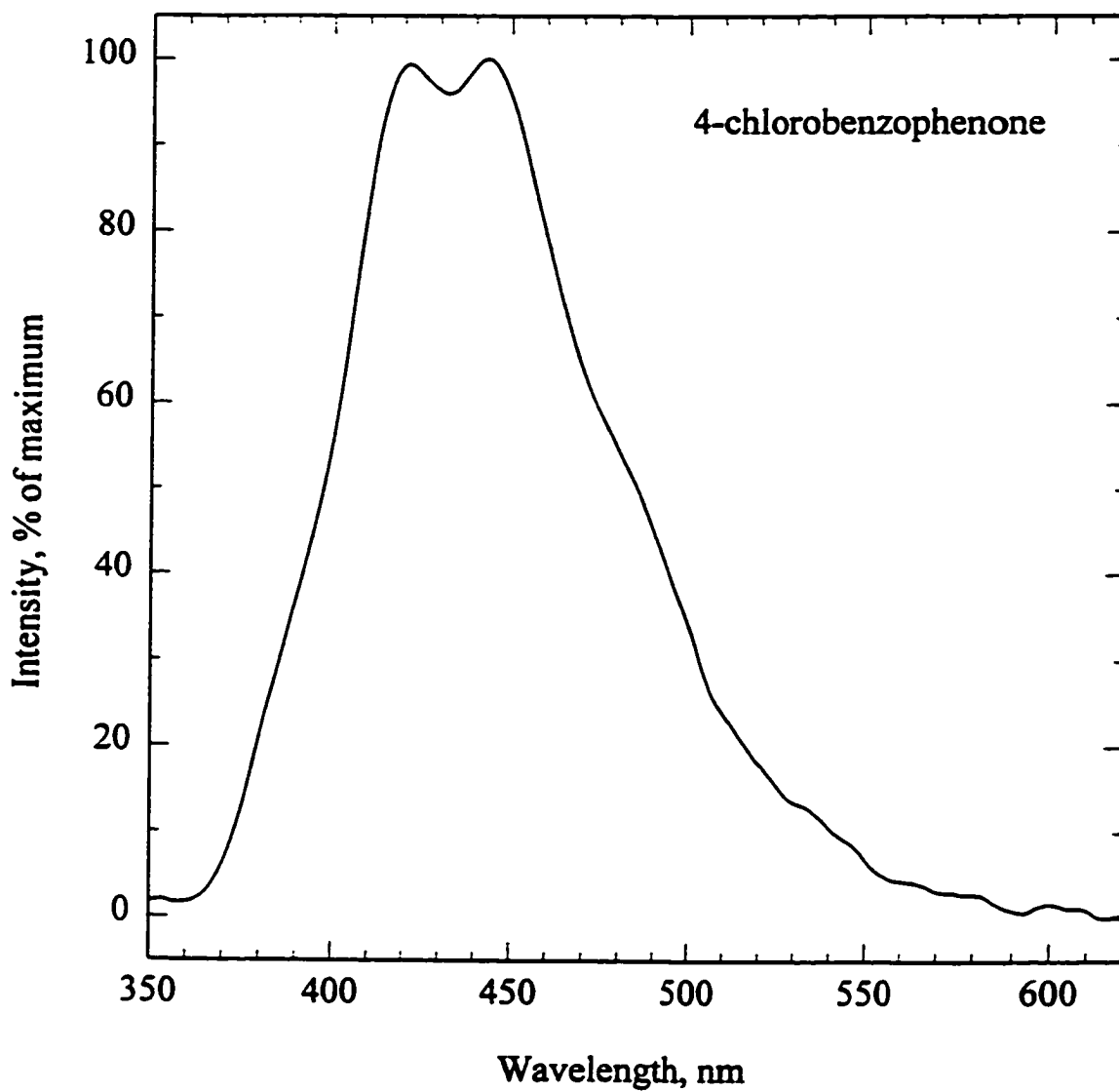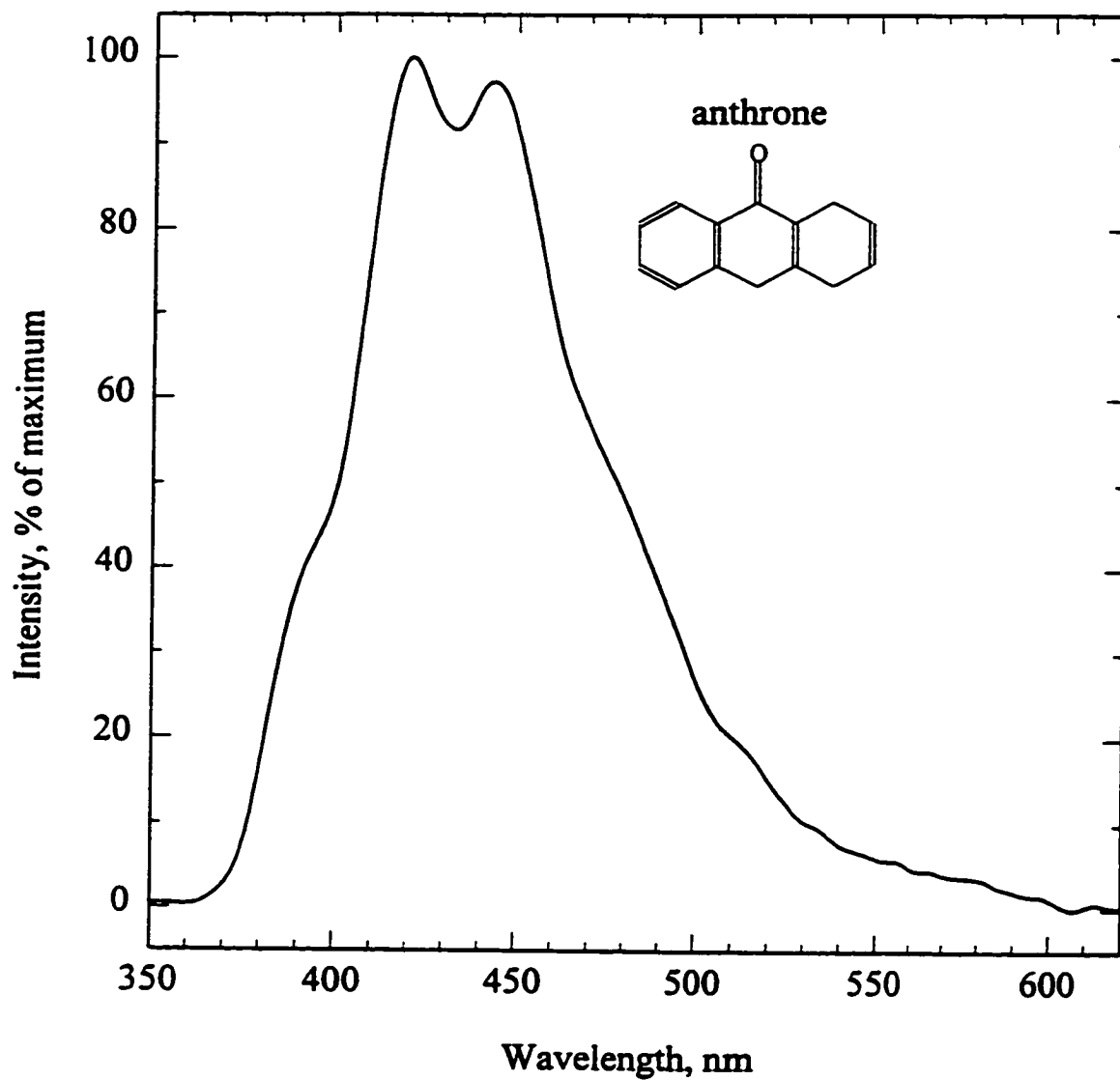
Figure 4.61 Gas-phase luminescence spectrum of anthrone in excited nitrogen obtained by using 1/8 meter grating monochromator, R-374 PMT and single-peak mode. Bandpass: 6.6 nm.

In excited nitrogen, 9-anthraldehyde shows relatively weak emission in the gas phase. The gas-phase luminescence spectrum of 9-anthraldehyde (Figure 4.62) has two main peaks at 22,471 cm^{-1} (445 nm) and 20,833 cm^{-1} (480 nm) with two shoulders at about 24,096 cm^{-1} (415 nm) and 19,230 cm^{-1} (520 nm). This spectrum is very similar to the fluorescence spectrum in rigid media in spectral shape and band position. Since the phosphorescence of 9-anthraldehyde lies in a long-wavelength region (650-850 nm), the fact that we could not observe it might simply be due to the wavelength range (400-700 nm) of the filter monochromator.

4.3.10 trans-Cinnamaldehyde and Dibenzosuberenone

To the best of our knowledge, the photophysical behavior of trans-cinnamaldehyde and dibenzosuberenone have not been investigated in solution or in the gas phase. In this study, both of these two compounds emit weakly in excited nitrogen. The gas-phase luminescence spectra of trans-cinnamaldehyde and dibenzosuberenone are shown in Figures 4.63 and 4.64, respectively. An examination of Figure 4.63 indicates that trans-cinnamaldehyde emits a similar spectrum as benzaldehyde in the gas phase, except for the red shift. The spectrum exhibits prominent peaks at about 25,063 cm^{-1} (399 nm), 23,366 cm^{-1} (428 nm), 21,739 cm^{-1} (460 nm) and 20,040 cm^{-1} (499 nm), respectively, and shows the appearance of aromatic C=O vibrational frequency of 1674 cm^{-1}. We assigned the present spectrum as that of trans-cinnamaldehyde phosphorescence from a T_1 (n,π^*) state. This means that the C=C group conjugating with the carbonyl group and the benzene ring does not change the nature of excited state in benzaldehyde, but does lower the energy
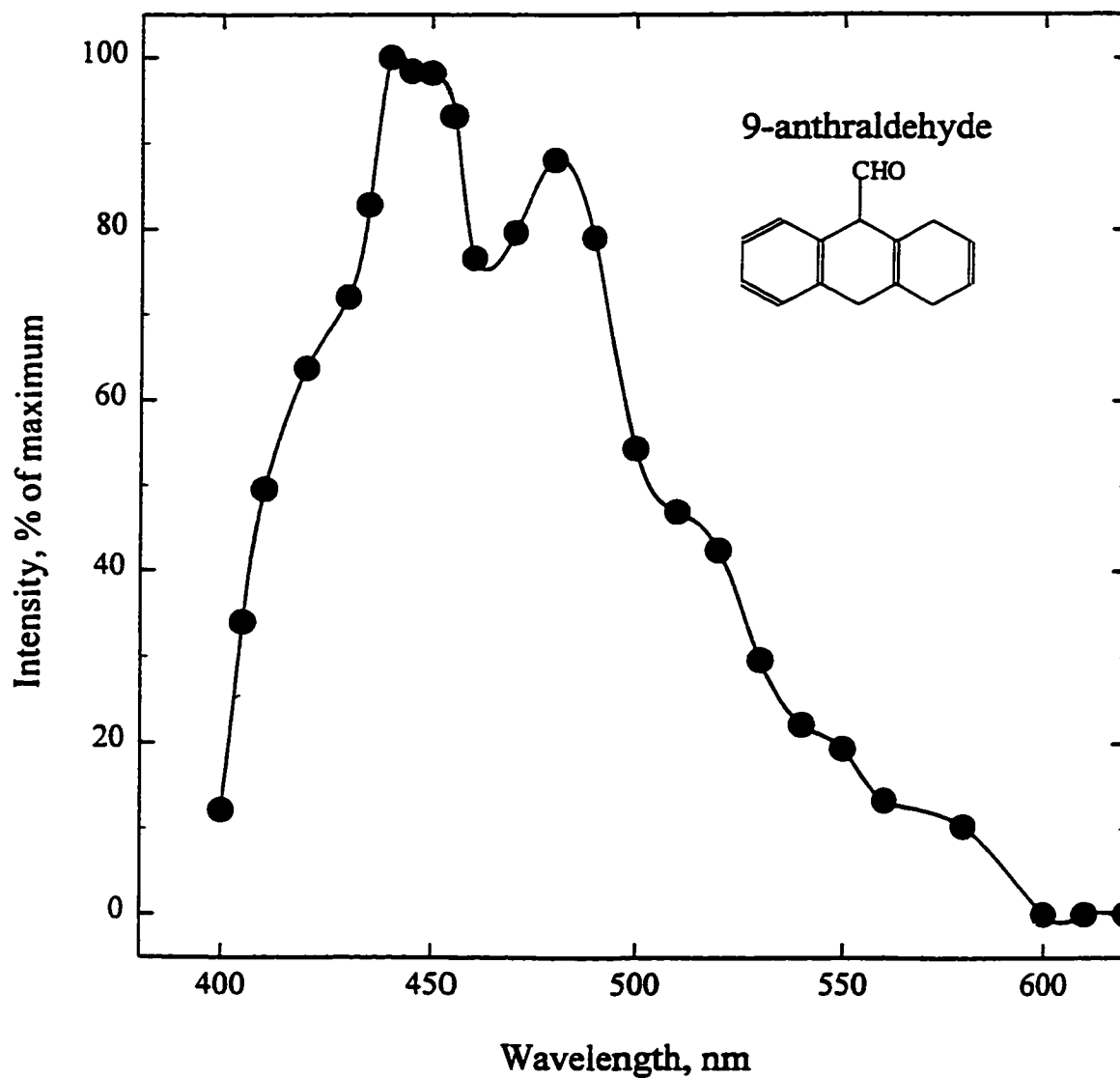
Figure 4.62 Gas-phase luminescence spectrum of 9-anthraldehyde in excited nitrogen obtained by using a filter monochromator, R-268 PMT and repeated injection mode. 2 mm slit (corresponding to a 13 nm bandpass at 400 nm).
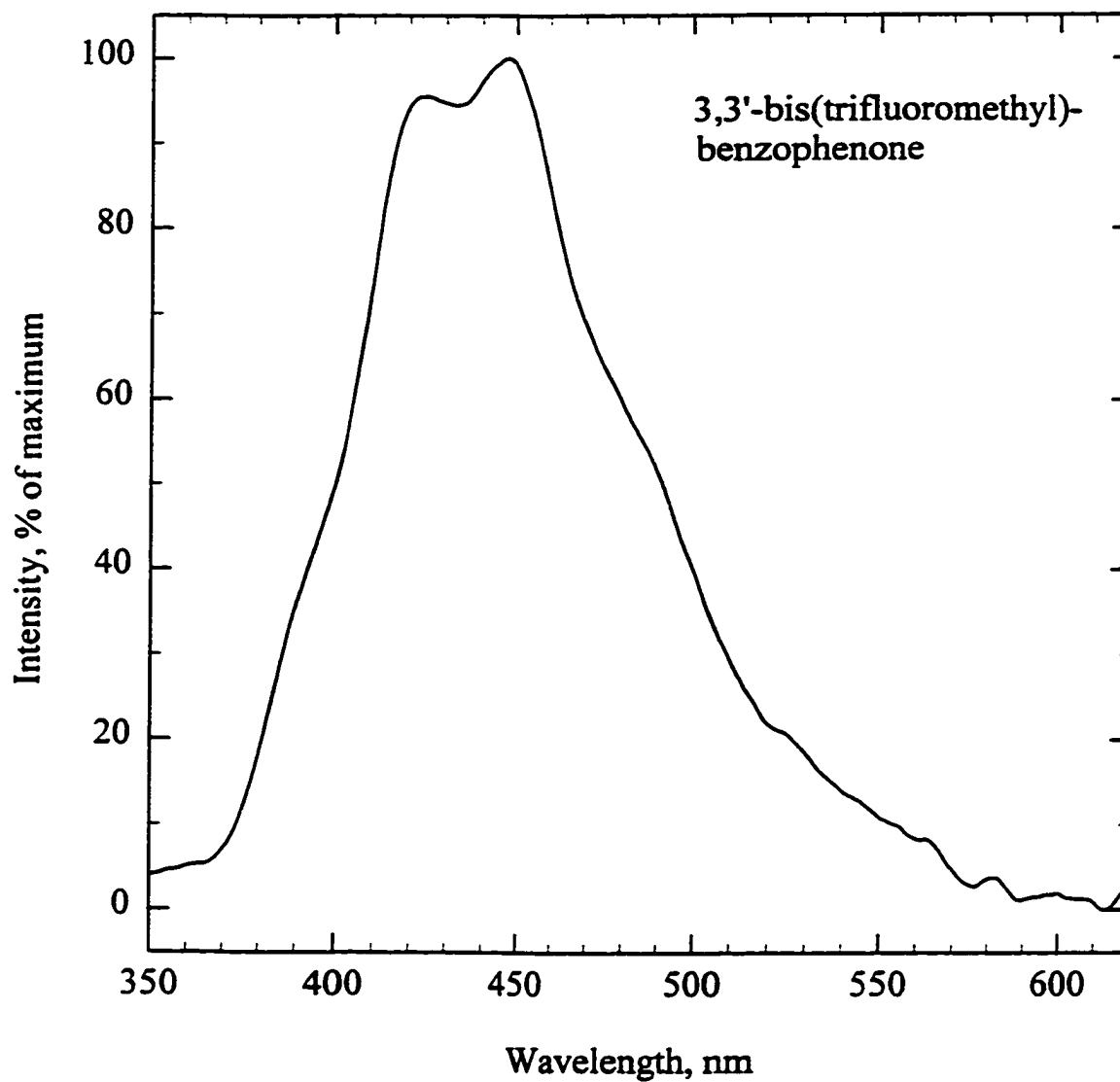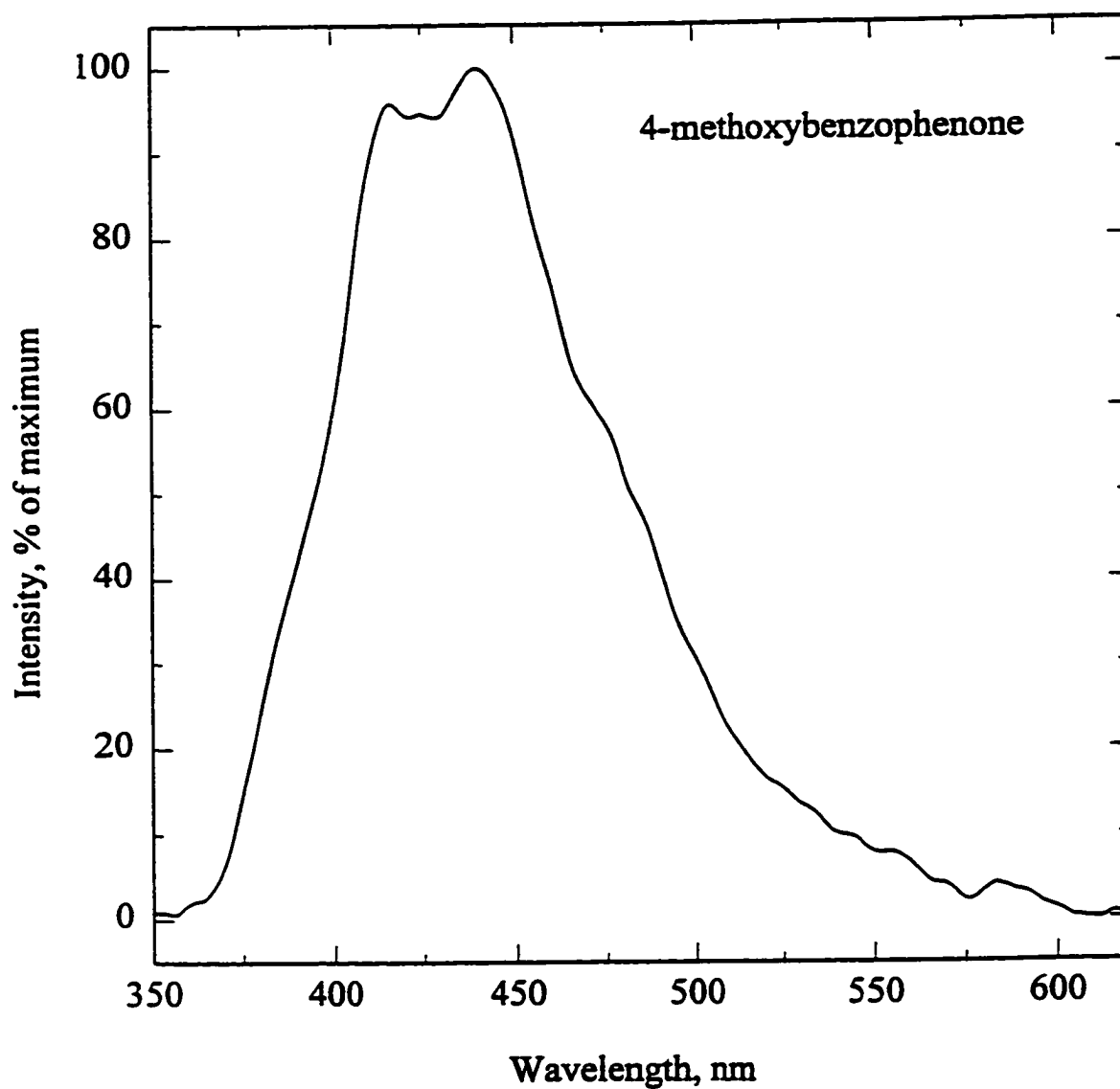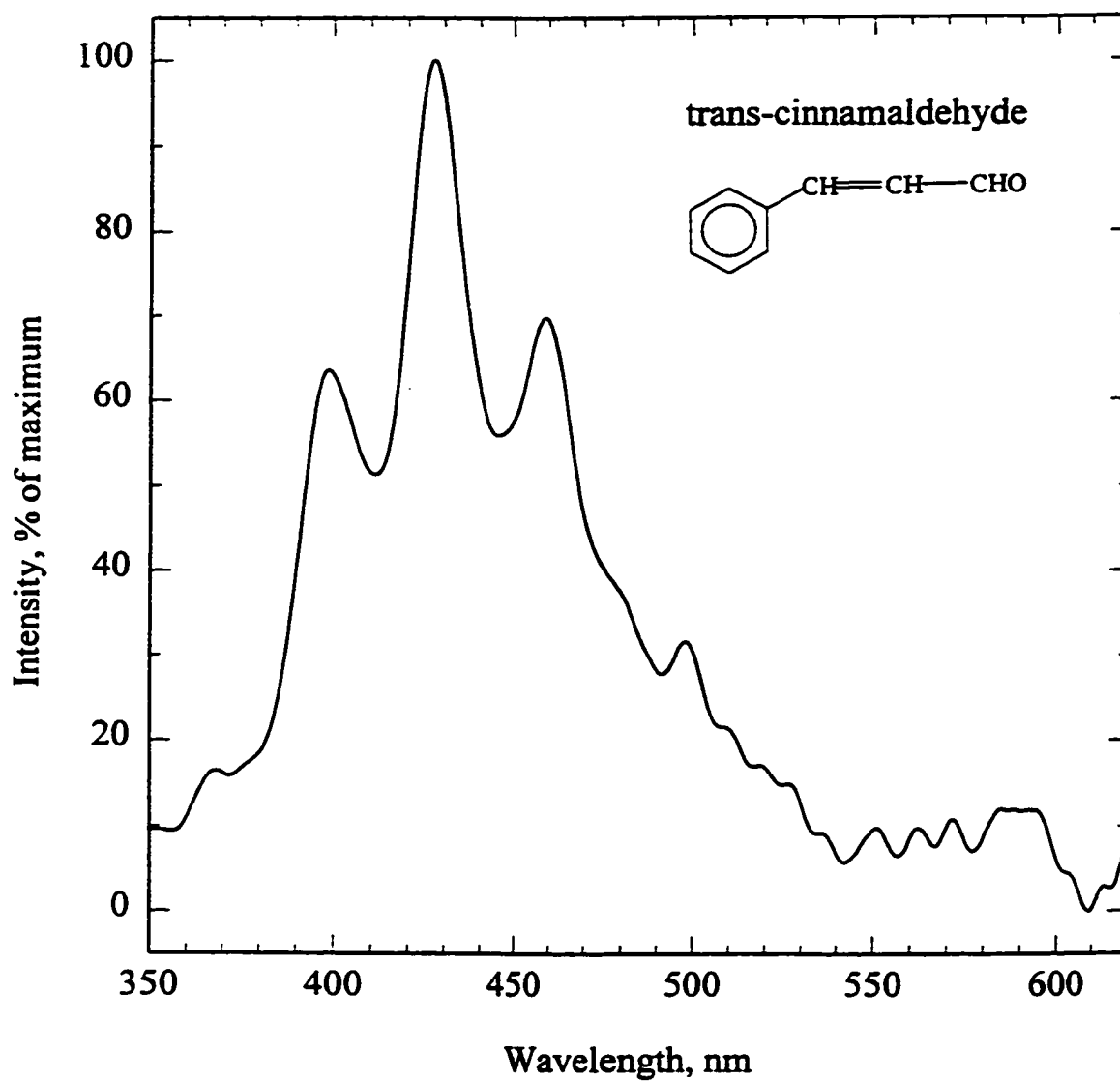
Figure 4.63   Gas-phase luminescence spectrum of trans-cinnamaldehyde in excited nitrogen obtained by using 1/8 meter grating monochromator, R-374 PMT and single-peak mode. Bandpass: 6.6 nm. Note: the features above 500 nm are due to noise.
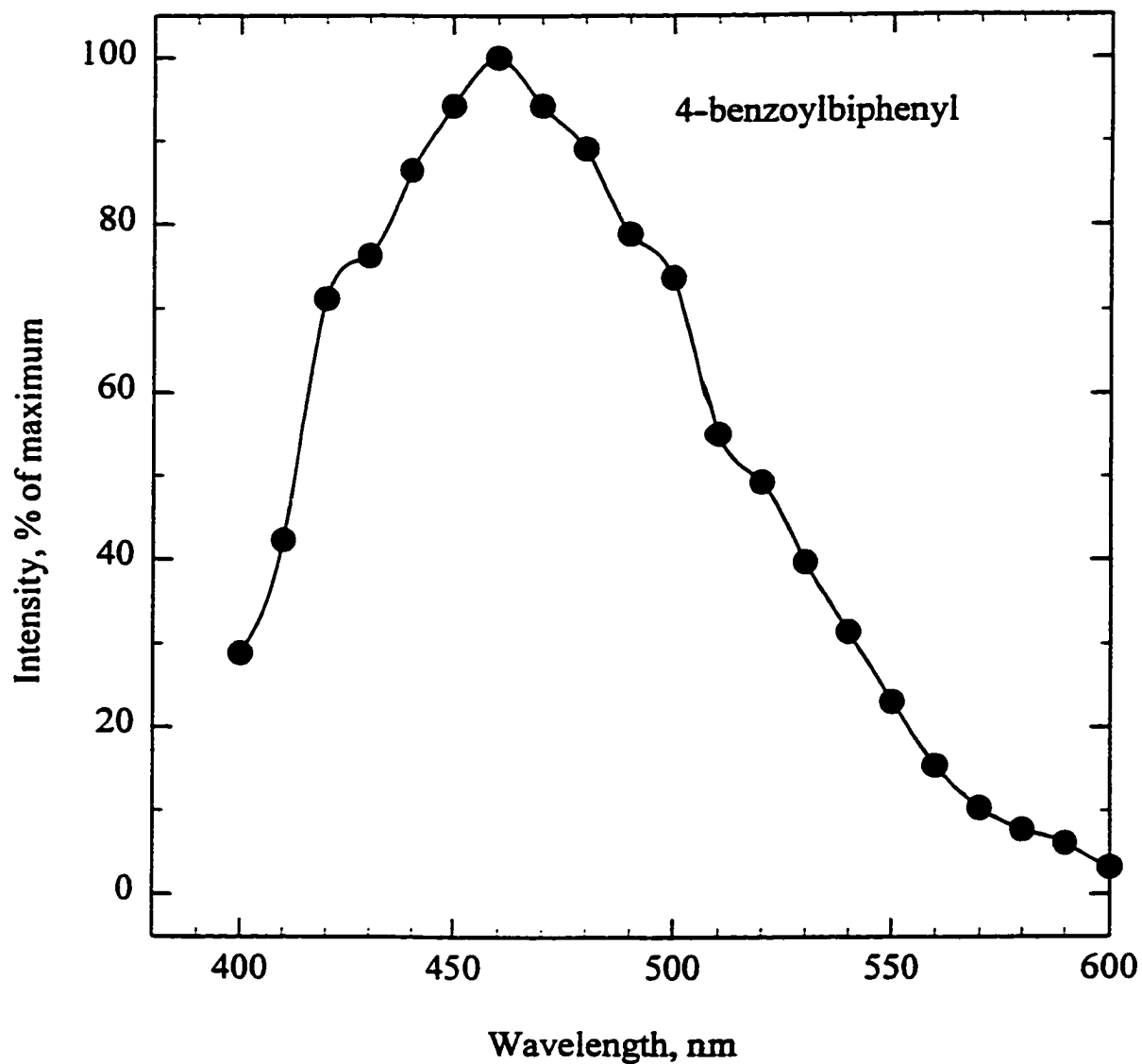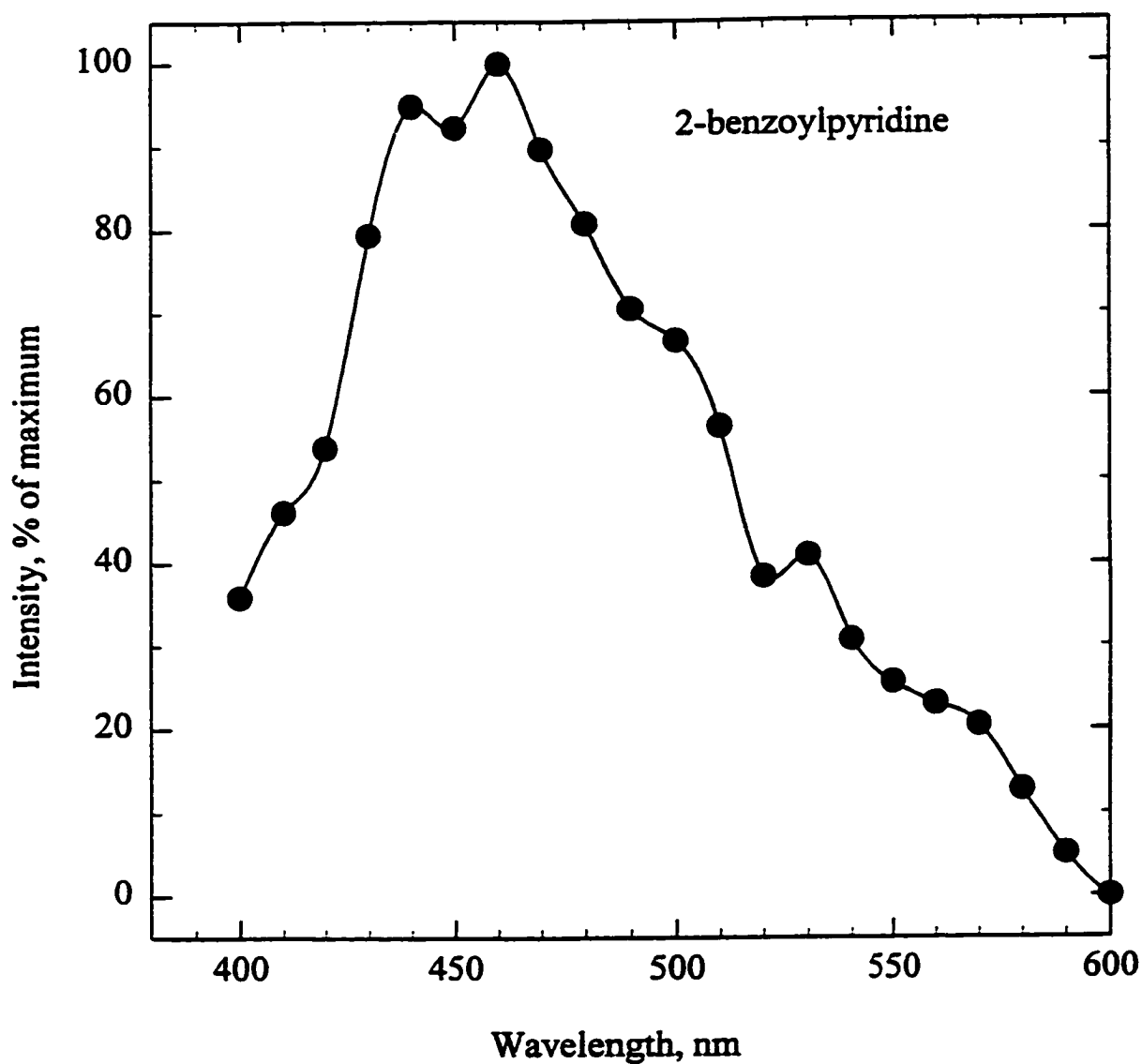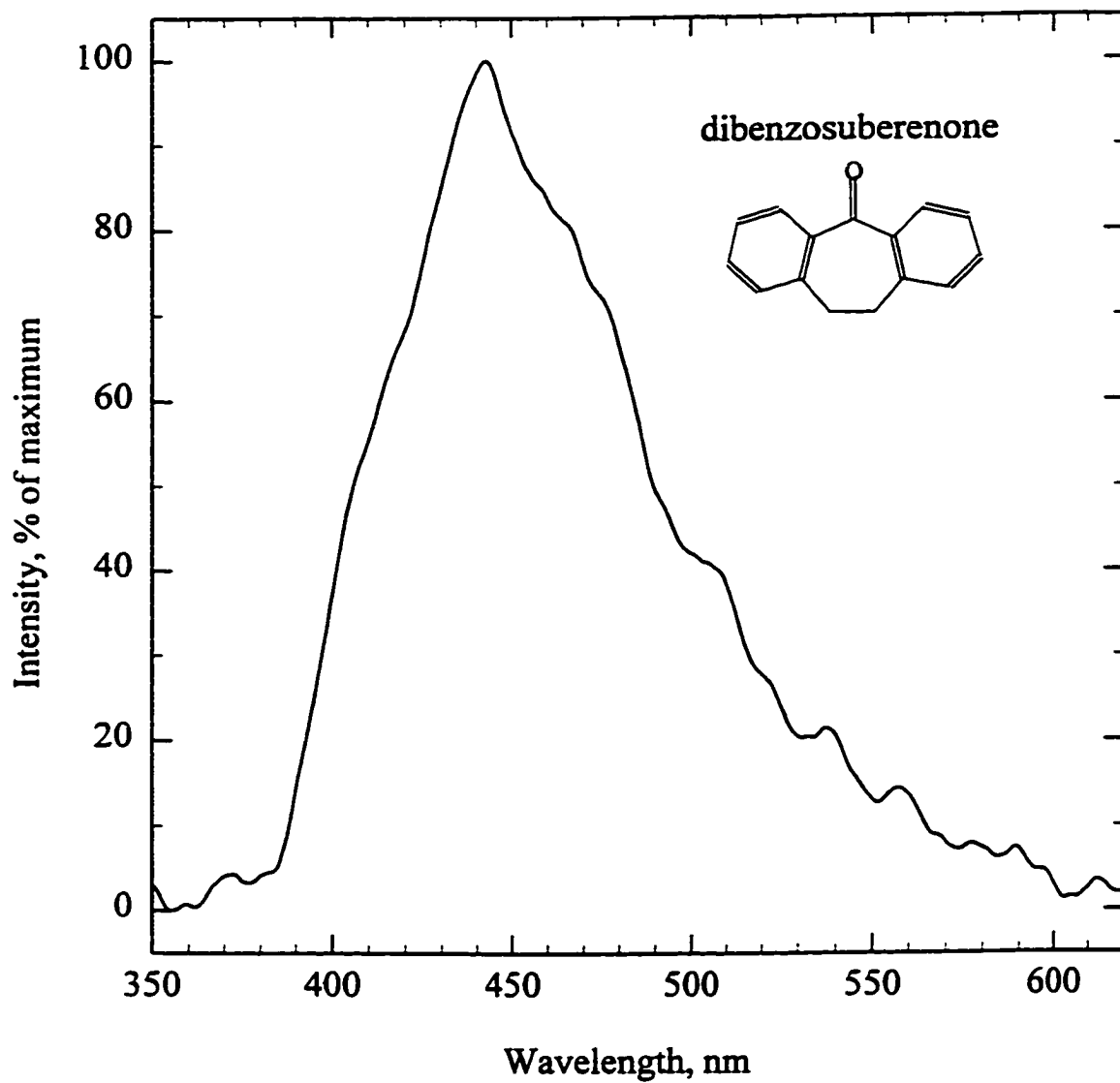
Figure 4.64 Gas-phase luminescence spectrum of dibenzosuberenone in excited nitrogen obtained by using 1/8 meter grating monochromator, R-374 PMT and single-peak mode. Bandpass: 12.6 nm. Ar doped into nitrogen: 100 mL/min.

of the excited triplet state because of the conjugative effect (59).

The gas-phase luminescence spectrum of dibenzosuberenone exhibits a broad band with a maximum at about 22,573 cm^{-1} (443 nm). No comparison can be made because there is no literature available concerning the luminescence spectrum of dibenzosuberenone. Since almost of all luminescing compounds investigated in this study emit mainly phosphorescence, we tentatively regard the gas-phase luminescence spectrum shown as that of dibenzosuberenone phosphorescence.

4.4 Triplet-State Energies of Aroyl Compounds in the Gas Phase

Intermolecular transfer of electronic energy has been applied to study new photochemical reactions, to direct the course of photochemical reactions and to elucidate the mechanisms of photochemical reactions. Triplet-triplet energy transfer is the most common and the most important type of energy transfer involved in organic photochemistry (62, 63). Knowledge of the electronic energy levels of compound may permit application of that compound as either a photosensitizer (donor) or a quencher (acceptor) in photochemical studies. For the selection of photosensitizers and quenchers. it is necessary to have available a series of compounds with triplet energies distributed over a large range.

A number of triplet state energies have been reported in the literature (137). However, most of these triplet state energies were measured in condensed phases. It is well known that solvent effects may change the nature of the lowest excited states (86) and cause significant spectral shifts (78). There are discrepancies among the values of

triplet energies because of the different polarity of solvents employed. Accurate values of triplet state energy obtained in the gas phase are still scarce. In this study, the easily detectable gas-phase phosphorescence of aroyl compounds in excited nitrogen permits measurement of this important photochemical parameter on isolated molecules.

The triplet energies can be estimated from the 0-0 band in singlet-triplet absorption spectra, from the 0-0 band in phosphorescence spectra, and from energy "titration" via triplet-triplet energy transfer. Phosphorescence is the most widely used of three common methods for determining triplet state energies, and gives the most definitive value. The triplet state energies listed in Table 4.5 were calculated from the highest energy 0-0 band maxima in the respective phosphorescence spectra. According to the Frank-Condon principle (63), if the triplet and ground states have significantly different geometries, the 0-0 band may not be the band of maximum intensity. As discussed, some aroyl compounds such as benzophenones and anthraquinones emit mainly phosphorescence from a triplet n,π^* state, but also weak E-type delayed fluorescence. In order to calculate triplet state energy, the identification of the 0-0 band of phosphorescence is important. For most of phosphorescence spectra such as these of the benzaldehydes, little difficulty was encountered in the assigning 0-0 band, since vibronic structure was usually well developed. In some other cases, e.g. of xanthone and some substituted acetophenones, the broadness of the bands made the precise assignment of the 0-0 band position more difficult.

From Table 4.5, our gas-phase values are slightly different from those measured in condensed phases; they are, however, in good agreement with literature values, where

available, for data obtained in the gas phase. A correlation was found between the n,π^* triplet state energies of several series of substituted aroyl compounds. Generally, for a given series, electron-donating substituents increase, while electron-withdrawing substituents decrease, the n,π^* triplet state energy. This correlation is illustrated in Figure 4.65, in which the triplet state energies of substituted acetophenones. benzaldehydes and benzophenones are plotted against Hammett substituent constants (σ) (137, 139, 140). A similar correlation was observed for the triplet state energies obtained in condensed phases (141). The substituent effect on the n,π^* triplet state energy has been rationalized in terms of variation in charge redistribution between the ground and excited states (142, 143) in which electron density on oxygen decreases upon excitation (78, 144).

However, in substituted anthraquinones, the substituent effect is not pronounced. This means that substituents on the aromatic rings do little to alter the character of excited states intrinsic to the anthraquinone molecule.

4.5 Ortho Effects

In the present study, the aroyl compounds having a hydrogen directly attached to the carbon substituted at the ortho position such as o-methylbenzaldehyde, o-methyl-acetophenone, o-methylbenzophenone and phthalic dicarboxaldehyde, did not luminesce to a significant extent, while the para- and meta- isomers of these compounds emitted almost as strongly as benzaldehyde (Table 2). This "ortho effect" was also observed in photophysical and photochemical studies by other researchers (83, 145, 146). The well-

Table 4.5   Triplet State Energies of Some Aroyl Compounds

Compound	Experimental Value[a], $E_T(g)$, kJ/mole	Literature Value, kJ/mole			Reference		
		$E_T(g)$[b]	$E_T(n)$[c]	$E_T(p)$[d]	$E_T(g)$	$E_T(n)$	$E_T(p)$
Benzaldehyde	301	301	301	298	82	137	137
Isophthalaldehyde	298						
Terephthal-dicarboxaldehyde	286		277			137	
3-Methylbenzaldehyde	300		302			137	
4-Methylbenzaldehyde	303		305	298		137	137
4-Ethylbenzaldehyde	302						
4-Isopropylbenzaldehyde	301						
2-Fluorobenzaldehyde	293		295			137	
3-Fluorobenzaldehyde	298		299			137	
4-Fluorobenzaldehyde	304	304	305		81	137	
2-Chlorobenzaldehyde	288		290			137	
4-Chlorobenzaldehyde	299	299	300		81	137	
2,6-Dichlorobenzaldehyde	290						
3-Cyanobenzaldehyde	295						
4-Cyanobenzaldehyde	288						
4-Acetoxybenzaldehyde	302						
3-Methoxybenzaldehyde	300						
4-Methoxybenzaldehyde	304	309	300	295	138	137	137
4-Ethoxybenzaldehyde	304						
Methyl 4-formylbenzoate	292						
4-Ethyl-formylbenzoate	292						
2-Chloroethyl 4-formylbenzoate	292						
2,2,2-Trifluoroethyl 4-formylbenzoate	292						
Heptyl 4-formylbenzoate	293						
Benzophenone	285	285	287	289	81	137	137
4-Methylbenzophenone	285		287	290		137	137
4-Methoxybenzophenone	288		287	290		137	137
3,3'-Bis(trifluoromethyl)-benzophenone	283		280	289		137	142
4-Chlorobenzophenone	285		286	288		137	137
2-Chlorobenzophoneone	285						
4,4-Dichlorobenzophenone	283		285	286		137	137
2-Benzoylpyridine	272		279	282		137	137
3-Benzoylpyridine	285		286	288		137	137

Table 4.5 (continued)

Compound	Experimental Value[a], $E_T(g)$, kJ/mole	Literature Value, kJ/mole			Reference		
		$E_T(g)^b$	$E_T(n)^c$	$E_T(p)^d$	$E_T(g)$	$E_T(n)$	$E_T(p)$
4-Benzoylpyridine	279		281	281		137	137
4-Benzoylbiphenyl	260			254			137
Acetophenone	304	304	310	311	81	137	137
3'-Methylacetophenone	304		306	303		137	137
4'-Methylacetophenone	305		305	305		137	137
4'-Fluoroacetophenone	305						
3-Acetylbenzonitrile	296		295	307		137	137
4-Acetylbenzonitrile	290		290	291		137	137
2-Acetylpyridine	289		293	296		137	137
4-Acetylpyridine	292		290	295		137	137
Anthraquinone	264	264	261	263	113	137	137
2-Methylanthraquinone	265		261			109	
2-Ethylanthraquinone	265						
1-Chloroanthraquinone	265		262			109	
Benz(g)isoquinoline-5,10-dione	265						
1,4,4a,9a-Tetrahydro-anthraquinone	265						
Anthrone	302			301			137
Xanthone	306		310	310		137	137
Thio-xanthene-9-one	315[e]		265			137	
9-Anthraldehyde	279[e]		182			136	
α-Tetralone	299		303	304		137	137
1,4-Naphthoquinone	246	245		241	117		137
2-Methyl-1,4-naphthoquinone	244	244			117		
trans-Cinnamaldehyde	300						
Dibenzosuberenone	270						

[a] Determined from the 0-0 band of the phosphorescence spectra;
[b] Triplet state energy measured in the gas phase;
[c] Triplet state energy measured in non-polar solvent;
[d] Triplet state energy measured in polar solvent;
[e] Phosphorescence origin questionable.
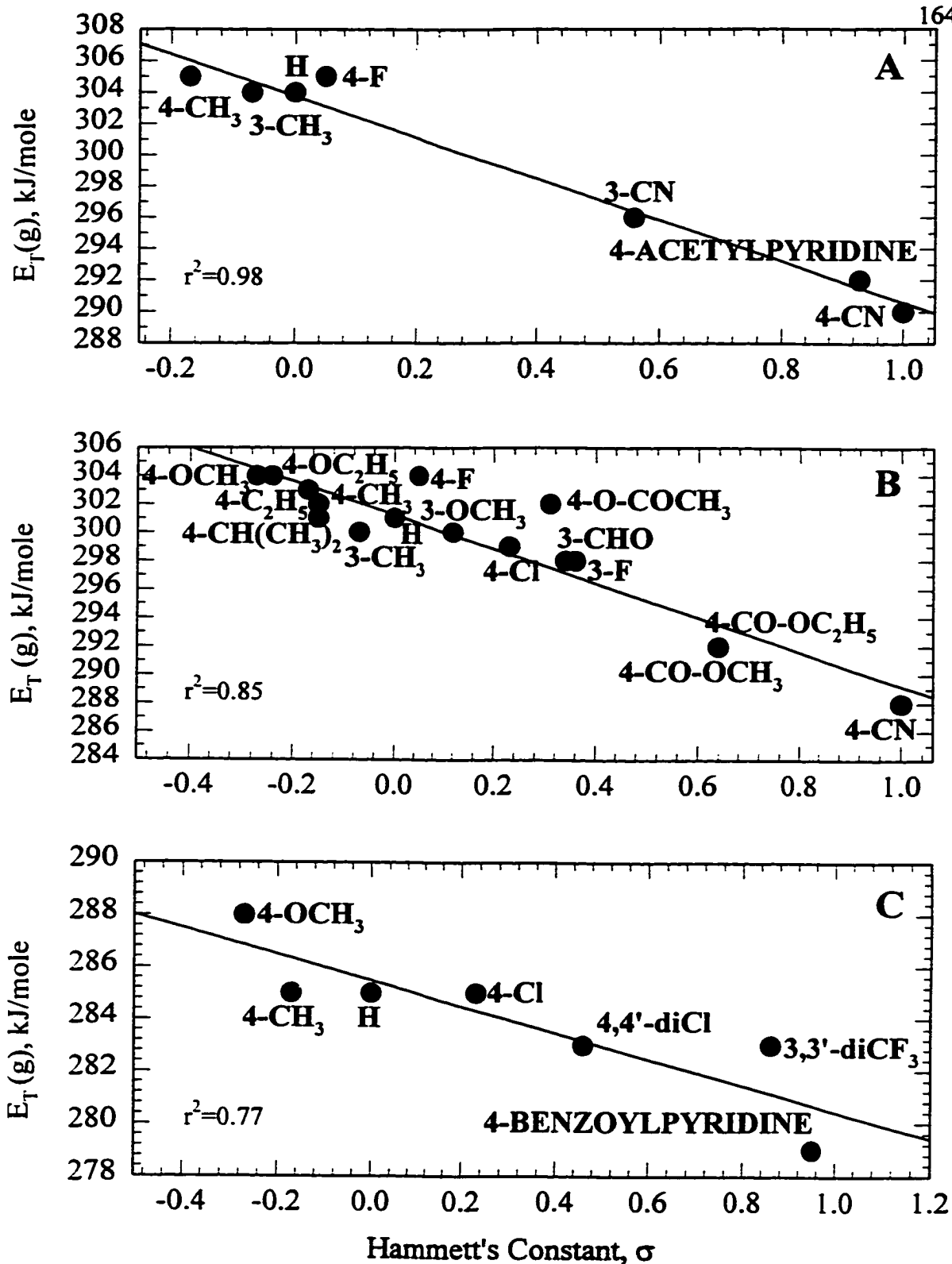
Figure 4.65 Substituent effects on the triplet energy (0-0 band) of substituted acetophenones (A), benzaldehydes (B) and benzophenones (C) in the gas phase.

known and much studied intramolecular hydrogen abstraction (photoenolization) has been used to explain this phenomenon (147-154). It is believed that there exist two triplet states, T (n,π^*) and T (π,π^*), below S_1 (n,π^*) and that they lie close to each other in the ~2000 cm^{-1} energy gap between S_1 and the lowest triplet state in aromatic carbonyl compounds (59, 62). Only T (n,π^*) states are reactive, while T (π,π^*) states are less reactive in hydrogen abstraction reaction (72, 154) in which the oxygen atom of the carbonyl group abstracts the hydrogen atom directly attached to carbon at the ortho position after excitation, leading to the formation of short-lived biradicals that decay to unstable enols (151, 153).

Another aroyl compound we have to mention is 2-cyanobenzaldehyde. This compound did not luminesce, while its para- and meta- isomers emit strongly. This may be attributed to another photochemical reaction.

4.6 A Speculative Mechanism for Luminescence of Aroyl Compounds in Excited Nitrogen

4.6.1 Background Luminescence in the ALD

Figure 4.66 shows the nitrogen background luminescence spectrum in the ALD. The emission was scanned between 200 and 800 nm under various experimental conditions, and solely consisted of the well-known nitrogen second positive band system. This system results from the radiative decay of triplet state nitrogen molecules: N_2 (C $^3\Pi_u$) $\rightarrow$ N_2 (B $^3\Pi_g$) over the range 300-400 nm with a maximum intensity at 337.1 nm. The background emission was very weak in this system, was barely visible to the dark-
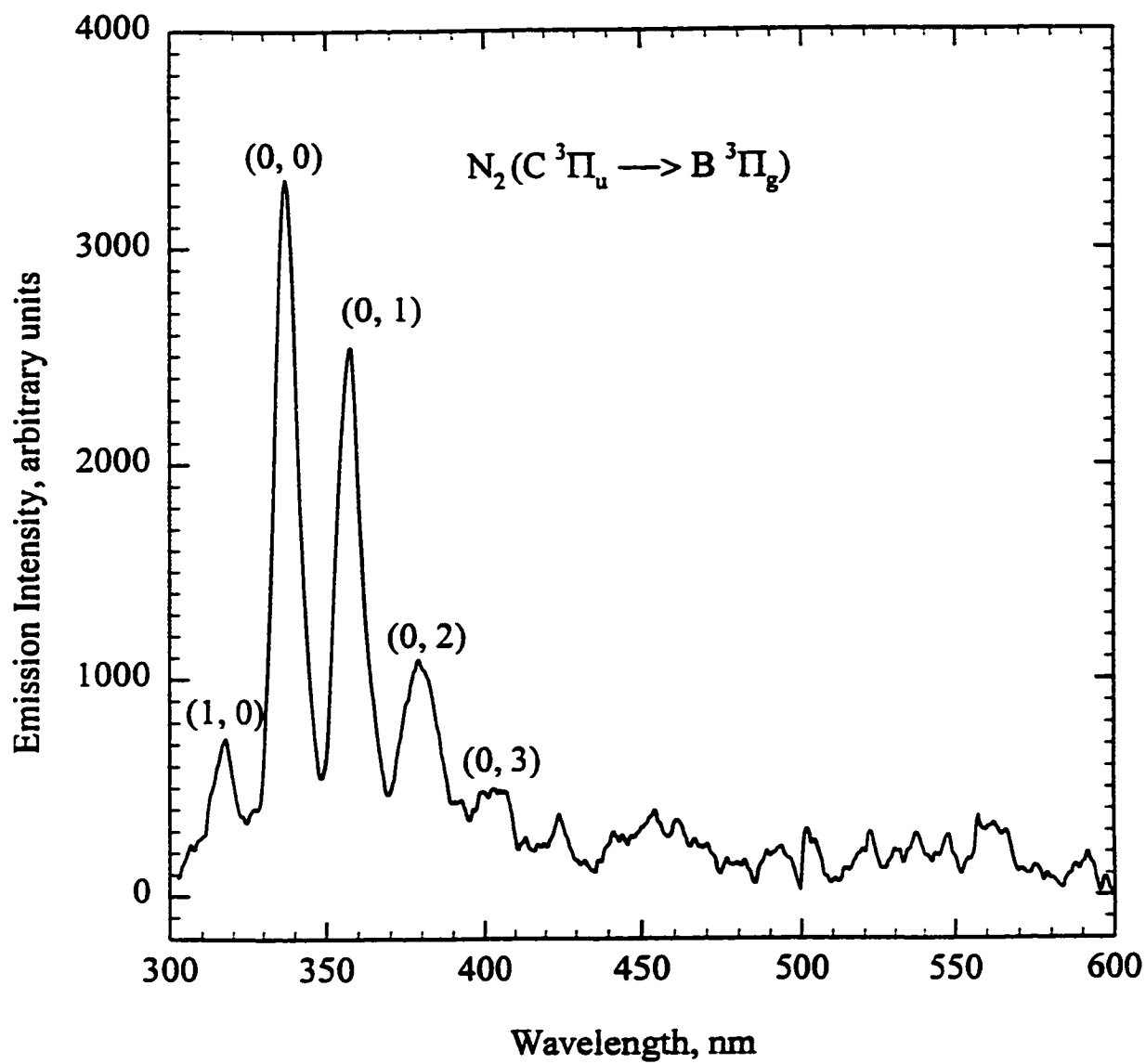
Figure 4.66 Nitrogen background spectrum in the ALD.

adapted eye and undetectable when the apparatus sensitivity was set for optimum recording of a luminescence spectrum. This is quite different from the dielectric discharge system in which a blue, flame-like nitrogen second positive emission was observed even under full room lights (28, 155). It has been shown in Figures 4.67 and 4.68 that the intensity at 337.1 nm of the nitrogen second positive emission increased with the applied DC voltage and the temperature. The nitrogen emission intensity as a function of pressure is shown in Figure 4.69. This study revealed that the emission intensity of the nitrogen second positive system increased as the pressure decreased but as the pressure was lowered, the DC voltage also had to be lowered because of sparking.

Our radioactively stimulated, high-voltage, low-current discharge was used as the excitation source. Molecular nitrogen was excited in this weak discharge (<35 nA), which is illustrated by a plot of discharge current versus applied voltage (Figure 4.70). No other nitrogen emission could be detected in the ALD system besides the nitrogen second positive system, although a careful search for the possible nitrogen first positive system $(N_2 \ (B \ ^3\Pi_g) \rightarrow N_2 \ (A \ ^3\Sigma_u^+))$ or the Vegard-Kaplan system $(N_2 \ (A \ ^3\Sigma_u^+) \rightarrow N_2 \ (X \ ^1\Sigma_g^+))$ was undertaken. This means that the second positive transition observed must generate only the low vibrational levels in the B state ($v<6$) from which no visible emission in the $N_2 \ (B \ ^3\Pi_g) \rightarrow N_2 \ (A \ ^3\Sigma_u^+)$ transition is observed (156). The absence of the Vegard-Kaplan band system $(N_2 \ (A \ ^3\Sigma_u^+) \rightarrow N_2 \ (X \ ^1\Sigma_g^+)$ may be due to some rapid reactions related to the $N_2 \ (A \ ^3\Sigma_u^+)$ state, or the low concentration of $N_2 \ (A \ ^3\Sigma_u^+)$ in the system (28, 35).
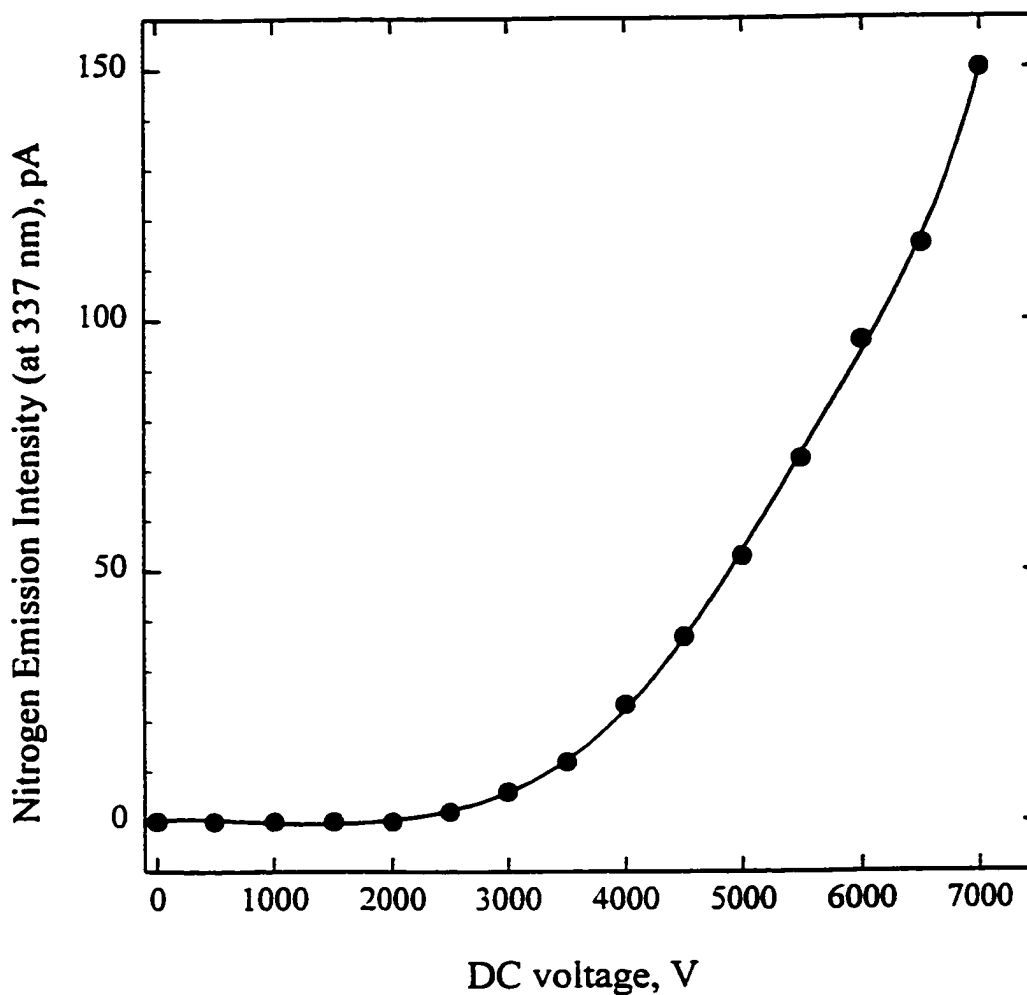
Figure 4.67 The nitrogen emission at 337 nm as a function of applied DC voltage. A 340 nm narrow-band interference filter used for monitoring the 337 nm band of nitrogen emission. Detector temperature: 200 °C; Nitrogen flow rate: 10 mL/min (carrier gas), 100 mL/min (make-up gas) and 50 mL/min (purge gas); PMT (R-374) voltage: -700 V.
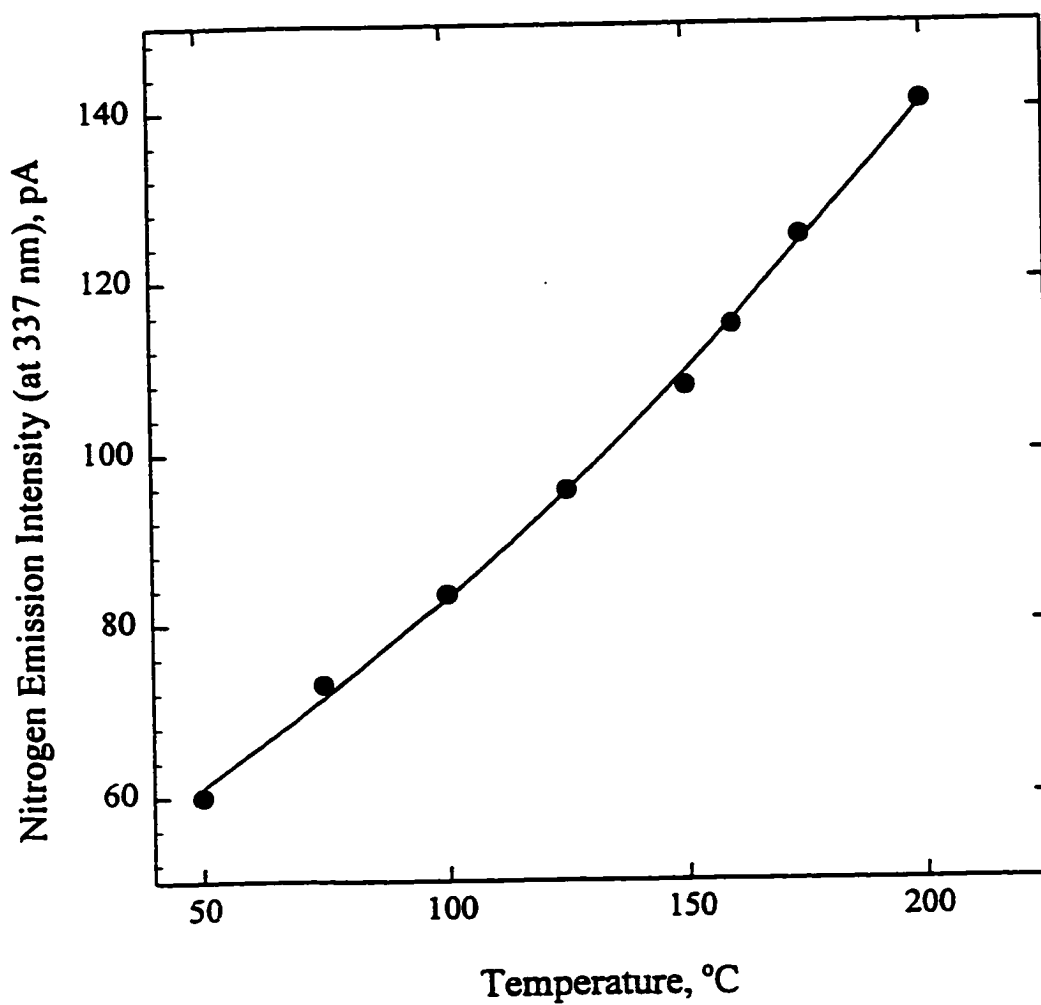
Figure 4.68   Temperature effect on the intensity of nitrogen emission at 337 nm. DC voltage: 7000 V. Other conditions as in Figure 4.67.
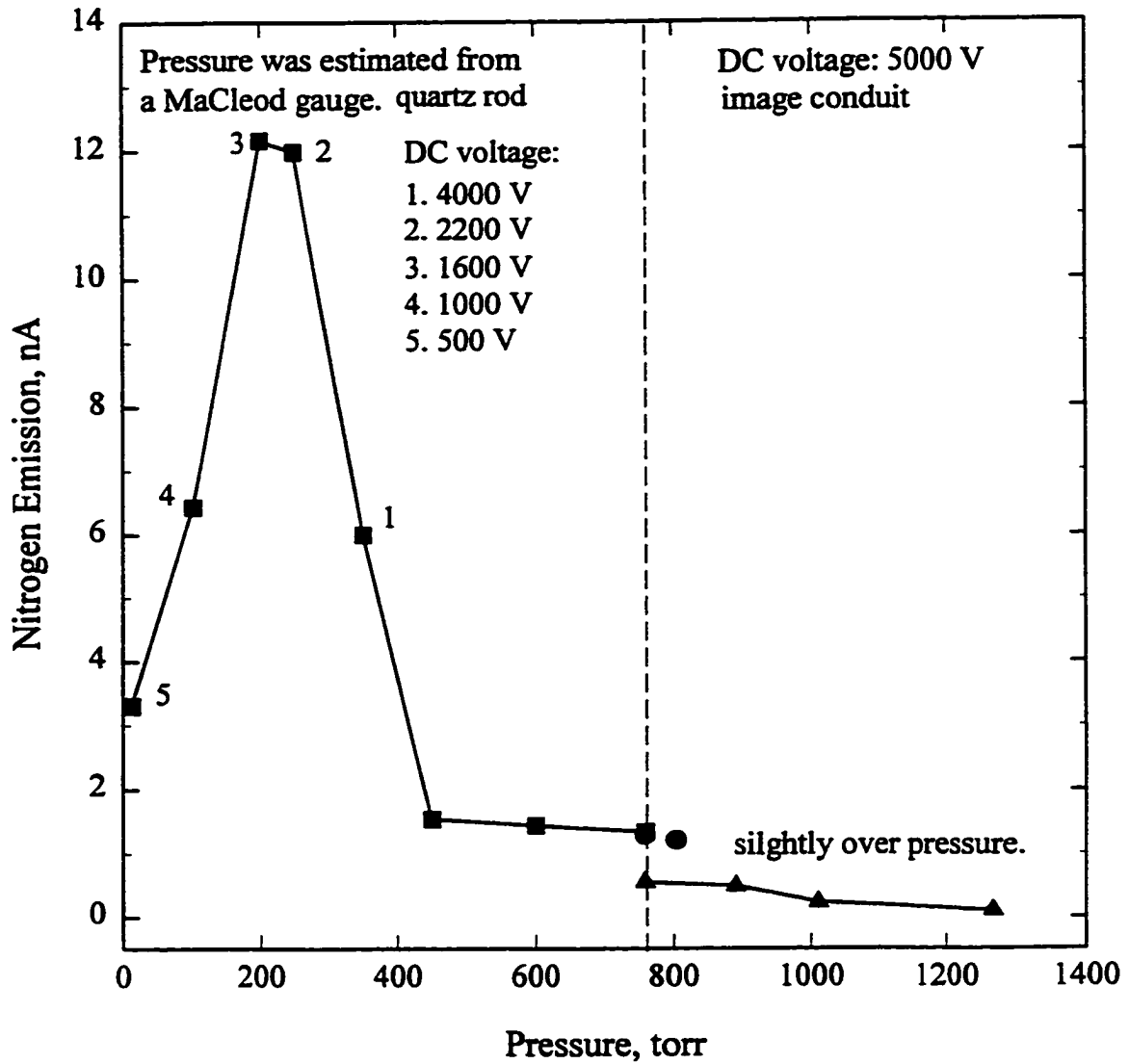
Figure 4.69   Nitrogen background emission in the ALD as a function of pressure. PMT (R-268) voltage: -600 V.
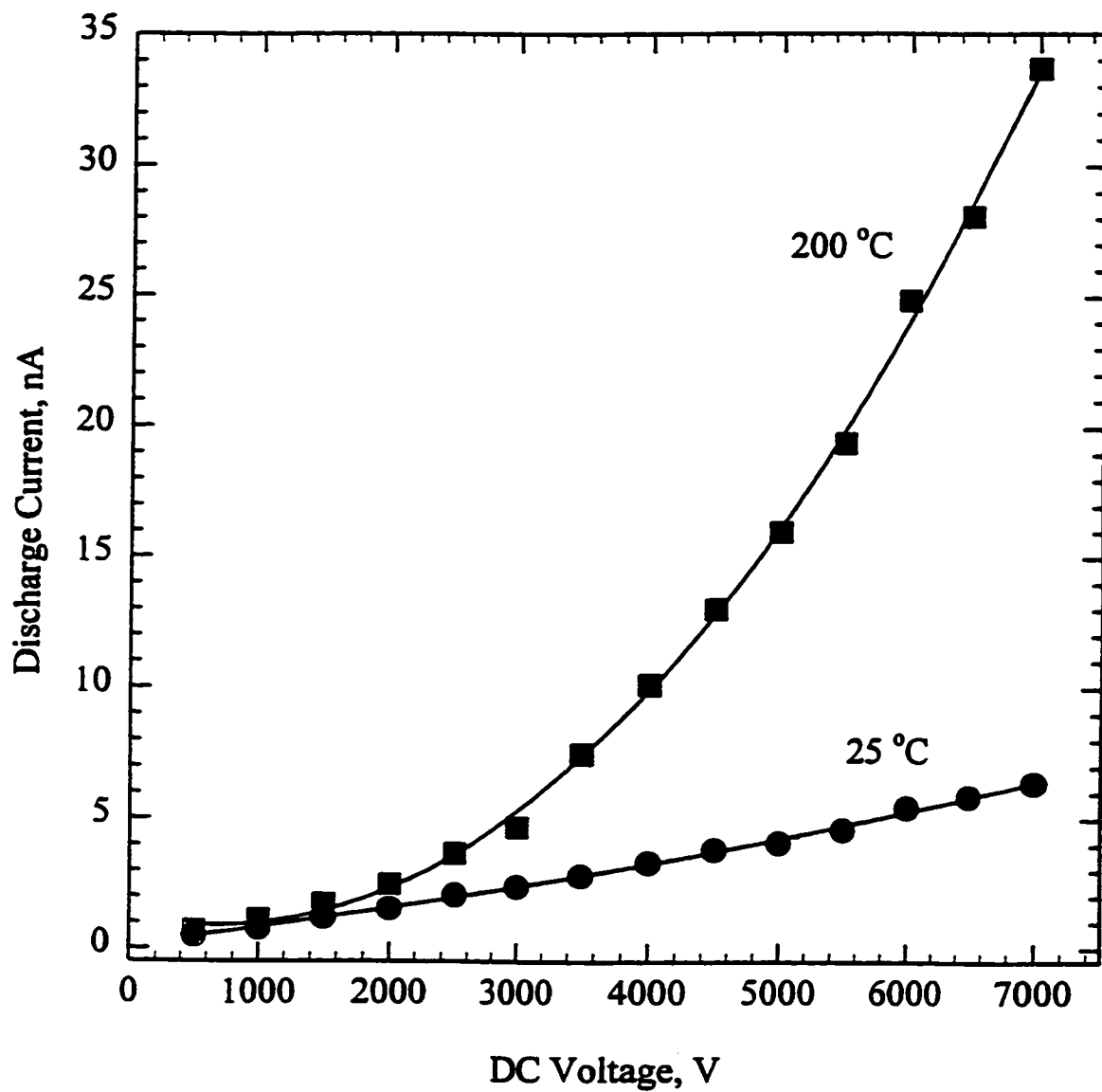
Figure 4.70   Discharge current in nitrogen as a function of applied DC voltage.

The partial energy level diagram of nitrogen is shown in Figure 4.71. The first triplet state, metastable N_2 (A $^3\Sigma_u^+$) with a long radiative lifetime ($\tau \leq 3.5$ sec at low pressure) (157), in its zero vibrational level, with 6.17 eV (594.9 kJ/mol) of energy above the N_2 (X $^1\Sigma_g^+$) ground state, can be excited from the ground state by electron exchange (21). The short-lived N_2 (B $^3\Pi_g$) triplet state ($\tau \sim 10$ ns) lying 7.35 eV (708.7 kJ/mol) above the ground state may also be excited from the singlet ground state by electron exchange (21). The energetic N_2 (C $^3\Pi_u$) state with a short radiative lifetime (0.1 ms-10 ns) and 11.03 eV (1063.5 kJ/mol) of energy may be populated on electron impact or triplet-triplet annihilation of N_2 (A $^3\Sigma_u^+$) (158):

$$N_2\ (A\ ^3\Sigma_u^+) + N_2\ (A\ ^3\Sigma_u^+) \rightarrow N_2\ (X\ ^1\Sigma_g^+) + N_2\ (C\ ^3\Pi_u) \qquad (4.1)$$
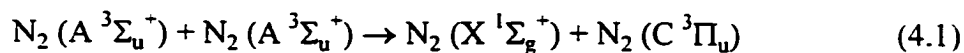
It has been confirmed that the luminescence of aroyl compounds such as benzaldehyde and anthraquinone was eliminated by shutting off the nitrogen flow or removing the β-ray source (Ni-63). However, much weaker aroyl luminescence can still occur even though no electric field was applied (44). It is reasonable to believe the excited states of nitrogen produced in the weak discharge were involved in the excitation. There could be different nitrogen excited-state species in this system. The question is which species is the potential excitation source for aroyl compounds and what is the possible mechanism for the excitation process.
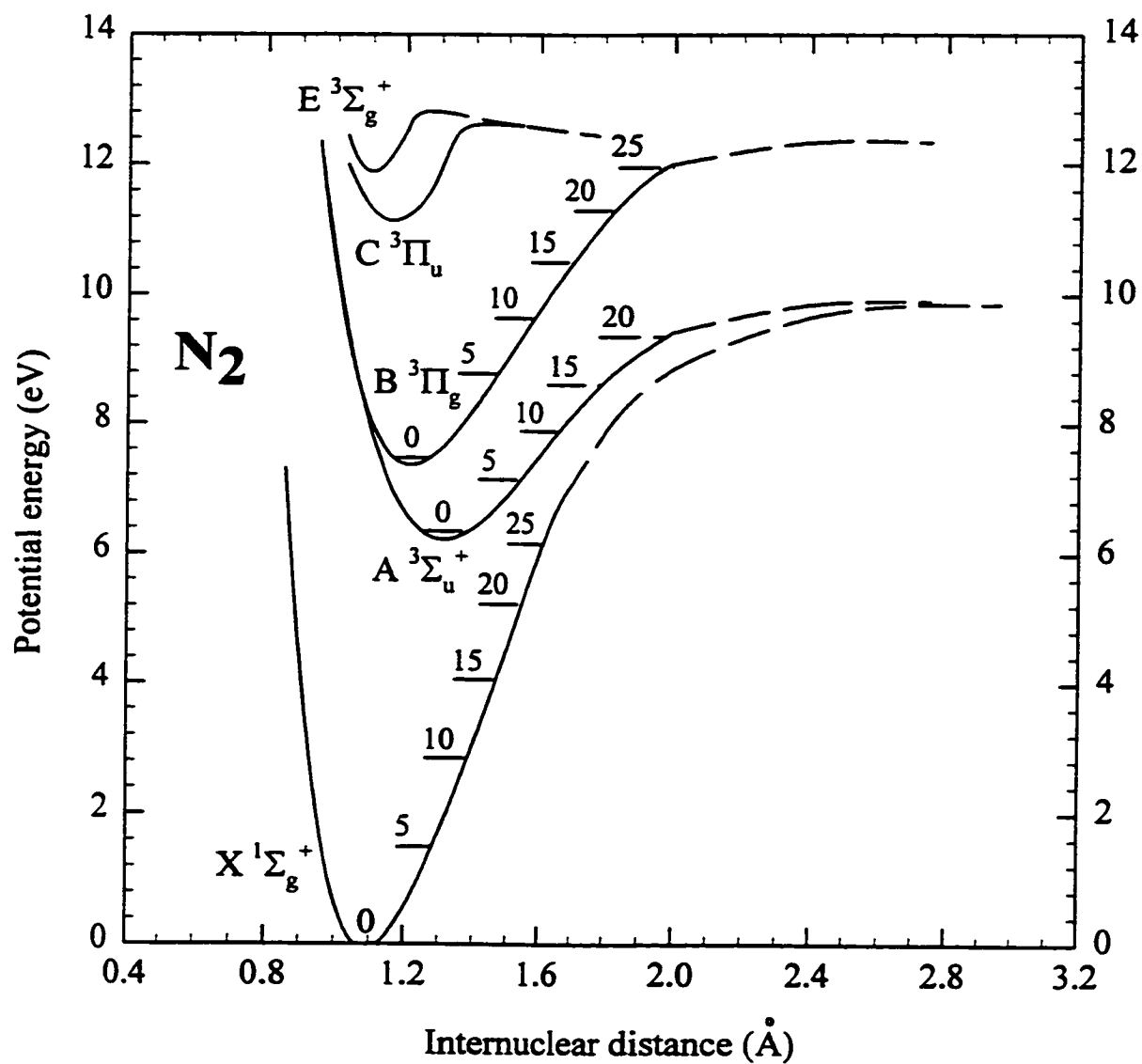
Figure 4.71 Energy level diagram of N_2 showing the energy levels of importance (from ref. 155).

4.6.2 Luminescence at Atmospheric Pressure: Evidence for Energy Transfer Mechanism

Phosphorescence originates from the lowest triplet state in a molecule which has long lifetime (10^{-4}-10 sec), and high probability of collisional transfer of energy with solvent molecules or impurity molecules. At a pressure of one atmosphere, a molecule experiences about 10^{10} collisions per second. As a consequence, excited molecules in the gas phase at ordinary pressure usually lose their energies by collision before they have a chance to phosphoresce. This is the reason for using very low pressures so that the collision frequency is greatly reduced and phosphorescence can be observed in the gas phase.

In this study, aroyl compounds exhibit intense phosphorescence in the gas phase at atmospheric or even higher pressure. Figure 4.72 shows the pressure effect on the relative intensity of the gas-phase phosphorescence of benzaldehyde under condition of a similar and constant level of nitrogen background emission which was obtained by adjusting the applied DC voltage. It was clearly shown that the emission intensity of benzaldehyde was enhanced as the pressure increased, but there was almost no effect on the spectral resolution (Figure 4. 73). These observations can be rationalized in terms of collisional excitation of benzaldehyde with energy transfer from an excited-state species of nitrogen instead of collisional quenching by these species.
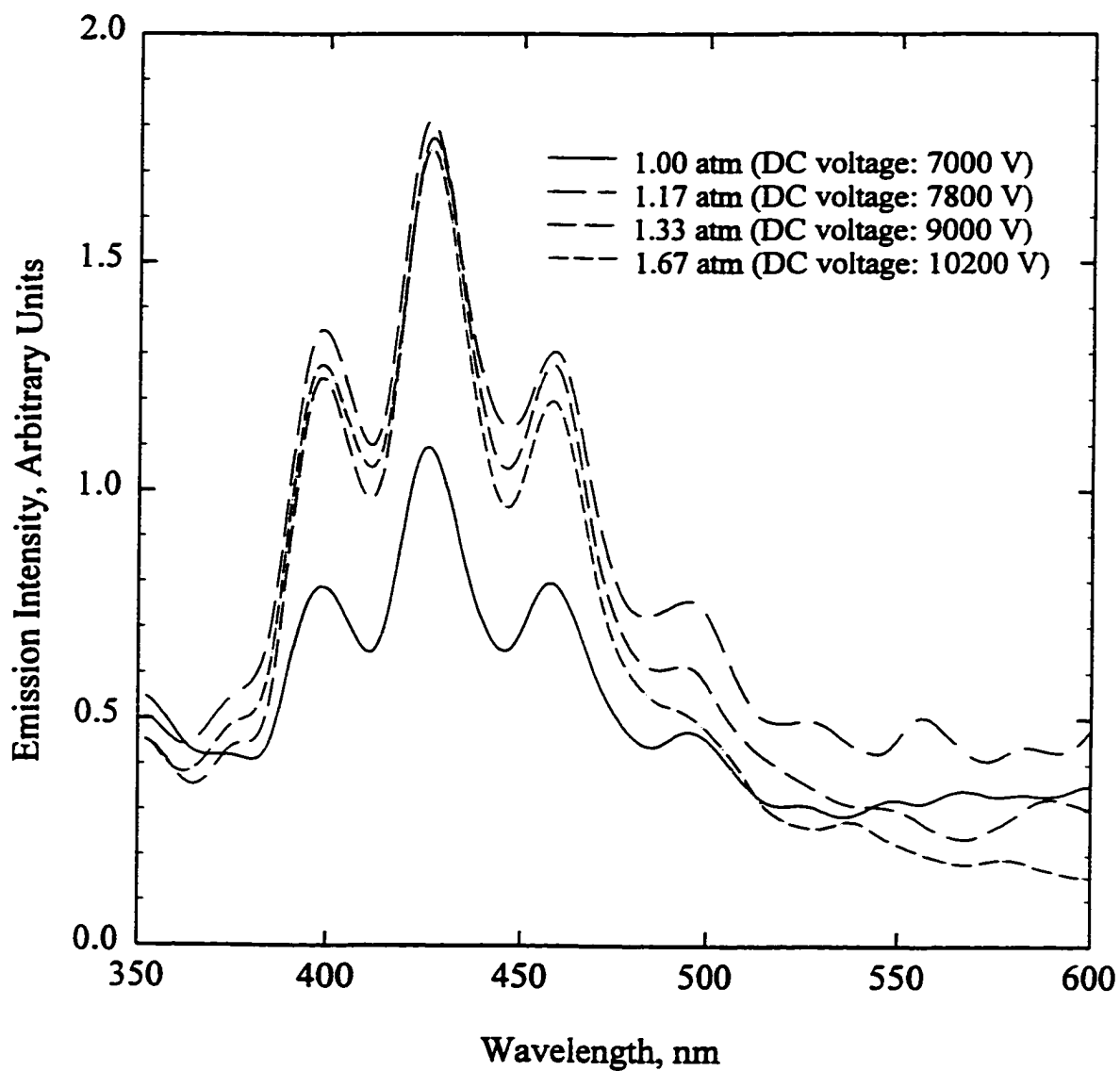
Figure 4.72   Pressure effect on the relative intensity of gas-phase phosphorescence of benzaldehyde. 1/8 meter grating monochromator with R-374 PMT and single-peak mode. Bandpass: 6.6 nm.
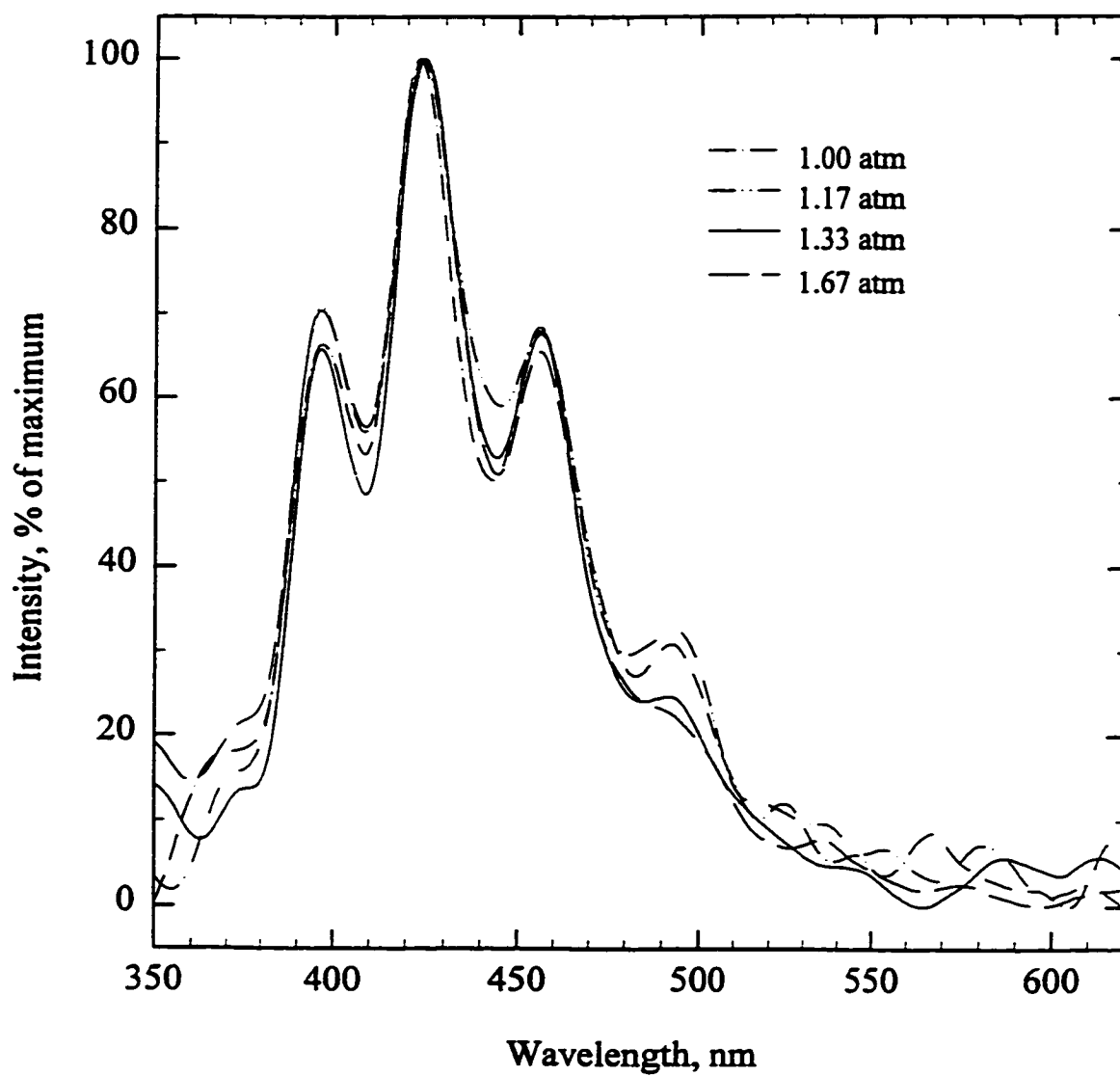
Figure 4.73 Pressure effect on the spectral resolution of gas-phase phosphorescence of benzaldehyde. Conditions as in Figure 4.72.

4.6.3 A Speculative Mechanism

The obvious question is which species is the potential energy carrier for excitation of aroyl compounds. The weak nitrogen background emission was solely from the so-called nitrogen second positive system (N_2 (C $^3\Pi_u$) $\rightarrow$ N_2 (B $^3\Pi_g$)). Therefore, the correlation between the nitrogen second positive emission and the aroyl luminescence was checked by varying the applied DC voltage (from 0 to 7000 V), temperature (from 70 to 200 °C) and pressure (from 1 to 1.67 atm), and the results are shown in Figures 4.74. 4.75, 4.76, respectively. These behaviors did not indicate that the N_2 (C $^3\Pi_u$) state is responsible for the collisional energy transfer to aroyl compounds. In addition, at low pressures, because of the short lifetimes of N_2 (C) (0.1 ms-10 ns) and N_2 (B) (~10 ns), their concentrations must be small, and it is doubtful that they contribute significantly to the excitation of aroyl compounds by energy transfer. On the other hand, N_2 (A $^3\Sigma_u^-$) has much longer lifetime ($\leq$ 3.5 sec) and greater stability toward deactivating collisions (21). Therefore, N_2(A) seemed to be the potential excitation source for aroyl compounds in the ALD system.

In the previous study, either the metastable triplet state molecules N_2 (A $^3\Sigma_u^-$) or the vibrationally excited ground-state molecules N_2 (X $^1\Sigma_g^+$) have been believed to be the principal energy carriers for atomic excitation in the nitrogen afterglow produced in dielectric discharge (28, 155). The technique to obtain an essentially pure N_2 (A $^3\Sigma_u^-$) source with minimal nitrogen atoms by the reaction $Ar^*(^3P_{0,2})$ + N_2 $\rightarrow$ $N_2(C)^*$ $\rightarrow$ $N_2(B)^*$ + hv $\rightarrow$ $N_2(A)^*$ + hv has been reported by Stedman, and co-workers, and the
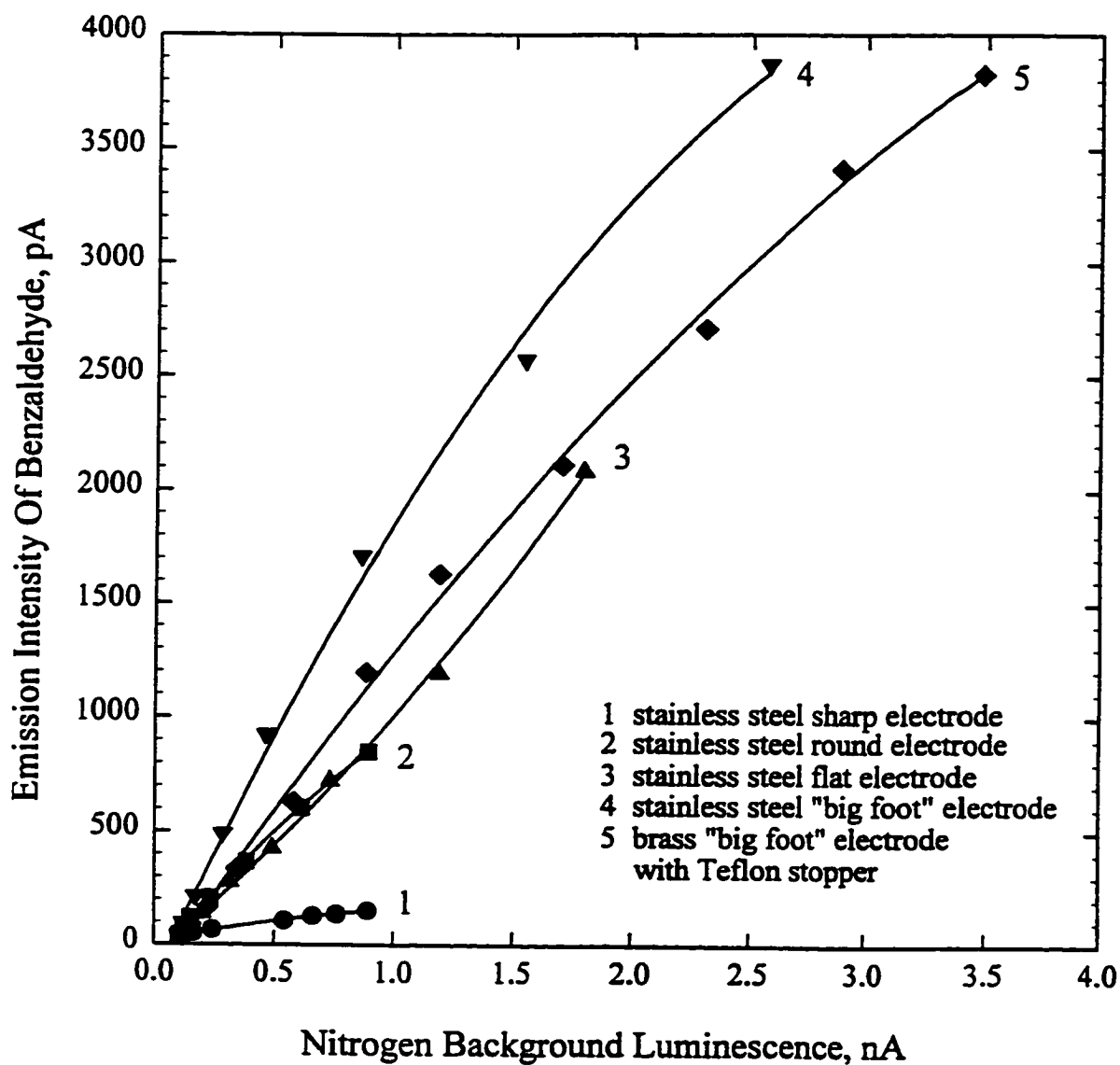
Figure 4.74   Emission intensity of benzaldehyde versus nitrogen background emission. Points shown were over an applied DC voltage range between 0 and 7000 V.
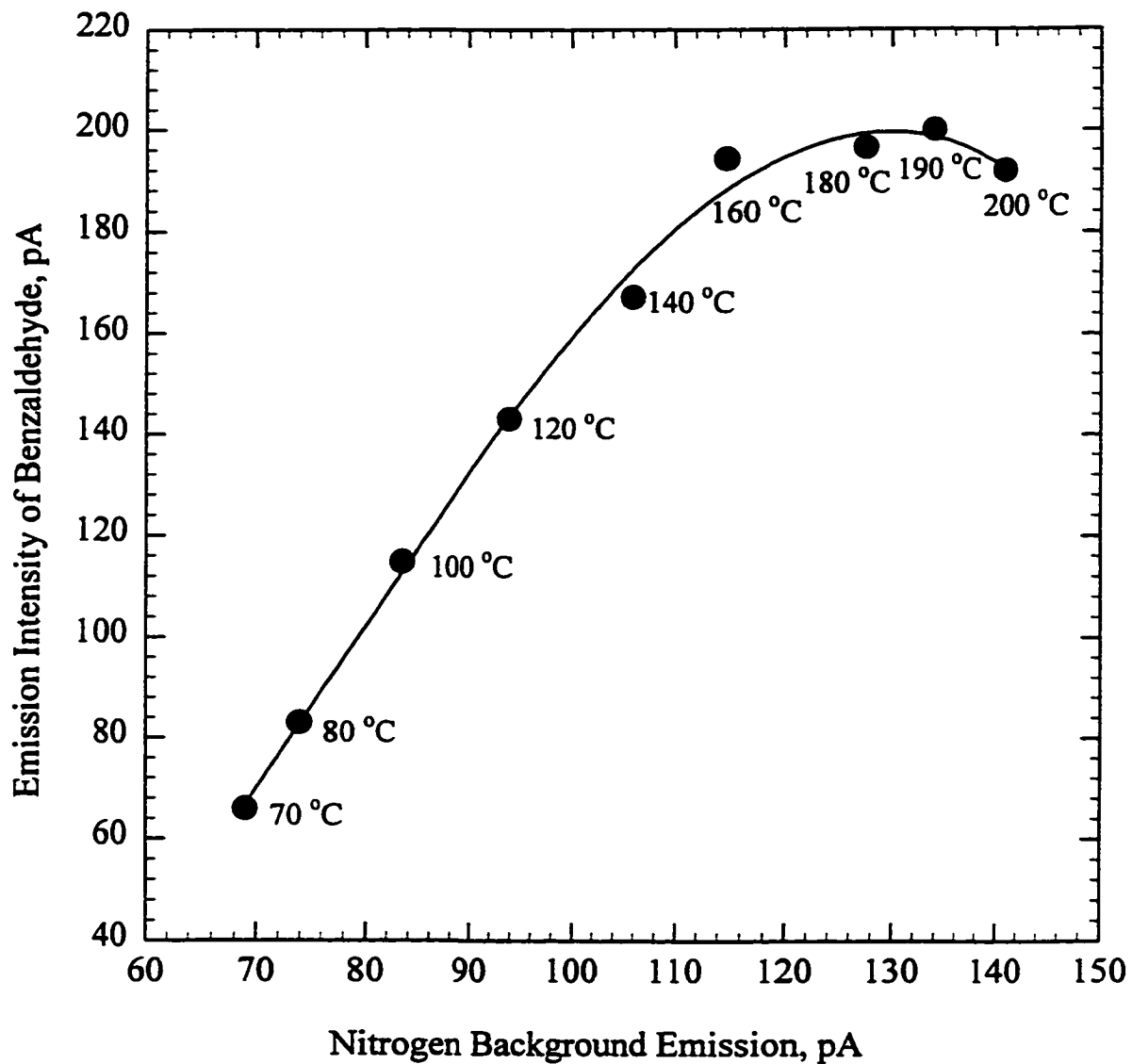
Figure 4.75 Emission intensity of benzaldehyde versus nitrogen background emission. Points shown were over a temperature range between 70 and 200 °C.
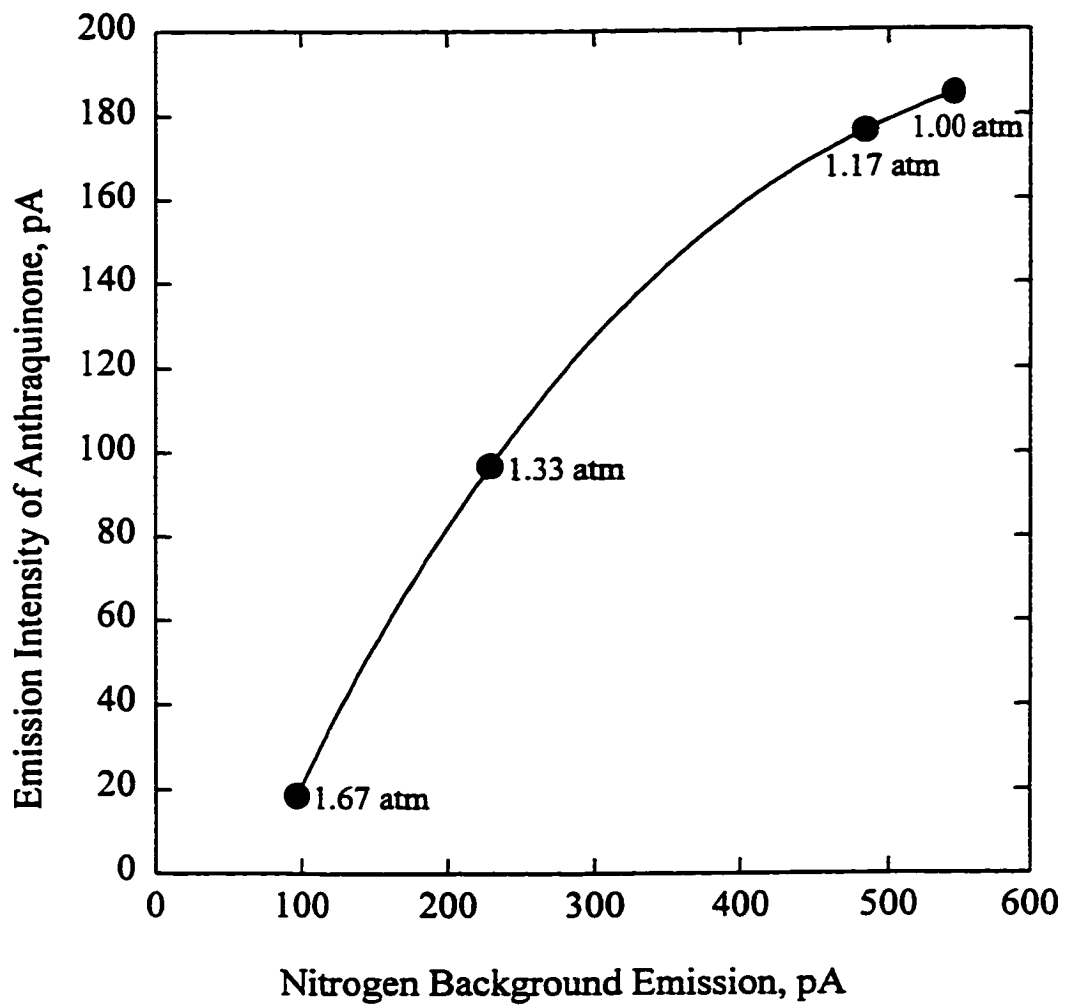
Figure 4.76 Emission intensity of anthraquinone versus nitrogen background emission. Points shown were over a pressure range between 1 and 1.67 atm.

N_2 (A $^3\Sigma_u^+$) source has been used as an efficient energy-transfer agent (157-159).

Devolder and co-workers (79, 160, 162) reported the observation of phosphorescence of

aromatic carbonyl compounds and hydrocarbons by the reaction with active nitrogen,

which was produced in a microwave discharge at low pressures. The excitation

mechanism they proposed was also related to the metastable N_2 (A $^3\Sigma_u^+$) state.

Generally, high-energy discharges, such as microwave discharges, produce large

amounts of nitrogen atoms, which then rapidly recombine to form metastable N_2 (A $^3\Sigma_u^-$).

Dielectric discharges with a discharge current of about 11.2 mA produce very few

nitrogen atoms (28). Instead, population of the N_2 (A $^3\Sigma_u^+$) state proceeds through an

excitation by the discharge to the N_2 (C $^3\Pi_u$) state. The formation of N_2 (A $^3\Sigma_u^-$) is

believed to result from the following two steps which are responsible for the second

positive and first positive spectra, respectively:

$$N_2 \text{ (C } ^3\Pi_u) \rightarrow N_2 \text{ (B } ^3\Pi_g) \text{ (second positive system)} \qquad (4.2)$$

$$N_2 \text{ (B } ^3\Pi_g) \rightarrow N_2 \text{ (A } ^3\Sigma_u^+) \text{ (first positive system)} \qquad (4.3)$$
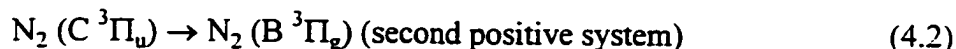
In this study, a very mild, low-energy discharge with a discharge current of ≤ 35 nA

—about 2.5 orders of magnitude lower than the electric-discharge current mentioned

above (28)—is used as an excitation source for nitrogen. It is believed that ground state

N_2 is excited mainly to the lowest triplet, metastable N_2 (A $^3\Sigma_u^+$) state by electron

exchange with the secondary electrons that are produced in the ionization of nitrogen by

β-particles emitted by the ^{63}Ni source. The N_2 (A $^3\Sigma_u^+$) formed is assumed responsible

for the excitation of the molecules of aroyl compounds by an efficient triplet-triplet

energy transfer process, and mainly for the formation of N_2 (C $^3\Pi_u$) by an energy pooling

process (158) following by the weak emission of the nitrogen second positive system. Therefore, the aroyl luminescence in excited nitrogen can be accounted for on the basis of the following mechanism:

(1) Nitrogen is ionized (and perhaps excited) by β-particles from the ^{63}Ni source. Thus, secondary electrons are produced:

$$\beta + N_2 \, (X \, ^1\Sigma_g^+) \rightarrow \beta' + N_2^+(X \, ^2\Sigma_g^+) + e^- \text{ (secondary electron)} \qquad (4.3)$$

$$\beta + N_2 \, (X \, ^1\Sigma_g^+) \rightarrow \beta' + N_2 \, (C \, ^3\Pi_u) \text{ (partially (21))} \qquad (4.4)$$
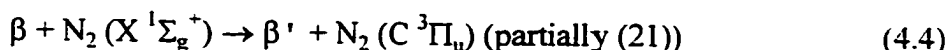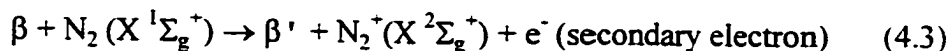
(2) The singlet ground state nitrogen is excited by secondary electrons accelerated by the high electric field (up to 1750 V/mm) to produce N_2 (A $^3\Sigma_u^+$):

$$N_2 \, (X \, ^1\Sigma_g^+) + e^- \text{ (fast)} \rightarrow N_2 \, (A \, ^3\Sigma_u^-) + e^- \text{ (slow)} \qquad (4.5)$$
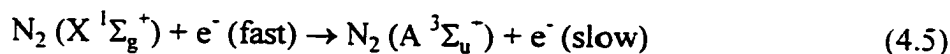
(3) This is followed by triplet-triplet energy transfer from N_2 (A $^3\Sigma_u^-$) to the molecules of aroyl compounds (A):

$$N_2 \, (A \, ^3\Sigma_u^+) + A \, (^1S_0) \rightarrow N_2 \, (X \, ^1\Sigma_g^+) + A \, (^3T_1) \qquad (4.6)$$
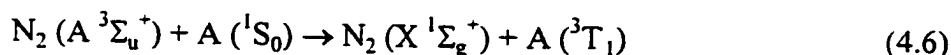
accompanied by energy pooling of N_2 (A $^3\Sigma_u^+$):

$$N_2 \, (A \, ^3\Sigma_u^+) + N_2 \, (A \, ^3\Sigma_u^+) \rightarrow N_2 \, (X \, ^1\Sigma_g^+) + N_2 \, (C \, ^3\Pi_u) \text{ (mainly)} \qquad (4.7)$$
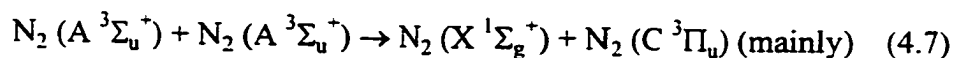
(4) Finally, the phosphorescence or E-type delayed fluorescence emission of aroyl compounds and the second positive system emission of nitrogen take place:

$$A \, (^3T_1) \rightarrow A \, (^1S_0) + h\nu \text{ (phosphorescence)} \qquad (4.8)$$

or $\qquad A \, (^1S_1) \rightarrow A \, (^1S_0) + h\nu \text{ (E-type fluorescence)} \qquad (4.9)$

and $\qquad N_2 \, (C \, ^3\Pi_u) \rightarrow N_2 \, (B \, ^3\Pi_g) \text{ (second positive system)} \qquad (4.10)$
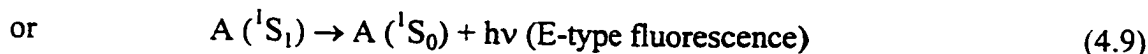
The metastable N_2 (A $^3\Sigma_u^+$) state as the excitation source for aroyl compounds in this study has long been used as a very efficient triplet energy agent, both in the gas phase

(21, 35, 155, 157, 159-163), and in matrices at 4.2 K (164).

4.7 An Attempt at Lifetime Measurements

The luminescence lifetime is an important characteristic associated with molecular emission. Lifetime measurements are basic to studies of quenching and energy transfer. In analytical chemistry, the combined luminescence and excitation spectra provide a valuable identification tool. However, luminescence lifetimes represent a potential probe for characterizing compounds. They offer the possibility of differentiating between various components in mixtures based on differences in lifetime since, frequently, compounds having very similar spectra can have greatly different lifetimes.

Phosphorescence lifetimes are longer than prompt fluorescence lifetimes and are relatively easy to measure. The simplest approach is to measure the phosphorescence signal as function of time after terminating of the exciting radiation (47). From the luminescence signal relative to the excitation pulse, information about the decay kinetics can be obtained. Figure 4.77 shows the high voltage pulse and the emission traces of the nitrogen second positive system and some typical aroyl compounds in the pulsed ALD (see experimental section in Chapter 2). The aroyl luminescence and the nitrogen emission decay curve (trace c-d in Figure 4.77) are shown in Figure 4.78. The half-life time $T_{1/2}$ is easy to read from oscilloscope traces. A more fundamental quantity is the mean lifetime τ, for an exponential decay, which is related to $T_{1/2}$ by

$$T_{1/2} = (1/k) \ln 2 = \tau (\ln 2) = 0.69319 \, \tau \qquad (4.11)$$

It can be calculated from the slope of a ln [A*]-versus-t plot (165). The calculated values
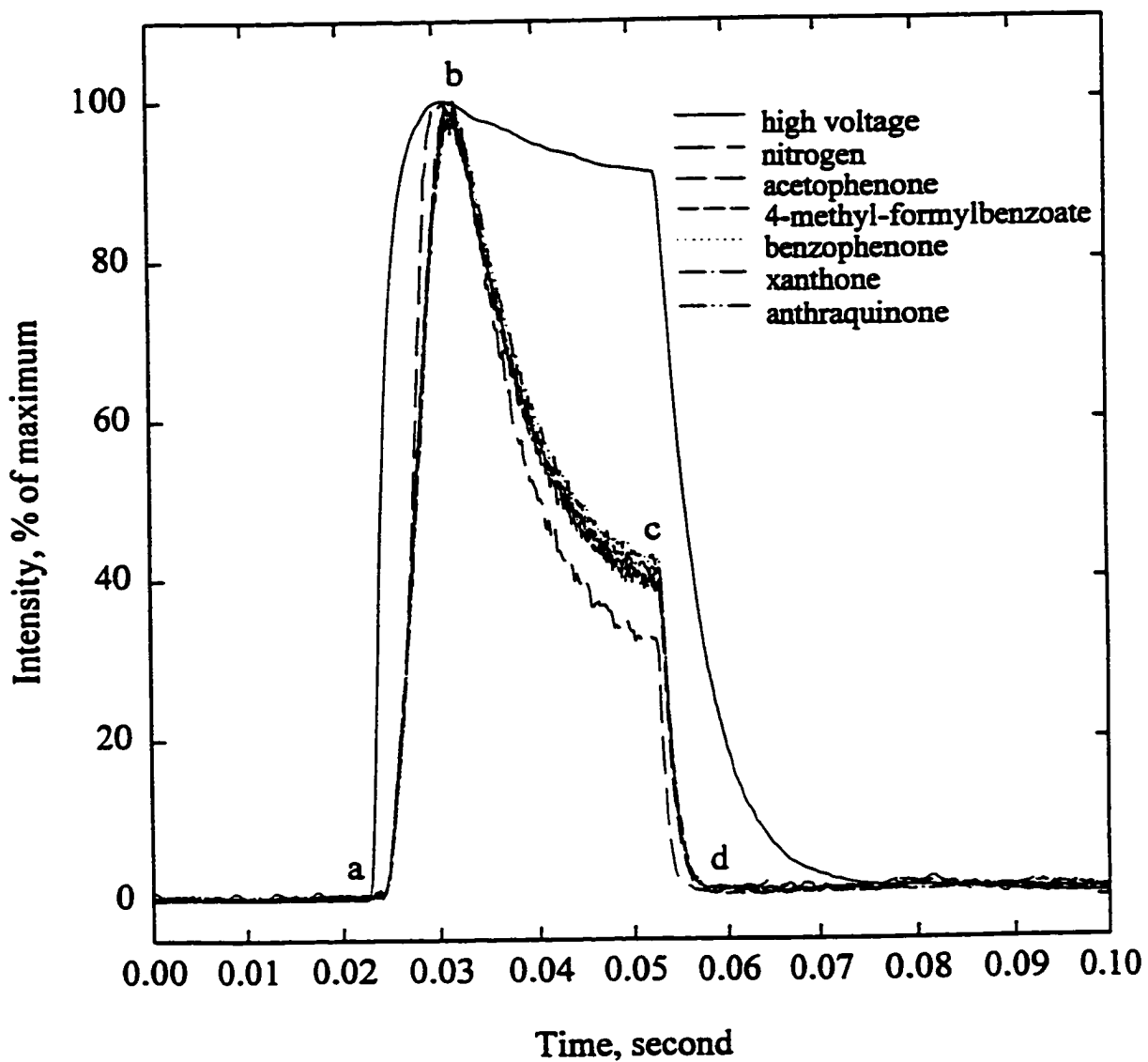
Figure 4.77 High voltage pulse and emission traces of the nitrogen second positive system and some aroyl compounds in the pulsed ALD. a-b: the high voltage pulse starts and produces nitrogen and aroyl emission; b-c: the pulsed DC voltage and the emissions stabilize; c-d: the high voltage pulse stops and the luminescence decays.
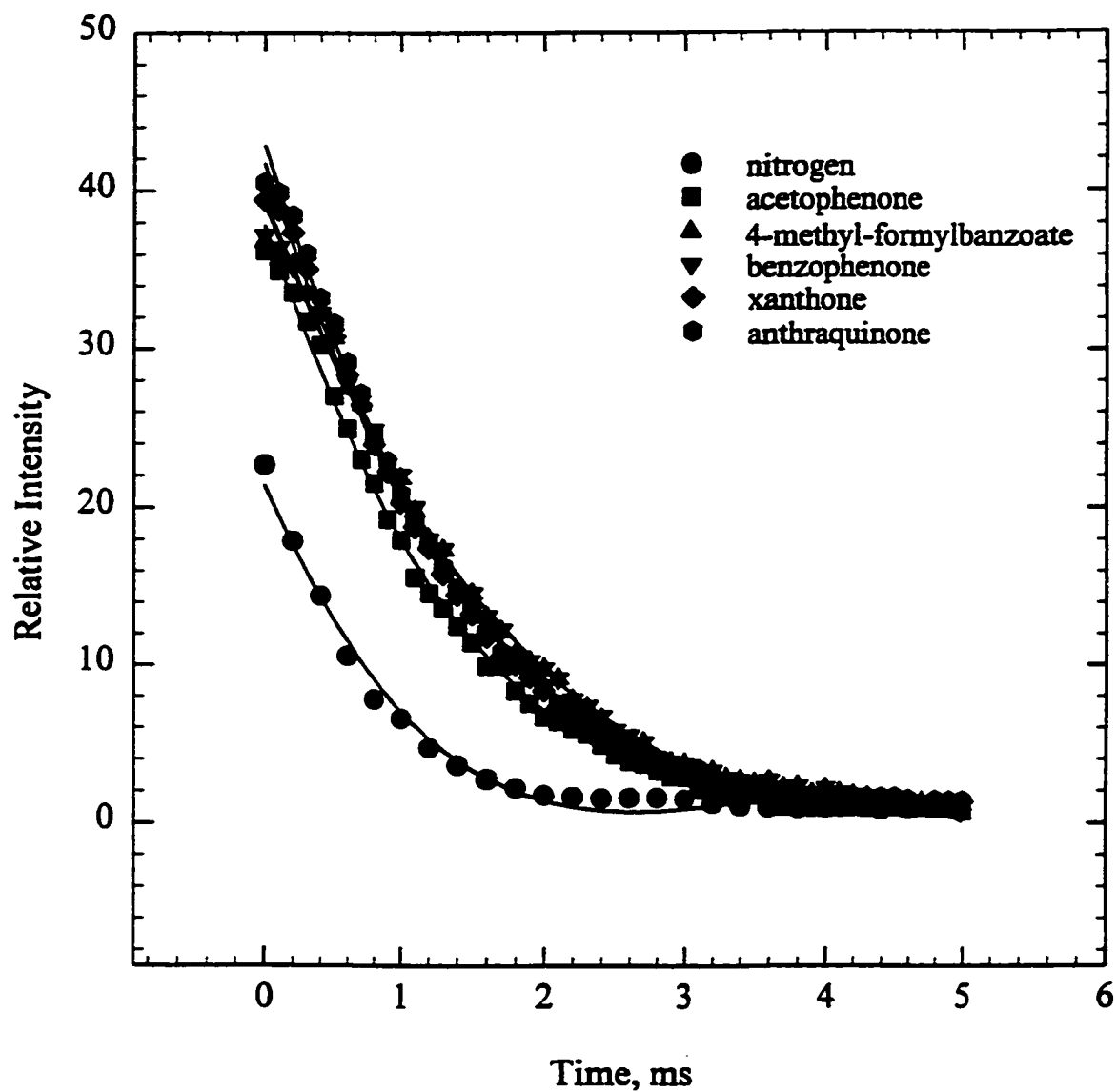
Figure 4.78 Decay curves of the nitrogen second positive system emission and aroyl luminescences.

for the nitrogen second positive system and the aroyl phosphorescence are about 1.2 ms

and 1.5 ms, respectively. From previously reported results, various aroyl compounds

have different lifetimes at low pressures (81, 82, 112). This suggests that in these cases

the measurements of luminescence lifetime are limited by slow processes of decay with a

lifetime of about 1 ms (i.e. the plasma decay), and the true lifetimes of the nitrogen

second positive system and the aroyl phosphorescences at atmospheric pressure are

smaller than 1 ms.

4.8   Quenching Effect

Luminescence quenching is a very general phenomenon, wherein the non-radiative

deactivation of an electronically excited molecule by a quencher molecule takes place

through various mechanisms. The investigation of quenching effects is an important

aspect of photochemstry as well as of analytical chemistry; any understanding will lead to

a more comprehensive description of photophysical and photochemical processes and a

rational design of detection devices for analytical work.

4.8.1 Quenching of Nitrogen Second Positive System and Benzaldehyde
Phosphorescence

In this study, the nitrogen second positive system is the sole, detectable background

emission. It is interesting to compare the quenching intensity of the nitrogen second

positive emission and of the aroyl phosphorescence by some common quenchers such as

oxygen and methane. Oxygen and methane play a role in photochemical and

photophysical studies and in gas chromatographic practice. The information from the

quenching study may help to understand the mechanism of aroyl phosphorescence excitation. Table 4.6 lists the concentration of four quenchers at 50% quenching, *i.e.* at a point where quenching has reduced a peak to 50% of its original size. A direct comparison of these data suggests that

Table 4.6 Comparison of Quenching of the Nitrogen Second Positive Emission and Benzaldehyde Phosphorescence Emission

Quencher	Concentration (μmol/s) of Quencher at 50% Quenching of	
	Nitrogen Second Positive System	**Benzaldehyde Phosphorescence**
Oxygen	50	0.0002
Hydrogen	6.8	1.6
Methane	50	0.9
Propane	2.9	0.4

benzaldehyde phosphorescence is subject to more severe quenching by these quenchers than the nitrogen second positive emission. A striking point is that oxygen is the strongest quencher of benzaldehyde phosphorescence but the weakest quencher of the nitrogen second positive system. This difference is clearly shown in Figure 4.79. It is therefore possible to speculate that the quenching mechanism of triplet benzaldehyde by triplet oxygen differs from that of triplet $N_2(C)$.

One of the most commonly used methods of presenting photochemical quenching data is the Stern-Volmer relation (72):

$$I_0/I_p = 1 + k_Q \tau [Q] \qquad (4.12)$$
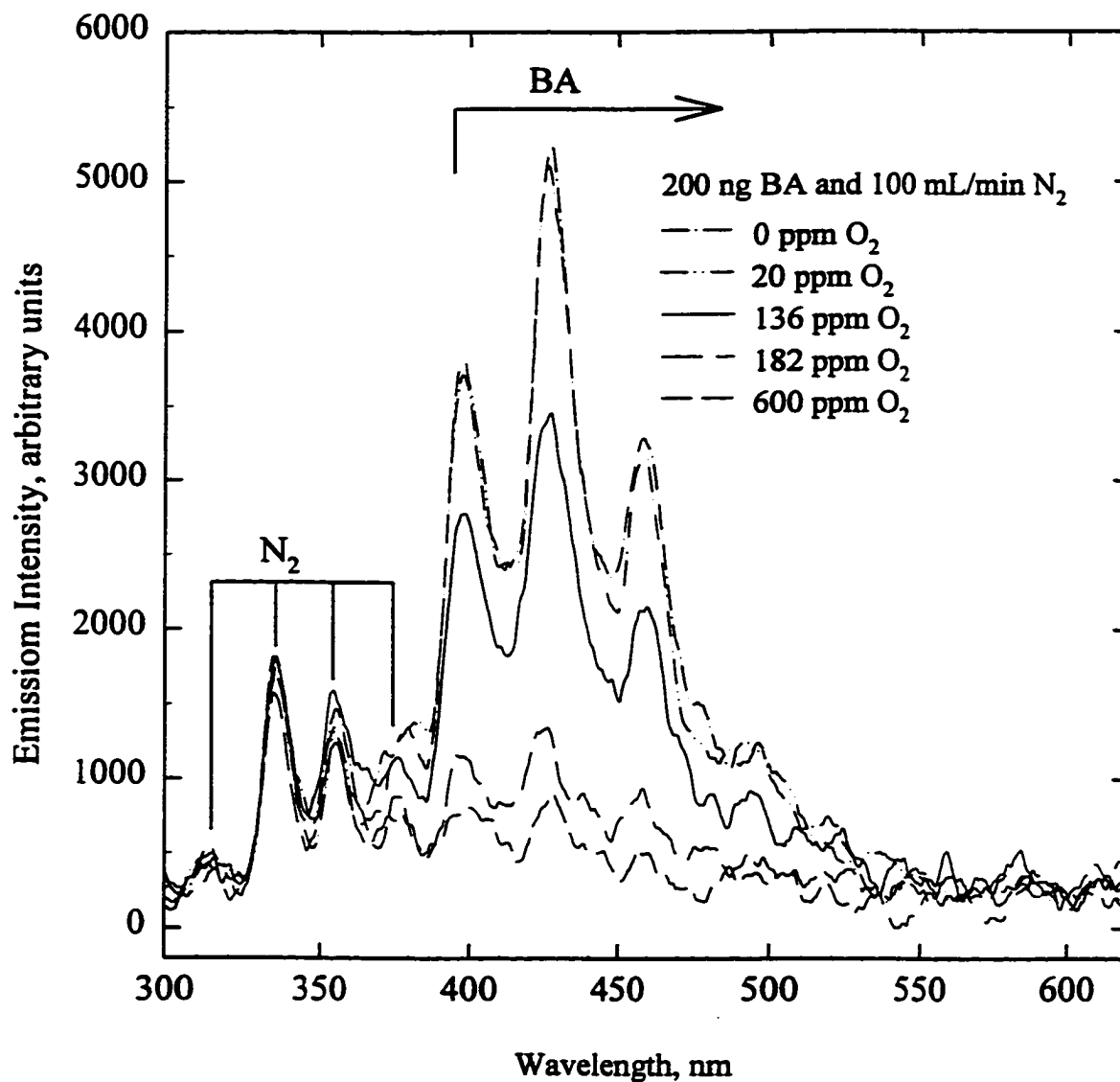
Figure 4.79   Gas-phase spectra of the nitrogen second positive system emission and benzaldehyde phosphorescence quenched by oxygen. Spectra were obtained by using 1/8 meter grating monochromator, R-374 PMT and single-peak mode. Bandpass: 6.6 nm.

where I_0 and I_p are the phosphorescence intensities in the absence and the presence of quencher, respectively. [Q] is the concentration of the quencher, τ is the lifetime of the triplet excited state, and k_Q is the quenching rate constant. Figures 4.80 presents the plots of I_0/I_p vs. [Q] for benzaldehyde phosphorescence, which were linear over the range of quencher concentration used. The normal Stern-Volmer plots for quenching of triplet $N_2(C)$ did not give a straight line, but the plots of I_0/I_p vs $[Q]^{1/2}$ (Figure 4.81) shows good linearity for the nitrogen second positive system emission, which may relate to the second order energy pooling reaction of producing $N_2(C)$ state (equation 4.7). This behavior again suggests different quenching mechanisms for triplet $N_2(C)$ and excited benzaldehyde. Unfortunately, the unknown lifetimes of the triplet $N_2(C)$ state and the excited benzaldehyde in this specific condition prevents the determination of absolute values for their quenching rate constants k_Q. But the $k_Q\tau$, a constant reflecting the efficiency of the quencher in deactivating the excited species, could be derived from the slope of the lines fitting the experimental data. The linear Stern-Volmer plots for quenching of benzaldehyde phosphorescence gave values for $k_Q\tau$ in the order $O_2 > C_3H_8 > CH_4 > H_2$.

4.8.2 Aroyl Luminescence Quenching by Oxygen

Molecular oxygen is a well-known and efficient quencher of fluorescence and phosphorescence (62, 63). In this study, the gas-phase luminescence of aroyl compounds was quenched strongly by trace amounts of oxygen in the carrier gas, or by the back-diffusion of atmospheric oxygen. The oxygen quenching effect was confirmed by the necessity of putting a valve in the exhaust line to keep the detector at a slight
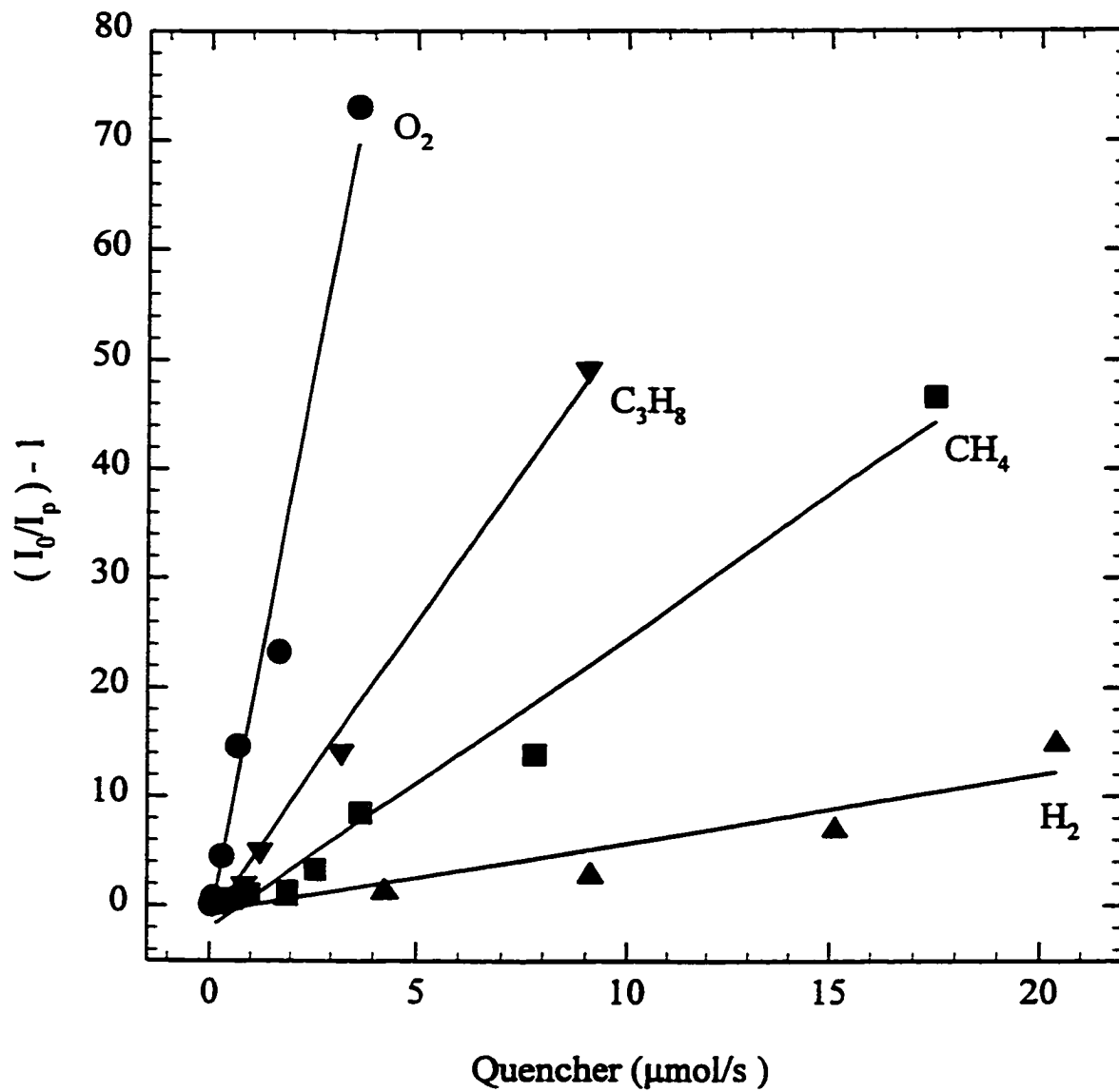
Figure 4.80 Stern-Volmer plots for quenching of benzaldehyde phosphorescence by oxygen, methane, hydrogen and propane.
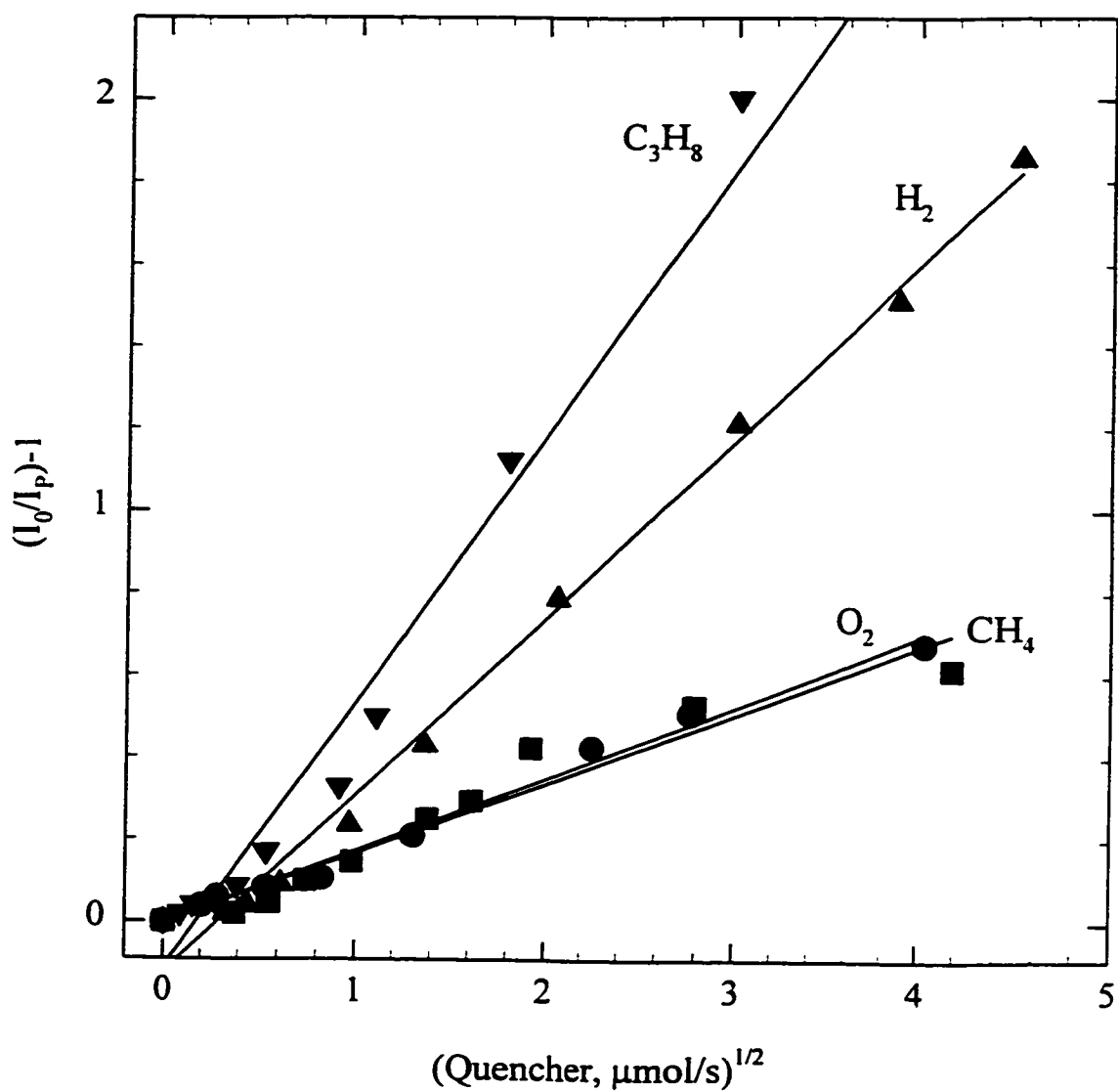
Fogure 4.81 Quenching of the nitrogen second positive system emission by oxygen, methane, hydrogen and propane.

overpressure for minimizing the back-diffusion of atmospheric oxygen, and the necessity of using a heated oxygen scavenger cartridge (Supelco) to purify the nitrogen. This was further confirmed by the slight increase of luminescence intensity of anthraquinone when increasing the pressure in the detector housing and keeping the nitrogen background emission at about the same level by adjusting DC voltages (Table 4.7).

Table 4.7 Anthraquinone Response in the ALD at High Pressures

Pressure, atm	DC Voltage, V	Nitrogen Background Emission, pA	Anthraquinone Response (4 ng), pA
1.00	5000	550.7	1108
1.33	6000	572.1	1240
1.67	7700	555.1	1337

As shown above, oxygen is a much stronger quencher to the aroyl triplet (A) than to the triplet N_2 (C) state. The triplet quenching mechanism by molecular oxygen may be physical or chemical in nature (63). The diradicaloid electron transfer and addition are probably the two most common chemical mechanisms:

Electron transfer $\quad A^* + O\text{-}O \rightarrow A^+ + O_2^-$ (4.13)

Diradical formation $\quad A^* + O\text{-}O \rightarrow A\text{-}O\text{-}O$ (4.14)
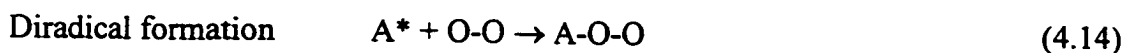
Physical quenching mechanisms include exciplex formation and energy transfer:

$^3A + {}^3O_2 \rightarrow$ exciplex $\rightarrow {}^1A + {}^1O_2 +$ heat (4.15)
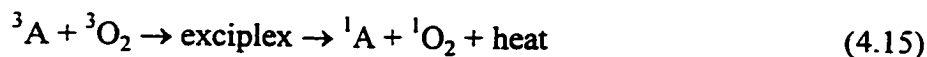
On the other hand, because of the long radiative lifetime of the triplet metastable N_2 (A $^3\Sigma_u^+$), this potential energy carrier for aroyl excitation may also be quenched by an

oxygen molecule through collisional quenching with energy transfer from N_2 (A $^3\Sigma_u^+$) (159):

$$N_2 \text{ (A } ^3\Sigma_u^+) + O_2 \text{ (}^3\Sigma) \rightarrow N_2 \text{ (X } ^1\Sigma_g^+) + 2O \text{ (}\Delta H = -96.4 \text{ kJ/mol)} \quad (4.16)$$
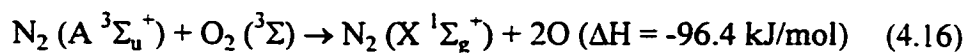
The available energy of N_2 (A) is sufficient to dissociate O_2.

4.8.3 Quenching of Aroyl Luminescence

Figures 4.82 and 4.83 show the quenching data of 16 typical aroyl compounds by two chosen quenchers, oxygen and methane, respectively. If all compounds and both figures are considered, the concentration of the strongest quencher at 50% quenching is about three times smaller than that of the weakest quencher. This suggests that the quenching behavior of all aroyl compounds tested is similar. However, there still is a correlation between the quenching intensity and compound structure, i.e., these compounds with similar structure were all quenched to a very similar degree (see an example shown in Figures 4.84 and 4.85), while different type compounds exhibited larger difference in quenching intensity by both oxygen and methane (Figures 4.86 and 4.87).

There also appeared to exist some correlation between the emission intensity of aroyl compounds and the concentration of quenchers at 50% quenching of aroyl phosphorescence, which is shown in Figures 4.88 and 4.89 for quenching by oxygen and methane respectively. From these results, it is reasonable to conclude that the stronger emitters are subject to more severe quenching by oxygen and methane than weaker emitters.
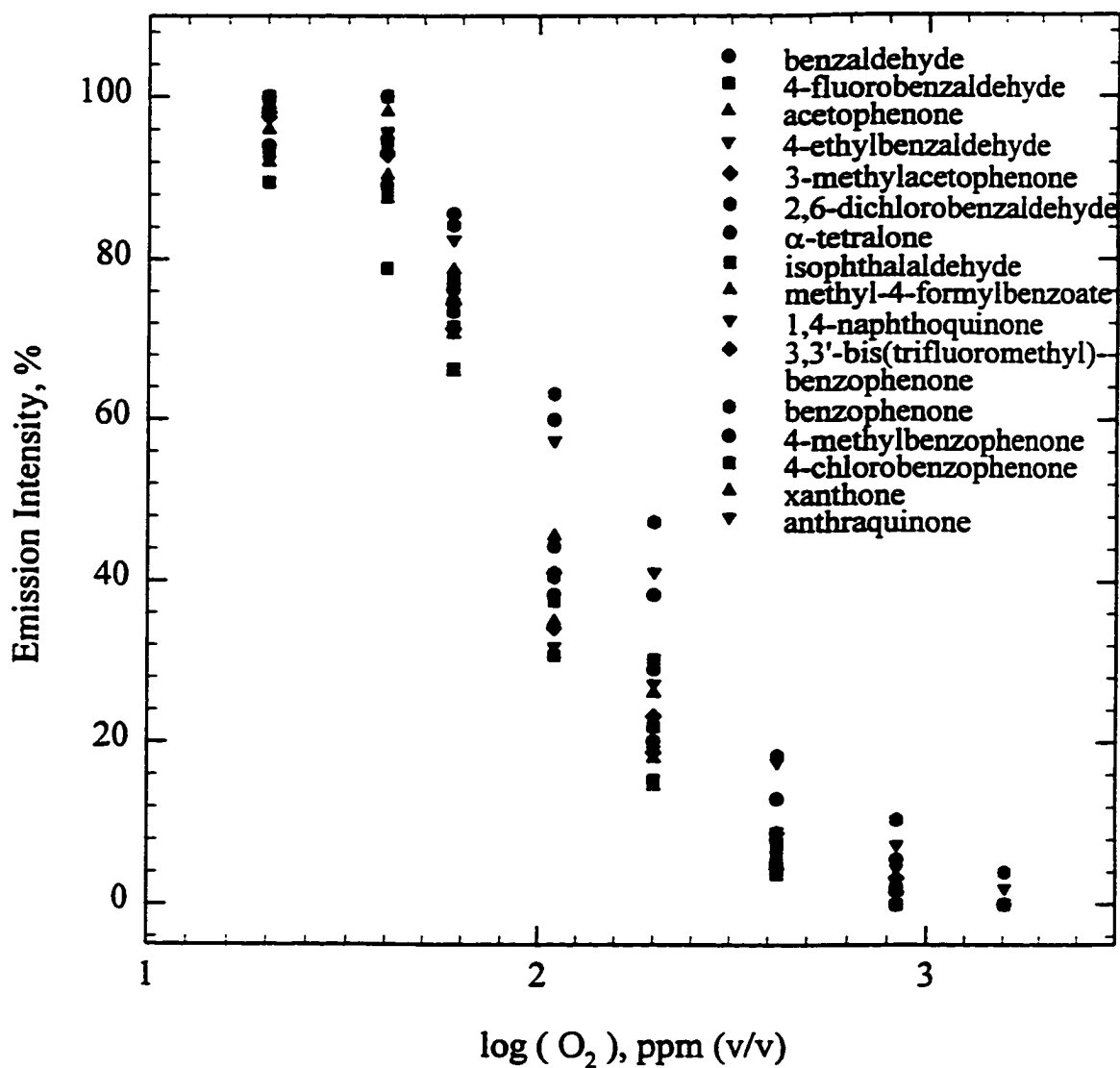
Figure 4.82   Quenching of sixteen typical aroyl compounds by oxygen. Aroyl compounds in order of elution: 2.5 ng benzaldehyde, 2.5 ng 4-fluorobenzaldehyde, 15 ng acetophenone, 2.5 ng 4-ethylbenzaldehyde, 10 ng 3-methylacetophenone, 50 ng 2,6-dichlorobenzaldehyde, 50 ng α-tetralone, 2.5 ng isophthalaldehyde, 2.5 ng methyl-4-formylbenzoate, 25 ng 1,4-naphthoquinone, 2 ng 3,3'-bis-(trifluoromethyl)benzophenone, 2 ng benzophenone, 1.5 ng 4-methyl-benzophenone, 2 ng 4-chlorobenzophenone, 0.2 ng xanthone and 0.35 ng anthraquinone.
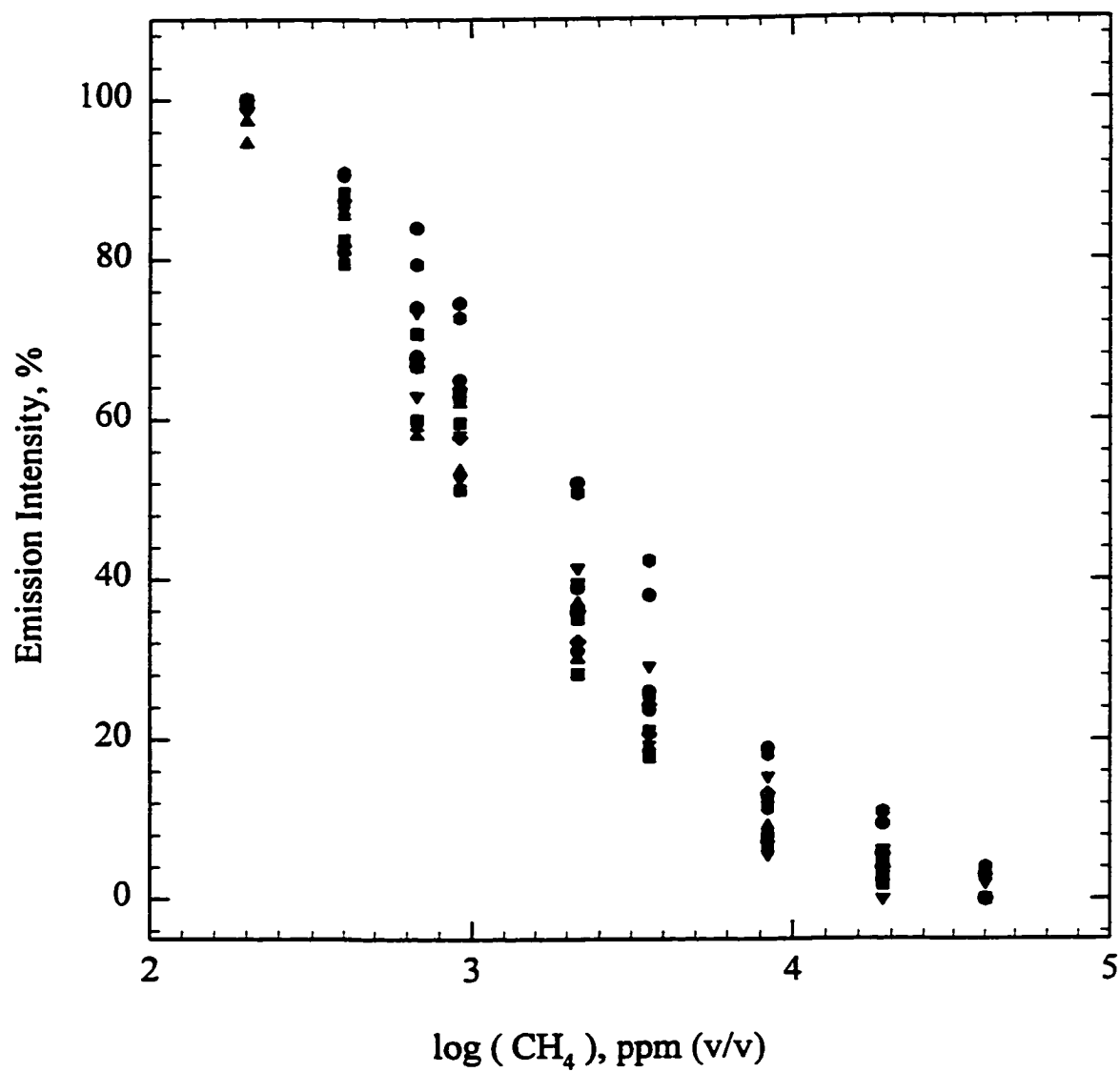
Figure 4.83   Quenching of sixteen typical aroyl compounds by methane. Aroyl compounds as in Figure 4.82.
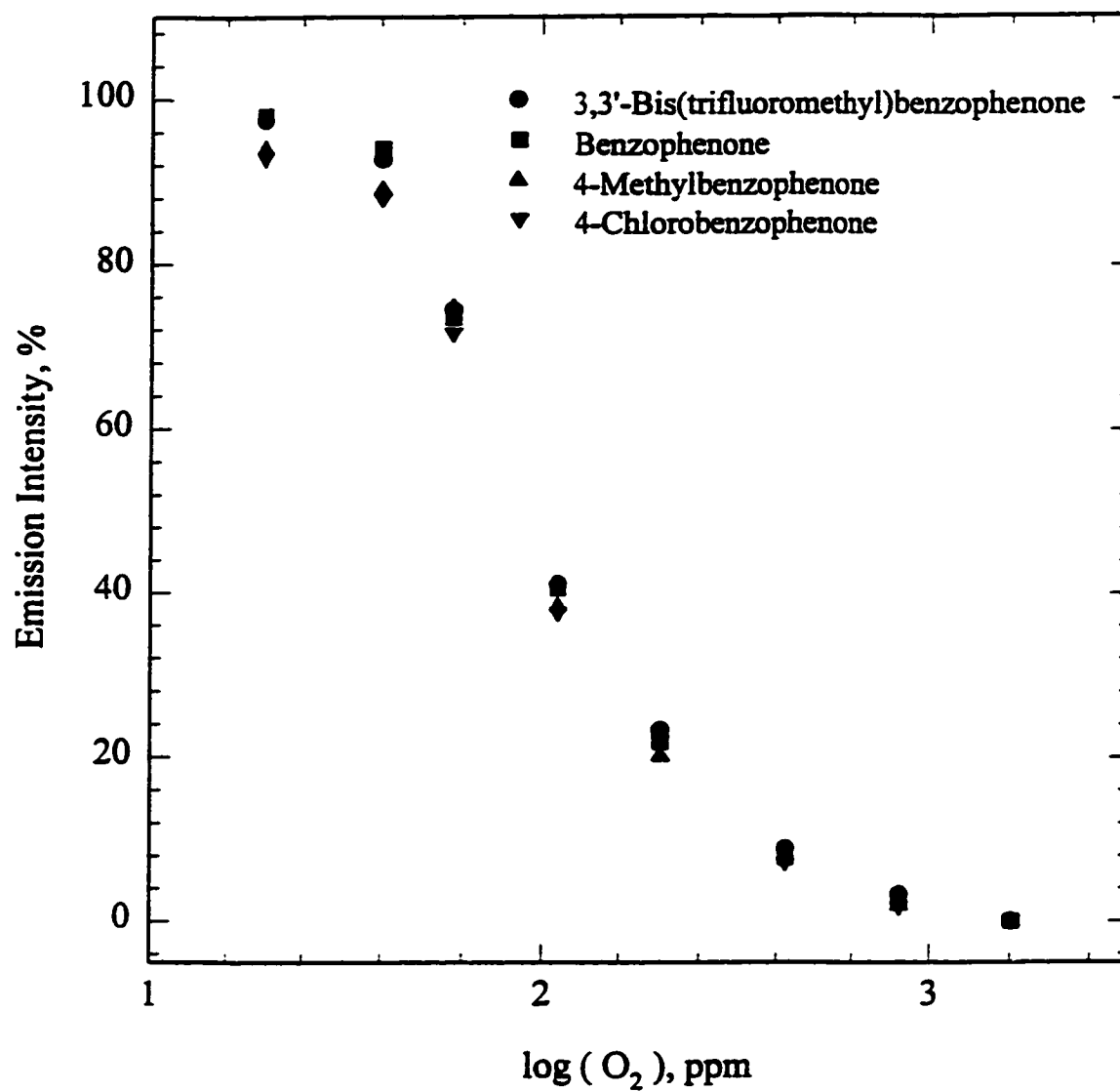
Figure 4.84   Quenching of four benzophenones by oxygen.
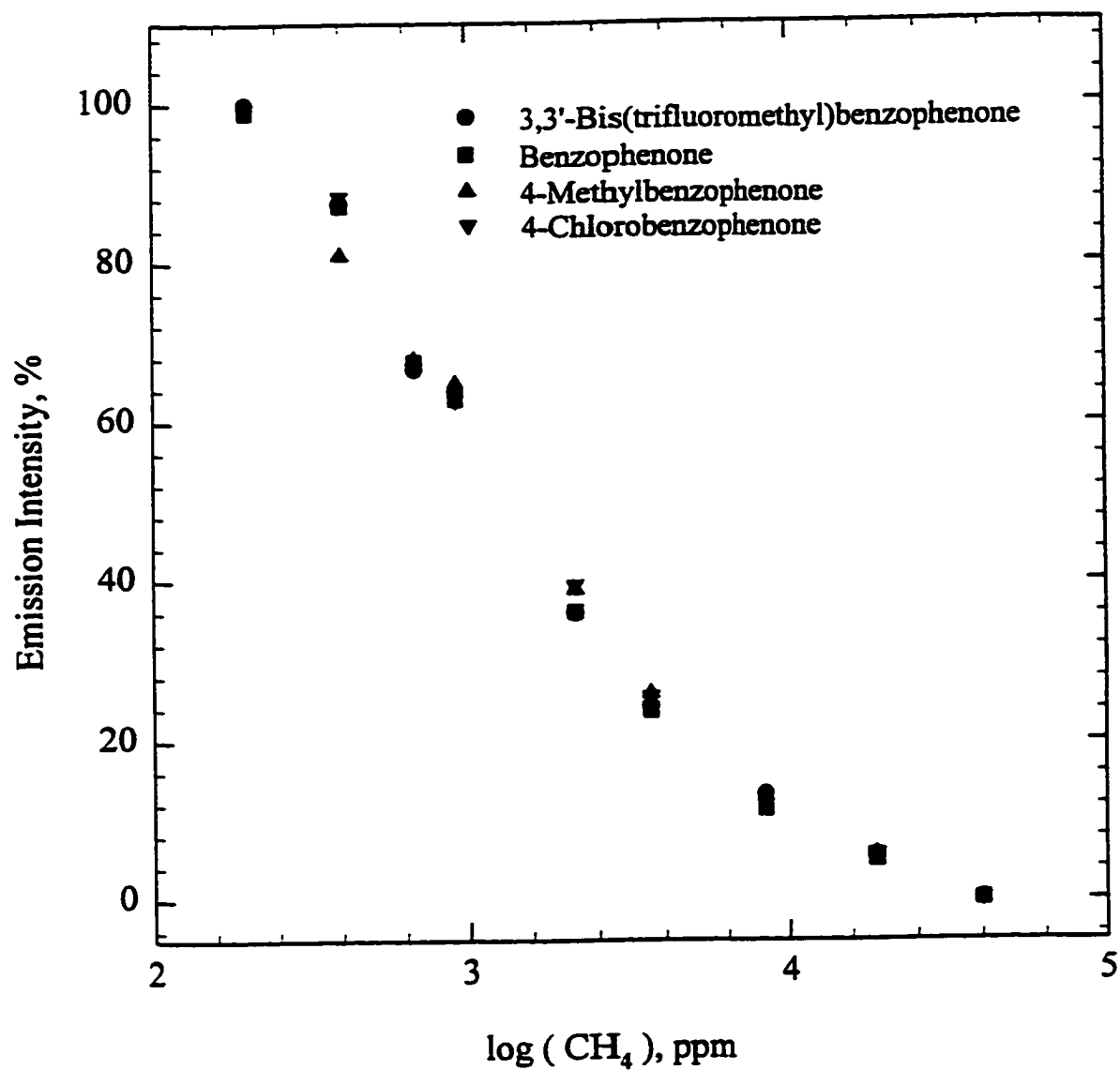
Figure 4.85 Quenching of four benzophenones by methane.
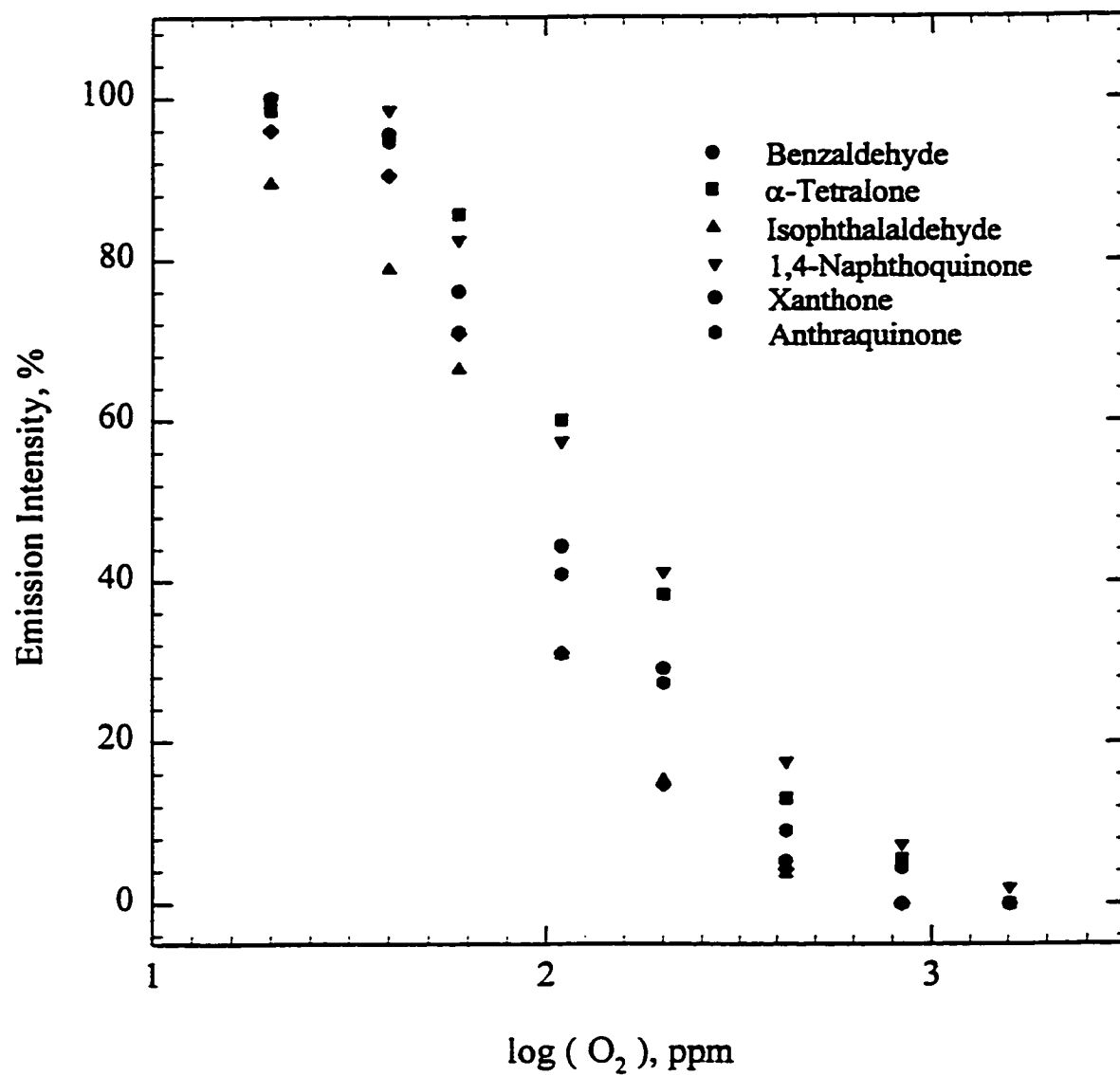
Figure 4.86 Quenching of six aroyl compounds of different types by oxygen.
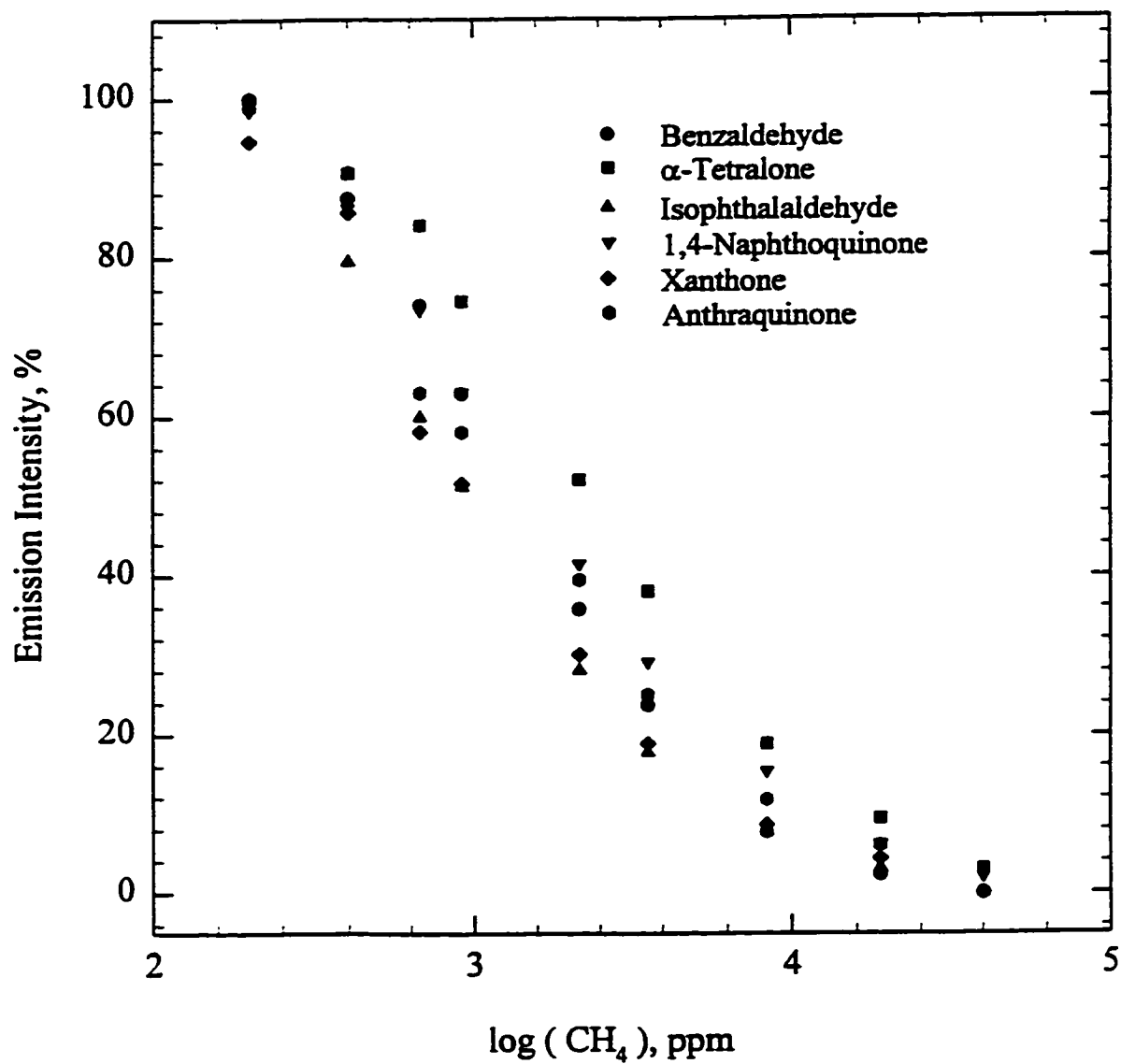
Figure 4.87   Quenching of six aroyl compounds of different types by methane.

4.9   Enhancement of Luminescence by Argon or Helium

Aroyl compounds were excited by triplet-triplet energy transfer from the $N_2(A)$ state and emitted phosphorescence or E-type delayed fluorescence. For whatever reason, the addition of small amounts of argon or helium to the carrier and excitation gas nitrogen can further enhance aroyl luminescence as well as nitrogen background emission (second positive system). Figures 4.90 and 4.91 show the gas-phase emission spectra in excited nitrogen doped with argon of the nitrogen second positive system and of benzaldehyde, respectively. An optimization was done on the argon or helium content in the nitrogen carrier. Figures 4.92 and 4.93 show the response and the S/N of benzaldehyde and nitrogen background emission vs. the argon and helium content in nitrogen, respectively. It is clearly demonstrated that the emission intensity of benzaldehyde was enhanced steadily as the argon content increased. In the case of doping with helium, it exhibited the same trend was observed except that a low content of helium (<10 mL/min) in nitrogen quenched the benzaldehyde emission. The S/N reached a maximum around 90 mL/min of doped argon flow and 60 mL/min of doped helium respectively. This argon or helium-doped ALD with improved sensitivity has been used in spectrum acquisition of some weak emitters (see section 4.3), and can be used in the determination of trace amounts of aroyls in the complex real-life samples after GC separation.

In addition to the analytical importance of the argon or helium-doped ALD, the interesting question is how the aroyl phosphorescence is enhanced in this system. In an argon photometric detector (Ar-PD) (46), argon metastables (11.7 eV) are produced in a mild, radioactively stimulated pure argon discharge by electron impact. Any analyte with
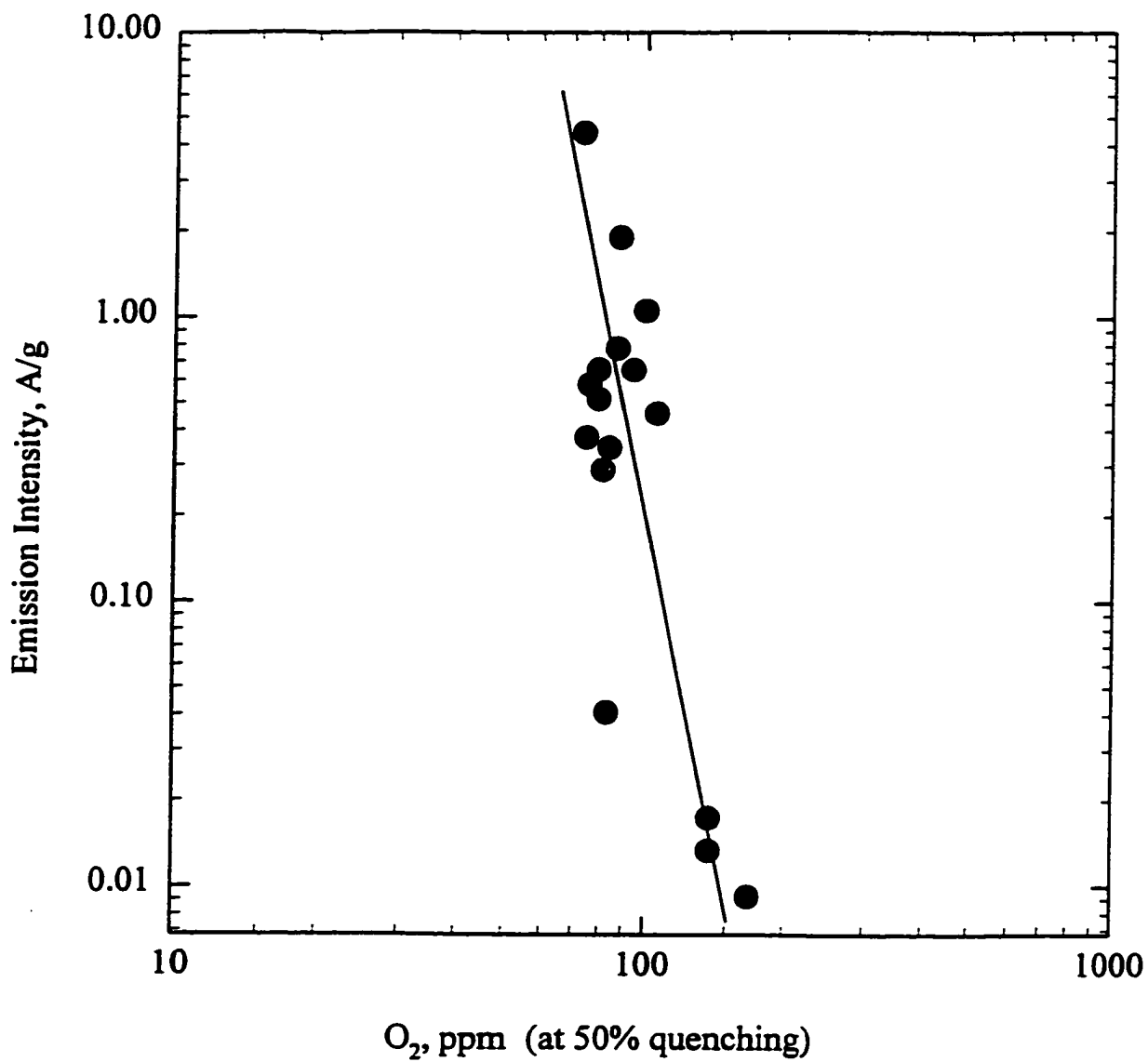
Figure 4.88 Dependence of oxygen concentration at 50% quenching of aroyl luminescence on the emission intensity of sixteen aroyl compounds. Compounds as in Figure 4.82.
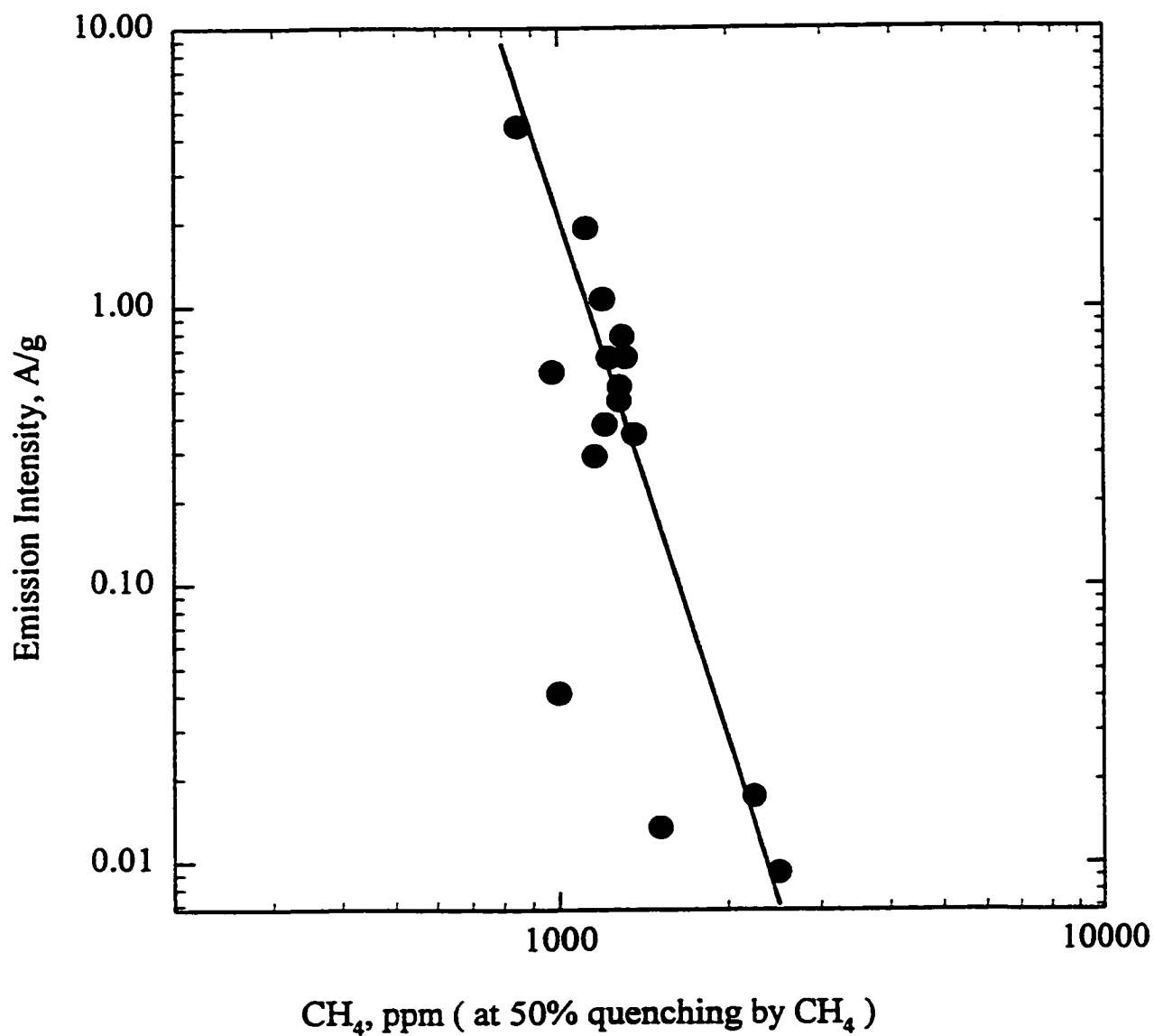
Figure 4.89   Dependence of methane concentration at 50% quenching of aroyl luminescence on the emission intensity of sixteen aroyl compounds. Compounds as in Figure 4.82.
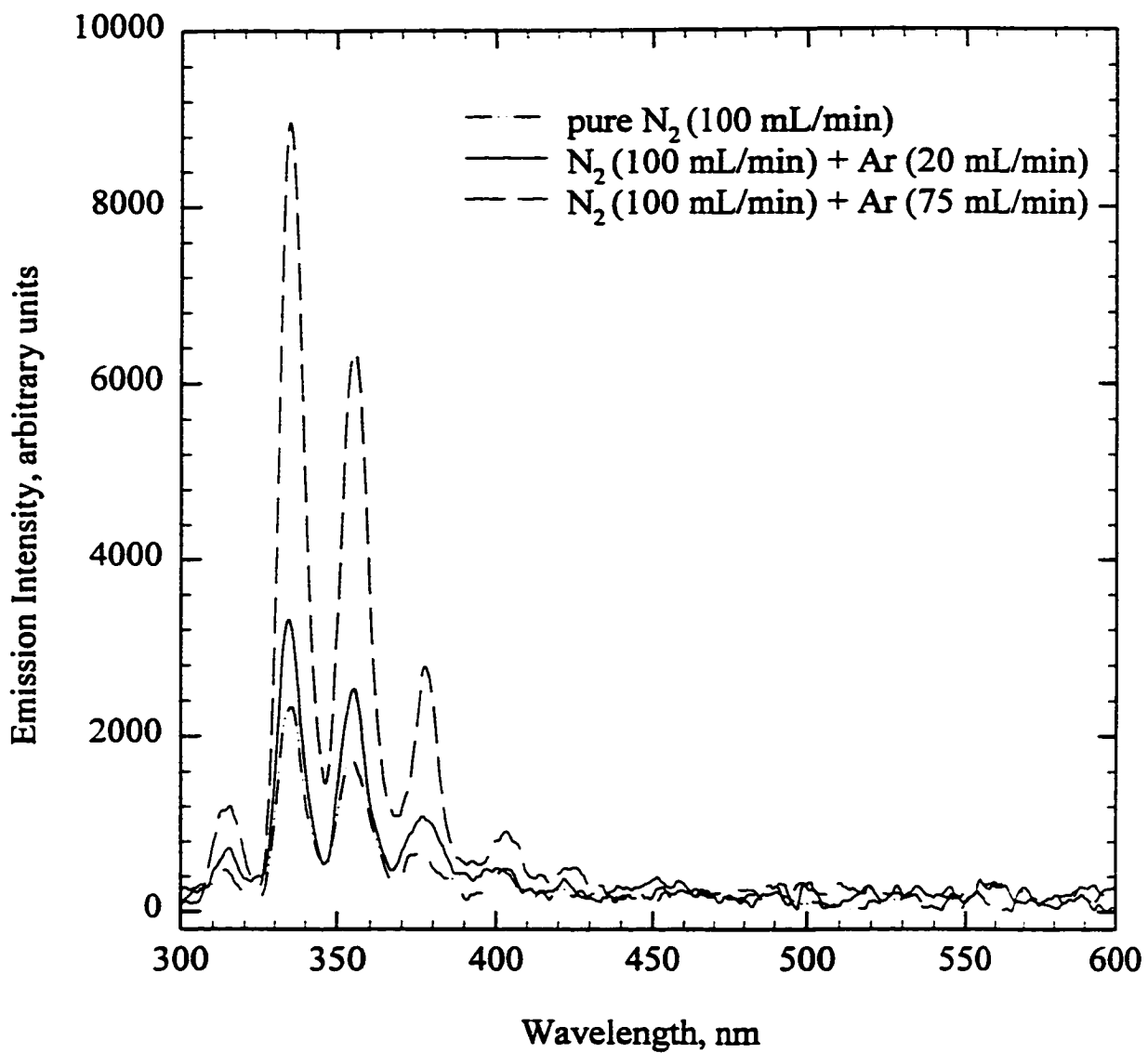
Figure 4.90 Spectra of the nitrogen second positive system emission with doped argon. 1/8 meter grating monochromator with R-374 PMT. Bandpass: 6.6 nm.
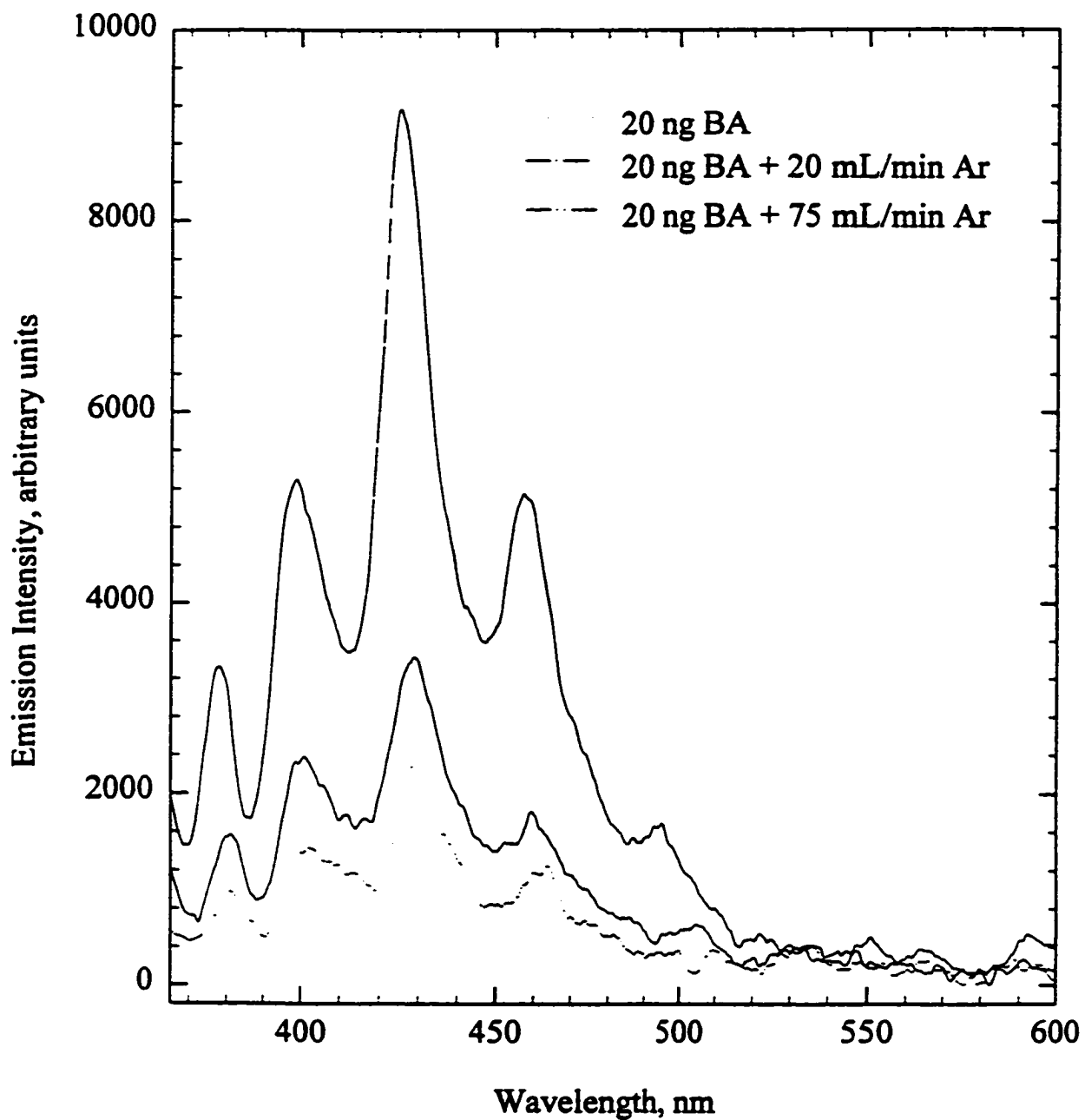
Figure 4.91 Gas-phase phosphorescence spectra of benzaldehyde in excited nitrogen doped with argon. 1/8 meter grating monochromator. R-374 PMT. Single-peak mode. Bandpass: 6.6 nm.
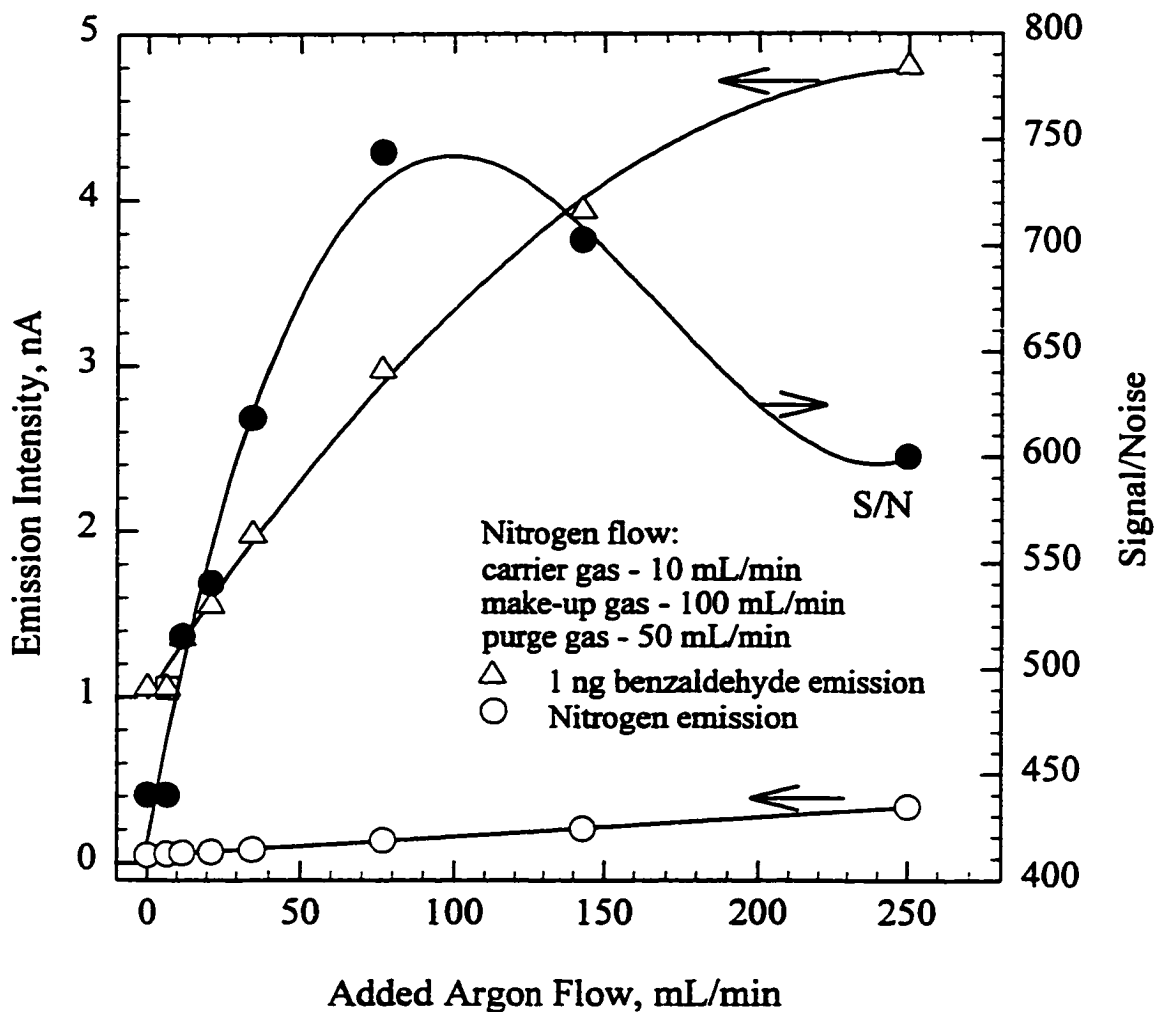
Figure 4.92   Dependence of benzaldehyde emission intensity, the nitrogen second positive system emission intensity, and the signal/noise ratio on added argon flow. The nitrogen second positive system emission was monitored with a 340 nm bandpass filter. DC voltage: 5000 V. PMT (R-268) voltage: -700 V.
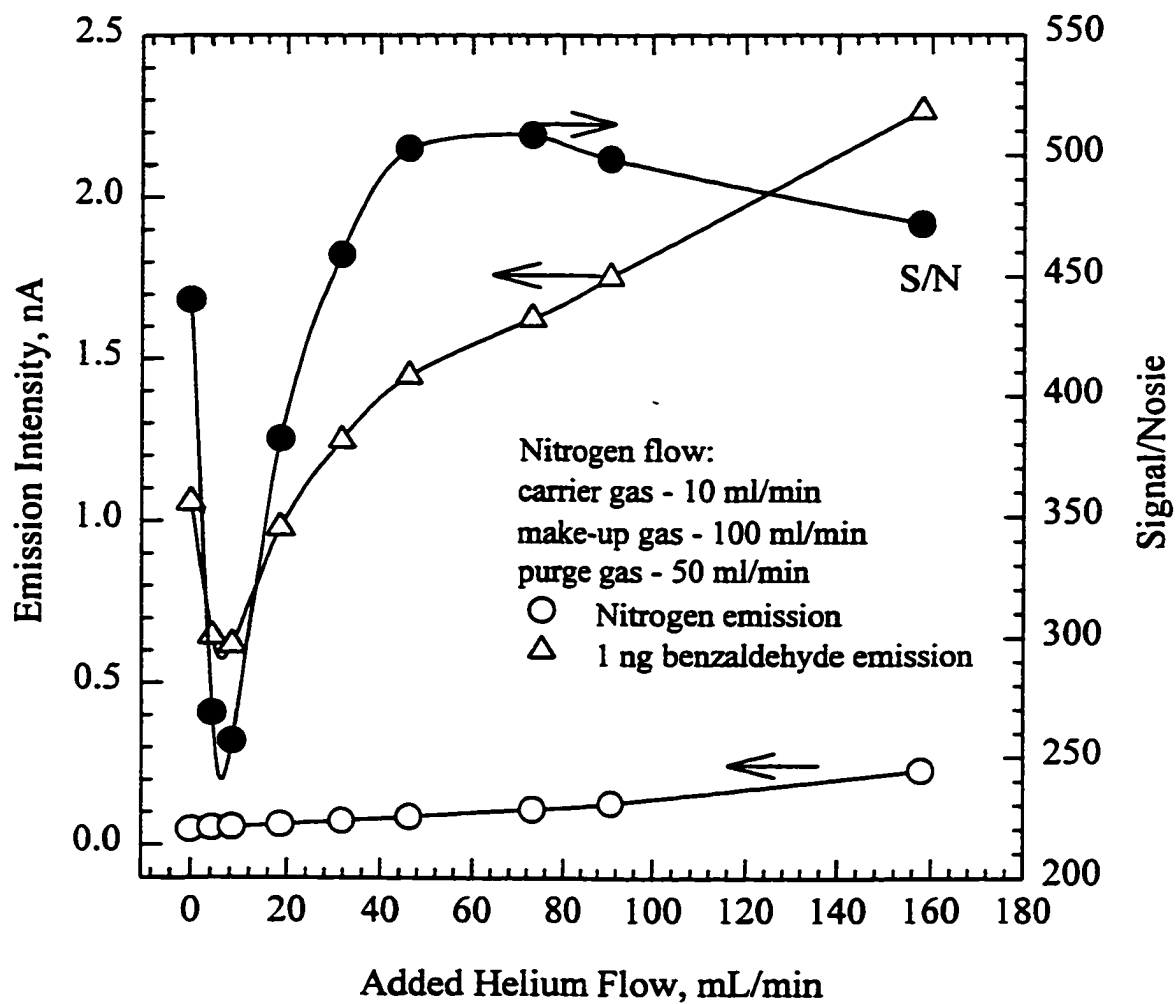
Figure 4.93 Dependence of benzaldehyde emission intensity, the nitrogen second positive system emission intensity, and the signal/noise ratio on added helium flow. Other conditions as in Figure 4.92.

an ionization potential below 11.7 eV, such as propane (ionization potential (IP): 11.1 eV) and benzaldehyde (IP: 9.52 eV), is ionized by metastable argon through Penning ionization. The increased electron concentration results in an increased concentration of argon metastables and of various other species in the plasma. Therefore, the emission increased. In this case, the enhanced nitrogen second positive emission accompaning the increased electric current is the only spectrum observed (Nitrogen is present at trace levels in argon gas, and also diffuses into the GC system from the atmosphere). However. in the present argon or helium-doped ALD system, the nitrogen content was much larger (Ar/N_2 (v/v): 1:1) or He/N_2: 0.6:1) than that in the Ar-PD system. When benzaldehyde was injected (and as well as an enhanced nitrogen second positive emission), there was an enhanced emission of benzaldehyde phosphorescence, while the electric current remained at about the same level. If the energy transfer mechanism for aroyl excitation is taken into account, the enhanced aroyl phosphorescence should result from an increased number of triplet metastable $N_2(A)$ states which can be produced by the reaction $Ar^*(^3P_{0,2}) + N_2 \rightarrow$ $N_2(C)^* \rightarrow N_2(B)^* + h\nu \rightarrow N_2(A)^* + h\nu$ (157, 159, 166, 167). This suggests that the aroyl excitation through energy transfer from the $N_2(A)$ state should be the major, if not the predominant, process, while Penning ionization of analyte is a very minor one in the argon or helium-doped ALD, at least as far as emission is concerned. What brings about the increase in emission is the increase in triplet N_2 (A) species generated by the noble-gas metastables. This was also confirmed by the lack of any significant increase in electric current when injecting other compounds with an IP below 11.7 eV such as propane, dodecane, acetone and hexane.

Further evidence for the proposed mechanism was the observation of the very intense second positive system emission as well as a few very weak transitions from the first positive system ($N_2(B) \rightarrow N_2(A)$) which mainly occurs in the red and near-infrared region (168). Figures 4.94 and 4.95 show the emission spectra of the intense second positive system and the weak first positive system in the argon and helium-doped ALD system, respectively. The similarity of Figures 4.94 and 4.95 supports the assumption of a similar mechanism for producing the $N_2(A)$ state for both argon and helium metastables. Unfortunately, due to our spectral limits of 200 and 800 nm, the main peaks were beyond our observation range. Another bit of supporting evidence was that the ratios of band intensity of the nitrogen second positive system to that of benzaldehyde phosphorescence kept about constant when doping argon into nitrogen carrier (Table 4.8).

Table 4.8 Dependence of the Ratios of Band Intensity of The Nitrogen Second Positive System to Benzaldehyde Phosphorescence on Doped Argon Flow

Ratio of Band Intensity	Doped Argon Flow (N_2 flow: 100 mL/min)		
	0 mL/min	20 mL/min	75 mL/min
$I_{337\ nm\ (N2)}/I_{427\ nm\ (BA)}$	0.91	0.90	0.95
$I_{357\ nm(N2)}/I_{397\ nm(BA)}$	1.13	1.03	1.22
$I_{381\ nm(N2)}/I_{460\ nm(BA)}$	0.53	0.54	0.50

This is in agreement with the reaction $Ar^*(^3P_{0,2}) + N_2 \rightarrow N_2(C)^* \rightarrow N_2(B)^* + h\nu \rightarrow N_2(A)^* + h\nu$ being responsible for the additional excitation of benzaldehyde phosphorescence.
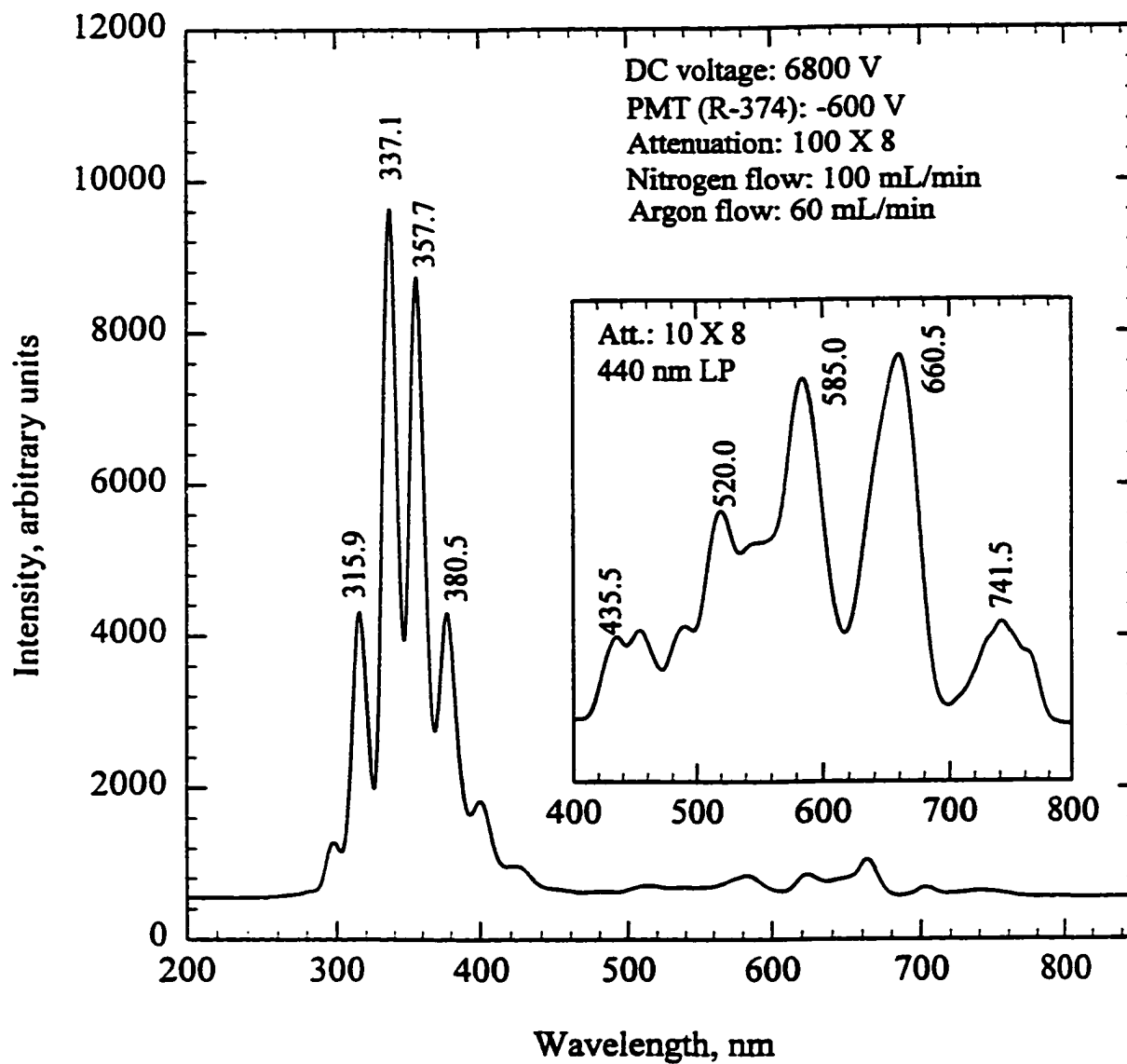
Figure 4.94 Background spectrum of nitrogen doped with argon in the ALD. 1/8 meter grating monochromator with R-374 PMT. Bandpass: 6.6 nm.
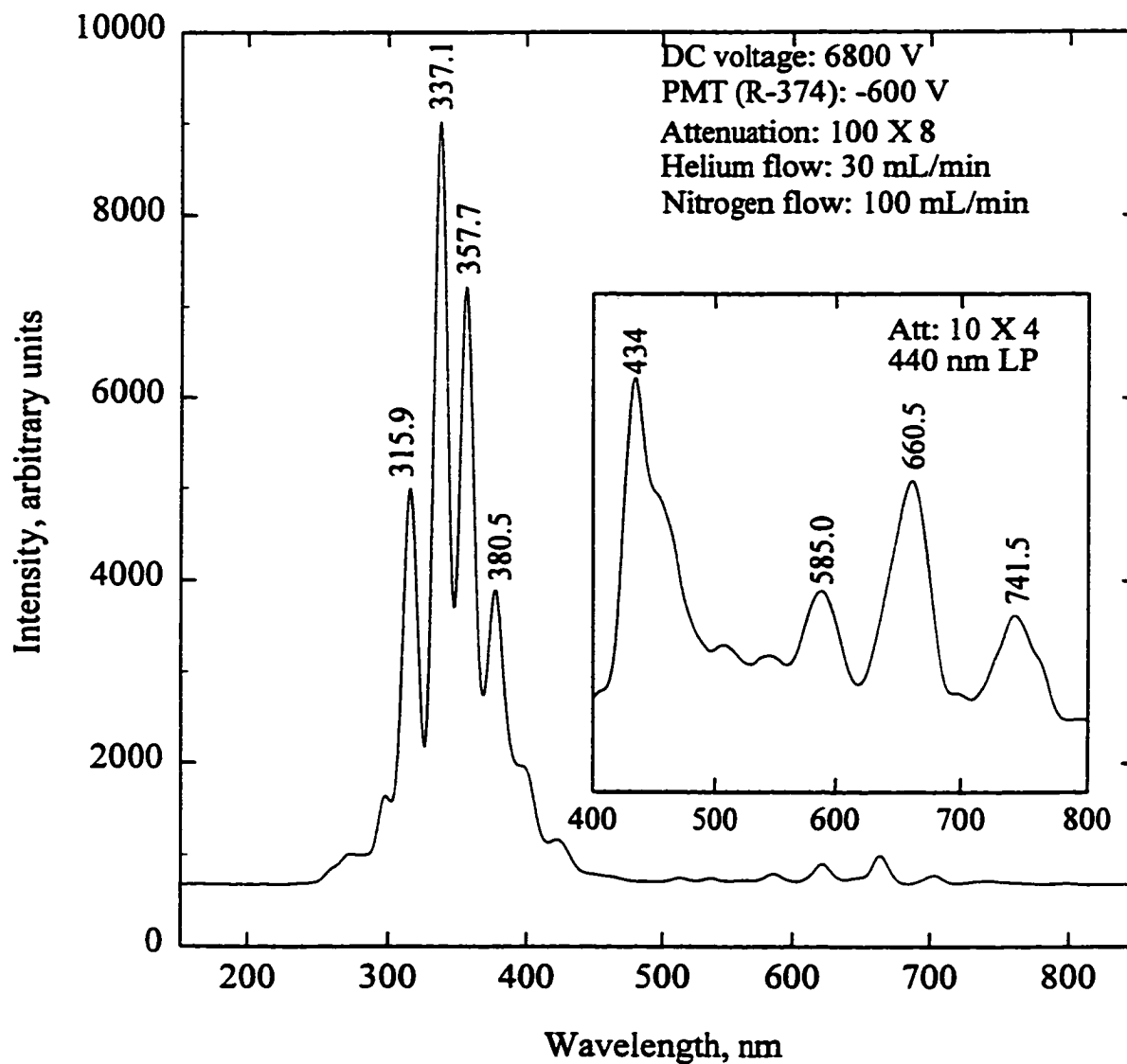
Figure 4.95 Background spectrum of nitrogen doped with helium in the ALD. 1/8 meter grating monochromator with R-374 PMT. Bandpass: 6.6 nm.

4.10 Conclusions

Phosphorescence in the gas phase is, as a rule, a very weak and very rare event. Almost all studies of the literature used reduced pressure in order to reduce quenching. In this study, however, the very intense gas-phase phosphorescences (or E-type delayed fluorescences) of certain types of aroyl compounds were observed in excited nitrogen at high temperature and atmospheric pressure. A novel, radioactively stimulated, high-voltage, low-current discharge in high-purity nitrogen was used to excite aroyl compounds. Our speculative luminescence mechanism for aroyl compounds suggests that ground state N_2 is excited to the triplet metastable $N_2(A)$ state by a fast electron, in a strong electric field, in the mild discharge (≤ 35 nA), and that this is followed by efficient triplet-triplet energy transfer from N_2 (A $^3\Sigma_u^+$) to the aroyl compounds. Doping argon into the nitrogen carrier increased the population of N_2 (A $^3\Sigma_u^+$) by reaction of metastable argon atoms with ground state N_2 and thus enhanced aroyl luminescence. Our novel excitation source represents a new method for obtaining large populations of emitting aroyl triplet states in the gas phase, which are extremely difficult to obtain by optical excitation.

The gas-phase luminescence spectra of some sixty compounds were recorded, and their triplet state energies were calculated. Most of these data had not been obtained before in the gas phase. The correlation between the n,π^* triplet state energy of a series of substituted aroyl compounds confirmed, for a given series, electron-donating substituents increase, while electron-withdrawing substituents decrease, the n,π^* triplet state energy. It was found that aroyl compounds having a hydrogen directly attached to carbon

substituted at the ortho position, such as o-methylbenzaldehyde, o-methylacetophenone and o-methylbenzophenone, did not luminesce to any significant extent, while the para- and meta- isomers of these compounds emitted almost as strongly as benzaldehyde. The "ortho effect" was observed in this study and had been rationalized in terms of the well-known and much studied intramolecular hydrogen abstraction (photoenolization). The quenching effects of the gas-phase phosphorescence of sixteen typical aroyl compounds by oxygen and hydrocarbons were also investigated. It was shown that gas-phase phosphorescence was subject to the most severe quenching by molecular oxygen, and that there was a small correlation between the quenching intensity and compound structure, *i.e.*, compounds of a similar structure were all quenched to a very similar degree, while different types of compounds exhibited larger differences in quenching intensity by both oxygen and methane.

Chapter 5

COMPOUND-SPECIFIC DETECTION AND QUANTITATION OF PERFECTLY CO-ELUTING ANALYTES IN DUAL-CHANNEL PHOTOMETRY

5.1 Filterless, Full Spectral Range, Compound-Specific Detection in Dual-Channel Photometry

5.1.1 Introduction

In the analysis of complex real-life samples, there is an increasing quest for greater selectivity. Dual-channel response ratios, including dual-detector response ratios and dual-wavelength response ratios of a single detector, have been used to improve selectivity in various analytical areas (169-174).

In addition to peak size and peak retention, response ratios add a third, chemical dimension to conventional chromatograms. Generally, response ratios can be used to check peak purity and identity, and to support derivative chromatograms of significantly higher selectivity. Aue and co-workers (173, 174) proposed the use of a computer algorithm for producing computer-mediated, i.e. "virtual" or "correlation" chromatograms of much improved selectivity in the analysis of various transition elements with a dual-channel FPD. The two channels monitor different wavelength ranges in accordance with analyte and interferent spectra. Based on response ratios, two different computer algorithms have been developed that either cancel peaks of one element (subtraction chromatograms) (175-177) or allow only peaks of a given response ratio access to the chromatogram (conditional-access or "Condac" chromatograms). The primary use of subtraction chromatograms lies in the suppression of matrix components

213

or interferents, and in the great increase in selectivity. In contrast, the use of CONDAC lies in the scanning of complex, computer-stored records of separation with the purpose of quickly finding the FPD-active elements of interest.

Condac chromatograms obtained from a dual-channel FPD will display only those peaks that contain the "dialed in" element to achieve element-specific detection. (The term "specific" used here retains its original analytical definition of "infinitely selective"). The interesting and also analytically important question here is: Can compound-specific detection be achieved in a single detector (i.e. a single-mechanism detector offering at least two distinct simultaneous signals)?

Theoretically, whenever the components of a sample differ in some physically measurable parameter —wavelength, mass, reaction rate, electrochemical potential, and the like— and whenever their intensity ratios in the two (optical, electronic, etc.) channels are (1) sufficiently different from one another and (2) sufficiently constant throughout the range of analytically important conditions (concentration, interference, etc.), compound-specific detection can be easily achieved. Analytically, such an approach simplifies the chromatogram and confirms that a particular peak does indeed represent the analyte of interest. Most importantly, though, the demonstration of single-compound specificity seemed a primarily conceptual task: for this reason it was one of the major objectives of this study. An additional objective was to achieve such specificity in the absence of any optical filter or spectrometer.

It is believed that an optical filter or, though at lower sensitivity, a spectrometer, is a prerequisite for achieving selectivity or specificity. For the dual-channel FPD, optical

filters are indeed needed to obtain the spectral difference between two channels (46). It became therefore rather interesting to investigate, in a generally applicable manner, whether Condac chromatograms could be produced from a dual-channel photometric detector in the absence of any spectral filters or light dispersive devices.

In order to test this basic idea, the dual-channel aroyl luminescence detector was used as a model system. The gas-phase luminescence spectra of aroyl compounds that this detector monitors are fairly broad and have been presented in Chapter 4. They occupy, very approximately, the same wavelength range. Nevertheless, their features are still characteristic of individual species. This means that, as model analytes, they promise the analyst a chance of obtaining compound-specific Condac chromatograms while at the same time posing the challenge of highly similar spectra. Thus, if the ALD should indeed prove capable of yielding Condac chromatograms from two filterless optical channels, it would seem reasonable to conclude that several other photometric detectors such as the UV-Vis absorption and fluorescence detectors should likewise be capable of providing virtually compound-specific responses.

5.1.2 Experimental

The dual-channel aroyl luminescence detector (Figure 2.3) was used in this study. The detector temperature was usually 200 °C, the operating DC voltage +6000 V. For most of the present study, the ALD was used without optical filters. One channel was fitted with an R-268, the other with an R-2228 Hamamatsu photomultiplier tube. Figure 5.1 shows the two PMT's typical radiant sensitivity in the range of interest. For purpose
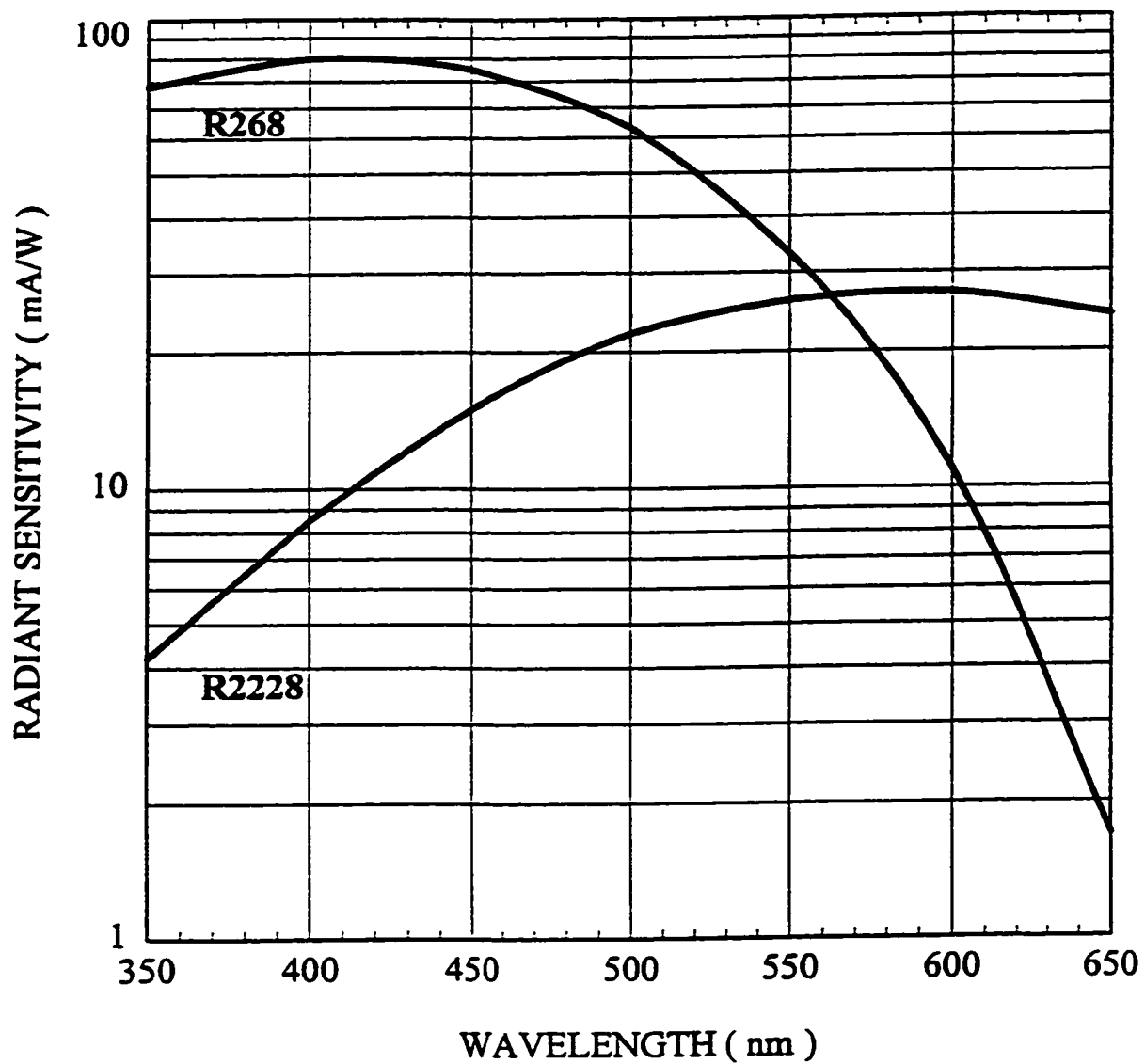
Figure 5.1   Nominal radiant sensitivity of two photomultiplier tubes (from ref. 178).

of comparison, the R-2228 PMT was replaced later with a combination of a 530-nm colored-glass longpass filter and a R-268 PMT.

The determination of response ratios used the "slope ratio" method (174) for "whole" peaks. The Condac algorithm (173) and the response-ratio chromatograms have been described (174); no changes were made to the computer hardware and software components.

5.1.3 Results and Discussion

A few 16-component mixtures of aroyl compounds were prepared for demonstrating the possibility of computer-mediated, compound-specific detection. even in the absence of optical filters. The choice of aroyls reflected different considerations: which responded well, which represented major versus minor structural differences. which fitted nicely and loosely into a simple demonstration chromatogram.

Figure 5.2 shows the two single-channel chromatograms of a typical mixture. topped by a whole-peak response ratio chromatogram (174). It is obvious that. as expected, the different radiant sensitivity profiles of the two PMT's used in this study have indeed generated differences in response ratio for sixteen components. The differences are not large. However, the question is whether they are large enough to produce Condac chromatograms by the computer algorithm. As the experiment clearly demonstrates, they are. Somewhat surprisingly, however, it was even possible to obtain from a single file, i.e., a single injection, the maximum possible complement of sixteen

individual Condac chromatograms. Seven of them are shown stacked up in the middle of Figure 5.3.

In the process of producing a Condac chromatogram (173), a numerical. "true" response ratio together with three quality parameters (thresholds) are put into the computer. The first parameter defines the fraction by which the determined response ratio is allowed to differ from the "true" one; the second defines what percentage of the 10-Hz data points within a Condac peak has to be accepted by the above criterion; and the third defines the minimum of time over which the other two conditions have to be met. The numerical values typically used to set these thresholds were 0.001, 90%, and 10 s. respectively.

For real-life tasks, the narrow space established by the above threshold values must be broadened due to the increased sample numbers and complexity, and chromatographic noise and overlap. This and the required precise reproducibility of response ratios may limit the number of single-compound Condac chromatograms obtained from one separation. It is also obvious that, if not most, at least many compound-specific chromatograms can be obtained from a single file/separation with relative ease. The measured response ratios of the 16-component mixture, at the particular setting of PMT voltage used, ranged from 0.430 for 1,4-naphthoquinone to 1.165 for xanthone. This is a fairly large gap, particularly in the case of spectral discrimination only provided by two photomultiplier cathodes. Many more compounds could easily fit into, and be safely differentiated within, this range.
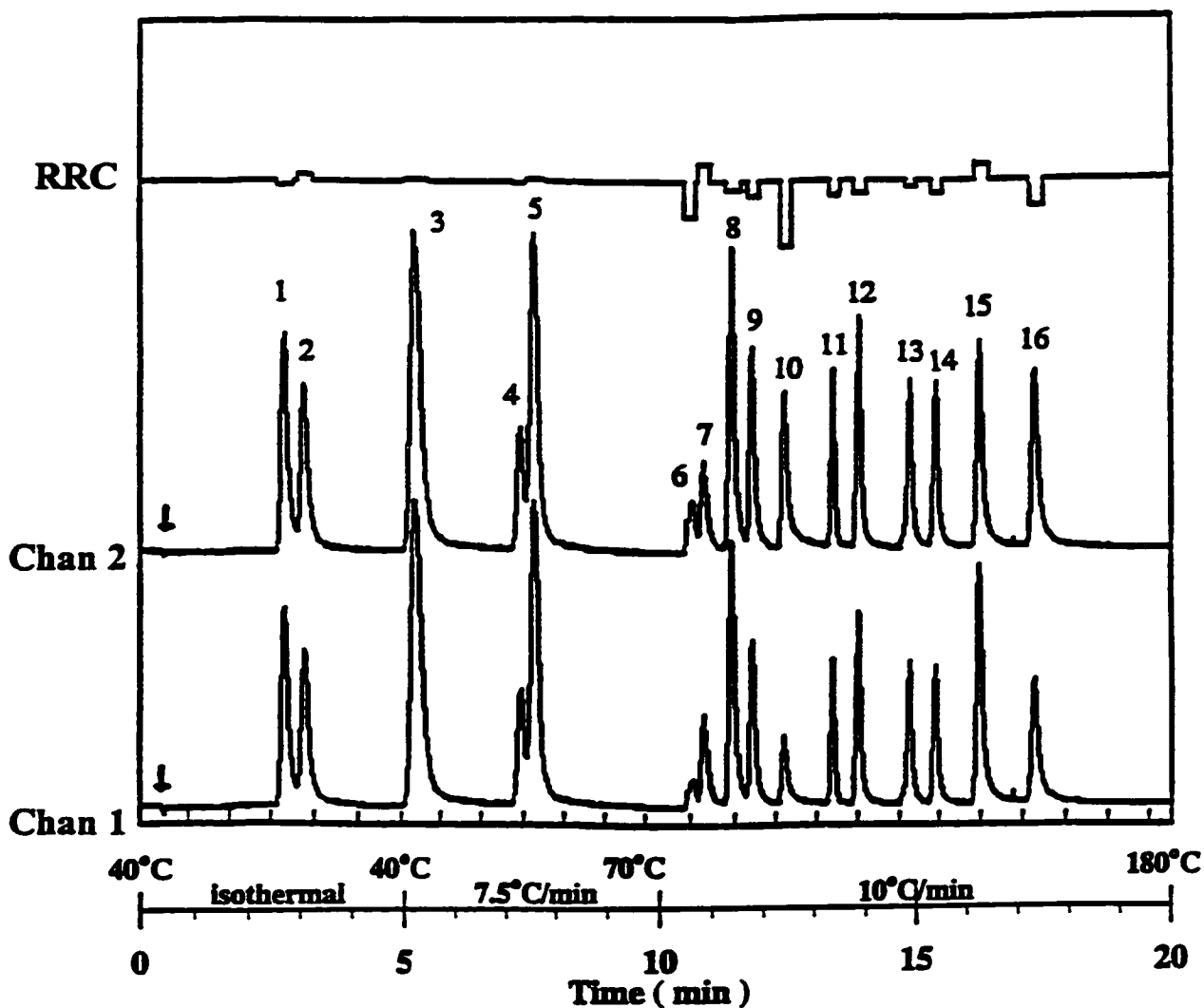
Figure 5.2 Screen-dump of individual channels and the slope-based, whole-peak response-ratio chromatogram (ref. 174) of a mixture of aroyl compounds; time/temperature scale added. Channel 1: PMT-268 (no filter, -600 V); Channel 2: PMT-2228 (no filter, -600 V). Compounds in order of elution: 0.5 μL hexane (solvent), 3 ng benzaldehyde (1), 3 ng 4-fluorobenzaldehyde (2), 18 ng acetophenone (3), 3 ng 4-ethylbenzaldehyde (4), 12 ng 3-methylacetophenone (5), 60 ng 2,6-dichlorobenzaldehyde (6), 60 ng α-tetralone (7), 3 ng isophthalaldehyde (8), 3 ng methyl-4-formylbenzoate (9), 30 ng 1,4-naphthoquinone (10), 3.2 ng 3,3'-bis(trifluoromethyl)-benzophenone (11), 2.4 ng benzophenone (12), 1.8 ng 4-methylbenzophenone (13), 2.4 ng 4-chlorobenzophenone (14), 0.3 ng xanthone (15) and 0.42 ng anthraquinone (16).
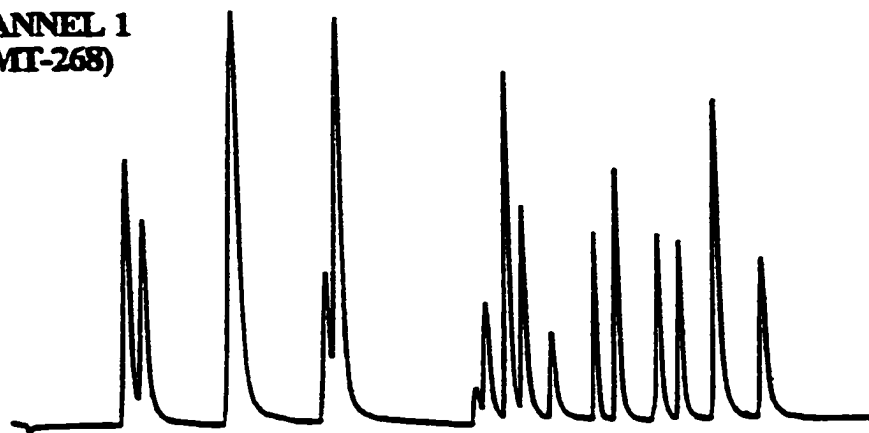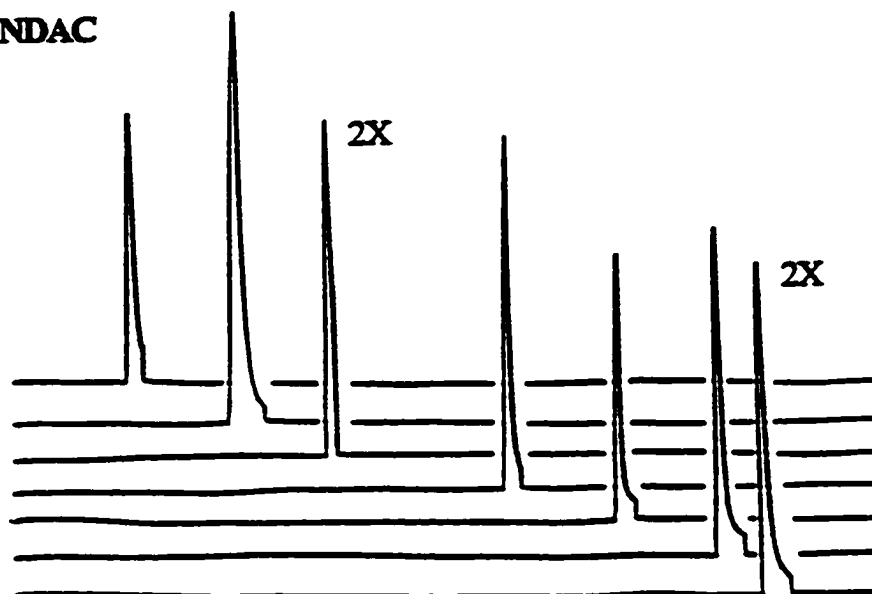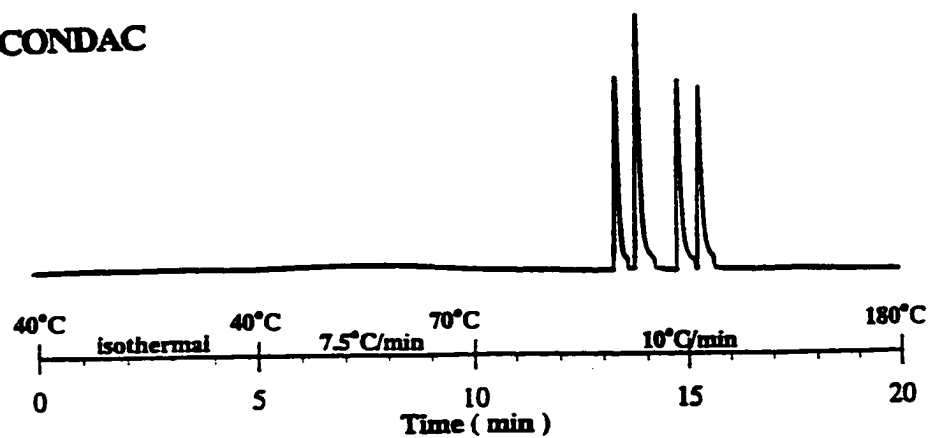
Figure 5.3   Selected single channel (top), single-Condac (middle) and group-Condac (bottom) chromatograms from one chromatographic separation. Conditions and compounds as in Figure 5.2.

Because of their spectral similarity, compounds of very similar structure are more likely to have very similar response ratios. An example is benzophenone and its 3.3'-bis(trifluoromethyl), 4-methyl, and 4-chloro derivatives. When the criterion of response ratio bandwidth is suitably relaxed, the four benzophenones with response ratios of 0.840. 0.835. 0,845 and 0.816, respectively, appear together on the Condac chromatogram. This is illustrated in the bottom section of Figure 5.3. Similar "group Condacs" may be used to indicate the probable structural similarity of peaks produced by an "unknown" sample. Given a two-dimensional data base of relative retention times and response-ratio windows, the identity of a peak may often be conveniently and tentatively addressed (see Chapter 6). The important point, however, is that such scant information can be obtained in the picogram to nanogram range, whereas measuring the (more informative) whole spectrum requires far more sample and far more time.

The range of response ratios measured by two different, filterless photomultiplier tubes is significantly narrower than the range accessible by using even a single, simple filter. The example given in Figure 5.4 shows chromatograms analogous to those of Figure 5.2, but now derived from nominally identical photomultipliers (both R-268 PMT's): one open (filterless) channel, the other in a channel fitted with a 530-nm longpass colored-glass filter. From the comparison of Figure 5.2 and Figure 5.4, it is obvious that the spread of response ratios has significantly widened. In this case, Condac chromatograms are therefore much easier to obtain. A much more extended spread of response ratios could be obtained by further spectral optimization which may involve the use of two filters, possibly of the interference type. These filters could yield a much more
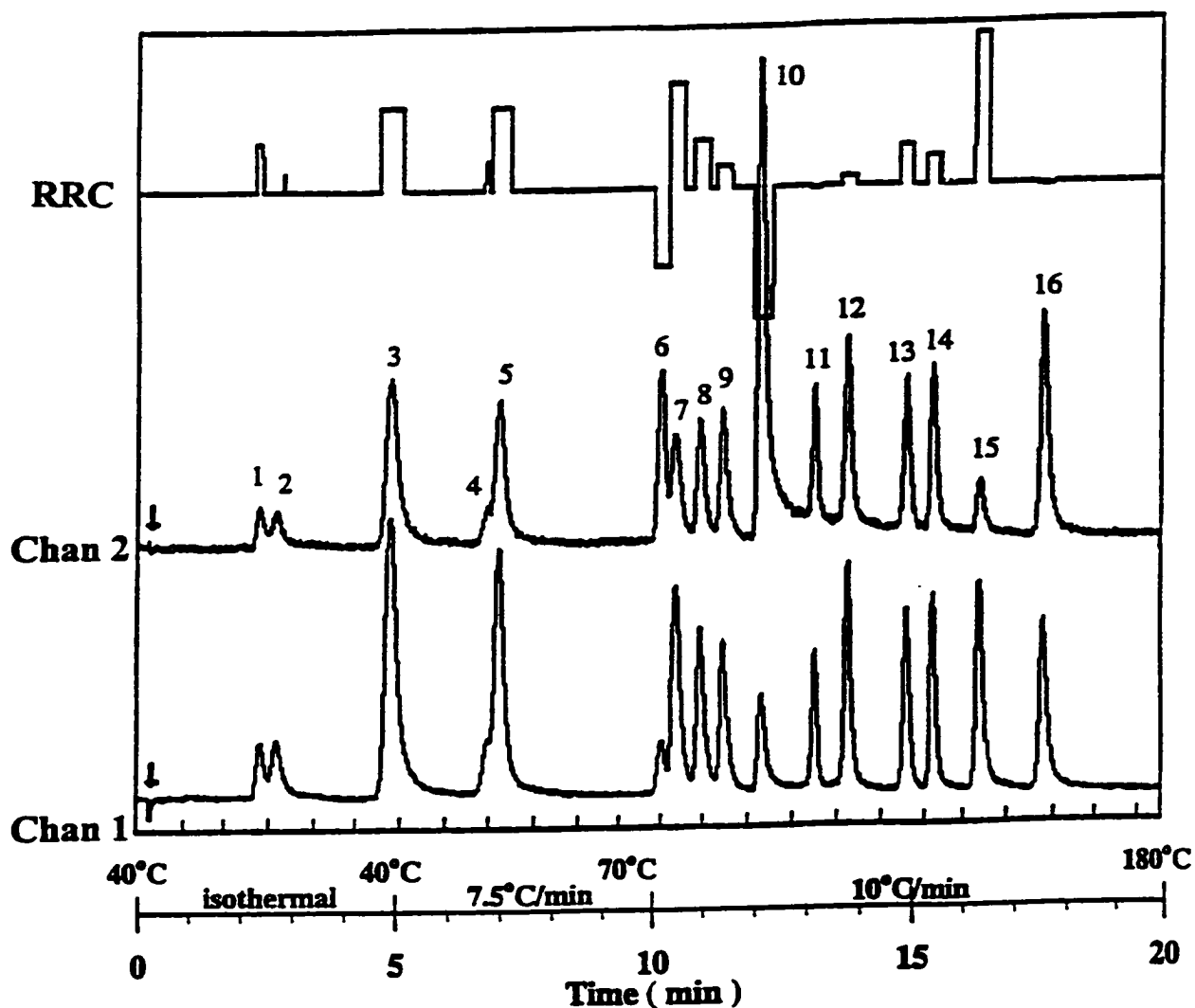
Figure 5.4 Individual channels and the slope-based, whole-peak response-ratio chromatogram of a mixture of aroyl compounds, comparable to Figure 5.2. Channel 1: PMT-268 (no filter, -600 V, attenuation: 8000 X); Channel 2: PMT-268 (530-nm longpass filter, -600 V, attenuation: 200 X). Compounds in order of elution: 0.5 μL hexane (solvent), 1 ng benzaldehyde (1), 1.2 ng 4-fluorobenzaldehyde (2), 25 ng acetophenone (3), 4 ng 4-ethylbenzaldehyde (4), 16 ng 3-methylacetophenone (5), 80 ng 2,6-dichlorobenzaldehyde (6), 80 ng α-tetralone (7), 4 ng isophthalaldehyde (8), 4 ng methyl-4-formylbenzoate (9), 40 ng 1,4-naphthoquinone (10),

3.2 ng 3,3'-bis(trifluoromethyl)benzophenone (11), 2.4 ng benzophenone (12), 2.4 ng 4-methylbenzophenone (13), 3.2 ng 4-chlorobenzophenone (14), 0.4 ng xanthone (15) and 0.56 ng anthraquinone (16).

rugged specificity for single (or spectrally related groups of) compounds.

Similar compound-specific behavior could be expected from other photometric detectors, say, UV-Vis absorption or fluorescence detectors. However. the analytical practicality of using response ratios depends on their constancy in the face of changing circumstances. Some additional experimental evidence shows that the aroyl-luminescence response ratios of all sixteen test compounds remained invariant throughout and beyond their conventional calibration curves, in accordance with expectations based on the singularity of their excited states. The constancy of aroyl response ratios was indeed never compromised, despite the large number of probed concentrations. Typically these concentrations ranged from close to the $S/N_{p-p}= 2$ detection limit to well beyond the end of the linear range. This is clearly shown in Figures 5.5 and 5.6. Figure 5.5 shows this perfect behavior for two different photomultipliers and no filter; Figure 5.6 shows the same for two similar photomultipliers, one of which resides behind a colored-glass filter. In order to avoid obscuring the graph, some compounds which are close to each other are presented not by horizontal lines, but merely by the numbers that identify them.

The relative standard deviation of the response ratio for any given compound over the whole tested concentration range —i.e. over 3 to 5 orders of magnitude depending on compound sensitivity— is, on average, $\pm$ 2.3% (lowest value 1.1%, highest value 5.6%). That puts it well within practical limits of Condac chromatography. Figures 5.5 and 5.6 also offer a good pictorial representation of the ample response space still available to new compounds, even in the filterless system. As mentioned before, gas-phase aroyl luminescence spectra show small spectral differences and a large overlap in the visible
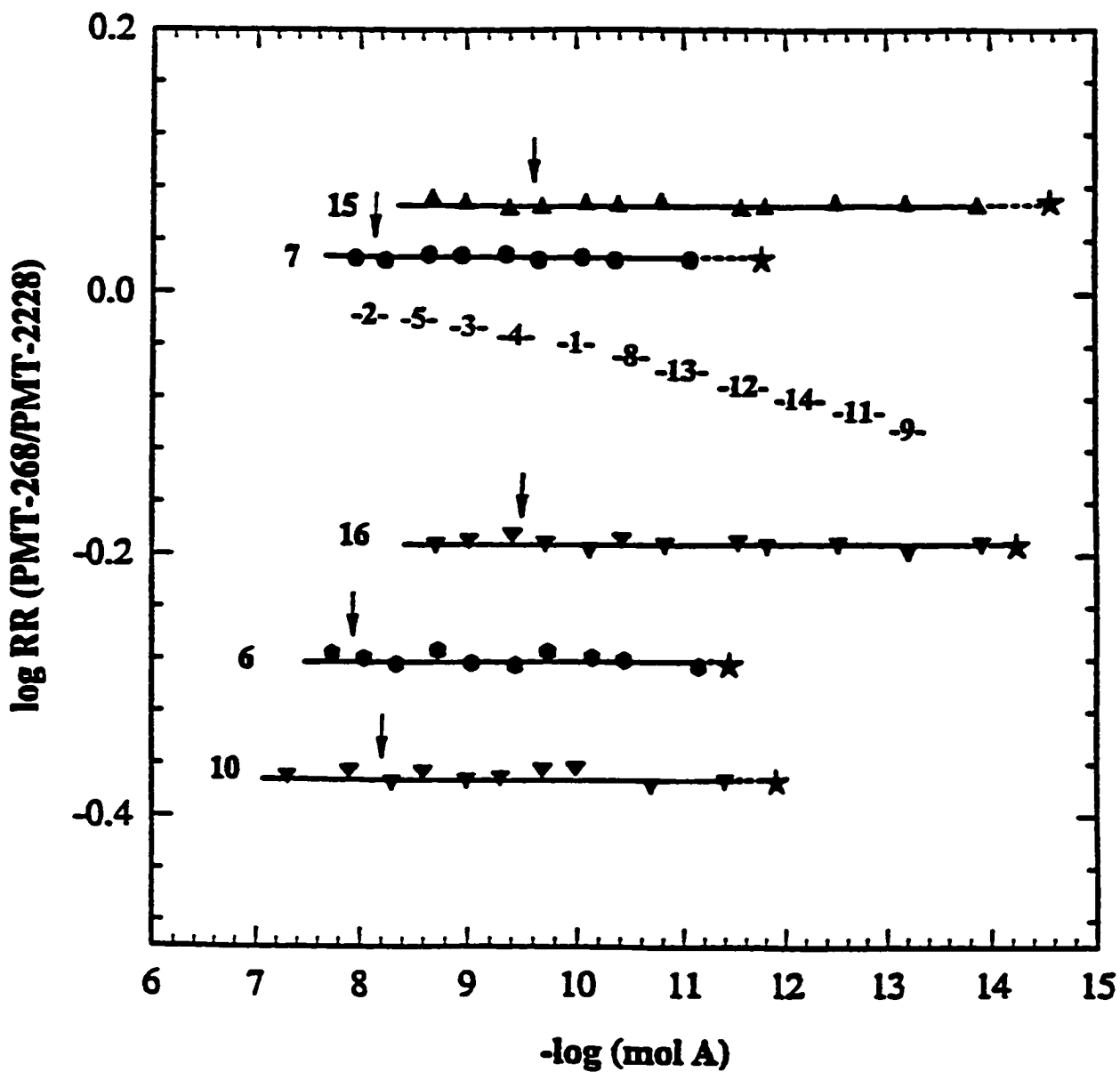
Figure 5.5   Whole-peak response ratio vs injected molar amount of 16 aroyl test compounds. First channel: PMT-268 (no filter, -850 V), second channel: PMT-2228 (no filter, -1000 V). Peak Nos. as in Figure 5.2. Data points for compounds closely approaching each other are omitted for clarity. Arrow: upper end of linear range (-10% deviation); Star: minimum detectable amount ($S/N_{p-p}=2$).
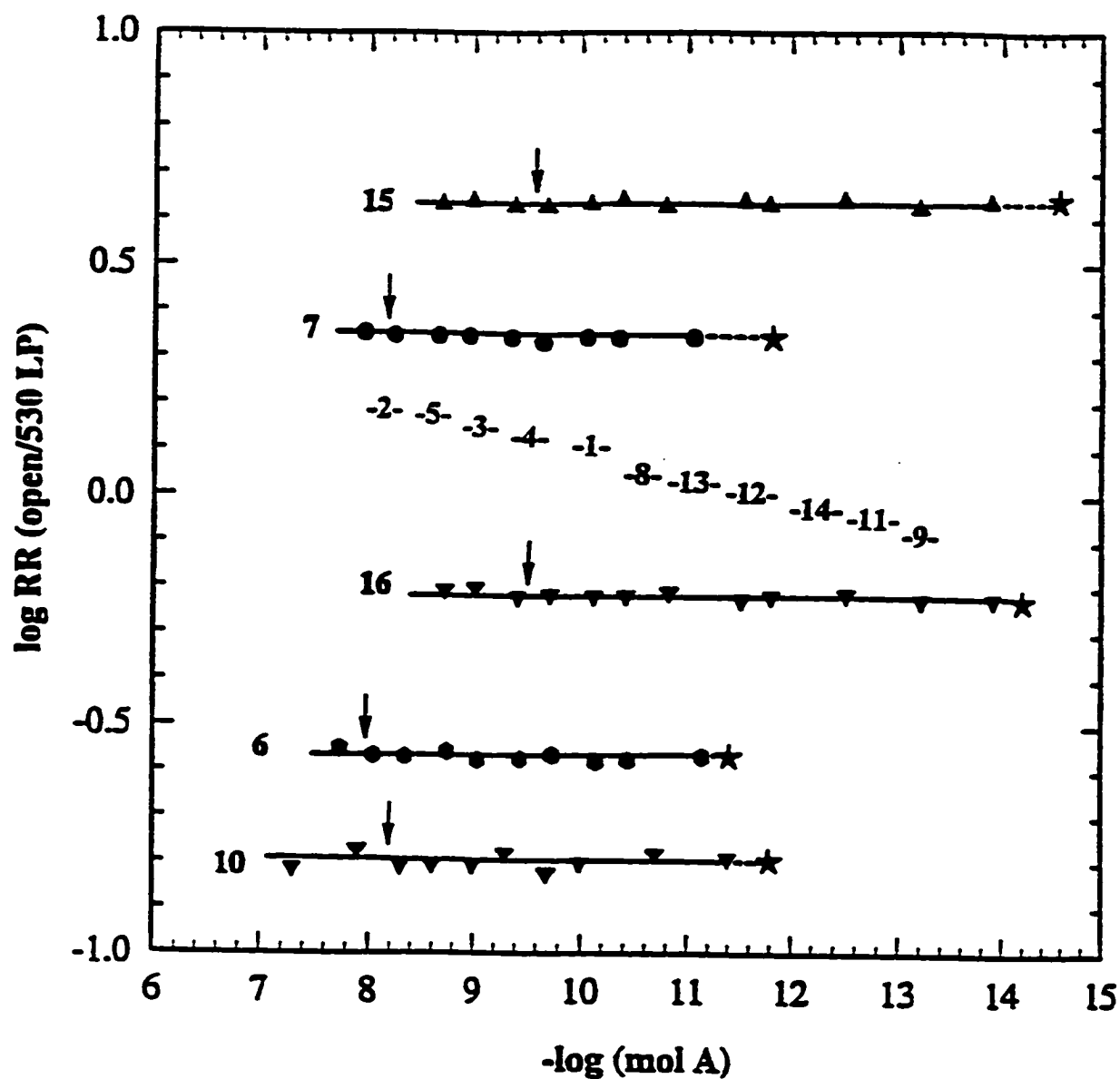
Figure 5.6 Whole-peak response ratio vs injected molar amount of 16 aroyl test compounds. First channel: PMT-268 (no filter, -850 V), second channel: PMT-268 (530-nm longpass filter, -850 V). Comparable to Figure 5.5.

region. In this regard they differ from typical flame-energized band spectra. The latter cover a much wider wavelength range with much less spectral overlap: they would hence be expected to expand even farther the response-ratio window.

This, plus the additional dimension provided by a chromatographic, i.e. largely resolved sample input, suggests that the filterless approach developed in this study can be used not just on the aroyl luminescence detector but on a variety of other "photometric" instruments and samples as well. Sometimes (e.g. in a destructive source such as a flame or plasma) the computer-mediated "specificity" will refer to single elements; sometimes (e.g. in a non-destructive source such as an absorption or as here, emission system) it will even refer to single compounds. Therefore, the basic supposition of this study has been sufficiently established.

5.1.4 Conclusions

The phosphorescence of aroyl compounds in excited nitrogen has been used as a model system to demonstrate that simple dual-channel detector responses that relate to analyte structure, e.g. those based on compound-specific spectra, can be used to obtain virtual chromatograms that display only a single, selected compound from among a multitude of separated ones. Many single-peak (or structurally defined multiple-peak) Condac chromatograms can thus be obtained from a single separation stored in computer memory. While this study was carried out on the aroyl luminescence detector, other types of "photometric" detectors—and, even beyond these, other types of compound-

responsive detection devices—should be capable of similar single-compound (or single-group) specificity.

This study has also demonstrated that it is possible to obtain spectrally based, virtual separations from a detector of full wavelength range that employs neither optical filters nor dispersive devices. The purpose of this demonstration was not to question the use of filters but to draw attention to how small a spectral difference can still be turned into a large analytical advantage.

5.2 Quantitation of Perfectly Co-eluting Analytes on Dual-Channel-Subtraction Chromatograms

5.2.1 Introduction

A peak is one of the commonest and most desirable forms of analytical response. Chromatographers generally try to achieve good resolution of components in a mixture as a prerequisite to quantitation. However, in the analysis of complex mixtures some of the peaks may overlap, partially or completely, due to similarities in the physical and chemical properties of the relevant constituents in the sample, even with carefully optimized chromatographic conditions. This overlap may cause difficulties in the precise quantitation of the components. In more severe situations, overlapping peaks may merge completely, appearing as a single peak; in this case, not only is quantitative analysis impossible, but also qualitative analysis is unreliable.

Conventional (mathematical) deconvolution of overlapping peaks has been the subject of much research over the years (see ref. 179-183 for several recent examples).

The purely mathematical deconvolution, including methods based on multivariate partial least squares, principal components and artificial neural networks, permit the quantitation of partially overlapping components without resorting to the use of pure compound standards, but these methods are not applicable in the case of perfectly co-eluting peaks. In addition, the application of these methods may also be somewhat limited by their requirement for fairly sophisticated chemometric techniques that may not be generally accessible to analysts. Yet, the analytical need for quantitating such peaks is both strong and widespread.

Some chromatographic detectors, particularly spectral ones, can be upgraded from being inherently selective to being tunably specific by a change from single-channel to dual-channel operation (173, 176). Tunable specificity implies that overlapping peaks can be quantified as if they were completely resolved, even if their retention times are identical. Technically, quantitation of perfectly co-eluting analytes is obtained from two subtraction chromatograms, each of which shows only one of the two co-eluting compounds (by subtracting the co-eluting compounds). Many different pairs of overlapping analytes (or analytes/interferents) can thus be algorithmically resolved from a single chromatographic separation stored in computer memory.

In this study, the dual-channel aroyl luminescence detector was used again as a demonstration system for quantitating two perfectly co-eluting model analytes (fluorobenzaldehyde isomers) from subtraction chromatograms. The reason that the dual-channel ALD was chosen as the testing system is that the gas-phase luminescence spectra of aroyl compounds are broad and fairly similar in shape and wavelength range. This is

particularly so in the case of positional isomers. The highly similar types of spectra would offer a much more challenging test due to the small difference in responses from the dual-channel ALD (compared with, e.g., the case of a dual-channel flame photometric detector in which the different responses of various elements would seem to offer much easier testing). In principle, the approach represents the gas chromatographic equivalent of the old two-component problem in solution spectrophotometry. In practice, the quantitation will be carried out, and its accuracy checked, on two differential chromatograms obtained from a dual-channel GC detector. To our knowledge, no explicit study of this kind exists in the literature, despite the presence of GC detectors suited to the task.

5.2.2 Experimental

In this study, the two channels were equipped with R-268 photomultiplier tubes behind a 420-nm shortpass and a 530-nm longpass interference filter, respectively (i.e. a rather crude optical arrangement that left much of the luminescence unused). The response ratio (the ratio of peak height or peak area in the two optical channels) was predetermined for each pure fluorobenzaldehyde isomer. It served as the algorithmic "magnification factor" that allowed a particular isomer to be deducted.

When an isomer mixture was chromatographed, the simultaneous outputs from the two optical channels were stored in computer memory. The second channel was scaled by the predetermined magnification factor (the response ratio of the interferent). Its subtraction from the first channel then annulled the respective isomer in the differential (subtraction) chromatogram. This procedure was repeated (still on the same data file) by

using the magnification ratio of the other isomer. In other words, this switches the roles of analyte and interferent. For a comparison of detection limits, the same file again was subjected to a software-based "channel swap". In essence, this switches the roles of the two channels. The entire process described above was then repeated. The computer interface and algorithms used are simple and have been reported earlier (173).

Solutions were prepared of 3-fluoro- and 4-fluorobenzaldehyde, and of 2-fluoro- and 4-fluorobenzaldehyde, either by themselves or in mixtures of weight ratios 1:3, 1:1 and 3:1, such that the data points would be conveniently spaced on two composite calibration curves for each pair of positional isomers. In a separate experiment, the same amount of one isomer was repeatedly injected in the presence of varying amounts of the other.

5.2.3 Results and Discussion

For this study, a large number of well-responding and overlapping analyte pairs was available. The three monofluoro isomers of benzaldehyde were selected as the co-eluting model analytes for their conceptual simplicity, good response, easy availability, reasonable chromatography, and adequate stability. As is common among substituted aromatics, the *ortho* isomer eluted first. It can, if desired, be easily separated from the closely eluting *meta/para* pair. For the current study, however, a column of very low resolution was deliberately used (see Chapter 2). Furthermore, the chromatographic separation was worsened by using a column temperature significantly lower than that required by the resolution optimum. Under these conditions, the three isomers merged.

Figure 5.7 shows as chromatographic example the 1:1 mixture of *meta-* and *para-*fluorobenzaldehyde, first as it appears in the two single channels, then as the individual components appear in the two subtraction chromatograms. Since both isomers phosphoresce with substantial intensity within both wavelength windows, and since the contribution of one isomer has been subtracted, it is not surprising that the individual subtraction peaks, as well as their sum, should be considerably smaller than the composite ones. However, this is not always the case. As will be demonstrated in a quantitative manner later, an inverted analyte peak in the subtraction chromatogram can actually be larger than either of the corresponding single-channel peaks.

Figure 5.8 shows the phosphorescence spectra of the three model isomers. The highly similar types of spectra explain why the difference in response ratios among the three isomers is not overly large.

Figures 5.9, 5.10 and 5.11 display the composite calibration curves of the three isomers. Within the linear range, the four calibration curves in each plot are identical. Since in each case one of them is that of the pure analyte, while the other three represent analyte in the presence of varying amounts of the overlapping isomer, it is obvious that the subtraction procedure provides accurate quantitation throughout the linear range. (For simplicity, some confirmatory calibration curves are not shown here, e.g. those of the *para* isomer from the *para/ortho* mixture.)

It has been shown that the calibration curves, beyond the linear range, diverge due to total sample load. The linear range of the pure analyte appears therefore longest, next
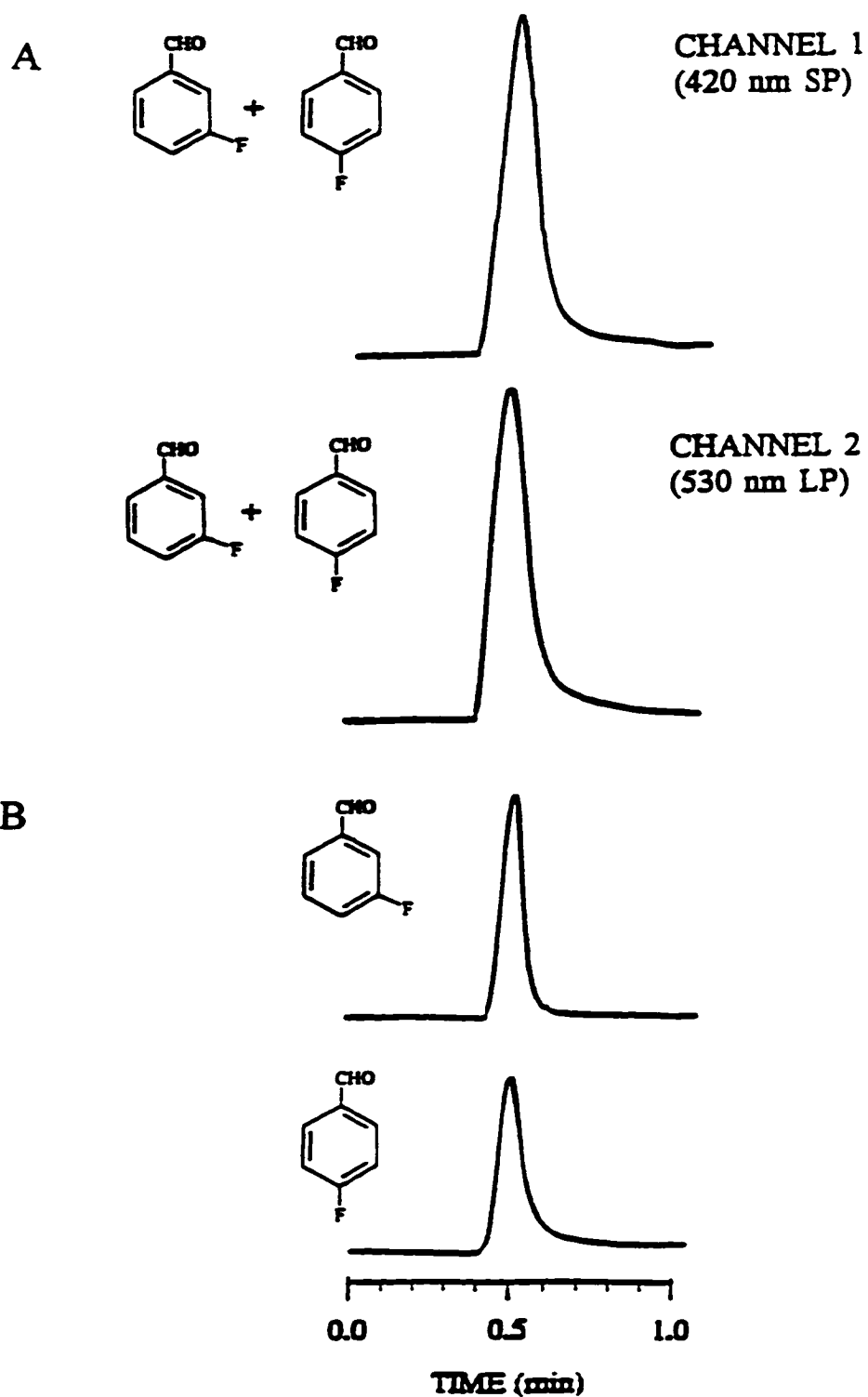
Figure 5.7   Typical peak shapes of an overlapping pair of fluorobenzaldehyde isomers, 20 ng each, appearing together in the two single channels (A), and appearing separated in the two subtraction chromatograms (B).

comes the analyte with the least amount of co-eluting isomer added. and so on. Conventional quantitation traditionally avoids non-linear behavior anyway; in the case of correlational quantitation, an additional caution zone, representing the maximum expected amount of overlapping material, should be established. This would not. however, unduly limit analytical applicability.

The detection limit also differs somewhat among calibrations based on single-channel and subtraction chromatograms. It is easy to see why. Let $R_A(1)$ be the response of the analyte in channel 1 and $R_A(S)$ its response in the subtraction chromatogram. With the response ratio RR between channels 1 and 2 defined as $RR_A = R_A(1)/R_A(2)$ for the analyte and $RR_I = R_I(1)/R_I(2)$ for the interferent, it is easy to show that

$$R_A(S) = R_A(1) \, (1-(RR_I/RR_A)) \tag{5.1}$$

In other words, if RR_I is smaller than RR_A, the response of the analyte in the subtraction chromatogram will be positive (a regular peak) and smaller than its response in the first-channel chromatogram, $R_A(1)$, would have been. If RR_I is larger than RR_A, however, $R_A(S)$ will be negative (an inverted peak). In absolute terms, the subtraction response $R_A(S)$ can then exceed the first-channel response $R_A(1)$.

The negative response can be prevented by a software-based channel swap. Aside from the direction of the peak, the trace analyst may find the detection limit an important parameter in the decision to swap or not to swap. Which of the two alternatives produces the lowest detection limit depends not only on the peak heights but also on the noise levels.
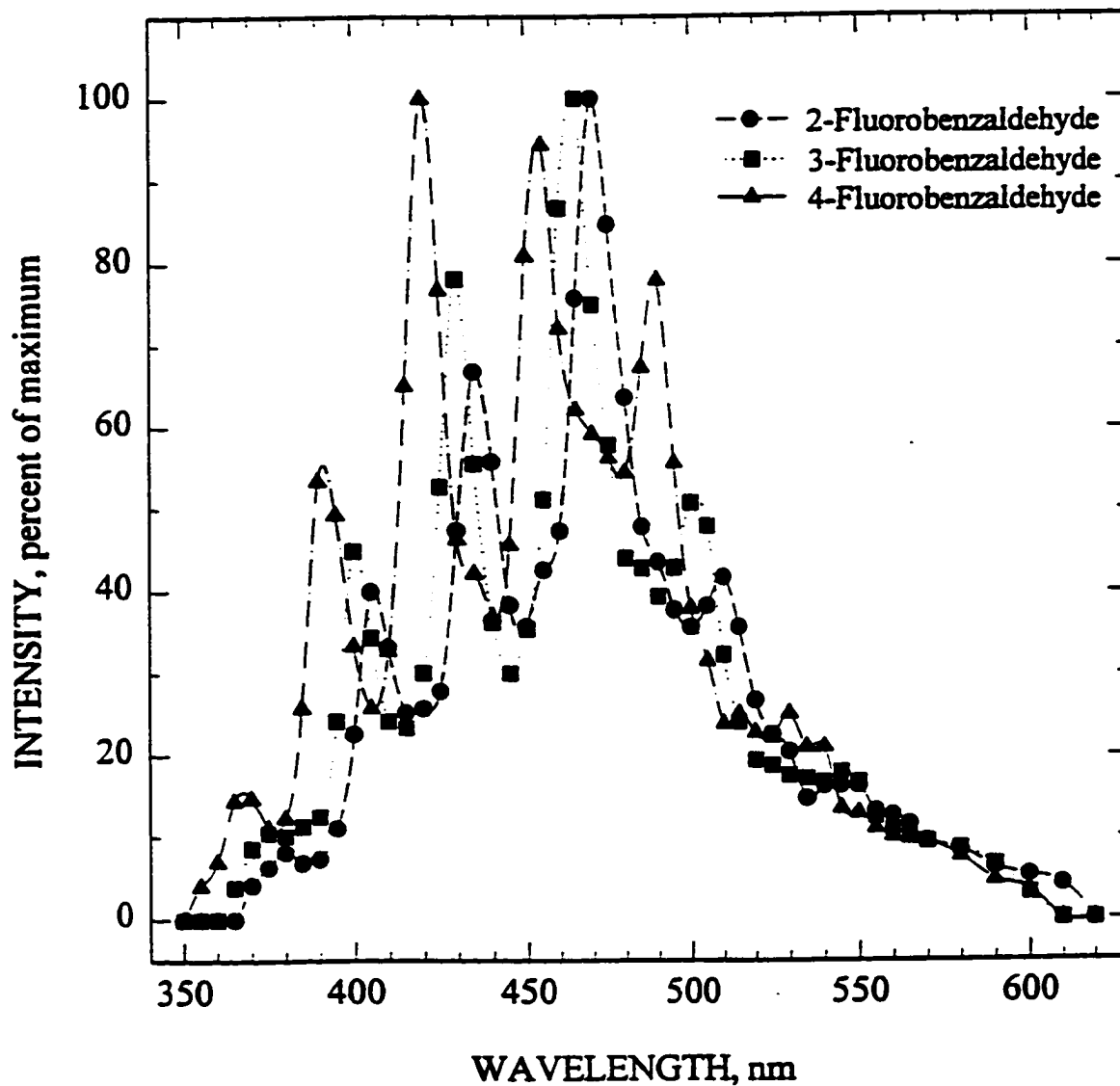
Figure 5.8　Normalized phosphorescence spectra of the three fluorobenzaldehydes in excited nitrogen obtained by using a 1/4 meter grating monochromator, R-374 PMT, a quartz rod as light guide, and the repeated-injection mode. Bandpass ca. 6.6 nm.
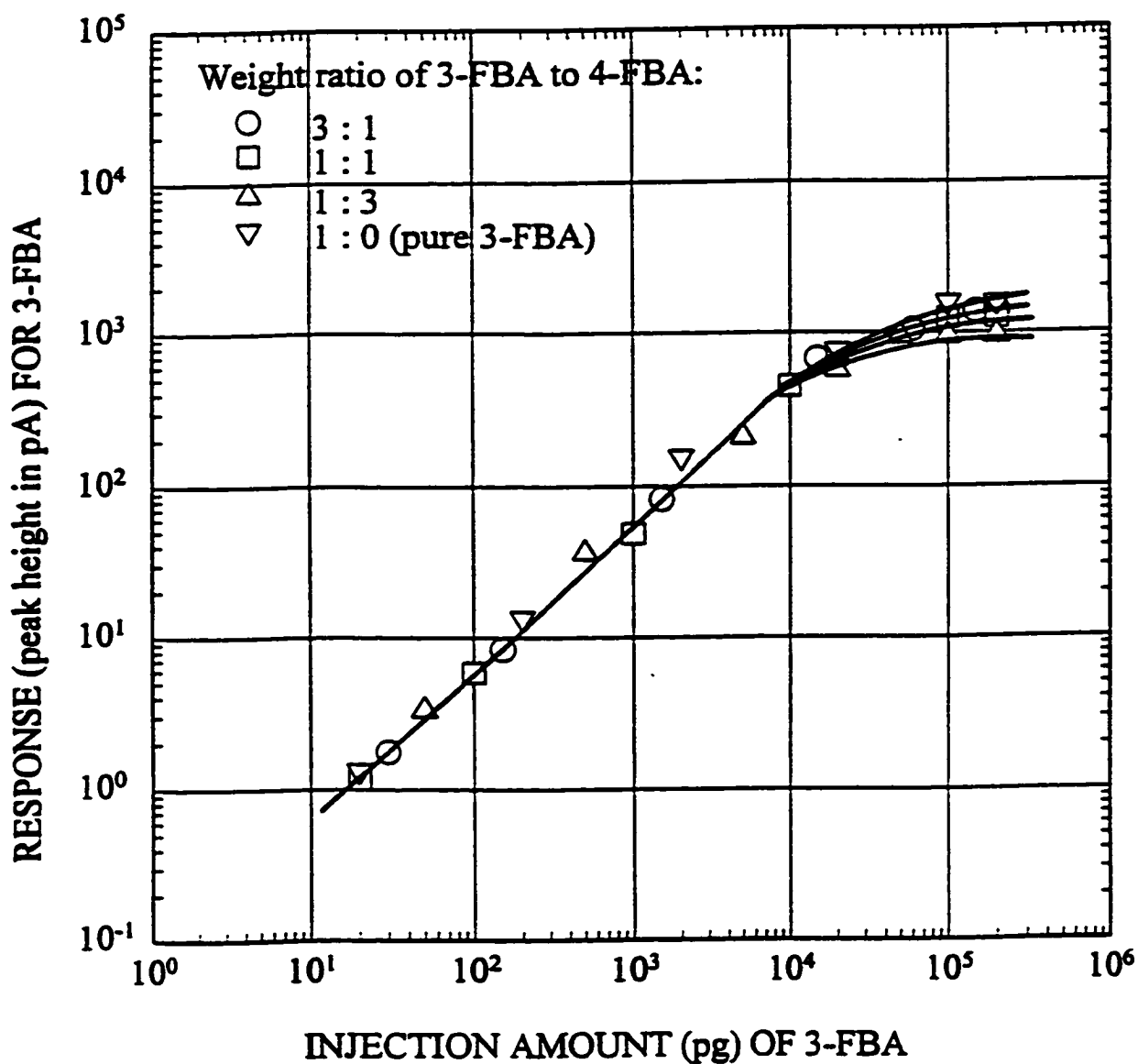
Figure 5.9 Composite calibration curve of 3-fluorobenzaldehyde, pure and in the presence of 0.3, 1 and 3 times the amount of the 4-fluorobenzaldehyde isomer, as measured from peak heights in subtraction chromatograms. The straight line is drawn at unity slope.
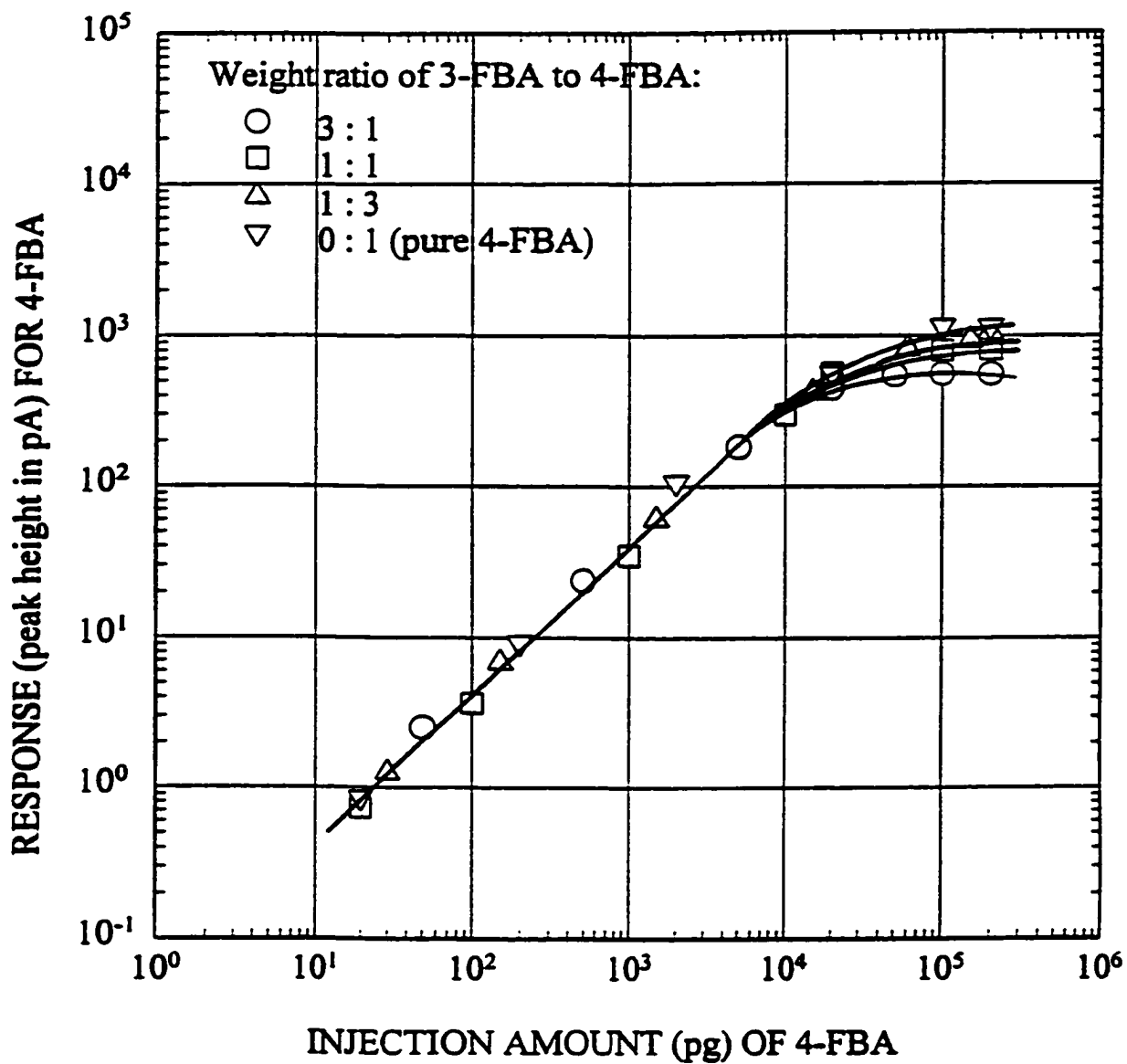
Figure 5.10   Composite calibration curve of 4-fluorobenzaldehyde, pure and in the presence of 3-fluorobenzaldehyde isomer. Otherwise similar to Figure 5.9.
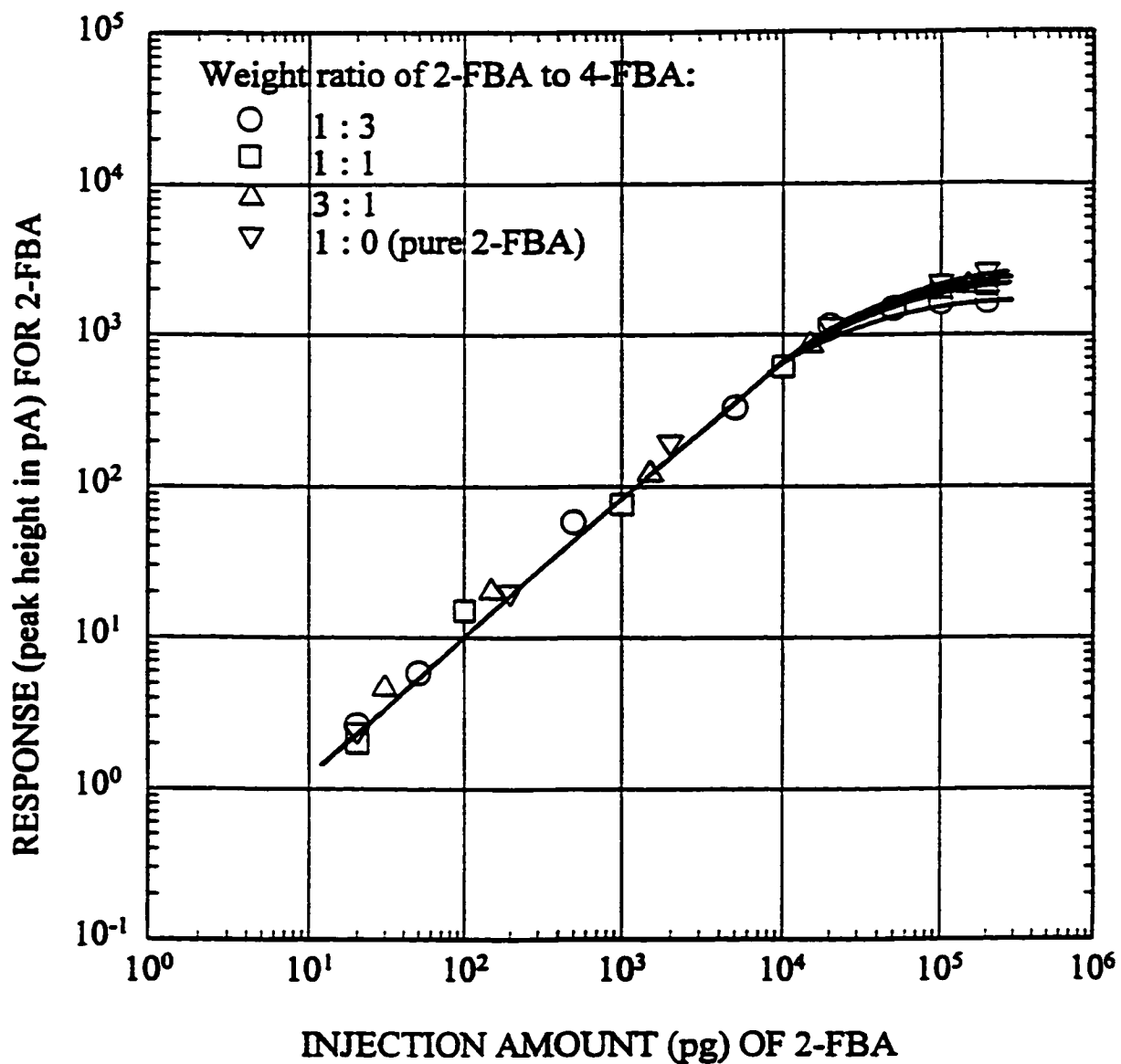
Figure 5.11 Composite calibration curve of 2-fluorobenzaldehyde, pure and in the presence of 4-fluorobenzaldehyde isomer. Otherwise similar to Figure 5.9.

In the aroyl luminescence detector, baseline noise is fundamental in nature. This conforms to a calculation (184) based on the molecular randomness of chemiluminescent events, and is numerically approximated by the square root of the photoelectron emission rate. The baseline noise of the subtraction chromatogram, N(S), is therefore larger than the noise of the first channel, N(1):

$$N(S) = N(1)\sqrt{1 + \left(\frac{N(2) \cdot RR_I}{N(1)}\right)^2} \qquad (5.2)$$

The detection limit of the pure analyte in the subtraction channel, DL(S), can hence be calculated from its detection limit in the first channel, DL(1):

$$DL(S) = DL(1)\frac{\sqrt{1 + \left(\frac{N(2) \cdot RR_I}{N(1)}\right)^2}}{\left|1 - \frac{RR_I}{RR_A}\right|} \qquad (5.3)$$

In Equation 5.3, if the analyte response in the subtraction chromatogram is negative, DL(S) would turn out to be negative as well. To avoid a negative value for the detection limit, the denominator is written as an absolute number. Equation 5.3 can be used to determine whether the two channels should be used as filed in computer memory or — if the analysis comes close to the detection limit — if they should be swapped before one is scaled and deducted from the other.

Table 5.1 lists the calculated detection limits for the three cases shown in Figures 5.9-5.11, as well as the detection limits for the same cases subsequent to a channel swap. Of the total number of thus scrutinized subtraction peaks, half are inverted (as they must

Table 5.1   A Comparison of Calculated Detection Limits

Analyte	DL(s)/DL(l)	
(interferent)	No channel swap	Channel swap
2-FBA (4-FBA)	0.90*	1.9
3-FBA (4-FBA)	1.5*	2.6
4-FBA (2-FBA)	2.5	1.6*

*= inverted (negative) peak.
FBA= fluorobenzaldehyde

be). In Table 5.1, the lower detection limits are associated with inverted peaks. This stems from the fact that (compared on the basis of similar-sized analyte peaks) one of the channels happens to display only about a tenth the noise level. If this channel is used as the "second channel", and if it happens to be multiplied by a relatively large magnification ratio, it will produce a fairly large negative peak in, but add only a small amount of noise to, the subtraction chromatogram. Thus it is possible, although rare, that the detection limit of the subtraction channel can actually be better than that of the first channel (DL(S)/DL(l)<1). One such case is shown in Table 5.1. The detection limits of all calculated cases were also experimentally determined. The measurements agreed with the calculated data of Table 5.1.

In order to explore analyte accuracy and precision over a wider range of such interference, and to check for the potential presence of systematic bias (which could result from a slightly inaccurate value of the response ratio used to suppress the

interferent), a constant amount of analyte was repeatedly measured in the presence of increasing amounts of overlapping isomer. This experiment is shown in Figure 5.12. It appears that, at least up to a ten-fold excess of overlapping isomer, the analyte is accurately measured. The precision (and accuracy) remains essentially that of the pure analyte which could be improved by the use of an automatic injector, or an internal standard, or both. Thus, as expected, correlational chromatography can provide accurate quantitation of completely overlapping peaks over a wide range of conditions. It should also have significant analytical applicability.

5.2.4 Scope and Limitation of the Method

The applicability of correlational chromatography is only limited by some (fairly obvious) conditions. One of the limitations is its requirement for pure component standards for the calculation of response ratios which are needed as scaling factors for the second channel. The second limitation is that the dual-channel response ratios of the two co-eluting compounds must differ significantly. If the response ratios are equal, the method does not work. If the response ratios are zero or infinity, the method is not needed. Other limitations include the phase shift and significantly different peak shapes between the two channels. In most cases such problems can be solved either by hardware or by software means.

It is obvious that the subtraction methodology can be used in wide variety of detector systems and in case of more than two co-eluting components. To quantitate three
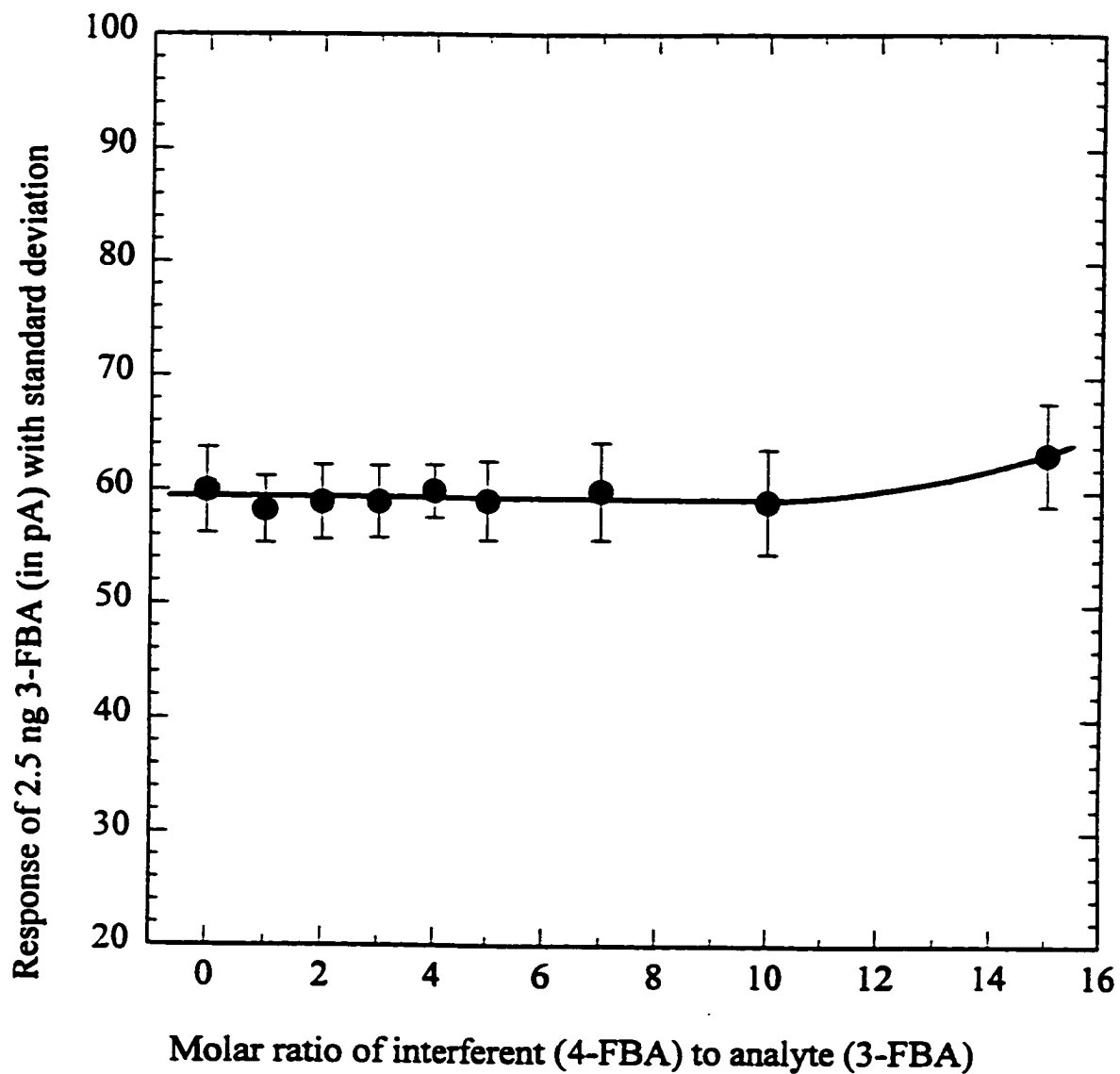
Figure 5.12   Replicate (5 X) quantitation with standard deviation bars of 2.5 ng 3-fluorobenzaldehyde, in the presence of 0 to 37.5 ng 4-fluorobenzaldehyde.

overlapping analytes requires three channels and three suitably different response ratios; four overlapping peaks require four detector dimensions and so forth. The general approach of dual-channel deduction methodology can be used in other ways as well. For example, the chromatogram-based purity check of a presumably interference-free analyte peak can be easily carried out by using this subtraction method. Since the response ratio of the analyte is known, its peak can be deducted from one of the two channels. Any peak still persisting in its place would therefore have to be that of a previously unrecognized interferent.

5.2.5 Conclusion

The dual-channel aroyl luminescence detector (ALD) was used as a demonstration system for quantitating two perfectly co-eluting model analytes (fluorobenzaldehyde isomers) from subtraction chromatograms. The linear part of the calibration curve of either *ortho-*, or *meta-* or *para-*fluorobenzaldehyde remained the same in the presence of 0.3- to 3-fold amounts of a co-eluting isomer. The accuracy of individual quantitation for two completely overlapping peaks was similar to that for a single peak: the error band started to increase only when the interfering isomer was present in more than a 10-fold excess. Formulas were developed, and experimentally confirmed, that allowed easy calculation of analyte peak size and detection limit in a subtraction chromatogram from corresponding single-channel data. The simple technique of resolving two peaks of identical retention into two quantifiable subtraction chromatograms is not restricted to the

ALD, but can be carried out on various types of dual-channel detectors. A similar technique can be employed to check the purity of analyte peaks.

Chapter 6

ANALYSIS OF AROYL COMPOUNDS OF COMPLEX MIXTURES BY COMBINED USE OF SPECTRAL RESPONSE RATIOS, RETENTION TIMES AND ON-LINE PHOSPHORESCENCE SPECTRA

6.1   Introduction

It was pointed out by Leathard and Shurlock in their 1970 monograph that methods of peak identification have developed much more slowly than most other aspects of gas chromatography (185). Even today there is no significant improvement in this area, and the analysis of some complex samples is frequently troubled by the presence of unknown peaks in the chromatogram.

Among the variety of peak identification techniques available (185), the methods of identification based on retention are the most commonly used and are well established due to their simplicity. In particular, identification of compounds by measurement of retention indices on two columns coated with stationary phases of different polarity is very often successful. However, rigorous identification from retention measurements is difficult, time-consuming, and ideally requires a specially designed instrument which can simultaneously use several columns. The unambiguous identification of a compound is often obtained by GC-MS, a powerful identification technique that requires expensive instrumentation not available in every laboratory. Unfortunately, apart from economic considerations, there are several fundamental limitations to the usefulness of this technique in analyzing of a complex mixture. These are:

244

1) In real-life samples, there are often found significant numbers of isomeric compounds. Their positive identification by mass spectral detection alone is often impossible. 2) Classical GC-MS has difficulties dealing with component overlap, i.e.. partial or complete co-elution. 3) In trace analysis, the vast dilution of eluate with carrier gas presents real experimental difficulties. 4) There are problems of condensation, memory-effects, sample loss, and decomposition associated with the GC-MS interface. For these reasons, it would be of practical importance to develop other means of identifying GC peaks.

Response ratios from dual- or multiple-channel GC detectors provide additional chemical information and can therefore aid the identification or confirmation of chromatographic peaks in qualitative analysis. Recently, a computer algorithm was developed for measuring the response ratios from a dual-channel flame photometric detector by our research group (174), and the calculated response ratios were successfully used to assess peak homogeneity, confirm peak identity, and facilitate subtraction and element-specific chromatograms (46). In this study, it was demonstrated that compound-specific detection can be easily achieved by using response ratios from the dual-channel aroyl luminescence detector, even from a filterless system (186). Therefore, response ratios from dual- or multiple-channel detectors can provide an additional criterion for unambiguous identification of components in a complex mixture, particularly if the response ratio is used in combination with retention time.

The spectral profile of chromatographic peaks is very important for confirming the identity of a suspected analyte or for indicating structural characteristics of an unknown

compound. Spectral information is of special value when environmental extracts containing hundreds of peaks are to be analyzed. And it becomes particularly useful when, for reasons of spectral similarity or lack of sensitivity, classic hyphenated techniques (GC-MS, GC-IR, etc.) fail to provide the desired information.

Recently, our research group demonstrated that single peaks from a dual-channel flame photometric detector can yield spectra that are amplitudinally accurate and of sufficient sensitivity (i.e., 5 pg of phosphorus produced a clearly recognizable HPO spectrum) and resolution to be of value for several types of qualitative analytical tasks (45). The direct applications of this technique include peak purity assessment and pre-run screening to determine the proper wavelength settings for optimum detection sensitivity. In addition, the ability to collect luminescence spectra on-line yields new types of diagnostic information for GC, and facilitates identification of components in a complex mixture. The methodology should be particularly applicable to cases where a compound can be obtained only as a gas chromatographic peak at trace level.

The research presented here investigates the possibility of analyzing of aroyl compounds in real-life samples by using spectral response ratios from the aroyl luminescence detector, in combination with retention times and on-line phosphorescence spectra, as a means of identification. This methodology was applied in the identification of some aroyl compounds in essential oils and a marine sediment sample.

6.2 Experimental

6.2.1 Data Manipulation

A particular version of the aroyl luminescence detector called triple-channel ALD (Figure 2.4) was used in this study to obtain phosphorescence spectra "on the fly", chart response ratios for two selectable wavelengths or wavelength regions, and carry out quantitative determination of aroyl compounds.

To keep the number of injections to a minimum and allow future manipulation of existing detector or monochromator signals, e.g., produce virtual chromatograms or spectra, the data streams are digitized and committed to computer memory via a lab-developed interface and software package called CHROM (46). It allows digital filtering, scaling, response ratio calculations, two-channel subtraction, printing or plotting, and export in ASCII format to a spreadsheet of the acquired chromatogram or spectra.

6.2.2 Sample Preparations

Essential Oil: Various amounts of pure essential oils were injected for the GC-ALD analysis.

Marine Sediment: A 2 g sediment sample was accurately weight on aluminum foil and transferred quantitatively into a prerinsed (with extracting solvent) extraction thimble. The sample was then extracted with 50 mL of dichloromethane in a specially-made extractor apparatus (187) for 16 hours. After the extraction was complete, the extract was preconcentrated and the final volume reduced to 1 mL, by evaporation in a stream of nitrogen, for analysis by GC-ALD. To provide a blank, a 2 g sand sample

obtained from Dalhousie campus was weighed in a crucible and heated in an oven at 600

°C for 2 hours. The same process of extraction, preconcentration and instrumental

analysis was used as in preparing the true sample.

6.3 Compound Identification Based on Spectral Response Ratios Combined with Retention Times and On-line Phosphorescence Spectra

6.3.1 Response Ratios and Retention Times of Some Standard Aroyls

Pure standards of eighteen aroyl compounds were prepared and chromatographed in

mixture on a 100 cm X 0.2 cm i. d. 5% Carbowax 20 M column. The choice of the 18

standard aroyls was based on different considerations: which responded well. which

represented major vs. minor structural differences, which fitted nicely into a simple

chromatogram, which were suspected analytes in the tested samples. Both optical

channels carried R-268 photomultiplier tubes; one of which was used in combination

with a 530-nm longpass filter. Other filter combinations can also be used. and yield

different response ratios. What is, of course, important is to use the <u>same</u> filter

combination for charting response ratios of components in both standards and real-life

samples.

Figure 6.1 shows the two single-channel chromatograms of an 18-component aroyl

standard mixture, topped by a whole-peak response-ratio chromatogram (174). It is

obvious that the eighteen aroyl standards offered significant differences in retention times

and response ratios. This is the basis of compound identification. A better pictorial

representation of the difference in retention times and response ratios is shown in a two-

dimensional log R (response ratio) vs . t_R (retention time) plot (Figure 6.2). It is clearly
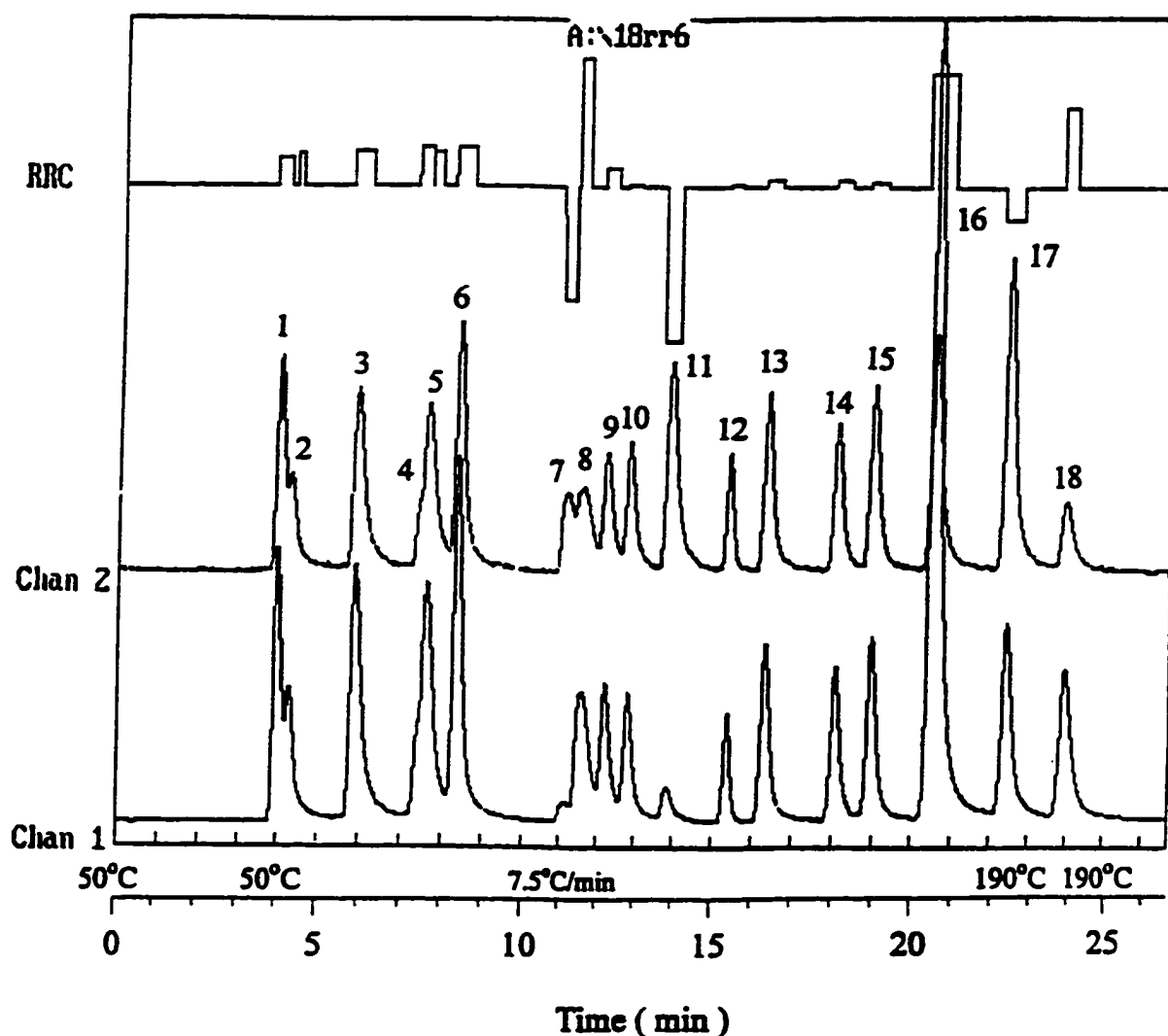
Figure 6.1 Individual channels and slope-based, whole-peak response ratio chromatogram of a 18-component standard mixture. Channel 1: PMT-268 (no filter, -800 V); Channel 2: PMT-268 (530-nm longpass filter, -800 V). Compounds in order of elution: 3 ng of benzaldehyde (1); 2 ng of 4-fluorobenzaldehyde (2), 18 ng of acetophenone (3); 3 ng of 4-ethylbenzaldehyde (4); 12 ng of 3-methylacetophenone (5); 1.8 ng of 4-isopropylbenzaldehyde (6); 60 ng of 2,6-dichlorobenzaldehyde (7); 60 ng of α-tetraone (8); 3 ng of isophthalaldehyde (9); 3 ng of 4-methyl-formylbenzoate (10); 30 ng of 1,4-naphthoquinone (11); 2.4 ng of 3.3'-bis(trifluoromethyl)benzophenone (12); 2.4 ng of benzophenone (13); 1.8 ng of 4-methylbenzophenone (14); 2.4 ng of 4-chlorobenzophenone (15); 0.42 ng of xanthone (16); 0.6 ng of anthraquinone (17) and 0.3 ng of thioxanthene-9-one (18).
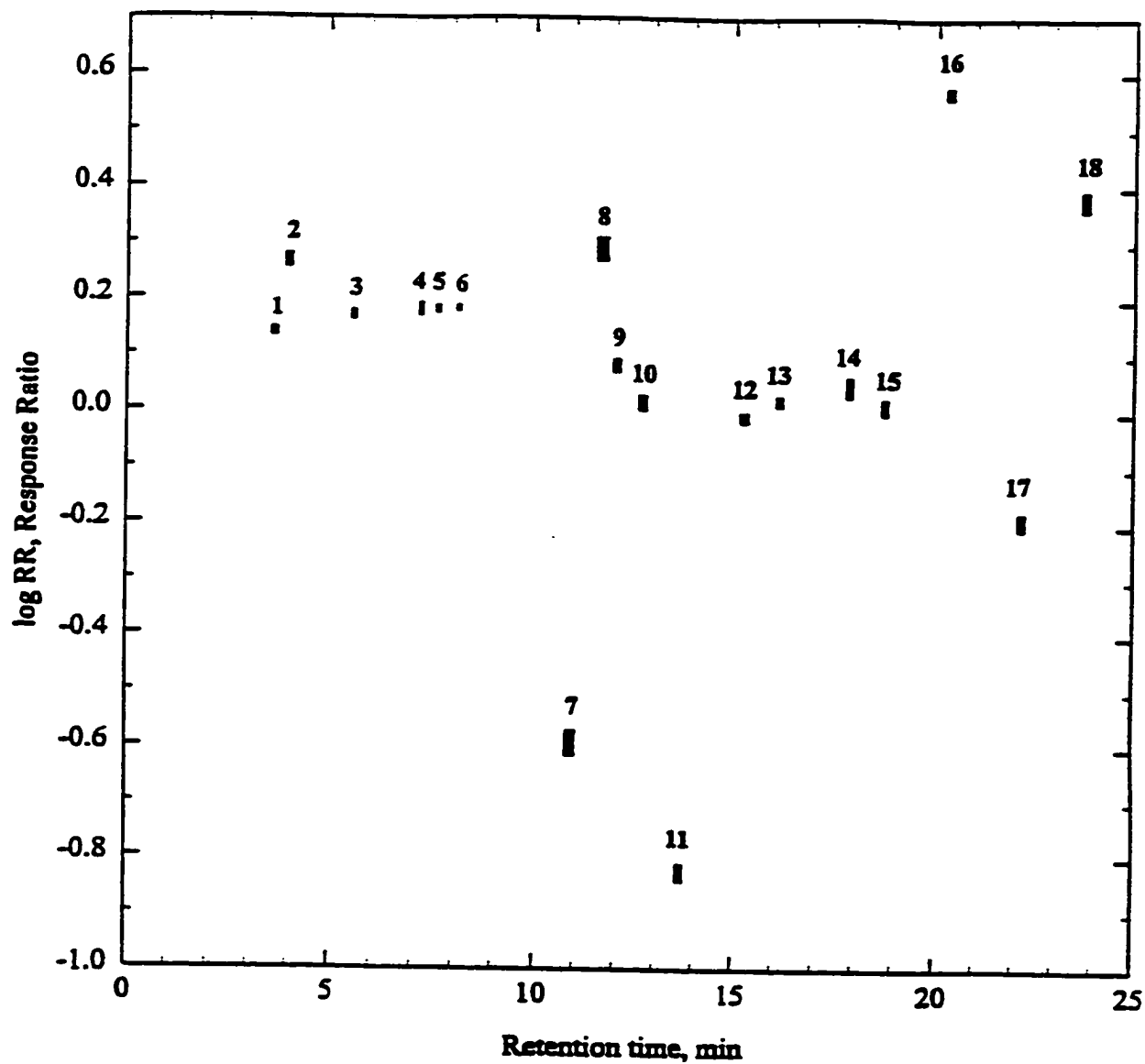
Figure 6.2   log RR (response ratio) vs. t_R (retention time), with standard deviation, for 18 typical aroyl compounds. Number of replicates: 10, except 5 for compounds 18. Peak Nos. and other conditions as in Figure 6.1.

shown that the reproducibility of response ratios was good, with relative standard deviations all in the range from 1.1-5.6%; and that ample response ratio space is still available for more compounds. However, it should be pointed out that the constancy of response ratios will depend on the stability of the PMT's radiant sensitivity and the constancy of the supply voltage. Reproducibility of retention times was also very good within one set of chromatographic conditions. Recent advances in GC instrumentation technology, i.e., narrower tolerances for flow-rates and temperature, can further improve retention time reproducibility.

6.3.2 Constancy of Spectral Response Ratios

The usefulness of spectral response ratios as identification criteria is strictly dependent on their reproducibility under different analytical conditions. It has been proven that the response ratios of 16 aroyl compounds (all that were tried) were invariant from close to their detection limit to well beyond their linear range (186). However, in analysis of a real-life sample it is not possible to ensure the complete absence of quenchers (a substance that reduces the luminescence of the analyte peak) in the ALD. An additional experiment was therefore carried out to check for the constancy of response ratios under quenching condition. Figure 6.3 shows the response ratios of 18 aroyl compounds challenged by increasing levels of quenchers. Clearly, the response ratios of all compounds remain constant in the presence of hydrocarbons that severely quenched most analyte peaks. This behavior is again in accordance with expectations based on the singularity of their excited states. A piece of supporting evidence is that the gas-phase

phosphorescence spectra of benzaldehyde under quenching conditions keep the same spectral features (while decreasing in emission intensity) in the presence of a quencher (Figure 6.4).

As discussed in Chapter 4, argon or helium can enhance the emission intensities of aroyl compounds in excited nitrogen. Figure 4.91 strongly suggests that the nature of the excited state of benzaldehyde did not change in excited nitrogen when doped with argon. Thus, it is reasonable to expect that the response ratios measured in the pure nitrogen system, and in nitrogen doped with argon, should be the same. This was confirmed by cross plotting (Figure 6.5), i.e., plotting the response ratios from the pure nitrogen system against those from the nitrogen/argon system. In Figure 6.5, almost all of the response ratios fall on the $45°$ line, which indicates that the response ratios from the two systems are identical within error limits. This behavior can be used to facilitate the measurement of response ratios of trace amount of components, or analytes subject to severe quenching, of a complex mixture.

6.3.3 On-line Wavelength-Resolved Phosphorescence Detection

The most obvious use of the on-line phosphorescence spectrum is to identify analytes based on their emission characteristics. As presented in Chapter 4, certain types of aroyls (e.g. benzaldehyde, benzophenone, anthraquinone and xanthone) emit mainly intense phosphorescence in the ALD. The gas-phase luminescence spectra of aroyl compounds are fairly broad and also occupy, very approximately, the same wavelength range (see Chapter 4). That notwithstanding, their features are still characteristic of
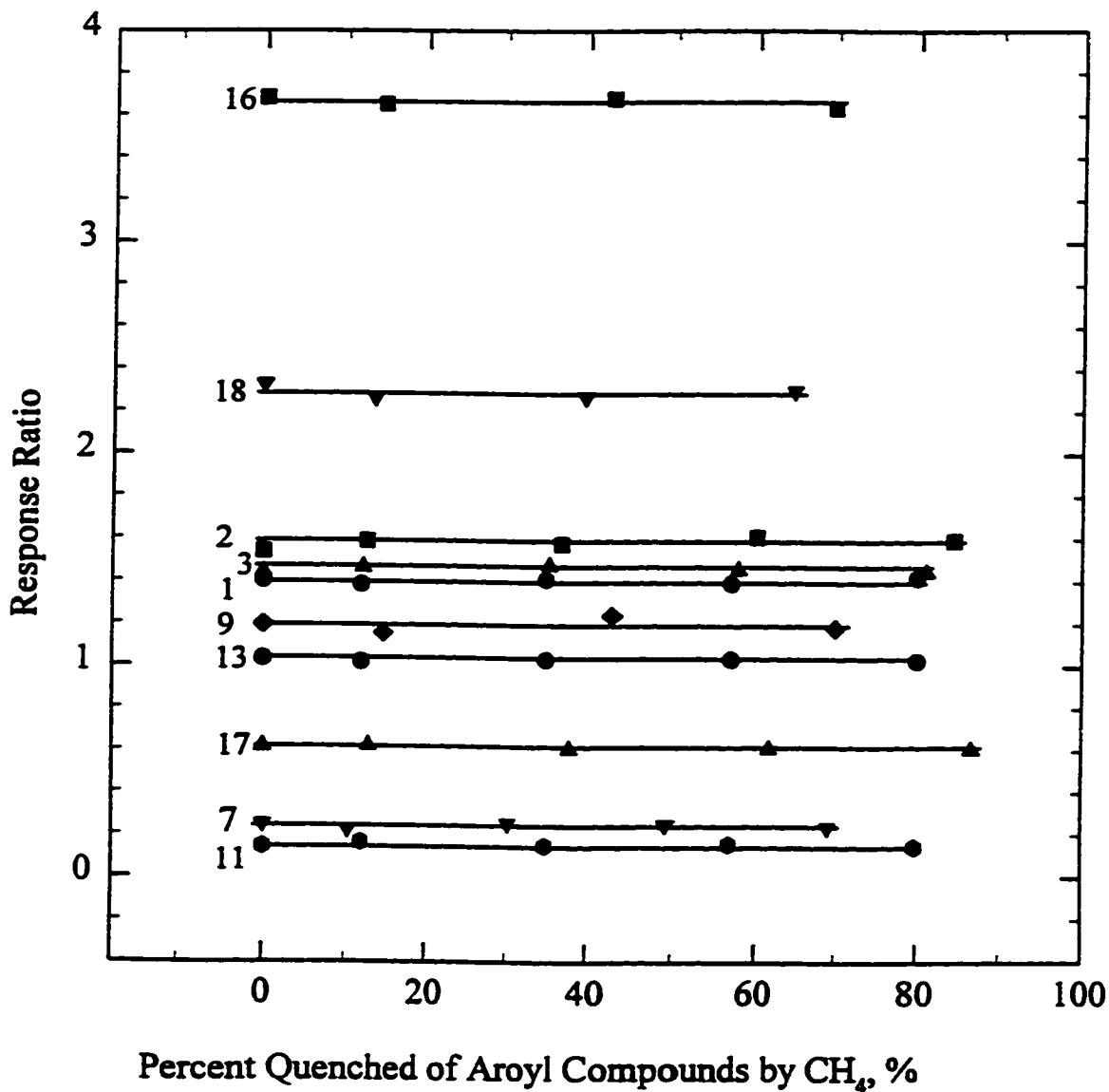
Figure 6.3 Constancy of response ratios of aroyl compounds at different quenching intensities. Methane flow: variable. Compound numbers and other conditions as in Figure 6.1. Data points for compounds closely approaching each other are omitted for clarity. The lines was drawn precisely horizontal.
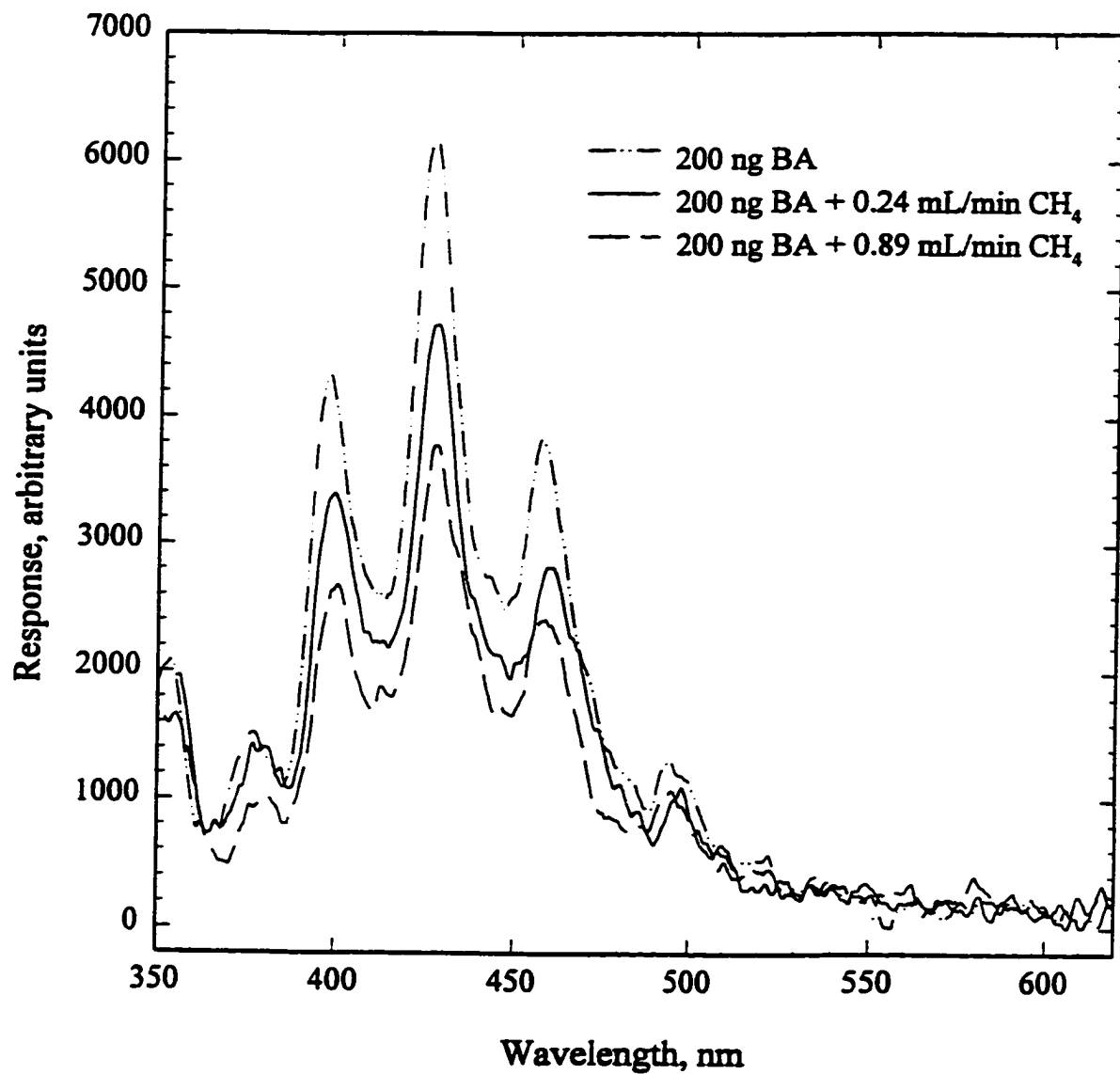
Figure 6.4 Gas-phase luminescence spectra of benzaldehyde at different quenching intensities. 1/8 meter grating monochromator. R-374 PMT. Single-peak mode. Bandpass: 6.6 nm.
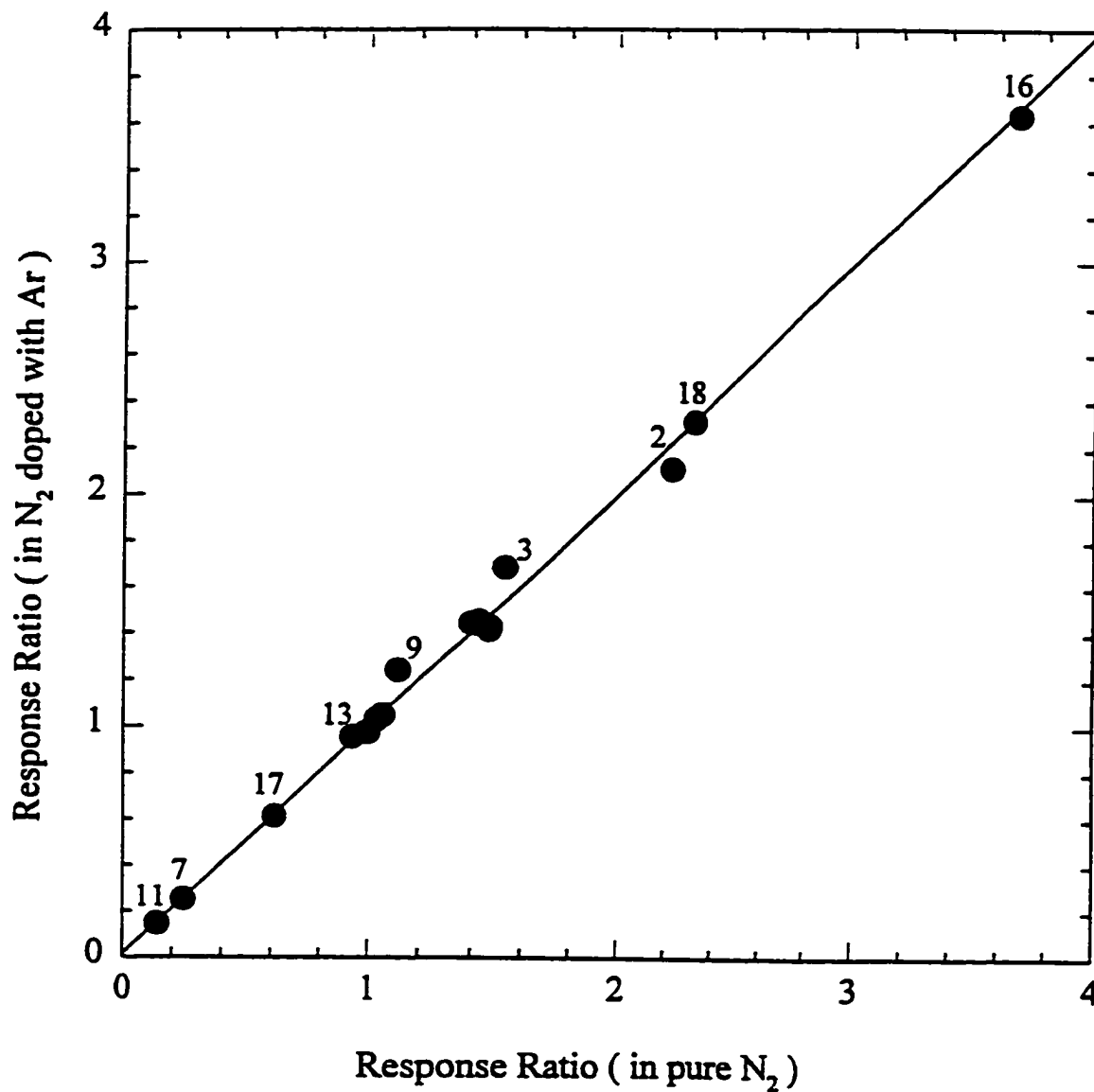
Figure 6.5 Cross plot of response ratios of 18 aroyl compounds in the pure nitrogen system versus the nitrogen/argon system. Compound numbers and other conditions as in Figure 6.1 except that some compound numbers have been omitted for clarity.

individual species. Thus they allow positive identification of aroyl compounds or at least indicate the basic luminescing structures (through spectral matching with standards). However, final compound identification will depend on the number and quality of library spectra available, as well as on the sensitivity of this method under conditions where the analytes are present in extremely low amount or are subject to severe quenching by co-eluting compounds.

In addition, on-line phosphorescence can also be used to check the peak purity. In such a measurement, a spectrum obtained from the front of a GC peak is compared with one from the back of this peak. If differences are observed between these spectra, then it is likely that the peak contains more than one compound.

6.4 Analysis of Aroyl Compounds in Essential Oils

6.4.1 Introduction

The so-called essential oils are complex mixtures of odorous and steam-volatile compounds which are deposited by plants and nowadays are widely used as aromas, flavor additives, air "fresheners", insect repellents, components of cosmetics such as perfumes and bath oil, therapeutic agents, etc. The main components of most essential oils have been identified: in part owing to the desire for increased scientific knowledge, in part due to requests for cheap synthetic substitutes. Gas chromatography has been the analytical tool of choice for separation and identification of essential oil components for many years. Traditionally, oil analysis has been performed mainly with flame ionization detection or with mass spectral detection (188, 189).

In FID response, the peak size roughly represents the weight fraction (really

reduced carbon content) of a volatile component. In contrast to this "general" type of response, a "selective" detector might provide a very different and possibly quite interesting picture. The most important effect of chromatograms from a selective detector is often not their information content but their perceptional and hence emotional impact. For instance, the extraordinary selectivity of the electron capture detector (ECD) is linked with various global scares such as the ozone hole. Without the ECD. nobody might have noticed or cared about, the presence of Freons in the atmosphere. Chances are that any new, highly selective, and highly sensitive detector might lead to similar consequences, simply by focusing attention on some previously hidden group of compounds present in environmental samples.

The aroyl luminescence detector (ALD) is one of the most selective of new sensing devices. Only certain types of aroyls respond in the ALD. However, there is little evidence for the presence of aroyls in essential oils, except for some well-known exceptions such as benzaldehyde and cuminaldehyde. Thus, it is quite interesting to use the ALD on a selection of essential oils to demonstrate the possibility of using spectral response ratios in combination with retention times and on-line spectra (when available) for identification of some aroyl components in these complex mixtures, and to answer some basic questions: 1) Do none or some or most of the essential oils contain aroyl components that respond in the ALD? If most this might raise or answer questions of plant biosynthesis, taxonomy, adulteration, characterization and quality control. 2) Is it possible to confirm the structure of suspected analytes—beyond the obvious criterion of retention—by using a simple, selective detector? If so, this might circumvent the

difficulties encountered with the classical GC-MS technique when, say, a minor aroyl peak and a major terpene peak overlap.

6.4.2 Results and Discussion

The triple-channel aroyl luminescence detector performed well. Sensitive determination of aroyl compounds could be achieved by replacing the spectral channel with a cooled PMT (Figure 2.4). Figure 6.6 shows the calibration curves of 16 typical aroyl compounds in the ALD. For most of these compounds, the minimum detectable amount were in the picogram region. The linear range was about four orders of magnitude.

GC-ALD Chromatograms of Some Essential Oils: Twenty-four pure essential oils, 0.2 µL of each, were directly injected for GC-ALD analysis. The highly sensitive and selective ALD provides chromatograms that are unique in appearance relative to those obtained with an FID (an example is shown in Figure 6.7). Only in three essential oils, bergamot, cypress and lemon, the concentrations of aroyl compounds were extremely low, which is evidenced by the lack of significant peaks in their GC-ALD chromatograms. The GC-ALD chromatograms of the other 21 essential oils are shown in Figure 6.8 (some peak identities are given in Table 6.2). It could be clearly demonstrated that trace amounts of aroyl compounds do exist in these essential oils, and that their GC-ALD patterns differ significantly from one another. The characteristic gas chromatograms could be used to discriminate between the different essential oils,
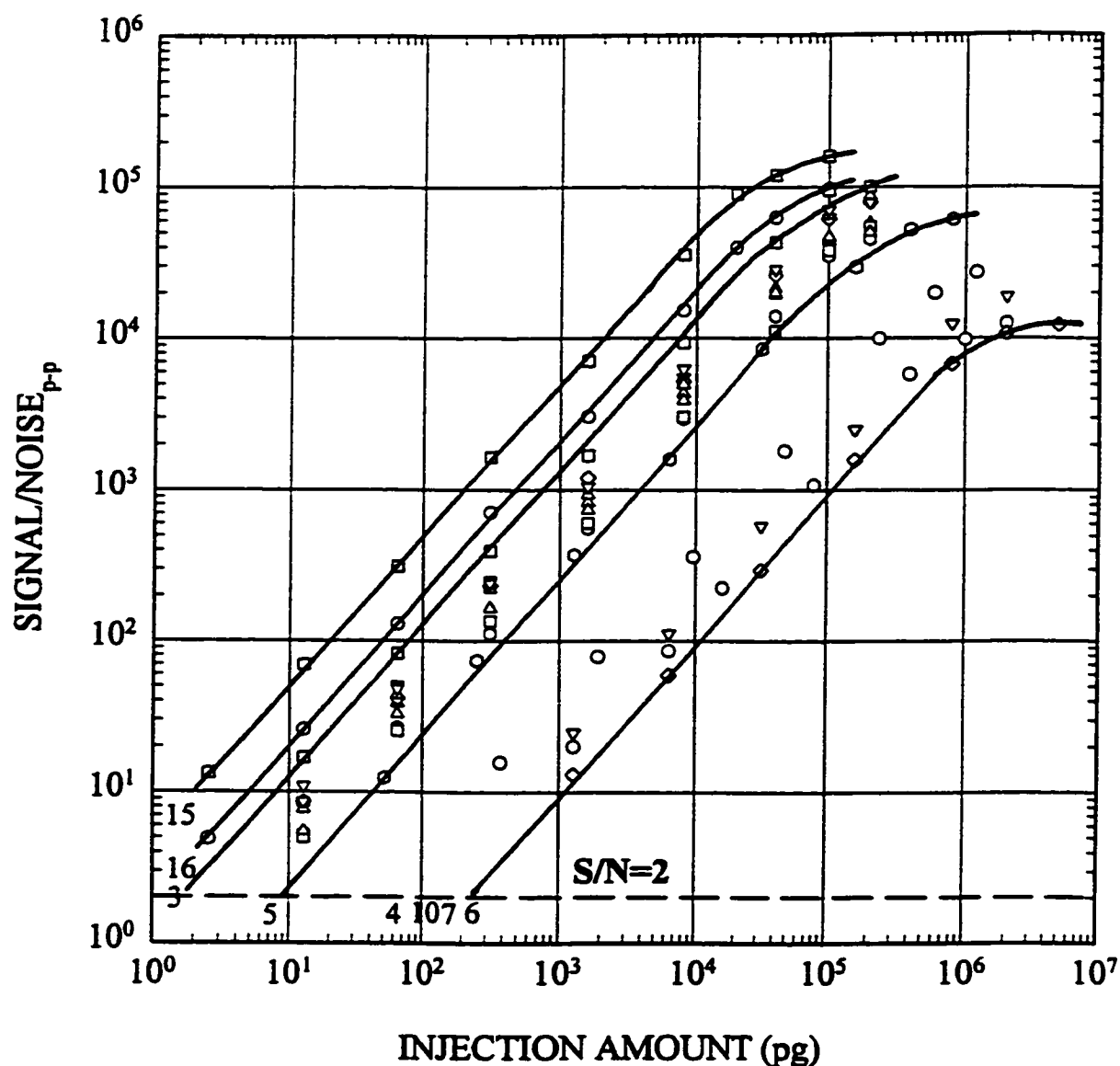
Figure 6.6   Calibration curves of 16 aroyl compounds. DC voltage: 5000 V; PMT-268 voltage: -850 V; Column temperature: 50 → 180 °C @ 7.5 °C/min. Compounds from left to right: xanthone (15); anthraquinone (16); 4-ethylbenzaldehyde (3); isophthalaldehyde (8); 4-methylbenzophenone (13); benzophenone (12); benzaldehyde (1); 4-chloro-benzophenone (14); 4-methyl-formylbenzoate (9); 4-fluorobenzaldehyde (2); 3,3'-bis-(trifluoromethyl)benzophenone (11); 3-methylacetophenone (5); acetophenone (4); 1,4-naphthoquinone (10); α-tetralone (7) and 2,6-dichlorobenzaldehyde (6). Numbers in parenthesis indicate the elution sequence. Numbers in the graph indicate some selected structures. The five calibration curves are drawn exactly at slpoe = 1; the rest are omitted for clarity.
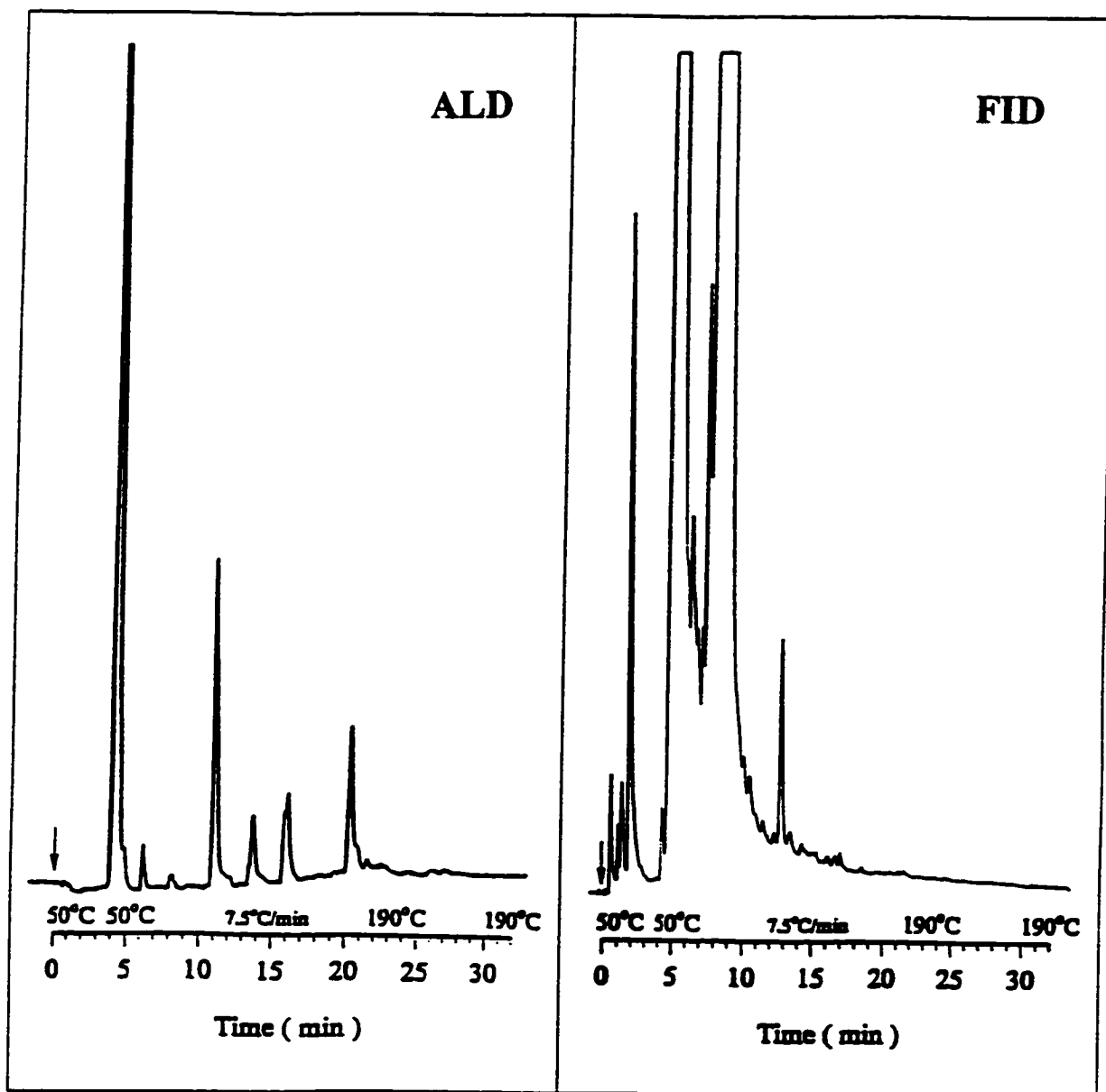
Figure 6.7   Gas chromatograms of 0.2 .μL peppermint oil.
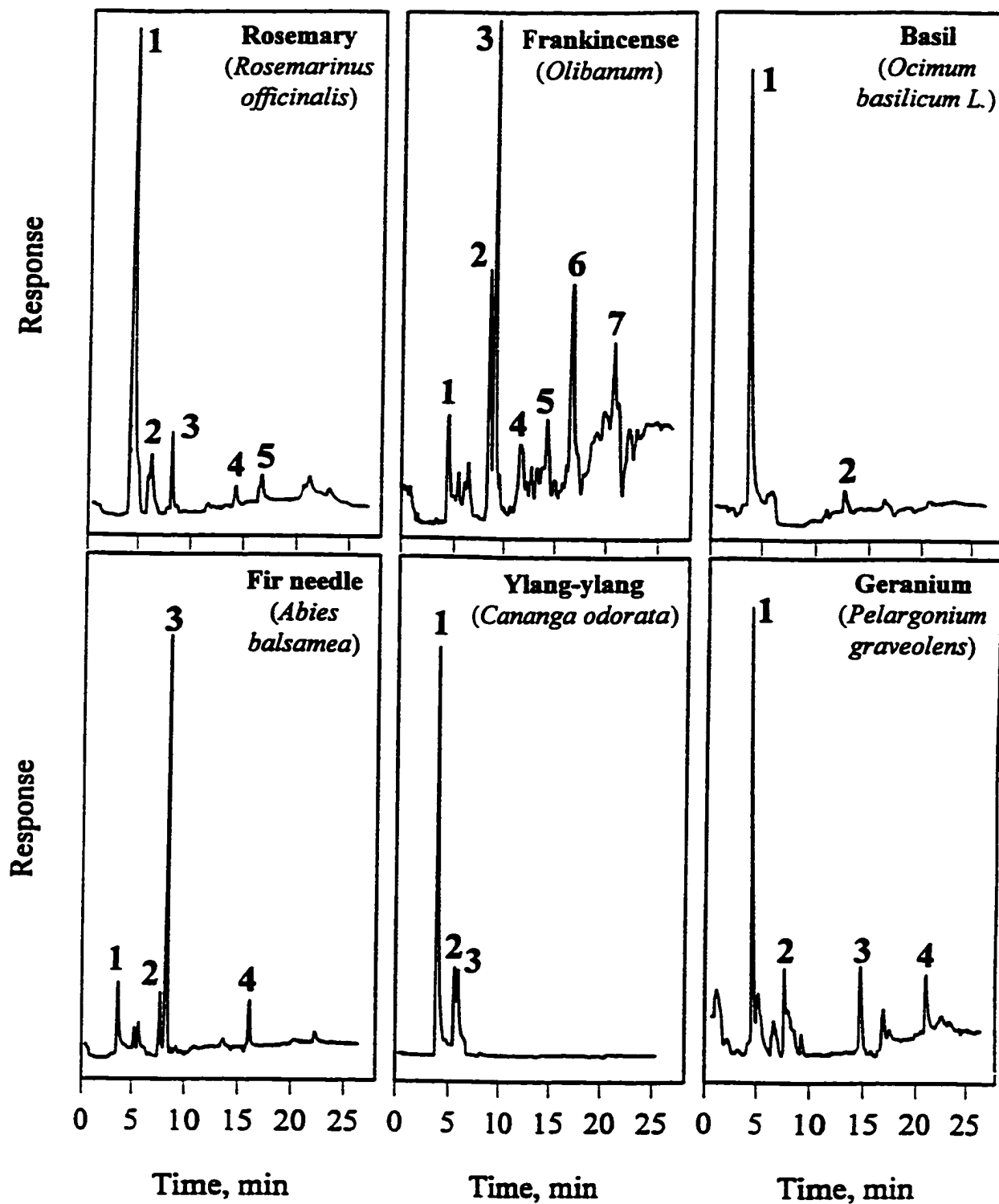
Figure 6.8   GC-ALD chromatograms of some essential oils. DC voltage: 5000 V; PMT-268 voltage: -700 V; Attenuation: variable; Sample amount: 0.2 µL each. Numbers indicate compounds in order of elution for discussion in the text; they do not indicate a particular compounds.
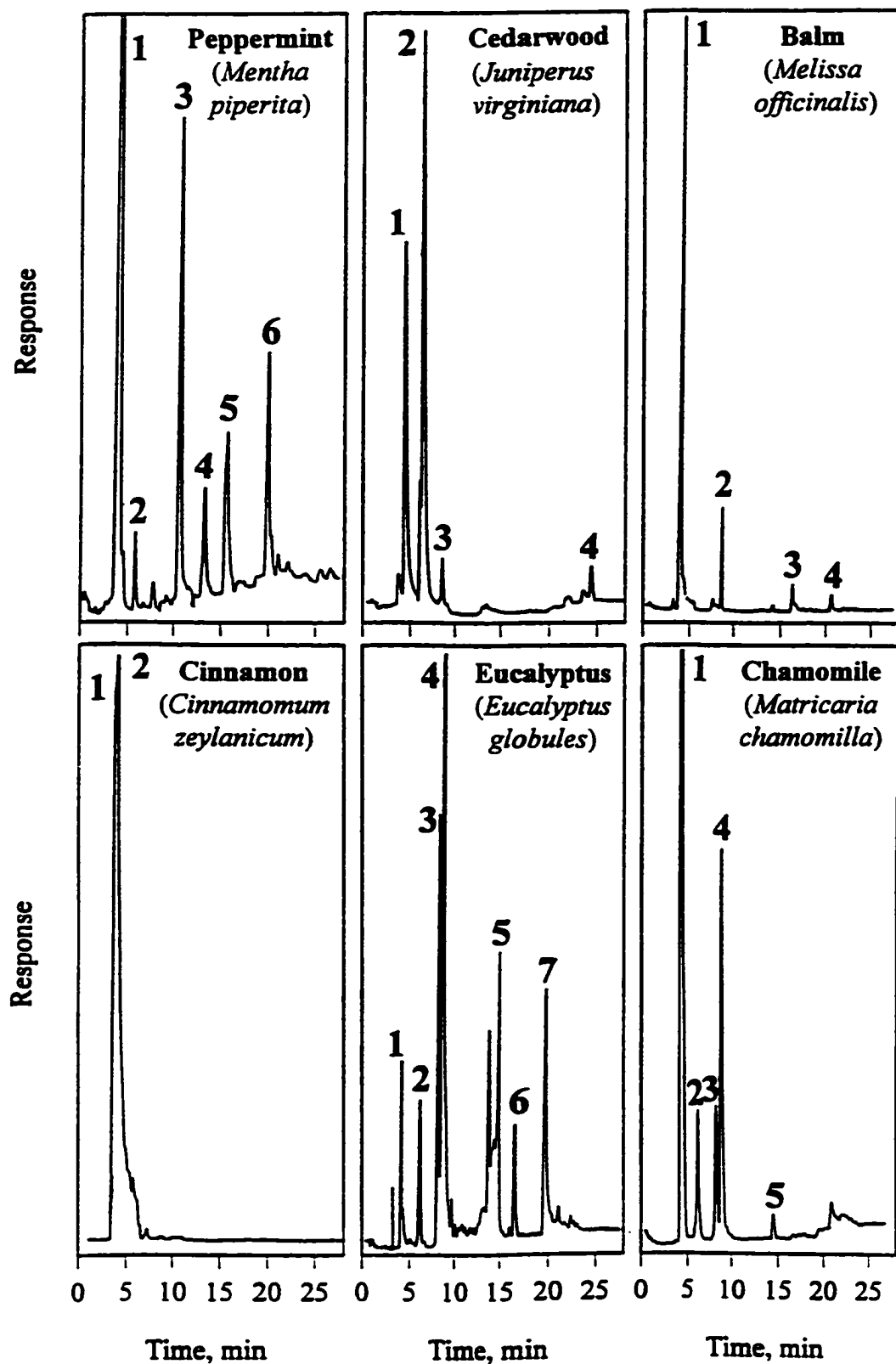
Figure 6.8   (continued)
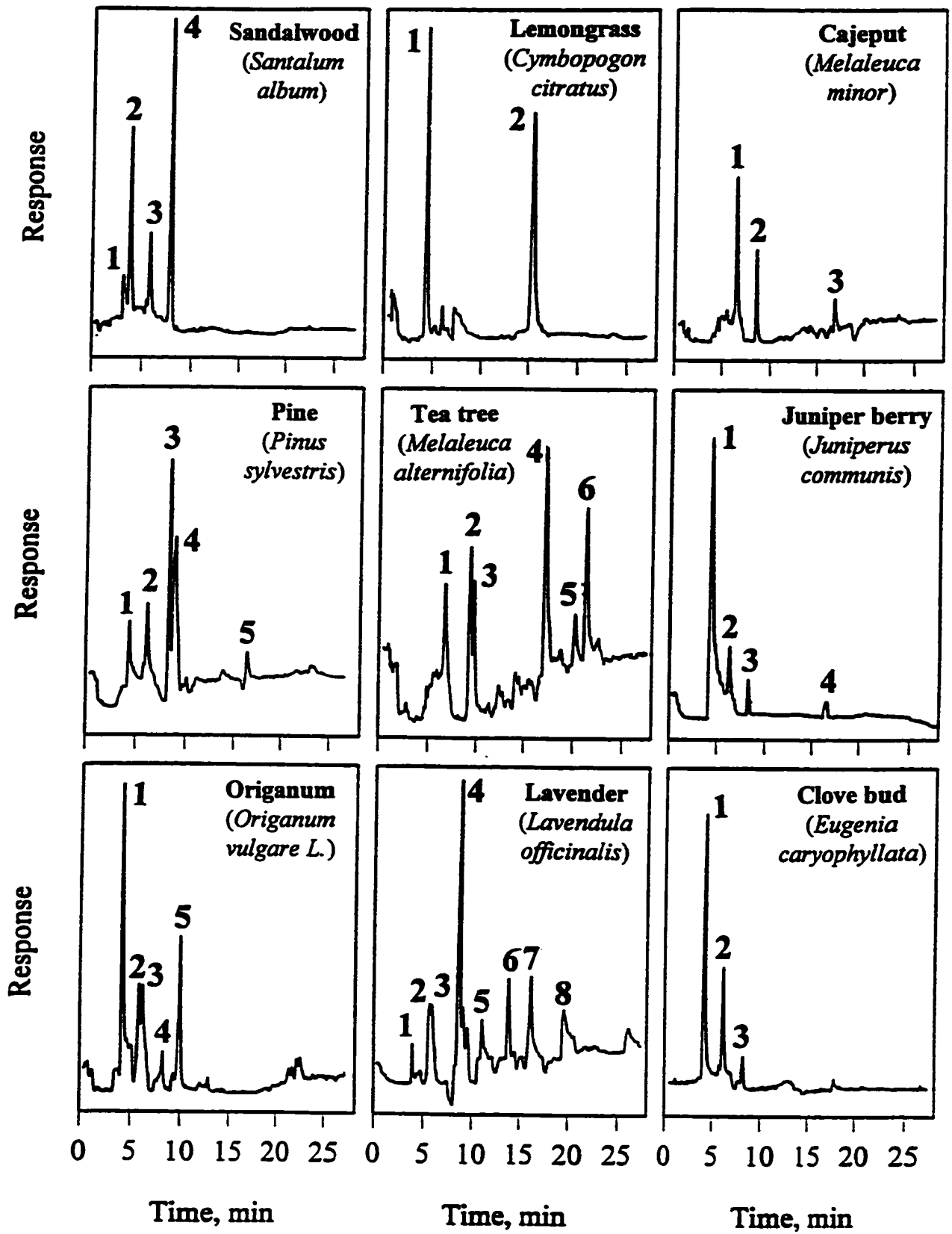
Figure 6.8   (continued)

or perhaps to distinguish their botanical origins or study the chemotaxonomic characters of various species.

Identification of Major Aroyl Compounds in Selected Essential Oils: The commercial differentiation of the grades of essential oils is mainly performed by determination of their chemical composition. The major components of most essential oils have been identified by GC-MS (188, 189). In this work, a simple, selective GC detector was applied to the analyses of trace aroyl components in selected (mainly inexpensive) essential oils.

All identifications were based on comparisons of the spectral response ratios, retention times and phosphorescence spectra of the pure standards (where possible) with those of the sample components under the same operating conditions. In this study, the same 18-component standard mixture and filter combination (channel 1: PMT-268/open and channel 2: PMT-268/530-nm LP filter) as in Section 6.3 were used to measure to response ratios and retention times. Figure 6.9, as an example, shows the individual channels and slope-based, whole-peak response-ratio chromatograms (174) of some of the essential oils. Table 6.1 lists the response ratios and retention times of aroyl components. The response ratios and retention times were the mean of five GC-ALD analyses of each essential oil with relative standard deviations ranging from 1.2 to 6.9%. Tentative identification was achieved by locating the suspected aroyl components in essential oils on the two-dimensional plot of log RR vs. t_R (Figure 6.2). The results are reported in Table 6.2.
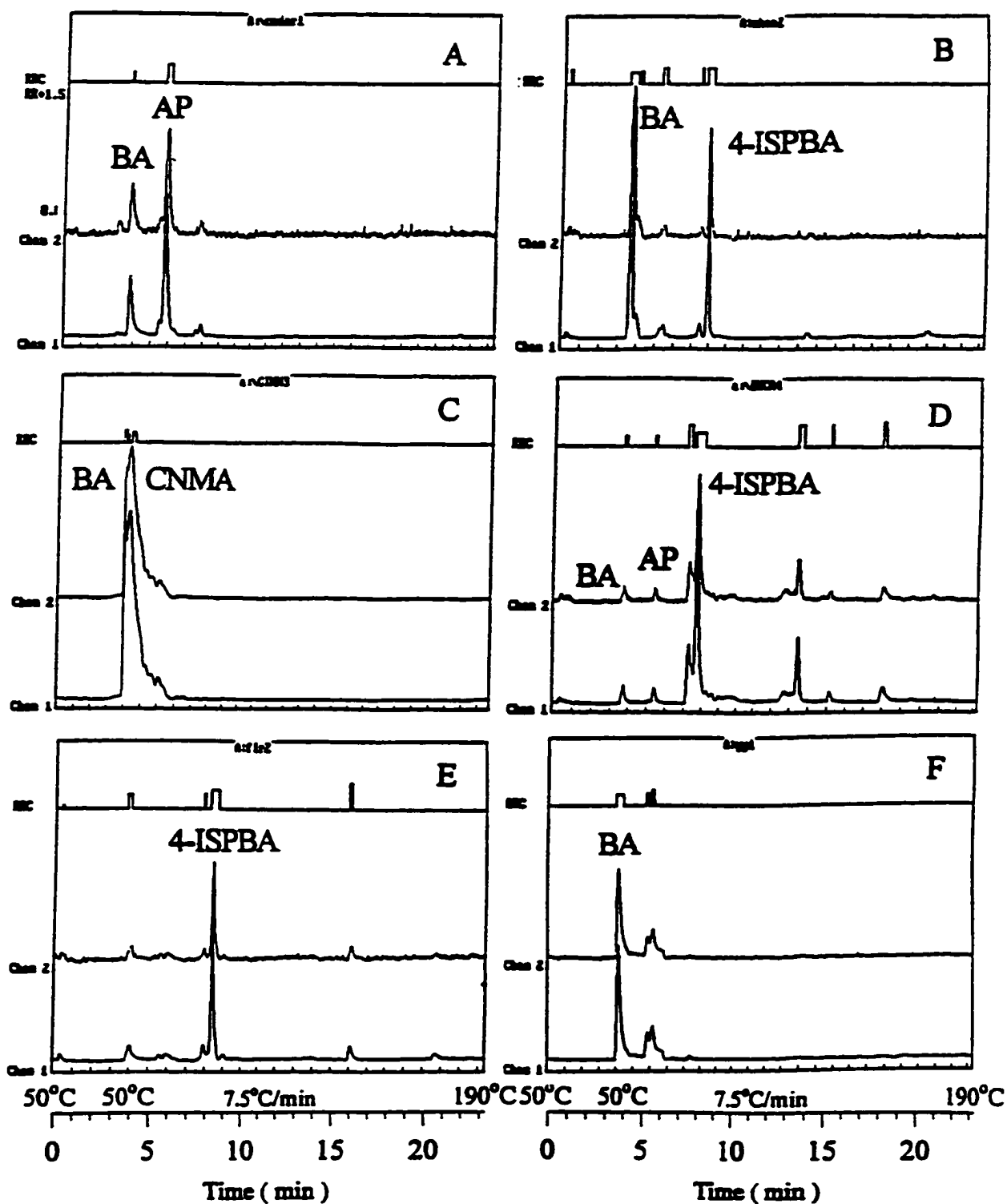
Figure 6.9 Individual channels and slope-based, whole-peak response ratio chromatograms of some essential oils. Channel 1: PMT-268 (no filter, -800 V); Channel 2: PMT-268 (530-nm longpass filter, -800 V). (A) cedar wood ; (B) chamomile; (C) cinnamon; (D) eucalyptus; (E) fir needle; (F) ylang-ylang. Abbreviations of compounds refer to component identification in Table 6.2.

Table 6.1   Response Ratios and Retention Times of Major Aroyl Components in Some Essential Oils

t_R (min)	Response Ratios (open/530-nm LP)[b]						
	Eucalyptus	Frank-incense	Geranium	Lavender	Lemongrass	Tea tree	Sandal-wood
3.0							0.659
3.5[a]	1.376	1.360	1.334		1.320		
3.6				1.114			
5.3							1.604
5.7	1.487						
7.0							
7.3[a]	1.677	1.625					1.428
8.1[a]	1.566	1.515		1.547		1.578	
14.2[a]	1.313	1.300	1.346	1.350	1.330		
16.7[a]	1.455	1.425		1.500		1.590	
16.8			1.640				
19.2	1.006						
20.8						1.222	

[a]   Retention times were the average values of these peaks after producing a single, non-broadened peak by co-injection.

[b]   Response ratios were measured from the two response-ratio channels of the triple-channel ALD: Channel 1: PMT-268, no filter, -750 V, attenuation: 100 X 1; Channel: 2: PMT-268, 530-nm longpass filter, -750 V, attenuation: 10 X 1.

Table 6.2 Aroyl Compounds Identified in Some Essential Oils with Response Ratios (RR) and Retention Times (t_R, min)

Essential Oil	Aroyl Compounds Identified [c] (Peak No. in Figure 6.8)									
	BA		CNMA		AP		4-ISPBA		BP	
	t_R	RR	t_R	RR	t_R	RR	t_R	RR	t_R	RR
Standard [a]	**3.7**	**1.376**	**4.0**	**1.285**	**5.6**	**1.474**	**8.2**	**1.529**	**16.2**	**1.059**
Balm	3.5 (1)	1.378								
Basil	3.8 (1)	1.387								
Cedar wood	3.7 (1)	1.336			5.7 (2)	1.443				
Cinnamon	3.9 (1) [b]	1.398	4.0 (2) [b]	1.230						
Chamomile	3.5 (1) [b]	1.321					8.1 (4)	1.498		
Clove bud	3.8 (1)	1.362								
Eucalyptus	3.5 (1)	1.339			5.7(2)	1.487	8.1 (4) [b]	1.566		
Fir needle							8.3 (3)	1.584		
Frankincense	3.5 (1)	1.360					8.1 (3)	1.515		
Geranium	3.5 (1)	1.334								
Juniper berry	3.6 (1)	1.346								
Lavender							8.1 (4)	1.547		
Lemongrass	3.5 (1)	1.320								
Peppermint	3.7 (1)	1.379							16.0(5)	1.049
Rosemary	3.5 (1)	1.388								
Tea tree							8.1 (2)	1.578		
Sandalwood					5.3 (3)	1.604				
Ylang-ylang	3.8 (1) [b]	1.371								

[a] Mean values from standard mixture. BA=benzaldehyde; CNMA=cinnamaldehyde; AP=acetophenone; 4-ISPBA=4-isopropylbenzaldehyde and BP=benzophenone.

[b] Identification was further confirmed by co-injection with an authentic standard and by comparing the on-line phosphorescence spectrum with that of an authentic standard.

[c] Identification confirmed by co-injection with an authentic standard.

The identities of Peak 1 in chamomile oil, Peaks 1 and 2 in cinnamon oil, Peak 4 in eucalyptus oil and Peak 1 in ylang-ylang oil were further confirmed by matching their on-line phosphorescence spectra (Figures 6.10-6.13) with those of standard compounds. The on-line luminescence spectra of Peaks 3 and 5 in eucalyptus oil are presented in Figure 6.14. Their response ratios, retention times and luminescence spectra did not match any of the standard compounds. Unfortunately, only a limited number of components in essential oils produced good spectra. The failure to obtain good on-line spectra for other components is due to severe quenching of emission intensities by far larger amount of co-eluting compounds. However, the spectral acquisition sensitivity could definitely be improved by using a good capillary column to eliminate quenching.

Interestingly, almost all of these tested essentials oils contained benzaldehyde, and some of them contained 4-isopropylbenzaldehyde (cuminaldehyde). From the results of the previous analyses reported, benzaldehyde was identified only in the essential oils of ylang-ylang tree (188, 190) and cinnamon (188, 191) and, obviously, cinnamaldehyde was determined to be one of the main constituents in cinnamon oil (188, 191). If reported in the literature, compounds showed up prominently in our samples. However, benzaldehyde, acetophenone and cuminaldehyde showed up in many more different oils than reported in the literature.

Conditional-access (Condac) chromatograms should permit the fast and facile identification of aroyl compounds in real-life sample analysis. Figures 6.15 and 6.16 display the examples of quickly finding cuminaldehyde in three different oils and three different aroyl components in eucalpytus oil, respectively.
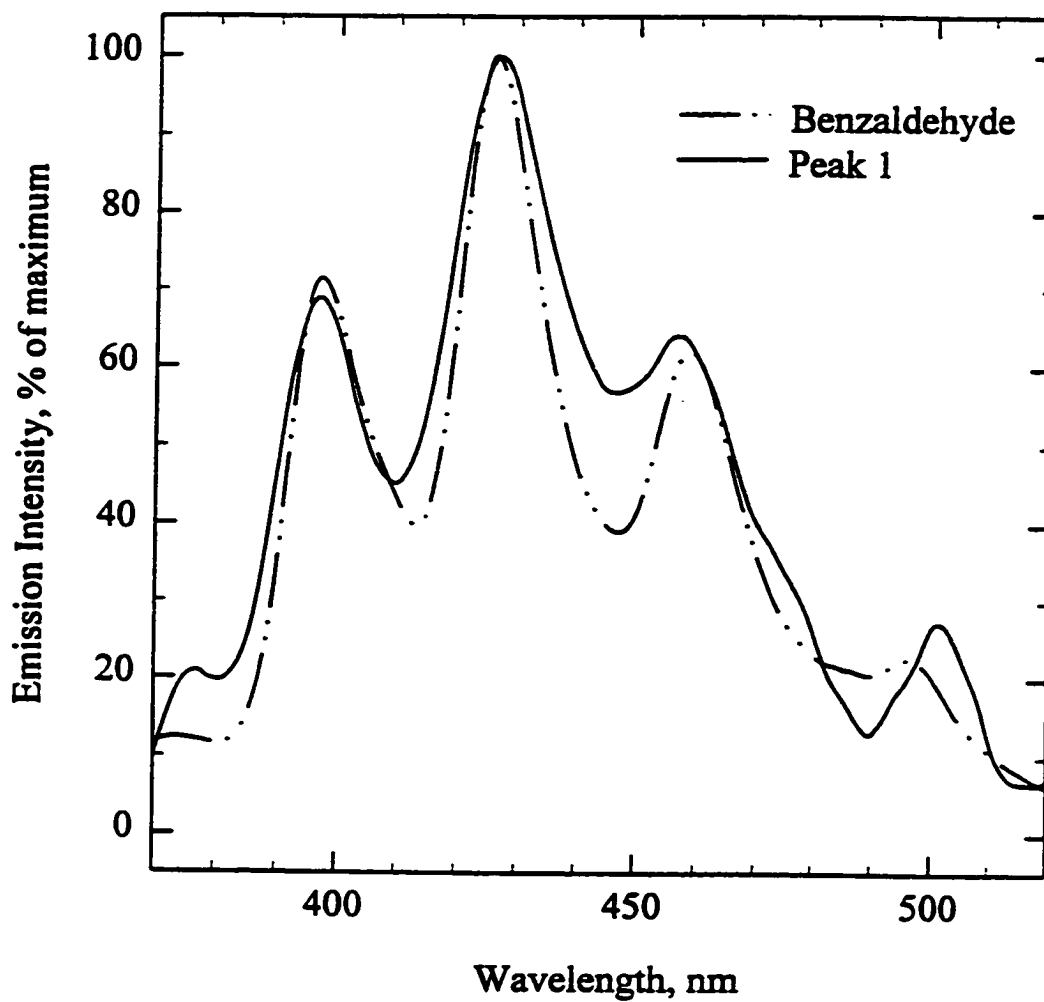
Figure 6.10   Gas-phase luminescence spectrum of Peak 1 in chamomile oil overlapping with that of benzaldehyde. 1/8 meter grating monochromator with an R-374 PMT, 1 mm slits and single-peak mode.
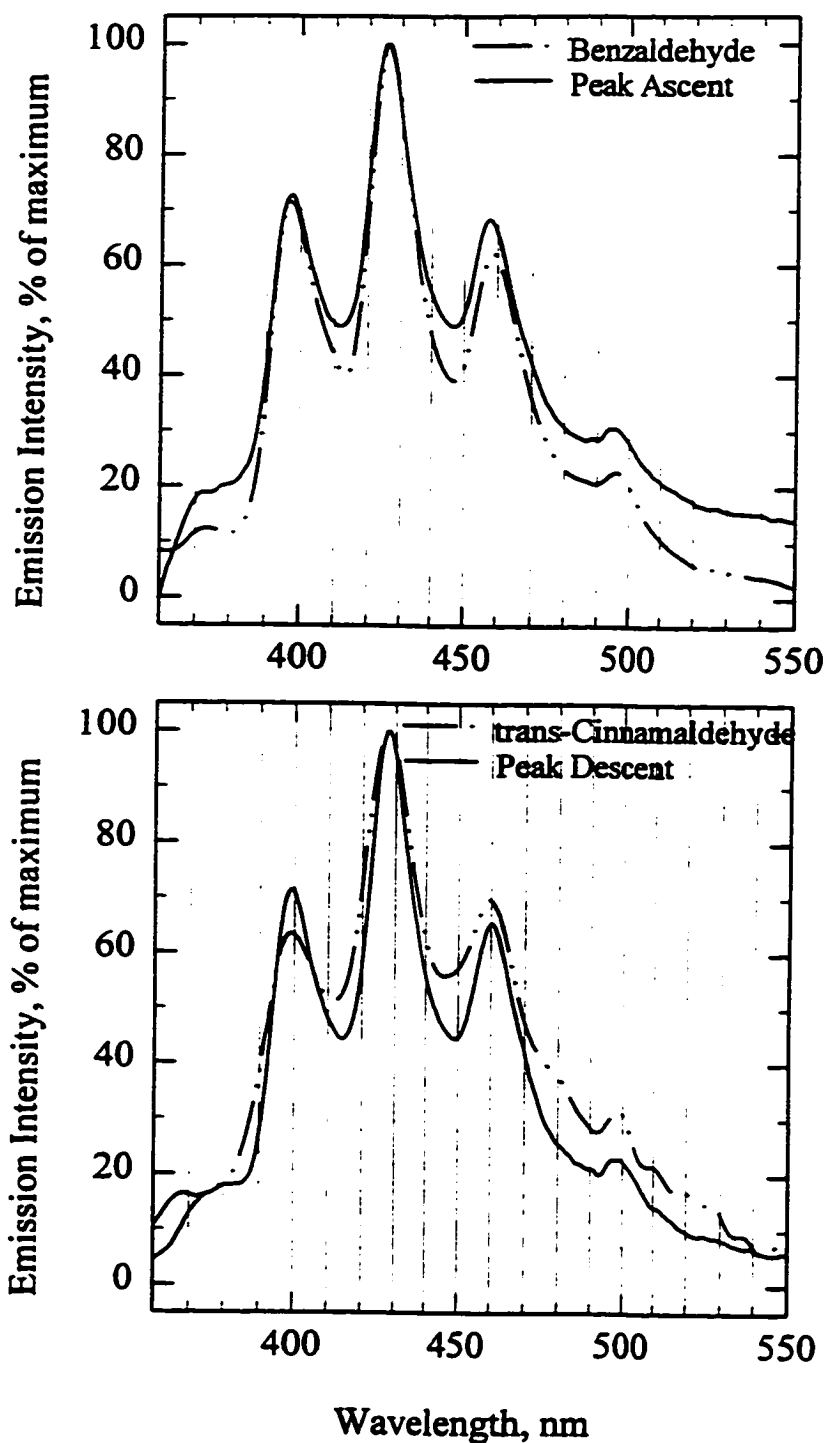
Figure 6.11   Gas-phase phosphorescence spectra of peak ascent in cinnamon oil overlapping with benzaldehyde spectrum (A) and peak descent in cinnamon oil overlapping with cinnamaldehyde spectrum (B). 1/8 meter grating monochromator with an R-374 PMT, 1 mm slits and single-peak mode.
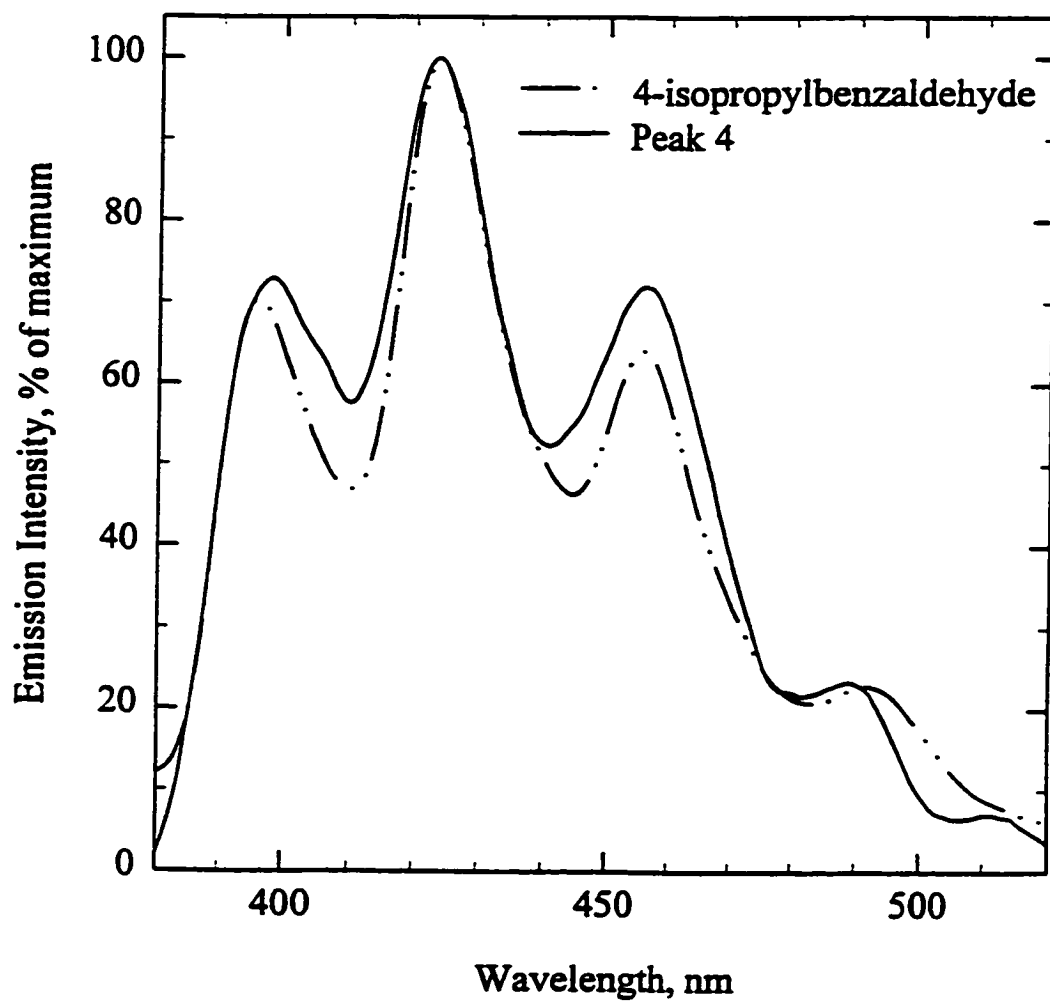
Figure 6.12 Gas-phase luminescence spectrum of Peak 4 in eucalyptus oil overlapping with that of 4-isopropylbenzaldehyde. 1/8 meter grating monochromator with an R-374 PMT, 1 mm slits and single-peak mode.
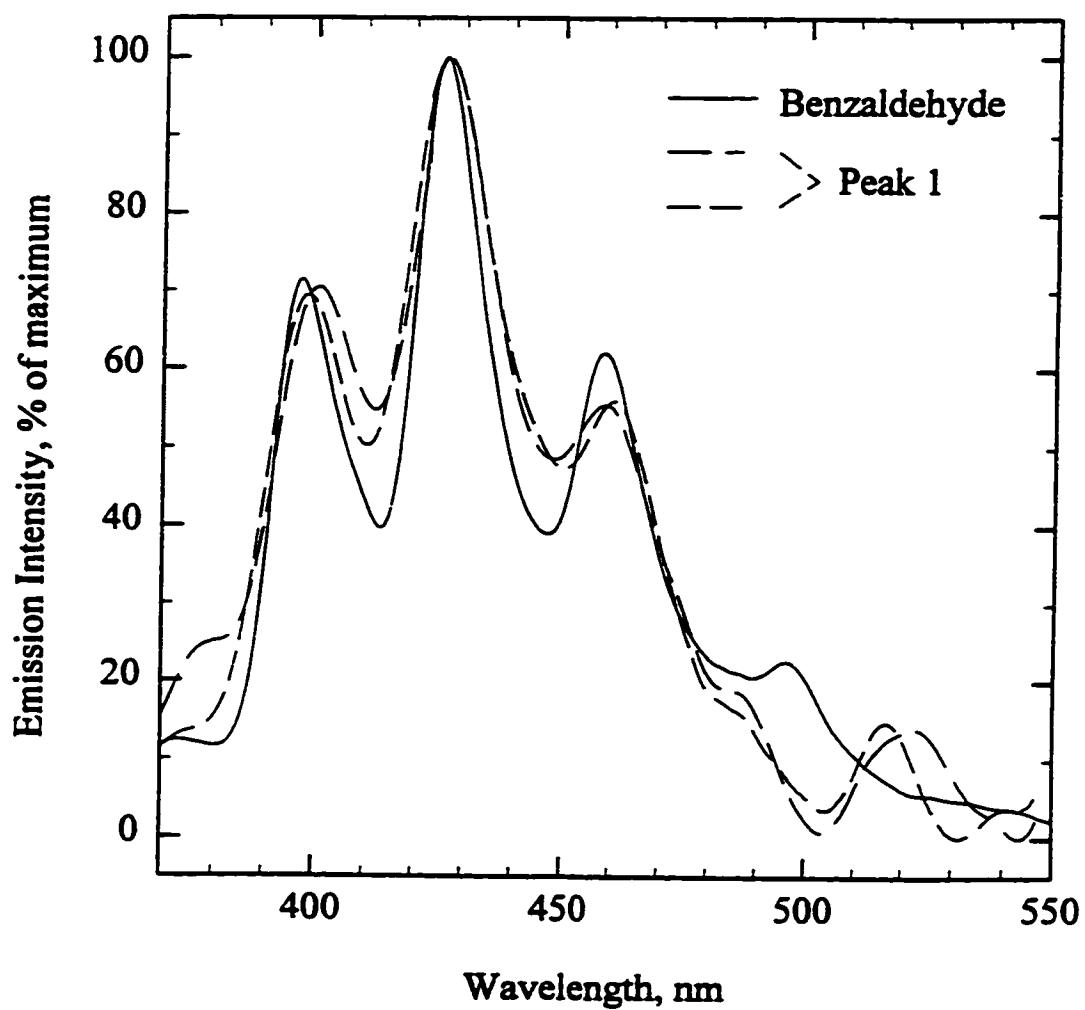
Figure 6.13 Gas-phase luminescence spectrum of Peak 1 in ylang-ylang oil overlapping with that of benzaldehyde. 1/8 meter grating monochromator with an R-374 PMT, 1 mm slits and single-peak mode.
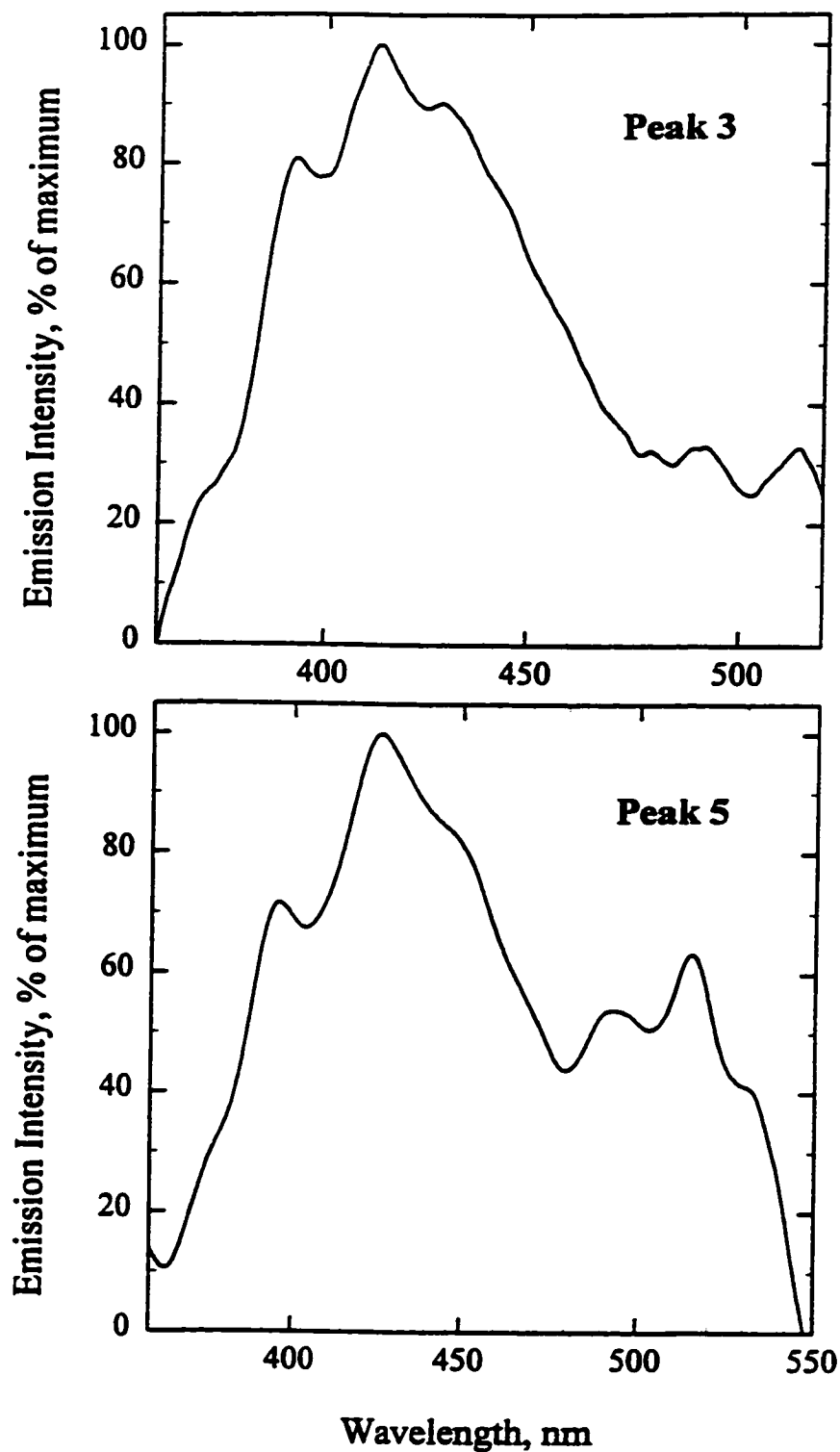
Figure 6.14 Gas-phase luminescence spectra of Peak 3 and Peak 5 in eucalpytus oil. 1/8 meter grating monochromator with an R-374 PMT, 1 mm slits and single-peak mode.

**Channel 1
(PMT-268/open)**

Chamomile Oil (A)

Eucalyptus Oil (B)

Fir needle Oil (C)

CONDAC

ISPBA in A

ISPBA in B

ISPBA in C

50°C 50°C   7.5°C/min   190°C

0   5   10   15   20 (min)
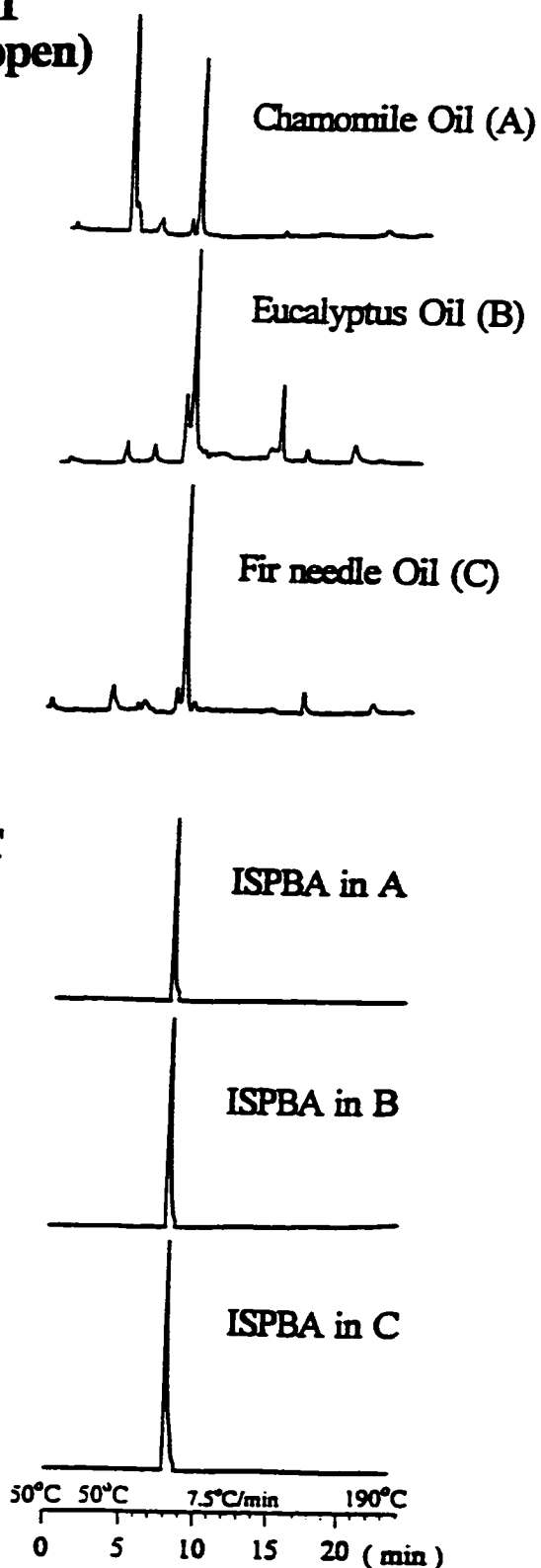
Figure 6.15   Upper half: Chromatograms of chamomile oil, eucalyptus oil and fir
needle oil. Lower half: CONDAC chromatograms for 4-isopropylbenzaldehyde (ISPBA)
in these essential oils.

Channel 1
(PMT-268/open)

Eucalyptus Oil

ISPBA

CONDAC

BA

AP

X 4

X 4

X 0.5

50°C   50°C   7.5°C/min   190°C

0   5   10   15   20   (min)
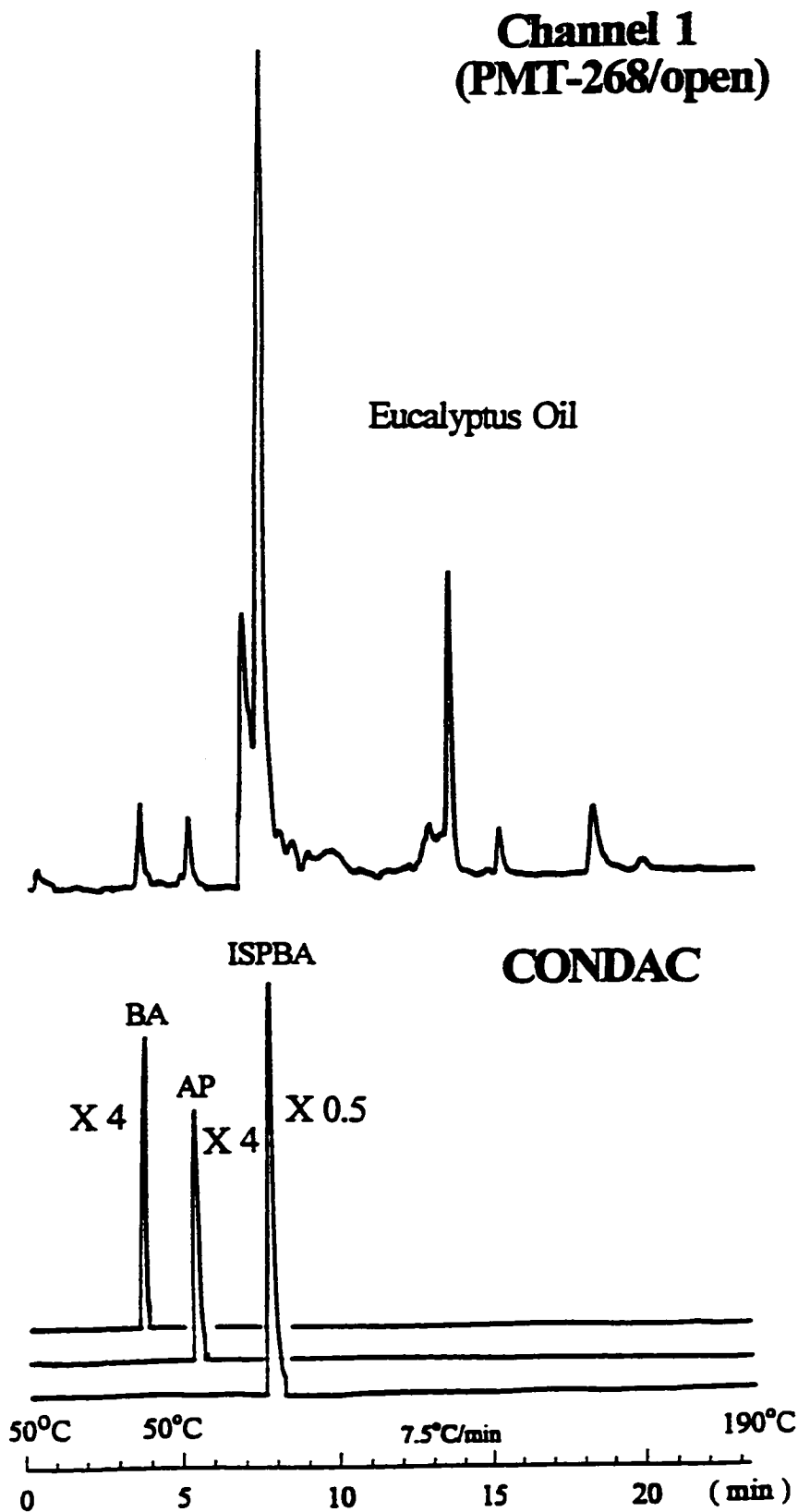
Figure 6.16   Selected single channel (top) and single-CONDAC (bottom) chromatograms for benzaldehyde (BA), acetophenone (AP) and 4-isopropylbenzaldehyde (ISPBA) in eucalyptus oil from one chromatographic separation.

Quantitation: The GC quantitative analysis of a real-life sample often shows strong matrix effects. Usually these matrix effects are attributed to the interaction of the detector or the analyte with some unidentified organic compounds contained in the sample. When such problems appear, the use of the standard addition procedure is recommended. This procedure is widely applied in atomic absorption and emission spectrometry, and has also found application in electrochemical analysis and other areas (192, 193).

In the present research—for the sake of simplicity and, more importantly, to demonstrate the extraordinary selectivity of the ALD—only a one-meter, 2 mm i.d. packed column was used for chromatographic separation. With mixtures containing as many components as an essential oil, it is therefore virtually certain that components will be incompletely separated. Therefore, quantification of some major aroyls in essential oils was achieved by using the standard addition procedure.

The prerequisite for carrying out the standard addition procedure is that the aroyl compounds still respond linearly in the ALD under quenching conditions. This was checked by measuring the calibration curves of two typical aroyls, benzaldehyde and benzophenone, while different levels of quencher (methane) were being introduced. As shown in Figures 6.17 and 6.18, the two aroyl compound still maintain straight calibration curves when up to about 75% of intensity has already been quenched..

In the standard addition procedure, equal volumes of the sample solution are taken, all but one are separately spiked with known, different amounts of the analyte, and all are
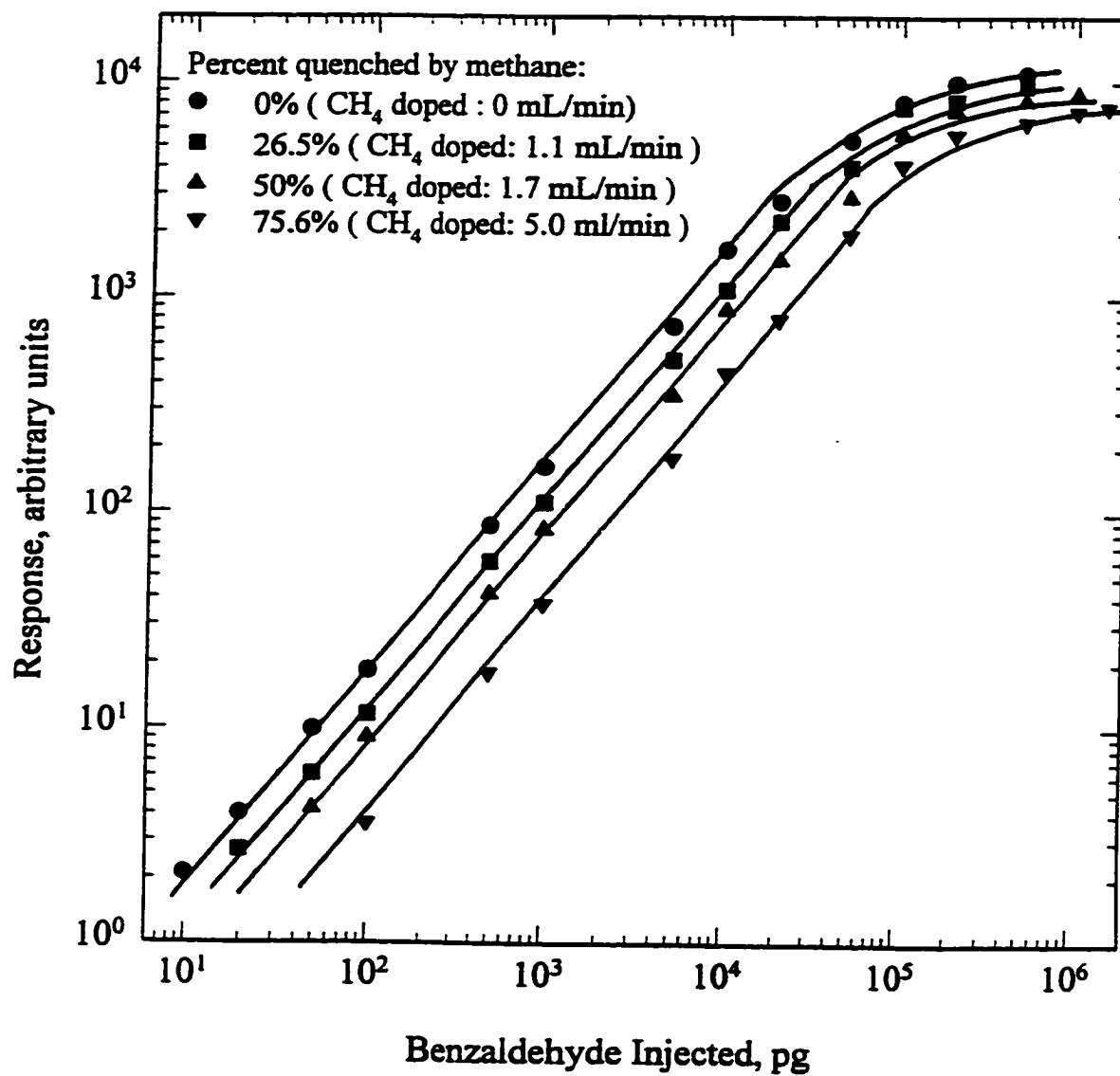
Figure 6.17 Calibration curves of benzaldehyde at different quenching intensities. Lines are drawn at unity slope.
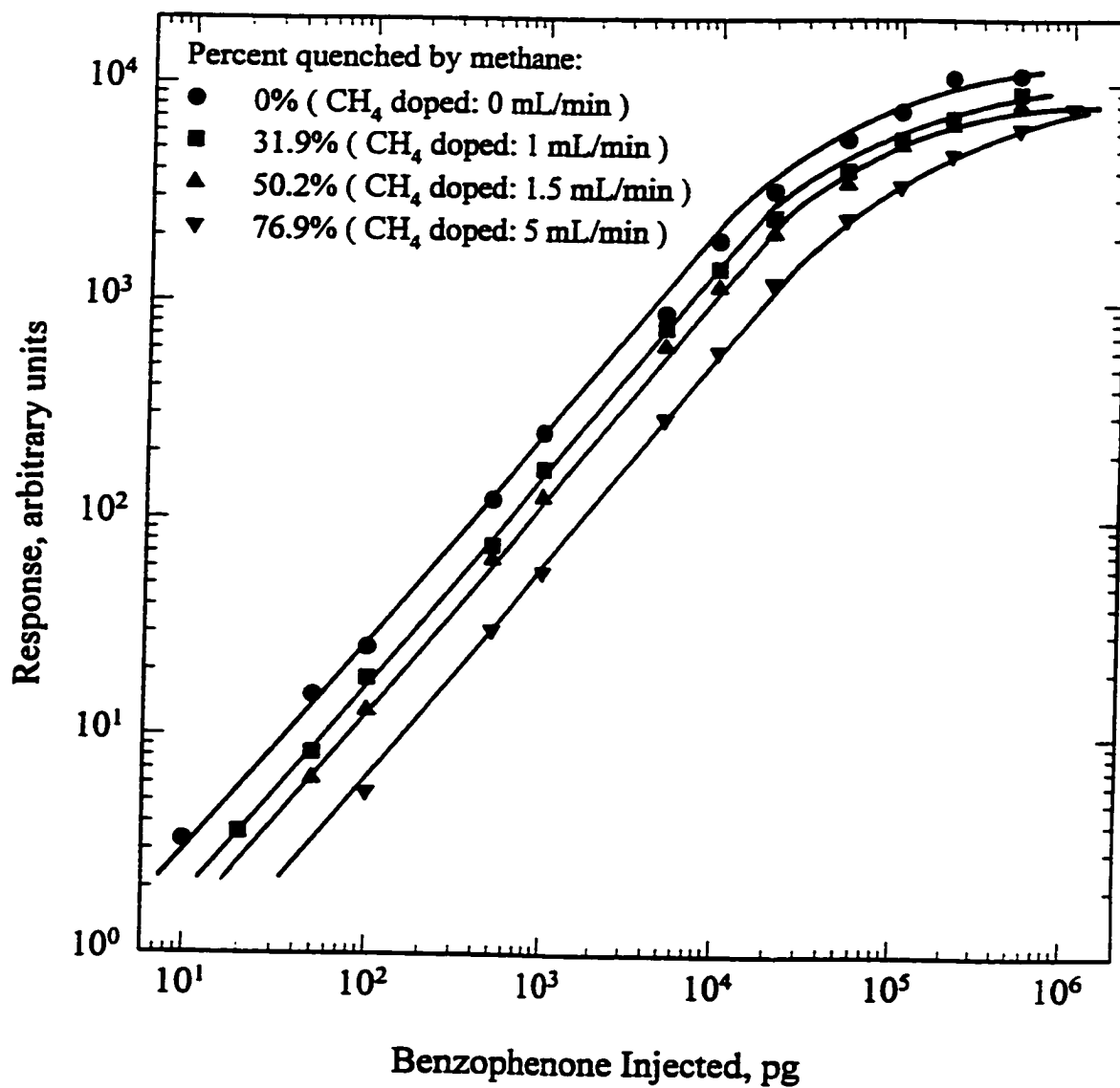
Figure 6.18 Calibration curves of benzophenone at different quenching intensities. Lines are drawn at unity slope.

then injected for GC-ALD analysis. One example of this procedure is shown in Figure 6.19. As usual, the signal is plotted on the ordinate; in this instance the abscissa is graduated in terms of the amounts of analyte added. The unweighed linear regression line is calculated by using the algorithm in Sigmaplot (Jandel Scientific, San Rafael, CA. USA). The negative intercept on the abscissa corresponds to the amount of the analyte in the test sample. The results are given in Table 6.3.

Table 6.3 Concentrations of Some Aroyl Compounds in Essential Oils

Essential Oil	Concentration, ppm (w/w)			
	Benzaldehyde	Acetophenone	4-isopropyl-benzaldehyde	Benzophenone
Balm	3.9×10^1			
Basil	6.8×10^1			
Cedar wood	7.9×10^0	3.5×10^1		
Chamomile	2.6×10^2		4.7×10^2	
Clove bud	7.7×10^0			
Eucalyptus	3.5×10^1	3.2×10^1	9.4×10^0	
Fir needle			5.4×10^2	
Juniper berry	1.6×10^2			
Peppermint	3.7×10^1			1.8×10^0
Rosemary	1.8×10^2			
Ylang-ylang	1.7×10^2			
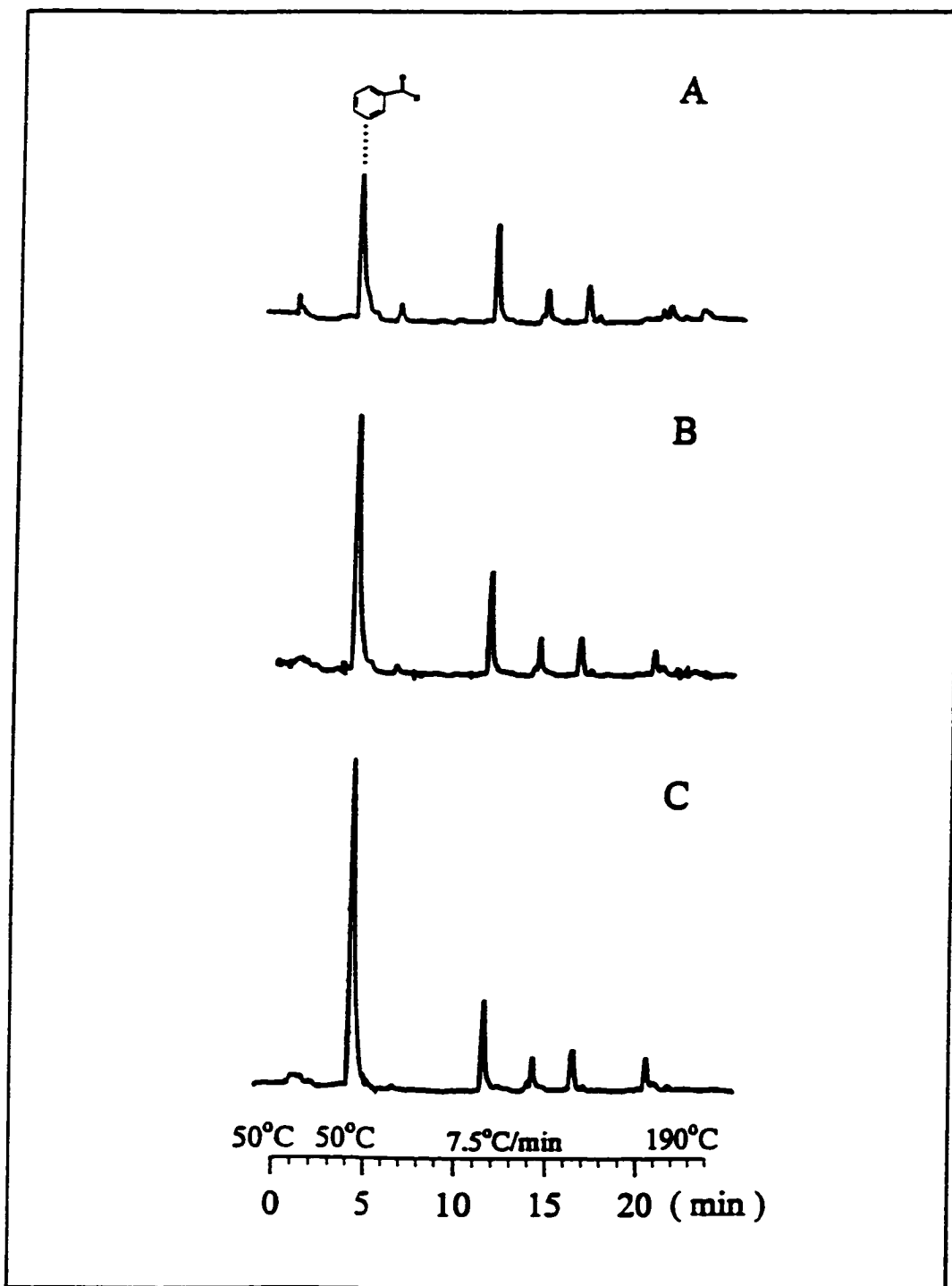
Figure 6.19 Quantitative analysis of benzaldehyde in peppermint oil by the standard addition method. (A) 0.2 μL peppermint oil; (B) 0.2 μL peppermint oil spiked with 4 ng benzaldehyde; (C) 0.2 μL peppermint oil spiked with 8 ng benzaldehyde.

One of the major advantages of the standard addition procedure is that it can avoid matrix interference effects. The quenching effects of aroyls in essential oils were further examined by comparing the responses of aroyl compounds in pure and diluted oil. Figure 6.20 clearly shows that the quenching both of benzaldehyde and 4-isopropyl-benzaldehyde in pure chamomile oil was severe: the peaks vary little in size after a 25-time dilution. The extent of quenching of benzaldehyde in different oils was, as could be expected, quite different. This behavior is shown in Figure 6.21. The necessity of using the standard addition procedure to eliminate the severe quenching effects in the analyses of aroyls in essential oils is illustrated in Figure 6.22. It clearly shows that the determined concentrations of benzaldehyde decreased as the injected sample amounts increased in the normal calibration curve procedure due to the larger amount of quenchers that co-eluted with benzaldehyde, while the concentrations determined by using standard addition method was independent of sample amount. While this study, in accord with its objections, used low-resolution chromatography and relatively large sample loads, practical analyses with the ALD should be carried out on a high-resolution column with relatively small loads, in order to minimize quenching effects.

It has been well established in the literature that components and component concentrations of essential oils can vary considerably with several variables such as time of year, geographic location, and tree type (194). Thus, the chemical composition and levels of aroyl compounds in these essential oils may serve to trace a source or even an adulteration.
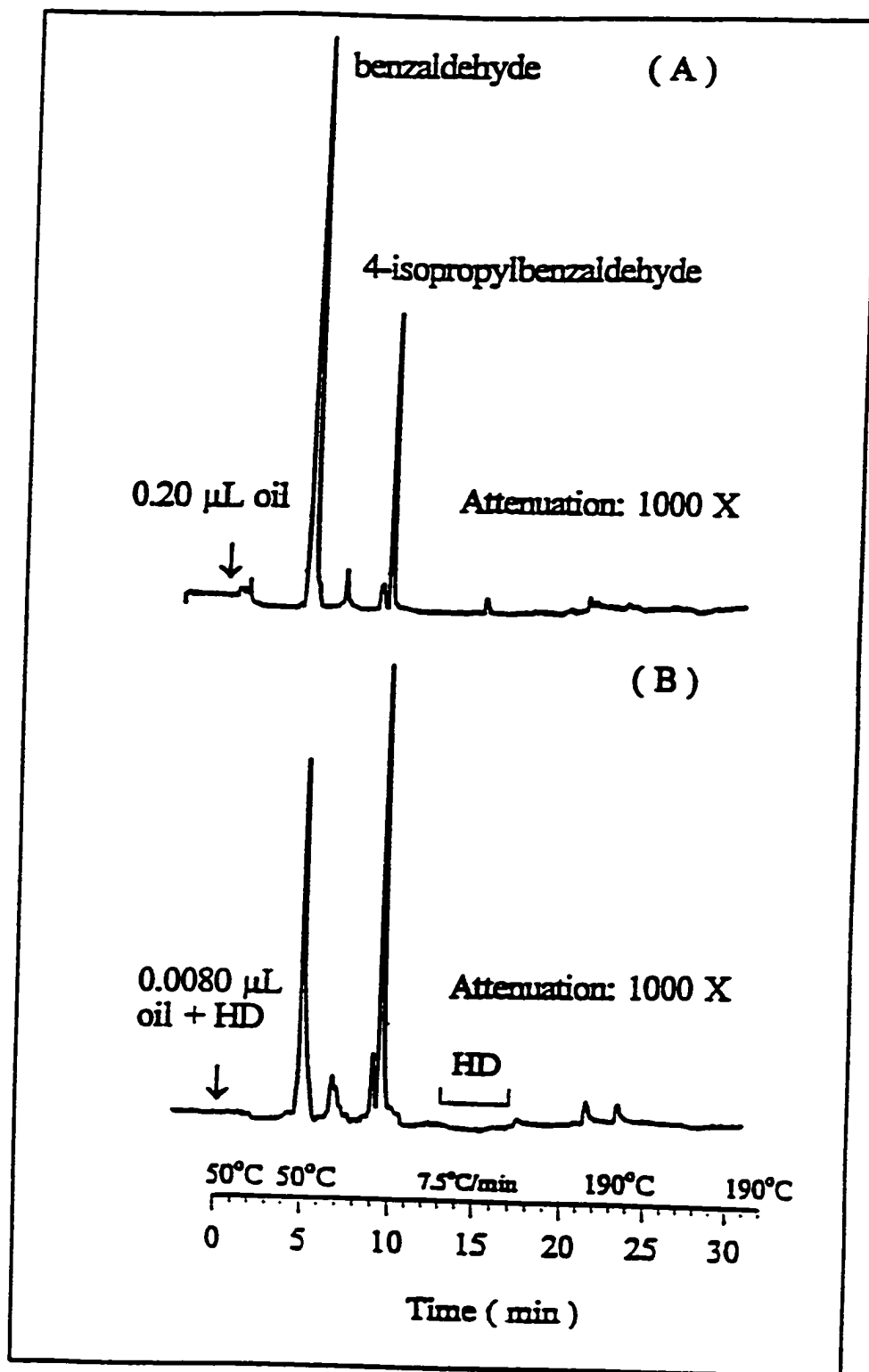
Figure 6.20   Gas chromatograms of chamomile oil showing quenching effects on different aroyl compounds. (A) 0.2 μL pure oil injected. (B) 0.2 μL hexadecane (HD) solution containing 0.008 μL oil.
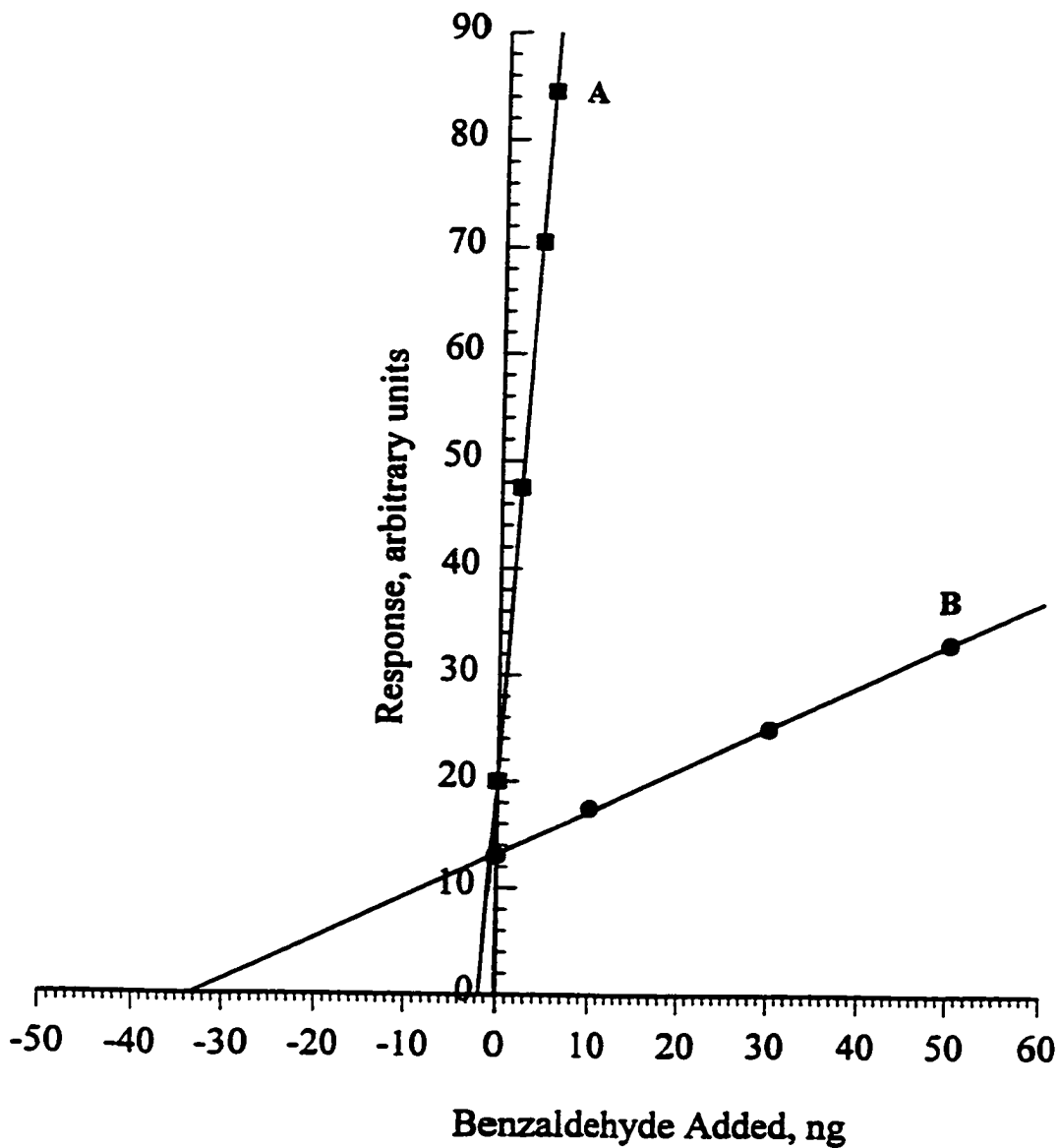
Figure 6.21 Standard addition plots for clove bud oil (A) and rosemary oil (B) showing different quenching effects on benzaldehyde.
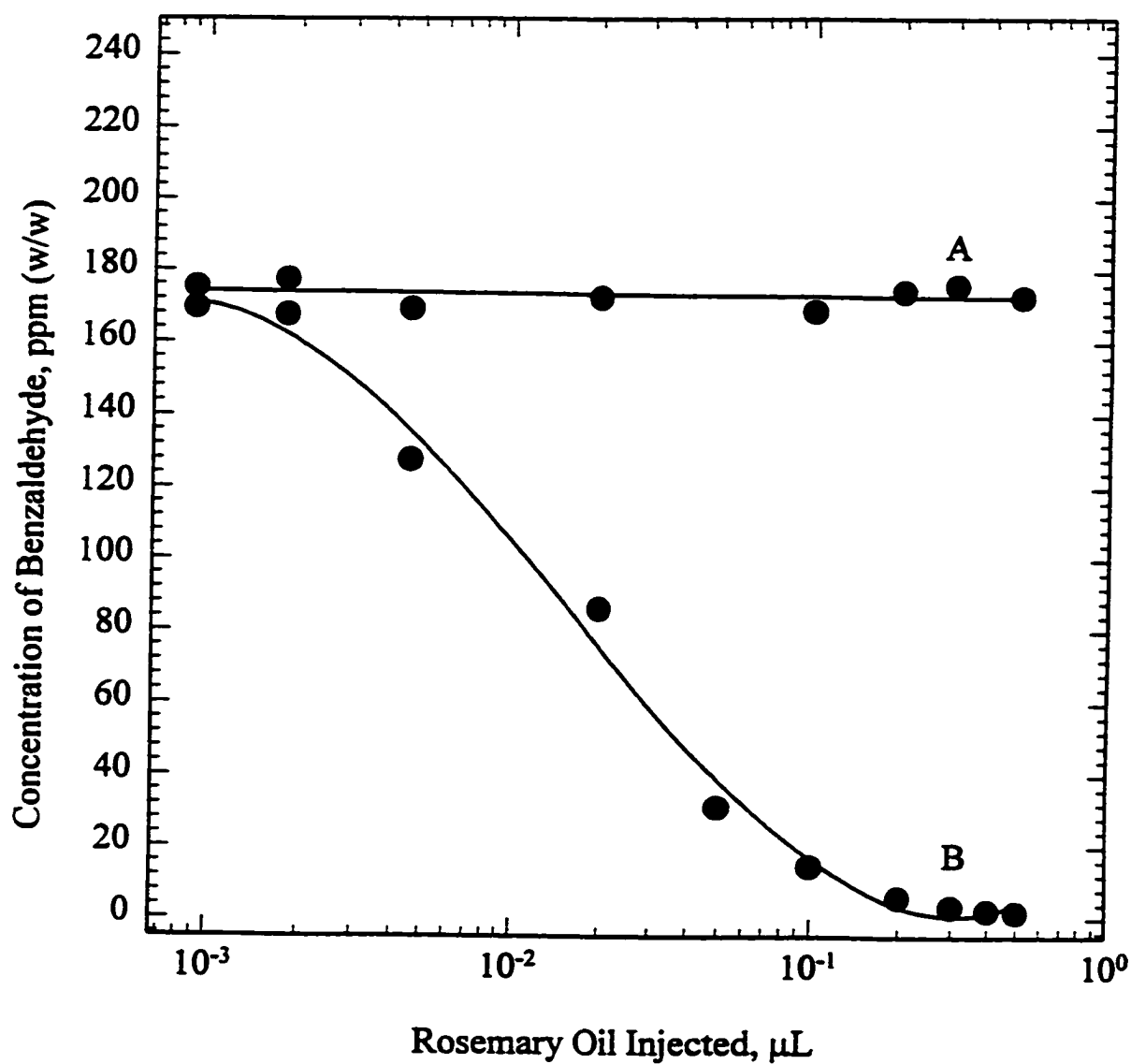
Figure 6.22   Effect of the analysis procedures on the determined concentrations of benzaldehyde in rosemary oil. (A) standard addition procedure. (B) normal calibration curve procedure.

6.5 Luminescent Aroyl Compounds in Marine Sediment

6.5.1 Introduction

As mentioned in Section 3.4.2, the oxidation products of polycyclic aromatic hydrocarbons (PAHs) such as polyaromatic quinones have been found to be more carcinogenic than their purely hydrocarbonaceous analogues (56). Hence, the risk assessment associated with their occurrence requires the determination of environmental levels in the different compartments. However, since the oxidation products of PAHs usually occur at concentration levels several orders of magnitude lower than the corresponding parent PAHs, the detection and quantification of these oxidation products at trace levels is often a difficult task. In general, the analysis of trace components in a complex environmental sample requires multistage enrichment and fractionation techniques prior to GC analysis.

Consequently, the present work demonstrates a relatively simple yet efficient technique for the analysis of some trace level PAH oxidation products in a marine sediment sample (PACS-1) by using the triple-channel ALD to collect phosphorescence spectra "on the fly" and chart spectral response ratios. These approaches, in combination with retention times, serve to demonstrate that, even at this high degree of selectivity (in the 10^6 range) and sensitivity (in the picogram detection limit range) and with many, far larger amounts of compounds co-eluting, it is possible to achieve positive identification of some aroyl compounds or their basic luminescing structures.

6.5.2 Results and Discussion

Extraction of marine sediment sample: The marine sediment (PACS-1). with certified values for trace metals and other constituents, was collected in the harbor of Esquimalt, B.C., Canada, and provided by Dr. Michael Siu at the National Research Council (Ottawa, Canada). Prior to extraction, the sample was kept at 4 °C in a refrigerator. For optimization of the extraction conditions, three different extracting solvents and different extraction times were evaluated in this study. Figure 6.23 shows the GC-ALD chromatograms of marine sediment (PACS-1) extracted with three different solvents. It was clearly shown that several luminescing aroyl compounds do exist in the marine sediment sample. In terms of peak numbers and intensities, dichloromethane and (1:1, v/v) acetone/cyclohexane showed no significant difference. However, with toluene as extracting solvent, the intensity of the first peak was significantly larger than those with other two solvents. On the contrary, the second peak was smaller. This means that toluene is not as efficient as dichloromethane and (1:1, v/v) acetone/cyclohexane for extracting the second component appearing in the chromatograms. On the other hand, it was confirmed by a blank test (Figure 6.24) that the increased intensity of the first component was probably due to the oxidation of toluene to benzaldehyde (see section of qualitative analysis). Therefore, toluene is not a suitable solvent to extract marine sediment for GC-ALD analysis. Thus, dichloromethane was selected as the extracting solvent in this study. The effect of the duration of extraction on the extraction efficiencies of two aroyl compounds in the sediment sample is presented in Figure 6.25. Because a very efficient, specially-made extractor was used (187), the extraction was very
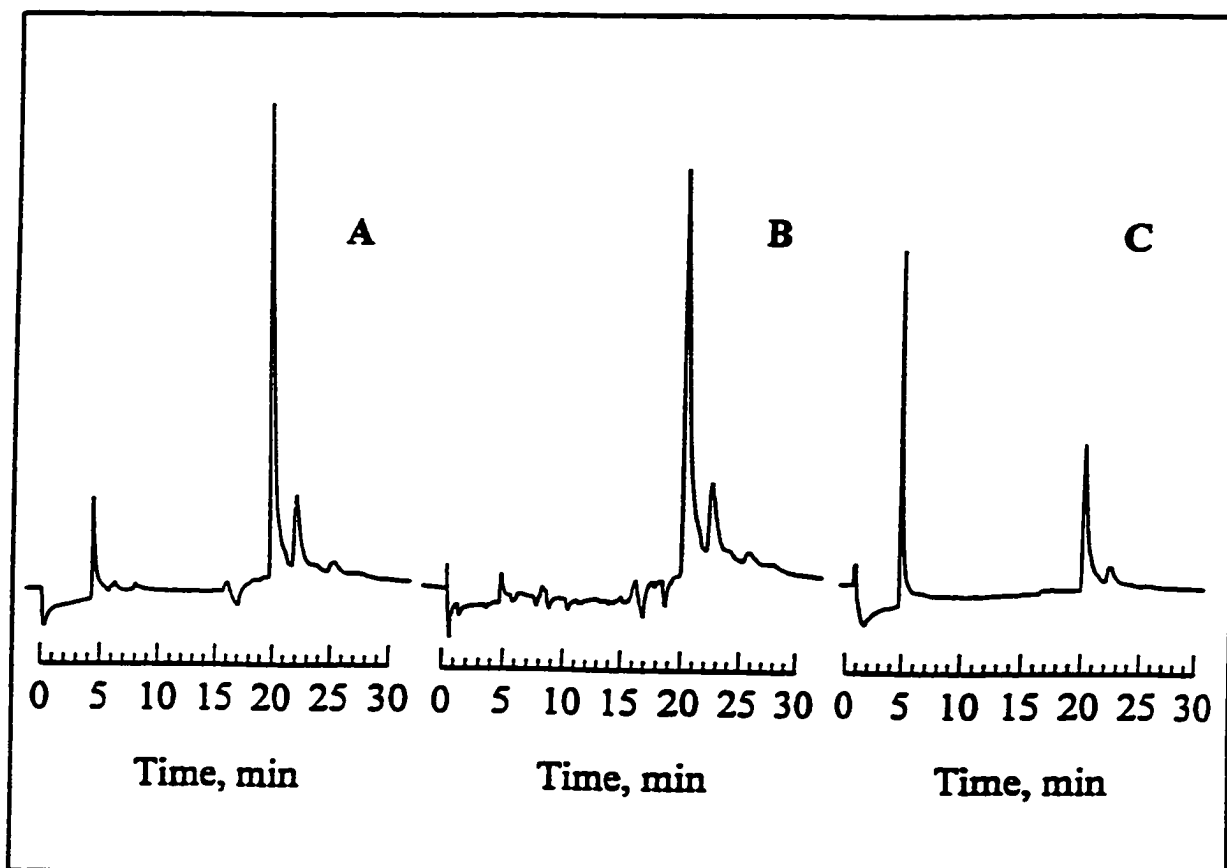
Figure 6.23 GC-ALD chromatograms of a marine sediment (PACS-1) extracted with three different extracting solvents: (A) dichloromethane; (B) acetone/cyclohexane (1:1, v/v) and (C) toluene. A 2 g marine sediment sample was extracted by 50 mL each of extracting solvents for 16 hours, then concentrated to 1 mL. 1 µL of extract was injected. DC voltage: 5000 V; PMT (R-268): 700 V; Column temperature: 50 °C → 190 °C @ 7.5 °C/min.
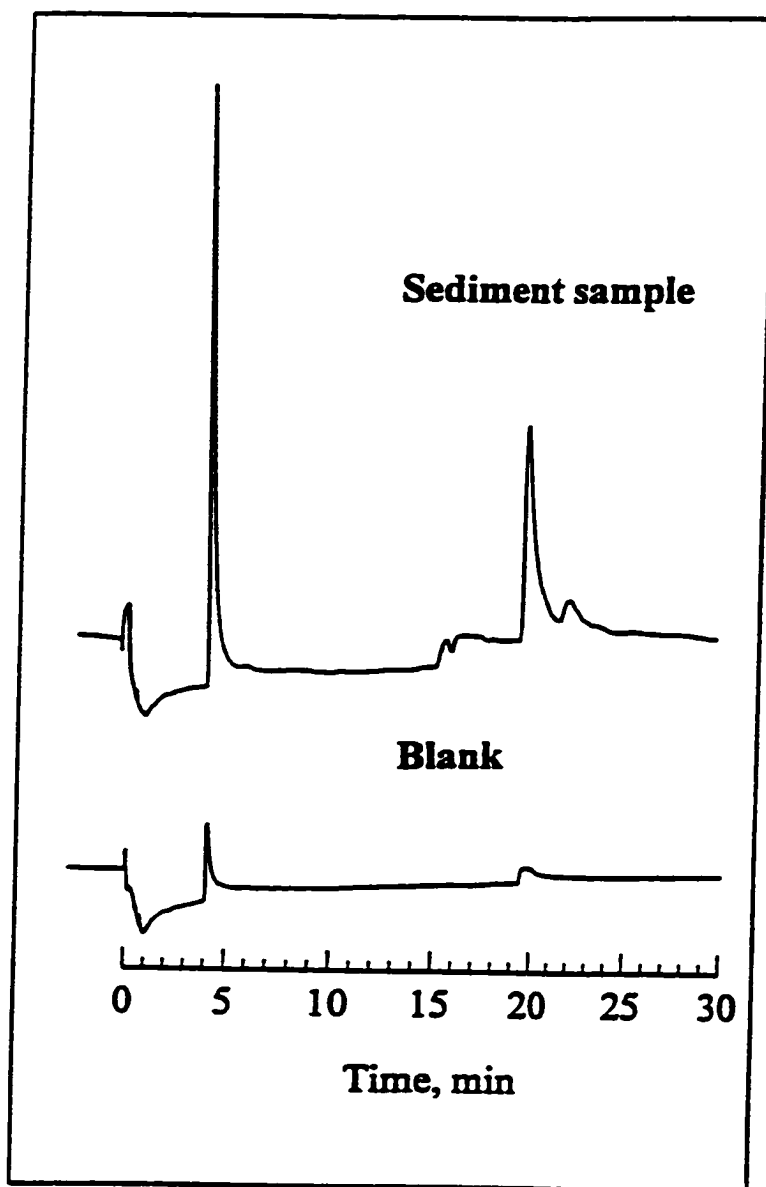
Figure 6.24   GC-ALD chromatograms of a marine sediment (PACS-1) extracted with toluene, and a blank (see Section 6.2.2). Other conditions as in Figure 6.23.
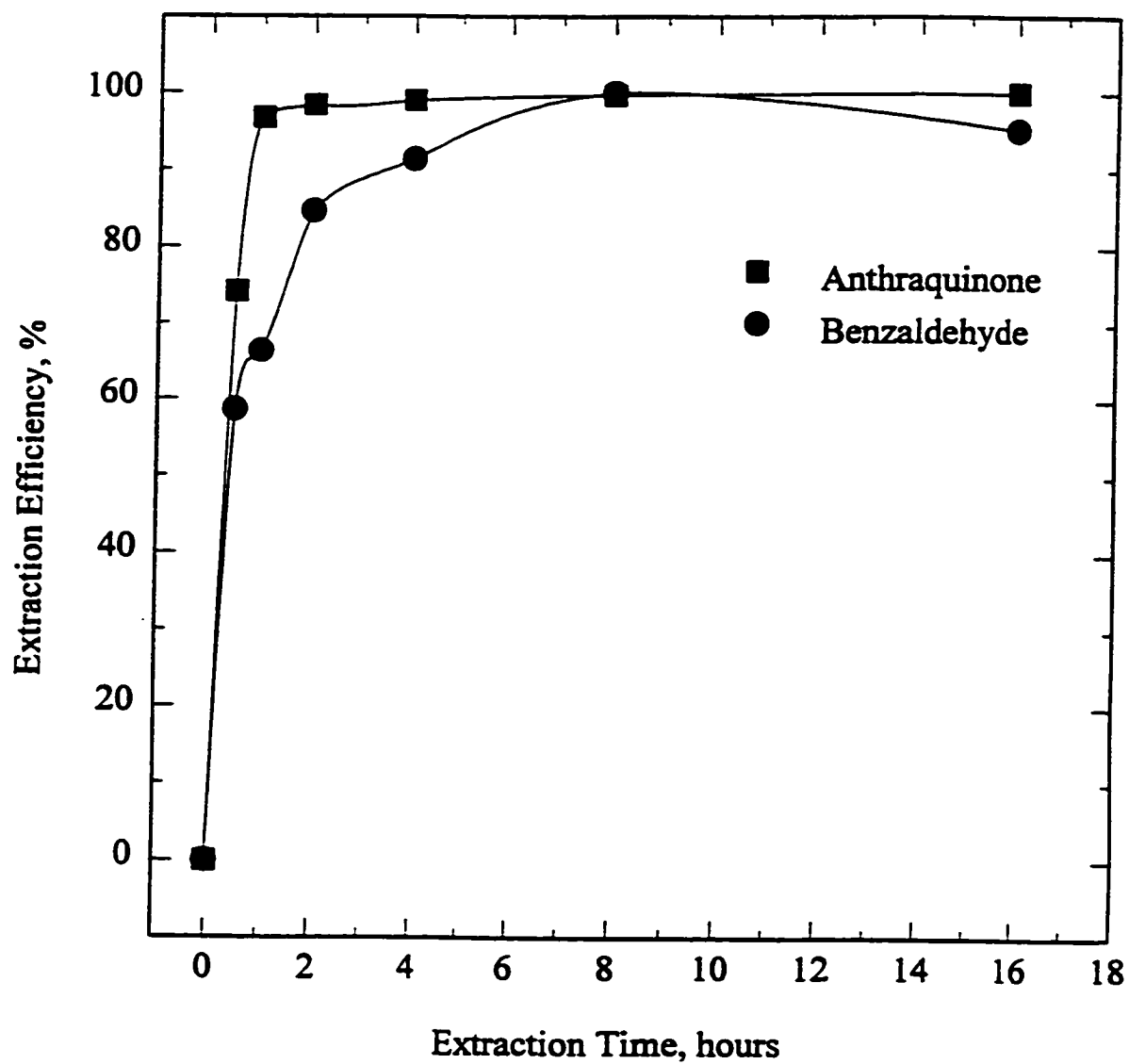
Figure 6.25 Dependence of extraction efficiencies of two aroyl compounds in the marine sediment (PACS-1) on the duration of extraction. Other conditions as in Figure 6.23.

fast and complete. However, a relatively long extraction time of 16 hours was used for the purpose of reducing solvent volume which was part of the preconcentraction process. As shown in Figure 6.26, the second extraction showed no significant peaks, indicting that the duration of extraction was sufficient to quantitatively recover the extractable compounds.

Qualitative analysis: The spectral response ratios from two response-ratio channels in the triple-channel ALD, in combination with retention times and on-line luminescence spectra, were used to identify the aroyl compounds in the marine sediment (PACS-1). In this study, an eight-component aroyl standard mixture was prepared for measuring the spectral response ratios and retention times. Two channels used R-268 photomultiplier tubes with two different filter combinations to get two sets of spectral response ratios for positive identification of suspected compounds. Table 6.4 reports retention times and spectral response ratios (and related relative standard deviations) for the eight components of the standard mixture. As already demonstrated in Section 6.3, reproducibility of response ratios was good, with relative standard deviations ranging from 0.5 to 5.4%. Reproducibility of retention times was also very good under the same operating conditions. However, the retention times and spectral response ratios (RR1) reported here are different from those in Section 6.3, because the column was replaced by a new 5% Carbowax 20M column and the two photomultiplier tubes were not the same tubes used in previous experiments.

As shown in Figure 6.26 (A), there are three major components in the marine sediment (PACS-1). These peaks were numbered 1 to 3 and are listed in Table 6.5 with
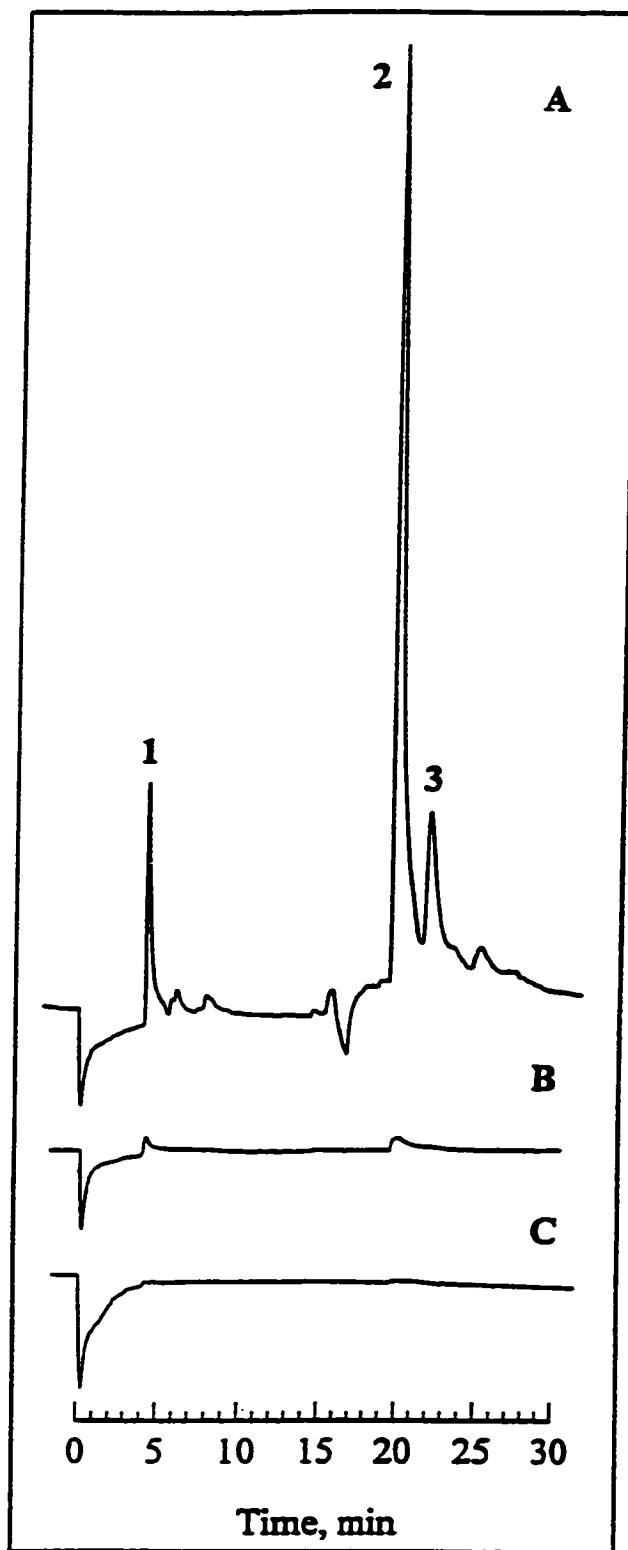
Figure 6.26 GC-ALD chromatograms of a marine sediment (PACS-1) extracted with dichloromethane. (A) first extraction. (B) second extraction. (C) blank. Other conditions as in Figure 6.23.

Table 6.4 **Retention Times and Spectral Response Ratios of Eight Components of a Standard Mixture**

Compounds	t_R (RSD,%) min (n=8)[c]	RR1 (RSD,%)[a] open/530-nm LP (n=4)[c]	RR2 (RSD,%)[b] 460-nm SP/515-nm LP (n=4)[c]
Benzaldehyde	3.2 (1.1)	1.993 (0.5)	1.010 (0.5)
Acetophenone	4.7 (1.1)	2.155 (5.4)	1.084 (3.6)
4-Ethylbenzaldehyde	6.0 (1.5)	2.115 (1.8)	1.180 (3.1)
Isophthalaldehyde	10.5 (0.8)	1.700 (0.9)	0.801 (0.8)
Benzophenone	14.2 (0.6)	1.602 (3.0)	0.678 (2.0)
Xanthone	18.4 (0.8)	5.668 (3.2)	2.973 (1.2)
Anthraquinone	20.3 (0.3)	0.955 (1.2)	0.310 (1.3)
Thio-xanthene-9-one	22.7 (0.2)	4.181 (0.7)	2.087 (4.2)

[a] RR1 was measured from the combination of Channel 1: PMT-268 (no filter, -800 V, attenuation: 10X2) and Channel 2: PMT-268 (530-nm longpass filter, -800 V, attenuation: 1X4).

[b] RR2 was measured from the combination of Channel 1: PMT-268 (460-nm shortpass filter, -800 V, attenuation: 10X2) and Channel 2: PMT-268 (515-nm longpass filter, -800 V, attenuation: 10X1).

[c] n=number of replicates.

their spectral response ratios, retention times and compound identification. The identification was made by comparing with the spectral response ratios and retention times of standard compounds under the same experimental conditions.

Peak 1 and Peak 2 were thus identified as benzaldehyde and anthraquinone. Standard and sample were in good agreement. The identification of Peak 2 was

Table 6.5 Aroyl Compounds in a Canadian Certified Marine Sediment (PACS-1)[a]

Peak No.	t_R (RSD,%) min (n=6)	RR1 (RSD,%) open/530-nm LP (n=3)	RR2 (RSD,%) 460-nm SP/515-nm LP (n=3)	Compound
1	3.2 (1.5)	1.989 (2.7)	1.017 (1.1)	Benzaldehyde[b]
2	20.3 (0.3)	0.953 (1.6)	0.313 (1.5)	Anthraquinone[c]
3	22.6 (0.1)	1.251 (3.1)	0.559 (3.4)	Unknown

[a] Experimental conditions as in Table 6.4.

[b] Identification was further confirmed by co-injection with a known standard.

[c] Identification was further confirmed by co-injection with a known standard and by comparing the on-line phosphorescence spectrum with that of a known standard.

further confirmed by matching its on-line phosphorescence spectrum with that of anthraquinone (Figure 6.27). The identification of anthraquinone in the marine sediment (PACS-1) agrees with those in other sediment samples (195, 196). Unfortunately, only Peak 2 produced an on-line spectrum of good quality. Peak 1 and Peak 3 failed to do so because of their weaker emission intensities, which may be due to the severe quenching effect of this complex mixture. However, it should be realized that the present research—for the sake of simplicity and, more importantly, for the sake of demonstrating the extraordinary selectivity of the ALD—used only a one-meter, 2 mm i.d. packed column. A good capillary column would have provided significantly larger plate numbers and signal/noise ratios. Also, a two-dimensional GC arrangement would likely have eliminated the quenching effects.
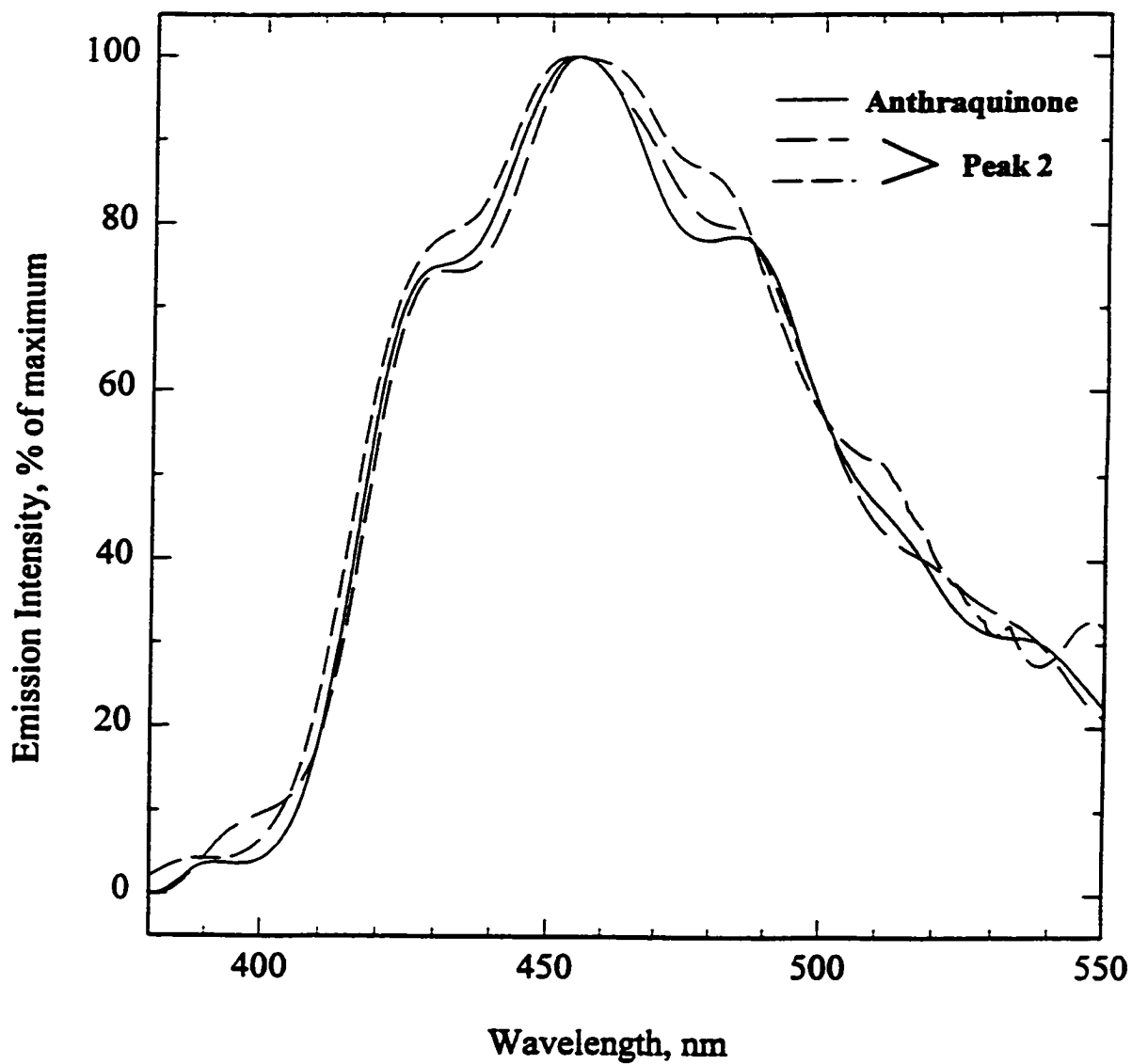
Figure 6.27 Gas-phase luminescence spectrum of a major component (Peak 2, run twice) in a Canadian certified marine sediment (PACS-1) overlapping with that of anthraquinone. 1/8 meter grating monochromator with R-374 PMT, 1 mm slits and single-peak mode. 100 mL/min argon was added into nitrogen flow to enhance the emission intensity.

For Peak 3, its retention time agreed with that of thio-xanthene-9-one. However, its two spectral response ratios were very different from the reference values.

Quantitation: In order to avoid matrix interference effects, the standard addition procedure was applied to determine the concentrations of benzaldehyde and anthraquinone in the marine sediment PACS-1 (instead of the conventional calibration plot).

In the standard addition procedure, equal volumes of the sample solution are taken, and all but one are separately spiked with known, different amounts of the analyte for GC-ALD analysis. The results are shown in Figure 6.28 and the concentrations are listed in Table 6.6. The relative standard deviations of the whole analytical procedure are 11.1% and 14.9% for benzaldehyde and anthraquinone, respectively. The concentration of anthraquinone in PACS-1 is about 150 times higher than that in another Canadian marine sediment HS-4 (195), but 5 to 18 times lower than that in a contaminated sediment (196).

As mentioned before, one of the major advantages of the standard addition procedure is that it can avoid matrix interference effects. An additional experiment confirmed that quenching occurred in the marine sediment PACS-1. This is clearly shown in Figure 6.29. The quenching of benzaldehyde and anthraquinone responses in the ALD was 70% and 31%, respectively. Consequently, the standard addition procedure did eliminate quenching effects and enabled quantitation to be carried out.
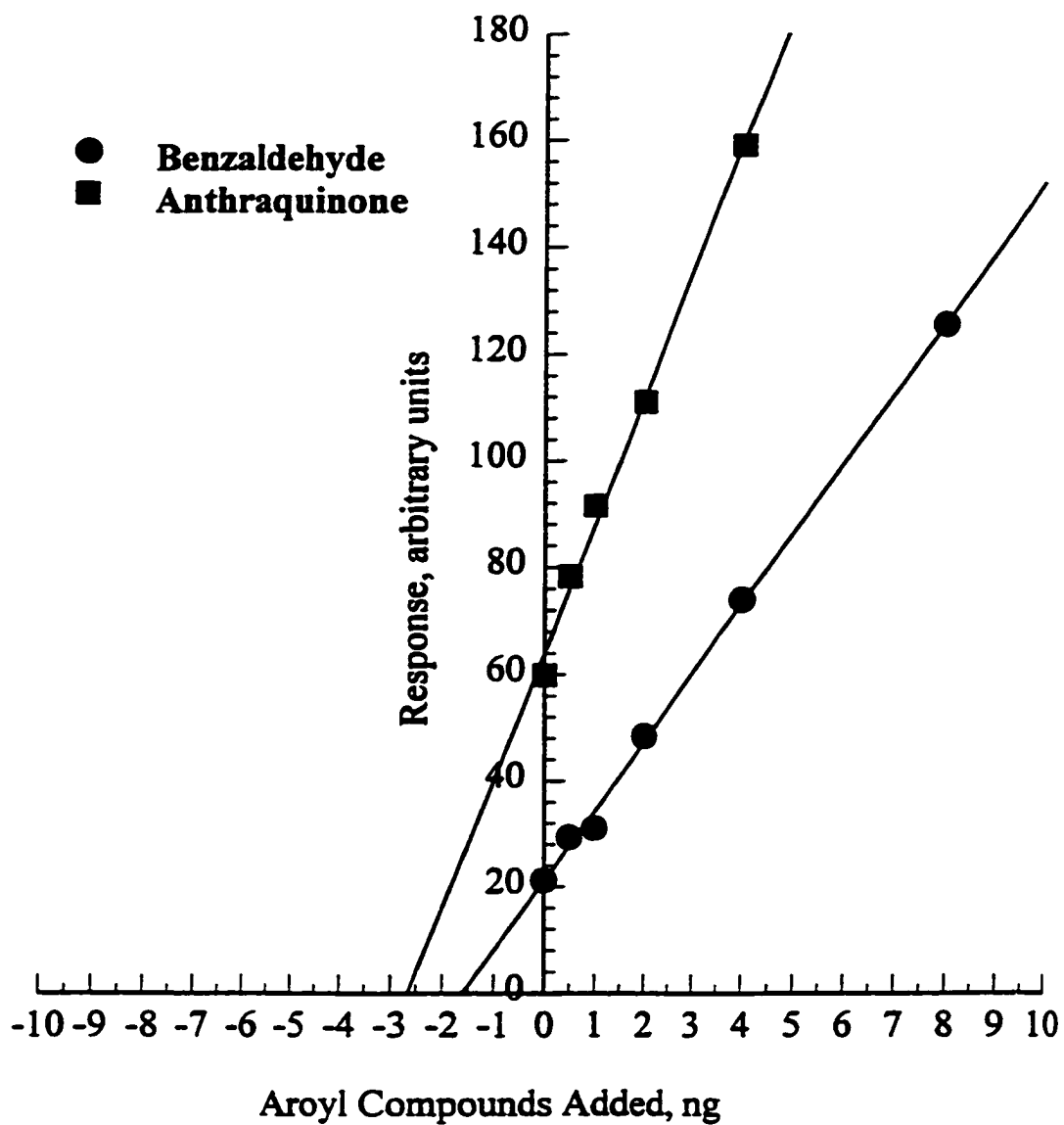
Figure 6.28 Plots of standard addition for determining concentrations of benzaldehyde and anthraquinone in the marine sediment PACS-1. Conditions as in Figure 6.23A.

Table 6.6   Concentrations of Benzaldehyde and Anthraquinone in the Marine Sediment Standard PACS-1

Peak No.	Compound	Concentration $(\mu g/g)^a$
1	Benzaldehyde	0.81 ± 0.09
2	Anthraquinone	1.34 ± 0.2

[a] Procedural relative standard deviations (n=3) are indicated as ± values.

6.6   Conclusions

A simple and rapid method for identifying aroyl compounds was developed. This method is based on spectral response ratios from the two response-ratio channels of the triple-channel aroyl luminescence detector, in combination with retention times and on-line phosphorescence spectra. Finally, the applicability of this methodology to the determination of aroyl compounds in essential oils and a marine sediment sample has been demonstrated. The method should be equally well applicable to the analysis of various other complex mixtures. The approach also serves to demonstrate that, even at this high degree of selectivity and sensitivity with many, far larger amounts of compounds co-eluting in a complex mixture, it is possible to achieve positive identification of some aroyl compounds or at least of their basic luminescing structures.

In the present research, for the sake of simplicity and, more importantly, for demonstrating the extraordinary selectivity of the ALD, only a one-meter, 2 mm i.d. packed column was used. For future routine analyses, a good capillary column or a multidimensional GC should used. The improved sensitivity would facilitate the
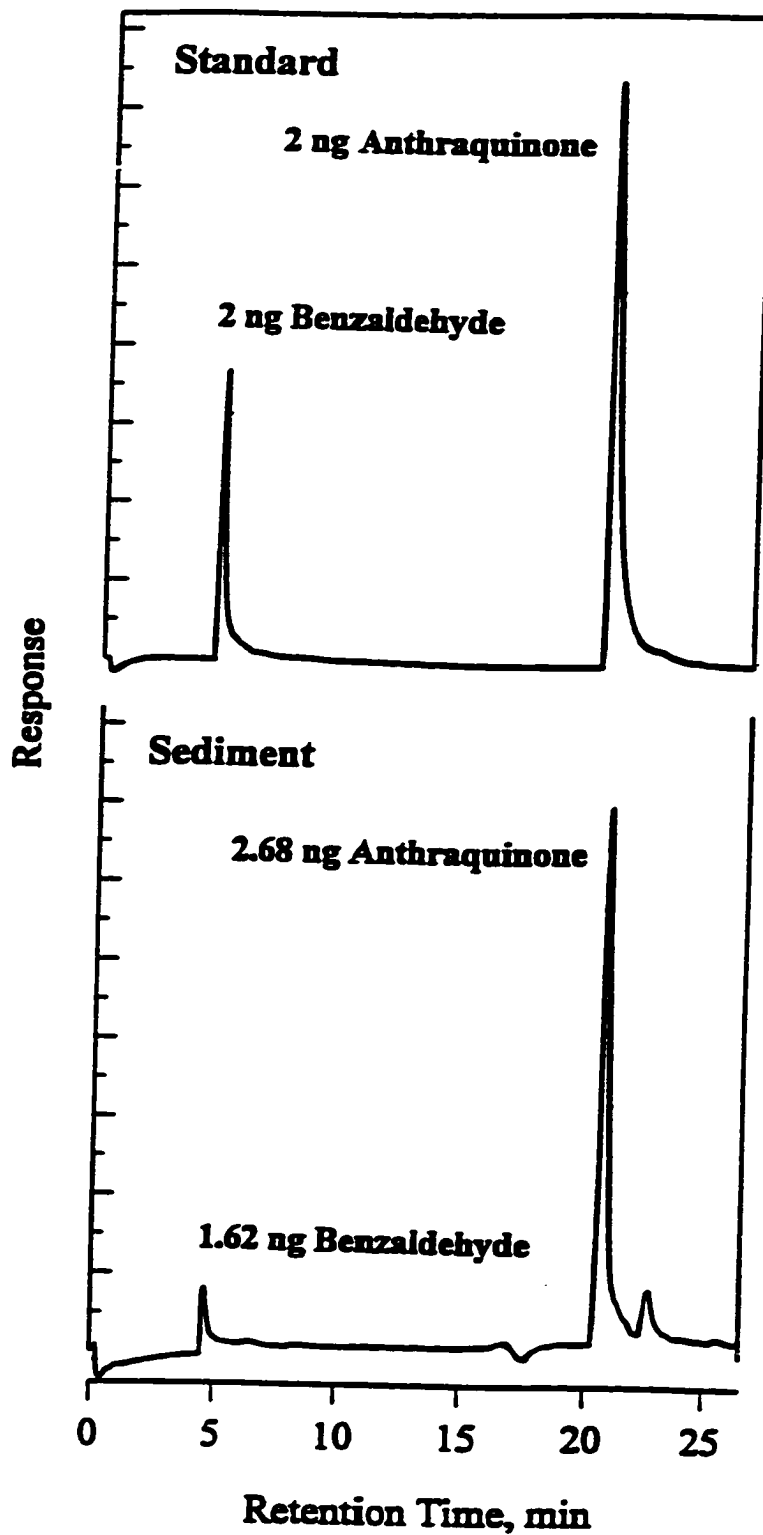
Figure 6.29   Quenching of aroyl compounds by components of the marine sediment standard PACS-1. Conditions as in Figure 6.23A.

measurement of response ratios and better the quality of on-line phosphorescence spectra. Thus this methodology shows much promise for the future.

6.7 Future Work

The prime objective of this research was achieved by demonstrating that the aroyl compounds in complex mixtures can be analyzed, in a triple-channel ALD, by using spectral response ratios, retention times, and one-line phosphorescence spectra. This can be done even at relatively low chromatographic resolution. In order for this methodology to be useful as an analytical tool for routine analyses, the following development work should be carried out.

(1)   There are several disadvantages in using absolute retention data, since they depend upon various column paraments such as flow rate, temperature and weight of liquid phase.   Instead, relative retentions should be used in order to ameliorate the variation of retention data and improve the reliability of the method.

(2)   In spite of the excellent sensitivity of the ALD, the severe quenching in the analysis of real-life samples can prevent the analyst from obtaining an on-line spectrum of good quality from a low-resolution packed column. For routine analysis, a good capillary column should be used. This would improve the chromatographic resolution and eliminate many incidents of quenching.

(3)   Final compound identification depends on the number and quality of library spectra available. The gas-phase luminescence spectra of more aroyl compounds should

be measured at various conditions to enrich the "spectrum library" that this work has

started.

REFERENCES

1.   M. Dressler, _Selective Gas Chromatographic Detector_, Journal of Chromatography Library 36, Elsevier, Amsterdam, 1986.

2.   H. H. Hill, Jr. and D.G. McMinn, _Detectors for Capillary Chromatography_, Chemical Analysis Serial 121, Wiley, New York, 1992.

3.   A. Zlatkis and C. F. Poole, _Electron Capture Theory and Practice in Chromatography_, Journal of Chromatography Library 20, Elsevier, Amsterdam, 1981.

4.   X. Y. Sun, B. Millier and W. A. Aue, _Can. J. Chem._, **70** (4), 1129 (1992).

5.   P. C. Uden, _J. Chromatogr.A_, **703**, 393 (1995).

6.   R. P. Evershed, _Mass Spectrom._, **10**, 181 (1981).

7.   G. A. Eiceman, H. H. Hill, Jr., B. Davanl and J. L. Gardea-Torresdey, _Anal. Chem._, **68**, 291R (1996).

8.   R. F. Zainullin and V. G. Berezkin, _Crit. Rev. Anal. Chem_ **22**, 183 (1991).

9.   M. A. Bush and K. W. Bush, _Spectrochimica Acta Rev_, **14**, 303 (1991).

10. P. Froehlich and E. L. Wehry, _Modern Fluorescence Spectroscopy_. Plenum Press. New York, 1981.

11. M. C. Bowman, M. Beroza, _Anal. Chem._, **40**, 535 (1968).

12. R. P. Cooney, J, D. Winefordner, _Anal. Chem._, **49**, 1057 (1977).

13. C. A. Gierczok, M. A. Heindorf and J. Allison, _Anal. Chem._, **56**, 2966 (1984).

14. L. F. Guilbault, R. Hohmann and E. L. Wehry, _J. Chromatogr._, **475**, 237 (1989).

15. A. K. Adams, D. L. Van Engelen and L. C. Thomas, _J. Chromatogr._, **303**, 341 (1984).

16. H. Bagheri and C. S. Creaser, _Anal. Chim. Acta_, **233**, 303 (1990).

17. V. B. Conrad, W. J. Carter, E. L. Wehry and G. Monantor, _Anal. Chem._, **55**, 1340, (1983).

18. J. M. Hayes and G. J. Small, *Anal. Chem.*, **54**, 1204 (1982).

19. B. V. Pepich, J. B. Callis, D. H. Burns, M. Gouterman and D. A. Kalman, *Anal. Chem.*, **58**, 2825 (1986).

20. J. W. Birks, *Chemiluminescence and Photochemical Reaction Detection in Chromatography*, VCH Publishers, New York, 1989.

21. A. N. Wright and C. A. Winkler, *Active Nitrogen*, Academic Press, New York and London, 1968.

22. A. P. D'Silva and V. A. Fassel, *Anal. Chem.*, **44**, 2115 (1972).

23. G. A. Capelle and D. G. Sutton, *Appl. Phys. Lett.*, **30**, 407 (1977).

24. G. A. Capelle and D. G. Sutton, *Rev. Sci. Instrum.*, **49**, 1124 (1978).

25. J. E. Melzer, J. L. Jordan and D. G. Sutton, *Anal. Chem.*, **52**, 348 (1980).

26. H. C. Na and T. M. Niemczyk, *Anal. Chem.*, **54**, 1839 (1982).

27. H. C. Na and T. M. Niemczyk, *Anal. Chem.*, **55**, 1240 (1983).

28. W. B. Dodge and R. O. Allen, *Anal. Chem.*, **53**, 1279 (1981).

29. A. P. D'Silva, G. W. Rice and V. A. Fassel, *Appl. Spectrosc.*, **34**, 578 (1980).

30. D. G. Sutton, J. E. Melzer and G. A. Capelle, *Anal. Chem.*, **50**, 1247 (1978).

31. D. G. Sutton, K. R. Westburg and J. E. Melzer, *Anal. Chem.*, **51**, 1399 (1979).

32. G. W. Rice, J. J. Richard, A. P. D'Silva and V. A. Fassel, *Anal. Chem.*, **53**, 1519 (1981).

33. G. W. Rice, J. J. Richard, A. P. D'Silva and V. A. Fassel, *J. Assoc. Off. Anal. Chem.*, **65**, 14 (1982).

34. J. E. Melzer and D. G. Sutton, *Appl. Spectrosc.*, **34**, 434 (1980).

35. R. Brown and C. A. Winkler, *Angew. Chem.*, **9** (3), 181 (1970).

36. G. W. Rice, A. P. D'Silva and V. A. Fassel, *Appl. Spectrosc.*, **38**, 149 (1984).

37. W. H. Hood and T. M. Niemczyk, *Anal. Chem.*, **58**, 210 (1986).

38. J. W. Mitchell, P. K. Wittman and A. M. Williams, *Anal. Chem.*, **58**, 371 (1986).

39. P. K. Wittman and J. W. Mitchell, *Appl. Spectrosc.*, **40**, 156 (1986).

40. H. A. Jurgensen, T. Yu and J. D. Winefordner, *Can. J. Spectrosc.*, **29**, 113 (1984).

41. Y. -Z. Tang and W. A. Aue, *J. Chromatogr.*, **409**, 243 (1987).

42. Y. -Z. Tang and W. A. Aue, *Mikrochim. Acta* [Wien], **II**, 21 (1987).

43. Y. -Z. Tang and W. A. Aue, *Mikrochim. Acta* [Wien], **II**, 29 (1987).

44. Y. -Z. Tang, *Doctoral Thesis*, Dalhousie University, 1987.

45. H. Singh and W. A. Aue, *J. Chromatogr.A*, **746**, 43 (1996).

46. X. -Y. Sun, *Doctoral Thesis*, Dalhousie University, 1993.

47. J. K. Rabek, *Experimental Methods in Photochemistry and Photophysics*, Part 2, John Wiley & Sons, New York, 1982.

48. R. E. Clement, F. I. Onuska, G. A. Eiceman and H. H. Hill, Jr., *Anal. Chem.*, **62**, 414R (1990).

48a. H. Simonis, *Ber.*, **45**, 1584 (1912).

49. W. F. Rogge, L. M. Hlldemann, M. A. Mazurek, G. R. Cass and B. R. T. Simonelt, *Environ. Sci. Technol.*, **28**, 1375 (1994).

50. T. Migake and T. Shibamoto, *J. Chromatogr. A*, **693**, 376 (1995).

51. A. Vairavamurthy, J. M. Roberts and L. Newman, *Atmosphere Environ.*, **26A**, 1965 (1992).

52. J. T. Coates, A. W. Elzerman and A. W. Garrison, *J. Assoc. Off. Anal. Chem.*, **69**, 110 (1986).

53. I. Blankenkorn, D. Meijer and R. V. Delft, *Fresenius Z. Anal. Chem.*, **343**, 497 (1992).

54. J. J. Gether and K. E. Thrane, *Anal. Chim. Acta*, **184**, 99 (1986).

55. T. Spitzer and S. Kuwatsuka, *Environ. Pollut.*, **62**, 63 (1989).

56. T. Spitzer and T. Takeuchi, *J. Chromatogr.A*, **710**, 109 (1995).

57. D. R. Knapp, *Handbook of Analytical Derivatization Reactions*, John Wiley & Sons, New York, 1979.

58. R. K. Marcus, *Glow Discharge Spectroscopies*, Plenum Press, New York, 1993.

59. R. S. Becker, *Theory and Interpretation of Fluorescence and Phosphorescence*, Wiley-Interscience, New York, 1969.

60. C. A. Parker, *Photoluminescence of Solutions*, Elsevier, New York. 1968.

61. J. D. Winefordner, S, G, Schulman, and T. C. O'Haver, *Luminescence Spectrometry in Analytical Chemistry*, Wiley-Interscience, New York, 1972.

62. J. B. Birks, *Photophysics of Aromatic Molecules*, Wiley-Interscience, New York. 1970.

63. N. J. Turro, *Modern Molecular Photochemistry*, Benjamin/Cummings, Menlo Park, CA, 1978.

64. S. G. Schulman, *Molecular Luminescence Spectroscopy: Methods and Application. Part II. Chapter 4*, Wiley, New York, 1988.

65. D. H. Levy, *Ann. Rev. Phys. Chem.*, **31**, 197 (1980).

66. V. L. Ermolaev, *Soviet Physics Uspekhi*, **80**, 333 (1963).

67. D. R. Kearns and W. A. Case, *J. Am. Chem. Soc.*, **88**, 5087 (1966).

68. A. Iuone and N. Ebara, *Chem. Phys. Lett.*, **109**, 27 (1984).

69. A. Iuone, *Chem. Lett.*, 2085 (1986).

70. N. Ohmori, T. Suzuki and M. Ito, *J. Phys. Chem.*, **92**, 1086 (1988).

71. T. Itoh, *Chem. Phays. Lett.*, **151**, 166 (1988).

72. J. A. Barltrop and J. D. Coyle, *Excited State in Organic Chemistry*, John Wiley & Sons, New York, 1975.

73. T. Takemura and H. Baba, *Bull. Chem. Soc. Jpn.*, **42**, 2756 (1969).

74. V. L. Ermolaev and A. Terenin, *J. Chem. Phys*, **55**, 698 (1958).

75. E. V. Donckt and C. Vogels, *Spectrochim. Acta*, **28A**, 1969 (1972).

76. L. Goodman, M. Lamotte and M. Koyanagi, *Chem. Phys.*, **47**, 329 (1980).

77. O. Sneh and O. Cheshnovsky, *J. Phys. Chem.* **95**, 7154 (1991).

78. E. Villa, A. Amirav, W. Chen and E. C. Lim, *Chem. Phys. Lett.*, **147**, 43 (1988).

79. P. Devolder, *C. R. Acad. Sc. Paris*, t.300, Serie II, **No. 4**, 133 (1985).

80. M. Koyanagi and L. Goodman, *Chem. Phys.*, **39**, 237 (1979).

81. T. Itoh, H. Baba and T. Takemura, *Bull. Chem. Soc. Jpn*, **51**, 2841 (1978).

82. Y. Hirata and E. C. Lim, *J. Chem. Phys.*, **72**, 5505 (1980).

83. S. Yamamoto, T. Ebata and M. Ito, *J. Phys. Chem.*, **94**, 5786 (1990).

84. Y. P. Sun, D. F. Sears, Jr., and J. Saltiel, *J. Am. Chem. Soc.* **111**, 706 (1989).

85. T. Itoh, *J. Chem. Phys.*, **87**, 4361 (1987).

86. G. Yamaguchi, Y. Kakinoki and H. Tsubomura, *Bull. Chem. Soc. Jpn*, **40**, 526 (1967).

87. G. Scharf and J. D. Winefordner, *Talanta*, **33**, 17 (1986).

88. R. Shimada and L. Goodman, *J. Chem. Phys.*, **43**, 2027 (1965).

89. W. A. Case and D. R. Kearns, *J. Chem. Phys.*, **52**, 2175 (1970).

90. S. K. Ghoshal, S. K. Sarkar and G. S. Kastha, *Bull. Chem. Soc. Jpn.*, **54**, 3556 (1981).

91. W. Siebrand and M. Z. Zgierski, A. Amirav, B. Fuchs A. Penner and E. C. Lim, *J. Chem. Phys.*, **95**, 3074 (1991).

92. N. C. Yang, D. S. McClure, S. L. Murov, J. J. Houser and R. Dusenbery, *J. Am. Chem. Soc.*, **89**, 5466 (1967).

93. T. Nakayama, K. Sakural and K. Hamanoue, *J. Chem. Soc. Faraday Trans.*, **87**, 1509 (1991).

94. R. Shimada and L. Goodman, *J. Chem. Phys.*, **43**, 2027 (1965).

95. R. E. Brown, L. A. Singer and J. H. Parks, *Chem. Phys. Lett.*, **14**, 193 (1972).

96. R. E. Brown, K. D. Legg, M. W. Wolf and L. A. Singer, *Anal. Chem.*, **46**, 1690 (1974).

97. P. F. Jones and A. R. Calloway, *Chem. Phys. Lett.*, **10**, 438 (1971).

98. N. A. Borisevich and V. V. Gruzinskii, *Dokl. Akad. Nauk SSSR*, **175**, 852 (1967).

99. A. V. Dorokhin and A. A. Kotov, *Opt. Spectrosc. (USSR).*, **51**, 617 (1981).

100. G. N. Lewis and M. Kasha, *J. Am. Chem. Soc.*, **66**, 2100, (1944).

101. C. A. Parker and C. G. Hatchard, *Analyst*, **87**, 664 (1962).

102. A. Kuboyama and S. Yabe, *Bull. Chem. Soc. Jpn.*, **40**, 2475 (1967).

103. H. R. Drott and H. H. Dearman, *J. Chem. Phys.*, **47**, 1869 (1967).

104. K. E. Drabe, H. Veenvliet and D. A. Wiersma, *Chem. Phys. Lett.*, **35**, 469 (1975).

105. O. S. Khall and L. Goodman, *J. Phys. Chem.*, **80**, 2179 (1976).

106. T. Murao and T. Azumi, *J. Chem. Phys.*, **70**, 4460 (1979).

107. K. Hamanoue, T. Nakayama, Y. Kajiwara, T. Yamaguchi and H. Teranishi, *J. Chem. Phys.*, **86**, 6654 (1987).

108. D. K. Palit, H. Pal, T. Mukherjee and J. P. Mittal, *J. Chem. Soc. Faraday Trans.*, **86**, 3861 (1990).

109. H. H. Dearman and A. Chan, *J. Chem. Phys.*, **44**, 416 (1966).

110. S. N. Singh and R. S. Singh, *Indian J. Pure Appl. Phys.*, **5**, 342 (1967).

111. P. Longin, *C. R. Acad. Sc. Paris*, **t.271**, 292 (1970).

112. K. L. Rogozhin, A. N. Rodionov and D. N. Shigorin, *Opt. Spektrosk.*, **52**, 952 (1982).

113. T. Itoh, *Spectrochim. Acta*, **42A**, 1083 (1986).

114. S. P. McGlynn, T. Azumi and M. Kinoshita, *Molecular Spectroscopy of the Triplet State*, Prentice-Hall, Inc., New Jersey, 1969.

115. S. A. Carlson and D. M. Hercules, *J. Am. Chem. Soc.*, **93**, 5611 (1971).

116. S. N. Singh and R. S. Singh, *Indian J. Pure Appl. Phys.*, **5**, 394 (1967).

117. T. Itoh and H. Baba, *Bull. Chem. Soc. Jpn.*, **52**, 3213 (1979).

118. T. Itoh and H. Baba, *Chem Phys.*, **51**, 179 (1980).

119. G. D. Baruah, S. N. Singh and R. S. Singh, *Bull. Chem. Soc. Jpn.*, **42**, 3572 (1969).

120. H. J. Pownall and J. R. Huber, *J. Am. Chem. Soc.*, **93**, 6429 (1971).

121. H. J. Pownall, R. E. Connors and J. R. Huber, *Chem. Phys. Lett.*, **22**, 403 (1973).

122. T. Terada, M. Koyanagi and Y. Kanda, *Bull. Chem. Soc. Jpn.*, **53**, 352 (1980).

123. A. Chakrabarti and N. Hirota, *J. Phys. Chem.*, **80**, 2966 (1976).

124. T. Terada, M. Koyanagi and Y. Kanda, *Chem. Phys. Lett.*, **72**, 408 (1980).

125. M. Koyanagi, T. Terada and K. Nakashima, *J. Chem. Phys.*, **89**, 7349 (1988).

126. K. Meier and H. Zweifel, *J. Photochem.*, **35**, 353 (1986).

127. N. C. Yang and S. Murov, *J. Chem. Phys.*, **45**, 4358 (1966).

128. Y. Kanda, J. Stanislaus and E. C. Lim, *J. Am. Chem. Soc.*, **91**, 5085 (1969).

129. N. Y. C. Chu and D. R. Kearns, *J. Am. Chem. Soc.*, **94**, 2619 (1972).

130. G. W. Suter and U. P. Wild, *Chem. Phys.*, **102**, 205 (1986).

131. A. M. Nishimura and J. S. Vincent, *Chem. Phys. Lett.*, **13**, 89 (1972).

132. T. F. Hunter, *Trans. Faraday Soc.*, **66**, 300 (1970).

133. J. C. Scaiano and C. W. B. Lee, *J. Photochem.*, **20**, 327 (1982).

134. N. C. Yang, *Pure Appl. Chem.*, **9**, 591 (1964).

135. D. A. Warwick and C. H. J. Wells, *Spectrochim. Acta*, **24A**, 589 (1968).

136. S. Hirayama, *J. Chem. Soc., Faraday Trans. 1*, **78**, 2411 (1982).

137. S. L. Murov, I. Carmichael and G. L. Hug, *Handbook of Photochemistry*, Marcel Dekker, Inc., New York, 1993.

138. T. Itoh, *J. Photochem. Photobiol. A*, **50**, 171 (1989).

139. R. W. Taft, Jr., N. C. Deno and P. S. Skell, *Ann. Rev. Phys. Chem.*, **9**, 287 (1958).

140. H. H. Jaffe, *J. Chem. Phys.*, **20**, 1554 (1952).

141. D. R. Arnold, *Adv. Photochem.*, **6**, 301 (1968).

142. W. J. Leigh, D. R. Arnold, R. W. R. Humphreys and P. C. Wong, *Can. J. Chem.*, **58**, 2537 (1980).

143. W. J. Leigh and D. R. Arnold, *J. Chem. Soc., Chem. Commun.*, 406 (1980).

144. R. M. Hochstrasser and L. J. Noe, *J. Mol. Spect.*, **38**, 175 (1971).

145. A. Beckett and G. Porter, *Trans. Faraday Soc.*, **59**, 2051 (1963).

146. S. Yamamoto, N. Hashimoto and M. Ito, *Bull. Chem. Soc. Jpn.*, **64**, 2202 (1991).

147. N. C. Yang and C. Rivas, *J. Am. Chem. Soc.*, **83**, 2213 (1961).

148. G. Porter and M. F. Tchir, *J. Chem. Soc. A*, 3772 (1971).

149. E. Block and R. Stevenson, *J. Chem. Soc. Perkin I*, 308 (1973).

150. P. J. Wagner and C. P. Chen, *J. Am. Chem. Soc.*, **98**, 239 (1976).

151. D. M. Findlay and M. F. Tchir, *J. Chem. Soc., Faraday Trans. 1*, **72**, 1096 (1976).

152. P. G. Sammes, *Tetrahedron*, **32**, 405 (1976).

153. R. Haag, J. Wirz and P. J. Wagner, *Helv. Chim. Acta*, **60**, 2595 (1977).

154. R. K. Das, M. V. Encinas, R. D. Small, Jr., and J. C. Scaiano, *J. Am. Chem. Soc.*, **101**, 6965 (1979).

155. T. Yu, K. Tanabe and J. D. Winefordner, *Anal. Chem. Acta*, **201**, 317 (1987).

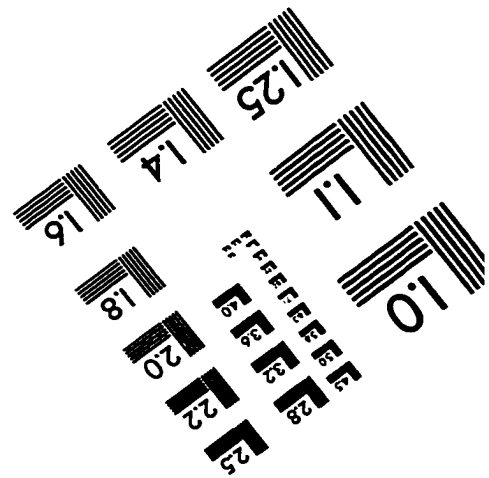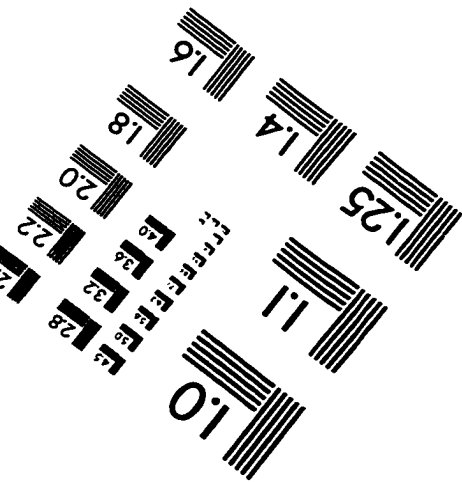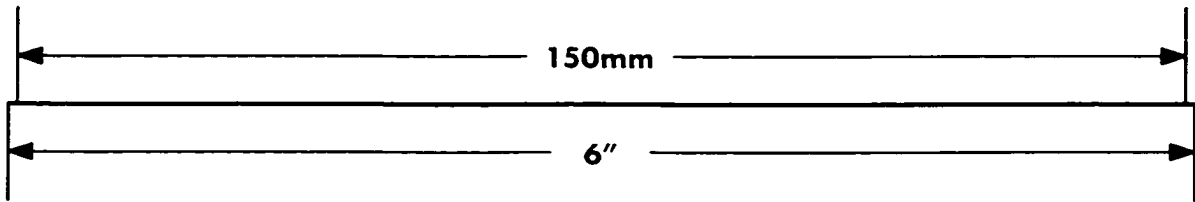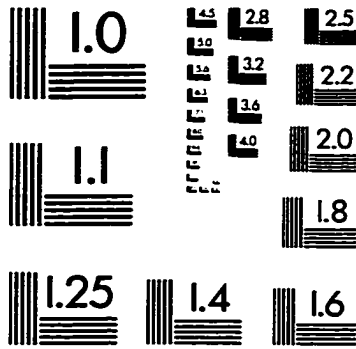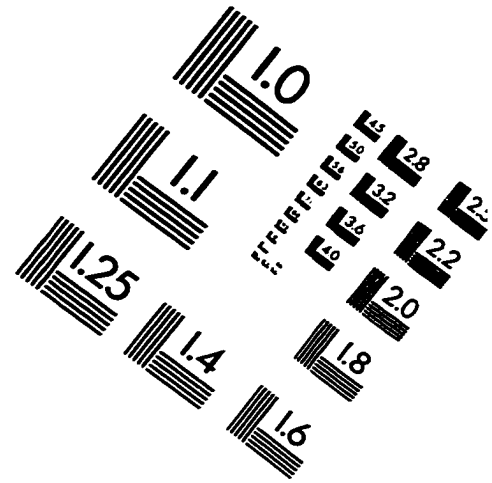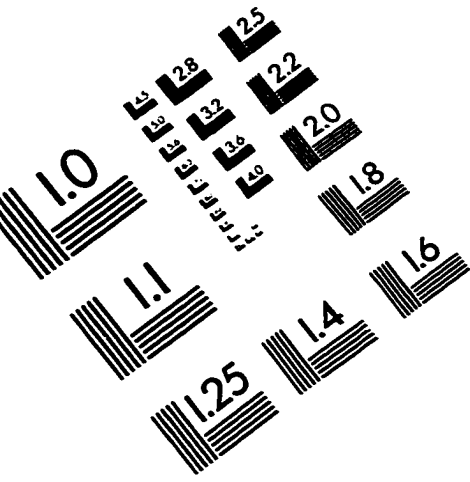156. O. Oldenberg, *J. Opt. Soc. Am.*, **61**, 1092 (1971).

157. J. A. Meyer and D. H. Klosterboer and D. W. Setser, *J. Chem. Phys.*, **55**, 2084 (1971).

158. D. H. Stedman and D. W. Setser, *J. Chem. Phys.*, **50**. 2256 (1969).

159. D. H. Stedman, J. A. Meyer and D. W. Setser, *J. Am. Chem. Soc.*, **90**, 6856 (1968).

160. P. Devolder, *Spectrochim. Acta*, **36A**, 783 (1980).

161. P. Devolder, O. Dessaux and P. Goudmand, *J. Photochem.*, **15**, 265 (1981).

162. J. Anketell and R. W. Nicholls, *Rev. Prog. Phys.*, **33**, 269 (1970).

163. M. F. Golde and B. A. Thrush, *Rev. Prog. Phys.*, **36**, 1285 (1973).

164. F. Valadier, E. Faure, R. Bergeron and J. Janin, *C. R. Acad. Sci.*, **265**, 1432 (1967).

165. J. N. Demas, *Excited State Lifetime Measurements*, Academic Press, New Yok, 1983.

166. D. H. Stedman and D. W. Setser, *Chem. Phys. Lett.*, **2**, 542 (1968).

167. D. W. Setser, D. H. Stedman and J. A. Coxon, *J. Chem. Phys.*, **53**, 1004 (1969).

168. R. W. B. Pearse and A. G. Gaydon, *The Indentification of Molecular Spectra*, Chapman & Hall, London, 1976.

169. M. C. Bowman and M. Beroza, *Anal. Chem.*, **40**, 1448 (1968).

170. V. A. Joonson and E. P. Loog, *J. Chromatogr.*, **120**, 285 (1976).

171. K. -P. Li and J. Arrington, *Anal. Chem.*, **51**, 287 (1979).

172. P. A. Webb, D. Ball and T. Thornton, *J. Chromatogr. Sci.*, **21**, 447 (1983).

173. W. A. Aue, B. Millier and X. -Y. Sun, *Anal. Chem.*, **63**, 2951 (1991).

174. B. Millier, X. -Y. Sun and W. A. Aue, *Anal. Chem.*, **65**, 104 (1993).

175. W. A. Aue, B. Millier and X. -Y. Sun, *Anal. Chem.*, **62**, 2453 (1990).

176. W. A. Aue, B. Millier and X. -Y. Sun, *Can. J. Chem.*, **70**, 1143 (1992).

177. W. A. Aue, H. Singh and B. Millier, *J. Chromatogr. A*, **719**, 468 (1996).

178. Catalogue, Hamamatsu Corporation, 250 Wood Avenue, Middlesex, N.J., 08846. USA.

179. Y.-Z. Liang, O. M. Kvalheim, H. R. Keller, D. L. Massart, P. Kiechle and F. Erni, *Anal. Chem.*, **64**, 946 (1992).

180. A. Fellinger, *Anal. Chem.*, **66**, 3306 (1994).

181. H. Miao, M. Yu and S. Hu, *J. Chromatogr. A*, **749**, 5 (1996).

182. A. Economou, P. R. Fielden and A. J. Packham, *Analyst*, **121**, 1015 (1996).

183. X. Shao, W. Cai, P. Sun, M. Zhang and G. Zhao, *Anal. Chem.*, **69**, 1722 (1997).

184. W. A. Aue, H. Singh and X. -Y. Sun, *J. Chromatogr. A*, **687**, 283 (1994).

185. D. A. Leathard and B. C. Shurlock, *Identification Techniques in Gas Chromatography*, Wiley, London, 1970.

186. Z. -P. Lin and W. A. Aue, *J. Chromatogr. A*, **742**, 143 (1996).

187. W. A. Aue, P. P. Wickramanayake and J. Mueller, *Anal. Chim. Acta*, **125**, 175 (1981).

188. Y. Masada, *Analysis of Essential Oils by Gas Chromatography and Mass Spectrometry*, John Wiley & Sons, Inc., New York, 1976.

189. R. P. Adams, *Identification of Essential Oils by Ion Trap Mass Spectrometry*, Academic Press, San Diego, CA, 1995.

190. E. E. Stashenko, N. Q. Prada and J. R. Martinez, *J. High Resol. Chromatogr.*, **19**, 353 (1996).

191. K. G. Millier, C. F. Poole and T. M. P. Pawlowski, *Chromatogr.*, **42**, 639 (1996).

192. J. C. Millier and J. N. Millier, *Statistics for Analytical Chemistry*, Ellis Horwood, Chichester, 2nd ed., 1987.

193. D. T. E. Hunt and A. L. Ailson, *The Chemical Analysis of Water. General Principles and Techniques*, Royal Society of Chemistry, Lodon, 2nd ed., 1986.

194. D. Simmons and R. F. Parsons, *Biochem. Syst. Ecol.*, **15**, 209 (1987).

195. P. Fernandez and J. M. Bayona, *J. Chromatogr.*, **625**, 141 (1992).

196. A. A. Mosi, K. J. Reimer and G. K. Eigendorf, *Talanta*, **44**, 985 (1997).

IMAGE EVALUATION
TEST TARGET (QA-3)

1.0

2.5
2.8
3.2
3.6
4.0
2.2
2.0
1.8
1.1
1.6
1.4
1.25

1.0
2.5
2.8
3.2
3.6
4.0
2.2
2.0
1.8
1.1
1.25
1.4
1.6

Center target

1.0
2.8
2.5
3.2
2.2
3.6
4.0
2.0
1.1
1.8
1.25
1.4
1.6

150mm

6"